Fluid Mechanics for Chemical Engineering

Fluid Mechanics for Chemical Engineering

Mathieu Mory

ISTE WILEY

First published 2011 in Great Britain and the United States by ISTE Ltd and John Wiley & Sons, Inc.

ISTE Ltd
27-37 St George's Road
London SW19 4EU
UK

www.iste.co.uk

John Wiley & Sons, Inc.
111 River Street
Hoboken, NJ 07030
USA

www.wiley.com

Library of Congress Cataloging-in-Publication Data

Mory, Mathieu.
Fluid mechanics for chemical engineering / Mathieu Mory.
p. cm.
Includes bibliographical references and index.
ISBN 978-1-84821-281-7 (hardback)
1. Chemical processes. 2. Fluid dynamics. I. Title.
TP155.7.M673 2011
660'.29--dc22

2010048940

British Library Cataloguing-in-Publication Data
A CIP record for this book is available from the British Library
ISBN 978-1-84821-281-7

Printed and bound in Great Britain by CPI Antony Rowe, Chippenham and Eastbourne.

Table of Contents

Preface

This book is mainly about fluid mechanics, but it is first intended to MSc and professionals who need to make use of fluid mechanics skills for applications pertaining to chemical and process engineering. This objective explains the presentation of fluid mechanics as given in this book. The foundations of the discipline are generally not set out, but the book endeavours to help students and professionals to use the tools of fluid mechanics in a pertinent way, while attempting to point out the key ideas associated with the concepts encountered.

As an example, the ability to use Navier-Stokes equations appropriately is more important, to most practitioners, than the ability to prove them. It is of course very interesting to have reflected upon that proof at some point, but this can be found in other books, and this is not the intended objective of this book. Besides, I will be very happy if this book can prove useful for specialists in fluid mechanics, giving them the opportunity to discover important applications of fluid mechanics in the field of chemical engineering.

The book is divided into three parts.

The first part is about the basics of fluid mechanics. Emphasis is on general theorems that constitute the tools used in the first instance by engineers. Chapter 2 forms the main foundation of that part, which then branches into short chapters tackling the key notions implemented by a specialist in process engineering (hydraulic circuits, pumps, rheometry, etc.). The concepts of dimensional analysis are also emphasized (Chapter 3).

The second part deals with mixing phenomena associated with turbulence. In that part, notions relating to turbulence are first presented. The problems associated with dispersion and mixing in connection with chemical reactions are then considered. The key notion, from a fundamental standpoint, regards the interrelation between the phenomena of turbulence and that of molecular diffusion, the latter being the actual cause for mixing that allows a chemical reaction to occur.

Toward the end of this part, elementary models for the simulation of reacting flows are also presented.

The third part presents the tools of fluid mechanics used in mechanical fluid/solid and fluid/fluid separation processes. Process unit operations considered include filtration, fluidization, and centrifugal separation. I have also tried to provide, in that part, means for understanding more complex approaches regarding the modeling of a solid particle's dynamics within a fluid flow (Chapter 16) and a presentation of the physics of a granular material, which will often be of interest to specialists in process engineering.

Although the whole treatment might not seem very ambitious, my goal was primarily to specify the elementary notions in fields related to fluid mechanics, in order to facilitate access to other, more specialized books.

This book draws its material chiefly from the courses I have been teaching for about 10 years at the École Nationale Supérieure en Génie des Technologies Industrielles, an engineering curriculum at the University of Pau and the Adour Region (UPPA) in the chemical and process engineering specialization. For the sake of consistency, I have endeavored to expand the coverage of the subject matter by complementing certain parts of my lectures. As this is an adaptation of a book previously published in French, and of course drawn from material originally taught to French students, there were of course issues regarding the references. I am fully aware that some of the literature in French will not be available to non-French speakers, and I apologise for this, but it would have been unfair not to keep these citations, as they were significant sources for writing the book. Wherever possible English substitutions to the French references have been provided, and where not, additional English textbooks have been suggested as a complement to the reading of the book.

I wish to thank the UPPA for giving me an opportunity to lecture in these topics. I am thankful to my colleagues S. Alexandrova, A. Saboni, and D. Graebling, from the UPPA, for their insightful discussions that proved invaluable to me while writing this book. Beyond this, their friendship has been a tremendous support for me throughout this critical work.

I have also used my experience in research and education while writing the various chapters of this book.

It is important to me to mention first my first teaching experiences, when I joined a team in Grenoble, teaching fluid mechanics at the École Nationale des Travaux Publics de l'Etat. The course taught by C. Le Provost, who was then in charge, emphasized the use and understanding of tools rather than the proof of

their validity. I have tried to emphasize and retain that approach as far as possible in this book. Later, I was lucky to receive an invaluable educational tutoring from R. Moreau, M. Favre-Marinet, and A. Temperville, at the École Nationale Supérieure d'Hydraulique et de Mécanique de Grenoble and at Joseph Fourier University.

This book also includes the legacy of the one year I spent (1988–1989) on secondment to the Centre d'Etudes et de Recherche de Grenoble (ALSTHOM group)[1], when I learnt a great deal alongside specialists in industrial hydraulics. My thanks to P. Chantrel, who was my supervisor and also to the whole team in this regard.

My thesis supervisor, E. Hopfinger, might not recognize much of himself in this book. Yet, I received my training, first and foremost, from him during my PhD years. He was instrumental in expanding my knowledge base. More importantly, by making himself available to me, he enabled me to get acquainted with the way he saw and tackled fluid mechanics. Those years were undoubtedly the richest and the most momentous in my professional life. I wish to express to him my recognition and my gratitude.

Lastly, I thank the experts who agreed to read this book and took time to offer very useful reviews in order to improve it and rectify errors. Jean-Luc Achard monitored the whole enterprise and I thank him for that, although I often cursed him during the editing stage for obvious reasons! Nevertheless, he has remained a true friend since 1982.

Mathieu Mory
January 2011

1 Now a subsidiary of the Environne'Tech company (http://cerg-fluides.com/)

Part I

Elements in Fluid Mechanics

Chapter 1

Local Equations of Fluid Mechanics

In this chapter, to begin with, we recall the Navier–Stokes equations that govern the flow of a Newtonian fluid. These equations explain the behavior of common fluids such as water or air. For a given force field and boundary conditions, the solution of Navier–Stokes equations controls both the flow velocity and pressure at any point and at any time in the domain under consideration. The Navier–Stokes equations are the most commonly used equations in fluid mechanics; they provide the knowledge of the flow of Newtonian fluids at the local level.

The solutions to Navier–Stokes equations are typically very difficult to arrive at. This fact is attested to by the extraordinary development of numerical computation in fluid mechanics. Only a few exact analytical solutions are known for Navier–Stokes equations. We present in this chapter some laminar flow solutions whose interpretation per se is essential in this regard. We then introduce the boundary layer concept. We conclude the chapter with a discussion on the uniqueness of solutions to Navier–Stokes equations, with special reference to the phenomenon of turbulence.

This being the introductory chapter, we have not included a prolonged discussion on continuum mechanics. The derivation of Navier–Stokes equations is available in other continuum mechanics or fluid mechanics books.[1] We have consciously avoided concentrating on the derivational aspects of Navier–Stokes equations as we

1 In particular, the well-known books by L.D. Landau and E.M. Lifshitz, *Fluid Mechanics* (2nd Edition, Butterworth-Heinemann, 1987) and by G.K. Batchelor, *An Introduction to Fluid Mechanics* (Cambridge University Press, 1967) provide an approach that complements the present book.

are convinced that it is far more important to understand the meaning of the different terms of these equations and to hence interpret the way they are applied in the study of fluid mechanics in general. In addition, we limit ourselves to introducing the only classical concept from continuum mechanics to be used in this book, namely, the ability to calculate the force acting through a surface passing through a point that lies inside a continuum, using the stress tensor. Hence, Chapter 1 partly serves as a collection of formulae, while proper physical principles are discussed in the remainder of this book. The reader might wish to read this chapter without pondering on it for long, and then may refer to it later, if necessary, for it may be insightful in such a case.

1.1. Forces, stress tensor, and pressure

Consider a domain, V, containing a fluid. The fluid's flow is controlled by various forces acting on it. The laws of mechanics help us to distinguish two types of forces:

– Body forces, which are exerted at every point in a domain. Weight is the most common body force.

– Forces that are transferred from one particle to another, at the boundary of and within the domain. These forces are expressed using the stress tensor. This is where the continuum concept intervenes.

The force at a point M in the continuum is associated with surface element ds whose orientation is given by the unit normal vector $\vec{n}$ (Figure 1.1). The force $\mathrm{d}\vec{F}$, which is proportional to the surface ds, varies when the orientation of the surface changes. It is determined at the point M using the stress tensor $[\Sigma]$, which is a symmetric,[2] 3×3 matrix:

$$[\Sigma] = \begin{pmatrix} \sigma_{xx} & \sigma_{xy} & \sigma_{xz} \\ \sigma_{xy} & \sigma_{yy} & \sigma_{yz} \\ \sigma_{xz} & \sigma_{yz} & \sigma_{zz} \end{pmatrix} \qquad [1.1]$$

2 The reader is referred to continuum mechanics textbooks for a justification of the symmetry of the stress tensor.

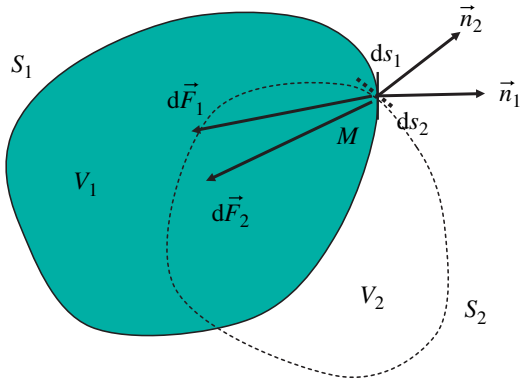

Figure 1.1. *Forces* $d\vec{F}_1$ *and* $d\vec{F}_2$ *exerted at a point M through two surface elements* ds_1 *and* ds_2*, whose orientations are given by normals* $\vec{n}_1$ *and* $\vec{n}_2$ *. Both* ds_1 *and* ds_2 *are elements of closed surfaces* S_1 *(solid line) and* S_2 *(dashed line), respectively, surrounding volumes* V_1 *and* V_2

The force through the surface element ds whose normal is $\vec{n}$ is written as:

$$d\vec{F} = \begin{pmatrix} dF_x \\ dF_y \\ dF_z \end{pmatrix} = [\Sigma]\vec{n}ds = ds \begin{pmatrix} \sigma_{xx} & \sigma_{xy} & \sigma_{xz} \\ \sigma_{xy} & \sigma_{yy} & \sigma_{yz} \\ \sigma_{xz} & \sigma_{yz} & \sigma_{zz} \end{pmatrix} \begin{pmatrix} n_x \\ n_y \\ n_z \end{pmatrix} \quad [1.2]$$

The force applied to a closed surface S surrounding an arbitrary volume V in the continuum (Figure 1.1) can be derived using the surface integral:

$$\vec{F} = \iint_S [\Sigma]\vec{n}ds \quad [1.3]$$

The concept of the stress tensor is inseparable from the mechanical principle of action and reaction. The normal vector $\vec{n}$ is oriented toward the exterior of the domain on which the force is applied. The direction of the force is reversed if one considers the force exerted by the domain V on the exterior. *Therefore, the domain under consideration should always be specified.* The force is exerted by the external environment through the surface of separation.

In equation [1.1] and [1.2], the stress tensor is expressed in a Cartesian coordinate system (O, x, y, z). In this coordinate system, the single-column matrices define the normal vector $\vec{n}$ and force $d\vec{F}$. We only have to multiply matrix $[\Sigma]$ by $\vec{n}$ to calculate the force.

The stress tensor embodies two notions: pressure and friction forces. For a Newtonian fluid, pressure is introduced by adding together the diagonal terms of the stress tensor:

$$p = -(\sigma_{xx} + \sigma_{yy} + \sigma_{zz})/3 \qquad [1.4]$$

We also introduce the stress deviator tensor [Σ′].

$$\begin{pmatrix} \sigma'_{xx} & \sigma'_{xy} & \sigma'_{xz} \\ \sigma'_{xy} & \sigma'_{yy} & \sigma'_{yz} \\ \sigma'_{xz} & \sigma'_{yz} & \sigma'_{zz} \end{pmatrix} = \begin{pmatrix} \sigma_{xx} + p & \sigma_{xy} & \sigma_{xz} \\ \sigma_{xy} & \sigma_{yy} + p & \sigma_{yz} \\ \sigma_{xz} & \sigma_{yz} & \sigma_{zz} + p \end{pmatrix} \qquad [1.5]$$

such that $\sigma'_{xx} + \sigma'_{yy} + \sigma'_{zz} = 0$. The stress deviator is associated with friction forces, whereas the pressure produces a force that is perpendicular to the surface element under consideration. Alternatively, the stress tensor can be expressed as:

$$[\Sigma] = \begin{pmatrix} -p & 0 & 0 \\ 0 & -p & 0 \\ 0 & 0 & -p \end{pmatrix} + [\Sigma'] \qquad [1.6]$$

Figure 1.1 depicts two volumes V_1 and V_2 surrounded by closed surfaces S_1 and S_2. At a point M belonging to both surfaces, the normals are different, and therefore the forces exerted on the surface elements, ds_1 and ds_2, are also different. The orientation of the force vectors shown in Figure 1.1 satisfies two properties. The forces are not perpendicular to the two surfaces onto which they are applied, if friction forces exist. However, they are not far from being perpendicular to the surfaces, and they are oriented toward the interior of the domain; this is because pressure forces are usually predominant in a fluid. Further, the forces exerted by the external environment on the volumes V_1 and V_2 push them toward the interior of the domain.

These concepts become more clear as and when they are used in specific cases, as done in subsequent sections of this chapter and other chapters of this book. The important point is to correctly use tensor calculus to calculate forces, using the stress tensor so as to obtain proper orientation of the normal vectors to the surfaces to assign a correct direction to the forces that are applied on the surface of a given volume.

1.2. Navier–Stokes equations in Cartesian coordinates

The fundamental law of dynamics for fluid flow in a continuum is given in Table 1.1 in a Cartesian coordinate system (O, x, y, z). The velocity vector is explained using its three velocity components (u_x, u_y, and u_z). The quantities (f_x, f_y, and f_z) are the three components of body forces, such as weight, $\rho\vec{g}$.

In mathematical terms, the system of equations shows the divergence of the stress tensor. For a continuum, the complete dynamic formulation of the mechanical problem requires that the stress tensor be known. Rheology is the discipline of mechanics which deals with the determination of the stress tensor for a given material, whether fluid or solid. In Chapter 7, we introduce some concepts of rheology, or rather rheometry. This discipline makes use of certain techniques (e.g. the use of rheometers) to determine the relationship that links the stress deviator tensor to the strain tensor or to the strain rate tensor, for a given material. This relationship is called "constitutive equation."

Local formulation of the fundamental law of mechanics:

$$\rho\left\{\frac{\partial u_x}{\partial t}+u_x\frac{\partial u_x}{\partial x}+u_y\frac{\partial u_x}{\partial y}+u_z\frac{\partial u_x}{\partial z}\right\}=\frac{\partial \sigma_{xx}}{\partial x}+\frac{\partial \sigma_{xy}}{\partial y}+\frac{\partial \sigma_{xz}}{\partial z}+f_x$$

$$\rho\left\{\frac{\partial u_y}{\partial t}+u_x\frac{\partial u_y}{\partial x}+u_y\frac{\partial u_y}{\partial y}+u_z\frac{\partial u_y}{\partial z}\right\}=\frac{\partial \sigma_{xy}}{\partial x}+\frac{\partial \sigma_{yy}}{\partial y}+\frac{\partial \sigma_{yz}}{\partial z}+f_y$$

$$\rho\left\{\frac{\partial u_z}{\partial t}+u_x\frac{\partial u_z}{\partial x}+u_y\frac{\partial u_z}{\partial y}+u_z\frac{\partial u_z}{\partial z}\right\}=\frac{\partial \sigma_{xz}}{\partial x}+\frac{\partial \sigma_{yz}}{\partial y}+\frac{\partial \sigma_{zz}}{\partial z}+f_z$$

Strain rate tensor:

$$[D]=\frac{1}{2}\begin{Bmatrix} D_{xx}=2\dfrac{\partial u_x}{\partial x} & D_{xy}=\left(\dfrac{\partial u_x}{\partial y}+\dfrac{\partial u_y}{\partial x}\right) & D_{xz}=\left(\dfrac{\partial u_x}{\partial z}+\dfrac{\partial u_z}{\partial x}\right) \\ D_{xy}=\left(\dfrac{\partial u_x}{\partial y}+\dfrac{\partial u_y}{\partial x}\right) & D_{yy}=2\dfrac{\partial u_y}{\partial y} & D_{yz}=\left(\dfrac{\partial u_y}{\partial z}+\dfrac{\partial u_z}{\partial y}\right) \\ D_{xz}=\left(\dfrac{\partial u_x}{\partial z}+\dfrac{\partial u_z}{\partial x}\right) & D_{yz}=\left(\dfrac{\partial u_y}{\partial z}+\dfrac{\partial u_z}{\partial y}\right) & D_{zz}=2\dfrac{\partial u_z}{\partial z} \end{Bmatrix}$$

Stress tensor for a Newtonian fluid:

$$[\Sigma]=\begin{Bmatrix} \sigma_{xx}=-p+2\mu\dfrac{\partial u_x}{\partial x} & \sigma_{xy}=\mu\left(\dfrac{\partial u_x}{\partial y}+\dfrac{\partial u_y}{\partial x}\right) & \sigma_{xz}=\mu\left(\dfrac{\partial u_x}{\partial z}+\dfrac{\partial u_z}{\partial x}\right) \\ \sigma_{xy}=\mu\left(\dfrac{\partial u_x}{\partial y}+\dfrac{\partial u_y}{\partial x}\right) & \sigma_{yy}=-p+2\mu\dfrac{\partial u_y}{\partial y} & \sigma_{yz}=\mu\left(\dfrac{\partial u_y}{\partial z}+\dfrac{\partial u_z}{\partial y}\right) \\ \sigma_{xz}=\mu\left(\dfrac{\partial u_x}{\partial z}+\dfrac{\partial u_z}{\partial x}\right) & \sigma_{yz}=\mu\left(\dfrac{\partial u_y}{\partial z}+\dfrac{\partial u_z}{\partial y}\right) & \sigma_{zz}=-p+2\mu\dfrac{\partial u_z}{\partial z} \end{Bmatrix}$$

Navier–Stokes equations: Conservation of momentum

$$\rho\left\{\frac{\partial u_x}{\partial t} + u_x\frac{\partial u_x}{\partial x} + u_y\frac{\partial u_x}{\partial y} + u_z\frac{\partial u_x}{\partial z}\right\} = -\frac{\partial p}{\partial x} + \mu\Delta u_x + f_x$$

$$\rho\left\{\frac{\partial u_y}{\partial t} + u_x\frac{\partial u_y}{\partial x} + u_y\frac{\partial u_y}{\partial y} + u_z\frac{\partial u_y}{\partial z}\right\} = -\frac{\partial p}{\partial y} + \mu\Delta u_y + f_y$$

$$\rho\left\{\frac{\partial u_z}{\partial t} + u_x\frac{\partial u_z}{\partial x} + u_y\frac{\partial u_z}{\partial y} + u_z\frac{\partial u_z}{\partial z}\right\} = -\frac{\partial p}{\partial z} + \mu\Delta u_z + f_z$$

Continuity equation: Conservation of mass

$$\frac{\partial \rho}{\partial t} + u_x\frac{\partial \rho}{\partial x} + u_y\frac{\partial \rho}{\partial y} + u_z\frac{\partial \rho}{\partial z} + \rho\left\{\frac{\partial u_x}{\partial x} + \frac{\partial u_y}{\partial y} + \frac{\partial u_z}{\partial z}\right\} = 0$$

State law

Incompressible fluid	**Compressible fluid**
$\frac{\partial u_x}{\partial x} + \frac{\partial u_y}{\partial y} + \frac{\partial u_z}{\partial z} = 0$	$\rho = \rho(P)$

Table 1.1. *Navier–Stokes formulation in a Cartesian coordinate system*

For Newtonian fluids the constitutive law is a linear relationship between the stress deviator tensor and the strain rate tensor:

$$[\Sigma'] = 2\mu[D] \qquad [1.7]$$

Table 1.1 sets out the strain rate tensor, $[D]$, as expressed in a Cartesian coordinate system. The constitutive equation [1.7] involves the dynamic viscosity of the fluid, μ (in kg m^{-1} s^{-1} or Pa s). We also introduce the kinematic viscosity, ν (in m^2 s^{-1}), defined by $\mu=\rho\nu$, where ρ is the mass density of the fluid (in kg m^{-3}).

For a Newtonian fluid, the Navier–Stokes equations are derived by introducing the constitutive equation [1.7] into the fundamental law of mechanics. The Navier–Stokes equations in a Cartesian coordinate system are also shown in Table 1.1.

In this book, we restrict our discussion basically to the principles of isothermal flows. When temperature varies within the domain, the heat equation must be added to the system of equations in Table 1.1. Here the physical properties of fluids are assumed to be constant, i.e. the numerical value of the viscosity at every point within the domain is linked to the fluid under consideration. The three Navier–Stokes equations contain five unknowns: pressure, three velocity components, and density. To determine the solution for a flow, the Navier–Stokes equations must therefore be complemented with two more equations:

– the continuity equation, which asserts the conservation of mass,

– the equation of state law specific to the fluid.

We can observe that in the flow patterns *of non-miscible, incompressible fluids*, the fluid density remains constant within each fluid particle that is followed along its path. The continuity equation implies that the divergence of the velocity vector is zero at any point. Density is a physical quantity that characterizes a fluid's specificity at every point in the domain. It can be inhomogeneous in space or variable with time without the fluid being compressible, as is the case when one considers flows of several non-miscible fluids (e.g. oil and water) or flows of fluids that show layered density in a natural environment (e.g. when salinity varies in seawater, the molecular diffusion of salt can be neglected at the time scales considered).

For an isothermal compressible fluid, the state law of the fluid links density with pressure.

The system of equations to be solved is surrounded with double bars in Table 1.1. It needs to be associated with boundary conditions. For a Newtonian fluid, such as water or air, with solid walls consisting of common materials, the boundary condition is a no-slip condition for the fluid at the wall.[3] The velocity of the fluid becomes zero on a fixed solid wall, or it equals the velocity of the wall if the latter is in motion.

In the following three sections, we present solutions to Navier–Stokes equations for classical laminar flows. These solutions are specific to an incompressible fluid of homogeneous mass density. The system to be solved is then reduced to the three Navier–Stokes equations, plus incompressibility.

---

3 The no-slip condition at the wall does not always hold. Particular properties of the materials making up the solid wall or fluids such as liquid polymers provide reasons regarding why the fluid slips along the wall.

1.3. The plane Poiseuille flow

The few known analytical solutions to Navier–Stokes equations are not obtained by integrating Navier–Stokes equations in their most general formulation. Typically, one merely verifies the existence of a simple solution satisfying simple assumptions of kinematics. These simplifications include an assumption that the velocity of certain components during the flow is nil and/or that the velocity and the pressure are independent from time or from certain space coordinates. We return to these assumptions toward the end of this chapter.

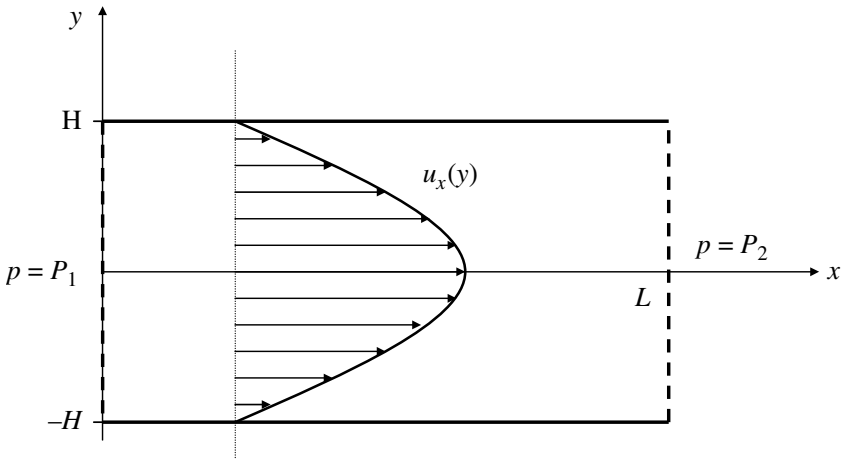

Figure 1.2. *Plane Poiseuille laminar flow*

For the plane Poiseuille flow, we consider (Figure 1.2) a fluid between two parallel planar walls located at $y = –H$ and $y = H$. The medium extends to infinity in the direction of O_z. Initially, the force of gravity is not taken into account. The flow is generated due to a difference in pressure between the inlet section (at $x = 0$) and the outlet section (at $x = L$). On the surfaces of both these sections, pressure is assumed to be uniform.

The boundary conditions for the problem are as follows:

– On solid walls, the normal and tangential components of the flow velocity equal zero:

$$u_x(x, y = H, z) = 0 \qquad u_y(x, y = H, z) = 0 \qquad u_z(x, y = H, z) = 0$$
$$u_x(x, y = -H, z) = 0 \qquad u_y(x, y = -H, z) = 0 \qquad u_z(x, y = -H, z) = 0 \qquad [1.8a]$$

– In the inlet and outlet sections, pressure is given as:

$$p(x = 0, y, z) = P_1 \qquad p(x = L, y, z) = P_2 \qquad [1.8b]$$

A steady, time-independent solution is what we intend. For the plane Poiseuille flow, the most obvious kinematic simplification is to assume the flow is unidirectional (i.e. only the u_x velocity component is non-zero). The second simplification is the assumption that the u_x velocity component is independent from z (plane flow). Lastly, it can be assumed intuitively that u_x is also independent from x; however, this property is also influenced by incompressibility. The structure of the flow is, therefore, simplified by using a solution in the form:

$$u_x(y) \qquad u_y(x, y, z) = 0 \qquad u_z(x, y, z) = 0 \qquad [1.9]$$

Based on all these assumptions, the three Navier–Stokes equations become considerably simplified:

$$\left.\begin{aligned} 0 &= -\frac{\partial p}{\partial x} + \mu \frac{\mathrm{d}^2 u_x}{\mathrm{d}y^2} \\ 0 &= -\frac{\partial p}{\partial y} \\ 0 &= -\frac{\partial p}{\partial z} \end{aligned}\right\} \qquad [1.10]$$

The partial-derivative symbols for pressure have been retained, but it is now clear that the pressure depends only on the space coordinate x. The pressure is uniform in any flow section that is perpendicular to the walls. This property is already verified using the inlet and outlet boundary conditions. For a solution of the form:

$$u_x(y) \qquad p(x) \qquad [1.11]$$

the principle of variable separation leads to:

$$\frac{\partial p}{\partial x} = \mu \frac{\mathrm{d}^2 u_x}{\mathrm{d}y^2} = \text{constant} \qquad [1.12]$$

The two successive integrations, with velocity boundary conditions [1.8a, 1.8b] on the side walls, yield:

$$u_x(y) = \frac{1}{2\mu} \frac{\partial p}{\partial x} \{y^2 - H^2\} \qquad [1.13]$$

We hence obtain the well-known result that the velocity profile for a Poiseuille flow has a parabolic shape.

The force exerted by the solid wall on the fluid is calculated using the stress tensor. On the upper wall ($y = H$), the outward normal to the fluid domain is the vector, (0, 1, 0). The force is calculated using equation [1.2] and the definition of the stress tensor (Table 1.1) for the velocity field [1.13] of the Poiseuille flow:

$$\mathrm{d}\vec{F} = \begin{pmatrix} \mathrm{d}F_x \\ \mathrm{d}F_y \\ \mathrm{d}F_z \end{pmatrix} = \mathrm{d}s \begin{pmatrix} \sigma_{xx} & \sigma_{xy} & \sigma_{xz} \\ \sigma_{xy} & \sigma_{yy} & \sigma_{yz} \\ \sigma_{xz} & \sigma_{yz} & \sigma_{zz} \end{pmatrix} \begin{pmatrix} 0 \\ 1 \\ 0 \end{pmatrix} = \mathrm{d}s \begin{pmatrix} \mu \dfrac{\partial u_x}{\partial y}(H) \\ -p(H) \\ 0 \end{pmatrix} = \mathrm{d}s \begin{pmatrix} \dfrac{\partial p}{\partial x} H \\ -p(H) \\ 0 \end{pmatrix} \qquad [1.14]$$

Solution [1.13] for the velocity field allows the force to be expressed as a function of the pressure field only.

The Poiseuille solution illustrates several important mechanical concepts, including the following:

– The flow is generated by the pressure gradient:

$$\frac{\partial p}{\partial x} = \frac{P_2 - P_1}{L} \qquad [1.15]$$

which is negative when $P_1 > P_2$, making the fluid flow along the O_x direction. The direction of the flow is opposite to that of the pressure gradient. The absolute value of the pressure gradient is called the regular head loss inside the pipe.

– The pressure is uniform in any plane that is perpendicular to the direction of the flow. The very general character of this property is further discussed in Chapter 2.

– At the solid wall, the flow is subjected to a friction force whose orientation is opposite to the direction of the flow. There exists a general relationship (equation [1.14]) between the pressure gradient and the frictional stress. We discuss this general relationship in Chapter 2 also. The pressure gradient makes it possible to overcome the friction force and facilitates fluid flow.

1.4. Navier–Stokes equations in cylindrical coordinates: Poiseuille flow in a circular cylindrical pipe

The Poiseuille flow in a circular cylindrical pipe is determined in the same fashion as detailed above. The main difference is the need to represent the equations in a cylindrical coordinate system, since the boundary conditions are most optimum in that coordinate system. The equations are given in Table 1.2, and Figure 1.3 indicates the way in which a point M in space is located through the distance r to an axis O_z, its abscissa z along that axis, and the angle θ. At that point, the flow velocity is determined by the components (u_r, u_θ, and u_z), represented on the basis of the three vectors $\vec{e}_r, \vec{e}_\theta, \vec{e}_z$ indicated in the figure. Therefore, the velocity vector is:

$$\vec{U} = u_r\vec{e}_r + u_\theta\vec{e}_\theta + u_z\vec{e}_z \qquad [1.16]$$

The azimutal component u_θ accounts for the rotation of point M around the O_z axis. The radial velocity component u_r, depending on its sign, transports a fluid particle toward the O_z axis or away from it. u_z is called axial component. The strain rate and stress tensors are written as:

$$[D] = \begin{pmatrix} D_{rr} & D_{r\theta} & D_{rz} \\ D_{r\theta} & D_{\theta\theta} & D_{\theta z} \\ D_{rz} & D_{\theta z} & D_{zz} \end{pmatrix} \quad \text{and} \quad [\Sigma] = \begin{pmatrix} \sigma_{rr} & \tau_{r\theta} & \tau_{rz} \\ \tau_{r\theta} & \sigma_{\theta\theta} & \tau_{\theta z} \\ \tau_{rz} & \tau_{\theta z} & \sigma_{zz} \end{pmatrix} \qquad [1.17]$$

To describe the steady flow in a circular tube, we visualize ourselves in a cylindrical coordinate system wherein the O_z axis coincides with the axis of the pipe (Figure 1.3). The radius of the pipe is denoted by R.

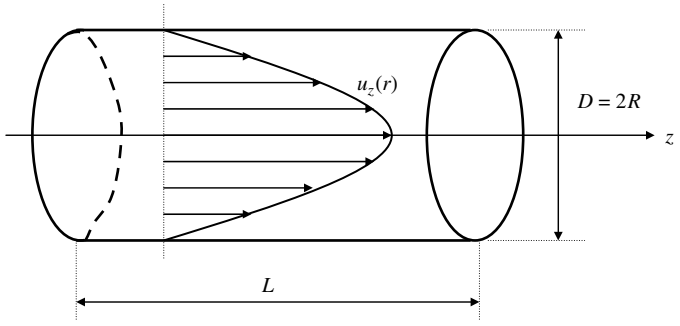

Figure 1.3. *Poiseuille laminar flow in a circular cylindrical tube*

The relevant boundary conditions to such a situation are:

– The velocity is zero at the solid wall of the tube

$$u_r(r=R,\theta,z)=0 \quad u_\theta(r=R,\theta,z)=0 \quad u_z(r=R,\theta,z)=0 \qquad [1.18a]$$

– In the inlet and outlet sections, the pressure is uniform:

$$p(r,\theta,z=0)=P_1 \quad p(r,\theta,z=L)=P_2 \qquad [1.18b]$$

From a kinematic standpoint, the simplest is to assume that the flow is unidirectional along the O_z direction. The assumption of flow axisymmetry leads us to emphasize that u_z does not depend on θ.

Local formulation of the fundamental law of mechanics:

$$\rho\left\{\frac{\partial u_r}{\partial t}+u_r\frac{\partial u_r}{\partial r}+\frac{u_\theta}{r}\frac{\partial u_r}{\partial \theta}+u_z\frac{\partial u_r}{\partial z}-\frac{u_\theta^2}{r}\right\}=-\frac{\partial p}{\partial r}$$
$$+\frac{1}{r}\frac{\partial(r\sigma'_{rr})}{\partial r}+\frac{1}{r}\frac{\partial \tau_{r\theta}}{\partial \theta}+\frac{\partial \tau_{rz}}{\partial z}-\frac{\sigma'_{\theta\theta}}{r}+f_r$$

$$\rho\left\{\frac{\partial u_\theta}{\partial t}+u_r\frac{\partial u_\theta}{\partial r}+\frac{u_\theta}{r}\frac{\partial u_\theta}{\partial \theta}+u_z\frac{\partial u_\theta}{\partial z}+\frac{u_r u_\theta}{r}\right\}=-\frac{1}{r}\frac{\partial p}{\partial \theta}$$
$$+\frac{1}{r^2}\frac{\partial(r^2\tau_{r\theta})}{\partial r}+\frac{1}{r}\frac{\partial \sigma'_{\theta\theta}}{\partial \theta}+\frac{\partial \tau_{\theta z}}{\partial z}+f_\theta$$

$$\rho\left\{\frac{\partial u_z}{\partial t}+u_r\frac{\partial u_z}{\partial r}+\frac{u_\theta}{r}\frac{\partial u_z}{\partial \theta}+u_z\frac{\partial u_z}{\partial z}\right\}=-\frac{\partial p}{\partial z}$$
$$+\frac{1}{r}\frac{\partial(r\tau_{rz})}{\partial r}+\frac{1}{r}\frac{\partial \tau_{\theta z}}{\partial \theta}+\frac{\partial \sigma'_{zz}}{\partial z}+f_z$$

Strain rate tensor:

$$[D]=\frac{1}{2}\begin{Bmatrix} 2\dfrac{\partial u_r}{\partial r} & \left(\dfrac{1}{r}\dfrac{\partial u_r}{\partial \theta}+r\dfrac{\partial}{\partial r}\left(\dfrac{u_\theta}{r}\right)\right) & \left(\dfrac{\partial u_r}{\partial z}+\dfrac{\partial u_z}{\partial r}\right) \\ \left(\dfrac{1}{r}\dfrac{\partial u_r}{\partial \theta}+r\dfrac{\partial}{\partial r}\left(\dfrac{u_\theta}{r}\right)\right) & 2\left(\dfrac{1}{r}\dfrac{\partial u_\theta}{\partial \theta}+\dfrac{u_r}{r}\right) & \left(\dfrac{\partial u_\theta}{\partial z}+\dfrac{1}{r}\dfrac{\partial u_z}{\partial \theta}\right) \\ \left(\dfrac{\partial u_r}{\partial z}+\dfrac{\partial u_z}{\partial r}\right) & \left(\dfrac{\partial u_\theta}{\partial z}+\dfrac{1}{r}\dfrac{\partial u_z}{\partial \theta}\right) & 2\dfrac{\partial u_z}{\partial z} \end{Bmatrix}$$

Stress tensor for a Newtonian fluid:

$$[\Sigma] = \begin{Bmatrix} -p + 2\mu\dfrac{\partial u_r}{\partial r} & \mu\left(\dfrac{1}{r}\dfrac{\partial u_r}{\partial \theta} + r\dfrac{\partial}{\partial r}\left(\dfrac{u_\theta}{r}\right)\right) & \mu\left(\dfrac{\partial u_r}{\partial z} + \dfrac{\partial u_z}{\partial r}\right) \\ \mu\left(\dfrac{1}{r}\dfrac{\partial u_r}{\partial \theta} + r\dfrac{\partial}{\partial r}\left(\dfrac{u_\theta}{r}\right)\right) & -p + 2\mu\left(\dfrac{1}{r}\dfrac{\partial u_\theta}{\partial \theta} + \dfrac{u_r}{r}\right) & \mu\left(\dfrac{\partial u_\theta}{\partial z} + \dfrac{1}{r}\dfrac{\partial u_z}{\partial \theta}\right) \\ \mu\left(\dfrac{\partial u_r}{\partial z} + \dfrac{\partial u_z}{\partial r}\right) & \mu\left(\dfrac{\partial u_\theta}{\partial z} + \dfrac{1}{r}\dfrac{\partial u_z}{\partial \theta}\right) & -p + 2\mu\dfrac{\partial u_z}{\partial z} \end{Bmatrix}$$

Navier–Stokes equation:

$$\rho\left\{\frac{\partial u_r}{\partial t} + u_r\frac{\partial u_r}{\partial r} + \frac{u_\theta}{r}\frac{\partial u_r}{\partial \theta} + u_z\frac{\partial u_r}{\partial z} - \frac{u_\theta^2}{r}\right\} = -\frac{\partial p}{\partial r} + f_r + \mu\left\{\frac{\partial}{\partial r}\left(\frac{1}{r}\frac{\partial (ru_r)}{\partial r}\right) + \frac{1}{r^2}\frac{\partial^2 u_r}{\partial \theta^2} + \frac{\partial^2 u_r}{\partial z^2} - \frac{2}{r^2}\frac{\partial u_\theta}{\partial \theta}\right\}$$

$$\rho\left\{\frac{\partial u_\theta}{\partial t} + u_r\frac{\partial u_\theta}{\partial r} + \frac{u_\theta}{r}\frac{\partial u_\theta}{\partial \theta} + u_z\frac{\partial u_\theta}{\partial z} + \frac{u_r u_\theta}{r}\right\} = -\frac{1}{r}\frac{\partial p}{\partial \theta} + f_\theta + \mu\left\{\frac{\partial}{\partial r}\left(\frac{1}{r}\frac{\partial (ru_\theta)}{\partial r}\right) + \frac{1}{r^2}\frac{\partial^2 u_\theta}{\partial \theta^2} + \frac{\partial^2 u_\theta}{\partial z^2} + \frac{2}{r^2}\frac{\partial u_r}{\partial \theta}\right\}$$

$$\rho\left\{\frac{\partial u_z}{\partial t} + u_r\frac{\partial u_z}{\partial r} + \frac{u_\theta}{r}\frac{\partial u_z}{\partial \theta} + u_z\frac{\partial u_z}{\partial z}\right\} = -\frac{\partial p}{\partial z} + f_z + \mu\left\{\frac{1}{r}\frac{\partial}{\partial r}\left(r\frac{\partial u_z}{\partial r}\right) + \frac{1}{r^2}\frac{\partial^2 u_z}{\partial \theta^2} + \frac{\partial^2 u_z}{\partial z^2}\right\}$$

Continuity equation:

$$\frac{\partial \rho}{\partial t} + u_r\frac{\partial \rho}{\partial r} + \frac{u_\theta}{r}\frac{\partial \rho}{\partial \theta} + u_z\frac{\partial \rho}{\partial z} = 0$$

Incompressibility:

$$\frac{1}{r}\frac{\partial (ru_r)}{\partial r} + \frac{1}{r}\frac{\partial u_\theta}{\partial \theta} + \frac{\partial u_z}{\partial z} = 0$$

Table 1.2. *Navier–Stokes formulation in a circular cylindrical coordinate system for an incompressible fluid*

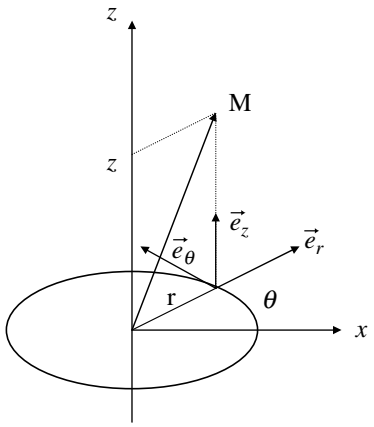

Figure 1.4. *Reference for the position of point M using its coordinates (r, θ, z) in a cylindrical coordinate system of axis O_z and definition of vectors $\vec{e}_r$, $\vec{e}_\theta$ and $\vec{e}_z$*

Incompressibility also signifies that u_z does not depend on z either, which leads to the conservation of the flow rate along the pipe. Therefore, we try a solution of the form:

$$u_r = 0 \qquad u_\theta = 0 \qquad u_z(r) \tag{1.19}$$

The Poiseuille flow in a cylindrical circular pipe is the solution of the set of equations surrounded by a double bar in Table 1.2. With equation [1.19], the Navier–Stokes equations are simplified into:

$$\left.\begin{aligned} 0 &= -\frac{\partial p}{\partial r} \\ 0 &= -\frac{\partial p}{\partial \theta} \\ 0 &= -\frac{\partial p}{\partial z} + \mu \frac{1}{r}\frac{\mathrm{d}}{\mathrm{d}r}\left(r\frac{\mathrm{d}u_z}{\mathrm{d}r}\right) \end{aligned}\right\} \tag{1.20}$$

Variable separation between the pressure, which depends only on z, and the axial velocity, which depends only on r, leads to the following results:

– The pressure is uniform in any flow section that is perpendicular to the direction of the flow, with a regular head loss:

$$\frac{\partial p}{\partial z} = \frac{P_2 - P_1}{L} = \text{constant} \tag{1.21}$$

– The axial velocity is such that:

$$u_z(r) = \frac{1}{4\mu}\frac{\partial p}{\partial z} r^2 + A\ln(r) + B \qquad [1.22]$$

The constant of integration, A, is zero so as to avoid an infinite velocity value on the pipe axis. The integration constant B ensures that the velocity is zero at the wall. Consequently:

$$u_z(r) = \frac{1}{4\mu}\frac{\partial p}{\partial z}\{r^2 - R^2\} \qquad [1.23]$$

– In the case for the plane Poiseuille flow, the stress exerted by the wall on the fluid is linked to the pressure gradient:

$$\mathrm{d}\vec{F} = \begin{pmatrix} \mathrm{d}F_r \\ \mathrm{d}F_\theta \\ \mathrm{d}F_z \end{pmatrix} = \mathrm{d}s \begin{pmatrix} \sigma_{rr} & \tau_{r\theta} & \tau_{rz} \\ \tau_{r\theta} & \sigma_{\theta\theta} & \tau_{\theta z} \\ \tau_{rz} & \tau_{\theta z} & \sigma_{zz} \end{pmatrix} \begin{pmatrix} 1 \\ 0 \\ 0 \end{pmatrix} = \mathrm{d}s \begin{pmatrix} -p(R) \\ 0 \\ \dfrac{\partial p}{\partial z}\dfrac{R}{2} \end{pmatrix} \qquad [1.24]$$

This is also calculated for the cylindrical coordinate system using equation [1.2] and the stress tensor (Table 1.2) for the velocity field [1.23] of the Poiseuille flow in a circular pipe.

– The flow rate varies linearly with the pressure gradient:

$$Q = \int_0^{2\pi} \mathrm{d}\theta \int_0^R u_z(r) r \mathrm{d}r = -\frac{\pi}{8\mu}\frac{\partial p}{\partial z} R^4 \qquad [1.25]$$

1.5. Plane Couette flow

For the Poiseuille flow presented in the previous two sections, the flow was induced by a pressure difference applied between the two ends of a straight pipe. The plane Couette flow makes it possible to study the way how a force is applied to move a solid wall, without pushing the fluid in contact with the wall, and can generate a flow due to viscosity. The fluid is held between two parallel plates of infinite length (Figure 1.5). One of the plates, at $z = 0$, is kept stationary. The other

plate ($z = H$) is subjected to a force by one surface τ_x along the O_x direction. This plate is set in motion and the fluid between the two plates, if it adheres to the wall, is entrained in the O_x direction due to friction between the layers of fluid. We wish to determine the profile of the flow and the link between the applied force and the velocity of the fluid. Such a configuration has an application in rheometry, as we discuss in Chapter 7.

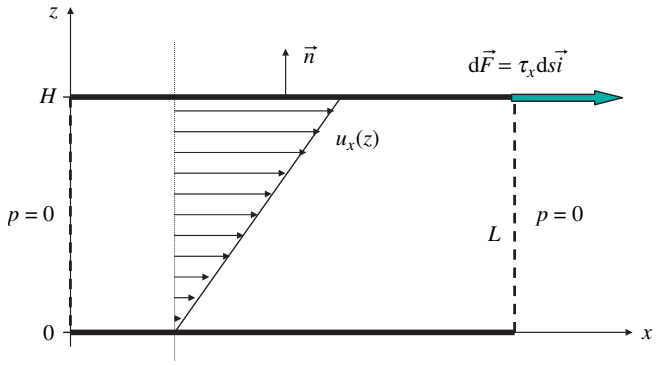

Figure 1.5. *Plane laminar Couette flow*

Along the lines of similar kinematic assumptions as with Poiseuille flows, and using incompressibility, one is naturally inclined to have a unidirectional flow along the O_x direction, in the form:

$$u_x(z) \qquad u_y(x,y,z) = 0 \qquad u_z(x,y,z) = 0 \qquad [1.26]$$

Navier–Stokes equations now simplify into:

$$\left.\begin{aligned} 0 &= -\frac{\partial p}{\partial x} + \mu \frac{d^2 u_x}{dz^2} \\ 0 &= -\frac{\partial p}{\partial y} \\ 0 &= -\frac{\partial p}{\partial z} \end{aligned}\right\} \qquad [1.27]$$

If no pressure gradient is operational along the O_x direction, the pressure is uniform in the entire fluid domain, and consequently has no dynamic role. This hence leads to:

$$u_x(z) = Az \qquad [1.28]$$

The velocity is zero at the lower wall. The constant of integration, A, is determined by the force exerted on the wall. That force is calculated by using (equation [1.2]) and representing the terms σ_{xz}, σ_{yz}, and σ_{zz} in the stress tensor (Table 1.1) as a function of the velocity field (equations [1.26] and [1.28]), taking into account the fact that the normal to the wall is oriented along the O_z direction. We hence obtain:

$$\mathrm{d}\vec{F} = \begin{pmatrix} \mathrm{d}F_x \\ \mathrm{d}F_y \\ \mathrm{d}F_z \end{pmatrix} = \mathrm{d}s \begin{pmatrix} \sigma_{xx} & \sigma_{xy} & \sigma_{xz} \\ \sigma_{xy} & \sigma_{yy} & \sigma_{yz} \\ \sigma_{xz} & \sigma_{yz} & \sigma_{zz} \end{pmatrix} \begin{pmatrix} 0 \\ 0 \\ 1 \end{pmatrix} = \mathrm{d}s \begin{pmatrix} \mu A \\ 0 \\ -p(H) \end{pmatrix} = \mathrm{d}s \begin{pmatrix} \tau_x \\ 0 \\ -p(H) \end{pmatrix} \qquad [1.29]$$

application of the frictional force (Figure 1.1) to the upper wall leads to:

$$u_x(z) = \frac{\tau_x}{\mu} z \qquad [1.30]$$

This is the profile of the plane Couette flow. If a pressure gradient is applied along the Ox direction, a plane Poiseuille-type solution (equation [1.13]) is superimposed onto the Couette flow [1.30].

1.6. The boundary layer concept

The boundary layer concept is introduced when dealing with a flow where the effect of viscosity is confined to the vicinity of solid walls. Such case is obtained when the flow's Reynolds number (introduced in Chapter 3) is sufficiently large.

Under these conditions, outside the boundary layer, the effect of viscosity is negligible.

The simplest boundary layer case is depicted in Figure 1.6(a). A uniform flow arrives in the O_x direction onto a semi-infinite flat that is parallel to the direction of the flow (half-plane $z = 0$, $x > L$). For $x < L$, the velocity is independent from any space coordinate ($u_x(x, y, z) = U$). If the fluid adheres to the wall, the velocity

will necessarily become zero on the plate ($u_x(x, y, 0) = 0$ for $x > L$). In the vicinity of the plate, viscosity gradually slows the fluid down as the distance from the leading edge increases (this is the ($x = L$, $z = 0$) line) in the $x > 0$ direction. Two boundary layers develop and thicken on either side of the plate when x increases. Outside the boundary layer, the flow is not affected by the plate, whereas a velocity gradient exists within the boundary layer. The boundary layer thickness, denoted by $\delta(x)$, is zero at the leading edge ($x = L$) and increases gradually when x increases.

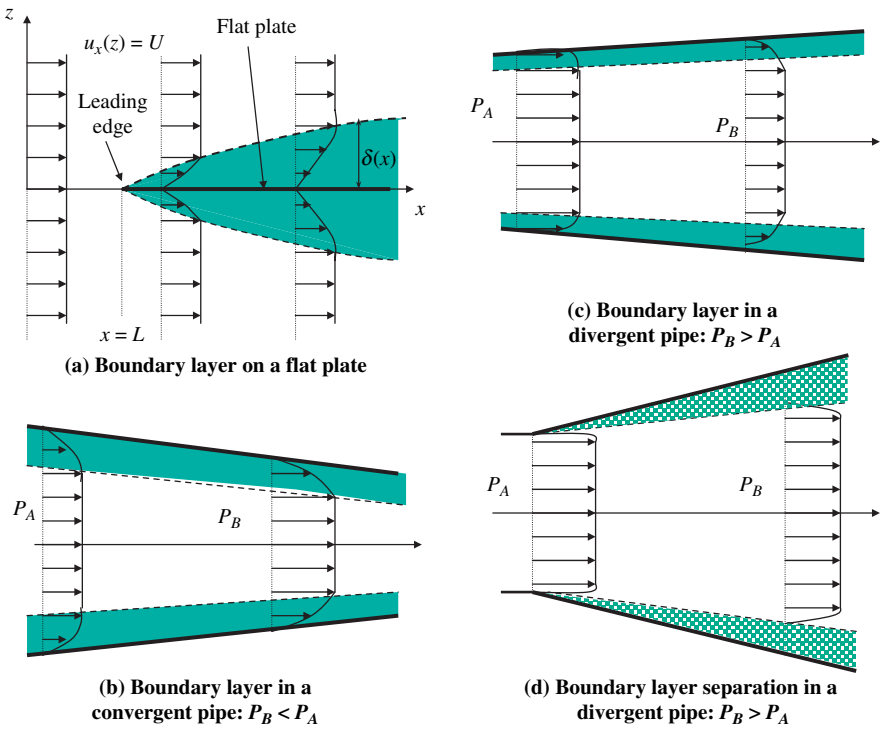

(a) Boundary layer on a flat plate

(c) Boundary layer in a divergent pipe: $P_B > P_A$

(b) Boundary layer in a convergent pipe: $P_B < P_A$

(d) Boundary layer separation in a divergent pipe: $P_B > P_A$

Figure 1.6. *Boundary layers in a flow along a solid wall. The boundary layer zone is delineated by the dashed lines and its inside is shaded*

The boundary layer concept is formalized when the thickness δ of the boundary layer is small compared to the geometrical dimensions of the zone of the flow that lies outside the boundary layer. Apart from the case (Figure 1.6(d)) where the boundary layer separates from the wall, the drawings of Figure 1.6 are distorted representations where the boundary layer thickness is exaggerated to show the inside of the boundary layer. The actual boundary layer thickness is very small compared

to the extent of the flow along O_z, in the flat plate case (Figure 1.6(a)), or to the width of the pipe (Figures 1.6(b) and 1.6(c)).

The main result from boundary layer theory (not derived herein) is that the pressure inside a boundary layer is equal to the pressure that prevails outside that boundary layer. This translates mathematically into the fact that the pressure gradient along the normal direction to the wall is zero inside the boundary layer:

$$\frac{\partial P}{\partial n} = 0 \qquad [1.31]$$

In the case of a flat plate boundary layer (Figure 1.6(a)), this equation is written as $\partial P / \partial z = 0$. It can be inferred from this that the pressure remains constant throughout the fluid, including inside the boundary layer.

For the configurations illustrated in Figures 1.6(b) and 1.6(c), the pressure is not constant within the fluid flow outside the boundary layer. Inside a convergent pipe, the pressure decreases when one follows a particle in its movement ($P_B < P_A$) as stated by Bernoulli's theorem (Chapter 2). The pressure decreases in the same manner inside the boundary layer. In a divergent pipe, the effect is reversed. The pressure increases when following the particle along its movement, in the fluid flow outside the boundary layer as well as inside the boundary layer ($P_B > P_A$). This is referred to as a boundary layer subjected to an "adverse pressure gradient." The more quickly the divergent widens, the more intense the adverse pressure gradient to which the boundary layer is subjected. When the adverse pressure gradient is too strong, this leads to the phenomenon of boundary layer separation (Figure 1.6(d)), which we describe in Chapter 4. This produces, in the vicinity of the walls, a zone that is stirred by turbulent motion but without an average flow rate. This is no longer a boundary layer, as its thickness has become much larger. In Chapter 4, we return to the essential differences between flows in convergent and divergent pipes, and to the effects of cross-sectional changes.

The property (equation [1.31]) of boundary layers regarding the pressure gradient is of the same nature as the property of pressure uniformity in planes perpendicular to the flow direction, which was observed for the Poiseuille and Couette solutions. Figure 1.6(a) shows that the boundary layer thickness on a flat plate grows with increasing values of x. At a sufficient distance from the inlet of a pipe, the boundary layer thickness eventually exceeds the diameter of the pipe. The flow reverts to the Poiseuille type solution presented previously, if the Reynolds number is sufficiently low to allow the flow to remain laminar. Such flows are termed "established laminar flows" or "developed flows", as the velocity field does not change any more when traveling downstream in the pipe, because the boundary

layers have spread enough to establish velocity gradients across the whole width of the pipe.

Regarding boundary layers, we limit ourselves in this book to discussing the essential property of boundary layers relating to the pressure field (equation [1.31]). The boundary layers on the surface of a solid wall or at the interface between two fluids with different properties (e.g. fluids of different densities or viscosities, or non-miscible fluids) play a key role in quantifying transfers of mass, heat, or momentum. It is at fluid/fluid or fluid/wall boundaries that transfers between media with different characteristics need to be determined, which necessarily involves boundary layers. It is, therefore, paradoxical not to discuss boundary layer phenomena further in a book intended to be used by process engineering specialists. We refer the readers to books dedicated to transfer phenomena,[4] where they will find a detailed description of boundary layer processes, in connection with interface transfer problems.

1.7. Solutions of Navier–Stokes equations where a gravity field is present, hydrostatic pressure

The simple solutions just described are only slightly modified when the gravity field is added as a body force. The kinematics of the flow remain unchanged. Only the pressure field is altered to incorporate the effect of gravity. Let us consider that the acceleration due to gravity has an arbitrary direction in the Cartesian coordinate system (O, x, y, z) in which the flow is described. The body force is written as:

$$\begin{pmatrix} f_x \\ f_y \\ f_z \end{pmatrix} = \begin{pmatrix} \rho g \alpha \\ \rho g \beta \\ \rho g \gamma \end{pmatrix} = \rho \vec{g} \quad \text{where in} \quad \alpha^2 + \beta^2 + \gamma^2 = 1 \qquad [1.32]$$

(α, β, and γ) are the components of one vector along which gravity is orientated.

4 In particular, the essential book, *Transfer Phenomena*, by R.B. Bird, W.E. Stewart, and E.N. Lightfoot, (John Wiley & Sons Inc., 2nd Edition, 2002) and the recent book, *Phénomènes de transfert en génie des procédés* by J.P. Couderc, C. Gourdon, and A. Liné (Lavoisier, 2008). A discussion of boundary layer flows is also given by L.D. Landau and E.M. Lifshitz, *Fluid Mechanics* (2nd Edition, Butterworth-Heinemann, 1987), and by G.K. Batchelor, *An Introduction to Fluid Mechanics* (Cambridge University Press, 1967).

When the fluid is incompressible and its mass density is uniform, Navier–Stokes equations can be written by introducing the gravity terms into the pressure gradient:

$$\rho\left\{\frac{\partial u_x}{\partial t}+u_x\frac{\partial u_x}{\partial x}+u_y\frac{\partial u_x}{\partial y}+u_z\frac{\partial u_x}{\partial z}\right\}=-\frac{\partial(p-\rho g\alpha x)}{\partial x}+\mu\Delta u_x$$

$$\rho\left\{\frac{\partial u_y}{\partial t}+u_x\frac{\partial u_y}{\partial x}+u_y\frac{\partial u_y}{\partial y}+u_z\frac{\partial u_y}{\partial z}\right\}=-\frac{\partial(p-\rho g\beta y)}{\partial y}+\mu\Delta u_y \qquad [1.33]$$

$$\rho\left\{\frac{\partial u_z}{\partial t}+u_x\frac{\partial u_z}{\partial x}+u_y\frac{\partial u_z}{\partial y}+u_z\frac{\partial u_z}{\partial z}\right\}=-\frac{\partial(p-\rho g\gamma z)}{\partial z}+\mu\Delta u_z$$

The solution to the problem is therefore the same as the one established previously, provided the pressure p is replaced at any point M with the quantity:

$$p'(x)=p(x,y,z)-\rho(\vec{g}\cdot\overrightarrow{OM})=p(x,y,z)-\rho g\{\alpha x+\beta y+\gamma z\} \qquad [1.34]$$

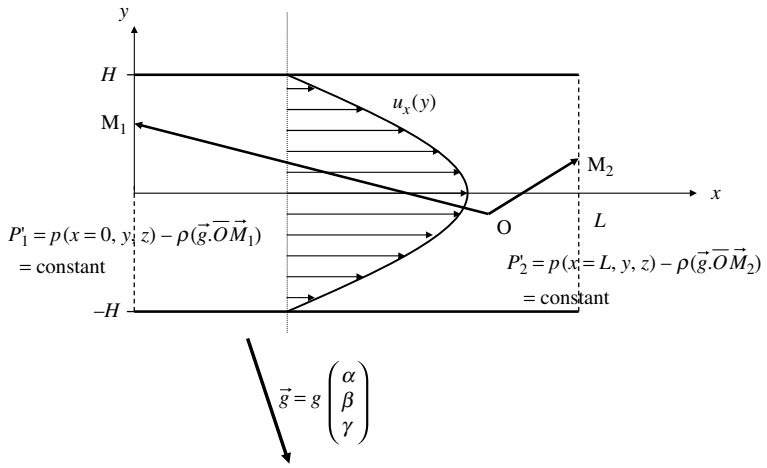

Figure 1.7. *Plane Poiseuille flow accounting for the gravity field*

In Figure 1.7, the modifications brought about by gravity in the case of a plane Poiseuille flow are depicted. The pipe is inclined within the gravity field.[5] Navier–Stokes equations in directions O_y and O_z now reduce to:

$$\begin{aligned}\frac{\partial(p-\rho g\beta y)}{\partial y}&=\frac{\partial(p-\rho g(\alpha x+\beta y+\gamma z))}{\partial y}=0\\ \frac{\partial(p-\rho g\beta y)}{\partial z}&=\frac{\partial(p-\rho g(\alpha x+\beta y+\gamma z))}{\partial z}=0\end{aligned}. \qquad [1.35]$$

Equations [1.34] and [1.35] involve the hydrostatic pressure:

$$p_{hyd}(x,y,z)=\rho(\vec{g}\cdot\overrightarrow{OM})=\rho g\{\alpha x+\beta y+\gamma z\} \qquad [1.36]$$

which is defined with respect to a reference point O, where it is taken to be zero. The quantity p' (equation [1.34]) is, at any point, the difference between the actual pressure and the hydrostatic pressure. It is uniform in any plane that is perpendicular to the flow direction (Figure 1.7), and only varies with x. The velocity profile in the pipe retains the same shape, since:

$$u_x(y)=\frac{1}{2\mu}\frac{\partial(p-p_{hyd})}{\partial x}\{y^2-H^2\} \qquad [1.37]$$

The regular head loss which generates the flow is:

$$\frac{\partial p'}{\partial x}=\frac{\partial(p-p_{hyd})}{\partial x}=\frac{P'_2-P'_1}{L}, \qquad [1.38]$$

where P'_1 and P'_2 are defined in Figure 1.7.

In many cases, the problem is indeed simplified by introducing the gravity term into the pressure term. That is equivalent to subtracting the hydrostatic pressure from the pressure value measured or calculated at any point. It should, however, be recalled that we introduced the gravity term into the pressure term under the assumption that the mass density of the fluid is homogeneous within the domain.

5 Attention should be paid to the notations for coordinate systems: here, the O_z direction is not the vertical direction related to the gravity field, as it is often defined, but rather a direction related to the axis of the pipe. It is not possible here to write $p'=p+\rho gz$…

That is no longer the case when a two-phase flow (air–water flow, free-surface flow) is considered. For a two-phase flow, it is typically not worthwhile to consider introducing gravity into the pressure term, although this could in theory be done in each phase separately. This would complicate the process of writing out the boundary conditions at the interface between the fluids.

1.8. Buoyancy force

The buoyancy force is the resultant of hydrostatic pressure forces exerted on a domain V, under the action of gravity, by the surrounding fluid. In the absence of flow, the pressure inside the fluid is the hydrostatic pressure, p_{hyd}, associated with the weight of the water column. Navier–Stokes equations now reduce to:

$$-\nabla p_{hyd} + \rho\vec{g} = \vec{0} \qquad [1.39]$$

The resultant of the pressure field exerted by the fluid on domain V is:

$$\vec{R} = -\iint_S p_{hyd}\vec{n}\mathrm{d}s \qquad [1.40]$$

S is the closed surface surrounding V and $\vec{n}$ is the outward normal to the domain on that surface (Figure 1.1). Following Ostrogradsky's theorem, and then using (equation [1.39]), we arrive at:

$$\iint_S p_{hyd}\vec{n}\mathrm{d}s = \iiint_V \nabla p_{hyd}\mathrm{d}v = \iiint_V \rho\vec{g}\mathrm{d}v \qquad [1.41]$$

We recover the buoyancy force:

$$\vec{R} = -\rho\vec{g}\iiint_V \mathrm{d}v \qquad [1.42]$$

whose magnitude equals the weight of the liquid volume displaced by the solid body and whose orientation is opposite to the direction of gravity. Thus, the buoyancy force corresponds to the integral of hydrostatic pressure forces exerted on a volume by the fluid located outside that volume.

It is important to establish the link between buoyancy force and hydrostatic pressure. The forces exerted by the movement of a fluid on an object contained in that fluid are in most cases calculated using pressure p', which is the difference between the absolute and hydrostatic pressures (equation [1.34]). The force calculated by integrating the pressure field, p', across the surface of the object is the one produced

by the fluid flowing around the object. It has a very clear point. The gravity force exerted on the object, which then has to be taken into account, is the difference between the weight of the object and the buoyancy force applied to the object.

1.9. Some conclusions on the solutions of Navier–Stokes equations

The three exact solutions of Navier–Stokes equations presented in this chapter have allowed us to familiarize ourselves with Navier–Stokes equations and to use the concept of stress for a Newtonian fluid. They also illustrate simple properties regarding pressure distribution within the flows.

One may recall the approach employed to establish these three solutions, by making assumptions about the kinematics of the flow to simplify the system of differential equations to be solved. In fact, we have merely checked that such solutions verify Navier–Stokes equations and the boundary conditions for each of the problems considered.

There are a few analytical solutions to Navier–Stokes equations. This explains why solving Navier–Stokes equations numerically has become a discipline per se in the field of fluid mechanics. However, notion of a "solution to Navier–Stokes equations" calls for further discussion.

For the three solutions presented in this chapter, can we assert that these are "the right solutions?" From a mathematical standpoint, it could be argued that these are exact solutions to Navier–Stokes equations, since they verify them and also verify the boundary conditions. Nonetheless, we cannot assert that these are necessarily the ones the experimenter will observe, even when achieving the experiment with the highest care.

It is possible to offer a simple explanation for this apparent paradox. To obtain the solutions described in this chapter, we have assumed the flow to be steady. In reality, the flow remains steady only if it is stable. The experimenter cannot avoid the superimposition of small disturbances onto the flow. When the flow is stable, such small disturbances will fade out in time, thus always reverting to the steady-state solution. The flow is unstable when flow conditions are such that some disturbances may grow in time and end up altering the flow altogether. In that case, Navier–Stokes solutions cannot remain steady for the selected experimental conditions. Thus, in the case of the flow inside a circular cylindrical pipe, it is found that the Poiseuille solution describes the flow adequately when the flow rate is sufficiently low. On the other hand, when it exceeds a certain value, the velocity field does not remain steady. This is the initial idea that helps one to understand why a flow becomes turbulent.

A conclusion of the above discussion is that expressing an exact solution to Navier–Stokes equations is not sufficient in itself. One also needs to be able to demonstrate, with all necessary rigor, that this solution is stable under the conditions considered. This requires mastering the theory of instability in fluid flows.[6]

We might consider that we have tried everything to discourage the reader finding exact solutions to Navier–Stokes equations. This is not true, although we did wish to show some of the limitations involved in this regard. In the following chapters, we also introduce some tools for treating problems of fluid mechanics without explicitly solving Navier–Stokes equations.

6 Besides the famous book by S. Chandrasekhar (*Hydrodynamics and hydromagnetic stability*, Dover Publications, 1961), we recommend the introductary chapters in the books by P.G. Drazin (*Hydrodynamic intability*, Cambridge University Press, 1981) and F. Charru (*Instabilités hydrodynamiques*, EDP Sciences, 2007).

Chapter 2

Global Theorems of Fluid Mechanics

For many applications, it is not necessary to have a detailed knowledge of the flow at all points in the domain. Global conservation relations enable engineers to determine the main characteristics of a flow. For instance, they provide clues about pressure changes induced in a flowing fluid and enable the calculation of forces on walls in contact with the fluid. They also help in estimating the head losses generated in some flows. Using these principles, some of the relations established in Chapter 1 while solving the local Navier–Stokes equations will be resolved.

It is essential for an engineer to handle global theorems. Generally speaking, this chapter is devoted to the global conservation of mass, momentum, and energy. As far as the notion of conservation is concerned, these three quantities are interpreted differently:

– Mass is necessarily conserved. This notion is articulated in this chapter through flow rate conservation relations.

– The conservation of momentum is more complex. In a steady state, considering a fluid domain, the momentum flux leaving the domain equals that entering the domain, if no force is exerted at the domain boundaries. The momentum theorem enables the evaluation of the forces exerted by a flow on a wall, or the estimation of the global head loss produced in a volume, depending on the circumstances.

– The notion of energy conservation is more subtle. Bernoulli's theorem embodies an energy conservation principle that proves quite useful in linking pressure changes to velocity changes. In real fluids, however, the assumption of energy conservation cannot be made that easily. The conservation of energy depends not only on viscosity, but also on the structure of flows. The flow might strongly

dissipate energy in certain areas, and negligibly in others. By introducing the kinetic energy balance in section 2.8, the physical principle that causes the dissipation of kinetic energy is explicitly set out.

For simplicity, all derivations in this chapter assume an incompressible fluid and homogeneous mass density.

2.1. Euler equations in an intrinsic coordinate system

The Euler equations are the equations of motion for an ideal fluid, that is, an inviscid fluid. They are easily deduced from the Navier–Stokes equations, simply by omitting the viscous terms.

General properties of the pressure field come to the fore when the Euler equations are written in an intrinsic coordinate system. Such a formulation is especially helpful when the flow is *steady*. In that case, the streamlines and particle paths are the same curved lines.

The intrinsic coordinate system is associated with the path of a particle. Considering a point M in the fluid that moves in time, its path follows the curve $\overrightarrow{OM}(t)$. The movement of the particle along its path can be characterized by the variation in time of its curvilinear abscissa, which is denoted by $s(t)$; this is actually the distance travelled along that line from an original position M_0, as a function of time.

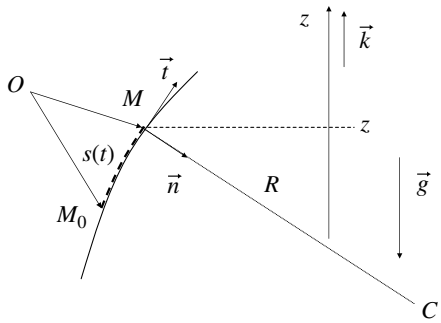

Figure 2.1. *Definition of the intrinsic coordinate system associated with the path of a fluid particle for a steady plane flow*

Some notions of differential geometry are necessary to prove what follows. So these can be recollected without proving them. If the position of point M is

described by its curvilinear abscissa, it is established that:

$$\frac{\mathrm{d}\overrightarrow{OM}}{\mathrm{d}s} = \vec{t} \qquad [2.1]$$

at *M*, the unit vector tangent to the path. The normal vector $\vec{n}$, directed toward the inside of the curve, is such that:

$$\frac{\mathrm{d}\vec{t}}{\mathrm{d}s} = \frac{\vec{n}}{R} \qquad [2.2]$$

where *R* is the radius of curvature of the path at point *M*, while its center of curvature is located at *C*.

At every point *M*, the intrinsic coordinate system comprises the unit vectors $\vec{t}$ and $\vec{n}$. It is important because velocity is tangential to the path:

$$\vec{V} = V\vec{t} \qquad [2.3]$$

In the intrinsic coordinate system, the Euler equations for a steady flow[1] are written along the tangential and normal directions, respectively, as:

$$\rho V \frac{\partial V}{\partial s} = f_s - \frac{\partial p}{\partial s} \qquad [2.4a]$$

$$\rho \frac{V^2}{R} = f_n - \frac{\partial p}{\partial n} \qquad [2.4b]$$

where f_s and f_n are the two components of body forces, e.g. weight. Proving these two equations is not very crucial. However, the global theorems that stem from these equations and the assumptions they require are worthy of further discussion. The first equation [2.4a] leads to Bernoulli's theorem. The second equation [2.4b] enables the derivation of important results on pressure changes around a point.

2.2. Bernoulli's theorem

If it is considered that the body force is the weight, then it can be written as $\vec{f} = -\rho g\vec{k}$, introducing a Cartesian coordinate system $(O,\vec{i},\vec{j},\vec{k})$, wherein $\vec{k}$ is the unit vector opposite to the direction of the gravity force (Figure 2.1). The definition

1 Here, we simplify the case of a flow within a plane.

of the intrinsic coordinate system then leads to:

$$f_s = -\rho g\vec{k}\cdot\vec{t} = -\rho g\vec{k}\cdot\frac{\mathrm{d}\overrightarrow{\mathrm{OM}}}{\mathrm{d}s} = -\rho g\frac{\mathrm{d}(\vec{k}\cdot\overrightarrow{\mathrm{OM}})}{\mathrm{d}s} = -\frac{\mathrm{d}(\rho g z)}{\mathrm{d}s} \qquad [2.5]$$

where z denotes the position of point M along the $\vec{k}$ axis of the fixed coordinate system (not in the intrinsic coordinate system). By substituting (equation [2.5]) into the first Euler equation [2.4a], we obtain:

$$\frac{\partial}{\partial s}\left\{\rho\frac{V^2}{2}+\rho g z+p\right\}=0 \qquad [2.6]$$

For a flow within the gravity field, the quantity:

$$H=\rho\frac{V^2}{2}+\rho g z+p \qquad [2.7]$$

is referred to as the "head" of the flow. It quantifies the energy of the flow per unit volume.[2] Its dimension is $kg\ m^{-1}\ s^{-2}$. Relation [2.6] means that the head is conserved along a path in a steady flow. This statement constitutes Bernoulli's theorem. In equation [2.7], three forms of energy are recognized: kinetic, potential, and pressure.

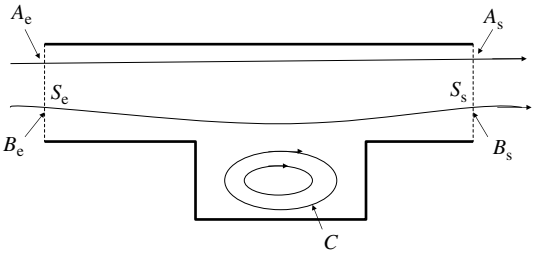

Figure 2.2. *Application of Bernoulli's theorem along a streamline*

This derivation of Bernoulli's theorem is quite interesting because it requires only the following assumptions: the fluid should be ideal and the flow must be steady. It is essential to bear in mind that in order to apply Bernoulli's theorem the

2 The term "head" often refers to the quantity $H/\rho g$, which is homogeneous to a length. This quantity is conveniently used when pressure changes are measured as water heights. Our definition is closer to the notion of energy. Either of these can be used, provided that consistency is maintained throughout.

path between two points in the flow needs to be known. The energy value is not necessarily identical along two different streamlines. There is no sense in using Bernoulli's theorem if the two points between which it is being applied are clearly not located on a common streamline. This is illustrated in Figure 2.2, which is a sketch of the flow in an enclosure, wherein a fluid enters through section S_e and exits through section S_s. Strictly, Bernoulli's theorem can only link energy between pairs of points (A_e, A_s) and (B_e, B_s), if the streamlines are well determined. In practice, the head is often uniform in the inlet section and is equal to the outlet head since the particles that come in are the ones that come out. However, there is no reason for the head at point C, which is located in a cavity where recirculation occurs, to be equal to the inlet head, as point C cannot be connected by a streamline to any point in the inlet section.

Another formulation of Bernoulli's theorem exists when the flow is irrotational (i.e. the curl of the velocity is zero at every point in the domain). This allows application to unsteady flows such as the propagation of waves on the sea. For a steady, irrotational flow, the head is the same at every point in the domain, and it is no longer necessary to check that the two points between which Bernoulli's theorem is being applied are connected by a streamline. However, the assumption of an irrotational flow is a substantial restriction; it precludes the recirculation depicted in Figure 2.2, for which the problem posed for the application of Bernoulli's theorem was already indicated.

2.3. Pressure variation in a direction normal to a streamline

If Euler's equation [2.4b] is considered along unit normal vector $\vec{n}$, some simple and useful properties regarding the pressure field can be established for a steady flow in two cases.

In the absence of gravity: pressure variation in a direction perpendicular to a curved streamline

If the gravity force is omitted, equation [2.4b] reduces to:

$$\rho \frac{V^2}{R} = -\frac{\partial p}{\partial n} \qquad [2.8]$$

When the particle path has finite curvature, since the normal vector is oriented toward the inside of the curve (Figure 2.1), the pressure increases from the inside to the outside of the curve.

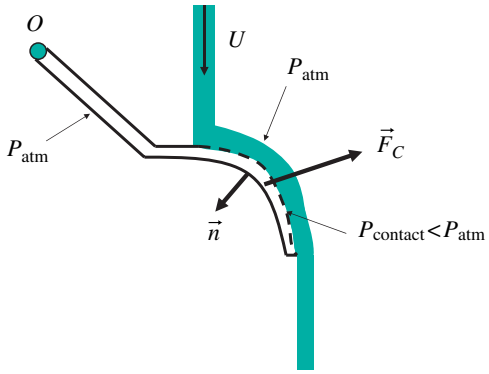

Figure 2.3. *Illustration of the effect of streamline curvature on the pressure field. The liquid flow exerts a force $\vec{F}_c$ on the convex face of a scoop*

The concept of centrifugal force lies behind this notion. This effect can be demonstrated simply by placing the back of a scoop in the jet of an open tap (Figure 2.3). Due to the curvature of the scoop, the pressure decreases inside the jet following a line directed radially along $\vec{n}$. Since atmospheric pressure prevails at the water–air interface, the pressure at the contact surface between the liquid and the scoop (dashed line) is lower than the atmospheric pressure. The integral of pressure forces acting on the scoop generates a force, $\vec{F}_c$, since the atmospheric pressure applies on the periphery of the scoop, except for the dashed-line liquid/scoop contact surface where the pressure is lower. If the scoop is held rotatably by an axis going through O, force $\vec{F}_c$ reduces the torque that needs to be applied in order to maintain the inclination of the scoop in the gravity field. The pressure gradient is proportional to the squared velocity (equation [2.8]). This effect can be felt manually if the jet flows sufficiently fast and the radius of curvature of the scoop is sufficiently small.

In the presence of gravity: hydrostatic pressure distribution in a parallel flow

Considering the case where gravity is taken into account, it is assumed that the movement occurs in a vertical plane containing the O_z axis. For a parallel flow, $R = \infty$, therefore equation [2.4b] becomes:

$$0 = f_n - \frac{\partial p}{\partial n} = -\rho g \vec{k} \cdot \vec{n} - \frac{\partial p}{\partial n} \qquad [2.9]$$

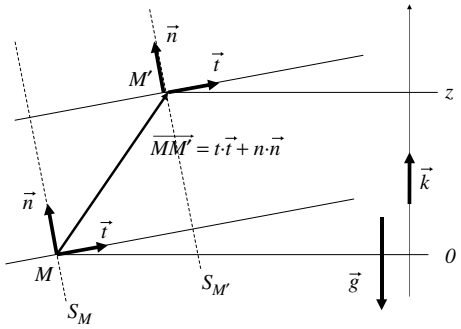

Figure 2.4. *Representation of the intrinsic coordinate system in the vicinity of a point around which the flow is parallel*

Let us consider a point M' in the vicinity of M, as depicted in Figure 2.4. Denoting with t and n its coordinates in the intrinsic coordinate system ($\vec{t}$, $\vec{n}$), it can be written as:

$$\overrightarrow{MM'} = t \cdot \vec{t} + n \cdot \vec{n} \qquad [2.10]$$

Using the notation z for the coordinate of M' along the gravity axis, $\vec{k}$, it can also be written as:

$$z = \vec{k} \cdot \overrightarrow{MM'} = t \cdot (\vec{t} \cdot \vec{k}) + n \cdot (\vec{n} \cdot \vec{k}) \qquad [2.11]$$

The dot products $(\vec{t} \cdot \vec{k})$ and $(\vec{n} \cdot \vec{k})$ are the cosines of the angles between $\vec{t}$ and $\vec{k}$, and between $\vec{n}$ and $\vec{k}$, respectively. Since the direction of the flow is known and the flow is parallel, the unit vectors of the intrinsic coordinate system $\vec{t}$ and $\vec{n}$ at M are the same as the ones at M', the angles are identical at any point near M, and consequently, it can be written as:

$$\frac{\partial z}{\partial n} = \frac{\partial t}{\partial n} \cdot (\vec{t} \cdot \vec{k}) + t \cdot \frac{\partial (\vec{t} \cdot \vec{k})}{\partial n} + \frac{\partial n}{\partial n} \cdot (\vec{n} \cdot \vec{k}) + n \cdot \frac{\partial (\vec{n} \cdot \vec{k})}{\partial n} = (\vec{n} \cdot \vec{k}) \qquad [2.12]$$

Equation [2.9] is therefore transformed into:

$$0 = -\rho g \vec{k} \cdot \vec{n} - \frac{\partial p}{\partial n} = -\frac{\partial}{\partial n}\{\rho g z + p\} \qquad [2.13]$$

This equation can be integrated in any plane that is perpendicular to the direction of the flow, yielding:

$$p(M') + \rho g \cdot \{z(M') - z(M)\} = p(M') - \rho \vec{g} \cdot \overrightarrow{MM'} = p(M) \qquad [2.14]$$

for two points M and M' located in the same plane S_M perpendicular to the direction of the flow. The constant of integration is the pressure at M. Relation [2.14] makes it possible to determine the pressure at any point in plane S_M if the pressure at a point within that plane is known. This property is very useful and will be frequently referred to. It enables the determination of the pressure field at any point in a parallel flow.

Relation [2.14] means that, for a parallel flow, the pressure variation is hydrostatic in any plane perpendicular to the direction of the flow. This property has already been highlighted for a Poiseuille flow within the gravity field (Chapter 1, section 1.7). It can be seen here that this property is much more general.

2.4. Momentum theorem

Consider a domain, D, bounded by a closed surface, S (Figure 2.5). Some portions of the surface, denoted by S_s, are solid walls, which do not permit fluid flow and the velocity of the fluid must be parallel to the wall. Other portions of the surface S_d are virtual surfaces within the fluid, which may allow flow through them. At any point M on surface S, the vector $\vec{n}$ is the normal vector to surface S oriented toward the outside of the domain.

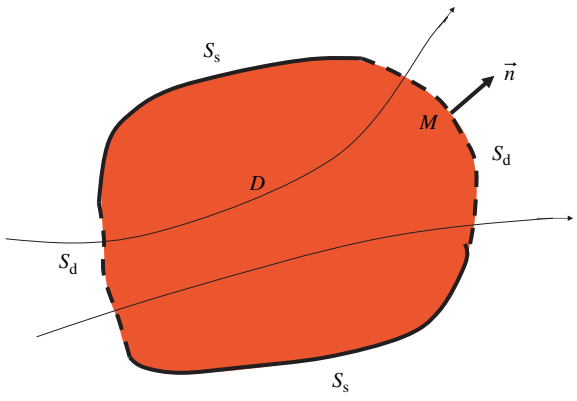

Figure 2.5. *Momentum theorem. Definition of a closed volume, D, of its envelope having solid surfaces S_s (solid lines) and throughflow surfaces S_d (dashed lines), and of the normal oriented toward the outside of the domain*

To explain the momentum theorem, it is assumed that the flow is steady and this is the only necessary assumption. It is by no means necessary for the fluid to be ideal, or even for the fluid's rheology to be Newtonian.[3]

The momentum theorem is established by integrating the local equations of motion on domain D, given in Chapter 1, which are written so as to exhibit the stress deviator, Σ' (the fluid is not necessarily Newtonian). We then obtain:

$$\iint_S \rho(\vec{U}\cdot\vec{n})\vec{U}\mathrm{d}s = -\iint_S p\vec{n}\mathrm{d}s + \iiint_D \vec{F}\mathrm{d}v + \iint_S \Sigma'\vec{n}\mathrm{d}s \qquad [2.15]$$

This expression exhibits different terms, which correspond to balances on the whole of volume D or on surface S. The term on the left-hand side is the *flux* (*or flow rate*) *of momentum* through surface S. This is only non-zero on the portions of surface S_d through which some flow occurs. Two contributions should be distinguished within the pressure term (the first term on the right-hand side): the integral over the throughflow surfaces S_d and that over solid surfaces S_s. On solid surfaces, we have:

$$\iint_{S_s} p\vec{n}\mathrm{d}s = \vec{R} \qquad [2.16]$$

which is the integral of the normal force exerted by the fluid on the solid wall.

The integral of body forces is the total weight of the fluid contained inside the domain, if gravity is the body force.

The integral of the stress deviator on surface S (last term in equation [2.14]) is the friction force exerted by the outside on the fluid, through the flow surfaces S_d, and on the solid surfaces S_s. In many cases, the friction force exerted through the flow surfaces is equal to zero. This is the case, for instance, when the flow is perpendicular to the throughflow surface. Here, these possible terms are neglected by writing:

$$\iint_S \Sigma'\vec{n}\mathrm{d}s \approx \iint_{Sd} \Sigma'\vec{n}\mathrm{d}s = -\vec{K} \qquad [2.17]$$

3 Exercise I in Chapter 7 uses the momentum theorem for a Bingham fluid.

The momentum balance can thus be written in the form:

$$\iint_{S_d} \left\{ \rho(\vec{U} \cdot \vec{n})\vec{U} + p\vec{n} \right\} \mathrm{d}s = -\vec{R} + \iiint_D \vec{F} \mathrm{d}v - \vec{K} \qquad [2.18]$$

Forces $\vec{R}$ and $\vec{K}$ are the global pressure and friction forces, respectively, *exerted by the flow on solid walls* (a minus sign appears in equation [2.17] in front of $\vec{K}$). The left-hand side of equation [2.18] represents the *impulse flux*. While applying the momentum theorem, it is important to specify whether the forces under consideration are the ones exerted by the flow on solid walls or the other way round. Sign errors frequently occur when there is lack of specificity in this respect. *To apply the momentum theorem, the first step is to specify domain D, throughflow surfaces S_d and solid surfaces S_s. Care must then be taken to orientate the normals in the proper direction.*

The momentum theorem is used to answer two types of questions:

1. Evaluating the forces applied by a flow on the solid walls that surround the fluid. A classical example is the flow in a bend (see Exercise I). Section 2.5 deals with the equally classical relation between regular head loss and wall friction for the flow inside a straight pipe. In both cases, the pressure changes between the different throughflow surfaces in the domain are known.

2. Evaluating pressure drops in a flow. The classical example of a sudden expansion is presented in section 2.6. Since there is a loss of energy, Bernoulli's theorem cannot be applied. An assumption usually enables the determination of the forces exerted by the flow on the solid walls, and the derivation therefrom of pressure changes between the inlet and outlet.

2.5. Evaluating friction for a steady-state flow in a straight pipe

Consider the flow in a straight pipe, whose walls are parallel to the O_x axis (Figure 2.6). Here, the cross-sectional geometry is arbitrary. In addition, the gravity forces are ignored and it is also assumed that the flow is unidirectional in the O_x direction. The momentum theorem applied to the closed domain bounded by the walls and the fluid inlet and outlet sections is written as:

$$\iint_{S_e+S_s} \left\{ \rho(\vec{U} \cdot \vec{n})\vec{U} + p\vec{n} \right\} \mathrm{d}s = -\vec{R} - \vec{K} \qquad [2.19]$$

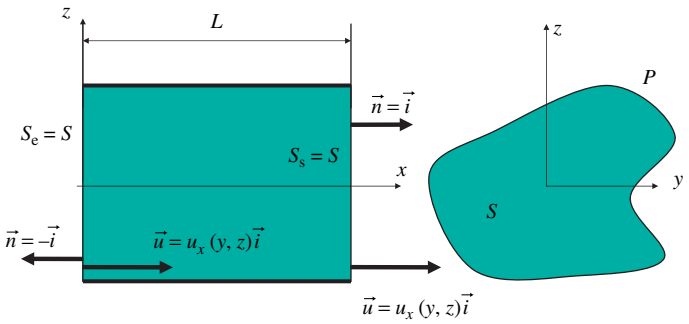

Figure 2.6. *Application of the momentum theorem to the fluid contained in a cylindrical pipe*

From the results of section 2.3, it can be stated that the pressure is uniform in the flow inlet and outlet sections, since the flow is parallel. Through mass conservation, the momentum fluxes between the inlet and the outlet cancel each other, as the direction of the unit normal vector is reversed between the inlet and outlet while the velocity profile is the same for both sections. We therefore deduce from equation [2.19] that:

$$\{p(L) - p(0)\} S\vec{i} = -\vec{R} - \vec{K} \qquad [2.20]$$

The inlet and outlet throughflow sections of the pipe have an area of S. Relation [2.20] is a vector relation. The pressure force $\vec{R}$ exerted by the flow on the solid side walls is perpendicular to vector $\vec{i}$, whereas the friction force, $\vec{K}$, is parallel to it. Consequently:

$$\{p(L) - p(0)\} S\vec{i} = -\vec{K} \quad \text{and} \quad \vec{R} = \vec{0} \qquad [2.21]$$

We assume that the friction stress τ exerted by the flow is uniform on the side wall. This assumption is questionable in the case of a complex cross-sectional geometry, but is wholly valid in the case of the plane Poiseuille flow or for the Poiseuille flow in a circular pipe. Therefore, it is written as:

$$\{p(L) - p(0)\} S\vec{i} = -\tau \cdot L \cdot P \cdot \vec{i} \qquad [2.22]$$

where P is the perimeter of a pipe section and PL is the wetted surface of the pipe. The friction stress exerted by the flow on the sidewall is thus expressed simply as a function of the pressure gradient:

$$\tau = \frac{\{p(0) - p(L)\}}{L} \frac{S}{P} \qquad [2.23]$$

As can be seen, the relations obtained in Chapter 1 for Poiseuille flows are solved in equation [2.23]. For a circular pipe, $S/P = R/2$, hence:

$$\tau = -\frac{\partial p}{\partial z}\frac{R}{2} \qquad [2.24]$$

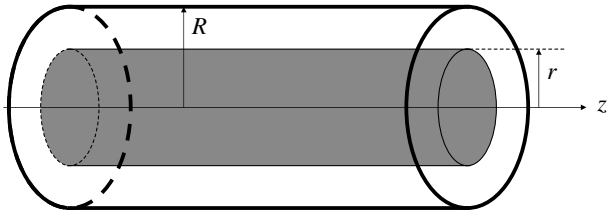

Figure 2.7. *Application of the momentum theorem on a virtual, circular cylindrical volume of radius r (shaded volume) contained within a pipe of radius R*

The momentum theorem is equally applicable to any circular cylindrical volume of radius r internal to the pipe (i.e. $r < R$) as sketched in Figure 2.7. It then enables the calculation of the friction stress exerted by the fluid contained inside the cylinder of radius r on the fluid contained outside that cylinder. Extrapolating equation [2.24] shows that this quantity varies linearly with the radius:

$$\tau(r) = -\frac{\partial p}{\partial z}\frac{r}{2} \qquad [2.25]$$

This remarkable result holds for a laminar flow as well as a turbulent flow. Such examples illustrate the power of momentum theorem; local knowledge of the flow is not always necessary to determine wall friction. However, the pressure gradient enables its determination.

2.6. Pressure drop in a sudden expansion (Borda calculation)

Consider the flow in a sudden expansion (Figure 2.8(a)) between two straight pipes whose walls are parallel to the O_x axis. In the expansion area, the flow is not parallel to the O_x direction. The domain to which the momentum theorem is applied (shaded domain in Figure 2.8(a)) is taken between the expansion section S_1 and a downstream section S_2 chosen sufficiently far away for the flow therein to become parallel again. Here, the gravity forces are ignored (the way gravity can be accounted for is discussed in section 2.7). Consequently, the pressure is uniform in sections S_1 and S_2, and is denoted by P_1 and P_2, respectively.

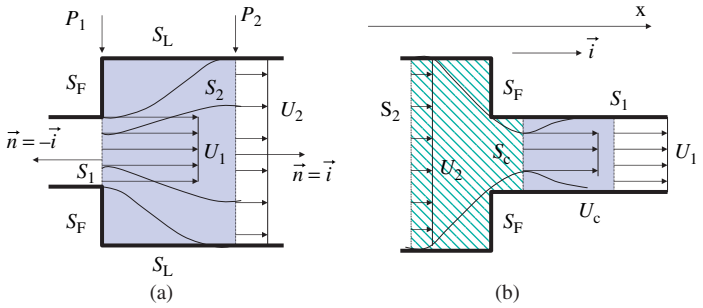

Figure 2.8. *(a) Sudden expansion and (b) restriction in a cylindrical pipe: geometrical definitions*

For a flow that is uniform in sections S_1 and S_2, and denoting the velocities by U_1 and U_2 , mass conservation is written as:

$$S_1U_1 = S_2U_2 \qquad [2.26]$$

The momentum theorem, of which only the projection onto vector $\vec{i}$ is considered here, is written as:

$$\{P_2 + \rho U_2^2\} S_2 \cdot \vec{i} - \{P_1 + \rho U_1^2\} S_1 \cdot \vec{i} = -\vec{R}_f - \vec{K} \qquad [2.27]$$

The pressure force on the sidewall S_L has disappeared as it is perpendicular to $\vec{i}$. Force $\vec{R}_f$ represents the pressure force on the solid wall S_F, which is the end wall surrounding throughflow section S_1. Borda's model assumes that the pressure also equals P_1 on S_F. The pressure force $\vec{R}_f$ is then given by:

$$\vec{R}_f = -P_1(S_2 - S_1)\vec{i} \qquad [2.28]$$

Lastly, the friction, $\vec{K}$, exerted by the flow on the sidewall is neglected. Using mass conservation [2.26] and property [2.28], it is inferred from [2.27] that:

$$\{P_2 - P_1\} S_2 = \rho \left\{ U_1^2 S_1 - U_1^2 \frac{S_1^2}{S_2^2} S_2 \right\} = \rho U_1^2 S_1 \left\{ 1 - \frac{S_1}{S_2} \right\} \qquad [2.29]$$

Neglecting friction can be easily justified: the distance between sections S_1 and S_2 is short and, consequently, the surface subjected to friction is limited. It is less straightforward to state that the pressure P_1 prevails all over surface S_F, due to

recirculation in that zone. However, the turbulence that reigns there contributes to homogenize the pressure, which settles at the level of pressure P_1 in the outlet.

Therefore, the momentum theorem makes it possible to calculate the pressure change between the inlet and outlet sections. The head change (equation [2.7]) between the inlet and outlet is then estimated (using [2.26] and [2.29]) based on the velocity in the inlet section only:

$$H_1 - H_2 = \left\{ P_1 + \rho \frac{U_1^2}{2} \right\} - \left\{ P_2 + \rho \frac{U_2^2}{2} \right\} = \frac{\rho U_1^2}{2} \left\{ 1 - \frac{S_1}{S_2} \right\}^2 \qquad [2.30]$$

This model, referred to as Borda's model, shows that the flow undergoes a loss of energy in a sudden expansion, since $H_1 > H_2$. Such dissipation is associated with the production of turbulence in the sudden expansion. Section 2.8, and further discussions in Chapter 8, explains the reasons that cause turbulence to dissipate energy.

Obviously, relation [2.30] does not hold if the direction of flow is reversed to consider the case of a sudden restriction. Otherwise, energy would need to be supplied to the flow in order to increase the head for the fluid particles. The situation of the flow in a sudden restriction is depicted schematically in Figure 2.8(b). The flow separates on the right angle of the restricted section's inlet edge. At first, it goes through a narrowed-down section of area $S_c < S_1$, then it spreads out. If the area S_c of the separation zone is known, mass conservation makes it possible to infer the velocity U_c, in the restriction. In the hatched zone corresponding to the restriction, the particles maintain their energy. Bernoulli's theorem, applied between sections S_2 and S_c, provides the pressure in the contracted section. Lastly, the momentum theorem, applied to the hatched domain, provides an estimate of the force applied by the flow on the end wall S_F. The head loss occurs within the shaded part in Figure 2.8(b), reverting to Borda's calculation described earlier and applying it to the expansion between S_c and S_1. The unknown needed to complete the calculations is the surface, S_c, of the contracted section. Calculation rules based on experimental data, for computing head losses in many expansion and restriction situations, can be found in the well-known handbook by Idel'Cik.[4]

The examples presented in the last two sections show that Bernoulli's theorem and the momentum theorem cannot always be applied simultaneously. When the momentum theorem is applied assuming that the pressures on the throughflow surfaces surrounding the domain considered are known, the forces on the walls can be deduced therefrom (as in section 2.5). When the forces are assumed known, the momentum theorem makes it possible to calculate the pressure change between the

4 I.E. Idel'Cik, 1960, *Mémento des pertes de charge* (translated from Russian), Editions Eyrolles, Paris.

inlet and outlet sections and to deduce the pressure drop therefrom. Energy is not always conserved, as seen in the case of sudden expansion.

2.7. Using the momentum theorem in the presence of gravity

The momentum theorem is written in equation [2.18] by exhibiting the body force, $\vec{F}$. The pressure to be considered in calculating the impulse flux (left-hand-side term in equation [2.18]) is then the absolute pressure. The calculation of integrals is typically not straightforward because the pressure varies with height due to the effect of gravity. To circumvent this difficulty without neglecting gravity, the impulse flux integrals are calculated using pressure p', which is equal to the difference between the absolute pressure and the hydrostatic pressure, p_{hyd}.

$$p'(M) = p(M) - p_{hyd}(M) \qquad [2.31]$$

The hydrostatic pressure, introduced in Chapter 1 (equation [1.36]), is written as:

$$p_{hyd}(M) = p_0 + \rho\vec{g}\cdot\overrightarrow{OM} \qquad [2.32]$$

where p_0 is a reference pressure taken at point O. Pressure p' is homogeneous in throughflow sections S_d if the flow is perpendicular to the throughflow section (see section 2.3), and the calculation of integrals poses no further difficulty. This very simple procedure enables a rigorous application of the momentum theorem in the presence of gravity, by omitting the gravity force in equation [2.18] of the momentum theorem.

2.8. Kinetic energy balance and dissipation

It is seen that a sudden expansion (Figure 2.8(a)) results in energy dissipation: the head decreases between the inlet and the outlet (equation [2.30]). The rate of energy dissipation evaluates how fast the kinetic energy is dissipated. For the sudden expansion, it is possible to estimate an average rate of kinetic energy dissipation per unit mass, $\overline{\varepsilon}$, by computing the ratio of the head change to the time of residence in the sudden expansion, namely:

$$\rho\overline{\varepsilon} = \frac{Q}{\text{Vol}}\{H_1 - H_2\} \qquad [2.33]$$

This formula involves the flow rate and the volume of the sudden expansion.

In reality, the rate of dissipation is a local physical notion that varies in both space and time. As will be seen hereinafter, turbulence dramatically increases the rate of energy dissipation, and hence its paramount importance in fluid mechanics. The rate of energy dissipation can be defined rigorously on the basis of the Navier–Stokes equations, by establishing the evolution equation for kinetic energy. For this derivation, it is assumed that the fluid is incompressible.[5] A tensor notation is used (Einstein's notation) where the velocity vector is expressed in the form u_i, with index i varying from 1 to 3 to designate the three space dimensions (namely $u_1 = u_x$, $u_2 = u_y$ and $u_3 = u_z$). The local equations can then be written as:

for incompressibility

$$\frac{\partial u_j}{\partial x_j} = \frac{\partial u_1}{\partial x_1} + \frac{\partial u_2}{\partial x_2} + \frac{\partial u_3}{\partial x_3} = 0 \qquad [2.34]$$

for the equations of dynamics

$$\rho\left\{\frac{\partial u_i}{\partial t} + u_j \frac{\partial u_i}{\partial x_j}\right\} = -\frac{\partial p}{\partial x_i} + \frac{\partial \sigma'_{ij}}{\partial x_j} \qquad [2.35]$$

While the tensor notation is convenient for subsequent calculations, it should be remembered that, in equations [2.34] and [2.35], the terms involving index j are summed for all three values of j, i.e. in equation [2.35],

$$u_j \frac{\partial u_i}{\partial x_j} = u_1 \frac{\partial u_i}{\partial x_1} + u_2 \frac{\partial u_i}{\partial x_2} + u_3 \frac{\partial u_i}{\partial x_3}$$

$$\frac{\partial \sigma'_{ij}}{\partial x_j} = \frac{\partial \sigma'_{i1}}{\partial x_1} + \frac{\partial \sigma'_{i2}}{\partial x_2} + \frac{\partial \sigma'_{i3}}{\partial x_3}$$

There are also three equations of dynamics for each value of index $i = 1$, 2, and 3. Equations [2.35] are written using the symbolic notation of the stress deviator, to simplify intermediate calculations. The expression of the stress tensor for a Newtonian fluid will be used later on.

By multiplying each of the equations [2.35] of dynamics by u_i, respectively, three equations are obtained for $i = 1$, 2, and 3.

---

5 The following discussion is much inspired by section 16 of the book of L.D. Landau and E.M. Lifshitz, *Fluid Mechanics* (2nd Edition, Butterworth-Heinemann, 1987), which is outstandingly clear.

$$\rho\left\{\frac{\partial}{\partial t}\left(\frac{u_i^2}{2}\right)+u_j\frac{\partial}{\partial x_j}\left(\frac{u_i^2}{2}\right)\right\}=-\frac{\partial p}{\partial x_i}u_i+u_i\frac{\partial \sigma'_{ij}}{\partial x_j} \qquad [2.36]$$

Summing these three equations over index *i* brings in the kinetic energy per unit volume:

$$e=\rho\left(\frac{u_i^2}{2}\right) \qquad [2.37]$$

whose evolution equation is:

$$\left\{\frac{\partial e}{\partial t}+u_j\frac{\partial e}{\partial x_j}\right\}=-\frac{\partial p}{\partial x_i}u_i+u_i\frac{\partial \sigma'_{ij}}{\partial x_j} \qquad [2.38]$$

Equations [2.37] and [2.38], and the subsequent ones, are now summed over indices *i* and *j*.

Differentiation formulae yield some simplifications, thanks to incompressibility:

$$\left.\begin{aligned} u_j\frac{\partial e}{\partial x_j}&=\frac{\partial(eu_j)}{\partial x_j}-e\frac{\partial u_j}{\partial x_j}=\frac{\partial(eu_j)}{\partial x_j}\\ \frac{\partial p}{\partial x_i}u_i&=\frac{\partial(pu_i)}{\partial x_i}-p\frac{\partial u_i}{\partial x_i}=\frac{\partial(pu_i)}{\partial x_i}\\ u_i\frac{\partial \sigma'_{ij}}{\partial x_j}&=\frac{\partial(u_i\sigma'_{ij})}{\partial x_j}-\sigma'_{ij}\frac{\partial(u_i)}{\partial x_j}\end{aligned}\right\} \qquad [2.39]$$

Evolution equation [2.38] for kinetic energy therefore becomes:

$$\frac{\partial e}{\partial t}=-\frac{\partial(eu_j)}{\partial x_j}-\frac{\partial(pu_i)}{\partial x_i}+\frac{\partial(u_i\sigma'_{ij})}{\partial x_j}-\sigma'_{ij}\frac{\partial(u_i)}{\partial x_j} \qquad [2.40]$$

that is:

$$\frac{\partial e}{\partial t}=-div\{(p+e)\vec{u}\}+div\{\Sigma'\vec{u}\}-\sigma'_{ij}\frac{\partial(u_i)}{\partial x_j} \qquad [2.41]$$

This formulation, which brings in the divergence of certain vectors, is attractive because, by integrating the equation over a volume *D*, it is possible, through Ostrogradsky's formula, to transform the volume integrals in some of the terms into integrals over surface *S*, which surrounds volume *D*. This results in the appearance

of flux terms through surface *S*. These transformations lead to:

$$\frac{\partial}{\partial t}\left\{\int_D e\mathrm{d}v\right\} = -\int_S (p+e)(\vec{u}\cdot\vec{n})\mathrm{d}s + \int_S (\Sigma'\vec{u})\cdot\vec{n}\mathrm{d}s - \int_D \sigma'_{ij}\frac{\partial(u_i)}{\partial x_j}\mathrm{d}v \qquad [2.42]$$

Finally, the symmetry of the stress tensor yields:

$$\frac{\partial}{\partial t}\left\{\int_D e\mathrm{d}v\right\} = -\int_S (p+e)(\vec{u}\cdot\vec{n})\mathrm{d}s + \int_S (\Sigma'\vec{n})\cdot\vec{u}\mathrm{d}s - \int_D \sigma'_{ij}\frac{\partial(u_i)}{\partial x_j}\mathrm{d}v \qquad [2.43]$$

The physical meaning of the different terms is worthy of some clarifications. From left to right, it is encountered in sequence:

– The rate of variation of the kinetic energy contained in the volume.

– The head flux through the surface surrounding the domain. Gravity forces may be incorporated into this term, through potential energy.

– The power of friction stresses at the boundaries.

– The rate of energy dissipation.

Now, specific attention is given to the fourth term, i.e. the rate of energy dissipation. For a Newtonian fluid, bringing the expression of the stress deviator tensor (Chapter 1, Table 1.1) in, the rate of energy dissipation, integrated over the volume, can be written as:

$$-\int_D \sigma'_{ij}\frac{\partial u_i}{\partial x_j}\mathrm{d}v = -\int_D \mu\left\{\frac{\partial u_i}{\partial x_j}+\frac{\partial u_j}{\partial x_i}\right\}\frac{\partial u_i}{\partial x_j}\mathrm{d}v = -\frac{\mu}{2}\int_D \left\{\frac{\partial u_i}{\partial x_j}+\frac{\partial u_j}{\partial x_i}\right\}^2 \mathrm{d}v \qquad [2.44]$$

since the summation takes place on both *i* and *j* indices. As a result, we arrive at the following conclusions:

– This quantity is always negative. Therefore, it is justified in referring to it as the rate of dissipation of kinetic energy, as it can only contribute to decrease kinetic energy.

– Energy dissipation is linked to velocity gradients. The larger the velocity gradients in the flow, the stronger the dissipation. It can therefore be anticipated that dissipation will be very large in a turbulent flow. The kinetic energy dissipated is thereby turned into heat. For fluids such as water or air, the warming induced by dissipation is very weak (see Exercise III at the end of this chapter). But for highly viscous fluids in configurations where the flow is strongly sheared, such as a liquid

polymer in an extruder, the amount of self-heating resulting from viscous dissipation can be very large.

– The dissipation rate per unit mass, denoted by ε, can thus be defined as a local quantity by:

$$\varepsilon = -\frac{\mu}{2\rho}\left\{\frac{\partial u_i}{\partial x_j} + \frac{\partial u_j}{\partial x_i}\right\}^2 \qquad [2.45]$$

The spatial distribution of this quantity is typically highly inhomogeneous. These aspects will be explained in Chapter 8, while dealing with the concepts of turbulence.

2.9. Application exercises

The exercises proposed below are applications of Bernoulli's theorem and the momentum theorem. As demonstrated in this chapter, these two theorems cannot always be applied simultaneously, because applying Bernoulli's theorem implies energy conservation, whereas energy is obviously not conserved if the momentum theorem is used to estimate a head loss. The first challenge is to know when and in which regions of a flow it can be considered that energy is conserved, and when the flow is dissipating energy. This will be explained in Chapter 4. The wording of the following exercises is deliberately kept somewhat ambiguous, because if it is indicated which of Bernoulli's theorem or the momentum theorem should be applied (specifying in which domain) there would no longer be an exercise to solve, but only calculations to perform.

Exercises 2.I–2.III and 2.V are classical ones. Exercise 2.IV compares the results of a local approach to those yielded by the global approach, establishing a link with Chapter 1. Exercises 2.VI and 2.VII are more complex. In those cases, the flow does not dissipate energy in certain subdomains, while in others it dissipates some. Based on Borda's model, it will be assumed that energy is conserved in regions where the flow is convergent (the available cross section diminishes) and that dissipation occurs in domains where a sudden expansion occurs.

Exercise 2.I: Force exerted on a bend

A circular cylindrical pipe whose diameter is 50 cm goes through a 90° bend. If the water flow rate in the pipe is 1 $m^3\ s^{-1}$, calculate the force applied by the flow onto the support (orientation and magnitude). The absolute pressure measured at the inlet of the bend is 2 bar and the air surrounding the pipe is assumed to be at a pressure of 1 bar.

Carry out the numerical application and discuss the way in which the ambient atmospheric pressure should be taken into account.

Exercise 2.II: Emptying a tank

Here, we analyze what can be learnt from the application of the Bernoulli's and momentum theorems when they are applied to the emptying of a tank in which the water level is H.

1. Establish Torricelli's formula, which gives the velocity of the fluid at its exit from the tank. For this question, it will be assumed that the pressure in the jet is the atmospheric pressure.

2. Using the results from section 2.3, explain which effect allows the pressure (within the gravity field) to actually settle at the atmospheric pressure in the jet at the tank outlet.

3. Calculate the force exerted on the walls of the tank. How would the tank behave if it was mounted on wheels and able to roll without friction?

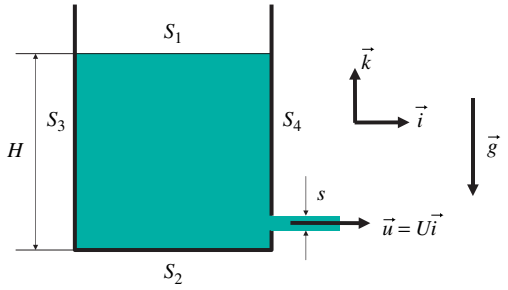

Figure 2.II.1

Exercise 2.III: Pressure drop in a sudden expansion and heating

Consider a sudden expansion such that $S_1 / S_2 = 1/3$. The inlet velocity is 5 m s^{-1}.

Determine:

– The head loss;

– The temperature rise;

The numerical application will be carried out with water as the fluid (mass density $\rho = 10^3$ kg m^{-3}, specific heat $C_p = 4.2\ 10^3$ J kg^{-1} K^{-1}).

Exercise 2.IV: Streaming flow on an inclined plane

Consider the streaming flow on an inclined plane lying at an angle α to the horizontal plane (imagine a river). Gravity is along the vertical axis. In a uniform flow regime, the thickness h of the fluid layer is invariant. It does not depend on coordinate x in the coordinate system indicated in the Figure 2.IV.1. The flow is assumed to be two-dimensional (that is, $u_x(x, z)$) and unidirectional ($u_y = u_z = 0$). ρ is the mass density of the fluid, and μ its dynamic viscosity.

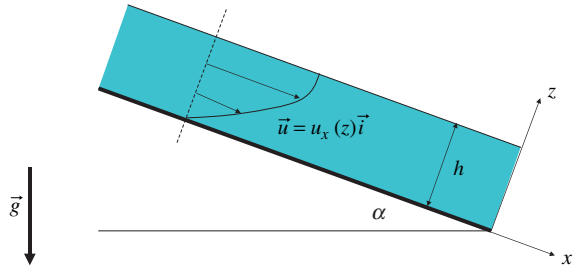

Figure 2.IV.1

Part 1 – Do not use the local solution of the Navier–Stokes equations

1. Why is the u_x velocity component independent from x?

2. Determine the pressure field.

3. Determine the head at every point in the liquid. Which term causes the head loss in the flow along a streamline?

4. Determine the friction stress exerted by the flow on the solid wall.

Part 2 – Use of the Navier–Stokes equations

1. Write out the Navier–Stokes equation for the u_x velocity component (along O_x), using the assumptions made about the kinematics of the flow and the results established in the first part?

2. Write out the boundary conditions on the bottom ($z = 0$) and at the free surface ($z = h$).

3. Determine the velocity profile, $u_x(z)$?

4. Calculate the friction stress exerted on the bottom by the flow, using a method other than the one used in Question 4 of Part 1?

5. Calculate height h as a function of the flow rate Q injected by unit width?

Exercise 2.V: Impact of a jet on a sloping plate

Consider, in a two-dimensional configuration, a jet of water that impinges on a flat plate defining an angle α with the direction of the incident flow (the jet impinges perpendicularly on the plate when $\alpha = \pi/2$). The upstream thickness of the jet is denoted by e and the thicknesses along the plate on either side of the incident jet's axis are denoted by e_1 and e_2. Besides the pressure of the gaseous atmosphere is denoted by p_o, which is also exerted on the rear side of the plate. The velocity in the incident jet is assumed to be uniform, which is denoted by U. At a sufficient distance from the incident jet's axis, velocities are also assumed to be uniform in the throughflow sections, and are denoted by U_1 and U_2.

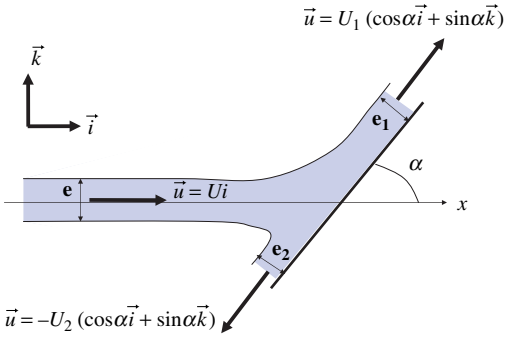

Figure 2.V.1

1. Determine:

– Thicknesses e_1 and e_2.

– Velocities U_1 and U_2.

– The force exerted on the plate.

The effect of gravity is neglected. It is assumed that energy is conserved and that the friction force exerted by the flow on the plate is negligible with respect to the pressure force. Justify the latter assumption.

2. If it was now assumed that the fluid particles undergo a head loss on impact, would thicknesses e_1 and e_2 be greater or smaller than the ones obtained in Question 1?

Exercise 2.VI: Operation of a hydro-ejector

This exercise aims to understand the principle of operation of a hydro-ejector, which is an apparatus used, for example, for cleaning the walls of a basin.

Part I – Jet from a submerged pump

In the first stage, we consider a simplified configuration where the apparatus simply consists of a submerged pump, which draws water from inside the basin and discharges it in the same basin in the form of a jet. The suction and discharge pipes are circular cylindrical pipes, which have the same diameter, $D_0 = 0.1$ m. Velocity U_j is assumed to be uniform at the outlet of the discharge line (Figure 2.VI.1). The axis of the apparatus is horizontal within the gravity field.

The characteristic of the pump is plotted in Figure 2.VI.2. The head/velocity relationship can be represented by a parabolic function

$$\Delta H_{\text{pump}} = P_{\max} - \alpha \rho U_j^2 / 2$$

with numerical values $P_{\max} = 10^5$ Pa and $\alpha = 9$.

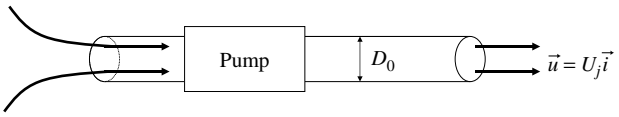

Figure 2.VI.1

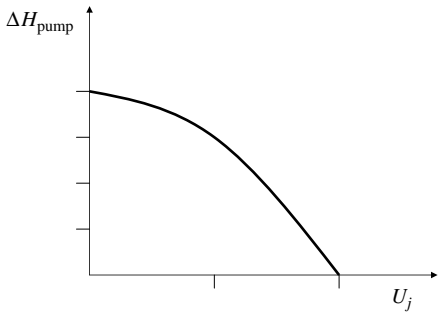

Figure 2.VI.2

1. State the operating conditions of the pump in terms of flow rate and head.

2. What is the momentum flux discharged by the apparatus?

Part II – The hydro-ejector

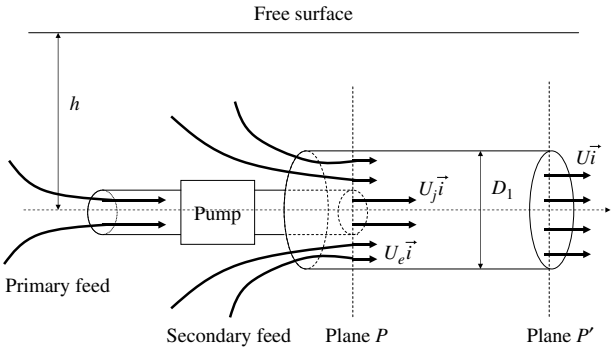

Figure 2.VI.3

To form a hydro-ejector (Figure 2.VI.3), the jet produced by the apparatus considered in part I is fed into a tube with diameter $D_1 = 0.2$ m, allowing a secondary supply by entrainment. In plane P, it is assumed that the jet produced by the primary supply (velocity U_j) is always uniform with $0 < r < D_0/2$; the same is true of the velocity U_e of the secondary feed with $D_0/2 < r < D_1/2$ in plane P. At the outlet of the hydro-ejector (plane P'), the velocity is assumed to be homogeneous, which is denoted by U. The length of the tube is not a parameter of the problem. It is assumed sufficiently large to allow the velocity field to become homogeneous, and sufficiently short to allow wall friction to be neglected.

For simplicity, it is assumed that the velocity U_j is the same as the one determined in Question 1. If Question 1 has not been solved, a value of $U_j = 4$ m s^{-1} may be used. The pressure value, however, is not necessarily the same. The axis of the hydro-ejector is located at a depth h under the free-surface level of the basin.

3. What indications can be provided regarding the pressure field in planes P and P'? (Numerical values will be calculated at the end of Question 5.)

4. Explain the mechanism that draws fluid through the secondary supply. State a first relation involving U_e.

5. Calculate the entrainment velocity U_e, the velocity U at the outlet of the hydro-ejector, and the numerical values of the pressure. Calculations will be facilitated by bringing in the ratio of the area of the primary jet to that of the hydro-ejector tube, $s = D_0^2/D_1^2 = 1/4$, as well as the velocity ratio, U_j/U_e.

6. What is the power consumption of the hydro-ejector? Compare this to an equivalent estimate that can be derived for the apparatus considered in part I.

7. Calculate the flow rate of the hydro-ejector, as well as the rate of momentum at the outlet of the hydro-ejector (plane P'). Explain one benefit of the hydro-ejector by comparing it to the configuration without a secondary supply tube as studied in part I.

Exercise 2.VII: Bypass flow

This exercise is inspired by cooling problems in an industrial facility. Part of the flow of a river is diverted and fed into a bypass channel that goes through a grid with which it exchanges heat. The exercise deals with the hydraulics problem: how is the flow rate distributed between the bypass channel and the river?

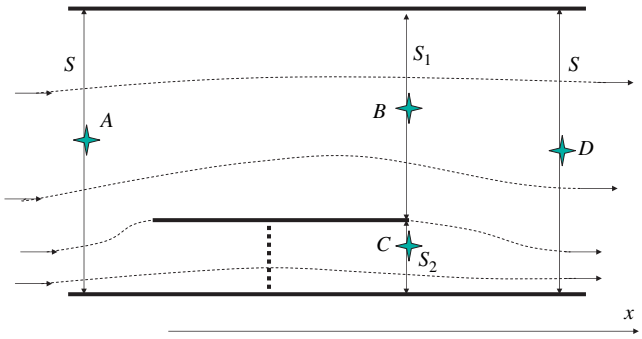

Figure 2.VII.1

For the solution of this problem, gravity will not be considered. The fluid is water. For simplicity, it is assumed that the channels are rectilinear in geometry, as shown in the Figure 2.VII.1, and wall friction is neglected. The grid induces a singular head loss in the flow, written as $\Delta H = K\rho U_2^2 / 2$. $K = 3$ will be used for the numerical applications.

We denote by $U = 1$ m s^{-1}, U_2 and U_1, respectively, the velocities in the inlet section (whose area is $S = 1{,}000$ m^2) containing point A, in the outlet section of the bypass channel (area $S_2 = 200$ m^2) containing point C, and in the outlet section of the other channel (area $S_1 = 800$ m^2) containing point B. The velocity is assumed to be uniform in all the sections considered. The pressure at A is $P_A = 1$ bar.

1. Justify why the pressure is the same at B and C.

2. By considering energy conservation (or non-conservation) between A and B, then between A and C, determine velocities U_2 and U_1. Deduce therefrom the difference in pressure, $P_A - P_B$, between points A and B.

3. It is assumed that the fluids are again completely mixed in the outlet section containing point D. Explain why the head cannot be conserved between B and D. By applying the momentum theorem on a domain to be specified, calculate the pressure difference, $P_B - P_D$, between points B and D.

Chapter 3

Dimensional Analysis

The treatment of this chapter goes far beyond the field of fluid mechanics. Although the concepts of dimensional analysis apply in all the fields of science, it finds extensive use in fluid mechanics as a tool for studying various phenomena. It, therefore, occupies center stage in this book. This chapter elaborates on several topics:

– It sets out the consequences of a system's behavior being independent from the system of units used to describe it. This idea is linked to the notion of homogeneity that should be verified by any mathematical expression describing a physical system.

– Dimensional analysis helps to establish the general form of a relation that exists between the various parameters involved in a problem. Let us consider the example of a fluid flow in a pipe with a diameter D and a length L, which we discuss later. This flow is generated by the pressure change between the inlet and outlet, shifting from P_1 to P_2. The streamwise velocity, U, is therefore expressed by a relation in the form $F(P_1, P_2, U, D, L, \nu, \rho, \ldots) = 0$ between the different physical parameters that define the system. Dimensional analysis shows that this relation should associate the parameters in a way respecting consistency in regards to units attached to the parameters. It also enables us to identify a reduction in the number of variables in the relation describing the system.

– An offshoot of dimensional analysis is the theory of similarities, which sets out a way to model a physical system at a different scale without altering its nature. This theory is commonly used in mechanics, as well as in chemical engineering, whenever a "pilot experiment" is involved. Similarity theory is based on defining "dimensionless numbers" to describe a physical phenomenon.

The principles of dimensional analysis are difficult to understand for a student who is studying them for the first time. This is natural because one apparently presumes to understand a phenomenon without actually being familiar with the equations which govern its behavior. The examples discussed in this chapter show that it is desirable to identify such equations correctly (even though we do not solve them) to count the parameters involved in a first stage and, to express relevant dimensionless numbers in a second stage. For the above-mentioned flow in a pipe, the parameter count is a consequence of the finding that the phenomenon is described using Navier–Stokes equations alone; solving them would suffice to arrive at the exact answer. The parameters involved in a problem may have different roles. A simple procedure, but one that is necessary to use dimensional analysis efficiently, consists of identifying the physical parameters that cause the phenomenon (the pressure difference between the ends of the pipe – why does the fluid flow inside the pipe?), those that characterize the consequence (the area-averaged streamwise velocity of the flow), and the other parameters (viscosity, geometrical dimensions, etc), which simply have an effect on the phenomenon.

3.1. Principle of dimensional analysis, Vaschy–Buckingham theorem

The Vaschy–Buckingham theorem is stated below:

> Consider a phenomenon involving n variables. Let those n variables, in turn, involve p units. The phenomenon can then be described by a relation linking $(n–p)$ dimensionless numbers.

Dimensional analysis, therefore, enables a reduction of the number of variables in the functional relation linking the physical quantities that describe the behavior of a system. To understand the Vaschy–Buckingham theorem, let us return to the example of the pipe flow. Initially, the system's parameters include the following:

– P_1 is the pressure at the pipe's inlet,

– P_2 is the pressure at the pipe's outlet,

– L is the length of the pipe,

– D is the diameter of the pipe,

– ν is the kinematic viscosity of the fluid, and

– U is the area-averaged streamwise velocity of the fluid.

The first five parameters are set by the user who wishes to make a fluid, whose properties he/she specifies, flow inside a chosen pipe. The sixth one, i.e. the velocity, is set based on the values of the previous five. It is this quantity (the unknown of the problem) that we want to determine based on the knowledge of

the other parameters. Other, more or less relevant, parameters such as those given below can also be taken into account:

– e, the roughness of the pipe (unit m), and

– the age of the captain (unit s) who actuates the valve.

Let us retain all these parameters.[1] We thus wish to express the velocity as a function of the other parameters, i.e. a functional of the form

$$U = F(P_1, P_2, D, L, e, \nu)$$

Including the quantity we wish to determine, we have $n = 7$ parameters in the functional, which are listed with their units in Table 3.1:

Parameter	U	P_1	P_2	L	D	e	ν
Unit	$m \cdot s^{-1}$	$Kg \cdot m^{-1} \cdot s^{-2}$	$kg \cdot m^{-1} \cdot s^{-2}$	m	m	m	$m^2 \cdot s^{-1}$

Table 3.1. *List of parameters, with their dimensions, involved in the flow in a cylindrical pipe (proposal no. 1)*

The parameters involve three units. The Vaschy–Buckingham theorem specifies that there exists, for determining the velocity, a functional relation between four dimensionless numbers. Dimensionless numbers are easily identified, starting by taking the ratio of quantities that have the same dimensions: P_1 / P_2, L / D, and e / D. These first three numbers are independent from one another, as each of them brings in at least one quantity that is not present in the others. The fourth dimensionless number necessarily involves the kinematic viscosity, which had not yet been taken into account, e.g. by writing UD / ν. The Vaschy–Buckingham theorem actually enables us to understand that the functional linking of all the seven parameters can be written in the form:

$$\frac{UD}{\nu} = F\left(\frac{P_1}{P_2}, \frac{L}{D}, \frac{e}{D}\right) \qquad [3.1]$$

Other formulations, involving different numbers, could also be used. Further, any other combination of dimensionless numbers can also be expressed using the four numbers we have defined.

1 Except, obviously, for the age of the captain. This silly proposal aims at pointing out that, for using dimensional analysis, we should tend to count only the parameters that are significant for the phenomenon and not all parameters that may eventually have an effect in some circumstances.

Although the Vashy–Buckingham theorem is not based on physics, using dimensional analysis should not rule out considering the physics; for, quite the contrary is true. Regarding the example treated here, it is very clear that expression [3.1] is unsustainable from a physical standpoint, because:

– We know that the flow is generated due to the pressure difference between the inlet and outlet. It would, therefore, be more judicious to obtain a functional of the form:

$$\frac{UD}{\nu} = F\left(\frac{P_1 - P_2}{P_2}, \frac{L}{D}, \frac{e}{D}\right) \qquad [3.2]$$

– Function [3.2] is not pertinent either, in a physical sense, as the solution depends on the pressure level P_2 at the outlet, rather than just the difference in pressure between the inlet and outlet. A review of the dimensions thus indicates that we are short of a parameter that involves mass.

The previous parameter count was intentionally incomplete; this is to convey the fact that reverting repeatedly to a physical analysis of a phenomena enables one to utilize dimensional analysis to express meaningful relations. The additional parameter involving the mass is easily obtained. One simply has to observe again that the phenomenon is governed by Navier–Stokes equations, which involve the density of the fluid (ρ). We therefore incorporate ρ into the parameter count, and withdraw P_2 since only the pressure difference between the inlet and the outlet modifies the velocity. This leads us to arrive at a functional between the parameters in Table 3.2.

Parameter	U	$P_1 - P_2$	ρ	L	D	e	ν
Unit	$m \cdot s^{-1}$	$kg \cdot m^{-1} \cdot s^{-2}$	$kg \cdot m^{-3}$	m	m	m	$m^2 \cdot s^{-1}$

Table 3.2. *List of parameters, with their dimensions, involved in the flow in a cylindrical pipe (proposal no. 2)*

Once again, four dimensionless numbers need to be determined. They are, for example:

$$\frac{\rho U^2}{P_1 - P_2} = F\left(\frac{UD}{\nu}, \frac{L}{D}, \frac{e}{D}\right) \qquad [3.3]$$

This functional is more appealing because it brings back quantities that have a physical meaning, such as kinetic energy, the pressure difference between the inlet and outlet, and the Reynolds number. Without having solved the equations of the problem, the use of simple results from the general principles of physics has

enabled us to bring to the fore some dimensionless numbers, which compare quantities that "interplay together within the principles of physics".

This can be taken even further, by calling upon a result that we have found before with Poiseuille flows: the flow rate is induced not by the pressure difference, but by the pressure difference per unit length of the pipe. This means that it is physically possible to introduce the quantity $(P_1 - P_2)/L$ alone, instead of the three parameters L, P_1, and P_2. Function [3.3] then reduces to a relation between three dimensionless numbers:

$$\frac{\rho U^2 L}{(P_1 - P_2) D} = F\left(\frac{UD}{\nu}, \frac{e}{D}\right) \qquad [3.4]$$

As seen in Chapter 4, the pressure drop laws for steady flows in pipes are expressed using a relation similar to this form, using the following dimensionless numbers:

$$\left.\begin{array}{ll} \text{– The linear pressure drop coefficient} & \lambda = \dfrac{2(P_1 - P_2) D}{\rho U^2 L} \\ \text{– The Reynolds number,} & \mathrm{Re} = \dfrac{UD}{\nu} \\ \text{– The relative roughness} & k = \dfrac{e}{D} \end{array}\right\} \quad [3.5]$$

Dimensional analysis, combined with simple physical considerations, makes it possible to set out numerous dimensional forms through which physical results can be expressed. It helps to number the parameters involved in a problem while removing extraneous ones. A fruitful use of the Vaschy–Buckingham theorem can only ensue from a meaningful parameter count. The lesser the parameters, the more informative the result from dimensional analysis will be.

The notion of independent parameters and independent dimensionless numbers needs to be emphasized. As each dimensionless number contained a quantity not present in the rest, we ensured that the defined dimensionless numbers are independent. By using Washy–Buckingham theorem, we usually want to investigate the dependence of one quantity (presently the flow velocity in the pipe) with other parameters. It is also important checking that these other parameters are independent. For the pipe flow problem, this notion is simple: the length and diameter are clearly independent, since we can choose the pipe length on the one hand and its diameter on the other. Nevertheless, adding the dynamics viscosity μ to the parameters in Table 3.2 would not be sensible, as it is simply linked by $\mu = \rho\nu$ to other parameters already taken into account. The notion of independence also leads to subtler questions. We have not taken temperature into account in the example

we have discussed above, although the principles of physics and experience indicate unequivocally that temperature influences changes in the flow rate for a given pressure drop. This is because temperature's only effect is to alter the viscosity. Insofar as thermal physics is not taken into account in the phenomenon, the equation that governs its dynamics is limited to the Navier–Stokes equation, while the temperature remains an indirect parameter of the problem. Identifying the nature of the physical phenomena governing a system is indispensable to perform a meaningful dimensional analysis of a problem.

Counting the units that appear in a problem can sometimes be complex. If, e.g. the units of length (m) and time (s) systematically appear in velocity-type parameters (m/s), then only one unit (m/s) should be counted, instead of two.[2]

3.1.1. *Example – the oscillating pendulum*

Consider the case of a pendulum, oscillating within the gravity field, whose oscillation frequency we wish to determine. The *a priori* parameters of the problem are the angular frequency, ω (s^{-1}) – the quantity to be determined – the pendulum's mass, M (kg), the length of the wire, l (m), the gravitational acceleration, g ($m \cdot s^{-2}$), and the maximum angle of oscillation, θ_o (dimensionless). Based on five parameters and three dimensions, there should therefore be two dimensionless numbers. The first is obviously[3] θ_o. The mass M, therefore, does not intervene in the physical problem, as no other parameter depends on the unit of mass. Consequent to this, the only option is to write:

$$\frac{\omega^2 l}{g} = F(\theta_o)$$

For small angles, we obtain the well-known pendulum relation:

$$\omega = A\sqrt{\frac{g}{l}}$$

Constant A is undetermined as per dimensional analysis. However, based on dimensional analysis the fact that the oscillation frequency is not dependent on the mass is justified.

---

2 This difficulty is encountered when solving Exercise 3.I at the end of this chapter.

3 Is the notion that simple? An angle is expressed by a unit (radians, degrees, etc.). For a dimensional analysis problem, we consider that an angle is a dimensionless quantity, because the length of a circular arc is the product of the angle by the radius. The angle, therefore, has no dimension as such.

3.2. Dimensional study of Navier–Stokes equations

The examples so far given, and the one we discuss fully in section 3.4 (the fall of a ball in a fluid under the effect of gravity), illustrate the fact that a problem can only be treated through dimensional analysis in a meaningful way if one comprehends the nature of its determining phenomena. In the case of the oscillating pendulum, e.g. it is necessary to realize that the pendulum oscillates because it is located within the gravity field. If this property is not identified, the error that results most often is the omission of the gravitational acceleration from the parameter count.

Dimensional analysis of the equations that govern a system enables the identification of the relevant dimensionless numbers for the problem. It also ensures that all parameters have been taken into account, and that they are independent. We illustrate this principle below with the example of Navier–Stokes equations, written in vector form:

$$\rho \frac{\partial \vec{u}}{\partial t} + \rho (\vec{u} \cdot \nabla) \vec{u} = -\nabla p - \rho g \vec{k} + \mu \Delta \vec{u} \qquad [3.6]$$

A critical interpretation of equation [3.6] helps us to generate a list of parameters involved in Navier–Stokes equations:

– the density, ρ, which we assume here to be homogeneous and constant,

– the gravitational acceleration, g,

– the dynamic viscosity, μ,

– the space dimensions (x, y, z), for which a length scale L is introduced,

– the velocity components (u_x, u_y, and u_z), whose scale is denoted by U,

– the pressure, p, whose scale we denote by P, and

– time t, whose scale is denoted by T.

Of the seven scales defined to represent the dynamics of Navier–Stokes equations, the first three are actual parameters of the problem. Their value is known and fixed, at least in the case where density is homogeneous. On the other hand, the length, velocity, pressure, and time scales are not defined precisely. The length scale can be defined arbitrarily using any existing geometrical dimensions (such as the diameter of the pipe), but this physical dimension is not necessarily a typical scale of the fluid flow. In complex cases (e.g. turbulence or boundary layer), several scales may exist in the flow. We shall assume in the present case that the length scale is the same along all the three directions in space. This is not necessarily correct (there may be the length and width of a pipe). The same considerations apply to the velocity dimensions.

The seven scales involve three units (time, length, and mass). Four dimensionless numbers should, therefore, be defined to represent the flow. These numbers are determined naturally by evaluating the order of magnitude of the various terms in Navier–Stokes equation. By writing:

$$\left.\begin{array}{c} \vec{u} = U\vec{u}' \\ (x,y,z) = L(x',y',z') \\ p = Pp' \\ t = Tt' \end{array}\right\}, \qquad [3.7]$$

we bring in the velocity, $\vec{u}'$, length scales (x',y', and z'), pressure p', and time t', which are dimensionless variables. Substituting [3.7] into [3.6] leads to:

$$\left(\rho\frac{U}{T}\right)\frac{\partial\vec{u}'}{\partial t'} + \left(\rho\frac{U^2}{L}\right)(\vec{u}'\cdot\nabla)\vec{u}' = -\left(\frac{P}{L}\right)\nabla p' - (\rho g)\vec{k} + \left(\mu\frac{U}{L^2}\right)\Delta\vec{u}' \qquad [3.8]$$

Dividing this equation by $\rho U^2 / L$ yields:

$$\left(\frac{L}{TU}\right)\frac{\partial\vec{u}'}{\partial t'} + (\vec{u}'\cdot\nabla)\vec{u}' = -\left(\frac{P}{\rho U^2}\right)\nabla p' - \left(\frac{gL}{U^2}\right)\vec{k} + \left(\frac{\mu}{\rho UL}\right)\Delta\vec{u}' \qquad [3.9]$$

Equation [3.9] naturally brings the four numbers we require, namely:

– the reduced frequency, $\gamma = \frac{L}{TU}$, which evaluates the significance of unsteadiness,

– the Euler number, $\mathrm{E} = \frac{P}{\rho U^2}$, which gives the ratio of pressure to kinetic energy,

– the Froude number, $\mathrm{Fr} = \frac{U^2}{gL}$, which evaluates kinetic energy in relation to variations in potential energy,

– the Reynolds number, $\mathrm{Re} = \frac{\rho UL}{\mu}$, which evaluates the effect of viscosity in the dynamics of the flow.

These four dimensionless numbers have a physical significance, because they compare the orders of magnitude of the different forces that govern the dynamics of the flow.

Navier–Stokes equations can, therefore, be regarded as a functional relationship between these four dimensionless numbers. The solution of Navier–Stokes equations depends on the values of the different dimensionless numbers. Unsteady effects are negligible if $\gamma << 1$. The gravitational force is negligible if $\mathrm{Fr} >> 1$. Lastly, dynamic equilibriums are independent from viscosity if $\mathrm{Re} >> 1$. This formulation means that the flow's length, velocity, pressure, and time scales are linked by a relation. For example, in the case where, simultaneously, $\gamma << 1$, $\mathrm{Fr} >> 1$ and $\mathrm{Re} >> 1$, the predominant terms in [3.9] are such that:

$$(\vec{u}'\cdot\nabla)\vec{u}' \quad \approx \quad -E\nabla p' \qquad [3.10]$$

The Euler number is of order 1 (if that is not the case, then the scales were improperly chosen). The flow is characterized by the exchanges between pressure energy and kinetic energy. This is the case of a flow governed by Bernoulli's theorem, for an ideal fluid, and in the absence of gravity.

The approach presented here is the most commonly used when two terms dominate the Navier–Stokes equation. The flow can then be characterized by the value of a single dimensionless number. This is illustrated in section 3.4 with the classical example of the fall of a ball in a viscous fluid (Stokes' experiment).

The Euler, Froude, and Reynolds numbers are well known. The reduced frequency is less; so, the time scale is often given on the basis of velocity and length scales by writing $T = L/U$ so that $\gamma = 1$. This relation is used for a turbulent flow. Time appears as an independent parameter in the case of oscillating flows such as, e.g. the flow generated by the oscillation of a wall at a given frequency.[4]

3.3. Similarity theory

Similarity theory is used to study a physical phenomenon at a reduced scale compared to the real scale (there are also cases where one wishes to enlarge the scale, although this is rather infrequent). The classical example in fluid mechanics is the use of wind tunnel models to study an aircraft prototype before considering its real-size construction. The same process is followed in chemical engineering when building a pilot experiment.

To represent a given phenomenon at a different scale, it should be ensured that the physics of the phenomenon is preserved through the change of scale. Depending on the case, the equations of continuum mechanics, Navier–Stokes equations, the transport equations for thermal energy, etc. will provide the appropriate framework to identify, through dimensional analysis, the dimensionless numbers characterizing

4 See Exercise 3.II at the end of this chapter.

the problem. If the dimensionless numbers retain the same value when changing from the real scale to the reduced scale, there is a guarantee that the same physical phenomenon is being represented.

As a continuation of the previous section, let us take the example of a flow governed by Navier–Stokes equations. In the steady-state case, the values of the Euler number, the Reynolds number, and the Froude number should be preserved through the change of scale. Denoting by U, L, P, ρ, and μ as the characteristic quantities of the real flow and U_m, L_m, P_m, ρ_m, and μ_m as the characteristic quantities of the "model" flow, the following relations should be verified:

$$\left.\begin{aligned} \frac{U_m}{U} &= \frac{\rho}{\rho_m}\frac{\mu_m}{\mu}\frac{L}{L_m} \\ \frac{U_m}{U} &= \sqrt{\frac{L_m}{L}} \\ \frac{P_m}{P} &= \frac{\rho_m}{\rho}\frac{L_m}{L} \end{aligned}\right\} \qquad [3.11]$$

bringing to the fore the consequences of the change in geometrical scale.

The first two relations (equality of Reynolds and Froude numbers) show that it is not possible to change the geometrical scale without changing the fluid (density and viscosity), if the first two conditions are to be fulfilled. If they are, the third condition will also be fulfilled in the flow, insofar as the full-scale and model-scale pressure boundary conditions are adapted to verify the latter condition.

In practice, it is rarely the case that all similarity conditions are verified. It is often necessary to identify the dimensionless numbers that are the most characteristic of the flow dynamics. The constraints associated with a change of fluid are usually rather stringent (cost, availability of products, toxicity, etc.). Quite often, in marine hydrodynamics, in aerospace, or for impact studies of natural flows, the Reynolds similarity is not enforced between the real scale and the scale model. However, care is taken to ensure that the Reynolds number is sufficiently large on the scale model, in order to be in a turbulent regime on the scale model as well as in real size. Since the effect of viscosity is small in both configurations, the difference in Reynolds number between the scale model and the real-size case is of less consequence for the structure of the flow. Studying a flow in air by simulating it on a scale model in water is an engineer's trick that allows a reduction in the Reynolds number difference between the real scale and the scale model (the kinematic viscosity of air is about 15 times greater than that of water).

3.4. An application example: fall velocity of a spherical particle in a viscous fluid at rest

We observe the fall, under the effect of gravity, of a spherical ball with a diameter D and a density ρ_p in a fluid with density ρ_f and kinematic viscosity ν. We assume that $\rho_p > \rho_f$ so that the particle has a falling movement within the fluid. After an acceleration phase, it is observed that the ball falls at a constant velocity, W_c. We wish to establish the dependence of W_c upon the parameters of the problem.

3.4.1. *Application of the Vaschy–Buckingham theorem*

As the ball is falling because it is located in the gravitational field, the acceleration due to gravity, g, should be added to the catalog of parameters suggested above. It is also clearly understood that the viscosity of the fluid is an important parameter. Friction forces slow down the particle and prevent it from exceeding a certain velocity. The catalog of parameters is listed in Table 3.3. With six parameters and three dimensions, the Vaschy–Buckingham theorem indicates that the fall dynamics of the ball is governed by three dimensionless numbers.

Parameter	W_c	D	ρ_p	ρ_f	g	ν
Unit	$m \cdot s^{-1}$	m	$kg \cdot m^{-3}$	$kg \cdot m^{-3}$	$m \cdot s^{-2}$	$m^2 \cdot s^{-1}$

Table 3.3. *List of parameters, with their dimensions, involved in the settling of a spherical particle in a viscous fluid (proposal no. 1)*

A simplistic, "blind" analysis of the dimensions of different parameters naturally leads us to suggest the following dimensionless numbers:

$$\frac{\rho_p}{\rho_f}, \frac{W_c D}{\nu} \text{ and } \frac{W_c^2}{gD} \qquad [3.12]$$

Such a suggestion is hardly acceptable from the standpoint of physics governing the fall of the ball. We have merely stated that the ball is falling because it is situated in the gravitational field and because $\rho_p > \rho_f$. To take this further, it is useful to consider, in sequence, two aspects of the phenomenon's physics:

1. The dynamics of the ball's fall, regarded as a solid system.
2. The dynamics of the flow past the ball, which slows down its fall.

3.4.2. *Forces exerted on the ball*

Three forces are exerted on the ball:

1. the weight $F_P = \rho_p \frac{\pi D^3}{6} g$ (downwards);

2. the buoyancy force exerted by the fluid $F_A = \rho_f \frac{\pi D^3}{6} g$ (upwards); and

3. the hydrodynamic force exerted by the fluid on the particle $F_R(W_c, D, \rho_f, \nu)$ (upwards). This hydrodynamic force does not depend directly on the density ρ_p of the particle, since it results from the flow of the fluid past the ball. It depends on it indirectly through W_c.

When the ball falls at a constant velocity, the equilibrium between these three forces is verified, in accordance with the fundamental law of dynamics. We can, therefore, write:

$$F_P - F_A - F_R = (\rho_p - \rho_f) g \frac{\pi D^3}{6} - F_R = 0 \qquad [3.13]$$

Not knowing $F_R(W_c, D, \rho_f, \nu)$, equation [3.13] does not seem to take us much further. However, it highlights the fact that the density of the particle, ρ_p, and the gravitational acceleration, g, only intervene in the problem through the quantity $(\rho_p - \rho_f) g$. Table 3.3 is therefore modified accordingly as presented in Table 3.4.

Parameter	W_c	D	$(\rho_p - \rho_f)g$	ρ_f	ν
Unit	$m \cdot s^{-1}$	m	$kg \cdot m^{-2} \cdot s^{-2}$	$kg \cdot m^{-3}$	$m^2 \cdot s^{-1}$

Table 3.4. *List of parameters, with their dimensions, involved in the settling of a spherical particle in a viscous fluid (proposal no. 2)*

The problem is thus described by only two dimensionless numbers. We introduce the following two dimensionless numbers:

1. Archimedes number $\quad \mathrm{Ar} = \frac{(\rho_p - \rho_f) g D^3}{\rho_f \nu^2}$ [3.14]

2. The Reynolds number $\quad \mathrm{Re} = \frac{W_c D}{\nu}$ [3.15]

The use of the Reynolds and Archimedes numbers stands out as the most natural among a number of possibilities. The fall velocity is the unknown of the problem, whose conditions are set by other parameters. Hence, the fall velocity is introduced only in the Reynolds number, while Archimedes number characterizes the properties of the ball and fluid (the conditions of the phenomenon).

Consequently, the fall velocity of the ball is governed by a relation between these two numbers:

$$\mathrm{Re} = \text{function}\{\mathrm{Ar}\} \qquad [3.16]$$

The formulation for determining the fall velocity is explicit, knowing the value of Archimedes number.

3.4.3. *The hydrodynamic force opposing the particle's movement relative to the fluid*

The analysis of the hydrodynamic force opposing the particle's movement relative to the fluid enables us to determine the dimensional form of the fall velocity in two asymptotical cases, when the Reynolds number is small or when it is large. The hydrodynamic force results from two contributions:

1. The viscous friction force $\quad F_v \approx \rho_f \nu \frac{W_c}{D} D^2 \qquad [3.17]$

2. The pressure force exerted on the surface of the ball $\quad F_p \approx PD^2 \qquad [3.18]$

Both these forces are proportional to the area of the ball, which is homogeneous to D^2. The viscous friction force involves the viscous stress for a Newtonian fluid (Table 1.1 of Chapter 1). We obtain [3.17] by estimating that the velocity gradient in the vicinity of the ball is of the order W_c/D, since W_c is the velocity scale and D is the only length scale in the problem. The length scale of movements generated in the fluid by the motion of the ball is necessarily similar to the size of the ball. The pressure field changes with the value of the Reynolds number.

3.4.4. *Fall velocity for a small Reynolds number*

When the Reynolds number is small, the dominant term in [3.9] is the viscous term. The Euler number has the order of the reciprocal of the Reynolds number, ($E \approx 1/\mathrm{Re}$). The dynamics of the flow is governed by equilibrium between

the pressure field and the viscous stress.[5] The pressure scale, then, has the same order of magnitude as the viscous stress:

$$P \approx \rho_f \nu \frac{W_c}{D} \qquad [3.19]$$

and the resistant hydrodynamic force is:

$$F_R = F_v + F_p \approx \rho_f \nu W_c D \qquad [3.20]$$

The equilibrium between the forces exerted on the ball (equation [3.13]) leads to the dimensional form of Stokes law:

$$W_c = A \frac{(\rho_p - \rho_f) g D^2}{\rho_f \nu} \qquad [3.21]$$

An exact calculation of the flow past the ball shows that the value of the constant is $A = 1/18$.

3.4.5. *Fall velocity for a large Reynolds number*

When the Reynolds number is large, the viscous term is negligible in [3.9]. The Euler number is of the order of 1, since we are in the situation described by [3.10]. The pressure scale is:

$$P \approx \rho_f W_c^2 \qquad [3.22]$$

Since the Reynolds number is large, the pressure force (equation [3.18]) outweighs the viscous force (equation [3.17]). The hydrodynamic force is:

$$F_R \approx F_p \approx \rho_f W_c^2 D^2 \,. \qquad [3.23]$$

The equilibrium between the forces exerted on the ball (equation [3.13]) now leads to Newton's law:

$$W_c = B \sqrt{\frac{(\rho_p - \rho_f)}{\rho_f} g D} \qquad [3.24]$$

Only the value of constant B is undetermined.

---

5 This category of flows, called "creeping flows", is abundantly documented, in particular for lubrication problems. Chapter 16 discusses creeping flows around a small particle.

The results of this application exercise are taken up again in section 14.1 of Chapter 14. As can be seen, dimensional analysis is very critical and crucial in the analysis of physical phenomena, at a first level by determining the association of physical parameters that enable results to be expressed, and at a second level, when the exact case arises, by predicting the dimensional form of physical laws for certain asymptotical situations. We have reached this second level in this example.

3.5. Application exercises

Exercise 3.I: Time of residence and chemical reaction in a stirred reactor

We are interested in performing, in a perfectly stirred reactor with volume V, the following chemical reaction:

$$A + B \rightarrow C + D,$$

which is a first-order reaction with respect to each of the constituents. The kinetics of the reaction are, therefore, written as:

$$\frac{d[A]}{dt} = \frac{d[B]}{dt} = -k \ [A] \ [B]$$

by incorporating the kinetic constant, k. Both constituents are fed at time $t = 0$ with concentrations $[A]_o$ and $[B]_o$.

Determine, by dimensional analysis reasoning, the order of magnitude of the residence time in the stirred reactor so that the concentration of product B at the reactor outlet is 1/100 of what it was at the inlet (it is assumed that $[A]_o > [B]_o$).

HINT.– This application of the Vaschy–Buckingham theorem leads us to question the notion of unit.

Exercise 3.II: Boundary layer on an oscillating plate

Consider a fluid bounded by a flat plate at its bottom. The plate oscillates at a vibration frequency ω in a horizontal plane (as indicated in Figure 2.II.1 by the double arrow). The magnitude of the plate's vibrational motion is $2a$. The fluid is a Newtonian fluid having a kinematic viscosity ν and a density ρ. Due to the effect of viscosity, the vibrational motion induces movements in the fluid, which are restricted to a boundary layer having a thickness δ.

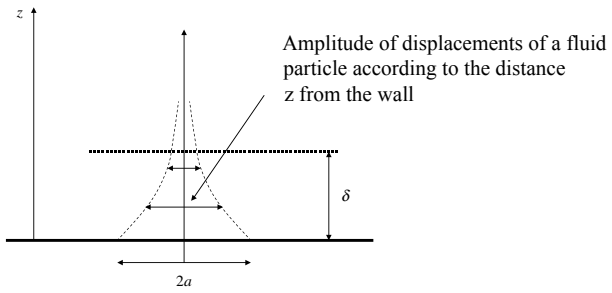

Figure 3.II.1. *Amplitude of displacements of a fluid particle according to the distance z from the wall*

1. Through dimensional analysis reasoning, determine a set of dimensionless numbers with which to express the dependency of δ on the parameters of the problem.

2. When the amplitude of oscillations is sufficiently small, experiments show that the thickness, δ, of the boundary layer does not depend on the amplitude $2a$ of the oscillations. Can you then provide a simple expression of the boundary layer thickness?

Exercise 3.III: Head capacity curve of a centrifugal pump

The head capacity curve of a pump, plotted in Figure 3.III.1, is described by the following function, which links the flow rate delivered Q with the head change ΔH between the inlet and outlet of the pump:

$$\Delta H = \Delta H_{\max,1} - \alpha_1 Q^2 \qquad [3.III.1]$$

with $\Delta H_{\max,1} = 10^5\,\text{Pa}$ and $\alpha_1 = 5.76\times10^9\,\text{Pa}\cdot\text{s}^2/\text{m}^6$. This pump has a rotor diameter $D_1 = 200$ mm and runs at a speed of 180 rpm.

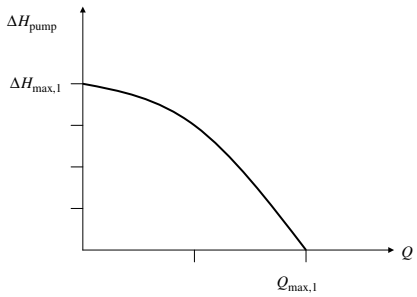

Figure 3.III.1. *Head capacity curve of pump 1*

1. What is the maximum flow rate deliverable by the pump, and what is the maximum height to which the pump can lift the fluid?

2. The company that manufactures this pump offers in its catalog another pump having a diameter D_2 = 150 mm, which runs at a speed of 150 rpm.

The two pumps are related by a scale factor, i.e. all geometrical dimensions are in proportion with the ratio of rotor diameters. For example, the diameters of the discharge ports are such that $d_1 / d_2 = D_1 / D_2$ (index 1 refers to pump 1 and index 2 to pump 2).

The flow conditions are such that the pumps operate in a turbulent regime, with a large Reynolds number. Which parameter can we infer that the head capacity curve is independent from?

As this company has not posted the head capacity curve of that second pump on its website, your boss asks you to determine it.

Demonstrate, by a dimensional analysis argument, that the head capacity curve of the second pump is of the form $\Delta H = \Delta H_{\max,2} - \alpha_2 Q^2$. Determine the values of $\Delta H_{\max,2}$, and α_2, having knowing those of $\Delta H_{\max,1}$, and α_1.

What are the maximum flow rate deliverable by pump 2, and the maximum height to which it can lift the fluid?

This exercise does not require any specific knowledge of the operation of centrifugal pumps, apart from understanding that it is the rotational speed of the rotor that produces the pumping action, and that the flow rate and head change between the inlet and outlet of the pump also depend on the geometrical dimensions of the device.

NOTE.– While many manufacturers express the output head as a water-column height, it is crucial in this exercise to express the head as an energy per unit volume ($H = P + \rho V^2 / 2$), as gravity has nothing to do with the pump's operation.

Chapter 4

Steady-State Hydraulic Circuits

4.1. Operating point of a hydraulic circuit

A hydraulic circuit encompasses all the elements that enable fluid circulation in an industrial system. It is made up of different elements such as:

– Pipes.

– Pumps to generate the flow.

– Blocking members, such as valves.

– Reactors.

The purpose of sizing a hydraulic circuit is usually to select the members of the circuit (pump, pipes, etc.) that enable the desired flow rate to be maintained in the circuit, for a known head change between the inlet and the outlet of the circuit.

In order to size a circuit, the engineer should consider two aspects:

1. *Evaluate the head change in the circuit*. Recall that the head is the fluid's energy per unit volume, and that this energy is the sum of the pressure energy, kinetic energy, and potential energy (Chapter 2, section 2.2):

$$H = p + \rho\frac{V^2}{2} + \rho g z \qquad [4.1]$$

(z is the altitude of the fluid in the direction opposite to that of gravity). Evaluating the head variations provides insight into the energy losses associated with the

various elements in the circuit. Energy losses per unit pipe length (referred to as "regular" or "frictional" head loss) are low in straight pipes, but cannot be neglected when pipe lengths are significant. Locally, large energy losses are also associated with particular items (valves, bends, cross-section expansions, etc.). These head drops, referred to as "singular head losses", need to be evaluated. A pump, on the other hand, adds energy to the flow: the fluid's head increases upon going through a pump.

2. *Evaluating the pressure change along a hydraulic circuit*. Care should be taken to prevent the pressure from dropping below the vapor pressure in a hydraulic circuit, so as to avoid cavitation. Cavitation is a phenomenon whereby a liquid boils due to a pressure drop, causing performance degradation, noise, and mechanical damage. We shall tackle the phenomenon of cavitation at the end of this chapter.

Plotting the "total head line" and the "pressure line" along a hydraulic circuit enables the engineer to identify the most sensitive elements. Quite often, a qualitative representation of the variations in these two lines, prior to a quantitative evaluation, provides a wealth of information.

Let us discuss, for example, a hydraulic circuit (Figure 4.1) that lifts water from a lower basin to an upper basin. The difference in altitude between the free-surface levels in the basins is h. The basins are assumed to have a large size; their level remains constant, and the velocity in each basin can be regarded as nil except in the immediate vicinity of the pipe's openings. The circuit includes ducts of various diameters, a pump, and a valve. Although it does not make much sense from a practical point of view, the diameter of the pipe is smaller between F and G than elsewhere in the circuit. This will enable us to describe the effect of the contraction (between E and F) and of the expansion (between G and H) on the total head and pressure lines.

The pressure and head at both ends of the circuit (at A and L) are easily determined. If the origin of the altitude is chosen at the free surface of the lower basin, both the pressure p and the head $H = p+\rho gz+\rho V^2/2$ equal the atmospheric pressure, P_{atm}, at A (the basin is large and the velocity is zero). At L, the pressure also equals P_{atm}, while the head equals $H = P_{atm}+\rho gh$. The pump generates the only head increase in the circuit (between C and D), allowing the fluid to be lifted from the lower basin to the upper basin.

Regular head losses occur along the pipes. The slopes of the total head line and of the pressure line are identical for the horizontal pipe sections (between B and C, and then between J and K). On the other hand, the pressure decreases more rapidly than the head in the sloping pipes (between D and E, then F and G, then H and I) because of gravity.

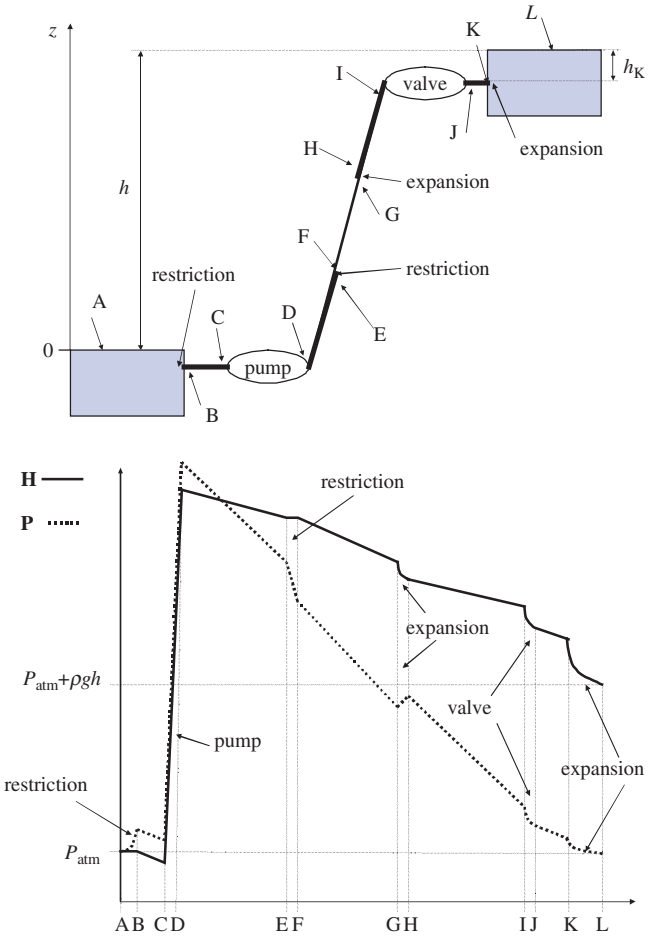

Figure 4.1. *Hydraulic circuit. Head line (solid) and pressure line (dotted)*

Passing through the valve (between I and J) generates a sudden head loss, called a singular head loss. As the cross-sections are identical at the inlet and outlet of the valve, the variation is the same for the head and the pressure.

A sudden expansion in cross-section causes a head loss, as we have seen with Borda's model (Chapter 2, section 2.6). The head decreases, but the pressure increases, between G and H. The expansion that corresponds to the arrival in the upper basin also causes a head loss. The flow is parallel; therefore the pressure is hydrostatic at K. Its value is $P_K = P_{atm}+\rho g h_K$, where h_K is the depth of the discharge end with respect to the free surface in the upper basin. The head loss between K and

L corresponds to the kinetic energy of the flow at the discharge end. All these behaviors are described in Borda's model. Head losses generated by cross-section contractions are typically smaller than those generated by expansions. For this reason, the head variation is taken to be zero between E and F, but the pressure decreases, through the application of Bernoulli's theorem, since the velocity increases. A contraction also occurs between A and B, and consequently it is postulated that the head is conserved. In Figure 4.1, the pressure increases between A and B, as is the case when B is sufficiently deep below A. The pressure increase due to gravity overcomes the pressure decrease associated with the acceleration of fluid in the contraction. The opposite behavior is observed if B is at a small depth below A.

This example shows how easy it is to plot, in a qualitative manner, the pressure and head variations in a hydraulic circuit. The theoretical foundation needed for sizing a hydraulic circuit has already been presented in the previous chapters, namely:

– The concept of head, including respective contributions from the pressure, kinetic energy, and potential energy.

– Bernoulli's theorem, which can be applied along those portions of the circuit where energy is conserved.

– The notion of a singular head loss, already encountered in the case of a sudden expansion (Borda's model). A head loss corresponds to a loss of energy. The differences between cross-sectional expansions and contractions, already considered in section 2.6, are again discussed in section 4.4. We retain here the basic idea that a substantial expansion in the cross-section of a pipe, in the direction of the flow, results in a head loss, whereas energy can be conserved in a cross-sectional contraction.

– Regular head losses in a straight pipe, already introduced for Poiseuille flows (sections 1.3 and 1.4) and discussed in Chapter 3 under the approach of dimensional analysis.

This chapter deals only with established regime (steady-state) flows in a hydraulic circuit. In this framework, we emphasize the difference between flows in convergent and divergent pipes, discuss the effect of turbulence on pipe flows, and tackle the problem of cavitation. Transient flows in hydraulic circuits will be dealt with in Chapter 6, when discussing water hammer phenomena.

In a steady-state regime, fluid flow in a hydraulic circuit is characterized by the flow rate Q. The flow rate is set by the head variations along the circuit. Since the head values (equation [4.1]) are known at the inlet (H_e) and at the outlet (H_s), the head difference between the outlet and inlet is equal to the sum of head differences

along the different portions of the circuit, which can be written as:

$$H_S - H_E = \sum_i \Delta H_{\text{pump},i}(Q) - \sum_j L_j \lambda_j \rho \frac{U_j^2}{2} \frac{1}{D_{H,j}} - \sum_k \zeta_k \rho \frac{U_k^2}{2} \qquad [4.2]$$

In this formulation, it is possible to distinguish pumps (sum over index *i*), which bring energy to the fluid, and head losses, which absorb some of it. One can also distinguish, among head losses, those associated with pipes (sum over index *j*), which absorb energy in proportion to their lengths, L_j, and those with the devices that are responsible for singular head drops (sum over index *k*). Some authors refer to equation [4.2] as the "generalized Bernoulli equation." We avoid this terminology since it can be recalled that the Bernoulli equation is connected to the notion of energy conservation. When energy is conserved, Bernoulli's theorem applies as a fluid particle is followed along a streamline. The same holds for establishing [4.2]. Determining the head variation $H_S - H_E$ between the inlet and the outlet is equivalent to following a fluid particle along the circuit, from the inlet to the outlet. Consequently, head variations across a pump are added, whereas head losses are subtracted.

In [4.2], we anticipate section 4.2 for determining head losses in straight pipes, and on section 4.4 for determining singular head losses. The unknown in equation [4.2] is the flow rate Q through the circuit, since the area-averaged streamwise velocities U_j and U_k are related to the flow rate via the available flow sections ($Q = U_j S_j = U_k S_k$). S_j is the through-flow section in straight pipes and S_k is the through-flow section at a characteristic point in the element causing the singular head loss. The operating point of the circuit is determined by deriving the flow rate from [4.2], which requires characterizing singular head losses by their head loss coefficients, ζ_k, and regular head losses by their regular head loss coefficients, λ_j. It is also necessary to know the head/capacity curves of the pumps installed in the circuit, $\Delta H_{\text{pump},i}(Q)$.

The notion of head is associated with that of power. For a pump, the hydraulic power consumed is:

$$\wp_{\text{hydraulic}} = Q \quad \Delta H_{\text{pump}} \qquad [4.3]$$

Since the head variation is an amount of energy per unit volume in a steady state, it is sufficient to multiply it by the volume flow rate.

For a closed circuit, we have $H_S = H_E$, and equation [4.2] is equivalent to writing that, in a steady state, the head contributed by the pumps cancels out the total head losses in the circuit.

Later in this chapter, we formally set out the tools used for sizing head losses. The elements used for selecting pumps are introduced in Chapter 5. Different types of pumps are presented (centrifugal pumps, axial pumps, positive displacement pumps), and the reasoning that guides the choice of a pump, based on the levels of flow rate and head to be delivered, is discussed.

4.2. Steady-state flows in straight pipes: regular head loss

Consider a straight pipe of length L, in which a fluid of density ρ and kinematic viscosity ν flows. The surface finish of the pipe is characterized by the roughness size, denoted by e (its dimension is a length). In the most generic case, the cross-sectional geometry of the pipe is arbitrary (rectangular, circular, etc.). A size representative of its "diameter" is defined by the hydraulic diameter D_H, which is based on the ratio of the cross-section's area, S, to its perimeter P:

$$D_H = \frac{4S}{P} \qquad [4.4]$$

The notion of a hydraulic diameter originates from the momentum theorem (Chapter 2, section 2.5). The factor 4 in [4.4] equates the hydraulic diameter with the physical diameter for a pipe of circular or square cross-section. For a rectangular pipe whose sides have lengths a and b, we have $D_H = 2ab/(a+b)$.

Dimensional analysis (described in Chapter 3) showed that the flow velocity U in the pipe is related to the regular head loss, $\Delta P/L$, via a functional involving the following three dimensionless numbers:

$$\left.\begin{array}{ll} \text{1. The linear pressure drop coefficient} & \lambda = \dfrac{2\Delta P D_H}{\rho U^2 L} \\ \text{2. The Reynolds number} & \mathrm{Re} = \dfrac{UD_H}{\nu} \\ \text{3. The relative roughness} & k = \dfrac{e}{D_H} \end{array}\right\} \qquad [4.5]$$

The velocity U is the area-averaged streamwise velocity in the pipe. We therefore write:

$$\frac{2\Delta P D_H}{\rho U^2 L} = F\left(\frac{UD_H}{\nu}, \frac{e}{D_H}\right) \qquad [4.6]$$

The form of the linear pressure drop coefficient prompts three remarks:

1. The factor 2 brings into λ the ratio of the change in pressure energy to the kinetic energy of the flow per unit volume.

2. The ratio D_H/L in the regular pressure drop coefficient accounts for the property that the flow velocity depends on the pressure change between the inlet and the outlet in proportion to the length of the pipe. The same flow rate is obtained if the pressure change and the length of the pipe are simultaneously doubled.

3. The linear pressure drop coefficient is related in a simple way to a friction coefficient. The momentum theorem (Chapter 2, section 2.5) established that the average friction stress τ exerted by the flow on the pipe is such that:

$$\tau = \frac{\Delta P}{L}\frac{S}{P} = \frac{\Delta P}{L}\frac{D_H}{4} \qquad [4.7]$$

The friction coefficient is then:

$$C_f = \frac{\tau}{\rho U^2} = \frac{\lambda}{8} \qquad [4.8]$$

This estimates the mean friction exerted by the flow on the wall. The value coincides with the local value at all points on the wall when the cross-section of the pipe is circular, or in the case of a plane flow. On the other hand, friction is inhomogeneous when the profile of the pipe has angles, in which case relation [4.8] estimates the mean friction over the perimeter of the pipe.

Figure 4.2 shows the Colebrook diagram of the variations in the linear pressure drop coefficient λ with the Reynolds number *Re* for various common values of the relative roughness *k*. When the streamwise velocity is known, the Colebrook diagram enables a direct determination of the head loss from the value of λ, since the Reynolds number and the relative roughness are known. It is useful to keep in mind that λ varies between 10^{-2} and 10^{-1} for typical engineering applications. The roughness of a pipe depends on the material from which the pipe is made, and also on its state of preparation. Orders of magnitude are provided in Table 4.1. In a turbulent regime, the analytical expression of the different curves is given by Colebrook's formula:

$$\frac{1}{\sqrt{\lambda}} = -2\log\left\{\frac{k}{3.71} + \frac{2.51}{\mathrm{Re}\sqrt{\lambda}}\right\} \qquad [4.9]$$

In case of a Reynolds number of very high value, the linear pressure drop coefficient becomes independent of the Reynolds number. Its value is determined by the relative roughness, which means that turbulence is driven by unevenness on the wall.

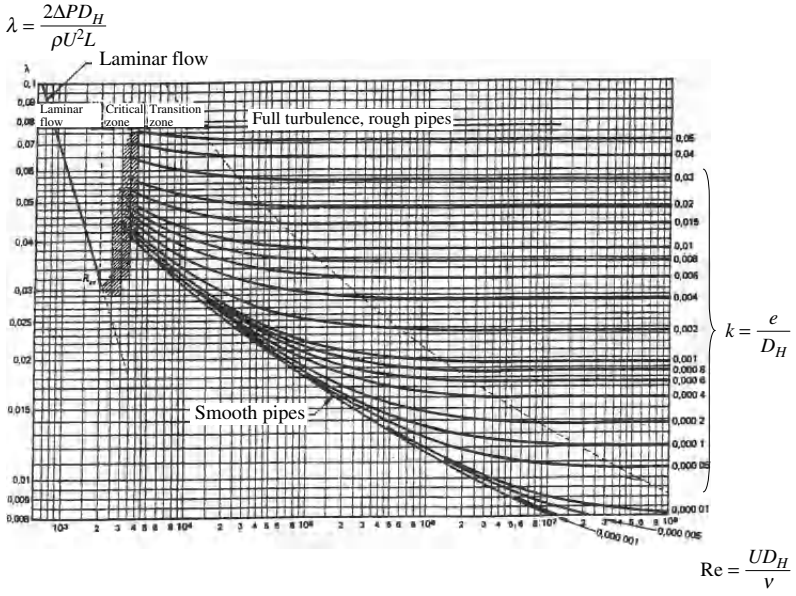

Figure 4.2. *Colebrook diagram. Figure reproduced from a photocopy from lecture notes by A. Bonazzi [BON 94]*

Material	Condition	e (in mm)
Brass, copper, aluminium, plastic materials, glass	Smooth, deposit-free	$e < 0.03$
Steel	New	$0.03 < e < 0.1$
	Slightly rusty	$0.1 < e < 0.2$
	Rusty	$0.2 < e < 0.3$
	Scale-coated	$0.5 < e < 2$
	Bituminized, new	$0.03 < e < 0.05$
	Bituminized, normal	$0.1 < e < 0.2$
	Galvanized	$e = 0.13$
Cast iron	New	$e = 0.25$
	Rusty	$1 < e < 1.5$
	Scale-coated	$e > 1.5$
	Bituminized, new	$0.03 < e < 0.05$
Concrete		$0.3 < e < 3$

Table 4.1. *Absolute roughness for pipes*

Using the Colebrook diagram to determine the area-averaged streamwise velocity based on a known head loss is not straightforward. However, by observing that the quantity $\mathrm{Re}\sqrt{\lambda}$ is independent of the velocity, it is possible to rewrite

Colebrook's formula [4.9] in the form:

$$\frac{1}{\sqrt{\lambda}} = -2\log\left\{\frac{e}{3.71D_H} + 2.51\sqrt{\frac{\rho L v^2}{2\Delta P D^3}}\right\} \qquad [4.10]$$

This alternative formulation enables us to calculate the linear pressure drop coefficient explicitly and to derive therefrom the value of the mean streamwise velocity.

On the Colebrook diagram, different classical flow regimes can be distinguished.

The smooth laminar regime. For $Re < 2000$, we obtain $\lambda = 64/\mathrm{Re}$. This result is accurate for the Poiseuille flow in a circular pipe (Chapter 1, section 1.4), as $D_H = 2R$ and $U = \Delta P R^2 / 8\rho\nu L$.

The smooth turbulent regime corresponds to the lower envelope of the bundle of curves in the Colebrook diagram, for $Re > 5 \times 10^3$. In the range $10^4 < Re < 10^5$, this curve is well described by the Blasius formula, $\lambda = (100\,\mathrm{Re})^{-1/4}$.

The rough turbulent regime corresponds to the conditions under which the linear pressure drop coefficient becomes independent of the Reynolds number (when the latter is sufficiently high). The value of λ then depends only on the roughness coefficient; that is, the zone to the right of the dashed curve on the Colebrook diagram.

The Colebrook diagram evaluates the head loss–flow rate relationship for all flow configurations in a straight pipe. This is made possible by the dimensionless representation of the diagram and by the use of the hydraulic diameter to represent the cross-section of the pipe. It provides a satisfactory estimate in many cases. More accurate and comprehensive evaluations can be found in the book by Idel'cik [IDE 60].

4.3. Turbulence in a pipe and velocity profile of the flow

The flow in a pipe becomes turbulent when its velocity exceeds a threshold defined by a critical value of the Reynolds number. For a circular pipe, the following criterion is agreed upon:

$$\mathrm{Re} = \frac{UD}{\nu} > 2000 \qquad [4.11]$$

The Reynolds number is defined using the area-averaged streamwise velocity and the diameter of the pipe. The onset of turbulence is related to the notion of flow instability. The Poiseuille flow does not remain steady if the Reynolds number

exceeds a value of a few thousand. Small disturbances in the flow, which are unavoidable, get amplified and render the flow unsteady. This principle has been described in the concluding part of Chapter 1.

Although a turbulent flow is by definition unsteady, the average profile of the flow in a pipe is defined by averaging, for example in time, the velocity measured at every point of the pipe. We will return to this approach in more detail in Chapter 8, which presents elementary notions regarding turbulence.

The three essential notions about turbulence that should be kept in mind for now are as follows:

1. *Turbulence mixes a fluid*. It therefore also "mixes velocities," hence a tendency to render the velocity field uniform immediately upon moving away from the walls.

2. *Turbulence reinforces viscous dissipation phenomena*. We have shown in section 2.8 of Chapter 2 (equation [2.45]) that the rate of kinetic energy dissipation per unit mass is, at any point in the flow:

$$\varepsilon = -\frac{\mu}{2\rho}\left\{\frac{\partial u_i}{\partial x_j}+\frac{\partial u_j}{\partial x_i}\right\}^2 \qquad [4.12]$$

This expression involves the square of the velocity gradients. Viscous dissipation is amplified in a turbulent flow because velocity gradients therein are strengthened. A knock-on effect of this result is an increase in the regular head loss.

3. *Wall friction is strongly reinforced in a turbulent flow*. This result ensues from the relationship between the regular head loss and the friction stress (equation [4.8]).

These three properties are manifest in the shape of the velocity profile for the pipe flow. In Figure 4.3, the parabolic profile of the laminar flow (Poiseuille solution) is compared to the typical average velocity profile for a turbulent flow. The turbulent flow is quasi-homogeneous in the central section of the pipe. This is coupled with a thin boundary layer on the walls, where the average velocity gradient is concentrated. For a fluid of viscosity ν flowing in a pipe with a diameter D, friction on the wall is much larger in a turbulent regime than in a laminar regime. The flow remains laminar only if its area-averaged streamwise velocity U_d is such that $U_d \mathrm{D}/\nu < 2000$. Transition from the laminar to the turbulent regime occurs upon increasing the mean streamwise velocity, and consequently the maximum velocity U_m is larger in the turbulent case than in the laminar case. The velocity gradient at the wall is also increased in a turbulent regime due to its being confined to a boundary layer on the wall, as shown in Figure 4.3.

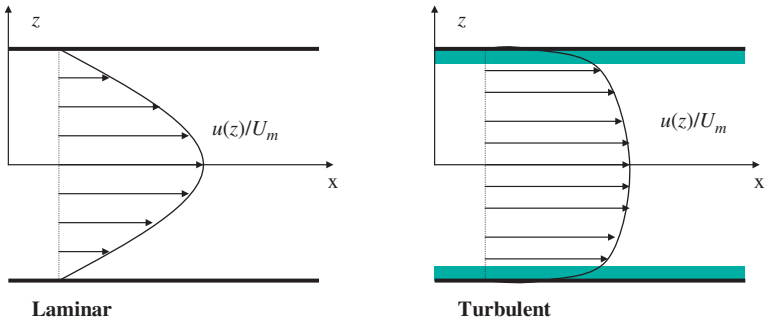

Figure 4.3. *Comparison of the velocity profile in a laminar regime with the average velocity profile in a turbulent regime for the flow in a straight pipe. U_m is the maximum velocity. For the turbulent case, the colored area indicates the boundary layer*

4.4. Singular head losses

Borda's calculation estimates the head loss of a flow in a sudden expansion. In Figure 4.4, we revisit the situations already examined in Chapter 2 (section 2.6), comparing the sudden expansion and sudden restriction cases.

The sudden expansion (Figure 4.4a) generates, in the shaded zone, a head loss whose value depends on the cross-section ratio:

$$H_1 - H_2 = \frac{\rho U_1^2}{2}\left\{1 - \frac{S_1}{S_2}\right\}^2 \qquad [4.13]$$

(Borda's model, equation [2.30] in Chapter 2). The most remarkable property of this relation is that it does not depend on viscosity. The sudden expansion causes a substantial, localized energy loss, which is consequently referred to as a *singular head loss*. A large part of the flow's kinetic energy is dissipated in the process. If this energy loss is compared to the head loss caused by friction in a cylindrical pipe, simple numeric applications (to be done as exercises) show that a substantial length of pipe would be needed to cause an energy loss of a level comparable to that generated by a sudden expansion.

For the sudden restriction (Figure 4.4b), the flow separates on the right-angle edge and first goes through the restricted section S_C, before expanding again to occupy the whole cross-section S_1 of the pipe. The ensuing head loss results due to the expansion between section S_C and section S_1 (shaded area). On the other hand, energy is conserved in the domain (hatched area) where the flow undergoes a restriction in available section.

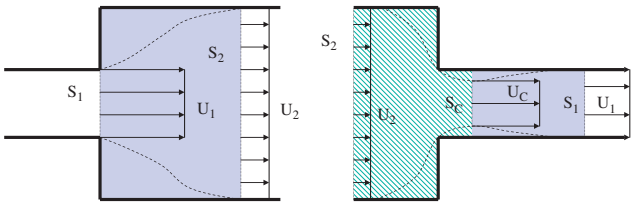

Figure 4.4. *Sudden expansion and restriction. The flow area is within the dashed curves. Head losses occur in the colored areas. Energy is conserved in the hatched area of Figure 4.4b*

Borda's model gives three general principles for the sizing of singular head losses:

– The singular head loss produced in a hydraulic circuit by various elements (valves, bends, obstacles, etc.) is regulated by kinetic energy. Any singular head loss is therefore quantified in the form:

$$\Delta H = \varsigma \frac{\rho U^2}{2}. \qquad [4.14]$$

The dimensionless parameter ς is the singular head drop coefficient. It mainly depends on the geometrical characteristics of the element considered. Its dependence on the viscosity (or the Reynolds number) is often secondary. Coefficient ς is determined for each element. In the *Mémento des pertes de charge* [IDE 60],[1] one can find values of the singular pressure drop coefficient ς for all sorts of elements that differ in their function, geometry, and size. The velocity U chosen to express the singular head loss is specified (usually on a chart) for each element:

– Singular head losses depend on the direction of the flow.

– We can recall, in summary, that singular head losses occur in areas where the cross-section available to the flow is enlarged, while energy is conserved in zones where the cross-section is restricted.[2]

1 Unfortunately, this book in Russian by I.E. Idel'cik has apparently not been translated into English.

2 Using the tables in Idel'cik's book, it can be established by calculation that the head loss is identical ($\zeta = 0.25$), for a given flow rate, through a sudden expansion or a sudden restriction such that $S_1/S_2 = 1/2$. This does not invalidate the above statement, which simply means that dissipation takes place in the shaded areas of Figure 4.4 and that energy is conserved in the hatched area.

Such different behavior of flows is encountered again when considering a pipe whose cross-section contracts or expands continuously in the direction of the flow. Both these configurations are illustrated in Figure 4.5, returning to a situation already discussed in Chapter 1 (section 1.6) where the boundary layer concept was first introduced. The important theoretical result regarding boundary layers is that the pressure in the boundary layer is equal to that prevailing outside the boundary layer. In a convergent pipe, (Figure 4.5a), the application of Bernoulli theorem between A and B shows that the pressure decreases when following a particle in its movement ($P_B = P_D < P_A = P_C$). Hence, the energy of a fluid particle located in the boundary layer decreases when the particle moves from position C to position D, because the particle's velocity is very low near the wall and its pressure energy decreases.

The same analysis when applied to the flow in a divergent pipe presents a difficulty (Figure 4.5b). S_A and S_B denote the flow sections containing points A and B. According to Bernoulli's theorem, the pressure increases for a particle moving from A to B, and the same holds for a particle in the boundary layer moving from C to D. The particle therefore has to increase head by the quantity $\rho U_A^2(1-(S_A/S_B)^2)/2$, through a mechanism of energy transfer from neighboring particles, in order to move from C to D, since its kinetic energy goes to zero at the wall. This is only possible if the widening of the available flow section takes place gradually. When this is not the case, the particle does not attain a sufficient level of energy to move from C to D. It is said that the particle in the boundary layer cannot "travel against the adverse pressure gradient." In that case, a separation of the flow from the pipe walls is observed. This situation is sketched in Figure 4.5c for the cases of a divergent pipe and of the flow past a cylinder. The separation produces recirculation flows and turbulence in the fluid zone between the separation line and the wall, inducing head loss. For a circular conical diffuser, the flow separates when the included angle of the cone exceeds a value of about 7°.

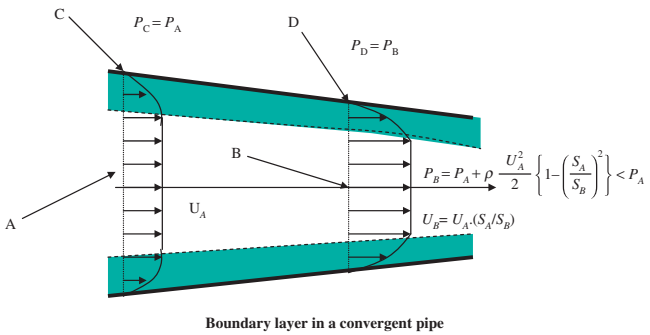

Figure 4.5a. *Flow and boundary layer in a convergent pipe. The boundary layer zone is shaded*

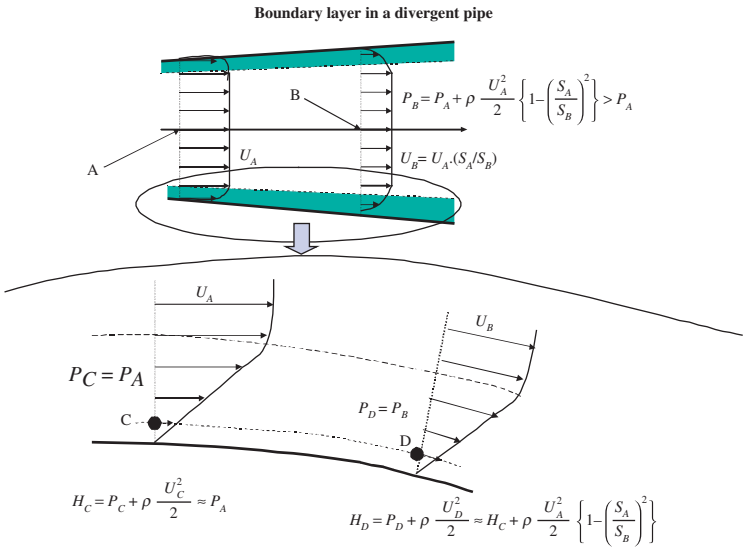

Figure 4.5b. *Flow and boundary layer in a divergent pipe. The boundary layer zone is colored. The energy of a particle in the boundary layer is bound to increase when the particle moves from C to D*

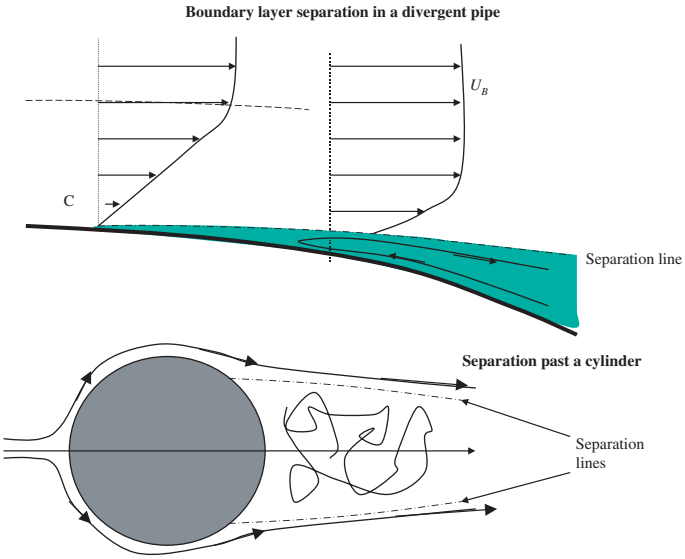

Figure 4.5c. *Boundary layer separation in a divergent pipe and past a cylinder*

4.5. Notions on cavitation

Cavitation is the local phenomenon of phase change that takes place in a liquid when the pressure at a point in the circuit becomes less than the vapor pressure P_v. This phenomenon, when it occurs, has numerous adverse effects, namely:

– Substantial noise. The existence of cavitation is easily detectable through its noise.

– Vibration.

– Performance degradation when cavitation occurs in a hydraulic machine.

– Erosion of the walls when cavitation occurs near them. Damage is caused by high-pressure impacts on solid surfaces. Dramatic deterioration, such as that shown in Figure 4.6, can be observed.

Figure 4.6. *Erosion due to cavitation on a propeller (left) and in a centrifugal pump impeller (right) (source: Wikipedia)*

Preventing cavitation is a permanent concern for engineers. In water at a temperature of 25°C, the vapor pressure is P_v = 32 mb = 3200 Pa. This low-pressure level can be reached very easily. It is necessary for the engineer to identify the potential low-pressure zones in a circuit, as indicated by pressure plots (for example in Figure 4.1). Low-pressure zones are primarily found:

– In the upper parts of a circuit, since the pressure decreases with altitude due to the effect of gravity.

– In those parts of the circuit where the flow section is restricted. This is often the case, for example, in valves. The pressure may drop significantly if the flow section of a pipe decreases from a value of S to S_c. Through mass conservation, the flow velocity U changes to $U_c = U.(S/S_c)$ in the contracted section. Applying Bernoulli's theorem between sections S and S_c leads to pressure decreases from P

to $P_c = P + \rho U^2 (1 - (S / S_c)^2) / 2$ in the contracted section. Numerical applications show that the pressure rapidly drops below P_v (even becoming theoretically negative) if the contraction ratio, S/S_c, is high enough. This triggers cavitation:

– At the center of vortices, which are low-pressure zones (as will be seen in Chapter 17).

– On the suction face of blades (the side of a propeller blade or wing where the pressure is lowest) in a hydraulic machine. Cavitation on propeller blades is a common phenomenon.

Remedies to cavitation stem from the analysis of the causes that produce it. They include:

– Raising the general pressurization level of a circuit when possible.

– Locating cavitation-prone components, such as valves, in the lower parts of circuits, and generally avoiding locating elements in the upper parts of a circuit unless it is necessary.

– Splitting pressure drops so as not to lower the pressure too abruptly, and locating pumps (which raise the pressure level) far enough upstream in the circuit.

4.6 Application exercises

Exercise 4.I: Regular head loss measurement and flow rate in a pipe

Consider a circular cylindrical pipe of diameter $D = 1$ m, descending from a height of $H = 200$ m over a length $L = 1$ km. At the top (point A), the pressure is measured at the lowest point in the cross-section, where it equals $P_A = 1.94$ bar. It is also measured at the bottom (point B), at the highest point in the cross-section, where the measured value is $P_B = 22.45$ bar.

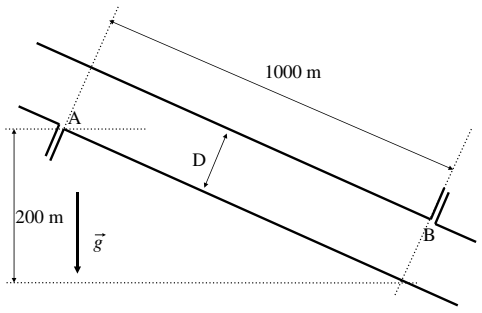

Figure 4.I.1

1. From these measurements, derive the regular head loss in the pipe (the fluid being water). In which direction does the fluid flow?

2. Assuming that the pipe is made of bituminized cast iron, evaluate the area-averaged streamwise velocity in the pipe.

Exercise 4.II: Head loss and cavitation in a hydraulic circuit

The aim is to size a circuit for lifting water between two basins whose levels differ by 20 m. The two basins are 2 km apart. The hydraulic circuit (Figure 4.II.1) that connects the two basins consists of cylindrical pipes made of bituminized cast iron with a square cross-section whose side length is denoted by a, a pump, and a valve. The main constraint is the ability to convey a flow rate of up to 100 l/s.

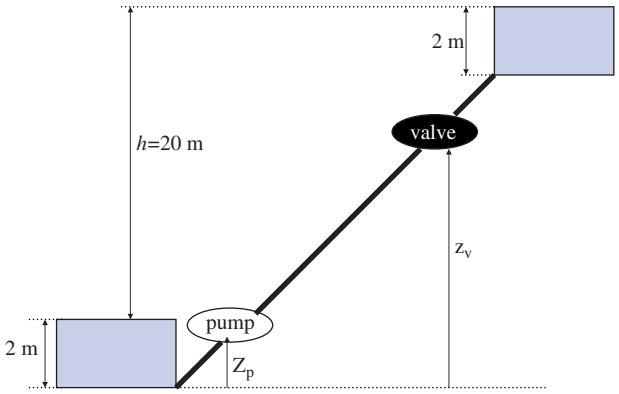

Figure 4.II.1

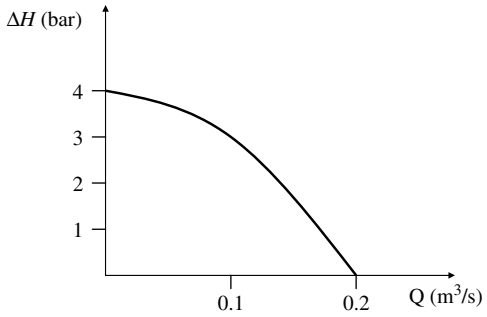

Figure 4.II.2

The pump we consider for use has the head/capacity curve in Figure II.2, which can be modelled by

$$\Delta H_{\text{pump}} = 4 \cdot 10^5 - 10^7 \cdot Q^2$$

where ΔH_{pump} is in Pa and Q in m^3/s. The flow rate is controlled using the valve, which varies the head to be delivered by the pump. It is envisaged to use a butterfly valve, whose pressure drop characteristics are given by Diagram 9.4 in *Mémento des pertes de charge* (Idel'cik), which is reproduced below.

1. Write the head loss versus flow rate relationship for the whole circuit. Head variations other than the regular head loss in the pipe, the singular head loss at the valve, and the head increase produced by the pump will be neglected.

2. In commercially available pipes, the dimension a of the section equals 10 cm, 20 cm, 30 cm, 40 cm, 50 cm, 60 cm, 70 cm, 80 cm, 90 cm, 1 m, etc. State the smallest value of a that allows for a flow rate greater than 100 l/s. For this evaluation, the head loss associated with the valve can be omitted. Why is that? For the different pipe diameters considered, comment upon the obtained variations in the regular head loss coefficient.

3. It is assumed from now on that $a = 0.3$ m. Estimate the angle by which the valve should open for a flow rate $Q = 70$ l/s. A first stage will consist in evaluating the head variation across the pump, the pipe, and the valve, and comparing the values obtained.

4. For the two opening angles $\delta = 70°$ and $\delta = 15°$, determine the flow rate and velocity in the pipe. Calculate the pressure variation between the inlet and the outlet of the valve, and between the inlet and the contracted section. Sketch the pressure changes inside the valve. Is it possible to observe cavitation in the contracted section without cavitation occurring at the valve outlet?

5. In Figure II.1, the pump is located before the valve. Sketch pressure changes in the circuit. Do the same when the valve is located before the pump. Which is the most judicious choice? In which part of the circuit should the pump and valve preferably be located?

NOTE.– The plate from Idel'cik's book is intentionally reproduced on the following page without further comment. The onus is on the user to train himself in decoding conventions by establishing links between tables, formulae, and diagrams.

Butterfly valve | **Chapter IX** | **Diagram 9.4**

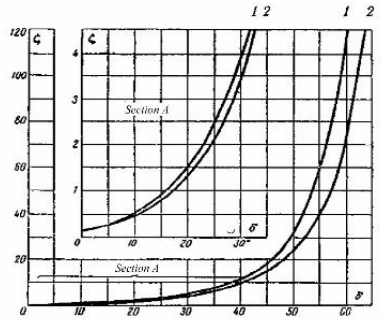

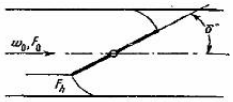

$$\zeta = \frac{\Delta H}{\frac{\gamma w_0^2}{2g}}$$ is determined based on the $\zeta = f(\delta^\circ)$ curve.

δ°	1 Circular pipe ζ	2 Rectangular pipe ζ	F_h/F_0
5	0,24	0,28	0,91
10	0,52	0,45	0,83
15	0,90	0,77	0,74
20	1,54	1,34	0,66
25	2,51	2,16	0,58
30	3,91	3,54	0,50
40	10,8	9,30	0,36
50	32,6	24,9	0,23
60	118	77,4	0,13
65	256	158	0,09
70	751	368	0,06
90	∞	∞	90

Figure 4.II.3

Exercise 4.III: Ventilation of a road tunnel

To ensure the replenishment of air in a road tunnel, fans are to be installed in order to produce an air stream between the two ends of the tunnel. The tunnel is $L = 10$ km long and its section is rectangular, with a width of 6 m and a height of 4 m. The tunnel is lined with concrete. The characteristics of the fluid flow should be chosen so as to renew the air completely in 1 h. The density of air will be taken equal to 1 kg/m^3 and its kinematic viscosity equal to 2×10^{-5} m^2/s.

1. State the values of the mean streamwise velocity and of the flow rate.
2. Calculate the overall head variation required from the fans.
3. What is the power of the fan?

Exercise 4.IV: Sizing a network of heating pipes

The object is to heat different shops in an industrial facility using a pulsed hot air system. The air is heated in a central furnace, and then conveyed to the shops via a trunk pipe crossing the factory, from which pipes (called secondary pipes) branch out to supply every shop. The dimensioning studied here should allow the provision of an identical flow rate to each shop, whether it is located at the beginning of the line or at the far end of the pipe. It is assumed that the pipes connecting the trunk line to the different shops are identical, and U denotes the area-averaged streamwise velocity, which is the same in all such pipes (whereas it varies in the trunk line). For simplicity, we denote by ΔP_n the regular head loss in the trunk line between the branching-off point leading to shop n–1 and the one leading to shop n (see Figure 4.IV.1). While regular head losses in the secondary pipes will be neglected (assuming their length is short), singular head losses in the secondary pipes will be taken into account and denoted by ΔH_n.

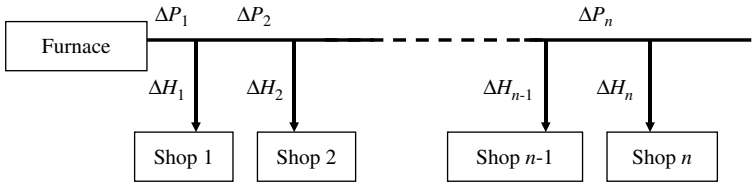

Figure 4.IV.1

1. Write out the head variation between the furnace outlet and the inlet of shop n. Justify that the singular pressure drop coefficient, $\zeta_{n,}$, defined by $\Delta H_n = \rho \zeta_n U^2 / 2$, should decrease as the secondary pipe considered gets further away from the furnace.

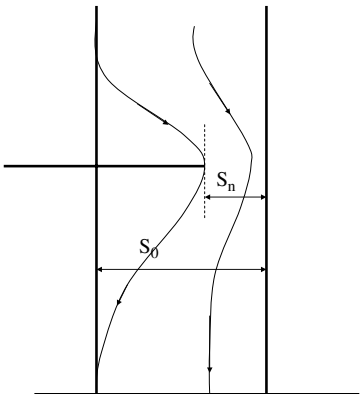

Figure 4.IV.2

2. Controlling the flow rate in each secondary pipe is achieved by adjusting a plate which partially blocks the cross-section of the secondary pipe (Figure IV.2). For secondary pipe n, express the singular head loss coefficient, ζ_n, as a function of the blocked cross-section S_n of the pipe and the unblocked cross-section S_o of the pipe.

3. Secondary pipe n–1 is blocked at 80% (that is, $S_{n-1}/S_o = 0.2$) and the regular head loss in the trunk line between the branching-off points for secondary pipes n–1 and n is $\Delta P_n = 5$ Pa. What should the blocking rate of secondary pipe n be? Use this result to explain that we are usually forced to block secondary pipes strongly in order to maintain the same flow rate in all secondary pipes. The fluid is air (density 1 kg/m^3, kinematic viscosity 2×10^{-5} m^2/s). The velocity in the secondary pipe is $U = 1.5$ m/s.

Exercise 4.V: Head, flow rate, and output of a hydroelectric power plant

A pipe draws water from a mountain lake and channels it to the turbine of a hydraulic power plant located 200 m below. The (cast iron) pipe has a length of 500 m and a diameter $D = 0.5$ m. The turbine discharges water into the open air through an aperture of the same diameter.

1. Express the head variation, $\Delta H_{\text{turbine}}$, between the inlet and the outlet of the turbine, taking into account the head losses in this hydraulic circuit.

2. Express the hydraulic power of the turbine as a function of the area-averaged streamwise velocity in the pipe.

3. Determine the streamwise velocity and the flow rate through the pipe under the condition where the hydraulic power of the turbine is at its maximum. It will be assumed that the flow in the pipe is of rough type, an assumption whose validity will be checked *a posteriori*.

Calculate the theoretical maximum hydraulic power of the plant. Provide an order of magnitude of the number of households that could be supplied with electricity by that plant.

In what proportion do the various head losses reduce the hydraulic power of the plant?

4.7. Bibliography

[BON 94] BONAZZI A., *Circuits hydrauliques*, ENSHMG, Institut National Polytechnique de Grenoble, 1994.

[IDE 60] IDEL'CIK I.E., *Mémento des pertes de charge* (translated from Russian), Paris, Editions Eyrolles, 1960.

Chapter 5

Pumps

This chapter is basically meant for pump users, i.e people who need to select a pump for a specific use. This requires an ability to identify the characteristics of the pumping work to be carried out (like what flow rate? what head? etc), to choose a suitable type of pump of the required size and, lastly, some knowledge of the precautions and difficulties involved in operating such devices in order to optimize their usage.

Engineers will not find in this chapter the tools required to design a pump. Nevertheless, the operating principles of each type of pump are described, as this is necessary to grasp the intricacies of the various issues mentioned above.[1]

With reference to classical applications of hydraulics, chemical engineering, and process engineering, two categories of pumps are presented in this chapter:

1. Turbo pumps, which are devices comprised of a rotor provided with blades. Within this category, centrifugal pumps and axial pumps are discussed. These two types of pumps lie at either end of the operating range of turbo pumps. Axial pumps allow for large flow rates in conditions where the head to be imparted on the fluid is small. Centrifugal pumps allow for smaller flow rates while imparting a larger head on the fluid.

2. Positive displacement pumps and peristaltic pumps, which are more particularly used in situations where it may be necessary to provide a large head increase at low and controlled flow rates.

---

1 Chapters 5 and 6 were written with the invaluable help of the lecture notes by A. Bonazzi, *Hydraulic Circuits*, ENSHMG, Institut National Polytechnique de Grenoble, 1994.

5.1. Centrifugal pumps

5.1.1. *Operating principle*

Figure 5.1 shows the classic layout of a centrifugal pump. The prime mover is the rotor, which spins at an angular velocity ω. The rotor draws the fluid through the suction tube, imparting a substantial rotational speed on the fluid particles that pass through it. On exiting the rotor, the fluid particles have a relative velocity which is tangent to the rotor blades. The plan-view sketch shows blades whose center of curvature is located on the rear of the blade with respect to the direction of rotation. The reverse situation may also occur. The absolute velocity of the fluid particles leaving the rotor is the sum of the relative velocity and the rotational velocity at the periphery of the rotor. The rotor mainly increases the head of the particles by increasing their kinetic energy via the rotational component. The pressure also needs to be increased, as there is a radial pressure gradient which balances the centrifugal force.[2]

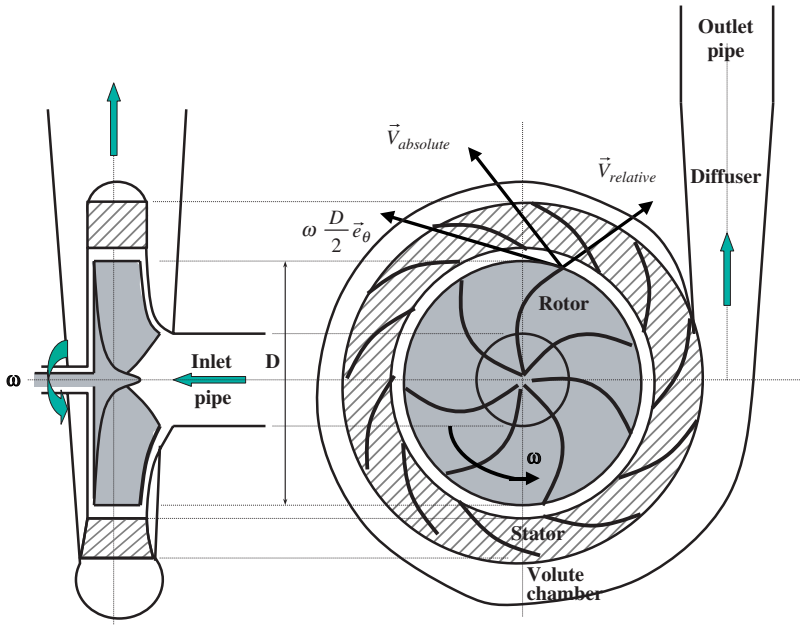

Figure 5.1. *Centrifugal pump. The movable, rotating part is shaded. The stator is hatched*

2 The pressure at the outer periphery of the rotor is higher than on the rotor axis because of the streamline curvature (Chapter 2, section 2.3). These properties are also discussed in Chapter 17, which is dedicated to centrifugal separation.

While the rotor is the key element in a centrifugal pump, the stator (whenever existing – all centrifugal pump are not equipped with a stator), the volute and the diffuser, downstream of the rotor, also have a dedicated function. On leaving the rotor, the head of the fluid particles carries a large proportion of kinetic energy, which needs to be converted into pressure energy while avoiding singular head losses as much as possible. It is known from Bernoulli's theorem that converting kinetic energy into pressure energy requires expanding the available crosssection in order to slow down the fluid while maintaining the flow rate. However, as we have also seen in Chapters 2 and 4, sudden expansions promote singular head losses. The stator, which channels the flow at the rotor's exit point, and the volute, which gradually widens the flow section of the fluid up to the point of pump discharge, are designed so as to reduce head losses as far as possible.

5.1.2. *Similarity laws and head/capacity curves*

The operating characteristics of a centrifugal pump are determined by an application of the momentum theorem, which provides a connection between the force exerted by the rotor blades on the fluid and the pressures and velocities at the inlet and outlet of the rotor. Such design work is not treated herein. We mainly wish to provide elements of understanding for the selection of a pump, with an emphasis on the dimensional forms of the sizing laws for a centrifugal pump.

5.1.2.1. *Head capacity curve of a pump*

Considering two pumps of strictly identical geometry, which only differ from each other by a scale factor, the size of each pump can then be characterized by the diameter of its rotor, respectively D_1 and D_2. In both pumps, the angles shown in engineering drawings are identical, and other lengths are proportional to D_1 and D_2. For example, the inlet and outlet diameters are such that $\Phi_{e,\,1}/\Phi_{e,\,2} = \Phi_{s,\,1}/\Phi_{s,\,2} = D_1/D_2$. The pump's operation is further characterized by angular rotational speeds ω_1 and ω_2, which may be different.

The pump's operating conditions are determined by the relationship between the flow rate, Q, delivered and the head increase, ΔH_{pump}, between the inlet and outlet of the pump. The relationship between these two quantities involves the angular rotational speed and the geometrical characteristics of the pump (lengths and angles, denoted by α). We can, therefore, write:

$$Q = Q(\Delta H_{\text{pump}}, \rho, \omega, D, \Phi_e, \Phi_s, \alpha, ...) \qquad [5.1]$$

Viscosity is ignored, under the assumption that centrifugal pumps typically operate in conditions where the flow is turbulent and, consequently, the Reynolds

number is large. The dimensional analysis of relation [5.1] shows that this relation is necessarily written as[3]:

$$\frac{\Delta H_{\text{pump}}}{\rho\omega^2 D^2} = \text{function}\left\{\frac{Q}{\omega D^3}, \frac{\Phi_e}{D}, \frac{\Phi_s}{D}, \alpha, ...\right\} \qquad [5.2]$$

The quantities implied by the ellipsis are other length ratios or angles characterizing the geometry of the pump.

Relation $\Delta H_{\text{pump}}(Q)$ is referred to as the "head capacity curve" of the pump. For a centrifugal pump, it typically displays the shape sketched in Figure 5.2. For the same pump, two head capacity curves, corresponding to two rotational speeds, have been plotted. In accordance with [5.2], these are similar, with a ratio that is proportional to ω for the abscissa axis (flow rate) and to ω^2 for the head.

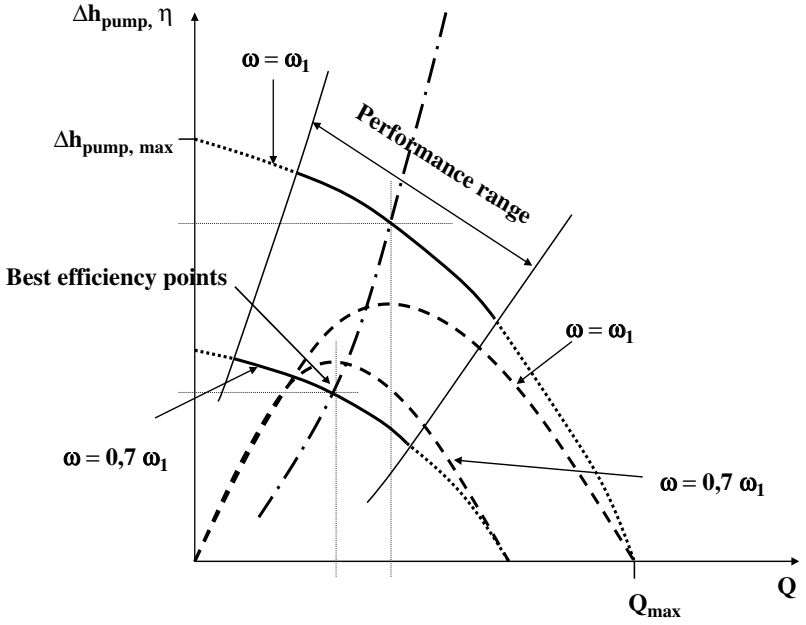

Figure 5.2. *Head capacity curves (____ or .....) and efficiency curves (- - - - -) for a centrifugal pump operating at rotational speeds $\omega = \omega_1$ and $\omega = 0.7\ \omega_1$ system curve (-.-.-.) indicates the best efficiency point of a head capacity curve*

3 It is essential to express the head delivered by the pump in Pascals and not to convert this quantity into a water-column height since the gravitational acceleration does not intervene in the operation of the pump (see Exercise 3.III of Chapter 3).

The characteristic curve is associated with two important values:

1. The maximum head, $\Delta H_{\text{pump,max}}$, is the largest head that can be provided to a fluid. In other words, a pump will be unable to carry fluid to a height greater than $\Delta H_{\text{pump,max}} / \rho g$. The flow rate through the pump reaches zero when the value of the head reaches $\Delta H_{\text{pump,max}}$.

2. The maximum flow rate, $Q_{\max}$, that the pump can deliver if the head change becomes zero.

5.1.2.2. *Efficiency*

The hydraulic power delivered by the pump is:

$$\wp_{\text{hydraul}} = Q\Delta H_{\text{pump}} \qquad [5.3]$$

This quantity reaches zero for both limiting conditions of the head capacity curve, where $\Delta H_{\text{pump}} = \Delta H_{\text{pump,max}}$ or $Q = Q_{\max}$. In reality, the pump consumes an additional power, $\wp_{machine}$, to drive the rotor while balancing mechanical friction in the bearings, and the loss of energy process in the electrical motor. The pump's overall efficiency is defined as:

$$\eta = \frac{Q\Delta H_{\text{pump}}}{\wp_{\text{machine}} + Q\Delta H_{\text{pump}}} \qquad [5.4]$$

For both head capacity curves, the variations of efficiency with the flow rate are plotted in Figure 5.2. Efficiency is zero for both the limiting conditions of operation.

The pump has an optimal operating point, corresponding to the flow rate and head for which efficiency is at its maximum. The operating conditions depicted in Figure 5.1 roughly correspond to the best efficiency point; the absolute velocity of the particles leaving the rotor and entering the stator is approximately parallel to the stator vanes. The flow is channeled into the stator under the best possible conditions to avoid head losses. In contrast, if the flow rate is low or if it is close to its maximum value, the fluid particles almost collide head-on onto the stator vanes. The head losses thus generated cause the fluid particles to lose some of the head they had built up inside the rotor.

It is recommended to operate a pump within flow rate and head intervals around the best efficiency point. Outside that range, efficiency levels deteriorate. Instabilities or difficulties in controlling operation during start-up or shutdown may also be encountered. Manufacturers delineate a "performance range" on head capacity curves, defining the recommended range of operation. This is represented

in Figure 5.2 by plotting the head capacity curves as a solid line within the performance range and as dashed lines outside it.

Dimensional form [5.2] also allows plotting, from a known head capacity curve of a pump (for D_1 and ω_1), the head capacity curve of another pump of similar geometrical design (for D_2 and ω_2). The second head capacity curve is derived from the first by an increase in the ratio $\omega_2 D_2^3 / \omega_1 D_1^3$ along the horizontal axis and of ratio $\omega_2^2 D_2^2 / \omega_1^2 D_1^2$ along the vertical axis.

5.1.2.3. *Forces exerted on the rotor of a centrifugal pump*

The forces applied to the rotor blades of a centrifugal pump are large, because the head increase is correspondingly associated with a rise in pressure. One can evaluate the order of magnitude of those forces by observing that the hydraulic power is related to the torque C exerted on the rotor:

$$\wp_{\text{hydraul}} = Q\Delta H_{\text{pump}} = C\omega \qquad [5.5]$$

We thus derive the torque and average force F exerted on the blades:

$$F \approx \frac{C}{D} \approx \rho\omega^2 D^5 \qquad [5.6]$$

This scaling law explains why large pumps are designed with particular attention being paid to the forces exerted on the structures.

5.1.2.4. *Pump specific speed*

A pump is characterized by its specific speed[4] which is defined by

$$n_s = n\frac{Q_{\text{design}}^{1/2}}{\left(\frac{\Delta H_{\text{design}}}{\rho g}\right)^{3/4}} \qquad [5.7]$$

where Q_{design} and ΔH_{design} are the flow rate and the head at the best efficiency point, respectively, and n is the rotational speed of the pump (usually given as a number of rpm: $n = 30\omega / \pi$). Using dimensional relation [5.2], the design flow rate and design

4 Caution: the specific speed is not a dimensionless quantity. The rotational speed is expressed in rpm and the flow rate in m^3/s. The quantity ρg appears in [5.7] to bring in, following common practice, the design operating head expressed in meters of water column height.

head are expressed as:

$$\begin{aligned} Q_{\text{design}} &= \text{A}\omega D^3 \\ \Delta H_{\text{design}} &= \text{B}\rho\omega^2 D^2 \end{aligned} \qquad [5.8]$$

Both A and B are dimensionless quantities that characterize the geometry of the pump. In accordance with the dimensional laws, it is observed that the specific speed depends neither on the size D of the pump nor on its rotational speed ω. It characterizes the geometrical design of the pump, as it depends only on angles α and scale ratios Φ_e / D, Φ_s / D given in [5.2]. Centrifugal pumps are typically characterized by specific speed values between 30 and 50.

5.1.3. *Implementation of a centrifugal pump*

5.1.3.1. *Priming of a centrifugal pump*

Centrifugal pumps have a well-known drawback, namely their priming for pumping a liquid. It is difficult to start the pump if the pump casing (and, therefore, the rotor) is not filled with liquid. The operating principle described in section 5.1.1 helps us to understand the reason behind this. Since the head acquired by the fluid inside the rotor is proportional to the rotational kinetic energy per unit volume, $\rho\omega^2 D^2$, the pump is unable to modify the upstream pressure field sufficiently to suck in the liquid if the rotor is filled with air, whose density is much lower. Some centrifugal pumps are provided with a device for filling the pump casing with liquid, either by manual pumping or by gravity.

5.1.3.2. *Cavitation in a centrifugal pump*

In a circuit, pressure reaches a minimum level at the inlet of each pump, which mandates preventative action against cavitation. Let us consider the example of Figure 5.3 that shows a pump moving a liquid from a lower basin to an upper basin. The head increase $\rho g h_{\text{tot}}$ between point A, which is located at the surface of the lower basin, and point D, which is located at the surface of the upper basin, is provided by the pump, which also has to compensate for the regular head losses in the pipes and the singular head losses (at the outlet into the upper basin, for example). Denoting by $\Delta H_{\text{c, tot}}$ the total head losses in the circuit, we therefore write:

$$\rho g h_{\text{tot}} = \Delta H_{\text{pump}} - \Delta H_{\text{c,tot}} \qquad [5.9]$$

(The basins are assumed to have large dimensions, and the velocity is zero at their surface.)

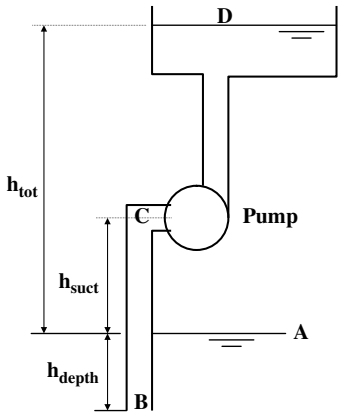

Figure 5.3. *Pumping between two basins whose water-level elevations differs by a height h_{tot}. To forestall cavitation, the elevation h_{suct} of the pump above the lower basin should not exceed the critical height $h_{suct,\ critical}$ given by [5.12]*

The pressure at a point C located in the pump's inlet is calculated by equating the head variation between points A and C to the head loss in the suction pipe, denoted by $\Delta H_{c,\ suct}$:

$$H_A - H_C = P_{atm} - \left\{ P_C + \rho \frac{U_C^2}{2} + \rho g h_{suct} \right\} = \Delta H_{c,suct} \qquad [5.10]$$

U_C is the velocity of the fluid at C and h_{suct} is the height of the pump's inlet relative to the free surface of the lower basin. Cavitation is avoided at the pump inlet if the pressure P_C is greater than the vapor pressure P_V, at any point C in the vicinity of the pump's inlet, which translates into the following condition:

$$\frac{P_{atm}}{\rho g} - h_{suct} - \frac{P_v}{\rho g} - \frac{\Delta H_{c,suct}}{\rho g} > \frac{U_C^2}{2g} \qquad [5.11]$$

Velocity U_c is not the mean streamwise velocity, but the local velocity at point C in the vicinity of the pump's inlet where it is at its maximum, and where the pressure is consequently at its minimum. Cavitation, if it occurs, will start at that point. The variation of quantity net positive suction head $\mathrm{NPSH}(Q) = U_C^2 / 2g$ with the flow rate is determined experimentally by pump manufacturers, by observing cavitation onset thresholds. The value of $\mathrm{NPSH}(Q)$ can be easily estimated by determining the value of the pump's height h_{suct}, relative to the free surface of the lower basin, for which cavitation appears; $\mathrm{NPSH}(Q) = U_C^2 / 2g$ corresponds to equality between both

terms in [5.11]. For the configuration of Figure 5.3, the NPSH value sets the maximum height of the pump, relative to the lower basin, which avoids the appearance of cavitation at the pump inlet, since [5.11] is equivalent to:

$$h_{\text{suct}} < h_{\text{suct,critical}} = \frac{P_{\text{atm}}}{\rho g} - \frac{P_{\text{v}}}{\rho g} - \frac{\Delta H_{\text{c,suct}}}{\rho g} - \text{NPSH}(Q) \qquad [5.12]$$

If this condition is verified, this risk of cavitation in the inlet pipe to the pump is avoided. On the other hand, engineering rules for positioning the suction depth h_{depth} are provided in order to avoid drawing air in, which may happen if a vortex is generated in the lower basin by the suction. Such rules compare the suction depth h_{depth} to the diameter of the pipe, the dimensions of the basin, and the distance from the suction port to the basin walls.

We emphasize the need to take into account the head loss $\Delta H_{\text{c, suct}}(Q)$ in the suction pipe, unless it is negligible, in order to estimate the NPSH. The variations of NPSH(Q) are often superimposed onto the head capacity chart of a pump, as depicted in Figure 5.4. The head delivered by the pump decreases with increasing flow rate, while the NPSH value increases.[5]

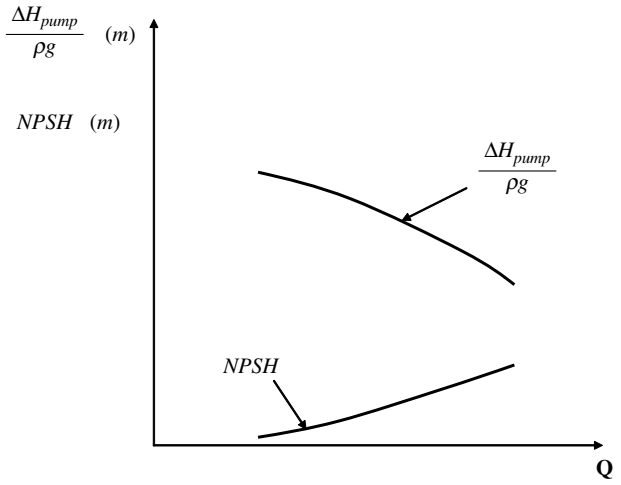

Figure 5.4. *Head capacity curve and variation of the NPSH with the flow rate supplied by a pump*

5 NPSH stands for "net positive suction head." Its unit is meters. In most cases, manufacturers also express the head increase supplied by a pump in meters.

For any configuration other than the one in Figure 5.3, knowing the NPSH(Q) curve makes it possible to assess the risk of cavitation at the pump's inlet. For that, one needs to know the pressure P_A and velocity U_A at one point in the circuit, the head change ΔH_{AE} between point A and the pump inlet E, and the elevation difference $(z_A - z_E)$ between points A and E. The head change between points A and E can be written in a similar manner to [5.10]:

$$\Delta H_{AE} = P_A + \rho \frac{U_A^2}{2} + \rho g(z_A - z_E) - P_E - \rho g \text{NPSH}(Q) \quad [5.13]$$

Cavitation is avoided if the pressure P_E is greater than the vapor pressure P_V at that point E in the pump's inlet where the velocity is at its maximum, i.e. if the following inequality is verified:

$$P_A + \rho \frac{U_A^2}{2} + \rho g(z_A - z_E) - P_V - \Delta H_{AE} > \rho g \text{NPSH}(Q) \quad [5.14]$$

5.1.3.3. *Implementing pumps in parallel or in series*

It is common practice, because a pump supplying both the required flow rate and head is not always commercially available, to use several pumps in a network, installing them in series or in parallel.

Two pumps are in series if the discharge port of one of them is connected to the suction port of the following one. Their flow rates are identical, and the heads produced are added together.

Two pumps are in parallel if their suction ports are directly connected together and their discharge pipes lead into a common manifold. The generated head is the same for both pumps, and the total flow rate is the sum of the flow rates through both pumps.

For parallel- or series-connected associations, it is recommended to employ pumps whose performance domains are close to one another. It is obvious that two pumps mounted in series should correspond to the same range of flow rate. Likewise, pumps that are mounted in parallel should correspond to compatible ranges of generated head. Significant discrepancies between the operating domains of the pumps (in their flow rate range for pumps installed in series, or in their head ranges for pumps installed in parallel) may give rise to operating conditions under which the efficiency of one pump deteriorates, or even to undesirable situations, such as a backward flow being observed in one of the pumps mounted in parallel.

5.2. Classification of turbo pumps and axial pumps

The principle of an axial pump is depicted in Figure 5.5. As this is also a turbo pump, the flow is generated by a rotating impeller whose inclined blades push the fluid along the axial direction defined by the orientation of the hub. On the upstream side, the nozzle channels the flow, and on the downstream side the straightener serves to avoid retaining a residual swirl in the fluid at the pump's outlet. Both these elements are stationary.

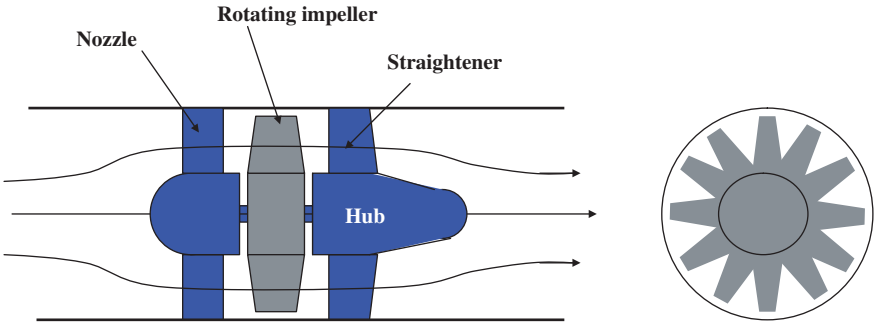

Figure 5.5. *Axial pump. The movable, rotating part is lightly shaded. The nozzle and straightener are more darkly shaded*

Similarity laws for axial pumps are of the same nature as for centrifugal pumps. The principles established in section 5.1.2 also apply to an axial pump. However, the operating ranges corresponding to axial pumps differ markedly. An axial pump supplies a larger flow rate for the same generated head. In other words, generally speaking, a centrifugal pump should be selected if the purpose is to increase the fluid's head, and an axial pump if a given flow rate is required for a limited head increase. This point is reflected in Figure 5.6, which classifies turbo-pumps based on the value of the specific speed n_s as defined by equation [5.7]. Typical values of n_s range from 200 to 300 for axial pumps, whereas they vary between 30 and 50 for centrifugal pumps. Mixed-flow pumps have intermediate values. While we do not treat those in this chapter, the mixed character of their design can be appreciated from the simplistic sketches lined up in Figure 5.6. The extreme case of an axial pump is the marine propeller, which produces no increase in pressure but only kinetic energy and a momentum flux that is used to propel the ship. Another common example of an axial pump is the underground car park fan, whose purpose is clearly to produce a mass flow to replenish ambient air. However, an axial flow pump is not able to compress gas. Gas compressors employ centrifugal pumps for common compression ratios (up to about 10 bars).

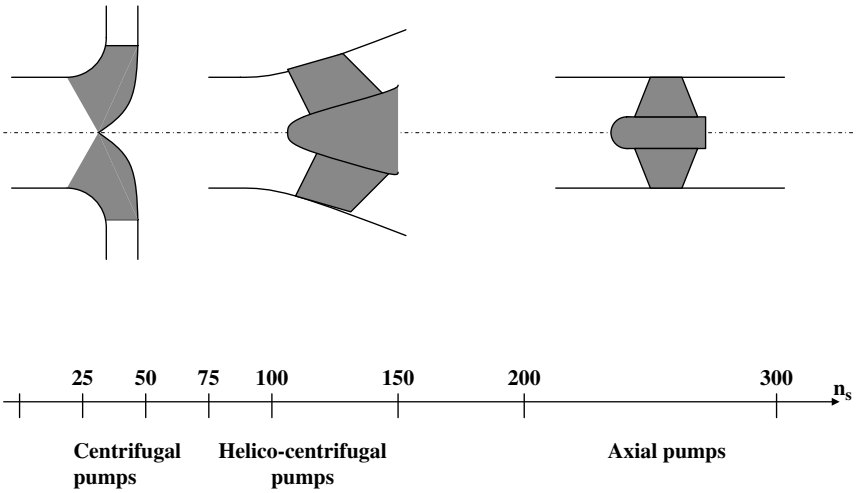

Figure 5.6. *Variation in the specific speed n_s of a turbo pump with geometrical design*

Other dissimilarities between axial and centrifugal pumps result from the differences between the specific speed for an axial pump and a centrifugal pump. The forces exerted on the blades of an axial pump are smaller, and the axial thrust exerted on the rotor of an axial pump is significantly lower than in a centrifugal pump. This results in different mechanical stress levels that have to be taken into account in terms of strength of the material with which the blades are constructed.

5.3. Positive displacement pumps

Positive displacement pumps cover a vast range of devices, which differ greatly in their design layout, in the pumped flow rates, and in the energy (head) supplied to the fluid. This category encompasses piston pumps (axial, rotary, etc.), gear pumps, sliding vane pumps, peristaltic pumps, etc. While turbo pumps are systematically used for pumping at high flow rates, there are also positive displacement pumps capable of pumping rates of the order of about 10 m^3/h. Some positive displacement pumps are also well suited for pumping at low rates (e.g. assay operations), unlike turbo pumps. Moreover, some positive displacement pumps can bring a fluid to a very high pressure (several tens or bars), well beyond the abilities of turbo pumps. Lastly, positive displacement pumps can pump a variety of fluids differing in rheology and nature (fluids that may or may not be loaded with particles), and can keep products out of direct contact with the pumping mechanism (peristaltic pumps for applications in chemistry, biology, or in medicine).

The operating principle of a positive displacement pump is shown in the sketch of a piston pump depicted in Figure 5.7.[6] The prime mover of the pump is a piston driven by a crank arm system which slides inside a cylinder enclosing a cavity. Its operation is associated with two valves. The movement of the piston produces a negative pressure in the cavity during the half-turn through which it is moving upwards. As soon as the difference between pressure P_{suct} inside the cavity and pressure P_{in} inside the inlet pipe reaches an optimal value, the valve isolating the inlet pipe from the cavity opens and the fluid is drawn into the cavity. The valve isolating the cavity from the outlet pipe is closed during the suction stroke. A symmetrical operation takes place during the stage when the piston is moving downwards. The inlet valve is closed, the valve between the cavity and the outlet pipe opens, and the fluid is discharged into the outlet pipe.

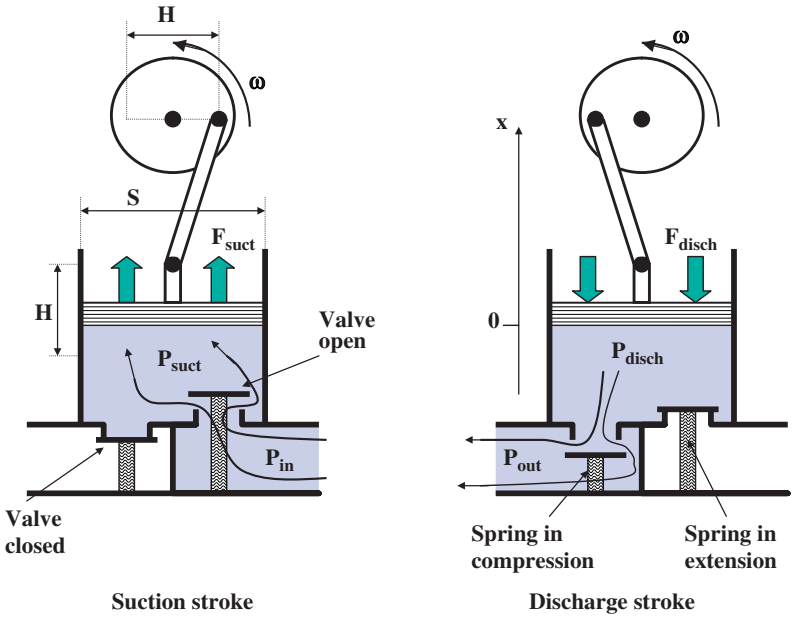

Figure 5.7. *Functional diagram of operation for a positive displacement piston pump*[6]

The pump operates cyclically. The amplitude H of the piston's vertical motion is equal to the diameter of the circle described by the point of attachment of the connection rod onto the rotary element. This determines the swept volume $V = HS$ during each cycle, S being the area of the piston in contact with the fluid. The phrase

6 Figure adapted from R. Joulié, *Mécanique des fluides appliquée*, Edition Ellipses, Paris, 1998, Chapter X.

"volumetric pump" used for such devices is thus clearly understood, since volume is the prime quantity used to characterize a positive displacement pump, based on geometrical values.

The second parameter determining the operation of the positive displacement pump is the rotational speed, ω, of the rotary element. This determines the duration $T = 2\pi/\omega$ of a suction/discharge cycle. The ability of the apparatus to execute that cycle at a specified speed depends on the torque applied to the crank arm assembly, which imparts on the piston a force $F(t)$ that varies during the cycle. When the rotary element turn at constant speed ($X_p(t) = H\cos(\omega t)$), the fundamental law of dynamics applied to the piston (the mass of the piston being denoted by M_p) can be written as:

$$M_p \frac{d^2 X_p(t)}{dt^2} = -M_p H \omega^2 \cos(\omega t) = F(t) + \{P(t) - P_{atm}\} S \qquad [5.15]$$

This relation links the force applied to the piston with the pressure variations $P(t)$ in the cavity during the cycle. The greater the amplitude of the force variations, the greater are the under pressure P_{suct} during the suction stroke and the over pressure P_{disch} during the discharge stroke inside the casing. The values of P_{suct} and P_{disch} should naturally coincide with the pressures allowing for the opening and closing of the valves. For hydrodynamic purposes, they should also allow the specified quantity of fluid to enter the cavity during the suction stroke and exit it during the discharge stroke. This is determined, among other factors, by the head losses associated with the valves. Without going into a detailed modeling of this system's operation, the present description of its principle helps us to understand the link between the force cycle applied to the piston, the period of one cycle, and the amplitude of the pressure variations produced. It is thus understood that, if the mechanical operating parameters of the pump are tailored to a given fluid, the positive displacement pump will be able to supply a large amount of pressure energy to the fluid, as indicated in the beginning of this section.

As already mentioned, there is a wide variety of positive displacement pumps. We have restricted ourselves to a description of their operating principle, emphasizing the "volumetric" character of such devices. One should mainly recall their ability to provide well-calibrated flow rates, including at low flow rates. The use of positive displacement pumps when it is necessary to compress a fluid at very high pressures, beyond what turbo pumps can achieve, should also be remembered.[7]

7 The book by Joulié (ibid.) presents numerous diagrams and photographs, enabling the reader to appreciate the diversity of the devices belonging to the category of positive displacement pumps.

To conclude, Figure 5.8 depicts the operation of a peristaltic pump. The selection of a pump is sometimes constrained by non-mechanical considerations. In a peristaltic pump, the fluid flows in a flexible pipe which is independent from the pump mechanism. The hose is inserted into a circular cavity against whose surface it is forced by cylindrical rollers attached to a rotating hub. These rollers squeeze the hose at regular intervals. The fluid contained in the hose is driven by the rotation of the rotary hub. One benefit of such an apparatus is that the fluid is not in contact with the pumping mechanism. After use, the hose can be replaced if necessary. Peristaltic pumps are very simple to use. The use of small peristaltic pumps is very common in chemistry and biology, whenever product containment is required for safety reasons, or when the products can prove harmful for the mechanical parts (abrasion, corrosion, etc.). Less widely known is the existence of peristaltic pumps of significant size, whose flow rates can reach several tens of m^3/h.

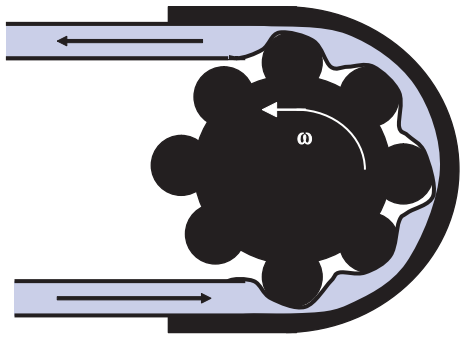

Figure 5.8. *Operating principle of a peristaltic pump*

Chapter 6

Transient Flows in Hydraulic Circuits: Water Hammers

This chapter deals with the most common "water hammer" phenomenon, which refers to vibration and noise occurring when a valve is abruptly closed in a hydraulic circuit. This phenomenon results from a strong disturbance in the pressure field in the vicinity of the valve, which is generated when the circuit is closed. This disturbance then propagates along the circuit in the form of a sound wave, creating discomfort due to the associated noise. It may also have more significant consequences, such as damage to, or failure of, the circuit.

In this chapter, we describe the water hammer phenomenon and the preventative devices. We also obtain the estimates of the over-pressures and of the phenomenon's characteristic times using simple methods.

Basically, this chapter introduces the notion of waves, particularly considering the case of sound waves. Waves have a fundamental role in fluid mechanics, irrespective of whether they are sound waves, surface gravity waves, or internal waves in oceanography and meteorology. Engineers cannot ignore wave propagation processes in fluid mechanics, and the wave water hammer phenomenon is an appropriate case study to introduce in this book on wave propagation in fluids.

6.1. Sound propagation in a rigid pipe

Let us consider the circuit depicted in Figure 6.1, composed of a straight rigid pipe of length L, with one end terminating at a valve, while the other opens into a tank of infinite volume. The initial condition is considered to be the steady draining

flow, in which the fluid flows with a velocity U inside the pipe. It is assumed that the valve is instantaneously closed at a time $t = 0$. The flow velocity immediately becomes zero at $x = L$. At that point in time, the velocity upstream of the valve remains equal to U, as it takes some time for the information about the valve closure to reach the pipe inlet.

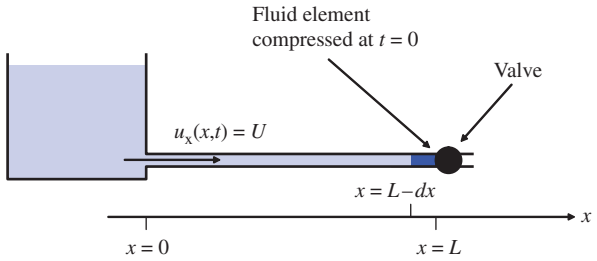

Figure 6.1. *Compression of the fluid brought about by the closure of a valve in a straight pipe*

The diameter of the pipe is small when compared to its length. Hence it is considered that the only non-zero velocity component in the flow is along the *Ox* axis. Other velocity components are assumed to be zero. Denoting by $u_x(t, x) = 0$ this velocity component at a point in the pipe at time t, the initial conditions of the problem are therefore:

$$u_x(t=0, x=L) = 0 \quad \text{and} \quad u_x(t=0, x<L) = U \qquad [6.1]$$

A small fluid element located between L-dx and L is necessarily compressed. It is only slightly squeezed in terms of volume, as the coefficient of isothermal compressibility of water is small,

$$\chi = \frac{\delta\rho}{\rho.\delta p} = 5\times10^{-10}\, Pa^{-1}, \qquad [6.2]$$

but the compression of the fluid volume in the vicinity of the valve produces a sharp pressure increase inside this element. The compressed fluid element then expands, generating a pressure wave that propagates in the upstream direction. Depending upon the boundary condition at the junction between the tank and the pipe, the pressure wave will be reflected back toward the valve, transmitted into the tank, or dissipated. To study the transient phenomenon we require an understanding of the propagation of pressure waves. This is equivalent to understanding sound propagation.

To study sound propagation in a fluid we need to superimpose a disturbance in pressure, velocity, and density onto the characteristics of the flow in its undisturbed state. This is determined when sound propagates in a rigid pipe, whose length is large compared to its diameter, considering the space and time variations of velocity, pressure, and density to depend only on time and on the x space coordinate. The only non-zero velocity component is also along Ox. We therefore consider the following variables:

$$p(x,t) = p_o + \tilde{p}(x,t), \quad \rho(x,t) = \rho_o + \tilde{\rho}(x,t), \quad u_x(x,t) = u_o + \tilde{u}_x(x,t). \qquad [6.3]$$

The quantities $\tilde{p}$, $\tilde{\rho}$, and $\tilde{u}_x$ represent the disturbance associated with the propagation of sound. Here, we consider the fluid at rest (i.e. $u_o = 0$) as the undisturbed state, with pressure p_o and density ρ_o. Although this case differs from the one explained in Figure 6.1, where the fluid is flowing in its undisturbed state, sound propagation is more basically introduced in this simpler case, and the other case of the water hammer phenomenon will then be easily treated. The space and time variations of the three variables are linked by mass conservation (continuity equation), the velocity component along Ox (Euler's equation), and compressibility (Chapter 1, Table 1.1).

We, therefore, write:

$$\begin{aligned}
&\frac{\partial \tilde{\rho}}{\partial t} + \frac{\partial}{\partial x}\{(\rho_o + \tilde{\rho})\tilde{u}_x\} = 0 \\
&(\rho_o + \tilde{\rho})\left\{\frac{\partial \tilde{u}_x}{\partial t} + \tilde{u}_x \frac{\partial \tilde{u}_x}{\partial x}\right\} = -\frac{\partial \tilde{p}}{\partial x} \\
&\chi = \frac{\tilde{\rho}}{(\rho_o + \tilde{\rho})\tilde{p}}
\end{aligned} \qquad [6.4]$$

Linearizing these equations with the three quantities $\tilde{p}$, $\tilde{\rho}$, and $\tilde{u}_x$ gives solutions that are simple, easy to interpret, and verifiable in nature, provided the amplitude of the waves remains small. It leads to simplifying system [6.4] into:

$$\begin{aligned}
&\frac{\partial \tilde{\rho}}{\partial t} + \rho_o \frac{\partial \tilde{u}_x}{\partial x} = 0 \\
&\rho_o \frac{\partial \tilde{u}_x}{\partial t} = -\frac{\partial \tilde{p}}{\partial x} \\
&\chi \rho_o \tilde{p} = \tilde{\rho}
\end{aligned} \qquad [6.5]$$

It can be proved, through substitutions, that the space and time variations of these three quantities are governed by the same partial differential equations, which can be written, for example, for the quantity $\tilde{p}$:

$$\chi\rho_o \frac{\partial^2 \tilde{p}}{\partial t^2} - \frac{\partial^2 \tilde{p}}{\partial x^2} = 0 \qquad [6.6]$$

By performing variable changes $\xi = x - at$ and $\psi = x + at$, with:

$$a = \frac{1}{\sqrt{\chi\rho_o}}, \qquad [6.7]$$

we establish that:

$$\frac{\partial^2 \tilde{p}}{\partial\xi\partial\psi} = 0 \ , \qquad [6.8]$$

so that the general solution is expressed in the form:

$$\tilde{p}(x,t) = F_p(x - at) + G_p(x + at) \qquad [6.9]$$

Functions F_p and G_p are determined on the basis of the initial and boundary conditions of the problem.

The solution is of the undulatory type, in the most fundamental sense of the notion of waves. For function F_p, for example, observing the time signal at point x_1 from time t_1 (by expressing $t = t_1 + t'$), the value of the function can be written as $F_p(x_1 - at) = F_p(x_1 - at_1 - at')$. It is readily verified that the same signal will be observed at point x_2 from time t_2, if $t_2 = t_1 + (x_2 - x_1)/a$. In other words, the phenomenon observed at one point in time, at a certain location, replicates itself in identical fashion at a later time, further along in the direction of propagation of the wave. The time delay is related to the spacing between the two points through the propagation speed a of the wave. The two functions F_p and G_p remain unmodified, respectively, if the observer moves at a velocity a or $-a$ in the Ox direction. F_p describes the propagation of a sound wave in the direction of increasing x, and G_p the propagation of a wave in the opposite direction. Equation [6.7] enables a calculation of the speed of sound in water, which, in the usual ambient conditions on earth ($\rho_o = 10^3\,\mathrm{kg\cdot m^{-3}}$, $\chi = 5\times10^{-10}\,\mathrm{Pa^{-1}}$), equals:

$$a = \frac{1}{\sqrt{\chi\rho_o}} = 1,414\,\mathrm{m\cdot s^{-1}} \qquad [6.10]$$

6.2. Over-pressures associated with a water hammer: characteristic time of a hydraulic circuit

Returning to the water hammer problem in the geometry depicted in Figure 6.1, the variations of quantities $\tilde{p}$, $\tilde{\rho}$, and $\tilde{u}_x$ are described by the same partial differential equation [6.6]. At any point in time, the values of $\tilde{p}$, $\tilde{\rho}$, and $\tilde{u}_x$ are linked through system [6.5]. In the previous section the partial differential equation [6.6] was expressed considering $\tilde{p}$ to underscore the fact that sound is a pressure disturbance which propagates in space. In the case of closure of a valve, depicted in Figure 6.1, the boundary and initial conditions are expressed in terms of velocity. This leads to solving the problem by considering equation [6.6] when derived for variable $\tilde{u}_x$. As is the case for pressure (equation [6.9]), the velocity disturbance is written in the form:

$$\tilde{u}_x(x,t) = F_u(x-at) + G_u(x+at) \qquad [6.11]$$

For the configuration shown in Figure 6.1, the initial conditions are:

$$\tilde{u}_x(x,0) = U \quad \text{and} \quad \frac{\partial \tilde{u}_x}{\partial t}(x,0) = 0 \quad \text{for} \quad x < L \qquad [6.12]$$

This means that, at the initial point in time, all fluid elements located between 0 and L, with the exception of the particle located at $x = L$, are not affected by the closure of the valve, and continue to flow at velocity U, which is the velocity of the previously established regime. Since the valve is closed from time $t = 0$ onwards, the boundary condition at $x = L$ is:

$$\tilde{u}_x(L,t) = 0 \quad \text{for} \quad t > 0 \qquad [6.13]$$

A singularity is observed in the solution at $x = L$ and time $t = 0$. The second boundary condition, at $x = 0$, is written in the form:

$$\frac{\partial \tilde{u}_x}{\partial t}(0,t) = a\frac{\partial \tilde{u}_x}{\partial x}(0,t) \qquad [6.14]$$

This means, as will be discussed below, that closure of the valve causes a disturbance, which escapes into the tank while, conversely, no disturbance enters the pipe from the tank. This is the simplest case that could be considered. The boundary condition at $x = 0$ (equation [6.14]) leads to:

$$F_u'(-at) = 0 \quad \text{for} \quad t > 0 \qquad [6.15]$$

Function F_u is therefore constant, and $\tilde{u}_x(x,t)$ can consequently be written as:

$$\tilde{u}_x(x,t) = G_u(x+at) \qquad [6.16]$$

Boundary condition [6.14] means that the solution consists solely in a wave that travels up the pipe between the valve and the tank.

The initial conditions [6.12] show that $G_u(x+at)$ is necessarily a piecewise-constant function, i.e. it is constant except for certain points where it is discontinuous. That solution is necessarily, with the boundary condition at $x = L$ (equation [6.13]):

$$\begin{aligned} &\tilde{u}_x(x,t) = U \quad \text{for} \quad x+at < L \\ &\tilde{u}_x(x,t) = 0 \quad \text{for} \quad x+at > L \end{aligned} \qquad [6.17]$$

Consequently, the solution simply appears as a velocity discontinuity which propagates from the valve to the reservoir.

The pressure disturbance is determined based on the velocity disturbance by substituting solution $\tilde{u}_x(x,t) = G_u(x+at)$ into the Euler equation:

$$\rho_o \frac{\partial \tilde{u}_x}{\partial t} = -\frac{\partial \tilde{p}}{\partial x} \qquad [6.18]$$

so that

$$\tilde{p}(x,t) = B - \rho_o a \tilde{u}_x(x,t) \qquad [6.19]$$

The constant of integration, B, is determined by considering that the pressure disturbance is zero in those zones where the velocity is that of the draining flow ($x + at < L$). Therefore, the pressure disturbance is given by:

$$\begin{aligned} &\tilde{p}(x,t) = 0 \quad \text{for} \quad x+at < L \\ &\tilde{p}(x,t) = \rho_o a U \quad \text{for} \quad x+at > L \end{aligned} \qquad [6.20]$$

Functions $\tilde{p}$ and $\tilde{u}_x$ are plotted in Figure 6.2 at time $t = 0$ and at a later time t. The undulatory nature of the solution is illustrated, even though in the present case we can see a significant change in the position of discontinuity in the velocity and pressure profiles. The speed of this displacement is the velocity a of the sound wave.

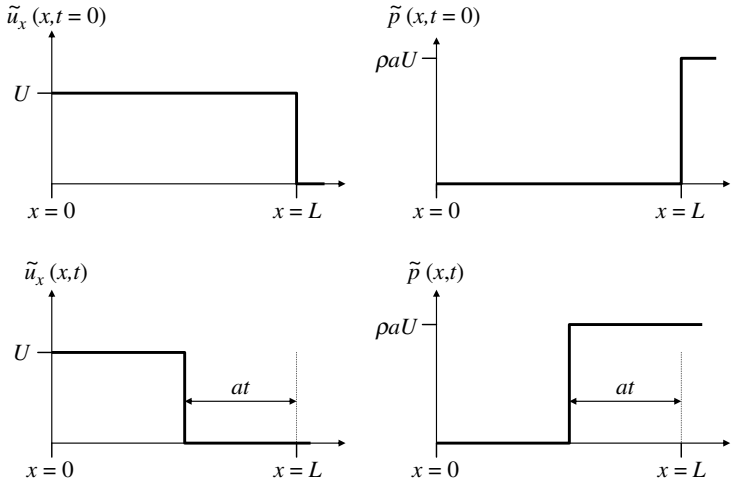

Figure 6.2. *Propagation of velocity and pressure discontinuity during water hammer phenomenon*

The main advantage of this model is that it arrives at an order of magnitude for the over-pressure generated by the instantaneous closure of a valve. Simple numerical calculations show that these over-pressures are very high, because the speed of sound is high. For a draining flow of velocity $U = 1\ \text{m}\cdot\text{s}^{-1}$, the over-pressure obtained is $P = \rho_o aU = 1.4 \times 10^6$ Pa, or 14 bars. This is a very high value, for relatively ordinary conditions. Hence, the water hammer phenomenon can damage pipes if they are not dimensioned to withstand such pressure variations.

The propagation model for pressure waves in a rigid pipe, presented in sections 6.1 and 6.2, is rudimentary. It is observed (Figure 6.2) that a constant over-pressure establishes itself in the pipe, once the disturbance is flushed out of the tank. In reality, there occurs an expansion. Furthermore, the disturbance is generally not entirely flushed out of the pipe into the reservoir. The wave is partially reflected at the mouth and travels back toward the valve in a reciprocating movement between the valve and the opening, resulting in a gradual dampening of the pressure. The entire water hammer phenomenon should, therefore, be seen as a sequence of alternating over- and under-pressure cycles. Over-pressures can bring about a failure of the pipe, whereas under-pressures are likely to generate cavitation.

The characteristic time of such reciprocating movements is:

$$t_c = \frac{2L}{a} \qquad [6.21]$$

This characteristic time is useful for determining the instantaneous or gradual nature of the valve closure. It can usually be considered that the closure of the valve is instantaneous, if the actual closure time t_f of the valve is less than t_c. Otherwise, the over-pressure generated is diminished, as compared to the instantaneous case. Table 6.1 summarizes the results that can be applied in practice.

Closure	Condition	Over-pressure
Instantaneous	$t_f < t_c$	$P = \rho_o a U$
Gradual	$t_f > t_c$	$P = \rho_o a U \frac{t_c}{t_f}$

Table 6.1. *Over-pressures generated during water hammer phenomenon for an instantaneous or gradual valve closure*

6.3. Linear elasticity of a solid body: sound propagation in an elastic pipe

In practice, the theory presented above needs to be complemented by considering the deformation of the pipe in the over-pressure zone. As illustrated in Figure 6.3, the over-pressure causes a swelling of the pipe. Even if it is small (the diagram exaggerates the deformation), this swelling increases the volume occupied by the fluid and reduces the level of the over-pressure. It is thus readily understood that the deformations of the pipe play a part in the problem. The over-pressure P in the pipe is balanced by a tension force $\vec{T}$, which stretches the ribbon in such a way that the perimeter of the pipe changes from πD to $\pi D'$. For a pipe whose material has an elastic behavior, the elongation is related in a simple way to the tensile stress σ associated with force $\vec{T}$ by a linear relationship:

$$\frac{D' - D}{D} = \frac{\sigma}{E} \qquad [6.22]$$

The proportionality coefficient E is referred to as the material's *Young's modulus*. It has the dimension of pressure.

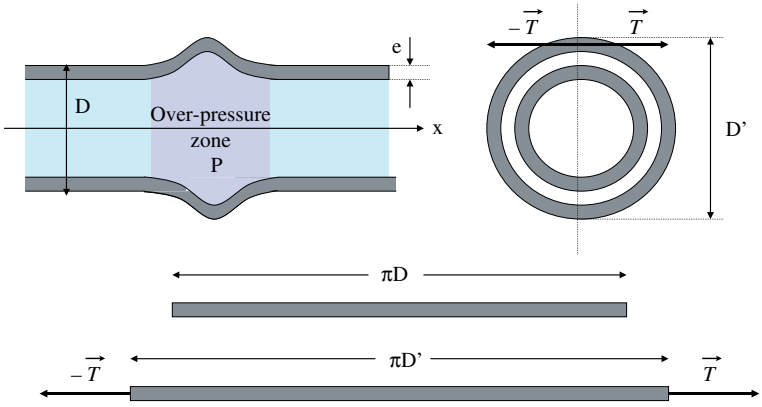

Figure 6.3. *Expansion of a pipe due to the effect of an over-pressure*

The water hammer principle is not altered when the effect of the pipe's elasticity is taken into account. But, the propagation speed of pressure waves is quantitatively diminished by the effect of elasticity. The celerity of the pressure waves is thus given by:

$$a = \frac{1}{\sqrt{\rho_o \left\{ \chi + \frac{D}{Ee} \right\}}}, \qquad [6.23]$$

where D denotes the diameter of the pipe and e its thickness (Figure 6.3). The results summarized in Table 6.2 remain valid if the wave speed given by [6.23] is applied. It is possible, through simple numerical calculations, to specify the conditions in which a pipe's elasticity cannot be neglected (see the exercise at the end of this chapter).

In Table 6.2, we provide the Young's moduli of different classic materials.[1]

1 The theory of elastic bodies also involves Poisson's modulus, which does not appear in this problem.

Material	**Young's modulus** ($N \cdot m^{-2}$)
Steel/iron	2×10^{11}
Cast iron	10^{11}
Aluminum	7×10^{10}
Lead	2×10^{10}
Copper	1.2×10^{11}
Concrete	4×10^{10}
Glass	5×10^{10}
PVC	10^{8}
Stiff rubber	8×10^{6}

Table 6.2. *Young's modulus for various common materials*

6.4. Water hammer prevention devices

Water hammer prevention devices serve two purposes:

1. Safeguarding against strong over-pressures, in order to limit their magnitude, and against under-pressures that might give rise to cavitation.

2. Dissipating disturbances that propagate inside the pipe. Disturbances should be lessened over time, and not be returned with a certain time.

Figure 6.4 presents various devices which provide protection against the water hammer phenomenon. All these operate on the principle of varying the liquid volume to reduce pressure variations. Such simple devices should be placed near the valve, so that they can act as soon as it is closed.

Relief valves and inlet check valves are simple devices that suppress the unsteady effects of an over-pressure or under-pressure, respectively. The relief valve is fitted against an aperture in the pipe by means of a spring whose stiffness is chosen so as to allow the valve to open, should the over-pressure exceed a limiting value. Some liquid is then forced out of the pipe, thus decreasing the pressure in the pipe. The inlet check valve operates in the opposite manner, opening inwards of the pipe when the pressure drops below a limiting value. The mass of the valves and the spring constants should be chosen in such a way that the characteristic frequency of the protective system differs from the characteristic frequency $1/t_c$ of the hydraulic

circuit, in order to prevent a resonance between the water hammer phenomenon and the protective system's response.

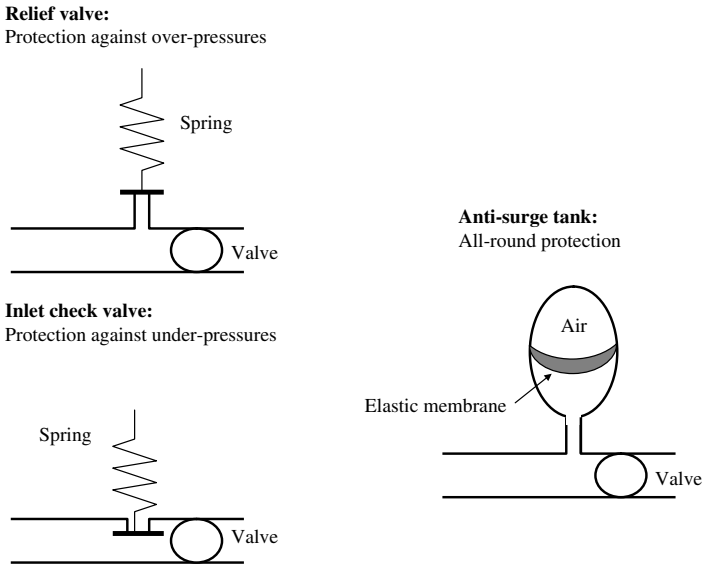

Figure 6.4. *Devices for protecting pipes against water hammers*

The anti-surge vessel consists of a self-contained protective device, which safeguards against both over- and under-pressures. The elastic membrane inside the tank, which isolates the liquid from a volume of air, moves under the effect of pressure changes, converting the pressure variations in the liquid into compressed air. At the same time, the membrane should be elastic to respond to pressure variations, and quickly contribute to the dissipation of pressure fluctuations.

Exercise

A steel pipe, 10 cm in diameter with a wall thickness of 3 mm, supplies to a basin at a flow rate of 30 $m^3\ h^{-1}$. The length of the pipe is 3 km.

1. Do we need to consider the elasticity of the pipe? What is the characteristic time of the pipe?

2. The valve closure time is 5 s. Evaluate pressure variations when the valve is closed. Should the pipe be equipped with a protection system against water hammers?

Chapter 7

Notions of Rheometry

This chapter is not dedicated to rheology as a discipline. We will not present, therefore, the classical rheological models, which describe the mechanical behavior of many materials.

We shall deal here with rheometry, which concerns the techniques for characterizing the rheological properties of materials. The physical principles underlying the design of rheometers are presented. Stating them here is justified for several reasons:

– It is important to be aware, within a fluid mechanics course, that not all fluids are Newtonian.

– The use of a rheometer should be familiar to an engineer, even one who does not specialize in rheology.

– The operating principle of rheometers is independent from the rheological models whose construction they make possible.

7.1. Rheology

Let us return to the local form, in a Cartesian coordinate system, of the fundamental law of mechanics for a continuum, already seen in Chapter 1 (Table 1.1). The equations are reproduced below, omitting body forces:

$$\rho\left\{\frac{\partial u_x}{\partial t}+u_x\frac{\partial u_x}{\partial x}+u_y\frac{\partial u_x}{\partial y}+u_z\frac{\partial u_x}{\partial z}\right\}=\frac{\partial \sigma_{xx}}{\partial x}+\frac{\partial \sigma_{xy}}{\partial y}+\frac{\partial \sigma_{xz}}{\partial z}$$

$$\rho\left\{\frac{\partial u_y}{\partial t}+u_x\frac{\partial u_y}{\partial x}+u_y\frac{\partial u_y}{\partial y}+u_z\frac{\partial u_y}{\partial z}\right\}=\frac{\partial \sigma_{xy}}{\partial x}+\frac{\partial \sigma_{yy}}{\partial y}+\frac{\partial \sigma_{yz}}{\partial z} \qquad [7.1]$$

$$\rho\left\{\frac{\partial u_z}{\partial t}+u_x\frac{\partial u_z}{\partial x}+u_y\frac{\partial u_z}{\partial y}+u_z\frac{\partial u_z}{\partial z}\right\}=\frac{\partial \sigma_{xz}}{\partial x}+\frac{\partial \sigma_{yz}}{\partial y}+\frac{\partial \sigma_{zz}}{\partial z}$$

They bring in the stress tensor $[\Sigma]$, which is a symmetrical 3×3 matrix. The mechanical behavior of a material is determined by the mathematical expression of the six terms in the stress tensor. The purpose of rheology is to establish these relations (called constitutive equations) between the stresses applied inside the material and the strains they cause. As such, rheology appears as a discipline situated "upstream" of mechanics. The equations for the fundamental law of dynamics can only be solved after determining the rheological behavior of the medium.

We recall, from Chapter 1, that the stress tensor $[\Sigma]$ can be used to express the transmission of forces inside the medium. Considering a volume V bounded by a closed surface S (Figure 7.1), the force exerted by the outside of the domain on the inside of the domain through the surface element, ds, centered on M is expressed as:

$$\mathrm{d}\vec{F}=\begin{pmatrix}\mathrm{d}F_x\\ \mathrm{d}F_y\\ \mathrm{d}F_z\end{pmatrix}=\mathrm{d}s[\Sigma]\vec{n}=\mathrm{d}s\begin{pmatrix}\sigma_{xx} & \sigma_{xy} & \sigma_{xz}\\ \sigma_{xy} & \sigma_{yy} & \sigma_{yz}\\ \sigma_{xz} & \sigma_{yz} & \sigma_{zz}\end{pmatrix}\begin{pmatrix}n_x\\ n_y\\ n_z\end{pmatrix} \qquad [7.2]$$

The total force exerted by the outside environment on domain V is derived from the surface integral:

$$\vec{F}=\iint_S([\Sigma]\vec{n})\,\mathrm{d}s \qquad [7.3]$$

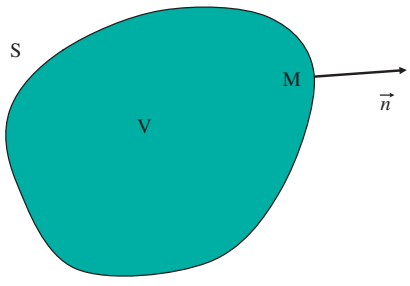

Figure 7.1. *Volume V bounded by a closed surface S.* $\vec{n}$ *is the outward normal to the domain at point M*

The concept of the stress tensor is inseparable from the mechanical principle of action and reaction. The normal vector $\vec{n}$ is oriented toward the outside of the domain on which the force is exerted. The force exerted by the domain V on the outside is in the opposite direction.

So far, we have merely recalled the notions introduced in Chapter 1. It is important to realize that a non-zero stress applied to a material implies the existence of a force capable of deforming it. Determining the stress tensor is only useful for a deformable material. For a rigid body, the stress distribution within the medium is unknown (and undeterminable) to begin with, but that is of no consequence. The movement of the body is described completely by the motion of its center of gravity and the rotation of the body. Describing these two movements only requires the knowledge of the body forces and the total forces applied to the walls of the body.

For a deformable material, let us consider, e.g. a slice of a material held between planes $z = 0$ and $z = h$. Two situations are shown in Figure 7.2: one for a solid and one for a fluid. While we rely here on the definitions that are given hereafter to define a solid and a fluid, common sense enables one to analyze the similarities and dissimilarities between both types of material. In both cases, the forces per unit surface exerted on the material are expressed as a function of the stresses at the upper interface and at the lower interface:

$$\frac{\mathrm{d}\vec{F}}{\mathrm{d}s}(z=h)=\begin{pmatrix}\sigma_{xz}(h)\\ \sigma_{yz}(h)\\ \sigma_{zz}(h)\end{pmatrix} \quad \text{and} \quad \frac{\mathrm{d}\vec{F}}{\mathrm{d}s}(z=0)=\begin{pmatrix}-\sigma_{xz}(0)\\ -\sigma_{yz}(0)\\ -\sigma_{zz}(0)\end{pmatrix} \qquad [7.4]$$

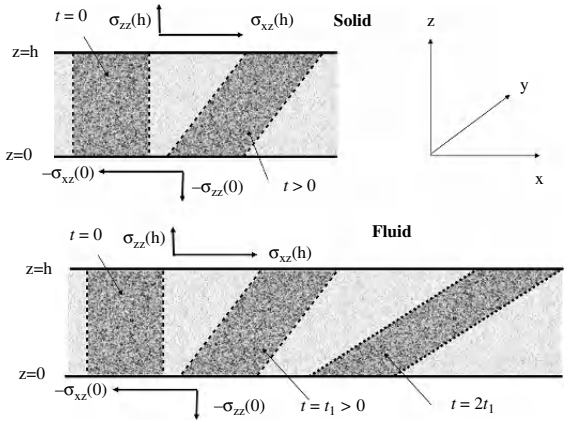

Figure 7.2. *Shear forces applied on a slice of material contained between two parallel planes, and outline of the variation in time of the strain depending on whether the material is a solid or a fluid*

The diagrams in Figure 7.2 assume that the magnitude of the stress is identical at the top and bottom along both the *Ox* and *Oz* directions (i.e. $\sigma_{xz}(h) = \sigma_{xz}(0)$ and $\sigma_{zz}(h) = \sigma_{zz}(0)$). This property is justified later. It serves as a basis to establish that the σ_{zz} stress can deform the material by squeezing it or stretching it, and that the σ_{xz} stress can deform it by shearing it in the *Oxz* plane. An initially rectangular volume element deforms into a slanted parallelepiped when a non-zero stress σ_{xz} is applied. Likewise, a non-zero stress σ_{yz} produces a shearing strain in the *Oyz* plane. For this reason, the σ_{xz}, σ_{xy}, and σ_{yz} stresses are referred to as shear stresses.

Figure 7.2 shows that the strains produced by a shear stress are different depending on whether the material is a solid or a fluid. For a solid, the strain is finite; the rectangle will quasi-instantaneously turn into a slanted parallelepiped, and come to rest in that state of strain. Consequently, to any stress state there is a corresponding strain state. The fluid, on the other hand, will flow. This means that the parallelepiped leans over even more as time goes on. To every stress state there is not a corresponding strain state, but a rate at which the parallelepiped leans over. This is referred to as a strain rate.

The purpose of rheology is to establish a link between stresses and strains, for a solid, and between stresses and strain rates, for a fluid. Rheometry concerns the experimental techniques that enable the characterization of such relationships. The design of a rheometer should first of all enable the application of uniform stresses throughout a material. This will result in a homogeneous strain. As we see hereinafter, a rheometer is sized in such a way that unsteady terms and inertial terms in the fundamental law of dynamics (left-hand terms in [7.1]) are zero or negligible.

7.2. Strain, strain rate, solids and fluids

Let us consider a point in a material, located at time $t = 0$ at *x, y,* and *z*. The motion of that material point is described by its trajectory:

$$X(t,x,y,z) = X_1(t,x_j),\ Y(t,x,y,z) = X_2(t,x_j) \text{ and } Z(t,x,y,z) = X_3(t,x_j). \qquad [7.5]$$

In the following discussion, we use tensor notation $X_i(t,x_j)$. The strains at a given point in a material are characterized on the basis of a comparison between the trajectories followed by three neighboring particles (Figure 7.3). The material is not deformed if the lengths and angles between three arbitrary points are conserved during the movement. Based on continuum mechanics, we introduce the 3 × 3 strain

tensor, which is written in tensor notation as:

$$\varepsilon_{ij} = \frac{1}{2}\left\{\frac{\partial X_i}{\partial x_j} + \frac{\partial X_j}{\partial x_i} + \frac{\partial X_i}{\partial x_k}\frac{\partial X_j}{\partial x_k}\right\} \qquad [7.6]$$

The derivative with respect to index k is summarized in [7.6] for the values $k = 1$, 2 and 3.

Therefore, a material is not deformed at x, y, and z if:

$$\varepsilon_{ij}(x, y, z) = 0 \qquad \forall i, j \qquad [7.7]$$

Likewise, we define the 3 × 3 strain rate tensor:

$$D_{ij} = \frac{1}{2}\left\{\frac{\partial u_i}{\partial x_j} + \frac{\partial u_j}{\partial x_i}\right\} \qquad [7.8]$$

which involves the velocity u_i. For small deformations, the strain tensor and the strain rate tensor are linked by:

$$D_{ij} \approx \frac{\partial \varepsilon_{ij}}{\partial t}. \qquad [7.9]$$

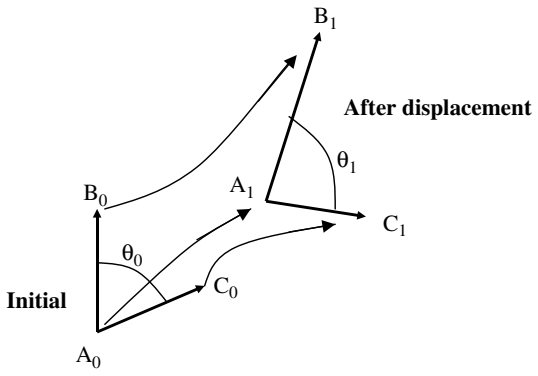

Figure 7.3. *Characterization of the deformation of a material by the displacements of three material points*

The constitutive equations of a material are the relationships between the stress tensor and the strain tensor, or between the stress tensor and the strain rate tensor.

Of course, the nature of the relationship differs according to whether the material is a solid or a fluid.

The assertions by Couarraze and Grossiord[1] for defining a solid or a fluid through their rheological characteristics are particularly clear:

– A substance is a solid if, when subjected to a constant stress that does not cause breakdown, it tends toward a condition of static equilibrium, for which its strain remains constant.

– A substance is a fluid if, when subjected to a constant stress, it never reaches a condition of static equilibrium. Its strain increases indefinitely; and hence the substance flows.

It follows from these definitions that strain tensor [7.7] characterizes the strain of a solid material subjected to stress. For a solid, the constitutive equation is a relation between the stress tensor and the strain tensor:

$$\sigma_{ij} = \text{function}\{\varepsilon_{mn}\} \qquad [7.10]$$

For a fluid, strain cannot characterize the response of the material to stress, since it keeps evolving in time. The constitutive equation is a relation between the stress tensor and the strain rate tensor [7.8]:

$$\sigma_{ij} = \text{function}\{D_{mn}\} \qquad [7.11]$$

These simple definitions conceal a sometimes subtler reality. The same material can be a solid under certain mechanical conditions and a fluid under others. Bingham plastics are materials that are solid as long as the applied stress remains below a critical level (which is called yield stress), and become fluid when the stress exceeds that level.[2] Certain paints, as well as some pasta-type foodstuffs, exhibit this type of behavior. In the natural environment or in purification plants, concentrated sludge also fits into this category. A thixotropic material modifies its rheological behavior over time even though the shear stress applied to it remains constant. A very common example is yogurt. It is solid when opened, and turns to liquid upon stirring, when the shear stress exceeds a finite yield stress. It does not recover its initial state as soon as the stirring ceases, but yeasts may, in time, recreate a solid structure if it is left to stand. Its behavior thus varies in time, depending on the stress cycle applied to it.

---

1 G. Couarraze and J.L. Grossiord, 1991, *Initiation à la rhéologie,* Lavoisier.

2 Exercise I at the end of this chapter deals with the flow of a Bingham fluid in a cylindrical pipe.

7.3. A rheology experiment: behavior of a material subjected to shear

To elucidate the principle of rheometry, we return to the experiment sketched in Figure 7.2. A slice of material is inserted between two parallel planes at $z = 0$ and $z = h$, which are subjected to stresses that are assumed to be homogeneous in the $z = 0$ and $z = h$ planes (no quantity depends on space variables x and y). The experiment is theoretical inasmuch as the planes are infinite. There is no edge effect, which any real experiment would require anyway.

The forces applied to the material per unit surface in the plane $z = h$ and in the plane $z = 0$ are given by [7.4]. We consider a case where stresses are kept constant in time, and we analyze the situation where the material's response is also independent from time. In the case of a solid, it will take a short while for the strain tensor to stabilize. In the case of a fluid, it is the strain rate tensor that will become independent with time after a short period.

Let us first consider the case of a fluid. Assuming that all motion is parallel to the Ox axis, the velocity field takes on the form

$$u_x(z) \quad \text{and} \quad u_y = u_z = 0 \qquad [7.12]$$

and the local equations for a continuum (equations [7.1]) reduce to:

$$\frac{\partial \sigma_{xz}}{\partial z} = 0$$

$$\frac{\partial \sigma_{yz}}{\partial z} = 0 \qquad [7.13]$$

$$\frac{\partial \sigma_{zz}}{\partial z} = 0$$

Stresses are, therefore, homogeneous throughout the layer, as a consequence of the steady-state character and of the kinematic assumptions. From this, it is inferred that the stress field is:

$$\sigma_{xz}(z) = \tau \ , \ \sigma_{yz}(z) = 0 \quad \text{and} \quad \sigma_{zz}(z) = P_0 \qquad [7.14]$$

the constant value, τ, is a reminder that stress σ_{xz} is a shear stress, while the notation P_0 of the other constant value indicates that stress incorporates the pressure force at the wall. It is verified that the forces applied on the top and bottom of the layer have the same magnitude and opposite directions, as had been shown in Figure 7.2.

The strain rate tensor is written, under the kinematic assumptions [7.12] (see Chapter 1, Table 1.1), as

$$[D] = \begin{pmatrix} 0 & 0 & \frac{1}{2}\frac{\partial u_x}{\partial z} \\ 0 & 0 & 0 \\ \frac{1}{2}\frac{\partial u_x}{\partial z} & 0 & 0 \end{pmatrix} \qquad [7.15]$$

its determination is principally based on the calculation of $D = (1/2)\partial u_x / \partial z$. The rheometry experiment enables the establishment of the relation

$$\tau = \tau(D) \qquad [7.16]$$

In practice, the movements of the surfaces that bound the material, rather than the strains or strain rates, are usually measured. If the bottom surface (at $z = 0$) is kept stationary, measuring the velocity $u_x(h)$ of the top surface leads to:

$$D = \frac{u_x(h)}{2h} \qquad [7.17]$$

Since stress is homogeneous within the material, the strain rate is necessarily homogeneous, too, when steady conditions are reached, as a consequence of the constitutive equation (equation [7.16]). The rheological properties of a material subjected to the effect of shear stress are readily determined using the relationship between the shear stress and the displacement of a wall.

The same properties hold for a solid. The rheology experiment consists in measuring the strains produced by the shear stress, τ, which is homogeneous within the material. Strain tensor [7.6] is written as:

$$[\varepsilon] = \begin{pmatrix} \frac{1}{2}\left(\frac{\partial X}{\partial z}\right)^2 & 0 & \frac{1}{2}\frac{\partial X}{\partial z} \\ 0 & 0 & 0 \\ \frac{1}{2}\frac{\partial X}{\partial z} & 0 & 0 \end{pmatrix} \qquad [7.18]$$

when the motion is parallel to the Ox axis (i.e. $X(z)$ and $Y = Z = 0$). It is determined solely from the value of $(1/2)\partial X / \partial z$, which will from now on be denoted by ε. For a solid, the rheometry experiment determines the relation:

$$\tau = \tau(\varepsilon). \qquad [7.19]$$

The fundamental principle of a rheological experiment is to generate uniform stress within the material. Since stress is a function of the strain or strain rate, the strain or strain rate is also necessarily uniform within the material, if the stress is so. The strain or strain rate can be estimated through a measurement of the displacements or velocities on the walls.

A rheometry experiment can be carried out in two ways:

1. In a "controlled stress rheometer", by applying a controlled stress and measuring the strain it induces. The rheological curve is obtained by carrying out such an experiment for various stress values.

2. In a "controlled strain rheometer", by prescribing a controlled strain and measuring the stress it causes. The rheological curve is obtained by carrying out such an experiment for various strain values.

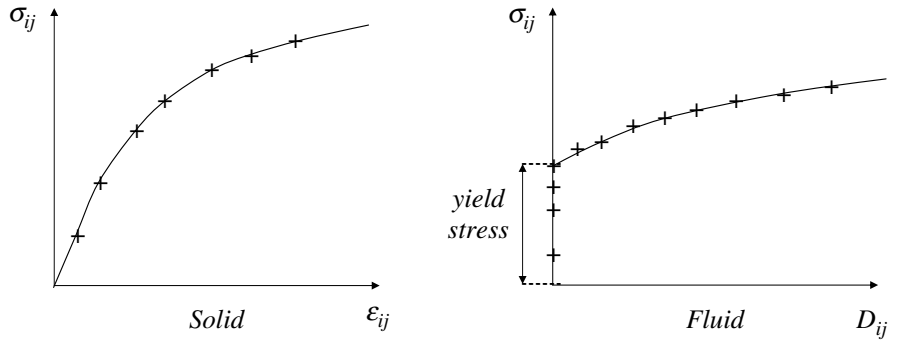

Figure 7.4. *Diagrammatic representation of the rheological curves for a solid and a fluid. The stress is a shear stress ($i \neq j$)*

Figure 7.4 depicts the type of curve obtained for a solid or a fluid; this type of chart is referred to as a "rheological curve". The experimental procedure is identical, although for a solid the stress depends on the strain, whereas in a fluid it varies with the strain rate. The stresses generated in usual rheometers are shear stresses (i.e. $i \neq j$). The stress σ_{ij} usually produces a strain ε_{ij} or a strain rate D_{ij} with the same indices. The theory that we have presented is for steady states. Specialists in rheology also carry out experiments in transient conditions.

– A creep test basically involves application of a constant stress from time $t = 0$, starting from zero stress and strain. The displacement or the rate of displacement of the walls is then measured over time.

– A stress–relaxation test is carried out by imposing a constant strain from time $t = 0$, starting from zero stress and strain. The evolution of stress is then measured over time.

We do not describe herein the possible interpretation of creep or stress–relaxation experiments. The rheometers used are designed to contain the material to be tested inside very narrow gaps, so as to be able to regard the strain (for a creep experiment) or the stress (for a relaxation experiment) as homogeneous during the transient regime under analysis.

7.4. The circular cylindrical rheometer (or Couette rheometer)

Rheometers often have a circular geometry. Their operating principle is identical to what has been described in the previous section. Thanks to the circular geometry, it is possible to partially avoid edge effect problems and to easily produce a quasi-uniform stress within the material. Figure 7.5 shows the layout of a circular cylindrical rheometer.[3] The material is inserted into the gap between the cylinders whose radii are R_1 and R_2. The outer cylinder is held stationary, while the inner cylinder can rotate about its symmetrical axis. The rheometry experiment is carried out by applying a known rotational moment, parallel to the cylinders' axis, which makes the inner cylinder revolve. Measuring the rotation or the rotation rate of the moving cylinder provides an estimate of the strain or strain rate, respectively, for a solid and a fluid.

The height, H, of the apparatus is sufficiently large, and the gap width R_2–R_1 sufficiently small, to be able to neglect edge effects at the top and bottom in the force balance. The displacements and stresses can be regarded as axisymmetric with respect to the Oz axis and independent from z. Therefore, in the cylindrical coordinate system with the Oz axis, the different variables depend not on variables θ and z, but only on r. Consequently, the stress tensor is written in the cylindrical coordinate system (Chapter 1, Table 1.2) as:

$$\begin{pmatrix} \sigma_{rr}(r) & \tau_{r\theta}(r) & \tau_{rz}(r) \\ \tau_{r\theta}(r) & \sigma_{\theta\theta}(r) & \tau_{\theta z}(r) \\ \tau_{rz}(r) & \tau_{\theta z}(r) & \sigma_{zz}(r) \end{pmatrix} \qquad [7.20]$$

3 In a similar fashion, the case of a cone/plate rheometer is treated in Exercise II at the end of this chapter.

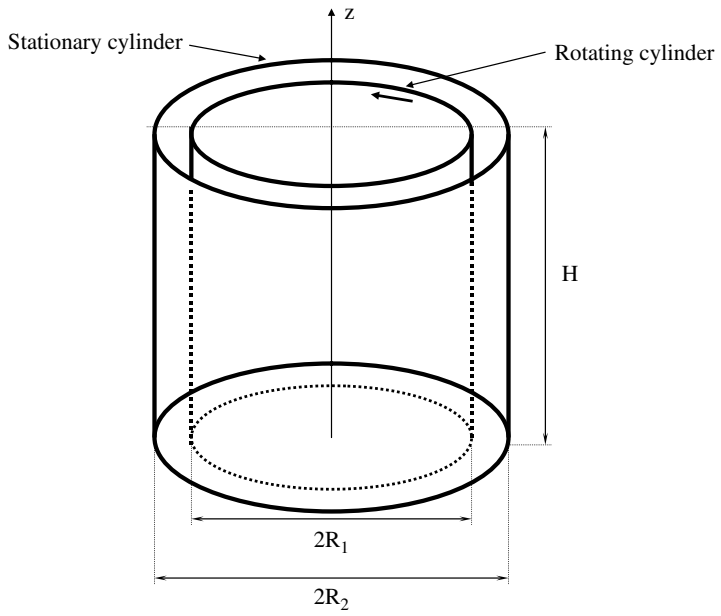

Figure 7.5. *Geometry of a circular cylindrical rheometer*

The force exerted by the inner cylinder on the material through a surface element, $\mathrm{d}z \cdot R_1 \cdot \mathrm{d}\theta$, whose outward normal is $-\vec{e}_r$, is written as:

$$\mathrm{d}\vec{F}(\theta) = -\begin{pmatrix} \sigma_{rr}(R_1) \\ \tau_{r\theta}(R_1) \\ \tau_{rz}(R_1) \end{pmatrix} R_1 \mathrm{d}\theta \mathrm{d}z \qquad [7.21]$$

The circular cylindrical rheometer only applies stresses to make the inner cylinder rotate and keep the outer cylinder fixed. No force is exerted along the *Oz* axis, and consequently, $\tau_{rz}(R_2) = 0$. The torque exerted on the entire contact surface of the inner cylinder is:

$$\overrightarrow{M} = \int_0^{2\pi} \mathrm{d}\theta \int_0^H \left\{ \overrightarrow{OM} \times \mathrm{d}\vec{F} \right\} R_1 \mathrm{d}z = \int_0^H \mathrm{d}z . R_1^2 \int_0^{2\pi} \begin{pmatrix} 1 \\ 0 \\ 0 \end{pmatrix} \times \begin{pmatrix} -\sigma_{rr}(R_1) \\ -\tau_{r\theta}(R_1) \\ 0 \end{pmatrix} \mathrm{d}\theta = \begin{pmatrix} 0 \\ 0 \\ -2\pi R_1^2 H \tau_{r\theta}(R_1) \end{pmatrix} \qquad [7.22]$$

The only non-zero component of the torque is a rotation moment about the *Oz* axis, associated with a shear stress, $\tau_{r\theta}$. Its magnitude is:

$$M_z = 2\pi R_1^2 H \tau_{r\theta}(R_1) \qquad [7.23]$$

The moment applied by the inner cylinder at the boundary of the material produces displacements only in the azimuthal direction. For a fluid, the axisymmetry of the flow simplifies the kinematics into:

$$u_r = 0, \quad u_\theta(r), \quad \text{and} \quad u_z = 0. \qquad [7.24]$$

Of the local equations for the fundamental law of dynamics in the cylindrical coordinate system (Table 1.2 of Chapter 1), the only relevant one here is on the azimuthal direction ($\vec{e}_\theta$), which reduces to:

$$0 = \frac{1}{r^2}\frac{\partial(r^2\tau_{r\theta})}{\partial r} \qquad [7.25]$$

Integrating it with [7.23] leads to[4]:

$$\tau_{r\theta}(r) = \frac{1}{r^2}\frac{M_z}{2\pi H} \qquad [7.26]$$

Unlike what was obtained for the planar geometry, stress is not homogeneous across the material, but its variations remain negligible if the gap width is small compared to the radii of the cylinders, i.e. if $(R_2 - R_1) << (R_2 + R_1)/2$. The stress within the gap can then be approximated by its average value:

$$\tau_{r\theta}(r) \approx \frac{2M_z}{\pi(R_1 + R_2)^2 H} \qquad [7.27]$$

For a fluid, the axisymmetric kinematics of the flow (equation [7.24]) leads to a simple expression of the strain rate tensor (Table 1.2 of Chapter 1):

4 Using relation [7.26], it can be established that the moment exerted by the inner cylinder of radius R_1 on the material is the exact opposite of that exerted on the material by the outer cylinder.

$$[D]=\begin{pmatrix} 0 & \frac{1}{2}\left(r\frac{\partial}{\partial r}\left(\frac{u_\theta}{r}\right)\right) & 0 \\ \frac{1}{2}\left(r\frac{\partial}{\partial r}\left(\frac{u_\theta}{r}\right)\right) & 0 & 0 \\ 0 & 0 & 0 \end{pmatrix} \qquad [7.28]$$

The only non-zero term in the strain rate tensor is $D_{r\theta} = (1/2)r\partial(u_\theta / r)/\partial r$. The rheometrical experiment enables the determination of the relationship between $D_{r\theta}$ and $\tau_{r\theta}$, with both remaining approximately homogeneous across the material. The average value of the magnitude of the strain rate is expressed by bringing in the angular rotational velocity, Ω, of the inner cylinder:

$$D_{r\theta} = \Omega\frac{(R_2 + R_1)}{4(R_2 - R_1)} \qquad [7.29]$$

since the outer cylinder is stationary ($u_\theta(R_2) = 0$),the inner cylinder rotates with velocity $u_\theta(R_1) = \Omega R_1$.

By studying the variations of the moment M_z with the angular rotational velocity, Ω, of the inner cylinder, we can thus plot the rheological curve $\tau_{r\theta} = \tau_{r\theta}(D_{r\theta})$, using [7.27] and [7.29]. For a Newtonian fluid, viscosity is simply determined by:

$$\mu = \frac{\tau_{r\theta}}{2D_{r\theta}} = \frac{4M_z(R_2 - R_1)}{\pi(R_1 + R_2)^3 H\Omega} \qquad [7.30]$$

The expressions that have just been established for determining the $D_{r\theta}$ term in the strain rate tensor rely on kinematic hypotheses (equation [7.24]) that assume the flow to be laminar, without secondary flow. It is within this framework that the use of a rheometer is valid. It should be emphasized that these hypotheses are not always verified.[5]

5 If the inner cylinder spins fast enough, an instability is triggered, which gives rise to a secondary flow made up of counter-rotating toroidal vortices stacked vertically inside the gap. The total solution is, therefore, not in the form given by [7.24]; instead, it has non-zero u_r and u_z velocity components. The Couette instability has prompted a number of studies to be taken up.

7.5. Application exercises

Exercise 7.1: Rheometry and flow of a Bingham fluid in a pipe

A pipe of length $L = 1000$ m and diameter $D = 0.2$ m is blocked by a liquid that has become congealed inside the pipe following a plant shutdown. We wish to determine the head loss required between the inlet and outlet to unblock the pipe.

The first step is to determine the rheological characteristics of the material, which has been sampled. The material is inserted into a circular cylindrical rheometer of height $H = 50$ mm, inner radius $R_1 = 19.5$ mm, and outer radius $R_2 = 20.5$ mm. The outer cylinder is stationary, while the inner cylinder can rotate about its symmetrical axis. The rheometer operates by imposing a known and controlled torque, M_z, to the inner cylinder and measuring its angular rotational speed, Ω, in a steady-state regime. The density of the material is $\rho = 2000$ kg/m^3.

1. For different values of torque M_z, readings have been taken of the angular rotational speed, Ω. The results are given in the table below.

M_z (10^{-4} N·m)	2.51	3.77	5.02	6.28	7.54	10.1	12.6	25.1
Ω (rd/s)	0	0	0	0	5	15	25	75

Plot the rheological curve of the material, i.e. the relationship between stress, $\tau_{r\theta}$, and strain rate, $D_{r\theta}$. Show that the rheological behavior is typical of a Bingham material, namely:

$$D_{r\theta} = 0 \quad \text{if} \quad 0 \le \tau_{r\theta} \le \tau_c$$
$$\tau_{r\theta} = \tau_c + 2\mu D_{r\theta} \quad \text{if} \quad \tau_{r\theta} \ge \tau_c$$

What does this rheological behavior mean, in simple terms? Determine τ_c (the yield stress) and μ (the viscosity) from the data in the table.

2. Returning to the problem of the blocked pipe, consider the flow in the cylindrical coordinate system whose Oz axis, which coincides with the axis of the pipe (see Figure 1.3 of Chapter 1), is oriented in the direction of the flow. By considering the non-zero component(s) in the velocity vector, verify that the only non-zero term in the strain rate tensor is D_{rz}. Set out the form of this term explicitly and explain why $D_{rz} \le 0$. Explain also why the only non-zero shear stress in the pipe is τ_{rz}, and why $\tau_{rz} \le 0$. It will be deduced there from that the rheological relation for the Bingham fluid can be written, for the flow of that fluid in a pipe, as:

$$D_{rz} = 0 \quad \text{if} \quad -\tau_c \le \tau_{rz} \le 0$$
$$\tau_{rz} = -\tau_c + 2\mu D_{rz} \quad \text{if} \quad \tau_{rz} \le -\tau_c$$

(Deriving the rheological relation between τ_{rz} and D_{rz} for the pipe flow from the rheological relation established between $\tau_{r\theta}$ and $D_{r\theta}$ in Question 1 by rheometry is not trivial. We will not dwell on that, being content with assuming an isotropic behavior of the material and finding that, in both cases, we are dealing with shear stresses and strain rates.)

3. By applying the momentum theorem, calculate the minimum pressure difference, ΔP, that should be applied between the inlet and outlet of the pipe to set the fluid in motion. By applying the momentum theorem on a domain to be specified, determine the variation of $\tau_{rz}(r)$ with r and ΔP. Justify the fact that the momentum theorem can be applied for a Bingham fluid.

4. A pressure difference is applied between the inlet and outlet of the pipe: ΔP = 1.2 bar. Explain why the material is solid in the central portion of the pipe, and why it is fluid in an annular domain adjacent to the wall. Determine the radius R_c within which the material is solid inside the pipe and beyond which it is liquid. Determine the velocity profile.

Exercise 7.II: Cone/plate rheometer

The purpose is to study the principle of the circular conical rheometer represented in the Figure 7.II.1 below. The material to be studied is inserted between a flat plate, which is held fixed, and a cone. The cone can rotate around the Oz axis. The apex of the cone contacts the plane.

It is considered here that the rheometer is employed to study a fluid. The cone is subjected to a rotational moment M_z about the Oz axis, and consequently rotates with an angular rotational speed Ω.

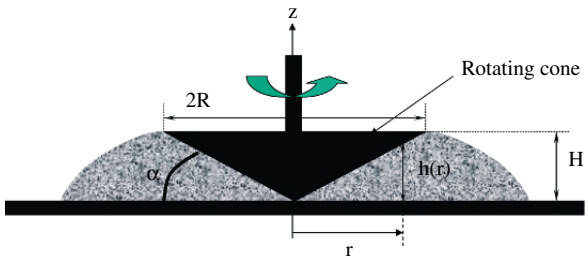

Figure 7.II.1

1. Let us first consider a Newtonian fluid, whose dynamic viscosity, μ, we wish to measure. List the parameters on which the measurement of the dynamic viscosity depends, making sure they are independent. Based on a dimensional

analysis argument, suggest dimensionless numbers that may be used to link the dynamic viscosity to the other parameters of the problem.

2. Setting the problem in a cylindrical coordinate system, express the boundary conditions and verify that a flow of the form

$$u_r(r,\theta,z)=0\ ,\ u_\theta(r,\theta,z)=\Omega r\frac{z}{h(r)}\ \text{and}\ \ u_z(r,\theta,z)=0$$

fulfils them. Here, $h(r)$ denotes the thickness of the gap at a distance r from the axis.

For this velocity field, after expressing $h(r)$, determine the different terms in the strain rate tensor. In the case where angle α is very small, justify that the $D_{z\theta}$ term is dominant in the strain rate tensor. Any comments?

3. The outward normal to the material on the surface of the cone is, in the cylindrical coordinate system

$$\begin{pmatrix}-\sin\alpha\\0\\\cos\alpha\end{pmatrix}$$

and the surface element on the cone is expressed as $(r\mathrm{d}\theta/\cos\alpha)\mathrm{d}r$.

Express the force by unit surface exerted by the cone on the material at any point on the surface of the cone. It will be postulated that $\tau_{r\theta}(r,\theta,z)=0$.

Write (in the form of an integral) the theoretical expression linking moment M_z to the stress.

Justify that $\tau_{z\theta}$ is uniform within the material and derive there from the relationship between the moment and the stress.

4. For a Newtonian fluid, determine the relationship between the dynamic viscosity, the moment and the angular velocity, for a conical viscosimeter.

NOTE.– Although the geometry of the rheometer would encourage, as a matter of principle, treating this problem in a spherical coordinate system, such a resolution requires setting the equations in a spherical coordinate system (not covered in this book), which does not make it any simpler either.

Part II

Mixing and Chemical Reactions

Chapter 8

Large Scales in Turbulence: Turbulent Diffusion – Dispersion

8.1. Introduction

All the five chapters in Part II are devoted to the phenomenon of turbulence and its applications to mixing and chemical reactions. We have already familiarized ourselves to some extent, in the first part, with the notion of turbulence, and discussed two of its characteristics:

1. Turbulence increases dissipation of kinetic energy in a fluid flow. We have observed this in pipe flows (Chapter 4); the regular head loss of the flow inside a pipe is larger when the flow is turbulent than when it is laminar. It was also shown (Chapter 2, section 2.8) that the rate of kinetic energy dissipation per unit volume depends on the square of its velocity gradients. The strengthening of velocity gradients in a turbulent flow is, therefore, directly responsible for this increase in dissipation.

2. Turbulence spatially homogenizes a quantity that is dispersed within a fluid. This mixing property also impacts the structure of velocity fields. For the turbulent flow in a pipe (Chapter 4, section 4.3), the average profile (of a turbulent flow) is more uniform than that of a laminar flow (Poiseuille solution). Conversely, the mean velocity gradient in the vicinity of the walls is larger in a turbulent flow than in a laminar flow. The increase in friction forces of the wall is correlated with that of head loss, in accordance with the momentum theorem (Chapter 2).

The aim of Part II is to introduce the elementary tools of turbulence, which will enable the understanding and modeling of the effects we have just described.

In this chapter, we provide a macroscopic description of turbulence, which corresponds, for example, to what is perceived by a person observing the large eddies in the turbulent wake downstream of an obstacle placed in a flow. We introduce the *root mean square (rms) turbulent velocity* and the *integral length scale*. These two quantities characterize the large scales, which are naturally observed in a turbulent flow. We shall additionally note, in the present and subsequent chapters of this second part, that other quantities introduced to account for the effect of turbulence are directly determined from the rms turbulent velocity and the integral length scale. This is the case for the rate of dissipation of the turbulent kinetic energy and for the turbulent diffusion coefficient. We present in this chapter two elementary tools for modeling turbulence, the *mixing length model* and the *k-ε model*. They basically make explicit the key role of the rms velocity and of the integral length scale in turbulent flow. Using these two models allows modeling turbulent dispersion in a flow..

Large scales in turbulence and the process of turbulent dispersion do not account for all the phenomena effected by turbulence. Dispersion is not equivalent to mixing, an important distinction while dealing with chemical reactions. Dispersing two products in a volume does not mean that they are mixed at the molecular scale and thus able to react together. In Chapter 10, we discuss mixing at molecular scale, which is due to the process of molecular diffusion. We show that turbulence actually accelerates the process of molecular diffusion upon splitting the fluid volumes into small-scale entities. The distinction between large scales and small scales in turbulence translates into the terms *macromixing* and *micromixing*, whose significance is discussed in Chapter 10. These concepts are extended in Chapter 11, where the size of the smallest scales within a turbulent flow is quantified, using Kolmogorov's theory. We finally introduce in Chapter 12, two classical models that are used in process engineering for the numerical simulation of mixing and chemical reaction in a turbulent flow.

Chapter 9 is actually a kind of sidetrack within this second part. It discusses the connection between the tools of turbulence introduced in Chapter 8 and two commonly used tools in chemical engineering, namely the residence time distribution (RTD) approach, and the rules pertaining to dimensioning a stirring process.

8.2. Concept of average in the turbulent sense, steady turbulence, and homogeneous turbulence

In essence, any quantity ϕ (e.g. a velocity component or the pressure) measured in a turbulent flow at any point (x, y, or z) is not constant. If the same experiment is carried out N times and that quantity is measured both at the same location in the flow and at the same time relative to the start of the experiment, the measured value

will vary from one experiment to another. Denoting $\varphi_i(t,x,y,z)$ as the value measured at time t and at point (x, y, z) during an experiment i, the average value of that quantity in the given location and time is defined by:

$$\overline{\phi}(t,x,y,z) = \frac{1}{N}\sum_{i=1}^{N}\phi_i(t,x,y,z) \qquad [8.1]$$

The average value thus defined is referred to as the "ensemble average" because it is estimated by carrying out independent and identical experiments. It is necessary to carry out a large number of experiments in order to estimate a reliable average value. The turbulent fluctuation measured during experiment i at the same location and at time t is then defined by:

$$\varphi'_i(t,x,y,z) = \varphi_i(t,x,y,z) - \overline{\varphi}(t,x,y,z) \qquad [8.2]$$

In the following discussion, a bar over a variable indicates that the quantity is turbulence-averaged and a "'" as a superscript of a variable means that it is the instantaneous turbulent fluctuation relative to the average value of the variable. From these definitions, it follows that the ensemble average of a turbulent fluctuation equals zero, i.e. we necessarily have:

$$\overline{\varphi'}(x,y,z,t) = 0 \qquad [8.3]$$

The magnitude of turbulent fluctuations is characterized by the variance of the measured quantity with respect to its average value:

$$\overline{\phi}_{\text{rms}}(t,x,y,z) = \sqrt{\frac{1}{N}\sum_{i=1}^{N}\left\{\phi_i(t,x,y,z) - \overline{\phi}(t,x,y,z)\right\}^2} \qquad [8.4]$$

This quantity is called the rms turbulent average.

In reality, however, the ensemble average of a quantity is difficult to determine, as it requires carrying out a sufficiently large number of experiments, beyond which it can be verified with a prescribed confidence that the estimated average no longer depends on the number of experiments. In the ensemble-average sense, the average quantity, $\overline{\varphi}$, depends in principle, with time and on the space coordinates. The average value varies with time when the driving force of the flow (e.g. the pump generating the flow) operates in a transient regime. It varies in space if one compares the values obtained from the boundary layer on the walls to those obtained away from.

In practice, turbulence is often studied in conditions where it can be regarded as "steady-state". This means that the ensemble averages of the different quantities we

are interested in (velocity components, pressure, etc.) are independent of the time at which their average value is estimated. This is usually the case in a stirring tank, if the rotational speed of the stirrers is kept constant. After a certain period of time elapsed following the start-up of stirring process, it is found that the stirring process inside the tank stabilizes at a constant level. This is referred to as steady-state turbulence, although velocity varies in both space and time. This is because the ensemble average of the velocity components and of the pressure is independent of time.

For steady-state turbulence, the average value and the rms value of the turbulent fluctuations in a quantity φ can be estimated using time averages computed on a recording of duration T:

$$\bar{\phi}(x,y,z) = \frac{1}{T}\int_{t}^{t+T} \phi(t',x,y,z)\mathrm{d}t'$$

$$\phi'(t,x,y,z) = \phi(t,x,y,z) - \bar{\phi}(x,y,z) \qquad [8.5]$$

$$\bar{\phi}_{\mathrm{rms}}(x,y,z) = \sqrt{\frac{1}{T}\int_{t}^{t+T} \left\{\phi(t',x,y,z) - \bar{\phi}\right\}^2 \mathrm{d}t'}$$

The steady-state nature of the turbulence can be verified by checking that the integrals in [8.5] do not depend on time t from which they are calculated. The recording duration of T should be sufficiently long for the calculated average value to be independent from T. From an experimental standpoint, studying steady-state turbulence constitutes a dramatic simplification. All that is needed is to carry out one experiment of sufficiently long duration.

Similarly, turbulence is said to be homogeneous when the average values do not depend on the point in space where they are measured.

We find that turbulence is described by determining its statistical characteristics. The statistical properties of turbulence can also be characterized by introducing the probability that an instantaneous value has a given value. The probability density function $p(\varphi)$ is defined such that $p(\phi)\mathrm{d}\phi$ is the probability for the variable to be between $\phi - \mathrm{d}\phi/2$ and $\phi + \mathrm{d}\phi/2$. It can be practically determined as follows:

$$p(\phi)\cdot\mathrm{d}\phi = \frac{\text{no. of values measured between } \phi - \mathrm{d}\phi/2 \text{ and } \phi + \mathrm{d}\phi/2}{\text{no. of values measured}}.$$

$$p(\phi)\cdot\mathrm{d}\phi = \frac{\text{time during which the value is between } \phi - \mathrm{d}\phi/2 \text{ and } \phi + \mathrm{d}\phi/2}{\text{recording time}} \qquad [8.6]$$

The first form relates to the notion of ensemble average, while the second refers, for steady-state turbulence, to the time average. The following properties result from the definition of probabilities:

$$\int_{-\infty}^{+\infty} p(\phi)\mathrm{d}\phi = 1$$

$$\overline{\phi} = \int_{-\infty}^{+\infty} \phi\, p(\phi)\mathrm{d}\phi \qquad [8.7]$$

$$\overline{\phi}_{\mathrm{rms}} = \sqrt{\int_{-\infty}^{+\infty} \left\{\phi - \overline{\phi}\right\}^2 p(\phi)\mathrm{d}\phi}$$

8.3. Average velocity and RMS turbulent velocity

The averaging notions introduced above can be directly applied to define the average value of a velocity component, its instantaneous turbulent fluctuation, and the rms turbulent velocity in the ensemble-average sense:

$$\overline{u}_x(t,x,y,z) = \frac{1}{N}\sum_{i=1}^{N} u_{x,i}(t,x,y,z)$$

$$u'_{x,i}(t,x,y,z) = u_{x,i}(t,x,y,z) - \overline{u}_x(t,x,y,z) \qquad [8.8]$$

$$\overline{u}_{x,\mathrm{rms}}(t,x,y,z) = \sqrt{\frac{1}{N}\sum_{i=1}^{N}\left\{u_{x,i}(t,x,y,z) - \overline{u}_x(t,x,y,z)\right\}^2}$$

For steady-state turbulence, we can also write

$$\overline{u}_x(x,y,z) = \frac{1}{T}\int_{t}^{t+T} u_x(t',x,y,z)\mathrm{d}t'$$

$$u_x'(t,x,y,z) = u_x(t,x,y,z) - \overline{u}_x(x,y,z) \qquad [8.9]$$

$$\overline{u}_{x,\mathrm{rms}}(x,y,z) = \sqrt{\frac{1}{T}\int_{t}^{t+T}\left\{u_x(t',x,y,z) - \overline{u}_x\right\}^2 \mathrm{d}t'}$$

The definitions written above for the velocity component, u_x, can be transposed to u_y and u_z. Turbulence is said to be isotropic if the statistical properties of the turbulent velocity field are independent from the velocity direction considered. In that case, $\overline{u}_{x,\mathrm{rms}} = \overline{u}_{y,\mathrm{rms}} = \overline{u}_{z,\mathrm{rms}}$. Turbulence often does not depart much from isotropic conditions. We place ourselves in such a situation, denoting turbulent velocity simply by u_{rms}, and also omitting the bar over that quantity. Turbulent velocity, u_{rms}, plays a major part in the theory of turbulence. It characterizes the level of turbulence, the importance of which is appreciated by noting that ρu_{rms}^2 is proportional to the kinetic energy of turbulence per unit volume. When the flow has a non-zero average velocity $\overline{u}$, the ratio $u_{\mathrm{rms}} / \overline{u}$ is called the "turbulence intensity."

8.4. Length scale of turbulence: integral scale

It is easily understood that a length scale is also necessary in order to describe the properties of turbulence. In the turbulent wake downstream of a bridge pier in a river, e.g. one can observe whirlpool movements whose size is of the same order of magnitude as the diameter of the bridge pier. Doubling the diameter of the bridge pier roughly doubles the size of the vortices. Figure 8.1 attempts to depict schematically this fact by representing the turbulent state observed in an obstacle on two different scales. If measurement points A and A′ occupy an identical position in both the cases, relative to the scale of the object, it is likely that the same average velocity and the same turbulent velocity at A and A′ can be measured if the velocity $\vec{u}$ upstream of the cylinders is identical. Nevertheless, the flow visualizations will be different, as vortices of very different sizes will be clearly perceived in both cases. Therefore, a length scale needs to be associated with the turbulent velocity scale u_{rms} in order to provide a minimum description of the statistical properties of turbulence.

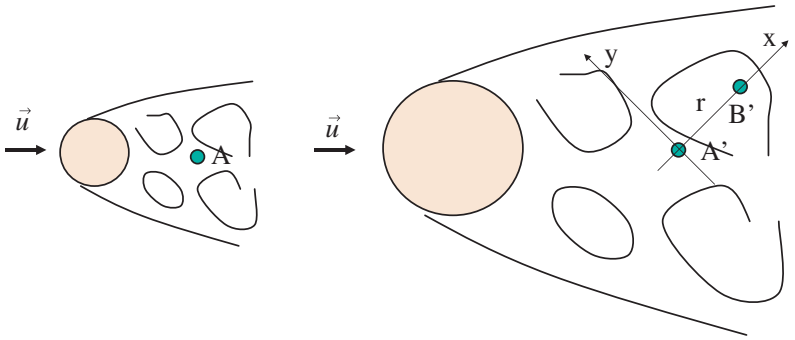

Figure 8.1. *Sketch of the turbulent wake downstream of an obstacle for two object sizes*

The length scale of the turbulence is linked to the notion of correlation. If two points are very close together, the velocity fluctuations measured simultaneously at those two points are almost identical at any time. On the other hand, if the two points are sufficiently spaced apart, it is difficult to link the velocities measured at the two points at the same time. The correlation scale varies from one flow to another, depending on the geometry of the system and the conditions in which the flow is generated. For example, for the flow behind a cylinder (Figure 8.1), the correlation of measurements taken at two points varies greatly depending on whether the distance between the two points is small or large with respect to the diameter of the cylinder. The scale of turbulence is associated with the notion of a "vortex". Literature on turbulence often refers to the concept of "turbulent eddies."

Several scales for turbulence are defined by the theories of turbulence. Here, we introduce the integral scale, based on the theory of homogeneous, isotropic turbulence. The coordinate system is illustrated in Figure 8.2(a). Considering two points spaced apart by a distance r along the Ox axis, the longitudinal components of the velocity fluctuations at x and $x+r$ are respectively the $u_x'(t,x,y,z)$ and $u_x'(t,x+r,y,z)$ components parallel to the Ox axis. The crosswise components are u_y' and u_z', of which only u_y' is shown. The longitudinal correlation is defined as the function:

$$f(r)=\frac{\overline{u_x'(t,x,y,z)u_x'(t,x+r,y,z)}}{\overline{u_x'(t,x,y,z)u_x'(t,x,y,z)}} \qquad [8.10]$$

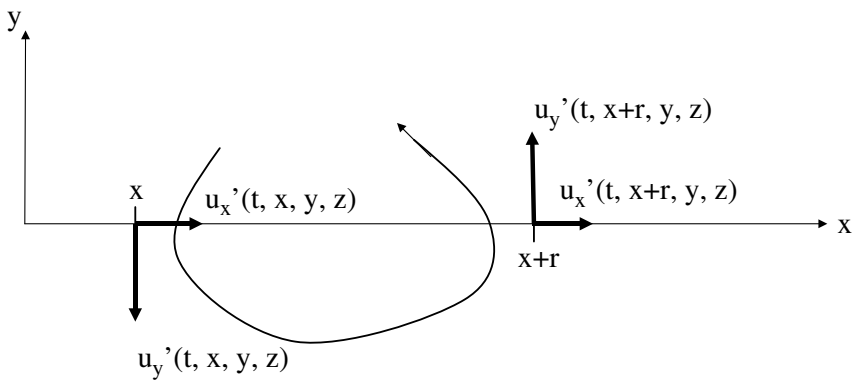

Figure 8.2(a). *Instantaneous velocity fluctuations at two points and notations used for computing the correlation function*

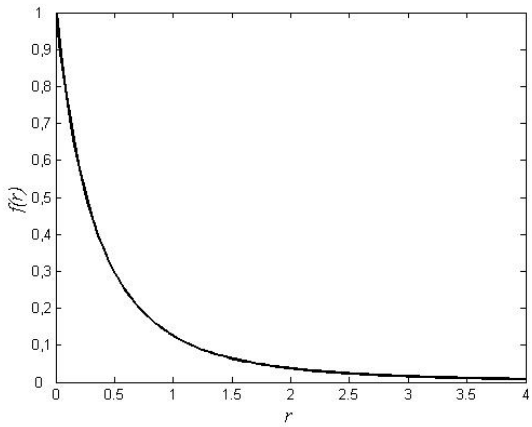

Figure 8.2(b). *Correlation function of turbulent fluctuations*

The numerator is the average value of the product of the algebraic values of the turbulent fluctuations measured at both points. The purpose of the denominator is to render the function $f(r)$ dimensionless. When the turbulence is homogeneous, the measured correlations are independent from the position of the origin of the coordinate system. We have placed ourselves within the framework of steady-state, homogeneous turbulence by writing in [8.10] that $f(r)$ is independent from t, x, y, and z. By writing that $f(r)$ depends only on the distance r between the two points, and not on the orientation of the Ox axis connecting them, we have also assumed the turbulence to be isotropic. We would obtain the same velocity correlation for any other orientation of the (O,x,y) coordinate system represented in Figure 8.1, provided that the distance between the two points A′ and B′ is identical. The property of isotropy in turbulence means that there is no preferred direction for turbulence. It is common knowledge to opt for the framework of steady, homogeneous, and isotropic turbulence[1], which forms the basis for statistical theories of turbulence. A correlation function is represented, in an idealized form, in Figure 8.2(b). By definition, $f(r = 0) = 1$ (perfect correlation, since both points are merged into one). The correlation function tends toward zero as the space between the two points increases. The transverse correlation function is defined by transposing [8.10] to the crosswise components u_y' or u_z' of the turbulent velocity fluctuations. Within the bounds of the theory of homogeneous, isotropic turbulence,

1 Within this framework, numerous theoretical developments have been established (see G.K. Batchelor, *The Theory of Homogeneous Turbulence*, 1953). We also recommend the book by M. Lesieur, *Turbulence in Fluids* (Springer-Verlag, 2007), the contents of which are more general than a Bachelor's presentation.

the longitudinal and transverse correlation functions are related to each other by a mathematical relation.[2] In Figure 8.2(b), the longitudinal correlation function $f(r)$ is always positive. Negative values of the correlation function are measured in some cases. This is easily understood for the crosswise correlation function, as the crosswise velocity components u_y' at x and $x+r$ are in opposite directions when the turbulent fluctuations are associated with a turbulent eddy whose size corresponds to the space between the two points, as shown in Figure 8.2(a).

The integral scale is defined by the integral of the correlation function

$$\ell_t = \int_0^\infty f(r)\mathrm{d}r \qquad [8.11]$$

This quantity is homogeneous with length. The integral scale plays a fundamental part in the theories of turbulence. Turbulent motion involves a wide range of length scales, the boundaries of which are often referred to as "large" and "small" vortices. We discuss this concept in Chapter 11. The integral scale provides an order of magnitude for the dimension of the most visible vortices in the turbulent flow. These are the largest ones, which contain most of the turbulent kinetic energy.

Lastly, we introduce the characteristic time of turbulence, τ_t, based on u_{rms} and ℓ_t:

$$\tau_t = \frac{\ell_t}{u_{\mathrm{rms}}} \qquad [8.12]$$

This time is often referred to as the "eddy turn-over time" of turbulence. It is interpreted as the time taken by a particle to perform a full rotation within the eddy.

We have seen in Chapters 2 and 4 that turbulence dramatically strengthens the dissipation of kinetic energy. This property results from the definition of the instantaneous rate of kinetic energy dissipation per unit volume:

$$\rho\varepsilon = \frac{\mu}{2}\left\{\frac{\partial(u_i)}{\partial x_j} + \frac{\partial(u_i)}{\partial x_j}\right\}^2 \qquad [8.13]$$

Here, we omit the minus sign that appears in equation [2.45] of Chapter 2, in order to use a positive rate of dissipation, as is customary in the studies of turbulence. Depending on their size, turbulence eddies contribute very differently to dissipation.

2 See the book by G.K. Batchelor, ibid.

Large-scale eddies have a large amount of kinetic energy, but the associated gradients are small. Small-scale eddies, on the other hand, produce very strong velocity gradients and account for the dissipation, despite their lower energy. Experimental observations have established that the rate of turbulent kinetic energy dissipation depends on the rms turbulent velocity and the integral scale, as expressed by the dimensional relation:

$$\varepsilon = A\frac{u_{\text{rms}}^3}{\ell_t} \qquad [8.14]$$

A is a constant of order O(1).[3]

Expression [8.14] of the rate of kinetic energy dissipation encompasses within it the property whereby a turbulent flow dissipates more than a laminar flow. For a laminar flow with characteristic scales of velocity u_{rms} and length ℓ_t, the rate of dissipation derived from [8.13] is $\varepsilon_{\text{lam}} \approx \nu(u_{\text{rms}}/\ell_t)^2$. Denoting by $\varepsilon_{\text{turb}}$ the rate of dissipation [8.14] in a turbulent flow leads to:

$$\frac{\varepsilon_{\text{turb}}}{\varepsilon_{\text{lam}}} \approx \frac{u_{\text{rms}}\ell_t}{\nu} \qquad [8.15]$$

The quantity:

$$\text{Re}_t = \frac{u_{\text{rms}}\ell_t}{\nu} \qquad [8.16]$$

is the turbulent Reynolds number, based on the scales of turbulence. There is a consensus in this regard, for various configurations, that a fully developed turbulent regime is reached if $\text{Re}_t > 100$. This criterion for transition to turbulence is more universal than any other criterion based on the overall characteristics of the flow (such as $\text{Re} = U_m D/\nu > 2{,}000$ for a flow with area-averaged streamwise velocity U_m in a pipe with diameter D). For $\text{Re}_t > 100$, relation [8.15] indicates that dissipation is indeed larger in a turbulent regime.

Relation [8.14] is of considerable importance for the phenomenon of turbulence. It is very important to be aware that dissipation does not depend on viscosity. The juxtaposition of [8.13] and [8.14] explains this paradox by indicating that the squared velocity gradients in a turbulent flow increase in inverse proportion to the viscosity, if viscosity decreases.

---

3 Density does not appear in [8.14]; ε is the rate of energy dissipation per unit mass.

We see hereinafter that the turbulent diffusion coefficient is also determined from the rms turbulent velocity u_{rms} and the integral scale ℓ_t. It is also be observed, in other chapters of the second part, that the properties of turbulence are essentially described by the knowledge of the two quantities u_{rms} and ℓ_t.

8.5. Turbulent flux of a scalar quantity: averaged diffusion equation

We now look at dispersion over time, by a turbulent flow, of a "passive scalar quantity" introduced into the fluid. The quantity is said to be passive if its presence does not alter the flow. This could be, for instance, a dye, a pollutant, or a chemical constituent that does not alter the mechanical properties of the fluid (density, viscosity, etc). Temperature is regarded as a passive scalar quantity when its variations in space are sufficiently small for viscosity variations to remain negligible and for spatial variations of density not to cause movement within the fluid (absence of natural convection).

Considering here a chemical constituent measured locally by its concentration $c(t,x,y,z)$, the dispersion of that quantity in space and time is described by an advection–diffusion equation accounting for its conservation:

$$\frac{\partial c}{\partial t} + \text{div}(c\vec{u}) = \kappa \Delta c \qquad [8.17]$$

κ is the coefficient of molecular diffusion.

Assuming provisionally that the flow has no turbulence-averaged component, velocity therefore accordingly gets reduced to turbulent fluctuations such as $u_x'(t,x,y,z)$, $u_y'(t,x,y,z)$, and $u_z'(t,x,y,z)$. Concentration, however, may be represented as the sum of the turbulence-averaged concentration and the concentration fluctuation:

$$c(t,x,y,z) = \overline{c}(t,x,y,z) + c'(t,x,y,z) \qquad [8.18]$$

In many cases, the aim is simply to determine the time and space evolution of the average concentration $\overline{c}(t,x,y,z)$, as illustrated in Figure 8.3 for the case where, at time $t = 0$, a product is introduced with uniform concentration C_0 inside a cylinder of radius R. Although the details of the dispersion process are complex, when dealing with a dye "spot" it is possible to view a mean area in which the product disperses in time. In the absence of an average flow, the position of the center of the spot is stationary. If the turbulence is homogeneous, the average dispersion of the spot is axisymmetric and the spot widens with time. Within the spot, turbulence-averaged concentration decreases as one moves further away from the center, and the

maximum turbulence-averaged concentration (obtained at all times in the center of the spot) decreases as a function of time.

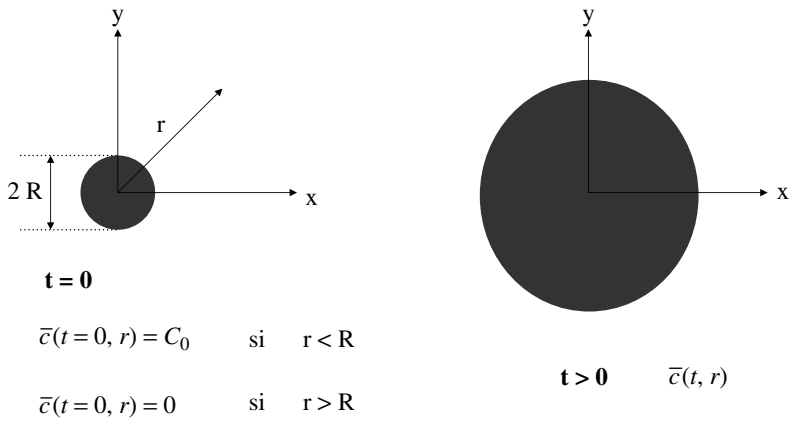

Figure 8.3. *Characterization of the average axisymmetric dispersion of a product in homogeneous turbulence with zero average velocity*

The process may be modeled by substituting [8.18] into [8.17]. Expanding the same leads to:

$$\frac{\partial \overline{c}}{\partial t}+\frac{\partial c'}{\partial t}+\frac{\partial(\overline{c}u_x')}{\partial x}+\frac{\partial(\overline{c}u_y')}{\partial y}+\frac{\partial(\overline{c}u_z')}{\partial z}+\frac{\partial(c'u_x')}{\partial x}+\frac{\partial(c'u_y')}{\partial y}+\frac{\partial(c'u_z')}{\partial z} = \kappa\Delta\overline{c}+\kappa\Delta c' \qquad [8.19]$$

Taking the turbulence average of this partial differential equation results in deletion of a few terms since, by definition, $\overline{c'}=0$, $\overline{u_x'}=0$, $\overline{u_y'}=0$, and $\overline{u_z'}=0$. However, the averages of double correlations $\overline{u_x'c'}$, $\overline{u_y'c'}$, and $\overline{u_z'c'}$ do not necessarily equal zero, as we see later. Reintroducing the turbulence-average velocity (for cases where it does not vanish), we thus derive the averaged advection–diffusion equation for describing the space and time evolution of the turbulence-average concentration:

$$\frac{\partial \overline{c}}{\partial t}+\overline{u}_x\frac{\partial \overline{c}}{\partial x}+\overline{u}_y\frac{\partial \overline{c}}{\partial y}+\overline{u}_z\frac{\partial \overline{c}}{\partial z}=-\frac{\partial \overline{u_x'c'}}{\partial x}-\frac{\partial \overline{u_y'c'}}{\partial y}-\frac{\partial \overline{u_z'c'}}{\partial z}+\kappa\Delta\overline{c} \qquad [8.20]$$

The double correlations $\overline{u_x'c'}$, $\overline{u_y'c'}$, and $\overline{u_z'c'}$ have a very simple physical meaning. They are the average turbulent fluxes of concentration per unit area, produced by the action of turbulence. $\overline{u_x'c'}$ is the turbulent flux per unit area

through a surface perpendicular to the *Ox* direction. A similar meaning ensues for $\overline{u_y'c'}$ and $\overline{u_z'c'}$.

The method used above to write out turbulence-averaged equations is entirely classical. While we have applied it to the dispersion of a passive scalar, it is also used for other quantities. Its application to Navier–Stokes equations leads to Reynolds equations:

$$\begin{aligned}
&\frac{\partial \overline{u}_x}{\partial t}+\overline{u}_x\frac{\partial \overline{u}_x}{\partial x}+\overline{u}_y\frac{\partial \overline{u}_x}{\partial y}+\overline{u}_z\frac{\partial \overline{u}_x}{\partial z}= \\
&\qquad -\frac{1}{\rho}\frac{\partial \overline{p}}{\partial x}-\frac{\partial \overline{u_x'u_x'}}{\partial x}-\frac{\partial \overline{u_x'u_y'}}{\partial y}-\frac{\partial \overline{u_x'u_z'}}{\partial z}+\nu\Delta\overline{u}_x+f_x \\
&\frac{\partial \overline{u}_y}{\partial t}+\overline{u}_x\frac{\partial \overline{u}_y}{\partial x}+\overline{u}_y\frac{\partial \overline{u}_y}{\partial y}+\overline{u}_z\frac{\partial \overline{u}_y}{\partial z}= \\
&\qquad -\frac{1}{\rho}\frac{\partial \overline{p}}{\partial y}-\frac{\partial \overline{u_x'u_y'}}{\partial x}-\frac{\partial \overline{u_y'u_y'}}{\partial y}-\frac{\partial \overline{u_y'u_z'}}{\partial z}+\nu\Delta\overline{u}_y+f_y \\
&\frac{\partial \overline{u}_z}{\partial t}+\overline{u}_x\frac{\partial \overline{u}_z}{\partial x}+\overline{u}_y\frac{\partial \overline{u}_z}{\partial y}+\overline{u}_z\frac{\partial \overline{u}_z}{\partial z}= \\
&\qquad -\frac{1}{\rho}\frac{\partial \overline{p}}{\partial z}-\frac{\partial \overline{u_x'u_z'}}{\partial x}-\frac{\partial \overline{u_y'u_z'}}{\partial y}-\frac{\partial \overline{u_z'u_z'}}{\partial z}+\nu\Delta\overline{u}_z+f_z
\end{aligned} \qquad [8.21]$$

The six double correlations $\overline{u_x'u_x'}$, $\overline{u_y'u_y'}$, $\overline{u_z'u_z'}$, $\overline{u_x'u_y'}$, $\overline{u_x'u_z'}$, and $\overline{u_y'u_z'}$ are called "Reynolds stresses," and are turbulent momentum fluxes.

The approach to turbulence modeling introduced above brings new turbulent flux terms into equations [8.20] and [8.21]. A "closure problem" arises for the system of equations, as it is necessary to model the $\overline{u_x'c'}$, $\overline{u_y'c'}$, and $\overline{u_z'c'}$ or $\overline{u_x'u_x'}$, $\overline{u_y'u_y'}$, $\overline{u_z'u_z'}$, $\overline{u_x'u_y'}$, $\overline{u_x'u_z'}$, and $\overline{u_y'u_z'}$ terms in order to solve the dispersion of a passive scalar or the Reynolds equations, respectively. We deal with this step in the following section, by presenting the mixing length model. Modeling turbulent fluxes is the key step to evaluate turbulence-generated transfers.

8.6. Modeling turbulent fluxes using the mixing length model

The mixing length model is the simplest approach to modeling the turbulent flux of a given quantity. The fundamental idea is that the turbulent flux of a quantity in a given direction is zero unless the average value of that quantity exhibits a non-zero gradient in that direction. Let us illustrate this concept by considering, as depicted in

Figure 8.4, that the average concentration is steady and only has a gradient along the *Oz* direction. Therefore, $\overline{c}$ depends only on *z*, and we consider the case in Figure 8.4, where $\mathrm{d}\overline{c} / \mathrm{d}z > 0$. For simplicity, we assume here that the flow has no turbulence-average component. The turbulent flux in the *Oz* direction is known through the $\overline{u_z'c'}$ correlation (the other correlations, $\overline{u_x'c'}$ and $\overline{u_y'c'}$, equal zero).

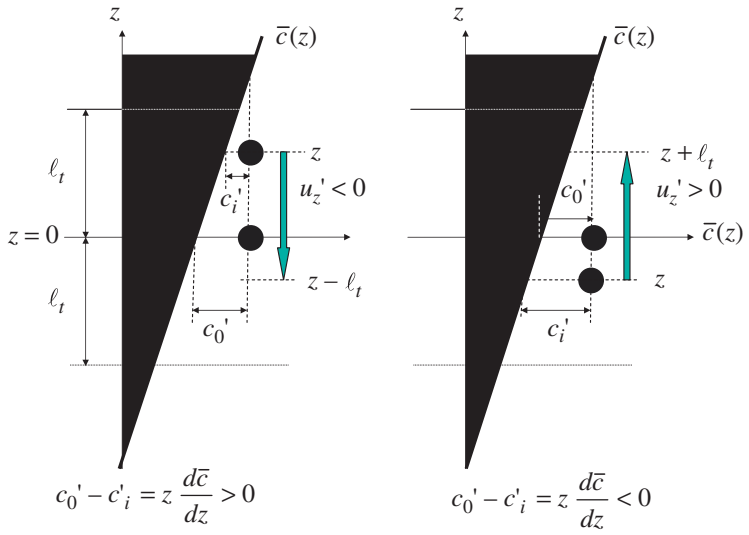

Figure 8.4. *Modeling of turbulent flux* $\overline{u_z'c'}$ *by the mixing length model in the case where* $\mathrm{d}\overline{c} / \mathrm{d}z > 0$. *The diagrams on the left and right describe the change in concentration fluctuation for a fluid particle carried downward or upward, respectively*

To calculate $\overline{u_z'c'}$ at a point *z*, the contributions to $\overline{u_z'c'}$ of particles from above (for which $u_z' < 0$) and of particles from below (for which $u_z' > 0$) are evaluated separately. This evaluation is performed using the probability density function introduced in section 8.1. Every value of the turbulent velocity, u_z', intervenes in average in proportion to the probability density function $p(u_z')$. The distribution will remain undetermined in the following; it will only be assumed to be symmetrical, i.e.:

$$p(u_z') = p(-u_z') \qquad [8.22]$$

The mixing length model involves a process whereby turbulence ensures movement of particles by a distance ℓ_t in the *Oz* direction with some of them being moved downward and others upward. In reality, mixing occurs on different scales.

We do not take into account this complexity, which does not affect the general idea underlying the model. The particles retain their concentration during these random motions, and subsequently mix into the surrounding fluid.

Let us consider a particle passing through the $z = 0$ plane from below (right-hand side of Figure 8.4). That particle is carried by a velocity $u_z' > 0$. Its initial position z was necessarily included in the interval $[-\ell_t, 0]$. Since no particular position within that interval is preferred, the probability for the initial position of the particle to be between $z - \mathrm{d}z/2$ and $z + \mathrm{d}z/2$ is dz / ℓ_t. Denoting by c_i' the difference between the concentration in the particle and the average concentration $\overline{c}(z)$ when it was initially at z, and by c_0' the difference with the average concentration $\overline{c}(0)$ when the particle passes through $z = 0$, the values of c_i' and c_0' differ due to the gradient of average concentration. The concentration fluctuation, c_0', is determined by assuming that the particle retains its concentration as it is being carried by the turbulent eddy. This is represented in Figure 8.4 by the grayscale gradation superimposed onto the variation of the average concentration $\overline{c}(z)$ in the Oz direction, while the color remains unmodified inside the particle. The concentration fluctuations, c_i' and c_0', are therefore linked together by:

$$\overline{c}(0) + c'_0 = \overline{c}(z) + c'_i \qquad [8.23]$$

Concentrations c_i' and c_0' are easy to evaluate graphically in Figure 8.4, and we deduce from [8.23] that:

$$c'_0(z) = \overline{c}(z) - \overline{c}(0) + c'_i \approx c'_i + z\frac{\mathrm{d}\overline{c}}{\mathrm{d}z}(0) \qquad [8.24]$$

by using Taylor's expansion to express the difference in average concentration between z and 0.

All particles passing with positive velocity through $z = 0$ contribute to the turbulent flux of concentration through the statistical average:

$$\begin{aligned}\overline{u_z' c'}_+ &= \int_0^\infty p(u_z') u_z' \left\{ \int_{-\ell_t}^0 c'_o \frac{\mathrm{d}z}{\ell_t} \right\} \mathrm{d}u_z' = \int_0^\infty p(u_z') u_z' \left\{ \int_{-\ell_t}^0 \left[c'_i + \frac{\mathrm{d}\overline{c}}{\mathrm{d}z} z \right] \frac{\mathrm{d}z}{\ell_t} \right\} \mathrm{d}u_z' \\ &= \int_0^\infty p(u_z') u_z' \left\{ \int_{-\ell_t}^0 c'_i \frac{\mathrm{d}z}{\ell_t} \right\} \mathrm{d}u_z' - \frac{\ell_t}{2} \frac{\mathrm{d}\overline{c}}{\mathrm{d}z} \int_0^\infty p(u_z') u_z' \mathrm{d}u_z'\end{aligned} \qquad [8.25]$$

Here, we have taken into account all possible velocities $u_z' > 0$, with their associated probability, as well as all possible initial positions of the fluid particle.

A similar calculation for particles going through $z = 0$ with a negative velocity provide a contribution to the turbulent flux of concentration amounting to:

$$\overline{u_z'c'}_- = \int_{-\infty}^{0} p(u_z')u_z' \left\{ \int_0^{\ell_t} c'_i \frac{\mathrm{d}z}{\ell_t} \right\} \mathrm{d}u_z' + \frac{\ell_t}{2} \frac{\mathrm{d}\overline{c}}{\mathrm{d}z} \int_{-\infty}^{0} p(u_z')u_z' \mathrm{d}u_z' \qquad [8.26]$$

The turbulent flux of concentration is the sum of these two contributions. We obtain:

$$\begin{aligned} \overline{u_z'c'} = \overline{u_z'c'}_+ + \overline{u_z'c'}_- &= -\frac{\ell_t}{2} \frac{\mathrm{d}\overline{c}}{\mathrm{d}z} \left\{ \int_0^{\infty} p(u_z')u_z' \mathrm{d}u_z' - \int_{-\infty}^{0} p(u_z')u_z' \mathrm{d}u_z' \right\} \\ &= -\frac{\ell_t}{2} \frac{\mathrm{d}\overline{c}}{\mathrm{d}z} \int_{-\infty}^{\infty} p(u_z')|u_z'| \mathrm{d}u_z' \end{aligned} \qquad [8.27]$$

In this expression, we have used the symmetry (equation [8.22]) of the probability density function $p(u_z')$. The contributions of c_i' vanish, since we must also consider all possible values of c_i', which cancel each other out because the fluctuations of u_z' and c_i' are uncorrelated. The result for the mixing length model is therefore written in the form:

$$\overline{u_z'c'}(z) = -\kappa_t \frac{\mathrm{d}\overline{c}}{\mathrm{d}z}(z) \qquad [8.28]$$

The properties underlying this relation are emphasized as follows:

– The existence of a non-zero turbulent flux of concentration depends on the existence of a gradient in the average concentration. When the average concentration is homogeneous in space, obviously $\overline{u_z'c'} = 0$, since there is nothing to mix.

– Relation [8.28], with its minus sign, is of the same nature as Fick's diffusion law: the direction of transfer is opposite to the direction of the gradient, so as to homogenize concentrations in space.

– The constant κ_t, called turbulent diffusion coefficient, has the dimension of a diffusion coefficient $(\mathrm{m}^2 \cdot \mathrm{s}^{-1})$. It has the order of magnitude of the product of the rms turbulent velocity by the integral scale of turbulence.[4] We write:

$$\kappa_t \approx u_{\mathrm{rms}} \ell_t \qquad [8.29]$$

4 The concept of molecular diffusion is similar to the mixing length model. In statistical physics, the molecular diffusion coefficient is proportional to the product of a velocity derived from the stirring velocity and a length given by the distance travelled by a particle before a collision with another particle.

Turbulent diffusion is much faster than molecular diffusion.

The mixing length model, therefore, leads to the following relations:

$$\overline{u_x\,'c'} = -\kappa_t \frac{\partial \overline{c}}{\partial x},\ \overline{u_y\,'c'} = -\kappa_t \frac{\partial \overline{c}}{\partial y},\ \text{and}\ \overline{u_z\,'c'} = -\kappa_t \frac{\partial \overline{c}}{\partial z} \qquad [8.30]$$

By substituting relations [8.30] into [8.20], the averaged advection-diffusion equation for the turbulence-average concentration becomes:

$$\frac{\partial \overline{c}}{\partial t} + \left(\overline{\vec{u}} \cdot \nabla\right)\overline{c} = \mathrm{div}\left\{\left(\kappa + \kappa_t\right)\nabla \overline{c}\right\} \qquad [8.31]$$

The turbulent and molecular diffusion coefficients add up together. The former is much larger than the latter, when the flow is turbulent.[5]

8.7. Turbulent dispersion

The elementary modeling of turbulence presented in this chapter associates turbulence with a diffusion process, which is quantified by the turbulent diffusion coefficient κ_t which is added to the molecular diffusion coefficient κ. An analysis of the diffusion equations enables us to distinguish the main properties of their solutions. From these, we deduce an evaluation of the characteristic time needed to perform a diffusion process up to a known length scale.

We present in section 8.9 an exact solution to the diffusion equation for the axisymmetrical diffusion of a dye spot and, in Chapter 9 (section 9.2), another exact solution for a unidirectional diffusion configuration. Those solutions substantiate the properties stated in the following.The first observation that can be elicited from examining [8.31] is that concentration varies with time, under the effect of diffusion, only in those zones where there exists a concentration gradient (incidentally, a constant gradient is not sufficient, since the Laplacian is a second derivative). One is thus led to investigate the gradient zones, which are found to widen with time. Figure 8.5 depicts a concentration gradient zone along a direction *Ox*, at two consecutive points in time, t_1 and t_2. Considering time t_1, for which the width of the

---

5 $(\kappa + \kappa_t)$ is placed in [8.31] inside the divergence term because, in many cases, turbulence is not homogeneous, so that u_{rms}, ℓ_t, and κ_t vary in space. The framework of homogeneous turbulence remains valid as long as the the spatial variations of u_{rms} and ℓ_t are small over a distance of the order of the integral scale. The *k*-ε model introduced in section 8.8 models the spatial variations of u_{rms} and ℓ_t.

gradient zone is $\delta(t_1)$, the diffusion process is quantified by the concentration flux at the center x_C of the gradient zone, which transfers concentration from the area located to the left of x_C to the area located to the right of x_C. The concentration distribution in the gradient zone changes with time, being linked to the diffusive flux through mass conservation:

$$(\kappa_t + \kappa)\frac{2\Delta C}{\delta(t_1)}\mathrm{d}t \approx -\frac{1}{2}\frac{\Delta C\delta(t_2)}{2} + \frac{1}{2}\frac{\Delta C\delta(t_1)}{2} + \Delta C\frac{(\delta(t_2)-\delta(t_1))}{2} \qquad [8.32]$$

The left-hand term is the order of magnitude of the amount of matter transferred during the time interval $\mathrm{d}t = t_2 - t_1$ from the left to the right through the x_C plane, whereas the right-hand term is the variation, between time points t_1 and t_2, of the concentration integral over interval $\left[x_C, x_C + \delta(t_2)/2\right]$, assuming the gradient to be homogeneous. The 2ΔC rise in concentration through the gradient zone remains constant in time, so that:

$$\frac{\partial\delta(t_1)}{\partial t} \approx 8\frac{\kappa_t + \kappa}{\delta(t_1)} \qquad [8.33]$$

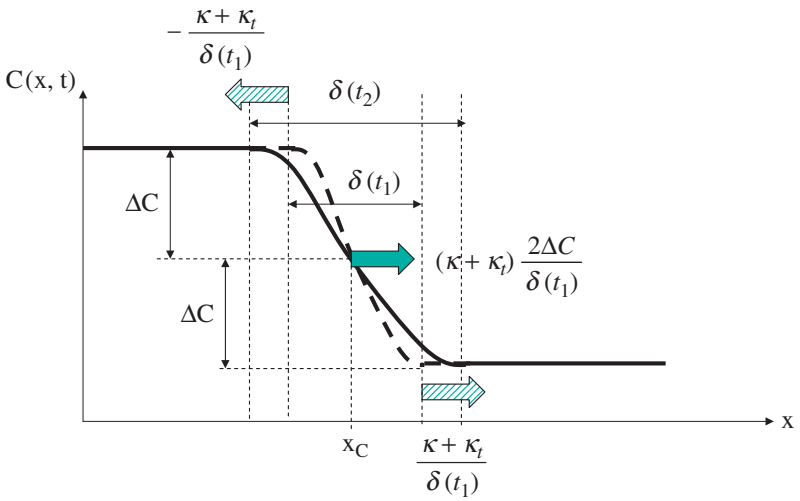

Figure 8.5. *Time evolution under the effect of diffusion, between time points t_1 and t_2, of the concentration within a zone where the concentration varies with a homogeneous gradient. The solid arrow represents the diffusive flux, while the hatched arrows show the displacement velocities of the boundaries of the concentration gradient zone*

The rate of expansion of the gradient zone is therefore proportional to $(\kappa_t + \kappa)/\delta(t_1)$, as represented in Figure 8.5. Integrating [8.33] leads to the widening law for the gradient zone:

$$\delta(t) \approx \sqrt{\delta_0^2 + A(\kappa_t + \kappa)t} \qquad [8.34]$$

where δ_0 is the width of the gradient zone at $t = 0$. The constant A depends on the criterion used to define the width of the gradient zone. Further, $A = 16$ when δ is defined based on the concentration gradient, as was the case when deriving [8.33]. The boundary of a dye spot is also often defined by the contour line along which the concentration equals a fraction of the maximum concentration at the center of the spot (in the example presented in section 8.9, $C_{\text{contour}} / C_{\max} = \exp(-1)$, and $A = 16$, too).

When $\delta_0 = 0$, we obtain:

$$\delta(t) = \sqrt{A(\kappa + \kappa_t)t} \qquad [8.35]$$

Thus, we recover the expression obtained for the particular solution presented in section 8.9. The square-root growth law of relations [8.34] and [8.35] is a general property of the solutions of diffusion equations. Taking the reciprocal of [8.35] yields an estimate of a diffusion time, which is the time required to diffuse a scalar quantity up to a length scale L:

$$\tau_{\text{diff}} \approx \frac{L^2}{\kappa + \kappa_t} \qquad [8.36]$$

This relation is used in the following chapters to analyze the mixing process in the context of a chemical reaction.

8.8. The k-ε model

The rms turbulent velocity and the integral length scale are the two elementary variables that describe the mixing and transfer processes brought about by turbulence. In practice, u_{rms} and ℓ_t may vary in space (in the case of inhomogeneous turbulence) and time (in the case of unsteady turbulence). Consequently, tools are needed to describe their evolution in time and space. The k-ε model is the most widely used model that deals with this problem. It is used in numerous computational fluid dynamics codes.

Variables k and ε are directly related to the rms turbulent velocity and to the integral scale. Variable k is the turbulent kinetic energy per unit mass, which is of the same order of magnitude as the squared rms turbulent velocity:

$$k = \frac{\overline{u}_x{}'^2 + \overline{u}_y{}'^2 + \overline{u}_z{}'^2}{2} \approx u_{\text{rms}}^2 \qquad [8.37]$$

Variable ε is the rate of turbulent kinetic energy dissipation per unit mass, which, based on [8.14], can be written as:

$$\varepsilon \approx \frac{u_{\text{rms}}^3}{\ell_t} \qquad [8.38]$$

Describing the evolution of k and ε in time and space is therefore equivalent to determining the variations of u_{rms} and ℓ_t.

The evolution equations for variables k and ε are obtained from the evolution equation for the kinetic energy (Chapter 2, section 2.8), by performing various modeling steps on which we will not elaborate here. We merely write out the result and comment on the physical meaning of the different terms:

$$\begin{aligned} &\frac{\partial k}{\partial t} + \overline{u}_j \frac{\partial k}{\partial x_j} = C_\mu \frac{k^2}{\varepsilon}\left\{\frac{\partial \overline{u}_i}{\partial x_j} + \frac{\partial \overline{u}_j}{\partial x_i}\right\}\frac{\partial \overline{u}_i}{\partial x_j} + \frac{\partial}{\partial x_j}\left\{\frac{C_\mu}{\sigma_k}\frac{k^2}{\varepsilon}\frac{\partial k}{\partial x_j}\right\} - \varepsilon \\ &\underbrace{\frac{\partial \varepsilon}{\partial t} + \overline{u}_j \frac{\partial \varepsilon}{\partial x_j}}_{\text{Advection}} = \underbrace{C_1 C_\mu k\left\{\frac{\partial \overline{u}_i}{\partial x_j} + \frac{\partial \overline{u}_j}{\partial x_i}\right\}\frac{\partial \overline{u}_i}{\partial x_j}}_{\text{Production}} + \underbrace{\frac{\partial}{\partial x_j}\left\{\frac{C_\mu}{\sigma_\varepsilon}\frac{k^2}{\varepsilon}\frac{\partial \varepsilon}{\partial x_j}\right\}}_{\text{Diffusion}} \underbrace{- C_2 \frac{\varepsilon^2}{k}}_{\text{Dissipation}} \end{aligned} \qquad [8.39]$$

In these equations, $\overline{u}_i$ denotes the components of the turbulence-average velocity. Equations [8.39] are summed over indices i and j. The k-ε model uses five constants C_μ, C_1, C_2, σ_k, and σ_ε, whose values were calibrated on the basis of reference experiments.[6] The quantity:

$$\nu_t = C_\mu \frac{k^2}{\varepsilon} \approx u_{\text{rms}} \ell_t \qquad [8.40]$$

is called the "turbulent viscosity." It brings back the notion of a turbulent diffusion coefficient, applied to momentum of the fluid particle.

---

6 The usual values of the constants in the k-ε model are $C_\mu = 0.09$, $C_1 = 1.44$, $C_2 = 1.92$, $\sigma_k = 1$, and $\sigma_\varepsilon = 1.21$. Exercise II at the end of this chapter employs the k-ε model on a grid-turbulence configuration. The exercise leads to a discussion on the value of C_2.

The Reynolds stresses appearing in the Reynolds equations [8.21], whose solution determines the turbulence-average velocity field, are modeled via the mixing length model (equation [8.28]) such as:

$$\overline{u_i' u_j'} = -\nu_t \left(\frac{\partial \overline{u}_i}{\partial x_j} + \frac{\partial \overline{u}_j}{\partial x_i} \right) \qquad [8.41]$$

The equations for k and ε are similar in their form. The physical meaning of the different terms is easily set out:

– The left-hand terms in the equations are the advection terms for k and ε.

– The first term on the right-hand side is a term of energy production by the gradient of the turbulence-average flow. Considering the equation for k, for a sheared, unidirectional averaged flow $\overline{u}_x(z)$, the production term reduces to $C_\mu (k^2/\varepsilon)(\mathrm{d}\overline{u}_x/\mathrm{d}z)^2$. This quantity is positive, meaning that any gradient in the average velocity generates turbulent kinetic energy. This term is particularly active in boundary layers, where the existence of a strong velocity gradient produces turbulence.

– In the second term on the right-hand side, we recognize a turbulent diffusion term, since it takes the form $\mathrm{div}(\kappa \cdot \nabla k)$ or $\mathrm{div}(\kappa \cdot \nabla \varepsilon)$. Diffusion is linked to the existence of gradients in turbulent kinetic energy and in the rate of turbulent kinetic energy dissipation, depending on the quantity considered. The diffusion coefficients, which are proportional to $k^2/\varepsilon = u_{\mathrm{rms}} \ell_t$, are dimensionally linked to the turbulent viscosity (equation [8.40]).

– The last term is always negative. It corresponds to dissipation. Regarding the equation for k, the dissipation term is simply the definition of the rate of dissipation. Regarding the equation for ε, dissipation takes place with the characteristic time of turbulence [8.12], since $\varepsilon^2/k = \varepsilon/\tau_t$.

It is important to note that the equations of the k-ε model are entirely governed by the values of u_{rms} and ℓ_t.

The simple mechanisms of the k-ε model provide for some qualitative understanding of the role played by turbulence in a circular cylindrical pipe (Figure 8.6(a)), at a sufficiently large Reynolds number. They also explain how turbulent kinetic energy is distributed in an established regime, where, sufficiently far from the pipe entrance, the flow and turbulence properties no longer depend on the streamwise coordinate and they only vary with the radial coordinate r. In the central part (lightly shaded in Figure 8.6(a)), the average velocity of the flow is uniform.

As a result, the production of turbulence therein is zero. In addition, dissipation is non-zero. The level of turbulence is maintained by a process of diffusion of turbulent kinetic energy from the boundary layer zone near the walls (darkly shaded) to the central zone, as indicated by the arrows. Turbulence is continuously produced in the boundary layer, where it stabilizes at a level for which production balances dissipation and diffusion toward the central zone. The diffusion of turbulent kinetic energy from the near-wall zone toward the axis of the pipe requires a radial gradient of turbulent kinetic energy such that $\partial k / \partial r > 0$. The $k(r)$ profile is depicted on the right in Figure 8.6(a). Experimental measurements are presented in Figure 8.6(b). The turbulent kinetic energy is plotted in dimensionless form, using the friction velocity u_* defined on the basis of the friction stress at the wall, $\tau(r = R) = \rho u_*^2$. Figure 8.6(b) also illustrates a very important result, namely that the friction velocity, in an established regime, sets the level of turbulence in a pipe.

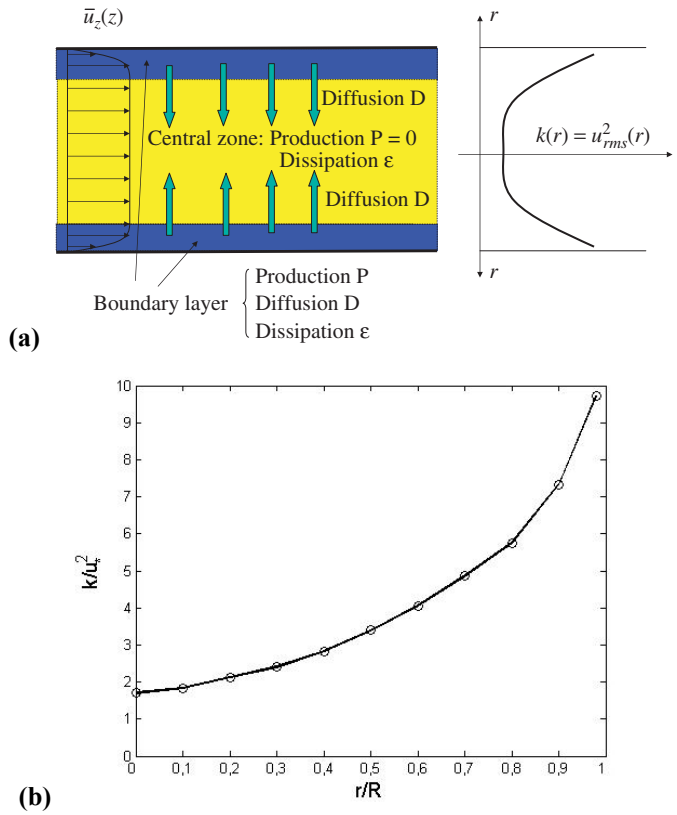

Figure 8.6. *(a) Sketch of the turbulence production, diffusion, and dissipation processes within a pipe flow, in an established regime. (b) Radial profiles of turbulent kinetic energy, based on Laufer's experimental data (1954)*

Equations [8.39] of the k-ε model are transport equations for the turbulent kinetic energy and its rate of dissipation. Their resolution depends on initial and boundary conditions fed into the calculation. For a steady-state flow regime, with the flow forcing being kept constant, solving the equations of the k-ε model with time brings out a transient regime during which the properties of turbulence evolve until they adjust, at all points in space, to the conditions of equilibrium between advection, production, dissipation, and diffusion. Such a transient regime can last for a long time if the initial conditions are far from the equilibrium conditions. For example, if the initial level of turbulence is high as compared to the steady-state value, it is necessary to wait till dissipation effects the desired change before finally adjusting to the steady-state conditions. While the initial conditions, in principle, pose no difficulty, setting boundary conditions remains a delicate task. When fluid is introduced into the computational domain, if the turbulence level at the inlet does not correspond to the actual conditions to be simulated, the solution computed within the domain in a steady-state regime will be affected.

8.9. Appendix: solution of a diffusion equation in cylindrical coordinates

In a simplified case where a product is introduced at time $t = 0$ along an axis Oz, it disperses over time by diffusion from that axis. Assuming that the distribution is initially homogeneous along the Oz axis, dispersion will be two-dimensional (at no time does it depend on the value of the z coordinate) and axisymmetrical around the axis. The concentration value at any given point depends only on the distance r from that point to the Oz axis and on time. Further, $C(t,r)$ is a solution of the diffusion equation written in the cylindrical coordinate system:

$$\frac{\partial C}{\partial t} = \kappa \Delta C = \kappa \frac{1}{r} \frac{\partial}{\partial r}\left(r \frac{\partial C}{\partial r} \right) \qquad [8.42]$$

For the initial condition $C(t = 0, r) = m_o \delta(r)$,[7] the solution is expressed as:

$$C(t,r) = \frac{m_o}{4\pi\kappa t} \exp\left\{ -\frac{r^2}{4\kappa t} \right\} \qquad [8.43]$$

7 The delta function $\delta(r)$ refers to the Dirac "function", which is infinite for $r = 0$, equal to zero for $r \neq 0$, and the integral of which from $r = 0$ to $r = \infty$ equals 1. In addition, m_o is the amount of dye per unit length.

The simplest proof consists in checking that [8.43] is a solution of [8.42] and that $C(t,r) \to m_o\delta(r)$ when $t \to 0$.[8]

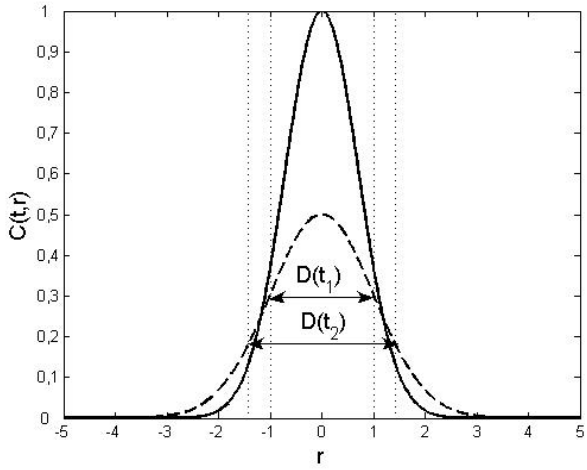

Figure 8.7. *Axisymmetrical diffusion of a dye initially introduced on an axis Oz. Solid line:* $4\kappa t_1 = 1$; *dashed line:* $4\kappa t_2 = 2$

Solution [8.43] is plotted in Figure 8.7 for two consecutive points in time. Further, $m_o / \kappa t$ has the dimension of a concentration. The term $1/4\pi\kappa t$ allows for mass conservation over time, as the amount of dye contained between two planes perpendicular to the *Oz* axis and spaced apart by a unit distance is:

$$\int_0^\infty 2\pi C(t,r) r \mathrm{d}r = m_o \qquad [8.44]$$

In addition, $\sqrt{\kappa t}$ has the dimension of a length. The form of solution [8.43] suggests that $D(t) = \sqrt{16\kappa t}$ could be regarded as a measure of the size of the dye spot at time *t*. The ratio of the concentration over the circle of radius $r = D(t)/2$ to the concentration on the axis is $C(t, D(t)/2) / C(t,0) = \exp(-1)$.

8 It is very difficult to obtain analytical solutions, except for a few sets of simple initial and boundary conditions. The use of Laplace's transform is, in principle, appealing. However, it can only be recommended if one can entrust some pal with the inverse Laplace transform of the solution, in order to revert to the real space, or if the case is simple enough for the inverse Laplace transform to be listed in available textbooks.

While the analytical solution for the initial condition whereby the dye is distributed evenly inside the cylinder of radius $r = 1$ is delicate to derive, its evolution in time is easily described with the help of the properties stated in section 8.7. For short time spans, the thickness of the diffusional zone (concentration gradient zone) increases according to the following law

$$\delta(t) = A\sqrt{\kappa t} \qquad [8.45]$$

as shown diagrammatically in Figure 8.8. When $\delta(t)$ reaches a size of the order of the initial radius of the cylinder ($r = 1$), the dye distribution takes on a Gaussian form approaching solution [8.43]. The maximum concentration at $r = 0$ then starts to decrease, and the diameter of the spot subsequently grows according to a law such that $D(t) \approx \sqrt{16\kappa t}$.

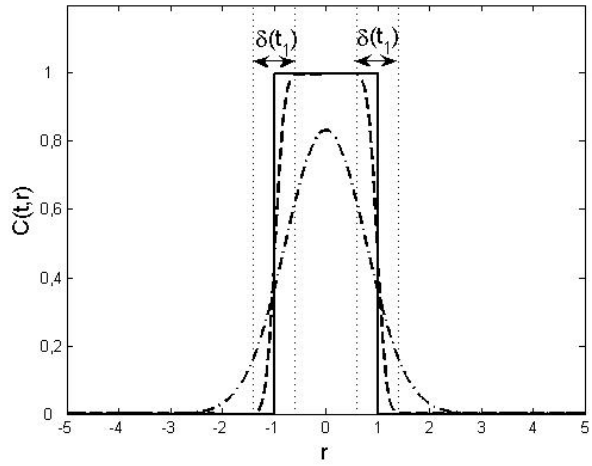

Figure 8.8. *Diffusion of an initially homogeneous dye "spot" in a cylinder of radius r = 1. Solid line: initial concentration; ----: concentration profile for a short time; and -.-.-: concentration profile for a long time*

8.10 Application exercises

Exercise 8.I: Dispersion of fluid streaks introduced into a pipe by a network of capillary tubes

Consider a circular cylindrical pipe of diameter $D = 2R$ in which water flows with an established velocity profile $\overline{u}_z(r)$ whose area-average velocity is $\overline{W}$.

A substance is introduced into plane $z = 0$ by a network of capillary tubes of diameter $d_o = 1$ mm, distributed over a square grid having a mesh size M. The goal is to evaluate the mesh size required to provide a homogeneous dispersion of the substance in the fluid at the pipe's exit ($z = L$).

We study the dispersion of the substance by laminar diffusion, and then by turbulent diffusion, in sequence. The molecular diffusion coefficient of the substance in water is $\kappa = 10^{-5}$ cm^2 s^{-1}.

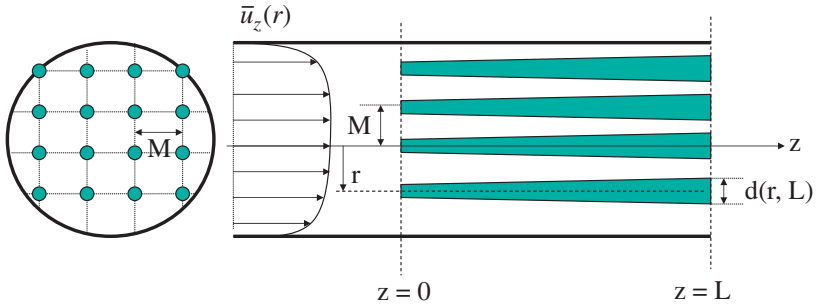

Figure 8.I.1

1. The substance introduced by the capillary tubes disperses inside the pipe in the form of streaks that expand as they move downstream in the pipe (increasing z). A homogeneous concentration distribution is reached when the diameter of the streaks becomes significantly greater than the spacing M between two adjacent streaks.

Prove that the expansion law for the streak whose axis is at a distance r from the axis of the pipe is written as

$$\mathrm{d}(r,z) = \sqrt{d_o^2 + 16(\kappa + \kappa_t)\frac{z}{\overline{u}_z(r)}}$$

$\overline{u}_z(r)$ is the average velocity of the fluid on the axis of the respective streak, and κ_t is the turbulent diffusivity. Which hypothesis is required in order to write this result?

2. The following numerical values are selected: $D = 0.1$ m, $\overline{W} = 0.1$ m s^{-1}, and $L = 20$ m. Although the Reynolds number is $\mathrm{Re} = \overline{W}D/\nu = 10^4$, it is assumed that the flow has been kept laminar. Express the velocity profile inside the pipe. What is the thickness, at the outlet ($z = L$) of the streak located on the axis of the pipe? In which part of the pipe is dispersion the least effective?

3. The following numerical values are selected: $D = 0.4$ m, $\overline{W} = 0.5$ m s^{-1}, and $L = 20$ m. The Reynolds number is $\mathrm{Re} = \overline{W}D/\nu = 2\times10^5$, and the flow is turbulent. We wish to evaluate the thickening of three streaks located at distances $(R-r) = 0.05R$, $(R-r) = 0.5R$, and $(R-r) = R$ from the pipe wall.

– Determine the friction stress τ exerted by the flow on the pipe wall, in order to derive there from the friction velocity u_* defined by the relation $\tau = \rho u_*^2$.

– Evaluate the velocity of the turbulence-average flow in each of the three streaks, using the logarithmic law (derived from boundary layer theories not covered in this book):

$$\overline{u}_z(r) = u_* \left\{ \frac{1}{0.4} \ln\left(\frac{u_*(R-r)}{\nu} \right) + 5.5 \right\}$$

Comment on the results.

– Evaluate the rms turbulent velocity in the three dye streaks, using the turbulent kinetic energy profile measured by Laufer (1954) (Figure 8.6(b) of this chapter).

– It is assumed that the integral scale varies linearly between the wall and the axis of the pipe according to the relation $\ell_t(r) = 0.1(R-r)$. Determine the turbulent diffusion coefficient for each of the streaks. Is it justified to neglect the molecular diffusion of the constituent?

– What is the diameter of the three streaks at their exit from the pipe? Suggest a value M for the capillary tube spacing providing a homogeneous dispersion of the substance over the crosssection at $z = L$.

Exercise 8.II: Grid turbulence and k-ε modeling

Consider the situation (see Figure 8.II.1) where turbulence is generated by channeling a flow through a grid. Turbulent energy is produced in the wake downstream the grid bars. Beyond this turbulent production zone ($x > x_o$), the turbulent energy carried by the flow decreases due to the effect of dissipation. The mean flow $\overline{u}_x = U$ is a uniform flow along the Ox direction, and the turbulent velocity $u_{\mathrm{rms}}(x)$ and integral scale $\ell_t(x)$ vary only with the x coordinate. The aim of this exercise is to describe such variations by studying the way they are modeled by the k-ε model. The values $u_{\mathrm{rms}}(x_o) = u_o$ and $\ell_t(x_o) = \ell_o$ are assumed known at the beginning of the dissipation zone.

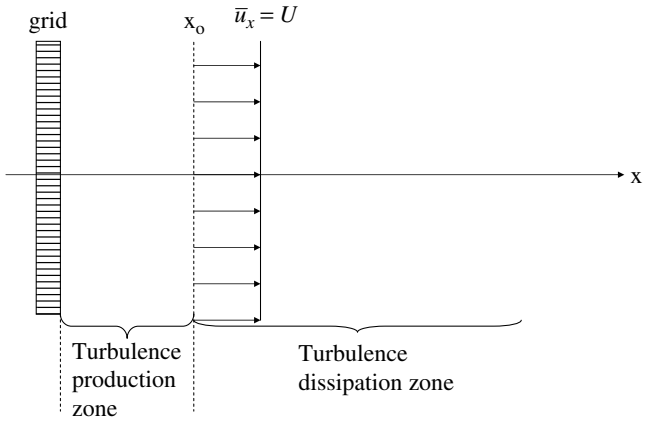

Figure 8.II.1

1. Write the equations of the k-ε model for this situation, retaining only non-zero terms. For the remainder of this exercise, diffusion terms in the Ox direction will be neglected (it will be easily verified, at the end of the exercise, that these terms are indeed negligible).

2. The equations of the k-ε model are coupled and nonlinear, which makes their resolution non-trivial. Prove that the two equations of the k-ε model can be combined to establish that:

$$\frac{\partial}{\partial t}\left(k\varepsilon^n\right) = 0 \text{ for } n = -1/C_2$$

This results in $\varepsilon(x)/\varepsilon_o = \left(k(x)/k_o\right)^{C_2}$. Use this relation to integrate the evolution equation for $k(x)$ and prove that:

$$\frac{k(x)}{k_o} = \left\{1 + (C_2 - 1)\frac{\varepsilon_o x}{k_o U}\right\}^{1/(1-C_2)}$$

$$\frac{\varepsilon(x)}{\varepsilon_o} = \left\{1 + (C_2 - 1)\frac{\varepsilon_o x}{k_o U}\right\}^{C_2/(1-C_2)}$$

3. Adapt the results obtained in Question 2 to determine the variations with x of the turbulent velocity $u_{\text{rms}}(x)$, of the integral scale $\ell_t(x)$, and of the turbulent Reynolds number $\text{Re}_t(x)$.

4. Comment upon the solution obtained when $C_2 = 2$. Why is it necessary that $C_2 < 2$ for the solution of the k-ε model to be physically meaningful?

For the usual k-ε model, $C_2 = 1.92$. Determine the variations with x of the turbulent velocity $u_{\text{rms}}(x)$, of the integral scale $\ell_t(x)$, and of the turbulent Reynolds number $\text{Re}_t(x)$ in this case, and comment on the solution.

Does the integral scale increase or diminish as the energy of turbulence decreases?

Chapter 9

Hydrodynamics and Residence Time Distribution – Stirring

We discuss in this chapter the link between the theory of turbulent diffusion/ dispersion presented in Chapter 8 and two classical tools of chemical engineering.

The first of these is the residence time distribution (RTD) method. This technique allows us to classify the dispersion properties of a constituent in a chemical reactor, with reference to ideal behaviors of simple reactors. The RTD theory does not explicitly associate a RTD with a flow configuration inside the reactor. We examine this particular issue when the flow is turbulent, by considering successively the cases of a tubular reactor with axial dispersion and of a continuous stirred tank reactor (CSTR). Matching up the dimensions of the reactor with the mean residence time and the velocity and length scales of turbulence allows the determination of the hydrodynamic conditions associated with either type of reactor, for which the RTD laws are recovered, using the turbulent dispersion concepts introduced in Chapter 8.

Section 9.2 of this chapter addresses the issue of stirring in a reactor. We introduce the primordial elements, from a mechanical point of view, for dimensioning a stirrer:

– The characterization of a stirrer by its power number and the link between this quantity and the rate of turbulent energy dissipation.

– The link between the mixing time and the rate of turbulent energy dissipation.

Both these concepts are recurrent in the dimensioning of stirrers, as observed by reading specialized textbooks.[1]

In this chapter, as in the previous one, we stress that the notion of mixing remains at the turbulent dispersion level. Mixing at the molecular scale, which enables chemical reactions to occur, is not necessarily carried out. We are thus dealing with "macromixing", as opposed to "micromixing", where mixing at the molecular level is carried out. Micromixing is discussed in Chapters 10–12.

9.1. Turbulence and residence time distribution

9.1.1. *Notion of residence time distribution*

The RTDs are a technique for analyzing the behavior of a reactor pertaining to the experimental protocol given in Figure 9.1. We consider a reactor of volume V in which chemical substances are introduced in a steady-state regime through one or more ports, and tapped via a single discharge pipe. A simple RTD experiment is carried out by injecting, at the reactor's inlet, a product over a very short period at time $t = 0$. If concentration is measured as a function of time in the zone of injection, its time variations assume the form of a delta function, as the product is carried away by the flow.

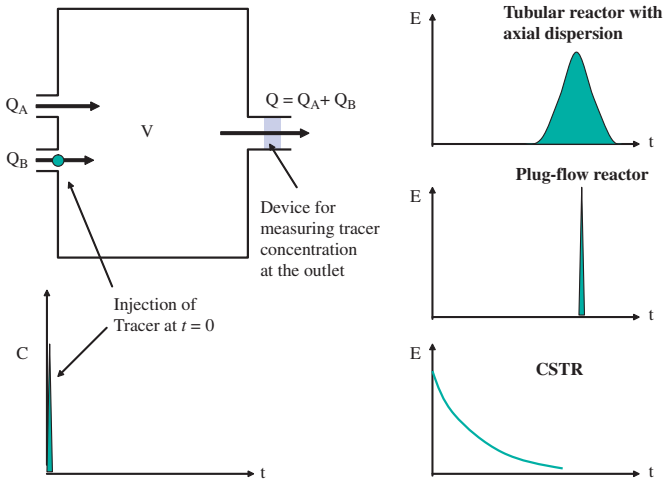

Figure 9.1. *Principle for determining the RTD of a reactor, and plots of three classical RTD functions*

1 See edited book *Agitation and Mélange*, by C. Xuereb, M. Poux, and J. Bertrand (Dunod, Paris, 2006).

The RTD experiment consists of measuring the time variations of concentration $C_s(t)$ in the outlet section of the reactor. Experimentally, the products injected are often ions, and the measurement of concentration level is performed by measuring the electrical conductivity at the reactor's outlet. What is actually plotted is the normalized concentration:

$$E(t) = \frac{C_s(t)}{\int_0^\infty C_s(t) \cdot \mathrm{d}t} \qquad [9.1]$$

which is the probability density function of the mass fraction of constituent leaving the reactor at time t after being introduced into the reactor (it can be verified that $\int_0^\infty E(t)\mathrm{d}t = 1$). The average value, $\tau_{\text{residence}} = \int_0^\infty tE(t)\mathrm{d}t$, is the mean residence time inside the reactor. The term residence time distribution (RTD) attached to $E(t)$ follows from these facts.

Three classical RTDs are plotted in Figure 9.1. Generally speaking, it is expected that the product will start leaving the reactor after a certain time, and that not all the injected product will leave the reactor at the same time. When the RTD varies with time as a Gaussian function whose maximum value is shifted with respect to the time of injection, it is recognized as the RTD of a tubular reactor with axial dispersion. We study this case in the following section. The other two classical RTD shown in Figure 9.1 correspond to the so-called "ideal" reactors, inasmuch as they represent simple limiting behaviors. The RTD of a "plug-flow reactor" is a delta function that is shifted in time with respect to the time of injection. All the particles that pass through the reactor have an identical history. This is the limiting behavior of a tubular reactor with axial dispersion, when axial dispersion becomes zero. In a "continuous stirred tank reactor (CSTR)", the stirring is ideally sufficiently effective to homogenize the average concentration inside the reactor after a very short time in comparison to the residence time. It can then be shown (this case is also discussed in section 9.1.2) that the RTD decreases exponentially with time.

9.1.2. *Modeling RTD via a turbulent diffusion approach: cases of a tubular reactor with axial dispersion and of a CSTR*

Consider a cylinder-shaped reactor (Figure 9.2), of length L and diameter D_R. By referring it as tubular, it is assumed that $D_R << L$. This reactor operates in a continuous regime with a steady-state flow rate, Q, going through it. The reactor is not necessarily empty. It may contain a packing, made up of solid elements, between which the fluid flows. The hydrodynamic regime is assumed to be turbulent. When the reactor does not contain a packing, turbulence is only generated

by the sudden expansion at the reactor's inlet and by friction due to the flow on the reactor wall. A packing serves to produce turbulence, through the head losses that it effects in the flow. We analyze a situation where turbulence is homogeneous. The turbulent velocity, u_{rms}, and the integral scale, ℓ_t, have identical values at all points in the reactor, and the turbulent diffusion coefficient $\kappa_t = u_{\text{rms}}\ell_t$ (equation [8.29] of Chapter 8) is therefore also homogeneous within the reactor. As a result, the flow inside the reactor spreads rapidly to become uniform over a through flow section of the reactor. Similarly, a volume containing a constituent, injected at the reactor's inlet, disperses inside the reactor in the form of a "spot," which is carried by the mean flow while expanding.

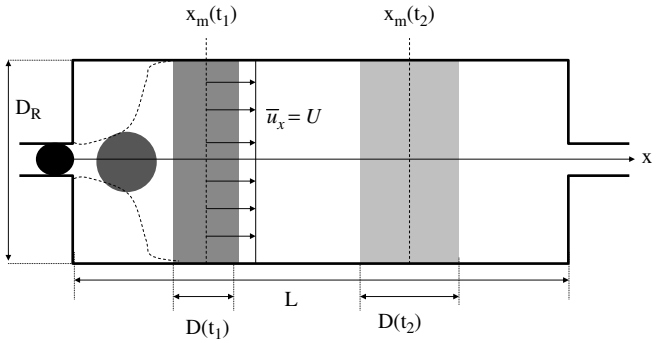

Figure 9.2. *Geometrical definitions for a tubular reactor*

Both these phenomena are depicted in Figure 9.2. The drawing is stretched in the lateral direction relative to the *Ox* direction, to better represent the detail of the flow in the through flow section. We denote by t_1 the period of time after which the dye spot and the flow have dispersed over the through flow section of the reactor. When turbulence is homogeneous and isotropic, the size of the spot is the same at time t_1 in the streamwise direction (along *Ox*) as in the cross-wise direction (perpendicularly to the *Ox* direction), which is not the case in Figure 9.2 because of distortion in the drawing. At a later time t_2, the spot would be carried along the *Ox* direction and expand in the streamwise direction. The time periods required to disperse the product in both the lateral (cross-wise) and axial (streamwise) directions of the tube are evaluated using the results obtained in Chapter 8 (equation [8.36]):

$$\tau_{\text{Disp,lateral}} = \frac{D_R^2}{\kappa_t}$$
$$\tau_{\text{Disp,axial}} = \frac{L^2}{\kappa_t} \qquad [9.2]$$

In these expressions, molecular diffusion has been neglected relative to turbulent diffusion. When the reactor is sufficiently long, ($D_R << L$), the distance after which the spot has dispersed laterally and the flow has become uniform over the available flow section is small compared to the length of the reactor, and the main process observed inside the reactor is the transport of the spot inside the reactor and its gradual expansion along the axial direction. It is this phenomenon that we model by employing the concept of turbulent dispersion introduced in Chapter 8. For this reactor, the mean residence time is related simply to velocity U of the mean flow:

$$\tau_{\text{residence}} = \frac{L}{U} \qquad [9.3]$$

The situation we are about to examine corresponds to the condition:

$$\tau_{\text{Disp,lateral}} << \tau_{\text{residence}} << \tau_{\text{Disp,axial}} \qquad [9.4]$$

The residence time in the reactor is sufficiently long for lateral dispersion to be regarded as instantaneous, but it is too short to give the product enough time to disperse over the whole length of the reactor. Condition [9.4] obviously requires the hypothesis $D_R << L$.

Figure 9.2 shows the geometrical characteristics of the evolution over time of the travel and growth of the spot. We denote by $x_m(t)$ the middle position of the spot at time t, and by $D(t)$ its thickness. Because of [9.4], the space and time evolution of the average concentration $\overline{c}(x,t)$ inside the reactor depend only on time and on the x coordinate. It is governed by the averaged diffusion equation (equation [8.31] of Chapter 8):

$$\frac{\partial \overline{c}}{\partial t} + U\frac{\partial \overline{c}}{\partial x} = \kappa_t \frac{\partial^2 \overline{c}}{\partial x^2} \qquad [9.5]$$

where molecular diffusion is neglected. The solution is required for the initial condition:

$$\overline{c}(x, t=0) = C_o \delta(x) \qquad [9.6]$$

(δ is the delta function and $x = 0$ coincides with the reactor's inlet.) With the variable change ($t' = t$, $x' = x - Ut$), [9.5] becomes:

$$\frac{\partial \overline{c}}{\partial t'} = \kappa_t \frac{\partial^2 \overline{c}}{\partial x'^2} \qquad [9.7]$$

The solution is determined by a method similar to the one described in section 8.9 of Chapter 8. For the initial condition [9.6], it is written as[2]:

$$\overline{c}(x,t) = \frac{\mathrm{A}}{\sqrt{t'}} \exp\left\{-\frac{x'^2}{4\kappa_t t'}\right\} = \frac{\mathrm{A}}{\sqrt{t}} \exp\left\{-\frac{(x-Ut)^2}{4\kappa_t t}\right\} \qquad [9.8]$$

To determine the RTD by substituting $\overline{c}(x,t)$ into [9.1], it is not necessary to know the constant A. The integral in the denominator of [9.1] is evaluated by observing that the total amount of constituent is equal to the flux of constituent integrated over time:

$$\int_{-\infty}^{+\infty} \overline{c}(x,t)\mathrm{d}x = U \int_{0}^{+\infty} \overline{c}(L,t)\mathrm{d}t \qquad [9.9]$$

Explicit calculation of the left-hand-side integral for solution [9.8] leads to:

$$\int_{0}^{+\infty} \overline{c}(L,t)\mathrm{d}t = \frac{\mathrm{A}}{U}\sqrt{4\pi\kappa_t} \qquad [9.10]$$

The RTD is then expressed as:

$$E(t) = \frac{U}{\sqrt{4\pi\kappa_t t}} \exp\left\{-\frac{(L-Ut)^2}{4\kappa_t t}\right\} \qquad [9.11]$$

We recover the classic form of the RTD for a tubular reactor with axial dispersion:

$$E(t) = \sqrt{\frac{Pe}{4\pi\tau_{\text{residence}} t}} \exp\left\{-Pe\frac{(\tau_{\text{residence}} - t)^2}{4\tau_{\text{residence}} t}\right\} \qquad [9.12]$$

using the residence time defined by [9.3] and the Péclet number[3],

---

2 Solution [9.8] mainly differs from solution [8.43] obtained in Chapter 8 in that, in the present case, the maximum concentration decreases as $1/\sqrt{t}$, whereas it decreases as $1/t$ for the solution given in Chapter 8. This difference ensures mass conservation in both cases. Here, diffusion is unidirectional along the *Ox* axis, whereas it is axisymmetric about an axis in Chapter 8.

3 The Péclet number thus defined is the one classically used in RTD models. It differs from the one more commonly introduced in turbulence theories, $Pe_t = \kappa_t / \kappa \approx (u_{\text{rms}}\ell_t)/\kappa$, where κ is the molecular diffusivity of constituents.

$$Pe = \frac{UL}{\kappa_t} \qquad [9.13]$$

The hypothesis [9.4], under which we have just recovered the RTD law for a tubular reactor with axial dispersion, can be restated in the form of a bounding of the turbulence intensity between two values comparing the dimensions of the reactor to the integral scale of turbulence:

$$\frac{D_R^2}{\ell_t L} << \frac{u_{\text{rms}}\tau_{\text{residence}}}{L} = \frac{u_{\text{rms}}}{U} << \frac{L}{\ell_t} \qquad [9.14]$$

Consider now the case of a CSTR. As indicated in section 9.1.1, the behavior of an ideal CSTR is observed when the dispersion inside the reactor is very fast with respect to the residence time. The average concentration, $\overline{c}$, is thus kept homogeneous irrespective of time inside the reactor. For a perfectly stirred reactor, we do not distinguish the axial dimension, L, from the lateral dimension, D_R, as we did for the tubular reactor ($D_R << L$), because the two scales are usually comparable. Using the dispersion time (equation [9.2]) for a single dimension L of the reactor, the hydrodynamic regime of a perfectly stirred reactor therefore corresponds to the following condition:

$$\tau_{\text{Disp}} << \tau_{\text{residence}}, \text{ i.e. } \frac{L}{\ell_t} << \frac{u_{\text{rms}}\tau_{\text{residence}}}{L} \qquad [9.15]$$

Under this condition, the average concentration, $\overline{c}$, of the injected product becomes homogeneous inside the reactor after a transient process, whose duration is of the order of τ_{Disp}, and then decreases with time as the product leaves the reactor. The variations $\overline{c}(t)$ are derived from the mass balance for the amount of product present inside the reactor:

$$V\frac{\mathrm{d}\overline{c}}{\mathrm{d}t} = -Q\overline{c} \qquad [9.16]$$

which can be readily integrated to establish the exponential decrease of the RTD in an ideal CSTR:

$$E(t) = \frac{1}{\tau_{\text{residence}}}\exp\left(-\frac{t}{\tau_{\text{residence}}}\right) \qquad [9.17]$$

The residence time depends on volume V of the reactor and flow rate Q through:

$$\tau_{\text{residence}} = \frac{V}{Q} \qquad [9.18]$$

Condition [9.15], which is associated with the regime of a CSTR, implies a high level of turbulence and/or a long residence time. If turbulence is only produced by the mean flow (friction on walls or head loss), the turbulence level produced is usually insufficient to verify [9.15]. For this reason, perfectly stirred reactors usually embody stirrers as the main source of turbulence, as explained in the following section.

We have determined in this section the hydrodynamic conditions on a turbulent flow that lead to the RTD laws of a CSTR or a tubular reactor with axial dispersion. The reverse analysis, for deriving turbulence characteristics of a flow from the measurement of a RTD, should be used with caution if it cannot be positively asserted that the flow is turbulent. A laminar flow (e.g. a Poiseuille flow) in a tubular reactor also produces an axial dispersion measured by a RTD, because the product injected on the pipe axis is carried faster than that injected near the walls. Clearly, it would be meaningless to derive turbulence characteristics from the measured RTD law.[4]

9.2. Stirring

9.2.1. *Mechanical characterization of a stirrer*

By stirrer, we generally mean a moving system (consisting of a rotor equipped with blades) which, when rotating, produces in a reactor a mean flow and some turbulence. Such a device obviously differs from a static mixer, wherein a complex geometrical configuration of the reactor forces the flow to acquire kinematics that promotes the mixing of fluid particles.[5]

4 The reader is referred to Chapter 15 of the book by J.P. Couderc, C. Gourdon, and A. Liné (*Phénomènes de transfert en génie des procédés*, Lavoisier, 2008) and in particular to its section 6, which explains how the non-uniformity of velocity profiles contributes to the dispersion of a tracer. This effect is less significant in turbulent flow than it is in laminar flow, as turbulence tends to render the velocity profile uniform (see Exercise 8.I of Chapter 8).

5 For static mixers, Chapters 12–14 in *Agitation et Mélange*, edited by C. Xuereb, M. Poux, and J. Bertrand (Dunod, Paris, 2006) might be perused.

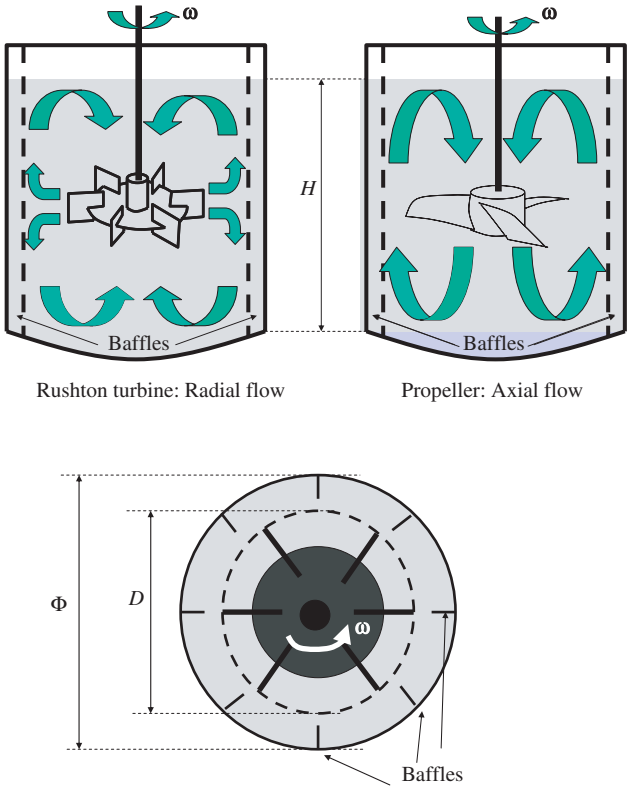

Figure 9.3. *Flow patterns generated in a reactor according to the type of moving stirring body*

The geometry (shape and dimension) of a stirrer and its insertion into a reactor influence the characteristics of a stirring system.[6] We limit ourselves here by indicating that the different stirrers are distinguished primarily by the nature of the flow produced inside the reactor, and underscoring the common features between stirrers and pumps (Chapter 5). The stirrer produces a recirculation flow within the vessel. An axial flow is produced by a propeller-type stirrer, as with an axial pump. When the plane containing the blades of the stirrer is parallel to the stirrer's axis of rotation, the rotation generates a centrifugal force, which ejects the fluid radially, in a similar fashion to a centrifugal pump. Figure 9.3 depicts the recirculations produced by a stirrer in a closed vessel, according to the type of moving stirring body. The rotation of the stirrer also generates a solid-body rotation movement of

6 Chapter 3 in *Agitation et Mélange* (*ibid*) presents a synthesis of the various stirring devices classically implemented.

the fluid inside the vessel, which is generally undesirable. First, the production of turbulence is linked to the difference between the rotational speed of the blades and the mean velocity of the flow. The rotation of the fluid reduces this difference. Additionally, the solid-body rotation of the fluid produces a radial pressure gradient. When the reactor is not entirely filled, the free surface may be dramatically deformed by the rotation of the fluid, and sometimes go down to the level of the stirrer.[7] The stirring system is, therefore, often associated with the provision of baffles against the vessel walls (Figure 9.3), the purpose of which is to reduce the solid-body rotation of the fluid.

The dimensional analysis describing the operation of a stirrer is akin to that performed for a pump (Chapter 5). For a stirrer whose moving body has a diameter D, arranged inside a tank of height H and diameter Φ, the different quantities characterizing the moving body in mechanical terms (mechanical power consumption, torque, or force exerted on the blades) depend exclusively on the three geometrical parameters cited previously, to which should be added the angular rotational speed $\omega = 2\pi N$ of the moving body, the density ρ, and the viscosity ν of the fluid. The mechanical power is the first quantity of interest to the engineer, as it determines the energy cost of the mixing method. The Vaschy–Buckingham theorem (Chapter 3) states that the power $\wp$ varies according to:

$$N_p = \frac{\wp}{\rho N^3 D^5} = \text{function}\left\{\text{Re} = \frac{ND^2}{\nu}, \frac{D}{\Phi}, \frac{H}{\Phi}, \ldots\right\} \qquad [9.19]$$

We use the rotational speed, N, of the moving body (in revolutions per second) rather than the angular rotational speed, ω, as is customary in the literature. The parameters implied in the ellipsis only involve other length ratios characterizing the geometry of the moving stirring body and of the vessel. The Reynolds number is based on the diameter of the moving body. The quantity N_p is called the power number. Figure 9.4 shows, for a stirrer, the aspect of the power number's variations with the Reynolds number. The turbulent regime is reached for a Reynolds number $\text{Re} > 10^4$, a condition easily exceeded for a typical stirring system in a low-viscosity liquid such as water. In the turbulent regime, the power number is independent from the Reynolds number. Its value depends on the geometry of the moving stirring body and of the vessel (diameter, height, and baffle geometry).

7 A description of these phenomena is given in section 17.2 of Chapter 17.

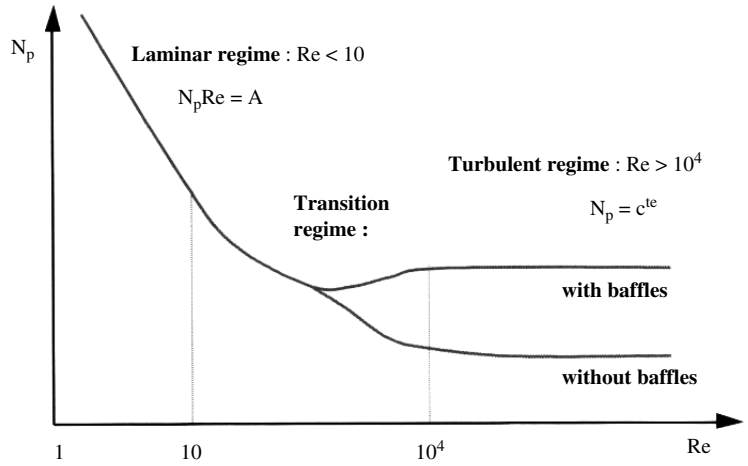

Figure 9.4. *Variation of the power number of a stirrer with the Reynolds number (figure reproduced from Agitation et Mélange, edited by C. Xuereb, M. Poux, and J. Bertrand (Dunod, Paris, 2006))*

Figure 9.4 indicates that the power number is larger if the stirrer is rotating inside a vessel provided with baffles than in the absence of baffles. As we have described earlier, the baffles serve to reduce the rotation of the fluid in the vessel. The difference in velocity between the rotating blades and the fluid is larger if the baffles are adequately dimensioned, and head losses and kinetic energy dissipation are greater then. The mechanical power consumed for the rotation of the stirring body is dissipated as heat within the fluid by turbulence. In a steady-state regime, the kinetic energy in the vessel is maintained and the energy balance equating the mechanical power consumed with the integral of the dissipation rate over volume V of the vessel provides an estimate of the average value of the kinetic energy dissipation rate:

$$\overline{\varepsilon} = \frac{\wp}{\rho V} \qquad [9.20]$$

For large Reynolds numbers, we therefore obtain $\overline{\varepsilon} \approx N_p N^3 D^5 / H\Phi^2$. A relationship between the power consumption and the characteristics of turbulence in the vessel is thus established, albeit a mere average estimate for ideally homogeneous turbulence.

The mechanical power dissipated by a stirrer results from the head loss phenomena associated with the rotation of the stirrer in the vessel. It is pertinent to correlate the aspect of the variations of the power number with the Reynolds number

(decrease of N_p with Re in a laminar regime, independence of N_p from Re in a highly turbulent regime) with variations plotted on the Colebrook diagram (Figure 4.2 of Chapter 4) for the head losses in pipe flows. These phenomena are similar. Knowing the power number enables us to calculate the dissipated power using:

$$\wp = N_p \rho N^3 D^5 \qquad [9.21]$$

In a turbulent regime, a simple hierarchy appears among the power numbers according to the nature of the stirrers. Rushton turbines, which produce substantial head loss, have a power number of the order of 4–5, whereas the power number of propeller-type stirrers is of the order of 0.3–1.

For reasons of mechanical strength of the moving body, it may be useful to determine the torque C exerted on the moving body or the average force F exerted on the blades. As we have established for pumps (Chapter 5, section 5.2), these two quantities are derived, for large Reynolds numbers, from the power number, since:

$$C = \frac{\wp}{2\pi N} = \frac{1}{2\pi} N_p \rho N^2 D^5 \qquad [9.22]$$

$$F \approx \frac{C}{D/2} = \frac{1}{\pi} N_p \rho N^2 D^4 \qquad [9.23]$$

The first relation is exact since the power is equal to the product of the torque by the angular rotational speed. The second relation provides an order of magnitude, as the torque is the product of the force by a length but the radius of the stirrer is only an estimate of the distance to the axis of the point of application of the force.

9.2.2. *Stirring and mixing time*

The dimensional dependence of the mixing time, τ_m, is similar to that [9.19] of the mechanical power consumed, except that the molecular diffusion of products is added thought the Schmidt number $\mathrm{Sc} = \nu/\kappa$. We, therefore, write:

$$N\tau_m = \text{function}\left\{\mathrm{Sc} = \frac{\nu}{\kappa}, \mathrm{Re} = \frac{ND^2}{\nu}, \frac{D}{\Phi}, \frac{H}{\Phi}, \ldots\right\} \qquad [9.24]$$

The mixing time, τ_m, is defined by a criterion stipulating the level of mixing that will be deemed sufficient. It is in general considered that the constituents are mixed if the variance of the concentration is less than a certain value. By including the diffusivity of products, formulation [9.24] is very general. It takes into account the

scale on which the mixing is performed: through turbulent dispersion at the level of the smallest scales of turbulence as analyzed in Chapter 8, or at the molecular level as discussed in Chapter 10.

9.2.3. *Emulsions and foams*

A classical and important application of stirring methods is the formation of foams and emulsions. The most common examples are in food processing. To prepare whipped cream, a beater is used to incorporate air into a liquid, in the form of microbubbles. The preparation of a mayonnaise sauce is somewhat subtler. First, a small quantity of oil is incorporated into an aqueous liquid (the egg yolk and mustard). The oil is dispersed by the beater in the form of droplets. When the level of oil exceeds a certain volume fraction, an inversion occurs. The oil becomes the continuous phase, while the water becomes the dispersed phase, because the volume of water is no longer sufficient to contain all the oil droplets.

The term emulsion refers to a mixture of two non-miscible liquids, one of which is dispersed within the other in the form of droplets. Foam is a mixture of microbubbles in a liquid. The physico-chemical properties of the products are important for stabilizing emulsions and foams. If the emulsion is not stabilized, the droplets coalesce when the stirring ceases and the emulsion gradually subsides. It is the function of the egg yolk to stabilize the mayonnaise. Anyone who ever prepared a mayonnaise or whisked egg whites will have understood that the beater is a precious utensil for achieving an emulsion or a foam/mousse. It is for this reason that we discuss this issue here.

From a mechanical point of view, understanding emulsion phenomena requires the introduction of important physical concepts such as surface tension between two fluids[8] and the notion of contact angle, when the interface between two fluids is in contact with a solid wall. These theoretical elements are summarized in section 9.3 of this chapter. We limit ourselves here with presenting the theoretical notions of mechanics involved in emulsion and foam phenomena, without touching upon considerations regarding the physico-chemical aspects of the phenomenon or the utilization of emulsion phenomena in process engineering.[9] The function of a beater for preparing an emulsion or foam is first and foremost to provide energy to split a gas or a liquid, forming bubbles or droplets. It is shown in section 9.3 of this chapter (equation [9.39]) that the equilibrium of a bubble or

8 More precisely, surface tension refers to a gas/liquid pair, and interfacial tension to a pair of non-miscible liquids.
9 Chapter 11 in *Agitation et Mélange* (ibid.) might be of use.

drop with radius a within a liquid requires an excess pressure inside the sphere relative to the outside pressure

$$\Delta P = \left(P_{\text{internal}} - P_{\text{external}}\right) = \frac{2\gamma}{a} \qquad [9.25]$$

which balances the surface tension force, γ, between the two phases. The smaller the bubble or drop is, the greater the energy provided needs to be. The gas inside the bubble needs to be more compressed, in relation to the smaller the diameter of the bubbles is. The surface tension between a liquid and air is of the order of several times 10^{-2} N m^{-1} (7.28×10^{-2} N m^{-1} for water and air, and 2×10^{-2} N m^{-1} for olive oil and air). For these fluids, the excess pressure inside the bubble is modest (40 Pa and 400 Pa for an air bubble in olive oil for respective radii of 1 mm and 100 μm). The energy required to produce foam is far greater than the energy per unit volume used to compress a gas, because a significant fraction of the mechanical energy consumed by the process is dissipated by the turbulence.

The important conclusion from emulsion and foam theory is that the more energy is provided, the smaller the radius a of the microbubbles or droplets is. In a turbulent flow, a bubble or droplet is deformed by eddies whose size is of the order of a. The shearing of the velocity field at that scale is likely to lead to splitting of the droplet or bubble if the kinetic energy of the eddy is greater than the energy that needs to be brought in to split the bubble and hence decrease its radius. This translates, in order-of-magnitude terms, into the inequality:

$$\rho u^2(a) \geq \frac{\gamma}{a} \qquad [9.26]$$

It is necessary to anticipate the results of Chapter 11 in order to evaluate the turbulent velocity $u(a)$. It will be established (equations [11.18] and [11.19] of Chapter 11) that the average kinetic energy per unit volume in a turbulent eddy of dimension a is fixed by the rate, ε, of dissipation per unit mass of the turbulent kinetic energy:

$$\rho u^2(a) \approx \rho(\varepsilon a)^{2/3} \qquad [9.27]$$

Equations [9.26] and [9.27], therefore, indicate that a bubble of radius a can be broken by turbulence if:

$$a \geq \left(\frac{\gamma}{\rho}\right)^{3/5} \varepsilon^{-2/5} \qquad [9.28]$$

This relation provides the order of magnitude of the minimum diameter of bubbles or drops generated when preparing foam or an emulsion[10]:

$$d_{\min} \approx \left(\frac{\gamma}{\rho}\right)^{3/5} \varepsilon^{-2/5} \qquad [9.29]$$

The characteristics of an emulsion depend to a large extent on the physico-chemical properties of the fluids involved, and also on the chemical additives used. Emulsifying surfactant products perform two functions. When they reduce surface tension, they help reduce the size of the bubbles and droplets. They also serve to stabilize the emulsion to prevent it from coalescing as soon as the stirring ceases. The first characteristic parameter of an emulsion is the volume fraction of each fluid. When a fluid is gradually incorporated into another which is being stirred, the incorporated fluid constitutes necessarily the dispersed phase and the receiving fluid the continuous phase, since the volume of the dispersed phase is smaller than that of the continuous phase. An inversion phenomenon may occur when the volumes of both phases become comparable. Surfactant additives also act to control phase inversion processes.

9.3. Appendix: interfaces and the notion of surface tension

9.3.1. *Interface between two non-miscible fluids and surface tension*

We consider an interface between two non-miscible fluids at rest. The forces exerted at the interface include a surface tension force parallel to the interface. Its intensity is quantified by the surface tension γ, whose dimension is a force per unit length (N m^{-1}). Figure 9.5 represents the surface tension force along an arbitrarily closed line C lying on the interface and bounding the surface element S. The tension force per unit length along C is:

$$\vec{T} = \gamma \ \vec{b} = \gamma \ \vec{t} \times \vec{n} \qquad [9.30]$$

The tension force is exerted on surface S, which, like a drum skin held by its rim, resists deflection. Further, $\vec{b}$ is the normal to curve C which is tangent to surface S and oriented outwards relative to surface S. The direction of the normal $\vec{n}$ to the surface is linked, by convention, to the direction of travel along curve C, given by

10 This relation is owed to Kolmogorov A.N. (*Dokl. Akad. Nauk*, 1949, Vol. 66, pp. 826–828) and Hinze J.O. (1955, *AIChE J.*, 1955, Vol. 1(3), 289–295). Experimental work has confirmed this dimensional dependence (Chen H.T. and Middleman S., 1967, *AIChE J.*, Vol. 13(5), 989–994).

the orientation of tangent $\vec{t}$, such that $\vec{t}, \vec{n}$, and $\vec{b}$ is a direct orthonormal coordinate system. The tension force per unit length is of constant magnitude, but its direction depends on the deflection of the surface. For a planar surface S, it is easy to show that the total tension force, obtained by integration along contour C, is zero. A non-zero total tension force is linked to the existence of a deflection of the interface. Its magnitude depends on the radii of curvature characterizing the deflection of the interface.

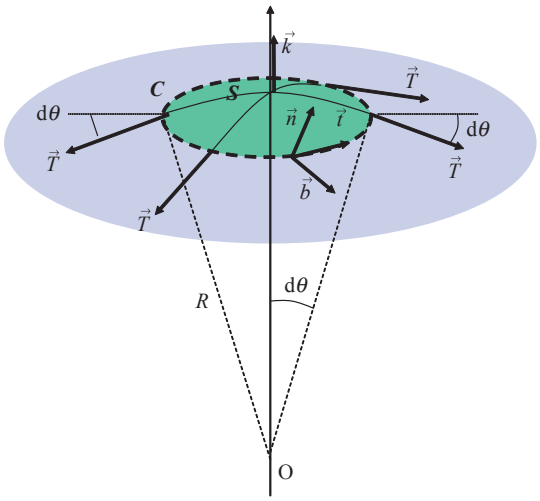

Figure 9.5. *Tension force at the interface between two non-miscible fluids*

For a spherical element of the surface whose center of curvature is at point O and whose radius of curvature is R, the tension force at different points of the curve C is represented in Figure 9.5. The surface is in mechanical equilibrium when the total force due to surface tension along contour C is balanced by the pressure forces exerted on S on either side of the interface. Denoting respectively by P_{convex} and P_{concave} the pressures on the convex and concave sides of the surface, the equilibrium between the forces is written as:

$$(P_{\text{concave}} - P_{\text{convex}})S\vec{k} - \gamma L \sin(\mathrm{d}\theta)\vec{k} = 0 \qquad [9.31]$$

For the spherical element given in Figure 9.5, $S = 2\pi R^2(1-\cos(\mathrm{d}\theta))$ and the perimeter of line C is $L = 2\pi R \sin(\mathrm{d}\theta)$. The sine of angle $\mathrm{d}\theta$ in the right-hand term in [9.31] corresponds to the projection of the tension force onto the vector $\vec{k}$ normal

to the apex of the surface element. For the limiting case of a small surface element ($d\theta \rightarrow 0$), [9.31] reduces to:

$$\Delta P = (P_{\text{concave}} - P_{\text{convex}}) = \frac{2\gamma}{R} \qquad [9.32]$$

The spherical surface element is in equilibrium if the deflection of the interface is associated with a rise in pressure through the interface that is inversely proportional to the radius of curvature. The pressure is greater on the concave side than on the convex side of the interface. For a non-spherical surface, relation [9.32] can be generalized by bringing in the radii of curvature along the principal directions of the surface[11]:

$$\Delta P = (P_{\text{concave}} - P_{\text{convex}}) = \gamma \left(\frac{1}{R_1} + \frac{1}{R_2} \right) \qquad [9.33]$$

The literature often provides an energy-based interpretation of surface tension, as γ has the dimension of an energy per unit surface (N m^{-1} = J m^{-2}). While this interpretation is meaningful as a rule, because the increase in the interfacial area is achieved under expenditure of energy, the interpretation in terms of energy is sometimes ambiguous, as discussed hereinafter with the example of Jurin's law.

9.3.2. *Equilibrium in the contact line between three phases, Jurin's law*

We now consider a line of contact between three media. This case is commonly of interest when it is considered that medium 1 is a solid and media 2 and 3 are two non-miscible fluids, such as, e.g. a liquid and air, or water and oil. The surface tensions γ_{12}, γ_{13}, and γ_{23} between the different media pairs are associated with three surface tension forces per unit length onto the line of triple contact, which in Figure 9.6 (where medium 3 is a gas) is the line perpendicular to the plane of figure and passing through point A. Each interface naturally tries to retract, and pulls the triple point, which explains the orientation of the vectors in Figure 9.6. If there exists a situation of three-phase equilibria for which the interface between the two fluids is attached onto the solid wall, the contact line can only move in the direction given by vector $\vec{k}$ in order to stabilize at a certain location. In that position, the equilibrium between the surface tension forces per length element of that line, projected onto direction $\vec{k}$, should be verified. It is written in the form:

$$\gamma_{12} + \gamma_{23} \cos\theta = \gamma_{13} \qquad [9.34]$$

11 This relation is called Laplace's formula, among other 'Laplace law or relations.'

The equilibrium contact angle θ, determined by the values of the three interfacial tensions, characterizes the respective affinity of both fluids for the solid. If $\gamma_{12} < \gamma_{13}$, then the affinity of the solid for fluid 2 is greater than that of the solid for fluid 3. That configuration is represented in Figure 9.6. The tension force γ_{13} pulls the triple line in the direction of vector $\vec{k}$. Two cases may then arise: (1) the surface tension between the two fluids is too weak ($\gamma_{23} < \gamma_{13} - \gamma_{12}$), and there can be no three-phase equilibria. Tension force γ_{13} pulls the triple line until the wall is entirely covered by fluid 2; and (2) if the surface tension between the two fluids is sufficient ($\gamma_{23} > \gamma_{13} - \gamma_{12}$), then there exists an equilibrium configuration such that $0 < \theta < \pi/2$. Fluid 2 covers the solid better than fluid 3 does (a liquid will be said to be "wetting the wall"). This situation can be adapted to the reverse case (if $\gamma_{12} > \gamma_{13}$) where the affinity of the solid for fluid 3 is greater than the one it exhibits for fluid 2. Fluid 3 tends to cover the wall. If the surface tension between the two fluids is too weak ($\gamma_{23} < \gamma_{12} - \gamma_{13}$), then fluid 3 covers the wall entirely. Three-phase equilibria is possible if the surface tension is sufficient ($\gamma_{23} > \gamma_{12} - \gamma_{13}$); the contact angle is such that $\pi/2 < \theta < \pi$. Lastly, in the case where $\gamma_{12} = \gamma_{13}$, both fluids have the same affinity for the solid. The equilibrium configurations are such that the interface between the two fluids is normal to the wall ($\theta = \pi/2$).

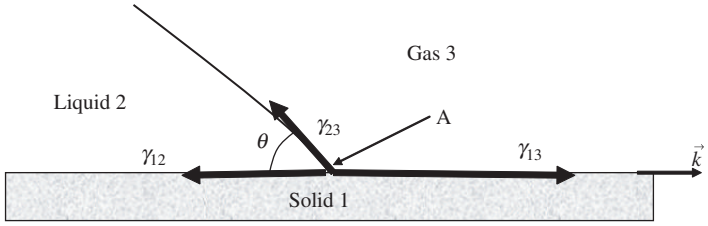

Figure 9.6. *Surface tension and contact angle between two fluids on a solid wall*

Relation [9.34] is known as the Young-Dupré law. While the values of surface tension between two fluids (γ_{23} in [9.34]) can be found for usual fluids in physical property tables for those fluids, data on the values of tensions γ_{12} and γ_{13} between each fluid and the solid are less accessible. Such quantities are difficult to measure. They depend on the surface finish of the solid wall, and vary dramatically in the presence of chemical additives deposited on the solid surface (an effect termed "pollution").

Writing the Young-Dupré law in the form:

$$\cos\theta = \frac{\gamma_{13} - \gamma_{12}}{\gamma_{23}} \qquad [9.35]$$

shows more clearly that the contact angle θ depends not only on the difference $\gamma_{13} - \gamma_{12}$, indicative of the relative affinity of the solid for either fluid, but also on the interfacial tension γ_{23} between the two fluids. It is important to mention this because, in practice, the interfacial tension between the two fluids is often altered in order to modify the wettability properties of a wall. If the affinity of the solid is greater for fluid 2 than for fluid 3 ($\gamma_{13} > \gamma_{12}$), a decrease in surface tension γ_{23} between the two fluids effects an increase in the value of cos θ, which means that angle θ diminishes. Fluid 2 will then cover the solid better, or even cover the wall entirely if the surface tension is sufficiently reduced. This is typically achieved by surfactant products, which are chemical molecules that position themselves on the interfaces due to radicals having an affinity for both fluids. Their presence at the interface alters the surface tension between the two fluids. Common surfactant products include detergents, which reduce surface tension between water and oil. If the affinity of the solid for water is comparatively better than it is for the oil, then the detergent enables water to better cover the solid surface, repelling the oil.

The Young-Dupré relation is the boundary condition that allows the determination of the shape of the surface between two fluids in contact with a solid wall, such as a liquid drop on a solid wall within a gas (dew) or an air bubble adhering to a solid wall within a liquid. It is important to emphasize that the Young-Dupré law is applicable only to the case where the triple line is at static equilibrium on the solid. When the triple line moves (if for example the dew drop slides down the wall), the concept of dynamic contact angle should be substituted for that of static contact angle for better results.[12]

One application of the above notions is the phenomenon of capillary rise of a liquid inside a thin tube of radius *a* immersed vertically in a basin, as depicted in Figure 9.7. It is observed that the liquid rises inside the tube until the gas/liquid interface stabilizes at a certain height *H*. When the radius of the tube is small compared to the capillary length:

$$\ell_c = \sqrt{\frac{\gamma}{\rho g}} \qquad [9.36]$$

12 See E.B. Dussan V., 1979, On the spreading of liquids on solid surfaces: Static and dynamic contact lines, *Ann. Rev. Fluid Mech.*,11: 371–400.

($a << \ell_c$), the effect of gravity in the vicinity of the interface between air and the liquid is negligible. The interface can be assimilated to a spherical meniscus for which the contact angle θ, a characteristic of the tube material, air, and the liquid, sets the radius of curvature R through a simple application of the trigonometric relations $a/R = \sin\alpha = \cos\theta$. The pressure below the meniscus is lower than the atmospheric pressure that prevails above it. Application of Laplace's law [9.33] in such a situation results in:

$$\Delta P = (P_{\text{atm}} - P_A) = \frac{2\gamma}{R} = \frac{2\gamma}{a}\cos\theta \qquad [9.37]$$

Hydrostatic equilibrium ($P_{\text{atm}} = P_A + \rho g H$) of the liquid between point A, which is located immediately below the meniscus, and a point B on the free surface of the basin, allows the determination of height H to which the liquid will rise inside the tube:

$$H = \frac{2\gamma}{\rho g a}\cos\theta \qquad [9.38]$$

This relation is known as Jurin's law. Such a simple experiment helps to explain physically the capillary rise phenomenon, which can be observed in a porous medium (e.g. a wall). The finer the pores in the porous medium, the higher the liquid rises.

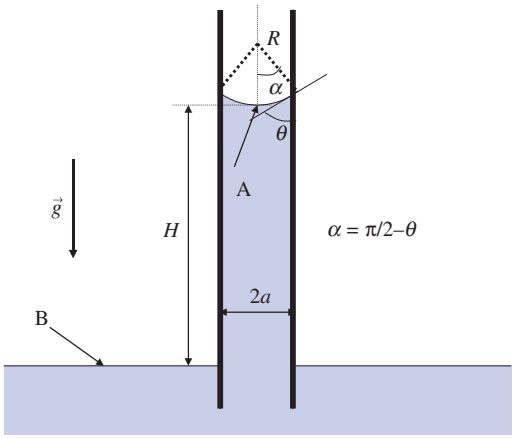

Figure 9.7. *Jurin's law characterizing the rise of a liquid inside a capillary tube*

An energy-based interpretation of Jurin's law is attractive, as it is found that the surface tension forces the liquid to rise by a certain height. However, the increase in the potential energy of a fluid particle is compensated for by the decrease in pressure. In other words, the rise of the liquid inside the tube is not associated with an increase in the energy of the liquid particles within the tube. Jurin's law actually emphasizes the balancing of the weight of the water column inside the tube ($\rho g H \pi a^2$) by projection onto the vertical axis of the surface tension force applied on the contour of the liquid's contact line with the tube ($2\pi a \gamma \cos\theta$). This is a balance between forces. The configuration leading to Jurin's law shows that the notion of interfacial energy, associated with surface tension and the area of the interface, does not always lead to a simple interpretation of the phenomena.

On the other hand, the energy-based interpretation of surface tension is meaningful if we consider a microbubble of radius a within a liquid at rest. The pressure inside the bubble is greater than that prevailing in the liquid, by virtue of [9.32]:

$$\Delta P = (P_{\text{internal}} - P_{\text{external}}) = \frac{2\gamma}{a} \qquad [9.39]$$

Some energy, therefore, needs to be provided to compress the gas. The smaller the bubble is, the more the energy is needed.[13] The excess pressure energy inside the bubble:

$$E = \frac{4\pi a^3}{3}\Delta P = \frac{2}{3}\gamma 4\pi a^2 \qquad [9.40]$$

is proportional to the product of surface tension by the area of the interface.

13 Interface modeling as presented in this section applies right down to bubbles and drops of a very small size. One can validly regard surface tension as independent from the deflections of the surface as long as the size of the drops or bubbles is greater than a few intermolecular distances, a dimension which has the same order of magnitude as the thickness of the interface (see G. Bruhat, *Thermodynamique*, Masson, 1968, pp. 363–364).

Chapter 10

Micromixing and Macromixing

10.1. Introduction

In this chapter and in the following chapters of the second part of this book, we discuss the mixing of chemical constituents by turbulence and their chemical reaction. The focus is first on the case of a reactor filled with a fluid in which two chemical constituents are present (Figure 10.1), but we assume provisionally that they do not react together. Initially, constituents A and B are dissolved in two distinct volumes separated by an interface; they are in contact only through that interface. We denote by V_A and V_B the volumes containing A and B, respectively, and by C_{A0} and C_{B0} the associated initial concentrations.

At time $t = 0$, stirring is initiated in the vessel using a moving body. Ideally, stirring is assumed to be homogeneous. This means that the mixing is performed in the same way at the center of the reactor as at its corners. It also means that, after a while, constituents are dispersed in identical fashion throughout the reactor. The concentration of constituents A and B, measured in a sample, is the same wherever the sample is taken in the reactor. If the concentrations of constituents A and B are represented by the yellow and blue colors, we would expect to see, at the macroscopic level, a green color in the reactor. However, this observation does not mean that the two products are in fact mixed, as illustrated in Figure 10.1, using varying grey levels. It is necessary to examine the distribution in space of products A and B at the molecular level in order to check that the mixing has actually taken place. Zooming in on a small volume element shows that, in some cases, volumes of fluid containing exclusively constituent A or constituent B are found to coexist therein. That is the case when constituents are initially in two different non-miscible fluids (such as some oils with water), for which the arrangement takes on the form

of an emulsion where droplets containing one of the products are dispersed within a continuous phase containing the other product. Figure 10.1 also illustrates another type of arrangement where both fluids stack themselves in the form of sheets resembling puff pastry. Such "non-mixing" characteristics can also be observed for miscible fluids, when the products have very low diffusivity, as will be seen later. Figure 10.1 depicts the fact that a macroscopic perception of mixing does not mean that the products are mixed at a molecular level. An analogy with an inkjet printer is helpful: the green color is produced by a relative density in blue- or yellow-colored pixels in a given area.

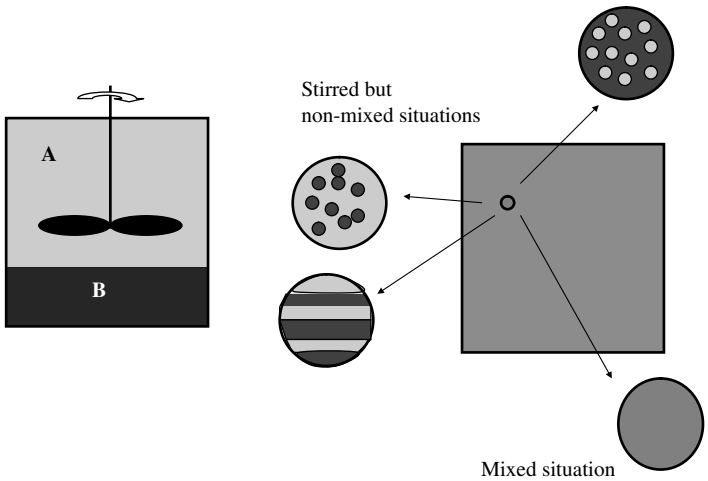

Figure 10.1. *Notions of dispersion and mixing in a perfectly stirred reactor*

These ideas have important consequences when a chemical reaction is now considered. In the case where the products are mixed at the molecular scale, they are in contact with each other at any point in the reactor, and the concentrations of products A and B become $C_{A0}V_A/(V_A+V_B)$ and $C_{A0}V_B/(V_A+V_B)$, respectively, due to dilution. In non-mixing situations, the products are only in contact at the interfaces between the two phases, and the concentrations remain equal to the initial values.

Dealing with mixing raises two preliminary questions:

1. What the mechanisms producing the mixing? The answer to this question needs to be provided with regard to chemical reactions.

2. How can the degree of mixing of constituents in a fluid be characterized? This entails introducing tools for its characterization.

We have to answer these questions before we presume to describe the dynamics of mixing and predict, for example, the durations required to mix two products. We shall hereafter exclusively discuss mixing produced by a developed turbulence. We will not deal with mixing in a laminar flow, although the basic concepts are identical.

10.2. Characterization of the mixture: segregation index

Suppose we can determine or measure, at all times and at any point $\vec{x}$, the concentration $C_A(\vec{x},t)$ of a constituent A. Since the flow is turbulent inside the reactor, the ensemble average concept introduced in Chapter 8 to describe turbulence can be used to define the probability density (PDF)[1] $P(C_A,\vec{x},t)$. $P(C_A,\vec{x},t)\mathrm{d}C_A$ then denotes the probability of measuring at $\vec{x}$, at time t, a concentration between $C_A - \mathrm{d}C_A/2$ and $C_A + \mathrm{d}C_A/2$. When the concentration distribution is homogeneous in the vessel, $P(C_A,\vec{x},t)$ does not depend on $\vec{x}$, and we simply write $P(C_A,t)$. This is the case that is presented in this chapter.

The general properties of probability densities apply, namely:

$$\int_0^\infty P(C_A,t)\mathrm{d}C_A = 1 \qquad [10.1]$$

$$\overline{C}_A(t) = \int_0^\infty C_A P(C_A,t)\mathrm{d}C_A \qquad [10.2]$$

$$\sigma_A^2(t) = \int_0^\infty (C_A - \overline{C}_A)^2 P(C_A,t)\mathrm{d}C_A \qquad [10.3]$$

where $\overline{C}_A(t)$ is the average concentration of constituent A and $\sigma_A^2(t)$ the variance attached to product A.

When two constituents are present in a fluid, and more particularly when they are likely to react with one another, it is necessary to introduce, in a similar way, the probability density function $P(C_A,C_B,t)$. The properties given by equations [10.1]–[10.3] can be immediately transposed. For example, to evaluate an average concentration, we write:

$$\overline{C}_A(t) = \int_0^\infty \left\{ \int_0^\infty C_A P(C_A,C_B,t)\mathrm{d}C_A \right\} \mathrm{d}C_B \qquad [10.4]$$

1 PDF stands for “probability density function”.

Lastly, the *segregation index* refers to function:

$$I(t) = \frac{\sigma_A^2(t)}{\sigma_A^2(t=0)} \qquad [10.5]$$

Let us now apply these notions to the case of the stirred reactor represented in Figure 10.1. When constituents A and B do not react, each product is conserved and the time evolutions of $P(C_A, t)$ and $P(C_B, t)$ can be described independently. For the case where product A is initially contained within volume V_A with concentration C_{Amax} and in volume V_B with concentration $C_{Amin,}$ the probability density function $P(C_A, t=0)$ at the initial time consists of two delta functions:

$$P(C_A, t=0) = 0 \quad \text{if} \quad C_A \neq C_{A\min} \quad \text{and} \quad C_A \neq C_{A\max}$$

$$P(C_{A\max}, t=0) = \frac{V_A}{V} \quad \text{and} \quad P(C_{A\min}, t=0) = 1 - \frac{V_A}{V}$$

with $V = V_A + V_B$. It follows that:

$$\begin{aligned}\overline{C}_A(t=0) &= C_{A\min} P(C_{A\min}, t=0) + C_{A\max} P(C_{A\max}, t=0) \\ &= C_{A\min} + (C_{A\max} - C_{A\min})\frac{V_A}{V}\end{aligned}$$

$$\sigma_A^2(t=0) = (C_{A\max} - C_{A\min})^2 \frac{V_A}{V}\left(1 - \frac{V_A}{V}\right)$$

In Figure 10.2, $P(C_A, t=0)$ has been plotted and the evolution over time of $P(C_A, t)$ is depicted in the absence of a chemical reaction. The average concentration is conserved, so that $\overline{C}_A$ is independent from time. It can be assumed that constituent A will be completely mixed and diluted in the volume at time $t \to \infty$.

Consequently, $P(C_A, t=\infty)$ is simply:

$$P(C_A, t=\infty) = 0 \quad \text{if} \quad C_A \neq \overline{C}_A$$

$$P(\overline{C}_A, t=\infty) = 1$$

It can be observed that $\sigma_A^2(t=\infty) = 0$, so that $I(t=\infty) = 0$ whereas $I(t=0) = 1$.

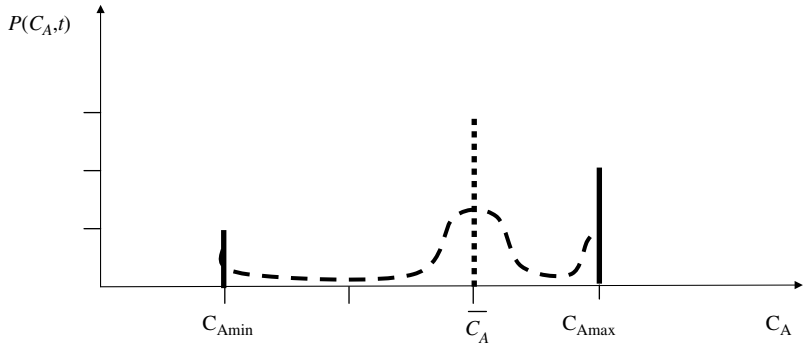

Figure 10.2. *Time evolution of the probability density function* $P(C_A, t)$ *during a mixing process in a stirred vessel.*
____: $P(C_A, t = 0)$; -----: $P(C_A, t > 0)$; .....: $P(C_A, t \to \infty)$

The aspect of the probability density function $P(C_A, t)$ represented in Figure 10.2 at an intermediate time during the mixing process is only indicative; many others might be envisaged, as we will see in Chapter 12. Nevertheless, it fulfils certain properties:

– The integral of function $P(C_A, t)$ over all concentrations should equal 1.[2]

– Function $P(C_A, t)$ verifies $P(C_A, t) = 0$ outside the interval $[C_{A\min}, C_{A\max}]$. If that was not the case, our process would separate rather than mix.

Function $P(C_A, t)$ varies in such a manner as to tend asymptotically toward the delta function in $C_A = \overline{C}_A$ for $t = \infty$. The variance decreases with time. The segregation index is a dimensionless function which decreases continuously from a value of 1 at time $t = 0$ to the value 0 when the mixture is obtained. It is therefore a good representation of the degree to which the mixing has been achieved.

Figure 10.3 shows the evolution in time of the probability density function $P(C_A, t)$ obtained by direct numerical simulation. The initial conditions are similar to those considered in the present section, although technical constraints on direct numerical simulation require an initial PDF that is smoother than the double delta function considered previously. It is found that the PDF varies in the form of a continuous function, a property which we will discuss in Chapter 12.

2 At $t = 0$ and at $t = \infty$, the representation shows the integral of the delta function.

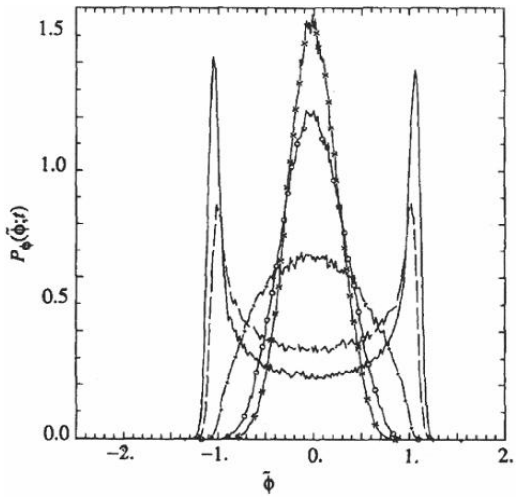

Figure 10.3. *Evolution over time of the probability density function* $P(C_A, t)$ *derived from the results of a direct numerical simulation of mixing in a stirred vessel (Eswaran and Pope, Physics of Fluids, Vol. 31(3), 506–520, 1988).*
---: $t / \tau_t = 0.22$ *; - - - :* $t / \tau_t = 0.42$ *; -+-:* $t / \tau_t = 0.83$ *;*
-o- : $t / \tau_t = 1.28$ *; -x- :* $t / \tau_t = 1.49$

10.3. The dynamics of mixing

The mixing of a product into a fluid flow results from two mechanisms: stirring, which regards to the advection of fluid particles, and molecular diffusion, which is characterized by a molecular diffusion coefficient D_A. In the absence of a chemical reaction, the evolution in time of the concentration field $C_A(\vec{x}, t)$ of a product A inside a fluid domain is governed by the transport equation:

$$\frac{dC_A}{dt} = \frac{\partial C_A}{\partial t} + \vec{u}.\nabla C_A = D_A \Delta C_A \qquad [10.6]$$

This is a conservation equation. The quantity is conserved over the reactor as a whole, if there is no exchange with the outside environment.

Equation [10.6] enables us to pinpoint the fundamental role of molecular diffusion in mixing processes. In the absence of molecular diffusion ($D_A = 0$), equation [10.6] reduces to:

$$\frac{dC_A}{dt} = \frac{\partial C_A}{\partial t} + \vec{u}.\nabla C_A = 0 \qquad [10.7]$$

which means that concentration is conserved in a fluid particle that is being followed during its movement. Consequently, there can be no mixing. The PDF $P(C_A, t)$ is independent of time. The flow merely advects fluid particles without changing their composition. We are therefore in a "non-mixing" situation as represented in Figure 10.1, where the fluid flow causes the fluid volumes contained in the domain to stretch, fold back, split up, or fragment, without however leading to mixing at the molecular scale.

We shall not discuss here the conditions that led to the two configurations illustrated in Figure 10.1. Rather, we wish to dwell on two concepts:

1. The first is that one should distinguish, when referring to mixing, the hydrodynamic process of dispersion, which in itself does not produce any mixing, from the mixing process, which requires molecular diffusion to bring the constituents into contact at the molecular scale. The term *stirring* means dispersion and the term *mixing* is used to describe the actual mixing through diffusion at the molecular scale.

2. The second concept, which we have intended to depict in Figure 10.1, is that advection of fluid particles by turbulence (*stirring*) causes a significant decrease in the characteristic sizes of the volumes containing constituents A and B. This property will accelerate mixing by dramatically reducing the diffusion times required to perform it.

These arguments are illustrated by Figure 10.4, which reproduces three figures from the outstanding book by Ottino.[3] The first illustration (Figure 10.4(a)) is an experimental observation[4] by laser-induced fluorescence of the instability at the interface between two superimposed fluid layers in parallel movement at different velocities. The Kelvin–Helmholtz instability results in the roll-up and stretching of flow threads through the generation of vortices at the interface. The second illustration (Figure 10.4(b)) reproduces the cover of this book, which shows a situation where the roll-up and stretching of flow threads end up occupying the entire space inside a cavity. These two illustrations, obtained experimentally, demonstrate the validity of the concepts described. The third illustration (Figure 10.4(c)) summarizes the different processes we have described. The initial mechanism is a stretching of flow threads, which leads to a "puff-pastry-like" striation of the domain Case (a). Case (c) depicts the way this process can subsequently lead to a fragmentation of the domain. Case (b) indicates the way the diffusion process is combined.

---

3 Ottino, J.M., *The Kinematics of Mixing: Stretching, Chaos and Transport*, Cambridge texts in applied mathematics, Cambridge University Press, 1989.
4 Koochesfani and Kimotakis, 1986, *J. Fluid Mech.*, 170, 83–112.

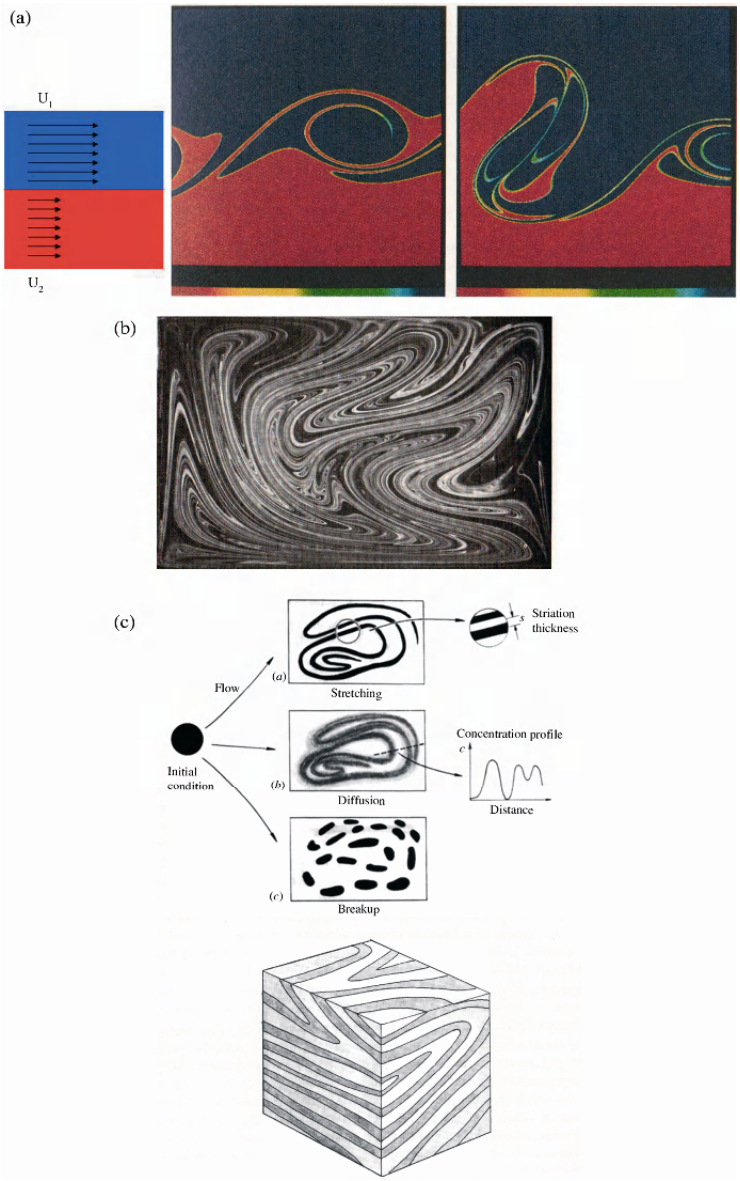

Figure 10.4. *Illustrations of the mixing processes initiated by the stretching and folding back of fluid threads in a flow. These three figures are excerpted from the book by Ottino (1989). (a) Stretching by Kelvin–Helmholtz instability at the interface between two fluids flowing in parallel with a velocity ratio $U_1/U_2 = 0.45$. (b) Stretching of a dye spot in a closed cavity where movement is generated by sinusoidal displacements at the boundaries. (c) Illustration of stretching: (a), diffusion phenomena (b), and fragmentation (c) during a mixing operation*

10.4. Homogenization of a scalar field by molecular diffusion: micromixing

Molecular diffusion is the only mechanism that can achieve the mixing by modifying the concentration of constituents inside fluid particles. It is this process that we examine now, with the aim of describing the way it occurs, but more importantly of determining the time span required to obtain it. We consider the situation depicted in Figure 10.1 where the stirring process has already fragmented the fluid domains containing products A and B into micro-elements of size ℓ_K. Stirring moves elementary cells relative to one another, without being able to modify their size, as this would require the existence of turbulent structures smaller than ℓ_K, or the ability to transfer products between elementary cells.

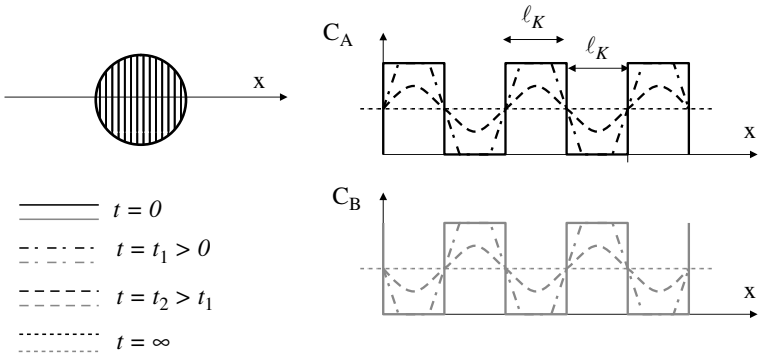

Figure 10.5. *Evolution in time of reagent concentrations under the effect of molecular diffusion. Products A and B are initially contained in streaks of thickness ℓ_K, and they are only in contact at the interface between streaks. Molecular diffusion transport the products along the Ox direction, producing their mixing while concentrations (dark grey for A and light grey for B) homogenize*

In order to characterize the time-dependent evolution of the spatial variations in concentration under the effect of molecular diffusion, we plot in Figure 10.5 the variations in the concentrations of products A and B along an axis *Ox*. Initially, the latter are periodic square functions with a characteristic scale ℓ_K. The evolution in time of the spatial variations in concentration under the effect of molecular diffusion is also represented in Figure 10.5. In the first stage, the concentration field varies at the vicinity of the discontinuity surfaces in the form of a gradient which decreases with time. The concentration level at the center of the elements decreases in the second stage, with spatial variations of concentration gradually taking on the shape of a sine wave whose amplitude decreases with increasing time. This classical behavior is observed when solving for the diffusion equations, as described in the appendix to Chapter 8. Dimensional analysis of the advection/diffusion equation

shows that the time required to homogenize the concentrations by diffusion is of the order of:

$$\tau_{\mathrm{D}} = \frac{\ell_K^2}{D}. \qquad [10.8]$$

where D denotes the molecular diffusion coefficient (assumed here to be the same for all constituents). Equation [10.8] is similar to equation [8.36] of Chapter 8, without considering the turbulent diffusion coefficient as it corresponds to stirring. The time τ_{D} is called the micromixing time. We will return to this terminology in section 10.6.

The main consequence of [10.8] is that the smaller the scale ℓ_K is, the faster the effect of molecular diffusion will be. Stirring accelerates the mixing process by fragmenting fluid domains at the scale ℓ_K. It helps this way in accelerating the diffusion process, which homogenizes the concentration fields in space. In order to determine how rapidly the mixing process takes place, we need to know the size of the smallest scales of turbulence, which we will denote by ℓ_K.

A second argument is regarding the concentration measurements in a fluid domain. Measuring a concentration $C_{\mathrm{A}}(\vec{x},t)$ at one point at a given time (as we have assumed in section 10.3) is a theoretical notion, as we necessarily measure the concentration over a volume surrounding that point. However, we can deduce from [10.8] that the concentrations in the measurement volume considered are quasi-instantaneously homogenized by molecular diffusion, if the measurement volume is small.

10.5. Diffusion and chemical reactions

We continue with the case described in Figure 10.5, now examining the speed with which the chemical reaction takes place. We denote by τ_{C} the chemical time, which is the time required to perform the chemical reaction when products A and B are mixed. Two limiting cases need to be considered, depending on the relative values of τ_{C} and τ_{D}.

If $\tau_{\mathrm{D}} << \tau_{\mathrm{C}}$, products A and B are mixed after the time τ_{D} has elapsed, but it can be seen that reagents A and B, although mixed together during the time interval $0 < t < \tau_{\mathrm{D}}$, have had almost no time to react with each other. The chemical reaction therefore progresses with the characteristic time τ_{C} after mixing has been effected. The mixing itself is very fast.

The reverse case, where $\tau_D >> \tau_C$, is somewhat more complex. This is illustrated in Figure 10.6, whose representation is similar to the one shown in Figure 10.5. The initial conditions are the same for both cases. The variations in reagent concentrations are plotted along the axis *Ox*. Since $\tau_C << \tau_D$, we assimilate the reaction into an instantaneous reaction. Both reagents A and B cannot coexist. They are in contact only through the interfaces $x = n\ell_K$ (where *n* is an integer), where they react for forming product P. Inside each elementary cell containing the reagents A or B, the diffusion process is similar to the one plotted in Figure 10.5, but product A never penetrates into the volume containing product B (and conversely for product B). Molecular diffusion transports the reagents to the interfaces, where the chemical reaction occurs. Thereby, molecular diffusion controls the rapidity of the transport and the progress of the chemical reaction.[5] The concentrations of products A and B diminish due to the consumption by the chemical reaction.

Lastly, in the case where the diffusion time τ_D is of the same order of magnitude as the characteristic time of the chemical reaction τ_C, the reaction takes place concurrently with the diffusion and reaction process. It can therefore be concluded, as a general statement, that the progress time of a chemical reaction τ_R is given by

$$\tau_R \approx \max\{\tau_D, \tau_C\}. \qquad [10.9]$$

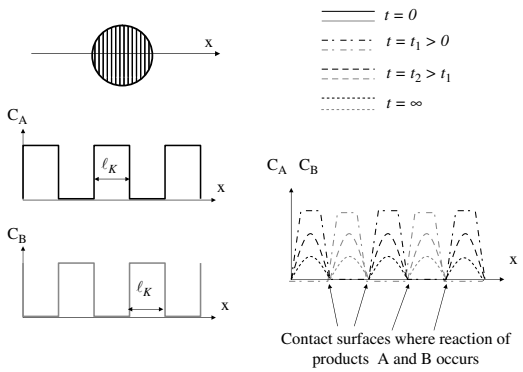

Figure 10.6. *Evolution in time of reagent concentrations under the combined effects of molecular diffusion and of an instantaneous chemical reaction. Products A and B are initially contained in streaks of thickness ℓ_K. During the whole process, they are only in contact at the interface between streaks where they react together. Molecular diffusion transport the products along the Ox direction, producing their mixing while concentrations (dark grey for A and light grey for B) decrease in time, while the products are consumed by the reaction*

5 A direct application of this case is found in combustion, with diffusion flames (see Exercise 11.III at the end of Chapter 11).

10.6. Macromixing, micromixing, and chemical reactions

A chemical reaction progresses as a result of three processes: chemical kinetics, which is characterized by the chemical time τ_C; micromixing, which is linked to molecular diffusion (characterized by the micromixing time τ_D – equation [10.8]); and macromixing (termed *stirring* in this chapter), which pertains to the process of turbulent dispersion as described in Chapter 8.

Macromixing refers to the processes of advection caused by the turbulent flow, which transport fluid particles and which, through the roll-up and stretching of sheets, assist in fragmenting the fluid phase into small-scale entities. As a result, concentration gradients within the fluid domain are considerably strengthened. These phenomena have already been described and illustrated in Figures 10.1 and 10.4.

Macromixing, produced by turbulence, involves different space and time scales. We have already discussed in Chapter 8 the large scale of turbulence, characterized by the integral scale ℓ_t and the turbulent velocity u_{rms}. With that is associated the time scale (equation [8.12]) which is referred to as the *eddy turn-over time of turbulence* as it gives an order of magnitude of the revolution time of an eddy at the large scale of turbulence:

$$\tau_t = \frac{\ell_t}{u_{\text{rms}}} . \qquad [10.10]$$

These space and time scales are not sufficient to describe the spatial variations in concentration, since they do not incorporate the process of domain fragmentation described in this chapter. It is necessary to consider the size ℓ_K, which is the smallest scale of turbulence that is present within the flow. Such small vortices are associated with a velocity u_K, which allows the introduction of the characteristic time of small-scale turbulence:

$$\tau_K = \frac{\ell_K}{u_K} . \qquad [10.11]$$

This time is characteristic of the relative motions of the small-scale fluid entities, adjacent to one another. These entities are produced by the fragmentation of the fluid phase under the effect of turbulence, and the relative motions serve to maintain spatial heterogeneity at small scales. Kolmogorov's theory, presented in Chapter 11, will help in quantifying ℓ_K, u_K, and τ_K.

It is finally necessary to include as a macromixing process, the dispersion of fluid particles at the overall scale of the reactor. The turbulent diffusion process

described in Chapter 8 allows us to quantify it. For a reactor of characteristic size L (its volume will be taken to be equal to $V = L^3$), the turbulent dispersion time τ_{disp} at the scale of the reactor is derived from equation [8.36]. Writing $L = \sqrt{\kappa_t \tau_{\text{disp}}}$, with turbulent diffusion coefficient $\kappa_t = u_{\text{rms}} \ell_t$, it follows that:

$$\tau_{\text{disp}} \approx \tau_t \left(\frac{L}{\ell_t} \right)^2 . \qquad [10.12]$$

This is the time required to homogeneously distribute small fluid particles throughout the reactor.

Generally speaking, the three characteristic times of macromixing in developed turbulence are such that:

$$\tau_K << \tau_t \leq \tau_{\text{disp}} . \qquad [10.13]$$

The first inequality will be established in Chapter 11. The second inequality results from $\ell_t < L$.

By extrapolating equation [10.9] we can estimate the progress time of a chemical reaction, where both molecular diffusion and turbulent dispersion are active. The progress of the chemical reaction will be controlled by the slowest of these processes, hence:

$$\tau_{\text{R}} \approx \max \left\{ \tau_{\text{D}}, \tau_{\text{C}}, \tau_{\text{K}}, \tau_{\text{t}}, \tau_{\text{disp}} \right\} . \qquad [10.14]$$

The configuration which we have so far considered (as shown in Figure 10.1) is that of a closed reactor. For an open reactor (with a flow passing through the reactor), the residence time inside the reactor also needs to be taken into account. This case will be considered in Chapter 12.

10.7. Experimental demonstration of the micromixing process

A simple experiment demonstrates the validity of the concepts of micromixing, by setting two reactions which compete for the consumption of a reagent. The experiment, in which we limit ourselves to establishing a balance of the reagents consumed at the end of the experiment, proves the fact that the degree of execution of each of the two reactions depends, for carefully selected conditions, on the micromixing of the constituents.[6]

6 These ideas and experiments were introduced by Fournier, M.C., Falk, L. and Villermaux J. (1996), *Chemical Engineering Science*, Vol. 51(22), pp. 5053–5064.

We consider the following two chemical reactions, for which products A and B are competing to consume product C:

A + C → D chemical time τ_{C1}

B + C → E chemical time τ_{C2}

The products A and B are introduced and mixed beforehand inside the reactor. We denote by C_{AB0} the initial concentrations of products A and B, which are assumed to be identical. The reaction can start as soon as reagent C is introduced, its initial concentration being denoted by C_{C0}. We consider the situation where products A and B are in strong excess, that is, $C_{C0} << C_{AB0}$. Both reactions are assumed to be of order 1 with respect to each of the constituents. The kinetic constants of both reactions are denoted by k_1 and k_2. It is assumed that the first reaction is much faster than the second, that is, $k_1 >> k_2$.

For this experiment, if, from time $t = 0$, product C is already perfectly mixed with products A and B, then product C will be almost totally consumed by reaction 1. The resolution of the kinetic equations shows that the concentrations of products A and B vary in time according to:

$$C_A(t) = C_{AB0} - \frac{k_1 C_{C0}}{(k_1 + k_2)}\{1 - \exp[-(k_1 + k_2)C_{AB0}t]\}$$

$$C_B(t) = C_{AB0} - \frac{k_2 C_{C0}}{(k_1 + k_2)}\{1 - \exp[-(k_1 + k_2)C_{AB0}t]\}$$

Final concentrations of products A and B are therefore, taking into account the fact that $k_1 >> k_2$ and $C_{C0} << C_{AB0}$:

$$C_A(t = \infty) = C_{AB0} - C_{C0}$$

$$C_B(t = \infty) = C_{AB0} - k_2 C_{C0} / k_1 \approx C_{AB0} \qquad [10.15]$$

These results are obtained if the characteristic times of micromixing and macromixing are small compared to the characteristic times of both reactions, $\tau_{C1} = 1/k_1 C_{AB0}$ for the first and $\tau_{C2} = 1/k_2 C_{AB0}$ for the second. Since $k_1 >> k_2$, we have $\tau_{C1} << \tau_{C2}$. Assuming that macromixing is performed properly, micromixing is not a limiting factor for either of the two chemical reactions if the characteristic time of micromixing (equation [10.8]) is sufficiently small compared to the chemical times, namely:

$$\tau_D \approx \frac{\ell_K^2}{D} << \tau_{C1} << \tau_{C2} \qquad [10.16]$$

In contrast, considering a situation where the small scales ℓ_K of turbulence are larger, and particularly in the case where $\tau_{C1} << \tau_D << \tau_{C2}$, the situation is such that micromixing limits the progress of reaction 1, whereas it has no effect on reaction 2. As a result, reaction 1 occurs more slowly, with the characteristic time τ_D of micromixing, while the kinetics of reaction 2 is not altered. Reagent C is consumed more slowly by reaction 1, and reacts more with product B. When reagent C has been completely consumed, it is found that product B has been consumed to a greater extent, and that more of product A is left, in comparison with the values [10.15] obtained in situations where there are no limits set for mixing.

In order to verify this effect, we require the ability to experimentally control the value ℓ_K of the smaller scales of turbulence. We have limited ourselves, in this chapter, to explaining the role played by the small scales of turbulence in the mixing process associated with a chemical reaction. In Chapter 11, we provide some necessary complements from the theory of turbulence, which will enable us to quantify ℓ_K.

Chapter 11

Small Scales in Turbulence

In Chapter 8, we characterized the large scales of turbulence by introducing the turbulent velocity u_{rms} and the integral scale ℓ_t. These two quantities are used to quantify two key processes of turbulence, the turbulent diffusion coefficient $\kappa_t \approx u_{\text{rms}}\ell_t$ (equation [8.29] of Chapter 8) and the kinetic energy dissipation rate in a turbulent flow:

$$\varepsilon = \frac{u_{\text{rms}}^3}{\ell_t} \qquad [11.1]$$

(equation [8.14] of Chapter 8). Again, the non-inclusion of viscosity in this relation is particularly noteworthy. This property, together with equation [11.1], constitutes the cornerstone of turbulence theories and of the concepts presented in this chapter.

The integral scale ℓ_t characterizes the size of large-scale motion observed in a turbulent flow. On a weather map, these are observed as cyclonic and anti-cyclonic eddies. Although it is the most visible, large-scale motion does not describe the entirety of turbulence-induced phenomena. Kolmogorov's theory, presented in this chapter, allows the determination of the Kolmogorov scale ℓ_K, which characterizes the size of the smallest eddies present in a turbulent flow.[1] This scale is used to evaluate the characteristic time of diffusion processes and apply the concepts of macromixing and micromixing introduced in Chapter 10 for a developed turbulence flow.

---

1 A more comprehensive presentation of Kolmogorov's theory can be found in the book by M. Lesieur, *Turbulence in Fluids* (Springer-Verlag, 2007).

11.1. Notion of signal processing, expansion of a time signal into Fourier series

Some notions of signal processing are necessary to understand that the spectral content is an essential characteristic of a random signal which neither the average value nor the variance accounts for.

This idea is illustrated in Figure 11.1. Figure 11.1(a) shows a velocity signal which is assumed to represent a turbulent flow, measured at one point as a function of time. After digitizing this signal at regular time intervals Δt, the digitized values were plotted in Figure 11.1(b), their order having been randomly modified. A curve passing through each of the points was then superimposed to this new signal. Since the same data was used in both plots, the values of $\overline{U}$ and u_{rms} are identical for both the plots. However, the two signals clearly differ. The oscillations are faster in Figure 11.1(b) than in Figure 11.1(a). Calculating a correlation time, analogous to the integral scale introduced in Chapter 8, would demonstrate that the correlation time calculated for the signal of Figure 11.1(b) is smaller than that of Figure 11.1(a). An analysis of the spectral content of the turbulent signal allows a finer characterization of turbulence than the statistical values $\overline{U}$, u_{rms}, and ℓ_t do.

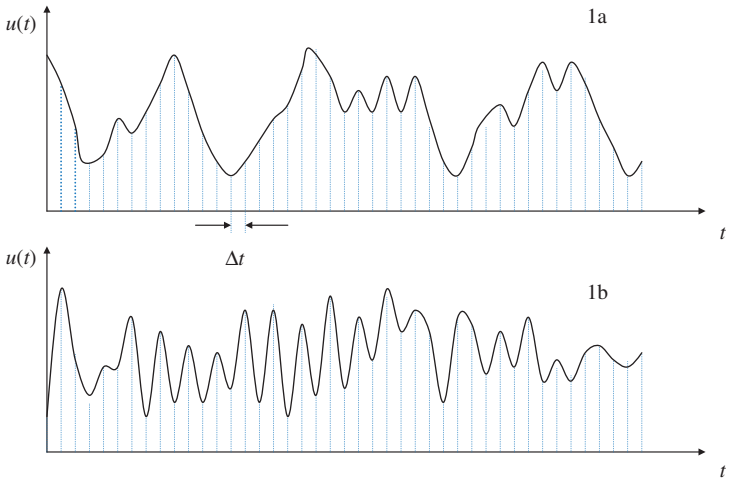

Figure 11.1. *Representation of a digitized turbulent signal. The digitized values in Figure 11.1(a) are plotted again in Figure 11.1(b), in a randomly modified order*

Expanding a time signal into Fourier series provides access to its spectral content. We consider the simplified case where the mean velocity is zero and we analyze the fluctuating velocity signal $u'(t)$ measured over a time interval $[0,T]$. The mathematical theory of Fourier series asserts that a continuous signal measured

over a time interval [0,*T*] can be written in an exact manner as an infinite series of sine functions:

$$u'(t) = \sum_{n=1}^{\infty} \left\{ a_n \cos\left(\frac{2\pi n}{T} t \right) + b_n \sin\left(\frac{2\pi n}{T} t \right) \right\} \qquad [11.2]$$

The coefficients of the series are calculated by integrals, using complex numbers formalism:

$$a_n + ib_n = \frac{2}{T} \int_0^T u'(t) \exp\left(i \frac{2\pi n}{T} t \right) \mathrm{d}t \qquad [11.3]$$

The expansion into Fourier series amounts to representing a signal using an infinite number of discrete frequencies $f_n = n/T$. Based on [11.3], it is easy to calculate, for every integer *n*, the terms of the sequence:

$$E\left(f_n = \frac{n}{T} \right) = \frac{T}{4} \{ a_n^2 + b_n^2 \} \qquad [11.4]$$

This sequence is called the energy spectrum of the random signal. The notion of energy related to this quantity will appear a little later.

It might seem paradoxical that the representation of the signal as a Fourier series should depend on the duration *T* of the signal, inasmuch as the content of the signal does not depend on its duration. A few simple examples using sine functions help establish that the spectral content of a sinusoid of frequency *f* exhibits significant positive values of $E(f_n = n/T)$ on the energy spectrum only for integer numbers *n* that are close to the value of fT. In other words, Fourier analysis enables the identification of the frequency of a sinusoidal signal, to the accuracy of discretization. For simple mechanical systems, the energy spectrum is discrete, which means that a finite number of frequencies are identified, for which $E(f_n) \neq 0$. Such a case is represented in Figure 11.2(a).

Figure 11.2(b) depicts the energy spectrum of a turbulent signal. This curve verifies several essential properties. Function $E(f_n)$ is always positive, as per its definition (equation [11.4]). It is also found that function $E(f_n)$ tends toward 0 for $n \to \infty$. This property results from the Parceval equality:

$$\frac{1}{4} \sum_{n=1}^{\infty} \{ a_n^2 + b_n^2 \} = \frac{1}{2} \frac{1}{T} \int_0^T u'^2(t) \mathrm{d}t \qquad [11.5]$$

which states that the series is convergent. The Parceval equality lends an energy-related meaning to $E(f)$:

$$\int_0^\infty E(f)\mathrm{d}f = \frac{1}{2}\frac{1}{T}\int_0^T u'^2(t)\mathrm{d}t \qquad [11.6]$$

since the right-hand-side term in [11.6] is the mean turbulent energy per unit mass.

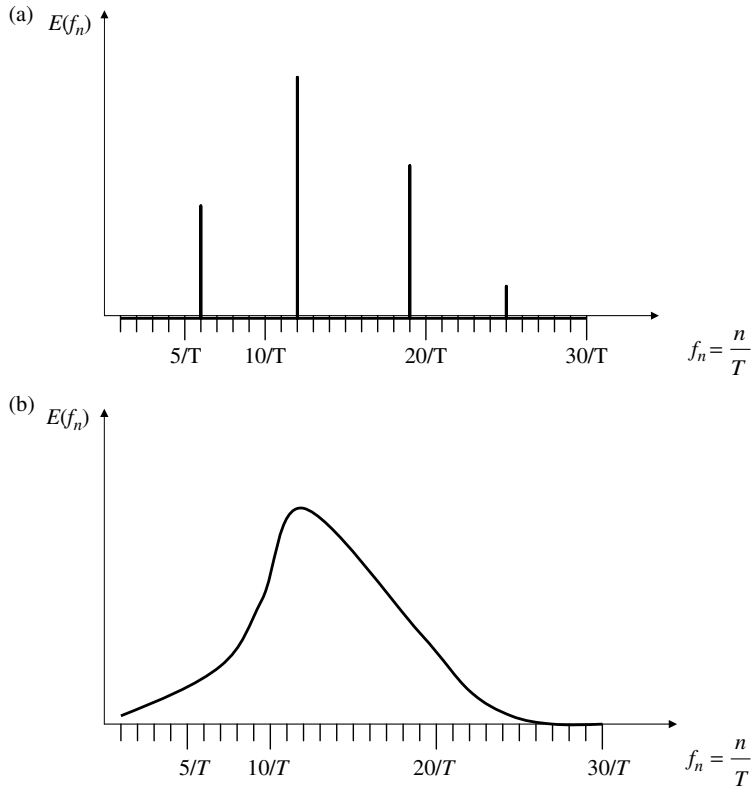

Figure 11.2. *Energy spectrum of a signal: (a) harmonic signal; (b) turbulent signal*

Unlike the "discrete" energy spectrum represented in Figure 11.2(a), the energy spectrum of a turbulent signal takes the form of a continuous curve, i.e. function $E(f)$ is non-zero and positive over a wide frequency band. This property allows us to ascertain whether a signal is turbulent, as chaos theories have shown. Kolmogorov's theory assumes that the shape of the energy spectrum over the frequency range is representative of a state of equilibrium of turbulence.

The frequency band $f_{\min} < f < f_{\max}$, in which the energy of the signal is held, can be determined in practice from the energy spectrum. It may for example be defined as the frequency band containing 99% of the signal's total energy:

$$\int_{f_{\min}}^{f_{\max}} E(f)\mathrm{d}f = 0.99\frac{1}{2}\frac{1}{T}\int_0^T u'^2(t)\mathrm{d}t \qquad [11.7]$$

11.2. Turbulent energy spectrum

Fluctuations of the velocity field in a turbulent flow vary both in space and time. It is this time–space information that is characterized using the energy spectrum of turbulence. If the variations of one turbulent velocity component $u'(x, t)$ are known over a length interval $[0, L]$ in a direction Ox at a given time t, the variations of $u'(x, t)$ may also be expanded into a Fourier series with respect to the space coordinate x.[2] Thus, [11.2] is extrapolated into:

$$u'(x,t) = \sum_{n=1}^{\infty}\left\{a_n(t)\cos\left(\frac{2\pi n}{L}x\right) + b_n(t)\sin\left(\frac{2\pi n}{L}\right)x\right\} \qquad [11.8]$$

Coefficients a_n and b_n are time dependent but, similarly to [11.3], we have:

$$a_n(t) + ib_n(t) = \frac{2}{L}\int_0^L u'(x,t)\exp\left(i\frac{2\pi n}{L}x\right)\mathrm{d}x \qquad [11.9]$$

Using an infinite number of discrete wave numbers $k_n = n/L$, the instantaneous energy spectrum is calculated as in [11.4]:

$$E(k_n,t) = \frac{L}{4}\left\{a_n^2(t) + b_n^2(t)\right\} \qquad [11.10]$$

For steady-state turbulence, the mean energy spectrum is obtained by time averaging over a time interval of duration T:

$$E\left(k_n = \frac{n}{L}\right) = \frac{1}{T}\int_0^T E(k_n,t)\mathrm{d}t \qquad [11.11]$$

2 This approach is linked to the notion of correlation treated in section 8.2 of Chapter 8 (see Figure 8.2(a)); however, we do not deal the same further here.

The Parceval equality gives an energy correspondence analogous to [11.6].

$$\int_0^\infty E(k)\mathrm{d}k = \frac{1}{2}\frac{1}{T}\frac{1}{L}\int_0^T \left\{\int_0^L u'^2(x,t)\mathrm{d}x\right\}\mathrm{d}t = \frac{1}{2}u_{\mathrm{rms}}^2 \qquad [11.12]$$

The energy spectrum, $E(k)$, provides some spatial information about the energy distribution, which is expressed figuratively by emphasizing that it allows us to know "the energy of turbulent eddies based on their size." The quantity $k = 1/\ell$ is the wave number associated with the size ℓ of a turbulent eddy. A large wave number corresponds to a small-sized eddy, and a small wave number to a large-sized eddy. From energy relation [11.12], it follows that the integral of the energy spectrum is finite. One can, therefore, define minimum and maximum wave numbers, respectively as k_{min} and k_{max}, between which the energy of turbulence is distributed. It can be verified that, usually, $k_{\mathrm{min}} \approx 1/\ell_t$. The wave number k_{max} is, for its part, associated with the smallest scale ℓ_K of turbulence. It is postulated that $k_{\mathrm{max}} = 1/\ell_K$.

11.3. Kolmogorov's theory

Kolmogorov's theory establishes that the energy spectrum has a "universal" form. In other words, the energy spectrum varies with the wave number in identical fashion in all turbulent flows, provided that the ℓ_K and ℓ_t scales are known.

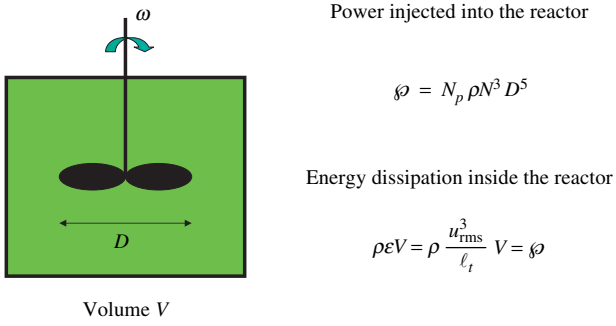

Figure 11.3. *Power injected as mechanical energy and dissipation in a perfectly stirred reactor in a steady-state regime*

Let us first consider the case of steady-state turbulence (the case of unsustained turbulence is discussed later). An energy source has to inject some energy at a rate equal to the rate ε of turbulent kinetic energy dissipation. That is what ideally occurs in a perfectly stirred reactor of volume V (Figure 11.3) in which a moving

body of diameter D rotating at a speed N (in revolutions per second) injects mechanical energy. The injected power is quantified by the power number N_p of the moving body (Chapter 9, equation [9.21]). In a (highly) ideal perfectly stirred reactor, the turbulent velocity u_{rms} and the integral scale ℓ_t are homogeneous. When the steady-state regime is reached, both u_{rms} and ℓ_t are stabilized at levels for which the energy provided by the moving body and the dissipation by turbulence balance each other:

$$\wp = N_p \rho N^3 D^5 = \rho \varepsilon V = \rho \frac{u_{rms}^3}{\ell_t} V \qquad [11.13]$$

This relation does not, by itself, enable the determination of the values of u_{rms} and ℓ_t. Complementary considerations need to be introduced in order to determine the integral scale ℓ_t, which mainly depends on the geometrical characteristics of the experimental apparatus (dimensions of the moving body, size, and geometry of the reactor). Nevertheless, equation [11.13] allows us to comprehend that the kinetic energy dissipation rate increases inside the reactor during the start-up stage of the moving body with the increase of turbulent kinetic energy. When the energy equilibrium is reached, the distribution of kinetic energy among the different scales of turbulence is also steady, and the turbulent kinetic energy spectrum takes on a steady-state form, as depicted in Figure 11.4. The integral of the energy spectrum over all wave numbers is equal to the mean turbulent energy per unit mass (equation [11.12]). Fully developed turbulent flow conditions are obtained when the turbulent Reynolds number $\mathrm{Re}_t = u_{rms} \ell_t / \nu$ (Chapter 8, equation [8.16]) is higher than 100. For such conditions, turbulent kinetic energy is distributed over a wide range of scales, which translates into $k_{max} / k_{min} >> 1$. This often leads to representing the energy spectrum using logarithmic scales, in order to represent the different scales with the same level of information.

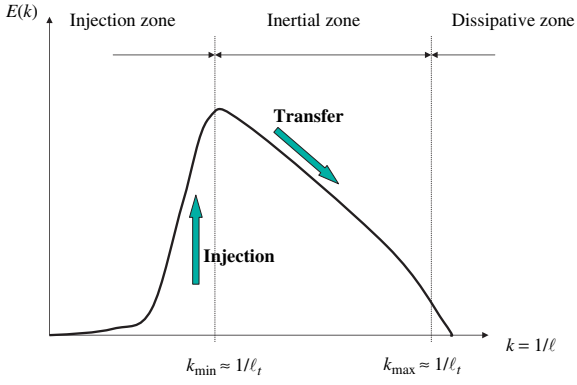

Figure 11.4. *Turbulent energy spectrum according to Kolmogorov's theory*

The starting point of Kolmogorov's theory is equation [11.1], which stipulates that the rate of turbulent kinetic energy dissipation is independent of viscosity and hence depends only on u_{rms} and ℓ_t:

$$\varepsilon = \frac{u_{\text{rms}}^3}{\ell_t} \qquad [11.14]$$

Consequent to this fact, it is deduced that dissipation occurs at small scales. It is easy to evaluate the order of magnitude of the different terms in Navier–Stokes equation, for any scale ℓ inside the interval covered by the turbulent energy spectrum ($\ell_{\text{K}} < \ell < \ell_t$). By associating velocity u_ℓ with length ℓ, the orders of magnitude of the various terms in Navier–Stokes equation can be evaluated:

$$\underset{O\left(\frac{u_\ell^2}{\ell}\right)}{\frac{\partial \vec{u}}{\partial t}} + \underset{O\left(\frac{u_\ell^2}{\ell}\right)}{(\vec{u}\cdot\nabla)\vec{u}} = -\frac{1}{\rho}\nabla p + \underset{O\left(\frac{\nu u_\ell}{\ell^2}\right)}{\nu\Delta\vec{u}} \qquad [11.15]$$

We thus find that the dissipation of turbulent kinetic energy is negligible for those scales ℓ for which $(u_\ell \ell)/\nu >> 1$, whereas it is dominant at scales such that $(u_\ell \ell)/\nu << 1$. In simplifying this observation, Kolmogorov considered that the turbulent kinetic energy is entirely dissipated at the scales $\ell < \ell_{\text{K}}$ and that, conversely, there is no turbulent kinetic energy dissipation at scales $\ell > \ell_{\text{K}}$. The consequences of this drastic simplification are not that important inasmuch as the energy spectrum is very wide ($k_{\max} / k_{\min} >> 1$), so that the transition zone is narrow compared to the energy spectrum as a whole. Kolmogorov then defines the size ℓ_{K} of the smaller scales in turbulence by the relation:

$$\frac{u_{\text{K}} \ell_{\text{K}}}{\nu} = 1 \qquad [11.16]$$

where u_{K} is the turbulent velocity of eddies of size ℓ_{K}.

The phenomenon of energy transfers is represented on the energy spectrum plotted in Figure 11.4. The energy injection occurs at larger scales, whose size is of the order of the integral scale ℓ_t. In a steady turbulence regime, the energy injected cannot be transferred to scales that are larger than ℓ_t, since that energy would then be impossible to dissipate. Energy is, therefore, transferred toward small scales (large wave numbers) in order to be dissipated there. Figure 11.4 includes a representation of the dissipation zone where energy level is very low. The most important part of the energy spectrum is the central zone, called the "inertial zone"

to express the fact that dissipation is negligible therein. This occupies the bulk of the wave number range covered by the energy spectrum. In a steady-state regime, Kolmogorov's theory determines the universal form of the spectrum inside the inertial zone by building on the property whereby the rate of transfer at any scale $\ell = 1/k$ in the inertial zone, toward the small scales, is equal to the rate of turbulent kinetic energy dissipation, ε. This leads to:

$$\varepsilon = \frac{u_\ell^2}{\tau_\ell} \quad \text{with} \quad \tau_\ell = \frac{\ell}{u_\ell} \qquad [11.17]$$

Such a formulation expresses the simple idea that transfer at any scale ℓ within the inertial zone depends only on the characteristics of turbulence at that scale. The turbulent structure can only transfer energy to a smaller scale to the extent of the energy u_ℓ^2 it contains and with its own characteristic time τ_ℓ. That is the reason for bringing in the characteristic time $\tau_\ell = \ell / u_\ell$.

In order to derive from [11.17] the form $E(k)$ of the energy spectrum, we use the correspondence $k = 1/\ell$ and establish a link between u_ℓ^2 and $E(k)$ by writing:

$$u_\ell^2 \approx E(k)\mathrm{d}k \approx E(k)k. \qquad [11.18]$$

The universal form of Kolmogorov's energy spectrum then ensues from [11.17] to [11.18]:

$$E(k) = \varepsilon^{2/3} k^{-5/3} \qquad [11.19]$$

It is found that the energy spectrum decreases within the inertial zone with increasing wave number. The inertial zone contains most of the turbulent kinetic energy relative to the energy contained in the injection zone and the dissipation zone. This is consistent with the shape of the spectrum, since integration of the energy spectrum over the inertial zone yields the turbulent kinetic energy:

$$\int_{k_{\min}=1/\ell_t}^{k_{\max}=1/\ell_K} E(k)\mathrm{d}k = \varepsilon^{2/3} \int_{k_{\min}=1/\ell_t}^{k_{\max}=1/\ell_K} k^{-5/3}\mathrm{d}k \approx \frac{3}{2}\varepsilon^{2/3}\ell_t^{2/3} = \frac{3}{2}u_{\mathrm{rms}}^2, \qquad [11.20]$$

by taking into account the fact that $k_{\max} / k_{\min} >> 1$ and also the definition of ε (equation [11.14]). The turbulent energy is indeed recovered (the factor 3 corresponds to the fact that all the three velocity components need to be accounted for).

The least obvious point in Kolmogorov's model is the relation $\mathrm{d}k \approx k = 1/\ell$ used in [11.18] to link u_ℓ^2 with $E(k)$. This is equivalent to using an integration step

that depends on the size of the object considered. This is not immediately understandable from a mathematical point of view. On the other hand, from a physical standpoint, it is easily acknowledged that it would not be meaningful to use a constant integration step, given the diversity of the scales contained within the inertial zone. One may also consider the fact that a spectral distribution is equivalent to constructing a histogram. It is natural, in a histogram, to classify events into categories that are representative of an identical condition. Let us draw a parallel with an example in economics, considering a population to be characterized by ranking the wealth of individuals for assets between €1000 and €1000 m. One is easily convinced that it makes sense not to put two persons who own €1000 and €10,000 into the same category. It also seems absurd to discriminate someone who owns €10 m from someone who has €10.01 m. Any interpretable statistics will necessarily use a variable step[3] to distinguish between people worth a thousand Euros from millionaires and billionaires. This is analogous to noting that, as a rule, one chooses a measurement unit that is comparable to the dimension of the object to be measured.

11.4. The Kolmogorov scale

Knowing the form of the Kolmogorov spectrum, the Kolmogorov scale can be readily calculated. Writing [11.18] and [11.19] for $k = 1/\ell_K$, it follows from [11.16] that:

$$\ell_K = \left(\frac{\nu^3}{\varepsilon}\right)^{1/4} = \ell_t \, \mathrm{Re}_t^{-3/4} \qquad [11.21]$$

with the turbulent Reynolds number:

$$\mathrm{Re}_t = (u_{\mathrm{rms}} \ell_t)/\nu \qquad [11.22]$$

Likewise, it can be established that:

$$u_K = \varepsilon^{1/3} \ell_K^{1/3} = u_{\mathrm{rms}} \, \mathrm{Re}_t^{-1/4} \qquad [11.23]$$

$$\tau_K = \frac{\ell_K}{u_K} = \tau_t \, \mathrm{Re}_t^{-1/2} << \tau_t \qquad [11.24]$$

The quantities evaluated using equations [11.21]–[11.24] vary with the turbulent Reynolds number. Recall the result from Chapter 8 whereby Re_t should be greater

3 By so doing, we can tacitly employ a representation based on logarithmic scales.

than 100 for the turbulence to be considered as in the developed stage. Equation [11.21] confirms that $k_{\max} / k_{\min} = \ell_t / \ell_K = \mathrm{Re}_t^{3/4} >> 1$ and it is found that the width of the energy spectrum diminishes with decreasing Reynolds number. Lastly, it is worth emphasizing that all quantities are determined on the basis of large-scale values, i.e. u_{rms} and ℓ_t.

We now discuss the case of unsustained turbulence. When the mechanism injecting turbulent kinetic energy is stopped (e.g. the rotating stirrer in a reactor is brought to rest), the turbulent kinetic energy diminishes over time due to dissipation. Figure 11.5 shows the evolution of the turbulent energy spectrum for an unsustained turbulence case. The energy spectrum at time $t = 0$ is the spectrum with the largest area. As time t increases, the energy decreases, so the area under the spectrum must diminish. The Reynolds number gradually decreases with time, but the shape remains as predicted by Kolmogorov's theory as long as $\mathrm{Re}_t > 100$. The width of the spectrum also diminishes over time (equation [11.21]). The spectrum's location along the horizontal axis corresponds to "$t > 0$" (solid line). It will be readily understood that the other two spectra plotted in dotted lines are not relevant. Due to the proportionality of the Kolmogorov energy spectrum to the rate of turbulent energy dissipation (equation [11.19]), such time evolutions of the spectrum would mean that the rate of dissipation remains unchanged (case 1) or increases (case 2) while the Reynolds number decreases.

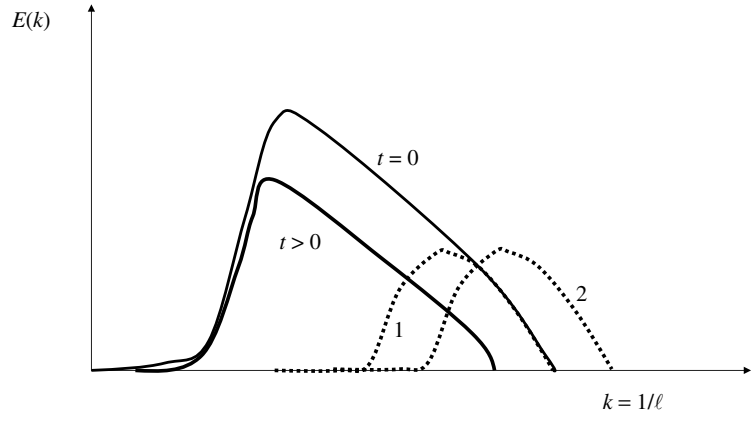

Figure 11.5. *Time evolution of the energy spectrum for an unsustained turbulence case. The relevant evolutionary pattern is plotted as a solid line*

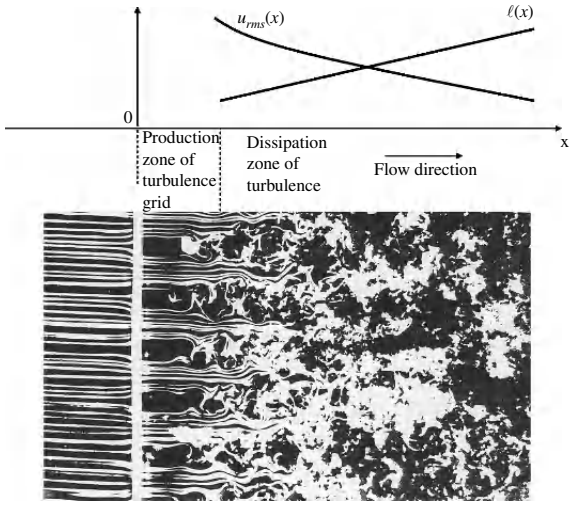

Figure 11.6. *Visualization of grid turbulence (Corke and Nagib, photograh from An Album of Fluid Motion, M. Van Dyke, The Parabolic Press, Stanford, California, 1982). The grid is at x = 0. The mean flow is in the x > 0 direction*

The time evolution of the energy spectrum, as plotted in Figure 11.5, may be set against typical observations that the integral length scale increases in decaying turbulence. In a basin, e.g. small-scale movements dissipate first while the large-scale motions take the maximum time to disappear, when the stirring is stopped. Another example is given by visualisations of grid turbulence flows, as displayed in Figure 11.6. Turbulence is produced in a wind tunnel by directing a homogenous flow through a grid (at $x = 0$). The visualization shows the instability of the jets over the first few lengths downstream of the grid, which develops into turbulent flow. The turbulent kinetic energy is produced in the rear of the grid. The phenomenon of turbulence described using the k–ε model (section 8.8 of Chapter 8) allows us to understand the dynamics of grid turbulence.[4] Downstream of the turbulent kinetic energy production zone, energy production becomes negligible. The mean flow has become uniform again, except in the boundary layers of the wind tunnel walls, but the production of energy near the wall is low compared to the level of turbulence generated by the grid. The turbulent diffusion of energy is also weak in that zone, because the grid produces a homogenous turbulent energy distribution in any plane parallel to the grid and perpendicular to the direction of the flow. The only gradient of turbulent kinetic energy is in the *Ox* direction, but the decrease in the downstream direction is sufficiently slow for diffusion to be neglected. The turbulent velocity $u_{\mathrm{rms}}(x)$, therefore, decreases in the downstream direction due to dissipation. This

4 This is treated in Exercise 8.II at the end of Chapter 8.

behavior is depicted in Figure 11.6. The integral scale of turbulence $\ell_t(x)$ increases with increasing x, a property that can be observed in the flow visualization shown in Figure 11.6.

11.5. Application to macromixing, micromixing, and chemical reaction

Now that we know how to estimate the size ℓ_K of the smallest scales of turbulence, it is simple to conclude by summing up the principles that govern mixing and chemical reactions in a flow with homogenous turbulence. Table 11.1 shows, for a chemical reaction, for micromixing (molecular diffusion), and for macromixing (dispersion at different scales), the characteristic times and the scales with which these various processes are associated. For a stirred reactor, the phenomenon involves six parameters of different nature:

– The fluid's properties: its viscosity ν and diffusivity D of reagents in that fluid.

– Turbulence, which is characterized by the scale ℓ_t and turbulent velocity u_{rms}.

– The scale L of the reactor.

– The characteristic time τ_c of the chemical reaction.

Phenomenon	Spatial scale	Characteristic time	Dimensionless numbers
Chemical reaction	Small scale $\ell_K = \ell_t \, \text{Re}_t^{-3/4}$	τ_c	**Damköhler** $Da = \dfrac{\tau_t}{\tau_c}$
Micromixing	Small scale $\ell_K = \ell_t \, \text{Re}_t^{-3/4}$	$\tau_D = \dfrac{\ell_K^2}{D} = \tau_t Sc \, \text{Re}_t^{-1/2}$	**Schmidt** $Sc = \dfrac{\nu}{D} = \dfrac{\tau_D}{\tau_K}$
Macromixing	Large scale ℓ_t	$\tau_t = \ell_t / u_{\text{rms}}$	**Reynolds** $\text{Re}_t = \dfrac{u_{\text{rms}} \ell_t}{\nu} = \dfrac{\tau_t^2}{\tau_K^2}$
	Small scale $\ell_K = \ell_t \, \text{Re}_t^{-3/4}$	$\tau_K = \tau_t \, \text{Re}_t^{-1/2}$	
	Dispersion in a reactor of size L	$\tau_{\text{disp}} = \dfrac{L^2}{\ell_t^2} \tau_t$	**Scale ratio** $\dfrac{L}{\ell_t} = \sqrt{\dfrac{\tau_{\text{disp}}}{\tau_t}}$

Table 11.1. *Spatial scales and characteristic times associated with the mixing and chemical reaction processes*

As these six parameters involve two dimensions (length and time), they lead to the expression of four dimensionless numbers, which are also given in Table 11.1.

These parameters influence five processes (chemical reaction, micromixing, and the three scales of macromixing), which also bring forth five characteristic times. It can be seen that the four dimensionless numbers can be expressed as a ratio of the time scales associated with the processes of micromixing, macromixing, and chemical reaction.

In Table 11.1, we associate the Damköhler number with the chemical reaction, which is restrictive since that number also involves the characteristic time of turbulence, τ_t. It is also restrictive associating the Schmidt number only to micromixing, since this number is the ratio of the characteristic time of micromixing to the characteristic time of small-scale macromixing. Nevertheless, the Damköhler number is the only one that involves chemistry, just as the Schmidt number is the only one that takes into account the diffusion process.

The Schmidt number depends only on the physical properties of a fluid. For an aqueous medium, the Schmidt number is usually of the order of $Sc = 10^3$. The physical meaning of this dimensionless number therefore renders micromixing more limiting than macromixing in an aqueous medium. On the other hand, in a gaseous medium such as air, the Schmidt number is usually of the order of $Sc = 1$, which means that there is no particular need to be concerned with micromixing if the macromixing processes are effective.

Lastly, we recall equation [10.14] of Chapter 10, which sets out explicitly that the advancement time of a chemical reaction is governed by the slowest process.

$$\tau_R \approx \max\{\tau_D, \tau_C, \tau_K, \tau_t, \tau_{disp}\} \qquad [11.25]$$

For an open reactor, this time will need to be compared to the residence time.

11.6. Application exercises

Exercise 11.1: Mixing in a continuous stirred tank reactor

Ethyl acetate reacts with soda in a CSTR as follows:

$$CH_3C_2H_5COO + NaOH \rightarrow C_2H_5OH + CH_3CO_2Na$$

The reaction is first order with respect to each of the constituents. This reaction's constant is $k = 200$ L mol^{-1} h^{-1}. In the following discussion, we denote ethyl acetate by A and soda by B. Both products are in solution in water. The diffusivities of the two constituents are, respectively, $D_A = 10^{-5}$ cm^2 s^{-1} and $D_B = 3.1 \times 10^{-5}$ cm^2 s^{-1}.

The reactor is a cube of volume $V = 1$ L. Both products enter the reactor at the same rate $Q = 15$ L h^{-1}, and have been prepared with the same concentration $C = 1$ mol L^{-1}.

Stirring inside the reactor is produced by a stirrer of diameter $d = 5$ cm, whose rotational speed is $N = 600$ rpm. It is assumed that the turbulent velocity u_{rms} and the integral scale ℓ_t of turbulence are homogenous inside the vessel. The mechanical power required to rotate the stirrer is $\wp = 0.4\rho N^3 d^5$ ($\wp$ being in W, ρ in kg m^{-3}, N in rotations/s, and d in meters). Assuming that this power is dissipated by turbulence, we deduce that $\wp = \rho V u_{\text{rms}}^3 / \ell_t$. In the following, we use the values $u_{\text{rms}} = 10.8$ cm s^{-1} and $\ell_t = 1$ cm, which verify the latter relation and for which the scale ℓ_t is commensurate with the size of the moving body. Based on this information, now:

1. Calculate the Reynolds number and the Kolmogorov scale.

2. Calculate the different time characteristics of the problem.

3. Is the mixing effective? What is the advancement time of the reaction? To what extent is the reaction completed at the reactor's outlet?

Exercise 11.II: Mixing and combustion

Consider the combustion reaction of methane in air

$$CH_4 + 2O_2 \rightarrow CO_2 + 2\,H_2O$$

1. The following data were found in the *Handbook of Physics and Chemistry* for the kinematic viscosity of air and diffusivity of methane in air.

Temperature T (K)	297	473	673
Diffusivity of CH_4 in air (cm^2 s^{-1})	0.106	0.485	0.899
Temperature T (K)	303	473	773
Kinematic viscosity of air (cm^2 s^{-1})	0.160	0.346	0.785

Justify that micromixing is not more limiting than macromixing for the chemical reaction.

2. The combustion reaction is more complex than summarized in the above reaction. Several reactions occur in sequence and in parallel. A global kinetic model establishes that the reaction rate can be evaluated by:

$$r = -\frac{\mathrm{d}[CH_4]}{\mathrm{d}t} = -\frac{1}{2}\frac{\mathrm{d}[O_2]}{\mathrm{d}t} = 1.3\times10^8 \exp\left(-\frac{E_a}{RT}\right)[CH_4]^{-0.3}\,[O_2]^{1.3}$$

The activation energy of the reaction is $E_a = 48.4$ kcal mol^{-1}. The reaction rate r is expressed as mol cm^{-3} s^{-1} and the concentrations as mol cm^{-3}. The universal gas constant is $R = 8.32$ J mol^{-1} K^{-1}. For a mixture of methane and oxygen in stoichiometric proportions, the characteristic time τ_c of the reaction is then expressed by:

$$\frac{1}{\tau_c} = -\frac{1}{[O_2]}\frac{d[O_2]}{dt} = -\frac{1}{[CH_4]}\frac{d[CH_4]}{dt} = 3.2\times10^8 \exp\left(\frac{-E_a}{RT}\right)$$

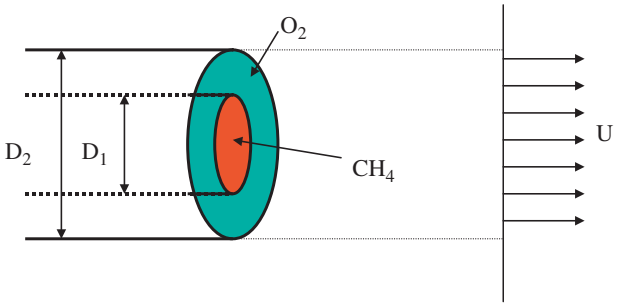

Figure 11.II.1

Consider a burner with two concentric injections (see Figure II.1). The fuel (CH_4) leaves through the central aperture of diameter $D_1 = 10$ cm. The oxidizer (O_2) exits through the annular aperture of diameter $D_2 = 20$ cm. The velocity of both fluids is identical ($U = 20$ m s^{-1}). The flow is turbulent and it is postulated that the characteristics of turbulence are such that $u_{rms} = 2$ m s^{-1} and $\ell_t = (D_2 - D_1)/4 = 2.5$ cm.

For two flame temperatures ($T = 1000$ K and $T = 2000$ K), discuss, based on a comparison between the characteristic time of the chemical kinetics and the characteristic times of mixing, to what extent the reaction can be considered as slow or fast relative to turbulent mixing.

What mechanism controls the combustion in each case?[5]

5 This exercise provides evidence of the fact that the kinetics (given by an Arrhenius law) is very sensitive to temperature. The temperatures achieved by combustion in pure oxygen are often much higher than for combustion in air, as no energy is consumed to heat nitrogen.

Exercise 11.III: Laminar and turbulent diffusion flames[6]

In this exercise, we study a combustion flame burning a gaseous fuel A in a gaseous oxidizer B. The oxidizer is air in an infinite environment, and the fuel is a gas which is fed into the oxidizer-filled environment through a cylindrical pipe of diameter $\phi = 3$ cm. The velocity of the fuel jet at the pipe exit is assumed to be uniform and denoted by $W = 10$ m s^{-1}. Reagent diffusivity $D = 1.5 \times 10^{-5}$ m^2 s^{-1} and the viscosity of the fluid, $\nu = 1.5 \times 10^{-5}$ m^2 s^{-1}, are used. The kinetics of the reaction is given by the chemical time $\tau_c = 10^{-5}$ s. If mixed, the reagents are assumed to be in stoichiometric proportions.

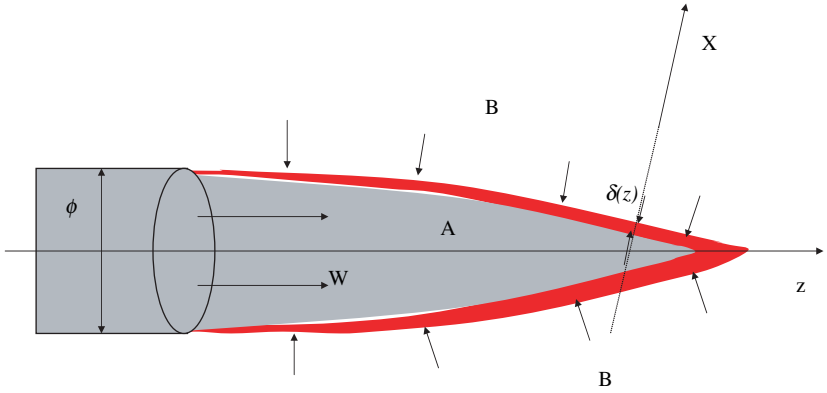

Figure 11.III.1

The laminar diffusion flame

When the kinetics is very fast, reagents A and B are only brought together within a thin mixing layer, which is the darker area represented in Figure III.1. That is the shape of the flame as seen by an observer, due to the radiation generated by combustion. Inside that, there is only fuel A, which is transported by the stream up the reaction layer. Outside, there is only the oxidizer, which is carried by diffusion into the reaction zone, as indicated by the small arrows. Both constituents diffuse into the mixing layer where they react together, hence the term "diffusion flame."

When the kinetics is infinitely fast, the shape of the flame can easily be obtained thanks to the Schvab-Zeldovitch function $Z = Y_A - Y_B$, defined on the basis of the fuel and oxidizer mass fractions Y_A and Y_B. Indeed, function Z is a solution of

6 The idea of including this exercise in this chapter came from reading the book by R. Borghi and M. Destriau, *La combustion et les flammes* (Lavoisier, 1995).

the following advection–diffusion equation (expressed in the cylindrical coordinate system based on the *Oz* axis, assuming that the flame is highly elongated, so that molecular diffusion occurs chiefly in the radial direction):

$$\frac{\partial}{\partial z}\{u_z Z\} = D\frac{1}{r}\frac{\partial}{\partial r}\left(r\frac{\partial Z}{\partial r}\right) \qquad [11.III.1]$$

The thickness, δ, of the reaction zone increases with z. In the mixing layer, the reagent concentrations qualitatively exhibit the shape plotted in Figure 11.III.2 along the crosswise direction X. A dimensional analysis of equation [11.III.1] indicates that the length of the flame L_f is in the form

$$\frac{L_f}{\phi} = \alpha\frac{W\phi}{D} \qquad [11.III.2]$$

where α is a constant.

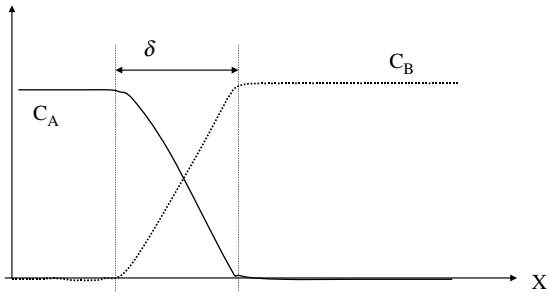

Figure 11.III.2

1. For a laminar flow, explain why the thickness, δ, of the mixing layer increases from the fuel injection orifice and why its value rapidly levels out at a maximum value. It will be easier to evaluate the time evolution $\delta(t)$ by noting that time t corresponds to a spatial displacement $z = Wt$ in the Oz direction.

2. Evaluate the maximum thickness of the reactive zone. Based on that value, justify that the kinetics of combustion can actually be considered instantaneous.

The turbulent flame

For simplicity, it is assumed that the properties of turbulence are homogenous in that part of the jet where the reaction occurs. The turbulent velocity and the integral scale will be chosen such that $u_{rms} = \beta W$ and $\ell = \gamma\varphi$, with $\beta = \gamma = 0.1$.

3. Due to turbulence, the shape of the flame remains similar to that charted in Figure III.1. Its dimensions are altered by the effect of turbulence, but that issue is examined in subsequent questions. The distribution of reagent concentrations within the mixing layer can still be represented by Figure 11.III.2, although its thickness is controlled by a turbulent diffusion/dispersion process. Based on the above, elucidate the turbulent diffusion coefficient.

To what extent do the plotted concentration profiles represent either the concentration of reagents in the fluid particles or the distribution of fluid particles containing a reagent that is not mixed with the other?

4. Evaluate $\delta(t)$ for time τ_t of turbulence and for time τ_D, which is characteristic of diffusion. Does either or both of these appear reasonable to you for estimating the thickness of the turbulent mixing layer and of the reaction zone? Can the chemical reaction still be considered instantaneous?

5. How is the flame's length modified in a turbulent regime relative to equation [11.III.2], which is representative of the laminar case (A dimensional law should be proposed here to correctly answer this question.)?

6. Is the turbulent flame shorter or longer than the laminar flame? Compare the advantages and disadvantages of a laminar and turbulent flame, in terms of energy.

Chapter 12

Micromixing Models

12.1. Introduction

We discuss in this chapter the numerical modeling of mixing and chemical reaction(s). For a turbulent flow, we have seen in the previous chapters that mixing at the molecular scale, which is necessary to perform the chemical reaction, involves very fine scale motions in the flow. These are so minute that currently it is hardly possible to carry out direct numerical simulations of reacting flows for Reynolds numbers typical of situations of practical interest. In order to treat industrial situations, coarser models have been developed. In this chapter, we focus on two such models, which, by implementing the concepts described in the previous chapters, model the mixing and chemical reaction of constituents in a fluid:

– the interaction by exchange with the mean (IEM) model, and

– the coalescence-dispersion (CD) model.

These classical models are nowadays embedded in certain numerical codes, and they are most commonly used in engineering processes. It is useful to know them, as well as the k-ε model summarized in Chapter 8.

The set of problems to be modeled is illustrated in Figure 12.1. Let us consider a reactor into which two volumes respectively containing chemicals A and B are injected. In a turbulent flow, the introduced fluid volumes split up to form elementary fluid particles (EFP). Their size is such that the concentrations of products are homogeneous in each EFP. It is through interactions between EFPs that mixing is modeled. When the products react with one another, chemical reaction(s) occurs within each EFP.

In order to implement the IEM and CD models, selecting a location sufficiently far from the point of injection enables us to assume that the splitting process has already taken place. When the Schmidt number is Sc = 1, the size of the EFPs is of the order of the Kolmogorov scale (the more complex case wherein $\mathrm{Sc} \neq 1$ is not addressed in this chapter).[1]

As shown in Figure 12.1, the model is constituted of two model entities, which compute in parallel between two time steps $n\Delta t_{\mathrm{Lag}}$ and $(n+1)\Delta t_{\mathrm{Lag}}$: (i) a Lagangian model computes the transport and dispersion in the fluid flow of EFPs; (ii) a mixing model computes the mixing between the EFPs contained at time $n\Delta t_{\mathrm{Lag}}$ inside a cell of the computation domain.

The Lagrangian model determines the positions $\vec{x}_{p,i}(\vec{x}_{p,i,0},t)$ by integrating for each EFP in the domain:

$$\frac{\mathrm{d}\vec{x}_{p,i}}{\mathrm{d}t} = \vec{u}(\vec{x}_{p,i},t) = \overline{\vec{u}}(\vec{x}_{p,i},t) + \vec{u}'(\vec{x}_{p,i},t) \qquad [12.1]$$

$\vec{x}_{p,i,0}$ is the position at time t = 0 of EFP number i. The vector $\vec{u}(\vec{x}_{p,i},t)$ is the velocity of the fluid at $\vec{x}_{p,i}$. In order to model turbulent dispersion (macromixing), the velocity $\vec{u}$ should be an instantaneous value of the velocity, taking into account the turbulence-average velocity of the flow as well as the instantaneous turbulent velocity. We do not describe in detail this aspect of the model, which is distinct from the mixing model, but we emphasize that the mixing model should be coupled with a Lagrangian model calculating the random movements of elementary fluid particles in order to take into account the turbulent dispersion process described in the previous chapters.

The mixing model (IEM or CD) implement a process of interactions between EFPs which exchanges, between two time steps $n\Delta t_{\mathrm{Lag}}$ and $(n+1)\Delta t_{\mathrm{Lag}}$, the products A and B among EFPs contained in each cell of the fluid domain mesh. The Lagrangian model determines at each time $n\Delta t_{\mathrm{Lag}}$ the EFPs contained in each cell, which is considered by the mixing model as a closed stirred tank reactor between times $n\Delta t_{\mathrm{Lag}}$ and $(n+1)\Delta t_{\mathrm{Lag}}$. The size of the fluid volumes constituting the domain mesh cells should be chosen sufficiently small for those fluid volumes to be regarded as perfectly stirred reactors, which means that interactions between EFPs can occur with the same probability regardless of their relative positions in the mesh cell. The mixing model modifies the concentrations in EFPs, as Figure 12.1

1 For $Sc > 1$, the size of the scales to be resolved is of the order of the Batchelor scale $\ell_B = Sc^{-1/2}\ell_K$. This is smaller than the Kolmogorov scale ℓ_K.

illustrates by showing the increase between times $n\Delta t_{\text{Lag}}$ and $(n+1)\Delta t_{\text{Lag}}$ in the proportion of EFPs with intermediate gray levels. The positions of EFPs in each cell are kept unchanged, and the Lagrangian model applies the displacements to the EFPs whose concentrations were modified by the mixing model.

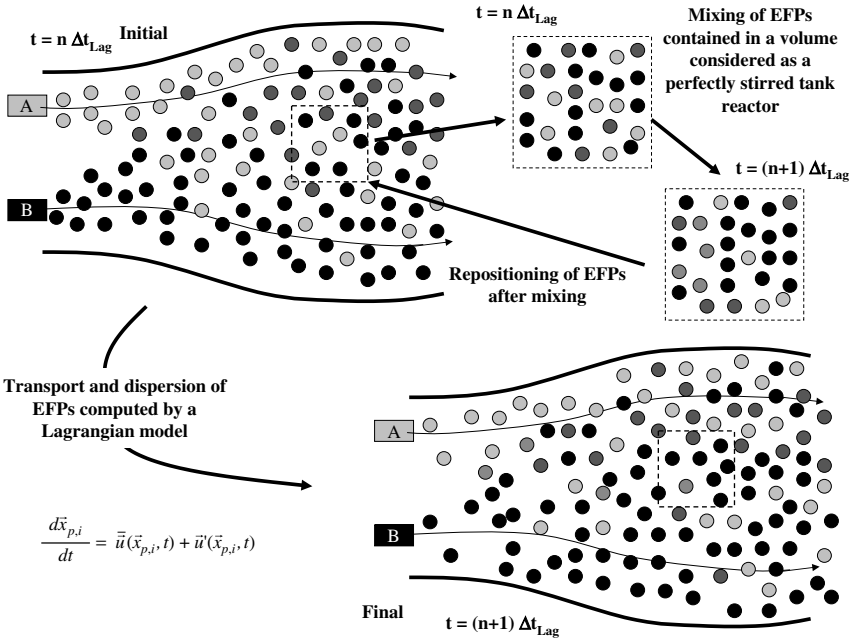

Figure 12.1. *Modeling mixing by associating a Lagrangian model, which calculates the movements of EFPs, with a model calculating their mixing in a fluid volume regarded as a perfectly stirred tank reactor*

In the next sections, we study both the CD, and then the IEM models, by implementing them in the configuration of a perfectly stirred reactor:

– Closed reactor: Mixing is characterized by the time evolution of $P(C_{\text{A}}, C_{\text{B}}, t)$.

– Open reactor in a steady-state regime (CSTR): Mixing is characterized by the difference between probability densities $P_E(C_{\text{A}}, C_{\text{B}})$ and $P(C_{\text{A}}, C_{\text{B}})$, respectively at the inlet and outlet of the reactor

In the closed-reactor case, the reactor initially contains (Figure 12.2(a)) a fluid volume V_{A} in which the concentrations are ($C_{\text{A}} = C_{\text{A0}}, C_{\text{B}} = 0$) and a fluid volume V_{B} in which the concentrations are ($C_{\text{A}} = 0, C_{\text{B}} = C_{\text{B0}}$). Further, $V = V_{\text{A}} + V_{\text{B}}$

denotes the volume of the reactor. It is assumed that both volumes are instantaneously fragmented into N_A and N_B EFPs in which the concentrations are ($C_A = C_{A0}, C_B = 0$) and ($C_A = 0, C_B = C_{B0}$), respectively. The EFPs are dispersed in a statistically homogeneous manner within the reactor. In Figure 12.2(a), the representation therefore exhibits both classes of EFPs dispersed inside the fluid, right from the time $t = 0$ from which mixing is modeled. The numbers of EFPs N_A and N_B are sufficiently large to provide a statistical representation that conforms to the relative proportions among constituents ($N_A / (N_A + N_B) = V_A / (V_A + V_B)$), without the need for the number of EFPs multiplied by their volumes to be equal to the initial volumes V_A and V_B. They are merely statistically representative samples. The carrier phase shown in Figure 12.2(a) is fictitious. Should a continuous carrier phase be taken into account, it would initially occupy a certain volume and be represented by a third category of EFPs with concentrations ($C_A = 0, C_B = 0$). Due to the action of the mixing model, the concentrations evolve in time within each EFP, as characterized by the time evolution of the probability density function (PDF) $P(C_A, C_B, t)$.

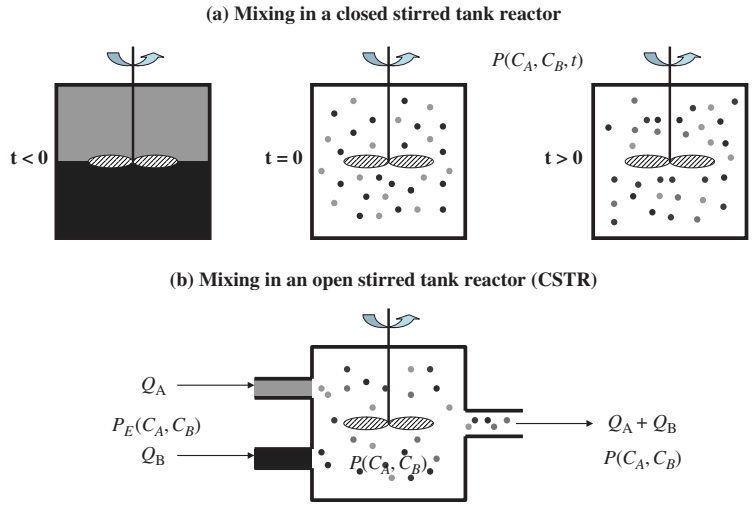

Figure 12.2. *Implementation process of mixing models in a perfectly stirred tank reactor. The fluid volume is fragmented into EFPs of the size of the Kolmogorov scale*

For the open reactor in a steady-state regime (Figure 12.2(b)), volume flow rates, Q_A and Q_B, are injected continuously with respective concentrations ($C_A = C_{A0}, C_B = 0$) and ($C_A = 0, C_B = C_{B0}$). It is also assumed that the fluid volumes are split into EFPs and are dispersed in a statistically homogeneous manner immediately upon entering the reactor. The concentrations in the EFPs vary with

time due to mixing while the EFPs are inside the reactor. Nevertheless, from the reactor is discharged a population of EFPs that have resided inside the reactor for variable durations, and whose statistical properties do not vary with time. For a CSTR, the PDF characterizing the population of EFPs at the outlet of the reactor, $P(C_A, C_B)$, is identical to the one that can be computed at any point in the reactor. The difference between $P(C_A, C_B)$ and the PDF $P_E(C_A, C_B)$ at the reactor's inlet provides a characterization of the degree of mixing.

Both the IEM and CD models address the statistics of EFP populations using the PDF $P(C_A, C_B, t)$ of finding in a EFP the concentrations C_A and C_B of the two products. We use here the tools introduced in Chapter 10 to express the average concentration:

$$\overline{C_A}(t) = \int_0^\infty \left\{ \int_0^\infty C_A P(C_A, C_B, t) \mathrm{d}C_A \right\} \mathrm{d}C_B \qquad [12.2]$$

and the variance:

$$\sigma_A^2(t) = \int_0^\infty \left\{ \int_0^\infty (C_A - \overline{C_A})^2 P(C_A, C_B, t) \mathrm{d}C_A \right\} \mathrm{d}C_B \qquad [12.3]$$

for product A. The same quantities are defined in a similar fashion for product B. We also have:

$$\int_0^\infty \left\{ \int_0^\infty P(C_A, C_B, t) \mathrm{d}C_A \right\} \mathrm{d}C_B = 1 \qquad [12.4]$$

Lastly, we define the segregation indices:

$$I_A(t) = \frac{\sigma_A^2(t)}{\sigma_A^2(t=0)} \text{ and } I_B(t) = \frac{\sigma_B^2(t)}{\sigma_B^2(t=0)} \qquad [12.5]$$

In the following discussion, we first present the CD model before discussing the IEM model. However, we discuss the non-reacting case beforehand.

12.2. CD model

12.2.1. *Principle*

In order to implement the CD model, we shall examine the case of a perfectly stirred reactor described in the previous section and illustrated by Figure 12.2. We hence consider the case of a closed reactor (without reaction, and then with reaction) and that of an open reactor sequentially.

An element specific to the CD model, in addition to the remarks accompanying Figure 12.2, is that the CD model defines an initial population of EFPs by assigning a number to each EFP. The time evolution of concentrations in each EFP is then monitored. The model thus ensures a perfect traceability of EFPs. The PDF $P(C_A, C_B, t)$ is reconstructed at every time step.

The CD model is implemented according to the following scenario:

– at every time T_{CD}, EFPs are randomly selected in pairs within the set of $2N = N_A + N_B$ EFPs contained in the domain; and

– for each pair of selected EFPs, the two EFPs are mixed (coalescence) and then the entity is split once again into two EFPs. The modified EFPs are placed back inside the volume at their initial positions.

For a pair of selected EFPs with numbers i and j, we denote by $C_{Ai}(kT_{CD})$, $C_{Bi}(kT_{CD})$, $C_{Aj}(kT_{CD})$, and $C_{Bj}(kT_{CD})$ the concentrations in the EFPs before operating the CD model for the $(k + 1)$th time. The concentrations after application of the CD process are:

$$\begin{aligned} C_{Ai}((k+1)T_{CD}) = C_{Aj}((k+1)T_{CD}) &= \frac{C_{Ai}(kT_{CD}) + C_{Aj}(kT_{CD})}{2} \\ C_{Bi}((k+1)T_{CD}) = C_{Bj}((k+1)T_{CD}) &= \frac{C_{Bi}(kT_{CD}) + C_{Bj}(kT_{CD})}{2} \end{aligned} \qquad [12.6]$$

The CD model is, by its very nature, a discrete model with respect to time. At every time step kT_{CD}, the PDF $P(C_A, C_B, kT_{CD})$ is computed by considering all the EFPs available in the domain.

Before we continue our discussion further, let us cite references to the contributions of Curl (1963) and Spielman and Levenspiel (1965) to the CD model. In France, the book by Villermaux (1993) is an authority on the subject matter.[2] A comprehensive review of mixing models is given in the book by Fox, definitely oriented toward their implementation in computational models.

2 Villermaux J., 1993, *Génie de la Réaction chimique* (Tec&Doc, Lavoisier, Paris). Villermaux J., 1986, "Mixing phenomena in stirred reactors", *Encyclopaedia of Fluid Mechanics*, Ch. 27 (Gulf Publishing Co., Houston). Curl R.L., 1963, *AIChE J.*, 9, 175. Spielman L.A. and Levenspiel O., 1965, *Chem. Eng. Sci.*, 20, 247. Fox R.O., 2003, *Computational models for turbulent reacting flows*, Cambridge University Press.

12.2.2. *CD model in a closed reactor without reaction*

If no chemical reaction is observed, the evolution of concentrations in the EFPs can be considered independently for each product. It is, therefore, simpler to consider a single constituent whose concentration is denoted by C. The generalization of several constituents is done later while dealing with the reacting case. We shall not encounter any particular difficulty in this regard. Initially, we again consider two categories of EFPs, one with concentration $C = C_0$ and another with concentration $C = 0$. For the initial situation depicted in Figure 12.3 where both types of EFPs are in equal numbers, the initial PDF is written as:

$$P(C, t = 0) = 0 \text{ if } C \neq 0 \text{ and } C \neq C_0$$

$$P(C = 0, t = 0) = 1/2 \qquad [12.7]$$

$$P(C = C_0, t = 0) = 1/2$$

The histogram shown in Figure 12.3 consists of two delta functions. Calculating the PDF $P(C, kT_{CD})$ "by hand" for the first two iterations (k = 1 and k = 2) enables us to describe the mixing process in the CD model.

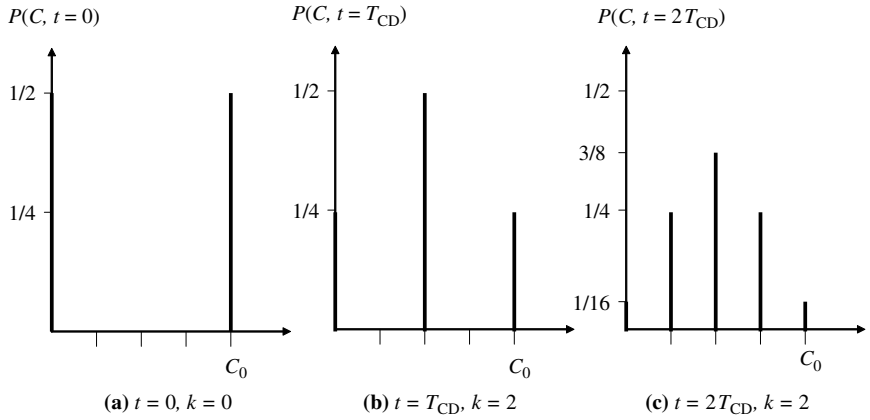

Figure 12.3. *Probability density functions* $P(C, kT_{CD})$ *resulting from the first two iterations (k = 1 and k = 2) of the CD model for the initial PDF represented in* (a)

Applying the CD model at time $t = T_{CD}$ (k = 1) to the initial distribution of EFPs [12.7] exhibits three types of EFPs, namely a mixture of EFPs with concentration $C = 0$ or of EFPs with concentration $C = C_0$ with a EFP of the same concentration,

or a mixture of a EFP of concentration $C = 0$ with a EFP of concentration $C = C_0$. In the first two cases, the concentrations inside the EFPs are not modified, whereas the concentration in the EFPs obtained by the third type of interaction is $C = C_0 / 2$. The PDF of the new EFP distribution is:

$$\begin{aligned}
&P(C,T_{CD}) = 0 \text{ if } C \neq 0, C \neq C_0, \text{ and } C \neq C_0 / 2 \\
&P(C = 0, T_{\mathrm{CD}}) = P(C = 0,0)P(C = 0,0) = 1/4 \\
&P(C = C_0, T_{\mathrm{CD}}) = P(C = C_0,0)P(C = C_0,0) = 1/4 \\
&P(C = C_0 / 2, T_{\mathrm{CD}}) = 2P(C = C_0,0)P(C = 0,0) = 1/2
\end{aligned} \qquad [12.8]$$

These probability values are obtained owing to the fact that the selection probabilities of the two EFPs forming a pair are independent from each other. For the third type of EFP, factor 2 appears because the EFP of concentration $C = 0$ may be the first one or the second one selected. The probability distribution $P(C, T_{\mathrm{CD}})$ has three delta functions (Figure 12.3(b)). It is verified that the sum of probabilities equals 1.

The PDF obtained after the second iteration is shown in Figure 12.3(c). We calculate the probability densities as:

$$\begin{aligned}
&P(C, 2T_{\mathrm{CD}}) = 0 \text{ if } C \neq 0, C \neq C_0, C \neq C_0 / 2, C \neq C_0 / 4, \text{ and } C \neq 3C_0 / 4 \\
&P(0, 2T_{\mathrm{CD}}) = P(0, T_{\mathrm{CD}})P(0, T_{\mathrm{CD}}) = 1/16 \\
&P(C_0, 2T_{\mathrm{CD}}) = P(C_0, T_{\mathrm{CD}})P(C_0, T_{\mathrm{CD}}) = 1/16 \\
&P(C_0 / 4, 2T_{\mathrm{CD}}) = 2P(0, T_{\mathrm{CD}})P(C_0 / 2, T_{\mathrm{CD}}) = 1/4 \\
&P(3C_0 / 4, 2T_{\mathrm{CD}}) = 2P(C_0 / 2, T_{\mathrm{CD}})P(C_0, T_{\mathrm{CD}}) = 1/4 \\
&P(C_0 / 2, 2T_{\mathrm{CD}}) = 2P(0, T_{\mathrm{CD}})P(C_0, T_{\mathrm{CD}}) + P(C_0 / 2, T_{\mathrm{CD}})P(C_0 / 2, T_{\mathrm{CD}}) = 3/8
\end{aligned} \qquad [12.9]$$

Detailing the probability calculations allows us to identify the EFP interactions from which the new distribution results. It is easy to imagine the form of the probability densities obtained from subsequent iterations. Additional lines appear in the histogram for the intermediary concentrations for which the PDF was non-zero. The distribution will include an increasing number of peaks, whose magnitudes will gradually decrease and eventually lead to a single delta function for the average concentration $C = C_0 / 2$.

The concept of the CD model is simple from a theoretical viewpoint. Its numerical implementation usually employs a Monte-Carlo method to perform the random selection of particle pairs whose PDF $P(C,t=kT_{\mathrm{CD}})$ is reconstructed at every iteration.

A time-continuous formalization of the CD model (considering a continuous function $P(C,t)$) enables the establishment of some interesting properties of the model. Assuming that $P(C,kT_{\mathrm{CD}})$ is known following the *k*th iteration of the CD model, it is verified that $P(C,(k+1)T_{\mathrm{CD}})$ is given by:

$$P(C,(k+1)T_{\mathrm{CD}}) = \int_0^{2C} 2P(C',kT_{\mathrm{CD}})P(2C-C',kT_{\mathrm{CD}})\mathrm{d}C' \qquad [12.10]$$

To this end, it is sufficient to note that the EFPs of concentration *C* resulting from the (*k* + 1)th iteration are products of all the CD processes between EFPs of concentration C' and $C''=2C-C'$, since $C=(C'+C'')/2$. The bounds of the integral are defined in [12.10] so as to include all possible interactions. Formally, C' or C'' can be defined outside the interval [0, C_0], since then $P(C',kT_{\mathrm{CD}})=0$ or $P(C'',kT_{\mathrm{CD}})=0$. Factor 2 appears in [12.10] by virtue of the argument invoked previously: concentration C′ can be selected first or second. It is also verified that:

$$\int_0^{\infty} P(C,(k+1)T_{\mathrm{CD}})\mathrm{d}C = 1$$

since, with changes in variables $C_1=C'$ and $C_2=2C-C'$:

$$\int_0^{\infty}\left\{\int_0^{2C} 2P(C',kT_{\mathrm{CD}})P(2C-C',kT_{\mathrm{CD}})\mathrm{d}C'\right\}\mathrm{d}C = \left\{\int_0^{\infty} P(C_1,kT_{\mathrm{CD}})\mathrm{d}C_1\right\}\left\{\int_0^{\infty} P(C_2,kT_{\mathrm{CD}})\mathrm{d}C_2\right\} = 1$$

Returning to [12.10], we obtain:

$$\frac{\left\{\int_0^{2C} 2P(C',kT_{\mathrm{CD}})P(2C-C',kT_{\mathrm{CD}})\mathrm{d}C'\right\} - P(C,kT_{\mathrm{CD}})}{T_{CD}} = \frac{P(C,(k+1)T_{\mathrm{CD}}) - P(C,kT_{\mathrm{CD}})}{T_{\mathrm{CD}}}$$

Going to the limit for $T_{CD} \to 0$ leads to the evolution equation for $P(C,t)$:

$$\frac{\partial P(C,t)}{\partial t} = \omega J \qquad [12.11]$$

with $\omega = 1/T_{CD}$ and:

$$J = \left\{ \int_0^{2C} 2P(C',t)P(2C-C',t)\mathrm{d}C' \right\} - P(C,t) \qquad [12.12]$$

Coefficient J is calculated as the time evolution progresses.

The CD model depends on the period T_{CD} (or, equivalently, on the frequency, ω), its only adjustable parameter. This sets the speed of mixing. Through somewhat tedious calculations, it can be shown that the segregation index decreases exponentially with time. By introducing the nth order moments of the PDF:

$$\mu_n(t) = \int_0^{\infty} C^n P(C,t)\mathrm{d}t \qquad [12.13]$$

writing [12.11] in the form:

$$\frac{1}{\omega}\frac{\partial P(C,t)}{\partial t} + P(C,t) = 2\int_0^{2C} P(C',t)P(2C-C',t)\mathrm{d}C' \qquad [12.14]$$

makes it possible to show that:

$$\begin{aligned} \frac{1}{\omega}\frac{\mathrm{d}\mu_n}{\mathrm{d}t} + \mu_n &= 2\int_0^{\infty} C^n \left[\int_0^{2C} P(C',t)P(2C-C',t)\mathrm{d}C' \right] \mathrm{d}C \\ &= \int_0^{\infty}\int_0^{\infty} \left(\frac{C'+C''}{2} \right)^n P(C',t)P(C'',t)\mathrm{d}C'\mathrm{d}C'' \\ &= \frac{1}{2^n}\sum_{i=0}^{n} \frac{n!}{i!(n-i)!} \int_0^{\infty} C'^i P(C',t)\mathrm{d}C' \int_0^{\infty} C''^{(n-i)} P(C'',t)\mathrm{d}C'' \end{aligned} \qquad [12.15]$$

That is:

$$\frac{1}{\omega}\frac{\mathrm{d}\mu_n}{\mathrm{d}t} + \mu_n = \frac{1}{2^n}\sum_{i=0}^{n} \frac{n!}{i!(n-i)!} \mu_i \mu_{n-i} \qquad [12.16]$$

This equality enables us to recover the following:

at order 0: $\mu_0(t) = \int_0^\infty P(C,t)\mathrm{d}t = 1$, and

at order 1: $\mathrm{d}\mu_1(t)/\mathrm{d}t = 0$,

which signifies the conservation of the constituent in the absence of a reaction:

at order 2: $(1/\omega)(\mathrm{d}\sigma^2(t)/\mathrm{d}t) = -(1/2)\sigma^2(t)$,

since the variance is written out as $\sigma^2(t) = \mu_2(t) - \mu_1^2$.

For the CD model, the segregation index decreases exponentially as a function of time:

$$I(t) = \frac{\sigma^2(t)}{\sigma^2(0)} = \exp\left(-\frac{\omega}{2}t\right) \qquad [12.17]$$

This result provides an alternative way of selecting the frequency $\omega = 1/T_{\mathrm{CD}}$ of the CD model.

12.2.3. *CD model in an open reactor without reaction*

The CD model is only modified to a minor extent when an open reactor is considered. For a reactor of volume $V = L^3$ through which a flow rate Q passes, the mean time of residence in the reactor is $\tau_{\mathrm{residence}} = V/Q$.

Recalling the results obtained in Chapter 10, macromixing can be regarded as perfect if:

$$\tau_{\mathrm{disp}} = \left(\frac{L}{\ell_t}\right)^2 \frac{\ell_t}{u_{\mathrm{rms}}} << \tau_{\mathrm{residence}} = \frac{V}{Q} \qquad [12.18]$$

We denote by $P_E(C,t)$ the PDF of the EFPs entering the reactor. Since the reactor is perfectly stirred at the macroscopic level, the PDF of the EFPs leaving the reactor is identical to the one that prevails homogeneously in the vessel, namely $P(C,t)$. In a steady-state regime, an identical number of EFPs should be entering and leaving the reactor at any given time. Denoting by N the number of EFPs per

unit volume, $n(C,t) = NP(C,t)$ is the density of EFP population as a function of concentration. The mass balance in the reactor is then written as:

$$V\frac{\partial n(C,t)}{\partial t} = VN\frac{\partial P(C,t)}{\partial t} = VN\omega J + Q\{NP_E(C,t) - NP(C,t)\} \qquad [12.19]$$

The last term is the difference between the incoming and outgoing fluxes for each level of concentration. Based on [12.19], the evolution equation [12.11] obtained for a closed reactor is changed into:

$$\frac{\partial P(C,t)}{\partial t} = \omega J + \frac{\{P_E(C,t) - P(C,t)\}}{\tau_{\text{residence}}} \qquad [12.20]$$

in which J is still given by [12.12].

In a steady-state regime, [12.20] is written as follows, using [12.12]:

$$\frac{\{P(C) - P_E(C)\}}{\omega\tau_{\text{residence}}} = \left\{2\int_0^{2C} P(C')P(2C - C')\mathrm{d}C'\right\} - P(C). \qquad [12.21]$$

Based on the same approach used in section 12.2.2 to arrive at [12.16], we obtain for the open reactor in a steady-state regime:

$$\mu_n + \frac{\mu_n - \mu_{nE}}{\omega\tau_{\text{residence}}} = \frac{1}{2^n}\sum_{i=0}^{n}\frac{n!}{i!(n-i)!}\mu_i\,\mu_{n-i} \qquad [12.22]$$

where μ_n is the nth order moment of the PDF $P(C)$ in the reactor and μ_{nE} the nth order moment of the PDF $P_E(C)$ at the reactor's inlet.

At order 1, equation [12.22] is equivalent to a trivial formulation of mass conservation $\mu_{nE} = \mu_n$ in a steady-state regime in the absence of a reaction. At order 2, it is established that the variance at the reactor's outlet $\sigma_S^2(t) = \mu_{2,S}(t) - \mu_{1,S}^2$ is related to the inlet variance $\sigma_E^2(t) = \mu_{2,E}(t) - \mu_{1,E}^2$ by:

$$\frac{\sigma_S^2}{\sigma_E^2} = \frac{1}{1 + \dfrac{\omega\tau_{\text{residence}}}{2}} \qquad [12.23]$$

This relation enables us to quantify the degree of advancement of mixing inside the reactor.

12.2.4. *CD model in the presence of a chemical reaction*

To conclude, we consider the chemical reaction A+B→P between two constituents. The kinetics of this reaction is described using the reaction rate $r(C_A, C_B)$, which characterizes the evolution of concentrations when the two products are mixed at the molecular level:

$$\frac{dC_A}{dt} = \frac{dC_B}{dt} = -r(C_A, C_B) \qquad [12.24]$$

This equation describes the chemical reaction which occurs inside each EFP. In order to describe the mixing and chemical reaction between the constituents, we need to consider the evolution of the PDF $P(C_A, C_B, t)$. With the aim of familiarizing ourselves with the joint PDF of the two concentrations, we illustrate with Figures 12.4 and12.5 the evolution of function $P(C_A, C_B, t)$ in two specific reactive cases.

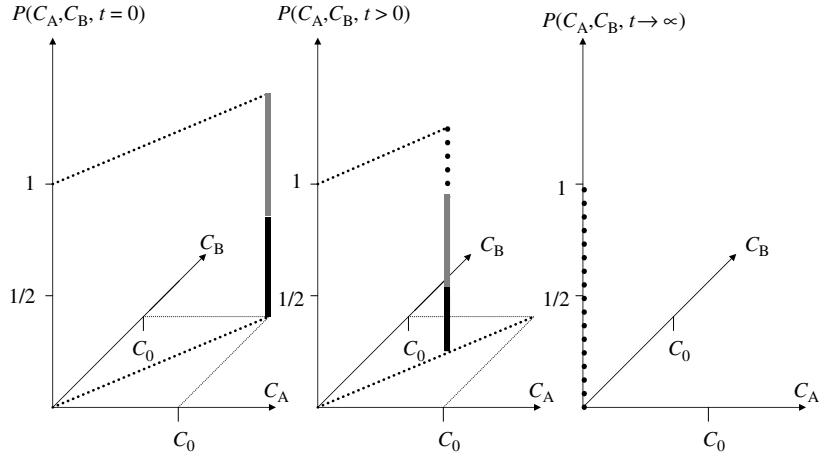

Figure 12.4. *Evolution in time of the PDF $P(C_A, C_B, t)$ for the chemical reaction of two constituents initially mixed in stoichiometric proportions at the molecular level. The gray level indicates the evolution of the relative fractions of products A (dark gray), B (light gray), and P (dotted gray) in EFPs as the chemical reaction progresses*

In the first case (Figure 12.4) the products are, at time $t = 0$, perfectly mixed and are in stoichiometric proportions. The population comprises a single type of EFP, in which the concentration of products is $C_A = C_B = C_0$. The PDF is represented by a single delta function. The consumption of products A and B by the chemical reaction causes both concentrations to decrease in identical proportions. The PDF

remains a delta function that moves in time along the bisector of axes (O, C_A) and (O, C_B) toward the vertical axis of the plot. For an infinite time, the reaction is complete and the delta function is on the vertical axis.

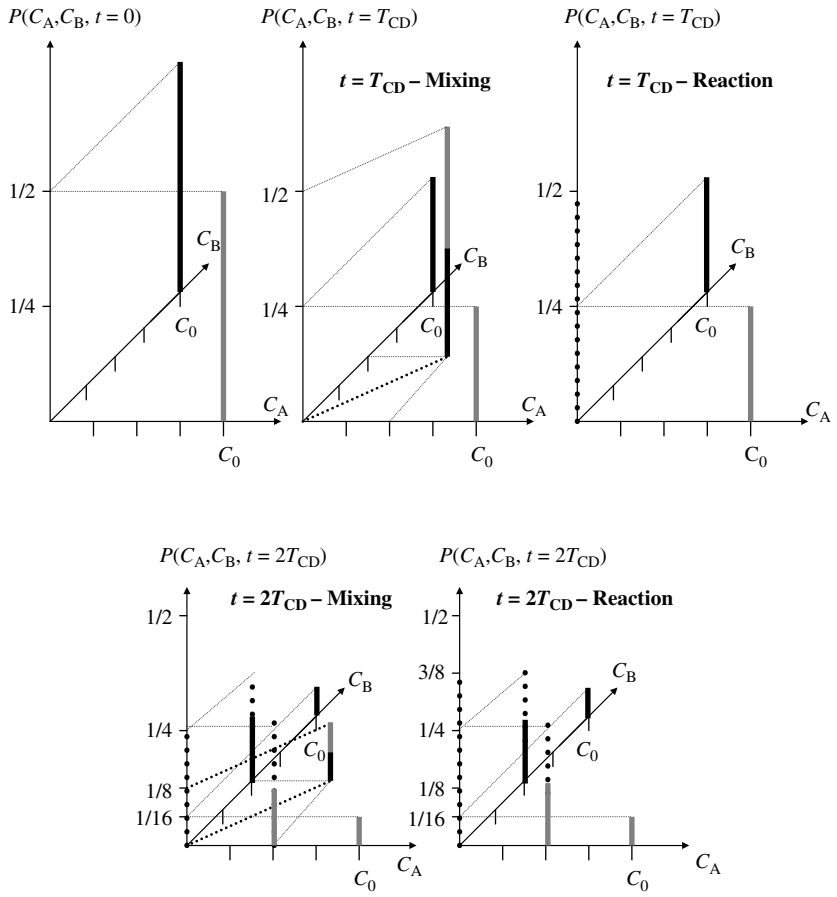

Figure 12.5. *Time evolution of the PDF* $P(C_A, C_B, t)$ *of two constituents in stoichiometric proportions, initially unmixed. The chemical reaction of the two constituents is instantaneous. The result of the first two iterations of the CD model is represented. The gray level indicates the evolution of the relative fractions of products A (dark gray), B (light gray), and P (dotted gray) in EFPs as the chemical reaction progresses*

We now consider in Figure 12.5 the unmixed situation where, at time $t = 0$, there are two classes of EFPs, the first category containing only product A at concentration C_0, and the second category only product B at the same concentration. EFPs of both types are initially present in equal quantities. It is assumed that the

reaction is instantaneous, which means that products A and B cannot coexist in a EFP; once they are brought into contact, they form product P. As far as the representation of PDFs is concerned, this means that it is not possible to have a non-zero value of the PDF anywhere else than on axes (O, C_A) and (O, C_B). As an extension of the unidirectional representation of Figure 12.3, we represent the evolution of $P(C_A, C_B, t)$ for the first two iterations of the CD model, distinguishing the mixing stage from the reaction stage that immediately follows it. For the mixing performed in the first iteration ($t = T_{CD}$), we recover the three delta functions shown in Figure 12.3. The third peak, positioned at $C_A = C_B = C_0 / 2$, is displaced by the action of the instantaneous chemical reaction along the vertical axis of the representation. The mixing stage of the second iteration ($t = 2T_{CD}$) exhibits six peaks (as opposed to five in Figure 12.3), but the principle of interactions among EFPs and associated probabilities is identical to what has been observed previously. The chemical reaction again displaces the new peak at $C_A = C_B = C_0 / 2$ on the vertical axis.

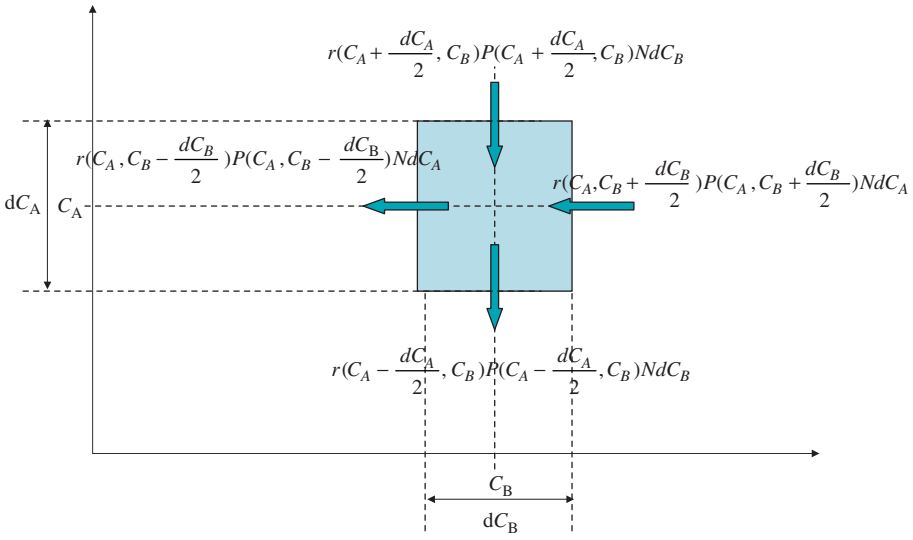

Figure 12.6. *Flux of EFPs, produced by a chemical reaction, entering and leaving a surface element* $dC_A dC_B$ *in the concentration space, centered in* (C_A, C_B)

Starting from the initial condition that is depicted in Figure 12.5, the situation where the reaction is not instantaneous calls for a more complex representation. The PDF is a surface covering a square of side C_0 in the (O, C_A, C_B) plane, which evolves with time. Figures 12.4 and 12.5 show that the chemical reaction deforms the PDF surfaces by displacing the non-zero values of the PDF toward the vertical

axis. In the simplest case represented by Figure 12.4, the displacement speed of the peak along the bisector has the components $-r(C_A, C_B)$ along the two axes (O, C_A), and (O, C_B). (The minus sign indicates the direction of displacement.) The reaction rate is thus associated with a notion of flux for representing the time evolution of the PDF. The population balance of the EFPs available in the surface element (Figure 12.6) centered on points (C_A, C_B) with sides (dC_A, dC_B) enables us to establish the form of the reaction term in the evolution equation of $P(C_A, C_B, t)$. Denoting by $n(C_A, C_B, t) = NP(C_A, C_B, t)$ the population density of EFPs in the reactor (N being the number of EFPs per unit volume), the time variation resulting from the chemical reaction inside the EFPs contained in that surface element within the concentrations plane is written out as:

$$\begin{aligned}&\{NP(C_A, C_B, t+dt) - NP(C_A, C_B, t)\}\, dC_A dC_B = \\ &\left\{ r\left(C_A + \frac{dC_A}{2}, C_B, t\right) P\left(C_A + \frac{dC_A}{2}, C_B, t\right) - r\left(C_A - \frac{dC_A}{2}, C_B, t\right) P\left(C_A - \frac{dC_A}{2}, C_B, t\right) \right\} N dC_B dt \\ &+ \left\{ r\left(C_A, C_B + \frac{dC_B}{2}, t\right) P\left(C_A, C_B + \frac{dC_B}{2}, t\right) - r\left(C_A, C_B - \frac{dC_B}{2}, t\right) P\left(C_A, C_B - \frac{dC_B}{2}, t\right) \right\} N dC_A dt\end{aligned} \quad [12.25]$$

This leads, for small values of dt, dC_A, and dC_B, to:

$$\frac{\partial P(C_A, C_B, t)}{\partial t} = \frac{\partial (rP)}{\partial C_A} + \frac{\partial (rP)}{\partial C_B} \quad [12.26]$$

The generalization of equation [12.11] to two constituents, including the chemical reaction term, can therefore be set out as:

$$\frac{\partial P(C_A, C_B, t)}{\partial t} = \omega J + \frac{\{P_E(C_A, C_B, t) - P(C_A, C_B, t)\}}{\tau_{\text{residence}}} + \frac{\partial (rP)}{\partial C_A} + \frac{\partial (rP)}{\partial C_B} \quad [12.27]$$

Coefficient J is the generalized form of [12.12]:

$$J = \left\{ 4 \int_0^{2C_A} \int_0^{2C_B} P(C_A', C_B', t) P(2C_A - C_A', 2C_B - C_B', t) dC_A' dC_B' \right\} - P(C_A, C_B, t) \quad [12.28]$$

Equations [12.27] and [12.28] are a generalized form, with two chemical constituents, of the equation known as Curl's equation:

$$\frac{\partial P(C,t)}{\partial t} - \frac{\partial (rP)}{\partial C} - \frac{\{P_E(C,t) - P(C,t)\}}{\tau_{\text{residence}}} = \omega J \qquad [12.29]$$

Despite its historical interest for the formalization of the CD model, Curl's equation is seldom used, as it models a reaction whose kinetics depends on the concentration of a single constituent.[3] Numerical models usually implement a Monte-Carlo method coupled to the generic algorithm of the model (equation [12.6]), rather than solving the evolution equation for the PDF.

12.3. Model of interaction by exchange with the mean

12.3.1. *Principle*

The model of interaction by exchange with the mean (IEM) is also a model based on the notion of EFPs and employing the PDFs of EFP populations. Unlike the CD model, the IEM model does not individually identify each EFP, but rather each class of EFPs. All EFPs initially having the same concentrations C_A and C_B will evolve in the same way under the IEM model, which was not the case with the CD model. Since the initial distribution $P(C_A, C_B, t = 0)$ of the population of EFPs is given, its subsequent evolution $P(C_A, C_B, t)$ will be limited to displacing the lines in the histogram.

The principle of the IEM model is simple: each EFP mixes with the EFPs located in its vicinity, with a characteristic exchange time denoted by T_{IEM}.

The evolution of the concentrations in each class of EFP is thus expressed as:

$$\begin{aligned} \frac{dC_A}{dt} &= -r(C_A, C_B) + \frac{\langle C_A \rangle(t) - C_A(t)}{T_{\text{IEM}}} \\ \frac{dC_B}{dt} &= -r(C_A, C_B) + \frac{\langle C_B \rangle(t) - C_B(t)}{T_{\text{IEM}}} \end{aligned} \qquad [12.30]$$

Unlike the CD model, the IEM model allows the chemical reaction to be immediately taken into account. Both $\langle C_A \rangle$ and $\langle C_B \rangle$ designate in [12.30] the average concentrations in the vicinity of the EFP. In a perfectly stirred reactor, these

3 In a number of books and publications, the reaction term in Curl's equation [12.29] is written with a positive sign. This error motivates, in part, our detailed derivation of the reaction term from the population balance (equation [12.25]).

average concentrations are the average concentrations in the reactor, since macromixing is assumed to have taken place.

In the presence of a chemical reaction, the average concentrations decrease in time. The delicate part in the IEM model lies in the fact that the average concentrations have to be recalculated with time. If this procedure is not performed properly, the model may not conserve mass. The sign of the mixing term is positive in [12.30]. If the average concentration is greater than the concentration in the EFP, mixing will effect an increase in the concentration of the EFP. The reverse behavior is observed if the average concentration is less than the concentration in the EFP.

Implementing the IEM model consists of solving equations [12.30] for every identified line in the initial PDF $P(C_A, C_B, t=0)$, i.e. for every pair of concentrations (C_A, C_B) such that $P(C_A, C_B, t=0) \neq 0$.

12.3.2. *IEM model without a chemical reaction*

We now consider the case of a closed reactor. As with the CD model, we consider a single constituent of concentration C and characterize its mixing into a solvent by the time evolution of the PDF $P(C,t)$. The implementation of the IEM model, in the absence of a chemical reaction, is particularly simple. As the initial distribution is made up of two categories of EFPs, the IEM model is, in this case, limited to calculating the time evolution of the concentration for two classes of EFPs, the first called "rich EFPs" having an initial concentration $C = C_0$, and the second called "lean EFPs" having an initial concentration $C = 0$.

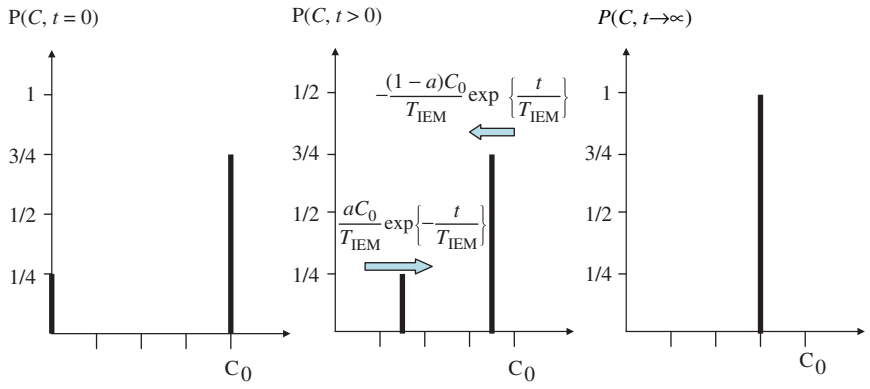

Figure 12.7. *Time evolution, obtained using the IEM model, of the PDF $P(C,t)$ characterizing the mixing of a non-reacting product in a closed reactor. The arrows and expressions characterize the displacement speed of both lines*

For the initial EFP distribution represented in Figure 12.7, the probability of having a rich EFP is $P(C_0, t=0) = a = 3/4$ and that of having a lean EFP is $P(0, t=0) = 1-a$. The average concentration is $\langle C \rangle = aC_0$. For both classes of EFPs, the evolution of the concentration in the EFPs is described by the same differential equation:

$$\frac{\mathrm{d}C}{\mathrm{d}t} = \frac{\langle C \rangle - C(t)}{T_{\mathrm{IEM}}} = \frac{aC_0 - C(t)}{T_{\mathrm{IEM}}} \qquad [12.31]$$

The reaction term is omitted, and the equation is simplified by the fact that the average concentration is constant with time. For both classes of EFPs, the general solution of [12.31] is identical:

$$C(t) = aC_0 + A\exp\{-t/T_{\mathrm{IEM}}\} \qquad [12.32])$$

The initial conditions for both types of EFPs determine the value of the constant of integrating A. The time evolution in both types of EFPs is then:

$$\text{Rich EFP: } C(t) = aC_0 + (1-a)C_0\exp\{-t/T_{\mathrm{IEM}}\} \text{ since } C(0) = C_0 \qquad [12.33]$$

$$\text{Lean EFP: } C(t) = aC_0\left[1-\exp\{-t/T_{\mathrm{IEM}}\}\right] \text{ since } C(0) = 0\,. \qquad [12.34]$$

Figure 12.7 shows the time evolution of the PDF. The evolution of the histogram is a simple displacement of the spectrum lines toward the position of the average concentration $\langle C \rangle = aC_0$ reached for $t \to \infty$. The displacement speed of a line is greater, the further it is from the average concentration $\langle C \rangle$.

It follows from [12.33] and 12.34] that variance decreases with time:

$$\begin{aligned}\sigma^2(t) = {} & P(C_0,0)\left[(1-a)C_0\exp\left\{-\frac{t}{T_{\mathrm{IEM}}}\right\}\right]^2 \\ & + P(0,0)\left[aC_0\exp\left\{-\frac{t}{T_{\mathrm{IEM}}}\right\}\right]^2 = C_0^2 a(1-a)\exp\left\{-\frac{2t}{T_{\mathrm{IEM}}}\right\}\end{aligned} \qquad [12.35]$$

As with the CD model, the segregation index decreases exponentially for the IEM model:

$$I(t) = \exp\left\{-\frac{2t}{T_{\mathrm{IEM}}}\right\} \qquad [12.36]$$

The decrease is identical for both models if the frequency, ω, of the CD model is such that $\omega / 2 = 2 / T_{\text{IEM}}$.

The case of an open reactor is significantly more complex. The tracking procedure of each class of EFP is identical, but even in a steady-state regime, the EFPs do not leave the CSTR with the same concentration, because not all EFPs stay in the reactor for the same period of time. It is necessary to bring in internal age distributions inside the reactor, using the concepts of residence time distributions.

In a steady-state regime, the PDF P_E at the reactor's inlet is related to the flow rate, Q_C, of a fluid in which the concentration is C_0 and to the flow rate, Q_0, of solvent (zero concentration):

$$\left.\begin{aligned} P_E(C_0) = P(C_0, t=0) &= \frac{Q_C}{Q_C + Q_0} = a \\ P_E(C=0) = P(0, t=0) &= \frac{Q_0}{Q_C + Q_0} = 1 - a \end{aligned}\right\} \qquad [12.37]$$

For both classes of EFPs, the concentration at the reactor's outlet is given by equations [12.33] and [12.34], by replacing time t with the internal age α of the EFPs when they leave the reactor:

$$\text{Rich EFP: } C_C(\alpha) = aC_0 + (1-a)C_0 \exp\{-\alpha / T_{\text{IEM}}\} \qquad [12.38]$$

$$\text{Lean EFP: } C_0(\alpha) = aC_0 \left[1 - \exp\{-\alpha / T_{\text{IEM}}\}\right] \qquad [12.39]$$

The theory of residence time distributions[4] demonstrates that the internal age distribution $I(\alpha)$ in a reactor is related to the residence time distribution $E(t)$ by:

$$I(\alpha) = \frac{1}{\tau_{\text{residence}}} \int_{\alpha}^{\infty} E(t)\mathrm{d}t \qquad [12.40]$$

For the CSTR, $E(t) = \exp(-t / \tau_{\text{residence}}) / \tau_{\text{residence}}$, wherein the residence time is defined by $\tau_{\text{residence}} = V / (Q_C + Q_0)$.

4 The book by J. Villermaux (*Génie de la Réaction chimique*, Tec&Doc, Lavoisier, Paris, 1993) presents a comprehensive explanation of the RTD method. Their use is also discussed by R. Prud'homme (*Flows of Reactive Fluids*, Springer-Verlag, 2010). A more advanced discussion of the implementation of internal-age distribution in computational models of mixing is given by Fox (*Computational Models for Turbulent Reacting Flows*, Cambridge University Press, 2003).

Consequently:

$$I(\alpha) = \frac{1}{\tau_{\text{residence}}} \exp(-\alpha / \tau_{\text{residence}}) \qquad [12.41]$$

The variance at the reactor's outlet can then be expressed by integrating the product of the internal age distribution and the obtained variance for each internal age α over all possible internal ages while taking [12.38] and [12.39] into account:

$$\begin{aligned}\sigma_S^2 &= P(C_0)\int_0^\infty \left(C_C(\alpha) - \langle C \rangle\right)^2 I(\alpha)\mathrm{d}\alpha + P(C=0)\int_0^\infty \left(C_0(\alpha) - \langle C \rangle\right)^2 I(\alpha)\mathrm{d}\alpha \\ &= C_0^2 a(1-a)\int_0^\infty \exp\left(-\frac{2\alpha}{T_{\text{IEM}}} - \frac{\alpha}{\tau_{\text{residence}}}\right)\frac{\mathrm{d}\alpha}{\tau_{\text{residence}}} \\ &= \frac{C_0^2 a(1-a)}{1 + \dfrac{2\tau_{\text{residence}}}{T_{\text{IEM}}}}\end{aligned} \qquad [12.42]$$

The inlet variance being $\sigma_E^2 = C_0^2 a(1-a)$, we eventually obtain:

$$\sigma_S^2 = \frac{\sigma_E^2}{1 + \dfrac{2\tau_{\text{residence}}}{T_{\text{IEM}}}} \qquad [12.43]$$

As with the closed-reactor configuration, this result is found to be identical to the one obtained via the CD model (equation [12.23]), if the frequency ω of the CD model is such that $\omega / 2 = 2 / T_{\text{IEM}}$.

12.3.3. *IEM model with a chemical reaction*

The implementation, within a numerical model, of the IEM model with a chemical reaction can prove delicate, even though the evolution equations (equation [12.30]) are simple. The average concentrations $\langle C_{\text{A}} \rangle(t)$ and $\langle C_{\text{B}} \rangle(t)$ evolve with time, and their values have to be recalculated at every time step. If this calculation is not performed accurately, the equations of the model will cause, through error, the production or consumption of products in addition to the effects of the reaction mechanism.

In a perfectly stirred closed reactor, it is easy to compute the average concentrations at any time:

$$\begin{aligned}\langle C_{\text{A}} \rangle(t) &= \int_0^\infty \int_0^\infty C_{\text{A}}(t, C_{\text{A0}}, C_{\text{B0}}) P(C_{\text{A0}}, C_{\text{B0}}, t=0)\mathrm{d}C_{\text{A0}}\mathrm{d}C_{\text{B0}} \\ \langle C_{\text{B}} \rangle(t) &= \int_0^\infty \int_0^\infty C_{\text{B}}(t, C_{\text{A0}}, C_{\text{B0}}) P(C_{\text{A0}}, C_{\text{B0}}, t=0)\mathrm{d}C_{\text{A0}}\mathrm{d}C_{\text{B0}}\end{aligned} \qquad [12.44]$$

Both $C_A(t, C_{A0}, C_{B0})$ and $C_B(t, C_{A0}, C_{B0})$ are the concentrations at time t in the EFPs whose initial concentrations were C_{A0} and C_{B0}. These concentrations are determined by a stepwise integration of equations [12.30], updating the average concentrations at every time step through the calculation of integrals [12.44]. In addition, $P(C_{A0}, C_{B0}, t = 0)$ is the initial PDF for the distribution of EFPs. An exercise given at the end of this chapter should allow the readers to familiarize themselves with the implementation of the model and to verify that the IEM model allows the various mixing and reaction processes to be tracked, depending upon whether the reaction is slow or fast compared to the mixing process.

Utilization of the IEM model is more delicate when an open reactor is considered, or when the reactor is non-homogeneous. It is essential to be specific about the domain that defines the vicinity of a EFP, so that the mass balance would not be distorted. We shall not discuss this fact further herein, as our concern is to draw attention of the reader on this relative disadvantage of the IEM model.

12.4. Conclusion

In this chapter, we have limited ourselves to describe only the CD and IEM models. These models are also commonly employed in numerical models. Provided that the characteristic time parameters specific to them (frequency ω for the CD model and time T_{IEM} for the IEM model) are carefully chosen, it is obvious that they are more or less successful in providing a representation of the dynamics of mixing and chemical reaction(s). However, the time evolution of the obtained PDFs $P(C_A, C_B, t)$ (illustrated in Figures 12.3 and 12.7 for the CD and IEM models, respectively) are far from representing the actual evolution of the PDFs demonstrated by direct numerical simulations, as shown among others in Figure 10.3 of Chapter 10. This is a definite drawback in the modeling of mixing and chemical reaction, insofar as the diversity of EFPs is not modeled satisfactorily, even if the evolution of average concentrations can be accessed via a parameterization of the models' characteristic times. Other models (Kerstein, 1991, for instance)[5] enable the modeling of time evolutions of the PDF in better agreement with direct numerical simulations, but such extensions are not discussed here. The reader by again refer to the book by Fox (*ibid.*) on the subject of computational modeling of reacting flows.

5 Kerstein A.R., 1991, *J. Fluid Mech.*, 213, 361–394.

12.5. Application exercise

Exercise 12.I: Implementation of the IEM model for a slow or fast chemical reaction

Consider a perfectly stirred reactor of volume V = 1 L, in which the stirrer maintains a homogeneous turbulence of characteristic velocity $u_{\text{rms}} = 10$ cm s^{-1} and of integral scale ℓ_t = 4 cm. The chemical reaction A + B → P is carried out therein, in an aqueous medium (kinematic viscosity $\nu = 10^{-2}$ cm^2 s^{-1}). The molecular diffusivity of all constituents is taken equal to $D = 10^{-5}$ cm^2 s^{-1}. Both constituents are introduced into the vessel in stoichiometric proportions and with the same concentration C_o = 1 mol L^{-1} at time t = 0, without being mixed.

We wish to model the progress of the chemical reaction using the IEM model.

1. Evaluate the micromixing time and the characteristic times of macromixing. It will be observed that the micromixing time is not significantly greater than the largest among macromixing times. Despite that, it will be postulated, for the implementation of the IEM model, that the macromixing is complete in the vessel at time t = 0.

2. The chemical reaction is a first-order reaction with respect to each of the constituents, so that the reaction rate is expressed as $r(C_A, C_B) = kC_AC_B$.

The IEM model is implemented by considering two types of EFPs at time t = 0, in which the time evolution of the concentrations in constituents A and B will be followed:

EFP 1: $C_{A1}(t)$ and $C_{B1}(t)$ refer to the concentrations of A and B in the EFP. Further, $C_{A1}(0) = C_0$ and $C_{B1}(0) = 0$.

EFP 2: $C_{A2}(t)$ and $C_{B2}(t)$ refer to the concentrations of A and B in the EFP. Further, $C_{A2}(0) = 0$ and $C_{B2}(0) = C_0$.

Write out the evolution equations for the concentrations in both types of EFPs according to the IEM model, taking into account the chemical reaction. At this stage, the values of the average concentrations will not be expressed. For the remainder, the time T_{IEM} of the IEM model will be taken equal to the micromixing time calculated in Question 1.

3. Calculate the average concentrations $\langle C_A \rangle(t)$ and $\langle C_B \rangle(t)$ as a function of $C_{A1}(t)$, $C_{B1}(t)$, $C_{A2}(t)$, and $C_{B2}(t)$. Justify that $C_{A1}(t) = C_{B2}(t)$ and $C_{B1}(t) = C_{A2}(t)$. Derive there from an expression of the evolution equations established in

Question 2, only involving for EFP #1 the concentrations $C_{A1}(t)$ and $C_{B1}(t)$. Similar findings hold for EFP #2.

4. Prove that

$$\mathrm{d}\left(C_{A1} - C_{B1}\right)/\mathrm{d}t = -\left(C_{A1} - C_{B1}/T_{IEM}\right)$$

and that, consequently,

$$C_{A1}(t) - C_{B1}(t) = C_o \exp(-t / T_{IEM}) .$$

5. The kinetic constant of the reaction is $k = 5\ \ 10^{-3}$ L·mol^{-1} s^{-1}. Justify that this is a slow reaction, and that the advancement of the reaction is not limited by mixing. Show that the mixing within the EFPs is performed in a time period of the order of several T_{IEM} . The concentration in the EFPs is then $C_o / 2$. There after, the reaction occurs in identical fashion within all EFPs.

6. The kinetic constant of the reaction is $k = 100\,\mathrm{L{\cdot}mol^{-1}\ s^{-1}}$. Justify that this is a fast reaction: concentration $C_{B1}(t)$ remains very low in EFP 1, just like concentration $C_{A2}(t)$ in EFP 2. Show that the result established in Question 4 makes it possible to prove that $\langle C_A \rangle(t) = (C_o/2)\exp(-t / T_{IEM})$. The advancement of the reaction is given by the micromixing time, and not by the kinetic constant of the reaction.

Part III

Mechanical Separation

Chapter 13

Physical Description of a Particulate Medium Dispersed Within a Fluid

13.1. Introduction

Part III of this book deals with the processes of mechanical separation. The implementation of a mechanical separation process is conceivable only if the materials to be separated can be clearly identified in space, so that mechanical forces exerted by one material upon the other can act to separate the two constituents. Mechanical separation methods, therefore, pertain to two- or three-phase media. Depending on the case, the terms solid/liquid or solid/gas separation will be used. Liquid/liquid separation, e.g. refers to the separation of two non-miscible liquids, such as oil and water.

Particles play a key role in many processes. In chemical engineering, catalytic reactors utilize catalysts, which are particles on the surface of which reactions occur. Major processing industries (plastic materials, ceramics, cement, paper, inks, etc.) operate based on their corresponding particulate materials. The same applies for the food processing industries also (powders, grains, beverage clarification, etc.). Lastly, in environmental studies, we may mention water treatment, gas scrubbing, incineration, and soil treatment processes, or indeed the problems of sedimentation in rivers, ports, and on beaches, all of which involve directly particulate media.

The different chapters of this third part present the mechanical principles used in different separation processes. This is discussed in the following order:

– membrane-based separation processes and filtration (Chapter 14);

– the behavior of particles within the gravity field (Chapter 15), by taking into account the different aspects: gravitational separation, the use of stirring to keep particles in suspension, the fluidization of a particle bed by an upward stream; and

– centrifugal separation (Chapter 17).

Chapters 16 and 18 discuss more academic matters. Chapter 16 deals with the movement of a solid particle in a fluid flow, while in Chapter 18 we introduce some essential notions on granular media. Such notions are useful to an engineer specializing in agri-food process engineering, to understand what happens inside a silo.

Our goal is not to treat these different processes on a technical level. This has already been addressed very well in other books. We shall not describe the variety of filtration devices, nor shall we address the issue of describing a gravity settler for water treatment. We, however, introduce the mechanical principles and tools used to describe them.

Particles, whether solid or fluid, are usually dispersed within a fluid. The fluid phase that contains the particles is referred to as the continuous phase, since it is possible to move throughout that phase while remaining within it. The gap between the density of the particles, denoted by ρ_p, and the density ρ_f of the continuous fluid phase is a key parameter of the particulate media under consideration, because this gap either intervenes directly in the study of mechanical separation (as in the case of gravitational or centrifugal separation or in fluidization) or because the mechanical stability of a deposited granular medium depends on it. The third essential parameter is the size D of the particles. The processes considered in this chapter are associated with a flow of the continuous fluid phase. The dynamic viscosity, μ_c, of the continuous fluid phase is, therefore, also a parameter to be taken into account. Lastly, for fluid particles, the flow of the continuous phase generates a flow inside the fluid particles and, in that case, it is also necessary to introduce the dynamic viscosity μ_d inside the dispersed fluid particles.

In this chapter, we introduce the tools for the characterization of a particulate medium. The list of mechanical parameters that we have just discussed is somewhat obvious. While in the following chapters we assume that the properties of these particles to be known, in the present chapter we see that, in reality, it is not always straightforward to determine them. On the one hand, particles are not always spherical. Quantifying their size necessitates the introduction of definitions, and measuring it requires the design of measuring apparatuses. On the other hand, solid particles gather under certain conditions to form clusters, while fluid particles can merge (coalescence). Thus, the size of particles can vary in space and time. By considering them as known quantities, in the following chapters, the size D of the

particles and their density ρ_p, these issues are discreetly set aside despite their huge importance. We address them in this first chapter of the third part.

Lastly, the particles, that we shall be dealing with this section are "small". This term, however, has no meaning per se, for a number of reasons. The size of a particle is given by its length quantified using an appropriate unit. The size of the particles that we consider in this section will vary from a few angstroms ($1\ \text{nm} = 10^{-9}\ \text{m}$) to a few millimeters ($1\ \text{cm} = 10^{-2}\text{m}$). The smallest ones are encountered when considering particles having a molecular scale, e.g. as in a seawater desalinisation process. The largest particles can be encountered when studying a catalyst inside a chemical reactor or waste particles being incinerated inside a furnace. Particle size can, therefore, vary by a factor of 10^7, which is obviously vast. Consequently, one cannot be too careful with regard to orders of magnitude, and we endeavor in this chapter to make the reader aware of this using a few trivial examples.

13.2. Solid particles

13.2.1. *Geometrical characterization of a particle*

Although rigid, the size of a solid particle is not easy to define if the particle is not spherical. However, its volume or area can be quantified, provided it is possible to measure the same. The size of the spherical particle is defined by its diameter D, based on which its volume V_p and area A_p are expressed by:

$$V_p = \frac{\pi}{6} D^3 \quad \text{and} \quad A_p = \pi D^2 \qquad [13.1]$$

We also define the specific area of the particle as the ratio of its area to its volume:

$$a_p = \frac{A_p}{V_p} \qquad [13.2]$$

For a sphere, $a_p = 6/D$. It is important to note that the specific area does not have the dimension of a length, but is instead represented as the reciprocal value of a particle's length. The smaller the particle, the greater will be its specific area. The relevance of this concept is apparent as we understand later on in this discussion.

Although we cannot simply define the size of a grain of arbitrary geometry, it is easier to define the size of a non-spherical particle by referring to its volume, its

surface, or its specific area. We therefore define:

– the diameter of a sphere having the same volume as the grain:

$$D_V = \left(6V_\mathrm{p}/\pi\right)^{1/3}$$

– the diameter of a sphere having the same area as the grain:

$$D_A = \left(A_\mathrm{p}/\pi\right)^{1/2}$$

– the diameter of a sphere having the same specific area as the grain:

$$D_a = \left(6/a_\mathrm{p}\right).$$

In short, the equivalent sphere is often used to define the size of a particle.

In this chapter, we consider particles whose size varies between a few angstroms and a centimeter:

$$1\ \mathrm{nm} = 10^{-9}\ \mathrm{m} < \mathrm{D} < 10^{-2}\ \mathrm{m} = 1\ \mathrm{cm}$$

Within this interval, the characteristics of a set of particles in terms of volume, area, specific area, and number vary dramatically. Let us consider, by way of an example, a mass $M = 1$ g of spherical sand particles of constant diameter D. This is very small; the total volume occupied by the solid is $V = 0.33$ cm^3 for a density $\rho_\mathrm{s} = 3{,}000$ kg·m^{-3}. For three particles of different diameters (10 nm, 1 μm, and 1 mm) Table 13.1 lists various characteristics.

D	Volume of a particle (m^3) $V_\mathrm{p} = \dfrac{\pi D^3}{6}$	Number of particles $N = \dfrac{M}{\rho_\mathrm{s}}\dfrac{6}{\pi D^3}$	Total area of the particles (m^2) $S = \dfrac{M}{\rho_\mathrm{s}}\dfrac{6}{D}$	Specific area (m^{-1}) $a_\mathrm{p} = 6/D$
10 nm	0.52×10^{-27}	6×10^{17}	200	6×10^{8}
1 μm	0.52×10^{-18}	6×10^{11}	2	6×10^{6}
1 mm	0.52×10^{-9}	600	0.002	6×10^{3}

Table 13.1. *Characteristics of a homogeneous set of spherical particles, with a diameter D and a density of $\rho_s = 3{,}000$ kg·m^{-3}. The total particle mass is M = 1g*

This table prompts several comments:

– The number of particles grows dramatically when their size diminishes.

– The area developed by all the particles increases very strongly when the size of the particles decreases. This point is essential where transfers or chemical reactions

are concerned, because transfers increase with the exchange area and reactions occur at the surface. Thus, the finer particles, which can occupy a limited mass or volume fraction in a set of particles, have a predominant role for transfers and chemical reactions.

– The specific area increases when the size of the particle decreases. The significance of this concept becomes apparent in view of the previous comment. The specific area is the exchange area for a given volume of particles. It, therefore, characterizes the exchange capability of a set of particles. The unit m^{-1} should be understood as equated with m^2/m^3.

13.2.2. *Grain size distribution in a granular medium*

A granular medium is, generally speaking, composed of grains of different sizes. Engineers most often characterize the size grading of a granular medium by sieving and weighing operations, the principle of which is elucidated in Figure 13.1. The characterization device uses a stack of N sieving baskets whose mesh diameter ϕ_i gradually decreases from the upper basket (number 1) to the lower basket (number N). A mass m_t of the granular medium to be characterized is placed in the upper basket (Figure 13.1(b)). The stack of baskets is placed on a vibrating machine (Figure 13.1(a)), which performs the operation of sieving particles, leading to their retention inside the various baskets according to their size. Basket number i collects a mass m_i of particles whose sizes range from ϕ_{i-1} to ϕ_i (Figure 13.1(c)).

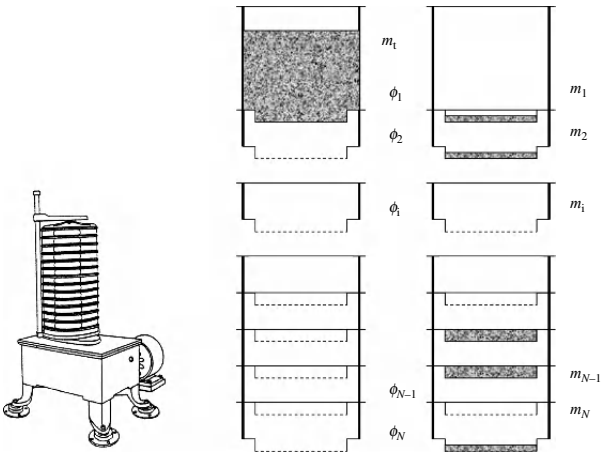

a. Rig for sieving a granular medium on a vibrating machine (after Perry, 1975)

b. Placement of particles in the upper sieve

c. Recovery and weighing of particles in the sieves according to their sizes

Figure 13.1. *Grain size characterization of a granular medium by a sieving and weighing method: experimental principle*

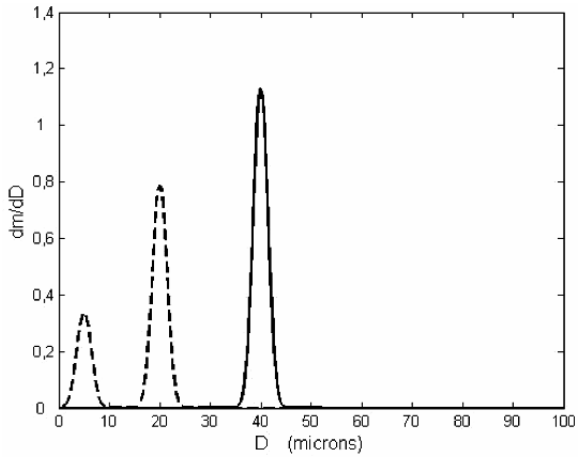

a. *Representation by mass density*

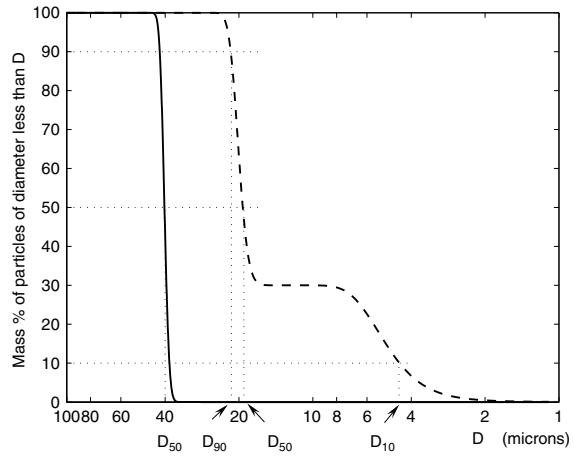

b. *Representation by accumulated mass*

Figure 13.2. *Grain size characterization of a granular medium by sieving and weighing methods: Grain size curves*

The results of such analyses are usually provided by an engineer by plotting, as a function of D, the mass percentage of particles whose size is less than D, as shown in Figure 13.2(b) for the grain size curves plotted in Figure 13.2(a). The solid line curve in Figure 13.2(a) shows a narrow distribution of particles around diameter $D = 40$ μm, designated as an unimodal particle distribution. The dashed line curve

displays a bimodal distribution with two particle size ranges, respectively, centred around diameters $D = 20$ μm and $D = 5$ μm. In Figure 13.2(b), the value given for diameter $D = \phi_i$ is simply the sum total of the masses in the baskets below basket i, as a proportion of the total mass m_t (multiplied by 100 to express the value as a percentage). It is common to represent this curve for decreasing values of the diameter, using a logarithmic scale for the horizontal axis (diameters). The semi-logarithmic representation allows a visualization of the grain size distribution with the same relative precision in all scale ranges, as illustrated by the comparison of Figures 13.2(a) and 13.2(b). The use of linear scales does not provide a good representation of the distribution in fine particles if the size grading is spread over sizes covering several orders of magnitude, between nanometers and centimeters. In connection with the semi-logarithmic representation of grain size distribution, the grain size characterization device according to the Association Française de NORmalisation (AFNOR) standard employs 21 sieves whose successive mesh sizes are: 40–50–63–100–125–160–200–250–315–400–500–630–800–1,000–1,250–1,600–2,000–2,500–3,150–4,000–5,000 (in μm).

Grain size curves of the type represented in Figure 13.2(b) are familiar to engineers, but their interpretation takes some getting used to. There are no particles in a diameter interval over which the curve is horizontal, and the faster the curve decreases in an interval, the greater the density of particles therein. The grain size distribution is often quantified on the basis of such curves, by determining the diameters D_{90}, D_{50}, and D_{10}, where D_X is defined as the size for which X% of the mass of particles has a diameter smaller than D_X. For particles whose grain size curve is plotted as a solid line in Figure 13.2(b), the three values $D_{10} = 36.6$ μm, $D_{50} = 40$ μm, and $D_{90} = 43.8$ μm explains satisfactorily the fact that the grain size distribution is unimodal, as shown in Figure 13.2(a). For the curves plotted in dashed lines, the three values $D_{10} = 4.5$ μm, $D_{50} = 19.2$ μm, and $D_{90} = 21.6$ μm poorly characterize the bimodal distribution observed in Figure 13.2(a), although the value of D_{10} enables us to detect the presence of fine particles while the values of D_{50} and D_{90} characterize the large ones.

More sophisticated apparatuses, which count particles according to their size, have been developed using electrical or optical techniques. Their use is more closely related to laboratories than to everyday engineering studies.

13.2.3. *Determination of a solid's density using a pycnometer*

Figure 13.3 illustrates the principle of a pycnometer, which is a simple device allowing measurement of the density of a solid or the average density of a granular medium, based on four weighing operations. The pycnometer is a container, of which the empty mass is first measured (operation 1), as well as the mass of the

container filled with water (operation 2). The fact that the container opens to the ambient air via a thin vertical tube guarantees a high precision on the volume of water that fills the pycnometer. Operations 1 and 2 allow the determination of the mass m_l of liquid that fills the container. The volume V_p of the container is derived there from, knowing the density of water. The mass m_s of the solid is determined by weighing it (operation 3), the last stage consisting of weighing (operation 4) the solid placed inside the water-filled pycnometer. The total mass weighed during operation 4 is the sum of the weight of liquid and the weight of solid in the pycnometer. From this, we can calculate the specific density $\rho_\mathrm{s}/\rho_\mathrm{l}$ of the solid with respect to water, since:

$$\frac{\rho_\mathrm{s}-\rho_\mathrm{l}}{\rho_\mathrm{s}}=\frac{m_\mathrm{tot}-m_\mathrm{l}}{m_\mathrm{s}} \qquad [13.3]$$

It is important to measure and control the temperature in order to obtain an accurate measurement. The variations of water density with temperature cause substantial errors if this is overlooked. It should also be realized that the density of the solid calculated using a pycnometer is the average density of the solid sample. It is obvious that the measurement principle does not enable the identification of density heterogeneities within the solid. In the case of a granular medium or porous material, the density measurement incorporates volumes of air that have not been forced out from the porous medium during operation 4 represented in Figure 13.3.

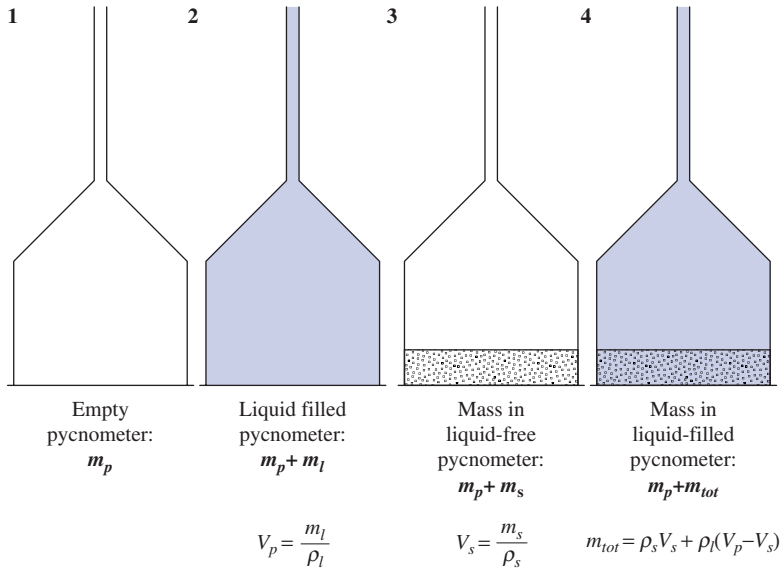

Figure 13.3. *Operating principle of a pycnometer*

13.2.4. Concentrations

Different definitions of concentration can be used to characterize the quantity of particles within a fluid. These different definitions are all related to the porosity ε, defined as the ratio of the fluid volume to the total volume. They include:

$$\text{Volume concentration} \quad C_{\text{V}} = \frac{\text{solid} \quad \text{volume}}{\text{total} \quad \text{volume}} = 1 - \varepsilon \qquad [13.4]$$

$$\text{Mass concentration} \quad C_{\text{M}} = \frac{\text{solid} \quad \text{mass}}{\text{total} \quad \text{volume}} = \rho_{\text{s}} C_{\text{V}} \qquad [13.5]$$

$$\text{Wet (or total) density} \quad \rho_h = \frac{\text{solid mass} + \text{fluid mass}}{\text{total} \quad \text{volume}} = \rho_{\text{f}} + \frac{\rho_{\text{s}} - \rho_{\text{f}}}{\rho_{\text{s}}} C_{\text{M}} \qquad [13.6]$$

Both the porosity and the volume concentration are dimensionless quantities. The mass concentration and wet density have the dimension $\text{kg}\cdot\text{m}^{-3}$. Another frequently used unit is g L^{-1} (the change of unit between $\text{kg}\cdot\text{m}^{-3}$ and g L^{-1} does not bring in a multiplicative constant). The M and V indices are generally omitted from the notations of the various concentrations, but the units are self-explanatory enough for guidance. In practice, the mass concentration is most commonly used and denoted by C.

It is useful to know a few reference values for porosity. In naturally occurring granular media, such as sands, porosity is between 0.3 and 0.5. The porosity value $\varepsilon = 0.3$ corresponds to a dense, highly packed ground. The term "loose sand" refers to a sand of relative density $\varepsilon = 0.5$. The force required to drive a pile in the ground increases considerably when passing from a loose soil to a dense soil. In filtration processes, porous media having a high porosity (ε of the order of 0.9) appear in some cases. Such products, called filter aids, help to maintain a higher level of permeability inside a granular porous medium by reducing its settling.

Even when dispersed at a low concentration, particles are very numerous and close to one another. Consider a set of particles dispersed in a homogeneous suspension in a given volume. For spherical particles of density ρ_{s} and diameter D with a mass concentration C, let us calculate the number N of particles per unit volume, the porosity ε, the wet density of the equivalent fluid ρ_h, and the average distance ℓ between the centers of two particles closest together. The following mathematical relations are established:

$$N = \frac{6C}{\pi \rho_{\text{s}}} \frac{1}{D^3}$$

$$\varepsilon = 1 - \frac{C}{\rho_s}$$

$$\ell \approx N^{-1/3} \qquad \text{so that} \qquad \frac{\ell}{D} \approx \left(\frac{\pi\rho_s}{6C}\right)^{1/3}$$

It can be noted that ℓ / D is independent from D. Table 13.2 recapitulates the values obtained for a set of solid particles of density ρ_s = 3,000 g L^{-1} immersed in a fluid of density ρ_f = 1,000 g L^{-1}, for various values of the concentration in particles. It can be seen that the particles are numerous (indeed, very numerous when the particle size is very small) for a volume concentration that remains low, and that porosity is not a defining indicator.

p	N (by m^3) for D = 1mm	C_V	ε	ρ_h (g L^{-1})	ℓ / D
1	6.4×10^5	0.0003	0.9997	1,000.6	11.6
10	6.4×10^6	0.0033	0.9967	1,006.6	5.4
100	6.4×10^7	0.0333	0.9667	1,066.6	2.5

Table 13.2. *Variations of the mass and volume concentrations, wet density, porosity, number of particles per unit volume, and average distance between particles, for particles of density ρ_s = 3,000 g L^{-1} dispersed in a fluid of density ρ_f = 1,000 g L^{-1}*

The second observation that stems from Table 13.2 is with reference to the proximity of particles to one another, which is strong (ℓ is the center-to-center distance, so that the shortest distance between surfaces is lower by a unit of D), even at a low concentration. The fluid flow between particles is constrained by the proximity of particles, as discussed in Chapter 14 within the context of gravitational sedimentation. The phenomena of hindered settling and turbidity currents are also described herein. When the particle concentration is sufficiently high, a two-phase fluid/particle medium flows, under certain conditions, like a homogeneous fluid whose density is the wet density (equation [13.6]).

13.2.5. *Formation of clusters, coagulation, and flocculation*

When particles are dispersed in a fluid, one can observe, under certain conditions, the formation of clusters. This phenomenon results from the action of interparticular forces of electrical origin, belonging to two types:

1. Van der Waals forces, which tend to draw two particles together. Very simplistically, these forces are the sum of the average forces exerted by the

fluctuating electrical dipoles consisting, for each atom in a particle, of its nucleus and electron cloud.

2. Electrostatic forces, which result from the fact that the particles are often negatively charged at their surface. These forces tend to repel two particles away from each other.

Clusters may form when Van der Waals forces overcome electrostatic forces.

The formation of clusters is an important phenomenon, as it modifies the size and density of particulate entities. We summarize here the main results from the theory of interparticular forces, called the DVLO theory by way of reference to its contributors (Deryaguin, Vervey, Landau, and Overbeck). A detailed presentation of this theory is outside the scope of the present book, as such presentation requires substantial theoretical developments.[1] This theory helps one to understand why particles are likely to form clusters in specific conditions. It is not, however, a predictive model of cluster formation, able to provide their number, size, and density.

In the following, we describe interparticular forces between two identical particles of radius *a*, as depicted in Figure 13.4. The distance between the particles is the distance *s*, taken from surface to surface.

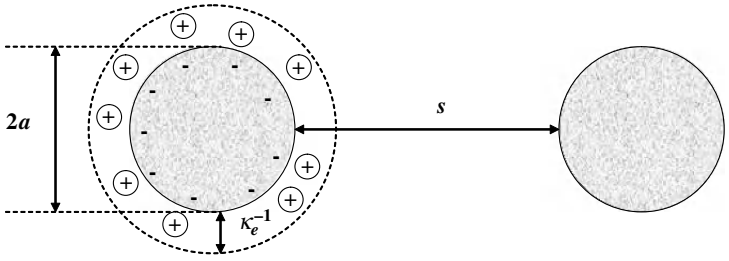

Figure 13.4. *Interparticular forces between two particles of equal radius a, dispersed in a fluid: geometrical notations. Minus signs represent negative electrical charges on the surface of the particles and plus signs denote positive ions within the fluid, which gather on the surface of the particle as a "double layer" of thickness* κ_e^{-1}

The action of Van der Waals forces is usually not quantified in terms of force, but rather in terms of interaction energy between two particles. For two spherical particles of radius *a*, the theory states that the Van der Waals interaction energy

1 See the chapter entitled "Petits volumes et grandes surfaces: l'univers des colloïdes", by Daniel and Audebert in *La juste argile* (Eds. Daoud and Williams, Editions de Physique, 1995). The book by Russel, Saville, and Schonwalter, *Colloidal Dispersions* (Cambridge University Press, 1989) enables further understanding.

varies with distance s between the particles according to the law:

$$E_{\text{vdw}}(s) = -\frac{A}{12}\frac{a}{s} \quad \text{for} \quad 0.3\text{nm} < s < a \qquad [13.7]$$

The constant A is Hamaker's constant. It depends on the composition of the particles and on the nature of the solvent in which they are dispersed. Its value is of the order of 10^{-20} J, with lower values in water than in air for the same particles.

For $s < 0.3$ nm, dipolar interaction forces become strongly repulsive (Born forces) due to the interpenetration of the two atoms' electron clouds. The negative value of the interaction energy in [13.7] means that the Van der Waals force between the particles is attractive. The particles would spontaneously place themselves at a distance $s = 0.3$ nm from each other if the Van der Waals forces and Born forces were the only to be considered, for it is at that distance that the interaction energy is the weakest. Equation [13.7] is valid for 0.3 nm $< s < a$. The formation of a cluster due to the effect of the Van der Waals forces therefore implies that the two particles have been brought sufficiently close to each other at some point in time.

It is found that particles are often negatively charged at their surface. These negative charges produce a negative electrostatic potential $-V_s$ at the surface of the particles. When the solid particles are dispersed in a liquid, the negative surface charges attract positive ions present in the liquid, which gather into a layer in the vicinity of the surface. The electrostatic potential produced by the particle, to which an adjacent particle is subjected, is in fact generated by this "double electrical layer", rather than solely by the charges on the surface of the particle. It not only depends on the charge density on the surface but also on the properties of the electrolyte. It can be shown, based on electrostatic theory, that the electrostatic interaction energy between two identical particles is written as:

$$E_e(s) = 2\pi\varepsilon_0\varepsilon a V_s^2 \exp\{-\kappa_e s\} \qquad [13.8]$$

The quantity $1/\kappa_e$ is homogeneous to a length. It is called the Debye length, and quantifies the thickness of the double layer. It can be evaluated using the relation:

$$\kappa_e^{-1} = \left\{\frac{\varepsilon_0\varepsilon kT}{2e^2 C_i N_A Z^2}\right\}^{1/2} \qquad [13.9]$$

The physical constants that appear in this relation are the electrical charge e of an electron,[2] Avogadro's number N_A, and the Boltzmann constant k. Further, ε_0 is the

2 We recall that $e = 1.60\times10^{-19}$ Coulomb, $1/4\pi\varepsilon_0 = 9\times10^9$, $N_A = 6.02\times10^{23}$ atoms mole^{-1}, and $k = 1.38\times10^{-23}$ J K^{-1}. The relative permittivity of water is $\varepsilon = 80$.

vacuum permittivity and ε is the relative permittivity of the solvent. The conditions intervene through the concentration C_i of positive ions in the fluid (in mol m^{-3}), their valence Z, and the absolute temperature T. At room temperature, the thickness of the double layer mainly depends on the concentration of positive ions within the fluid. It is interesting to comment on a few simple evaluations of the Debye length. For Na^+ ions in water at 25°C, $\kappa_e^{-1} = 0.4$ nm for $C_i = 0.6$ mol L^{-1}, whereas $\kappa_e^{-1} = 3$ nm for $C_i = 10^{-2}$ mol L^{-1}. The first condition corresponds to the average salinity of seawater (about 35 g L^{-1}). We shall consider both these conditions for the examples treated hereinafter.

Specific rigs enable the measurement of the electrical potential V_s on the surface of the particle. It is usually of the order of a few millivolts. The surface charge corresponding to the potential V_s can be estimated using the electrostatic relation:

$$Q = -2\pi\varepsilon_0\varepsilon a V_s \qquad [13.10]$$

since the electrostatic interaction energy is the product of the electrostatic potential for a given spacing of the two particles and the charge. An electrical charge equivalent to that of 28 electrons distributed over the surface of a particle of radius 1 μm produces a surface potential close to 1 mV.

The electrostatic interaction energy is positive and decreases with s, which implies that the electrostatic force is repulsive. The lowest energy level is obtained when the particles are infinitely distant from each other.

Equations [13.7]–[13.9] allow simple calculations to be performed in order to evaluate the ability of the particles to form clusters. To that end, it is sufficient to plot the variations with s of the total interaction energy:

$$E_t(s) = E_{vdw}(s) + E_e(s) \qquad [13.11]$$

Figure 13.5 represents the results obtained for two typical conditions. The radius of the particles is $a = 1$ μm. The particles are placed in water and Hamaker's constant is assumed to be equal to $A = 10^{-20}$ J. The energy levels plotted are rendered dimensionless by the energy due to Brownian movement, kT, in order to get reasonable values along the vertical axis and to recall that the interaction energy between particles and the energy of Brownian movement[3] are of comparable orders of magnitude.

3 Physical principles of Brownian movement are introduced in section 15.4.

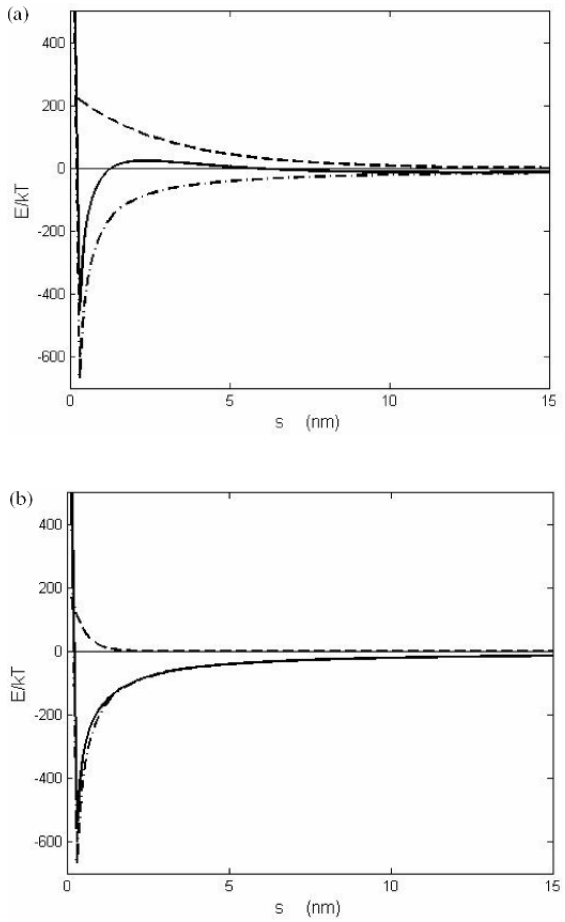

Figure 13.5. *Interaction energy vs. distance between two particles placed in water. Radius of the particles a = 1 μm. Hamaker's constant A = 10^{-20} J.*
Key: E_{vdw} , '-.-.-.'; $E_{e,}$ '----'; E_t, '____'.
a. V_s = 15 mV, κ_e^{-1} = 3 nm. b. V_s = 15 mV, and κ_e^{-1} = 0.4 nm

The first case (Figure 13.5(a)) is classical. It is often presented as an example of a result from the DVLO theory. The Debye length is rather large, meaning that there are few ions in the solvent. The Van der Waals force dominates at short distances, while the electrostatic force prevails when the particles are a little further apart. The energy minimum is observed at $s = 0.3$ nm. The particles may form a cluster in which particles are very close together ($s = 0.3$ nm). The absolute value of the energy minimum for $s = 0.3$ nm is large compared to the energy of Brownian movement, which means that the cluster is stable and dense, if it forms.

The curve $E_t(s)$ exhibits a positive maximum for a gap of the order of 2–3 nm. Particles must therefore have an amount of kinetic energy (either Brownian movement energy or mechanical stirring) larger than about 20 times the Brownian movement energy in order to pass that potential barrier and constitute a cluster with a spacing s = 0.3 nm between particles, called a "coagulation cluster". It is also observed that the total energy $E_t(s)$ exhibits a negative minimum for a gap of the order of 10–15 nm. This minimum is equivalent, in absolute value, to only a few times the Brownian movement energy. It corresponds to a cluster that is not very dense or very stable, called a "flocculation cluster."

For the same surface potential, but with a smaller Debye length, we have plotted in Figure 13.5(b) the variations of the different energies with s. This condition corresponds typically to a situation observed in seawater. The presence of a substantial quantity of ions within the solvent causes the electrostatic energy to decrease very rapidly. The Van der Waals force dominates for all values of the gap s, and coagulation clusters form spontaneously if the stirring within the solvent enables the particles to get sufficiently close to one another.

Equation [13.8] shows that an increase in the surface potential causes the repulsive force between the particles to increase, and is therefore unfavourable to the formation of clusters. Equations [13.7]–[13.11] hardly help to grasp the effect of the particle size on the formation of clusters. Both the electrostatic interaction energy and the van de Waals energy increase linearly with radius a of the particle, so that one might think that the obtained charts will simply be enlargements of those presented in Figure 13.5 if the size of the particles is varied. The energy minima corresponding to coagulation and flocculation clusters would thus be increased if the particle size increased, along with the level of the potential barrier to be passed. However, reality is different. A larger particle may have a negative surface charge greater than that of a smaller particle. The surface electrostatic potential is larger, so that the electrostatic force is more strongly increased than indicated by the linear variation with a of equation [13.8]. The important result is that particles are more likely to form clusters, the smaller their size is. For marine or river sediments, it is generally observed that particles of a size less than 60 μm form clusters. Those sediments are grouped under the appellation of cohesive sediments, or more commonly silts. Sediments of a size greater than 60 μm are ranged in the category of sands and non-cohesive sediments. We have seen that the presence of positive ions in the fluid promotes the formation of clusters. It is thus observed that the formation of flocs is enhanced in seawater in comparison to fresh water.

The DVLO theory effectively enables us to determine whether particles are liable to form clusters. The most delicate variable to access is the surface electrical potential, or equivalently the negative surface charge of particles. Still, this theory does not suffice to predict whether the particles will actually form flocculates under

specific conditions. A statistical model describing particle motion needs to be associated with the DVLO theory in order to quantify the probability for the particles to move toward one another. The concentration of particles obviously promotes the formation of clusters. So does the level of stirring, as it increases the probability of particles to move toward one another and supplies energy to the particles for passing potential barriers, if required. When the stirring energy is substantial, that energy is also capable of breaking up flocs.

13.3 Fluid particles

Fluid particles differ from solid particles in two respects:

1. They deform under the effect of the forces applied on their surface (gravity, pressure, friction stress, etc.).

2. When the particle is moving relative to the fluid, the frictional stress on the surface of the particle induces a movement inside the particle. Mechanics requires continuity of velocity and continuity of stress at the interface between the two fluids.

The third part of this book is mainly dedicated to studying phenomena involving solid particles. The differences between solid and fluid particles are only discussed twice in the next chapters. We shall study in section 15.3 the role of movements internal to fluid particle in the gravitational sedimentation of a fluid particle within a fluid at rest. Then, in section 17.7.2, we also discuss the centrifugation of an oil drop in a hydrocyclone, but the particle will then be considered sufficiently small for its deformation to be neglected.

In the following, we discuss the geometrical deformation of a fluid particle. As already mentioned in the introduction section of this chapter, the physical parameters governing the flows inside and outside a particle are densities ρ_p and ρ_f, dynamic viscosities μ_d and μ_c, and the particle diameter D. Dynamic parameters are the relative velocity U of the particle with respect to the fluid and the gravitational acceleration g, which will come into play if $\rho_p \neq \rho_f$. In order to describe the shape of the interface between two fluids, surface tension γ also has to be taken into account. This quantity was introduced in section 9.3.1 in the case of a gas/liquid interface.

Laplace equation [9.32] assumes uniform pressure outside the fluid particle. When $\rho_p \neq \rho_f$, the difference in the hydrostatic pressure applied by the exterior fluid on the particle at its bottom and at its top cannot modify the shape of the fluid particle if it is small compared with the pressure difference between inside and outside. This condition is met when the particle diameter D is less than the capillary length. Deformation of the surface by the effect of gravity is negligible and the

particle keeps its spherical shape thanks to surface tension. The capillary length, introduced with equation [9.36] for a gas/liquid interface, can be generalized to the case of any two fluids by writing:

$$\ell_c = \sqrt{\frac{\gamma}{\Delta\rho g}} \quad \text{with} \quad \Delta\rho = |\rho_p - \rho_f| \qquad [13.12]$$

The ratio of the particle diameter to the capillary length is evaluated by the Eötvös number[4]:

$$Eo = \frac{\Delta\rho g D^2}{\gamma} \qquad [13.13]$$

The relative displacement of the particle with respect to the surrounding fluid also deforms the fluid particle if the pressure variations around the particle caused by the relative motion of the fluid particle become significant compared to the effect of surface tension. For a fluid particle settling under the effect of gravity when $\rho_p \neq \rho_f$, the diagram presented by Clift, Grace and Weber[5] displays the different shapes of fluid particles observed, depending on the Eötvös number and on the Reynolds number:

$$\mathrm{Re} = \frac{UD}{\nu_c} \qquad [13.14]$$

U is the relative velocity of the fluid particle with respect to the fluid and $\nu_c = \mu_c / \rho_c$ is the kinematic viscosity of the continuous phase. The drawings superimposed onto the graph in Figure 13.6 show the various shapes encountered. The particles designated as spherical are such that the ratio of the smallest distance to the largest distance between two parallel planes enclosing the bubble is greater than 0.9. The essential result from Figure 13.6 is that a fluid particle has to be sufficiently small in order to be considered as remaining spherical. The diagram shows that a fluid particle is spherical when $\mathrm{Re} < 1$, for any value of the Eötvös number. For the results presented in the Figure, the velocity U is however not an independent parameter, as the particle settles in the gravity field. The condition $\mathrm{Re} < 1$ rely to a small fluid particle, as will be seen in section 15.3, which is devoted to the gravity settling of fluid particles.

Figure 13.6 is valid to gas bubbles in a liquid ($\rho_p/\rho_f << 1$ and $\kappa = \mu_d/\mu_c << 1$) and to drops of liquid that are non-miscible in another liquid (both ρ_p/ρ_f and κ are

4 This number is also called the Bond number.
5 R. Clift, J.R. Grace and M.E. Weber, *Bubble, Drops and Particules*, Academic Press, 1978.

usually of the order of 1). The diagram cannot be used for a liquid drop falling within a gas ($\rho_p/\rho_f >> 1$ and $\kappa >> 1$). A drop falling through air assumes an ellipsoidal shape, significantly flattened in the direction of the relative velocity, as soon as its size exceeds 1 mm.[6]

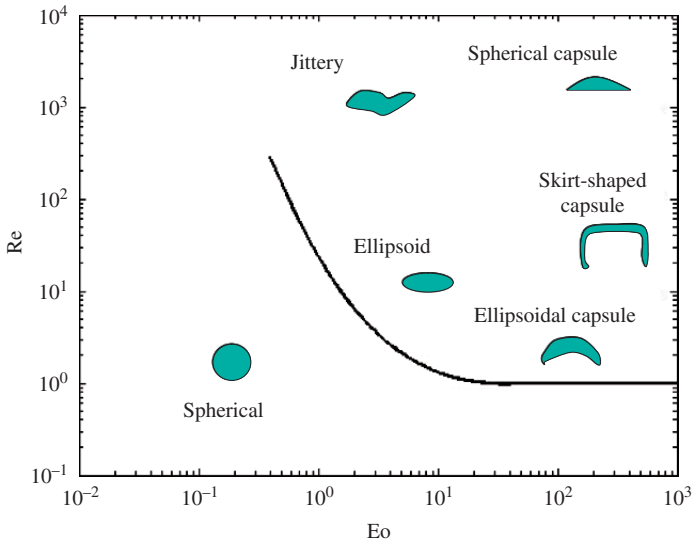

Figure 13.6. *Shape of a bubble or drop moving in a fluid under the effect of gravity and the difference in density. The curve delineates the parameters for which the bubble is spherical (figure adapted from Clift, Grace, and Weber,see footnote 5.)*

Fluid particles dispersed in a fluid, whether they are gas bubbles in a liquid or drops of liquid dispersed in a gas, are also likely to coalesce and constitute larger fluid particles. The coalescence phenomenon has a few common traits with the formation of clusters of solid particles as discussed in the previous section. Its occurrence depends on several parameters:

– The proximity of the bubbles or drops to one another. It, therefore, depends closely on the volume fraction of the dispersed phase within the continuous phase. The values given in Table 13.2 show that the particles are very close to one another, even for very low values of the volume fraction of the dispersed phase. Consequently, it is possible only to observe dispersions of fluid particles for very low values of the volume fraction of the dispersed phase (1% at the most). Beyond

6 The book by Clift, Grace, and Weber, *Bubbles, Drops and Particles* (ibid.) devotes its Chapter 7 to the dynamics of ellipsoidal fluid particles. This book is a major reference on the topic of fluid particles.

that, coalescence systematically occurs, leading to larger entities, or even to the formation of pockets.

– The probability of the bubbles or drops colliding with one another. This naturally depends on the level of stirring in the fluid. For bubbles having an upward motion under the effect of gravity in a fluid at rest, it can also be observed that a bubble accelerates when it is in the near-wake of a bubble located above it. This phenomenon promotes coalescence.

The coalescence phenomenon depends on gas/liquid surface tension. It is observed that the Weber number, which is the ratio of the kinetic energy to the pressure difference [9.32] between the inside and outside of the fluid particle:

$$We = \frac{\rho U^2 D}{\gamma} \qquad [13.15]$$

has a significant influence on coalescence phenomena.

A turbulent flow is also capable of fragmenting bubbles or drops. We have presented in section 9.2.3, the model by Kolomogorov and by Hinze, which rely the maximum diameter of fluid particles in an emulsion to the rate of turbulent energy dissipation and to surface tension. In the same way, indicated for the formation of clusters in a dispersion of solid particles, it is difficult to determine the bubble or drop size in a dispersion of fluid particles. We will not discuss this issue any further in this book, and hence refer the reader to more specialized volumes.[7]

13.4. Mass balance of a mechanical separation process

Mass balance is the preliminary step to study of any mechanical separation process. This aspect does not occupy center stage in this book, which is not intended as a book about process dimensioning but is limited to the mechanical aspects of such processes.

It is nonetheless important to recall how essential the mass balance is. The dimensioning of a mechanical separation apparatus derive from the entire process, and the mass balance of the process quite often dictates the choice of a mechanical separation technique and its implementation. It is easy to understand that the classical technology of the car oil filter, which traps particles on the upstream side of the filter, is adequate because the mass of particles to be trapped by the filter is very

7 See the book by E.E. Michaelides, *Particles, Bubbles & Drops* (World Scientific, 2006) and the paper by J. Fabre and A. Liné, "Modeling of two-phase slug flow" (*Annual Rev. Fluid Mech.,* 24, 21–46, 1992).

small. It will thus be possible to drive 10,000 or 20,000 km before replacing the oil filter. However, when tonnes of solid particles need to be retained in order to treat wastewater, the dimensioning and implementation of the mechanical process are immediately constrained by the mass to be treated, and in a peripheral way by the issues of managing and handling such quantities.

In Figure 13.7, the overall mass balance in a mechanical separation apparatus is depicted. The apparatus is supplied, at a volume flow rate Q_a that remains constant with time, with a fluid that carries solid particles with a concentration C_a at the inlet. The inlet mass rate of solid particles is $\dot{m}_a = Q_a C_a$. The sketch represents several possible configurations. The apparatus has two outlets through which fluid flow rates Q_{s1} and Q_{s2} leave, carrying solid particles with concentrations C_{s1} and C_{s2}, respectively. The fluid balance across the apparatus dictates that $Q = Q_{s1} + Q_{s2}$. If the apparatus retains a fraction of the solid particles, the mass $M_s(t)$ retained increases in time. The mass balance of the apparatus for solid particles is written as:

$$\frac{\mathrm{d}M_s}{\mathrm{d}t} = Q_a C_a - \{Q_{s1} C_{s1} + Q_{s2} C_{s2}\} \qquad [13.16]$$

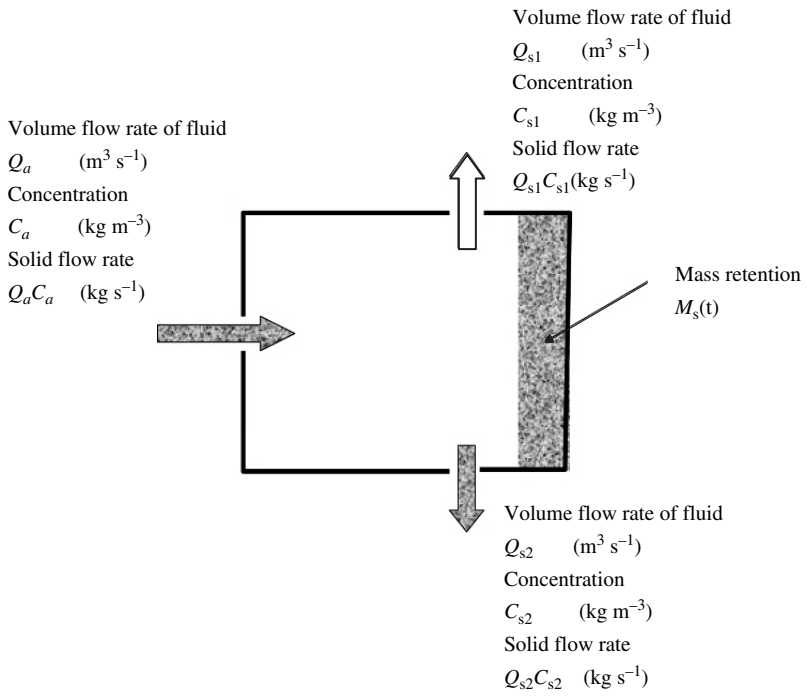

Figure 13.7. *Mass balance for a mechanical separation process*

It is vital to estimate the rate of solid feed $Q_a C_a$ before studying a mechanical separation process. Moderate concentrations in suspension, associated with large fluid flow rates, produce considerable masses of solids. A few figures regarding the river Gironde illustrate this fact. The river has an average flow rate of the order of 1,000 $m^3\ s^{-1}$ and carries 2.2×10^6 ton/yr of solid matter, which corresponds to an average concentration in suspension of the order of 60 mg L^{-1}. This value, which lends to the waters of the Gironde a turbid appearance (one cannot see through them), seems modest at a first glance. Such figures pertaining to river hydrodynamics are also relevant to process engineering practitioners. The mass flow rate is 60 kg s^{-1}. An engineer will easily realize that (s)he will have to manage substantial volumes of solid materials if they tap, for whatever purpose, a fraction of the liquid flow of the Gironde over a long period. If the mass $M_s(t)$ retained in the apparatus grows rapidly, clogging of the mechanical separation apparatus may occur quickly, and the implementation of the process will be essentially conditioned by the removal of particles from the apparatus.

Figure 13.7 comprises two outlets, which may perform different functions. If the purpose of the apparatus is to clarify the liquid, with a view to discharging through outlet 1 the particle-free liquid, the separation efficiency E may be characterized by bringing in the ratio of the rate of solids leaving through outlet 1 to the feed rate of solids:

$$E = 1 - \frac{Q_{s1} C_{s1}}{Q_a C_a} \qquad [13.17]$$

An efficiency equal to 1 means that the objective of separation has been reached, although that figure will need to be correlated to the ratio of fluid flow rates, Q_{s1} / Q_a. If $Q_{s1} / Q_a << 1$, the clarification will have been carried out at the expense of a substantial drop in the liquid flow rate leaving through outlet 1.

It is also possible to assign grain size sorting objectives to outlets 1 and 2. In the case of a bimodal distribution of solid particles in the fluid, one may wish to discharge through outlet 2 all solid particles whose size exceeds a certain diameter, while discharging through outlet 1 the largest possible fraction of small particles present in the fluid.

Chapter 14

Flows in Porous Media

This chapter deals with the physical principles that govern flows in porous media. Such flows have a wide range of applications in oil extraction, civil engineering and geomechanics (mechanical behavior of soils), or in hydrogeology (water resources). In the process field, filtration is widely used in the agri-food and environment industries (water treatment, dust removal, etc.).

Having introduced in the first section the characteristic parameters of the geometrical structure of a porous medium, we establish Darcy's law, which links the flux through a porous medium to the pressure gradient that is applied. The characteristic hydrodynamic parameter of a porous medium is its permeability. In section 14.5, we establish the Kozeny–Carman formula, which models permeability according to the geometrical parameters of the porous medium. Darcy's model is extended in section 14.6 to the turbulent regime, introducing Ergun's relation, which describes the flow in highly permeable porous media. Applications treated more directly in this chapter are the filtration processes. We introduce the notion of membrane resistance to filtration and discuss the case of filtration by pressing (section 14.7), whereby by compressing the porous medium, the liquid held inside the porous medium gets drained. That process couples the flow in the porous medium to the mechanical behaviour of the solid skeleton constituting the porous medium.

Membrane separation processes are not restricted to the mechanical principles discussed in this chapter. Different terminologies (microfiltration, ultrafiltration, nanofiltration, reverse osmosis, etc.) point to the fact that separation mechanisms change as particles become smaller and membranes become denser. The smaller the particles are, the greater the pressures used in membrane separation processes

will be. Physico-chemical processes intervene (diffusivity, solubility of products in the membrane), and transport through the membrane is governed by both the pressure gradient and the diffusion phenomena. We merely skim such phenomena[1] in section 14.8 by describing the reverse osmosis process used to separate particles of molecular size.

14.1. Consolidated porous media, non-consolidated porous media, and geometrical characterization

A porous medium is a granular medium in which grains (or fibers) are in contact with one another. In such a medium, interstitial spaces are called *pores*. The granular medium is assumed to be rigid and in mechanical equilibrium. Two types of porous medium can be distinguished:

1. Consolidated porous media: here, the contact (cohesive) forces between elementary grains maintain the mechanical stability of the material. Usual examples of consolidated porous media include calcareous rocks, clays, vegetable, and animal tissues. The deformation or mechanical equilibrium of the porous medium is not a concern, unless its mechanical breakdown under the effect of strong forces is considered.

2. Non-consolidated porous media: here, the grains are not fused together. They are stacked in a stable equilibrium configuration under the effect of the grains' weight and of the buoyancy force applied by the liquid contained in the pores. The mechanical equilibrium of the grains may be upset if a sufficient pressure gradient is applied in the opposite direction to the reduced gravity force (difference between the weight of the grains and the buoyancy force). Bed fluidization then occurs, a phenomenon that we study in Chapter 15. Classical examples of non-consolidated porous media include deposited beds of sand, glass balls, asbestos fiber, or glass wool, etc.

The flow in a porous medium mainly depends on the size of the pores and the volume they occupy inside the material. The heterogeneity of the pores can also be an important parameter; very fine pores, through which the fluid transits with difficulty, may coexist with wider pores and with larger fractures providing pathways through which the flow is facilitated. The detail knowledge of the geometrical characteristics of a porous medium is usually not available. Concept might be introduced to define them in a statistical way, but they remain of limited value if no apparatuses are available to measure them. Permeability is the key physical parameter that quantifies the flow inside the porous medium. Quite often,

1 See the book by J. Mulder (*Basic Principles of Membrane Technology*, Springer, 1996) which specifically deals with membrane separation.

engineers merely estimate the permeability of a porous medium by performing direct measurements of the discharge flow through a porous medium sample, without having access to geometrical data regarding the porous medium (see the laboratory permeameters described in section 14.3.1).

The permeability of a porous medium depends on geometrical parameters that involve only length dimensions:

– The "size of the pores": the notion of pore distribution according to their size can be arrived at in a manner similar to that used for the grain size distribution introduced in Chapter 13; however, the difficulty lies in translating this concept into a measurement apparatus. For a deposited granular material, it is common practice to consider that the characteristic size of the pores is of the order of magnitude of the grain size, when the grain size distribution is unimodal.

– The "total porosity", is defined as the ratio of the void volume in a porous medium to the total volume

$$\varepsilon = (\text{empty volume}/\text{total volume}) = 1 - (\text{solid volume}/\text{total volume})$$

– The "accessible porosity": some pores inside the porous medium may be enclaves unconnected to the outside, and the fluid cannot flow through them. Accessible porosity, defined on the basis of the volume of accessible pores, is written as:

$$\varepsilon_a = \text{accessible pore volume}/\text{total volume}$$

Accessible porosity is the relevant parameter in the study of hydrodynamics. It can be measured using a laboratory porosimeter, which measures the volume of a fluid that can be introduced into the porous medium. Accessible porosity can also be evaluated by both volume and mass measurements of a porous medium, if the density of the grains constituting the porous medium (measurable using a pycnometer) is known. The accuracy of this procedure implies the ability to ensure that accessible pores are filled with air or water, not a two-phase air/water mixture.

– The "specific area" (a_s) is defined as the ratio of the area between solid and void to the total volume of the sample. Its unit is m^{-1}. The smaller the size of the grains or pores is, the larger the specific area is. The specific area is important for evaluating a transfer capacity between the solid of the porous medium and the fluid. The larger the specific area is, the easier the transfers will be.

– *The tortuosity factor t*: this dimensionless quantity is defined as the ratio of the length of the path travelled by a fluid particle crossing the sample to the thickness of the sample. It is estimated statistically.

The concept of a porous medium supposes that the grains forming the porous medium are small. This notion is only meaningful in the context of a flow inside the porous medium. "Small" signifies that the flow inside the porous medium is slow. The Reynolds number, calculated from the velocity of the flow inside the porous medium, the characteristic size of the pores and the kinematic viscosity of the fluid, should be sufficiently small for the flow inside the porous medium to be laminar.

14.2. Darcy's law

Consider the principle of the experiment depicted in Figure 14.1. The porous medium, whose properties (grain sizes and porosity) are homogeneous in space, is bounded by two planes perpendicular to the *Oz* axis. The thickness of the layer is denoted by *L*. The material is immersed in a fluid, which saturates the interior of the porous medium.

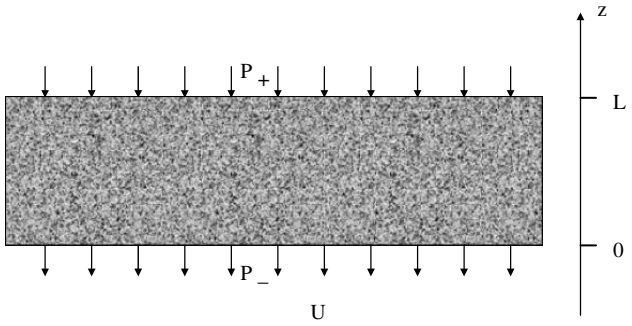

Figure 14.1. *Flow in a porous medium*

If a homogeneous pressure difference $\Delta P = (P_+ - P_-) > 0$ is applied between the two sides of the porous layer, it is easy to arrive experimentally at the following observations:

– The pressure differential ΔP produces a fluid flow rate through the porous medium, oriented from the side where the pressure is highest toward the side where it is lowest.

– The discharge velocity U varies linearly with the regular head loss $\Delta P/L$, for a given fluid and a given porous medium.

– For a given porous medium, the discharge velocity U decreases in inverse proportion to the dynamic viscosity μ of the fluid.

These simple observations lead to Darcy's law, which is written, for the configuration of Figure 14.1, in absolute values:

$$\frac{\mu U}{k} = \frac{\Delta P}{L} \qquad [14.1]$$

Darcy's law involves coefficient k, which is the intrinsic permeability of the porous medium. Its dimension is square meters. This quantity depends on the dimensions of the porous medium (grain or pore size) and on the geometrical characteristics (porosity, tortuosity) defined in the previous section.

Darcy's law is generalized to three dimensions (3D) by writing:

$$\frac{\mu}{k}\vec{u} = -\nabla p \qquad [14.2]$$

The velocity of the flow is parallel and in the opposite direction to the pressure gradient, as observed in the previous unidirectional configuration. The 3D formulation is useful, for instance, to study oil extraction from an oilfield. If the permeability is homogeneous in space and if the fluid is incompressible, the pressure field is the solution to the Dirichlet problem:

$$\Delta p = 0 \qquad [14.3]$$

for a known distribution of the pressure field at the boundaries of the domain. Darcy's law allows the velocities in the porous medium to be derived there from.

A second level of generalization, often useful in practice, occurs where body forces are applied to the fluid. We then write:

$$\frac{\mu}{k}\vec{u} = -\nabla p + \vec{F} \qquad [14.4]$$

In the case where the body force is represented by weight, [14.4] becomes:

$$\frac{\mu}{k}\vec{u} = -\nabla p + \rho\vec{g} \qquad [14.5]$$

where ρ is the density of the fluid. Equations [14.4] and [14.5] can be easily recovered by a comparison with Navier–Stokes equations. Only the pressure term and the body force remain unchanged. The left-hand side is substituted for the acceleration and viscous terms.

14.3. Examples of application of Darcy's law

14.3.1. *Laboratory permeameters*

Permeameters are instruments which, by an application of Darcy's law, allow the measurement of the intrinsic permeability of a porous medium. Two such examples are presented here. In both cases, the flow inside the porous medium is produced by the force of gravity.

14.3.1.1. *Constant head permeameter*

Figure 14.2 presents the principle of a constant head permeameter. The porous medium layer, of thickness L, is set in the lower tank. The water level in the upper tank is kept constant using an overflow pan. The liquid flows upward inside the porous medium, from bottom-up. The fluid is discharged using the same overflow principle that maintains the water level constant above the porous medium. As the upstream and downstream water levels are constant, the pressure difference ΔP between the bottom and top of the porous medium is also constant.

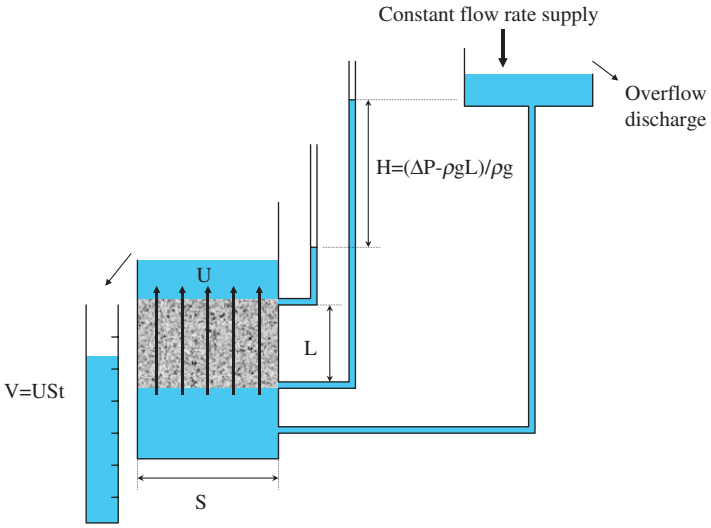

Figure 14.2. *Constant head permeameter*

The flow within the porous medium is produced by the head difference, $\Delta H = \Delta P - \rho g L$, between the bottom and top of the porous medium. This quantity is easily measured using height difference H (i.e. $\Delta H = \rho g H$) between the water levels in two piezometric tubes connected to the bottom and top of the porous

medium, respectively. If $H = 0$, the fluid is at hydrostatic equilibrium and the fluid does not flow through the porous medium. An upward flow, of discharge velocity U, is generated if $H > 0$. The flow rate Q is constant and is evaluated by measuring the volume $V(t)$ of water collected in a test tube after passing through the porous medium ($Q = V(t)/t$). The permeability of the porous medium is simply deduced from Darcy's law:

$$k = \frac{L}{\Delta H}\mu U = \frac{\mu QL}{S\rho gH} \qquad [14.6]$$

Here, S designates the cross-section of the porous medium.

14.3.1.2. *Variable head permeameter*

In order to understand the operation of a variable head permeameter, it is useful to start by studying the situation depicted in Figure 14.3. A liquid layer of initial thickness h_0 is placed on top of a layer of porous medium of thickness L, which is saturated with liquid. The weight of the water layer overlying the porous medium applies an overpressure to the upper side of the porous medium, generating a transient flow through the porous medium. The thickness $h(t)$ of the water layer on top of the filter medium decreases over time, as well as the discharge velocity $U(t)$. Atmospheric pressure serves as the pressure applied on the upper side of the liquid layer and at the exit of the porous medium.

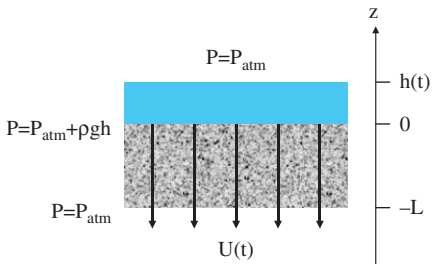

Figure 14.3. *Unsteady filtration under the effect of gravity*

With the conventions from Figure 14.3, Darcy's law [14.5] applicable to the porous medium ($-L < z < 0$) can be written as:

$$\frac{\mu}{k}u = -\frac{\partial p}{\partial z} - \rho g \qquad [14.7]$$

Through mass conservation, the velocity component u is necessarily independent from z. It is equal to the discharge velocity $U(t)$. The first integral of [14.7] from $z = -L$ to $z = 0$ is, therefore, written as:

$$\frac{\mu}{k} LU(t) = -p(z=0,t) + p(z=-L,t) - \rho gL \qquad [14.8]$$

Within the liquid layer on top of the porous medium ($0 < z < h(t)$), the pressure distribution is hydrostatic if the filtration process is sufficiently slow. We thus write:

$$0 = -\frac{\partial p}{\partial z} - \rho g \quad \text{for} \quad 0 < z < h(t) \qquad [14.9]$$

so that:

$$p(z=h(t),t) - p(z=0,t) = -\rho g h(t). \qquad [14.10]$$

Since the pressure of the liquid is equal to the atmospheric pressure P_{atm} at both the free surface ($z = h(t)$) and the underside of the porous medium ($z = -L$), summing [14.8] and [14.10] leads to:

$$-\frac{\mu}{k} U(t) L = \rho g \left(h(t) + L \right) \qquad [14.11]$$

Although it is not necessary to calculate the pressure on the upper side of the porous medium, its value (given in Figure 14.3) is determined by a simple hydrostatic calculation. The throughflow velocity $U(t)$ is negative. Measuring the flow rate $Q(t) = -U(t)S$ through the porous medium (S being the filtration area) then allows the permeability k to be evaluated as:

$$k = \frac{\mu Q(t) L}{S \rho g \left(L + h(t) \right)} \qquad [14.12]$$

The quantity $\rho g \left(L + h \right)$ is the head variation through the porous medium, which generates the flow. The thickness of the porous medium intervenes because the thickness of the water layer inside the porous medium also generates a pressure gradient.

The configuration of Figure 14.3 can be solved in a similar manner for $-L < h(t) < 0$, a situation which corresponds to the draining of the porous medium (much like the final stage of draining coffee grounds in a machine operated using

gravitational forces). The effective thickness of the filter medium is simply the thickness of the water layer $L+h(t)$, and that same height determines the pressure force due to gravity. Equation [14.8] is thus transposed into:

$$\frac{\mu}{k}U(t)(L+h(t)) = -p(z=h(t)) + p(z=-L) - \rho g\,(L+h(t)) \qquad [14.13]$$

Since $p(z=h(t)) = p(z=-L) = P_{atm}$, the filtration velocity is constant during the draining process:

$$U = \frac{\rho g k}{\mu} \qquad [14.14]$$

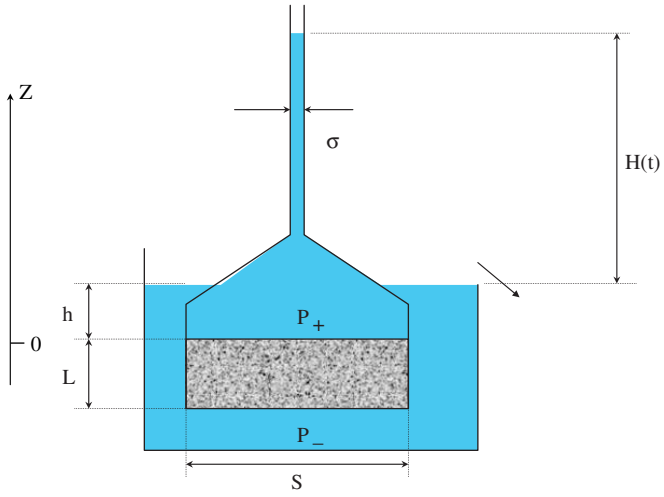

Figure 14.4. *Variable head permeameter*

Let us now consider the variable head permeameter illustrated in Figure 14.4. The pressure P_+ upstream of the porous medium is due to the water level in the upper tube. The hydrostatic calculation hence yields:

$$P_+ = P_{atm} + \rho g\,(h + H(t)) \qquad [14.15]$$

The downstream pressure is kept constant by the overflow device:

$$P_- = P_{atm} + \rho g\,(h + L) \qquad [14.16]$$

The time evolution of $H(t)$ is determined taking into account the fact that the flow rate is connected, through mass conservation, to the rate of displacement of the free surface in the feed tube (σ being the section thereof):

$$Q(t) = -SU(t) = -\sigma \frac{\mathrm{d}H}{\mathrm{d}t} \qquad [14.17]$$

Using [14.15]–[14.17], equation [14.8] leads to a first-order linear differential equation:

$$\frac{\mu}{k}\frac{\sigma L}{S}\frac{\mathrm{d}H(t)}{\mathrm{d}t} = -\rho g H(t) \qquad [14.18]$$

the solution of which is:

$$H(t) = H(0)\exp\left\{-\frac{kS\rho g}{\mu L\sigma}t\right\} \qquad [14.19]$$

A simple reading of the water height in the upper tube at two different times allows the permeability to be calculated by:

$$k = \frac{\mu L\sigma}{S\rho g t}\ln\left\{\frac{H(0)}{H(t)}\right\} \qquad [14.20]$$

Hydraulics practitioners often employ hydraulic conductivity $K = \rho g k / \mu$. This quantity has the dimension of a velocity.[2] Hydraulic conductivity is modified, for a given porous medium, if the viscosity of the liquid flowing through it changes. In contrast, intrinsic permeability depends only on the geometrical structure of the porous medium.

14.3.2. *Membrane resistance to filtration*

Elementary filtration theory is built upon Darcy's law. It is common for a filtration device to be comprised of several homogeneous filtering layers stacked upon one another. Each filter medium is characterized by its thickness H_f and

2 The UK and American literature on porous medium flows often calls "permeability" the quantity we know as hydraulic conductivity. The quantity k/μ (units m^3 s/kg) is also found introduced with the name of permeability. We advise the reader being careful with these different definitions. It is quite easy passing from one definition to another, as the definition of permeability is readily identified by examining the units.

permeability k_f. For the case represented in Figure 14.5, the filter comprises two layers, whose respective characteristics are designated by indices 1 and 2.

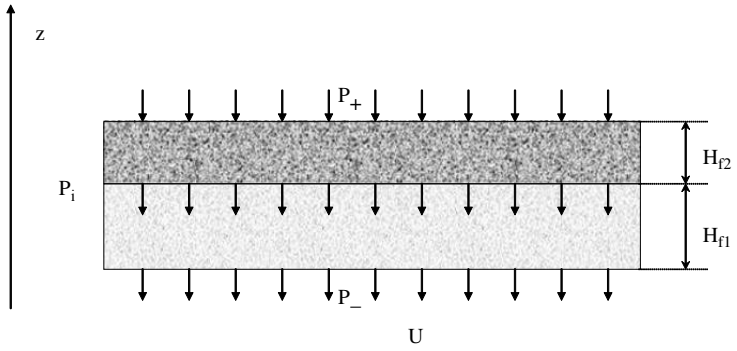

Figure 14.5. *Filtration device with two layers of a filter medium*

The continuity of the flow rate over the thickness of the filtration domain dictates that the throughflow velocity be independent from z, i.e. $u(z) = U$. Integrating Darcy's law over each of the two porous media can be written by a direct adaptation of [14.8] to the notations of Figure 14.5. The force of gravity is oriented downward, parallel to the Oz axis. We obtain:

$$P_+ - P_i = -\mu U \frac{H_{f2}}{k_{f2}} - \rho g H_{f2} \qquad [14.21]$$

$$P_i - P_- = -\mu U \frac{H_{f1}}{k_{f1}} - \rho g H_{f1} \qquad [14.22]$$

Summing [14.21] and [14.22] leads to:

$$\Delta P = P_+ - P_- = -\mu U \left(R_{f1} + R_{f2} \right) - \rho g \left(H_{f1} + H_{f2} \right) \qquad [14.23]$$

This relation links the total pressure variation $\Delta P = P_+ - P_-$ between the ends of the filtration system to the produced flow rate $Q(t) = -SU(t)$ (where S is the filtration area). The gravity term takes into account the contribution of the weight of the water column restricted to the thickness of the filter media. Relation [14.23] brings in quantities:

$$R_f = \frac{H_f}{k_f} \qquad [14.24]$$

for porous media 1 and 2, which are referred to as membrane resistance to filtration. The higher the membrane resistance to filtration, the lower is the discharge flow rate for a same head variation between both sides of the porous medium. It is found, based on [14.23], that the resistance to filtration of the different layers of filter medium can be simply added to evaluate the overall resistance to filtration of the whole device. This property explains why the notion of membrane resistance to filtration is used for dimensioning filtration devices.

14.3.3. *Dead-end filtration and cross-flow filtration*

Filtration processes can be categorized into dead-end and cross-flow filtration processes, both types being represented in Figure 14.6.

In dead-end filtration, the entirety of the fluid upstream of the filter medium passes through the membrane. Particles whose size is greater than the dimension of the pores accumulate on the upstream side of the filter, forming a cake which thickens over time (thickness $H_g(t)$). This layer of particles has to be taken into account for calculating the permeate flow rate, as if it was an additional layer of the filter medium. The resistance of the cake against filtration, $R_g = H_g(t)/k_g$, increases as it grows thicker. The flow rate, therefore, decreases in time.

The cross-flow filtration device (Figure 14.6(b)) aims to avoid the deposition of particles on the upstream side of the membrane and the associated resistance to filtration. Parallel to the surface of the filter, a flow is maintained, whose velocity is much higher than the velocity of the permeate flow induced by the pressure difference through the filter. The fluid and particles essentially just travel along the surface of the filter, and a small fraction of the fluid flow rate passes through the membrane. The friction of the tangential flow on the filter wall is used to re-entrain the particles that are deposited on the filter, in order to prevent the formation of a cake which would diminish the filtration flow rate. Cross-flow filtration reduces the phenomenon of membrane clogging.

The choice of dead-end or cross-flow filtration depends on the separation objective that is decided prior to selection of the filtration process. In wastewater treatment, e.g. the liquid discharged into the environment first has to be cleared of a large fraction of its particles. Dead-end filtration devices, such as filter presses, allow for the recovery of sludge for further treatment. As far as the supply of drinking water is concerned, it is the quality of the permeate flow that matters. At the end of the treatment chain, the concentration of particles within the fluid to be treated is low, and the particles to be removed are very minute. The membranes used are dense, and the ultimate water filtration is usually of the cross-flow type. This provides for good control over clogging phenomena.

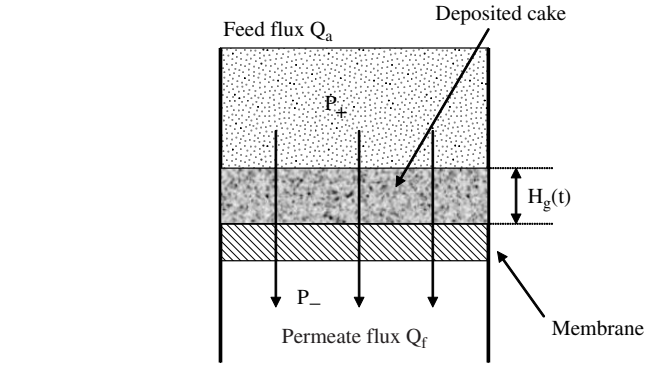

(a) Dead-end filtration

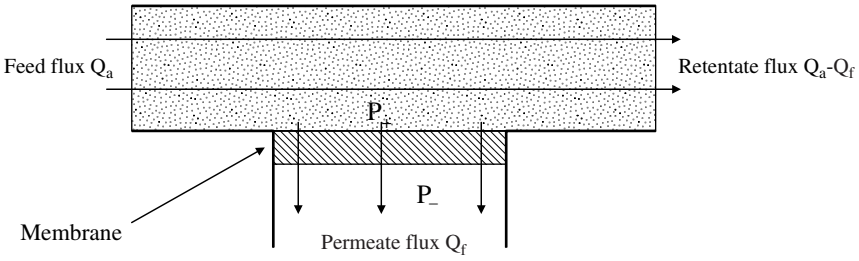

(b) Cross-flow filtration

Figure 14.6. *Dead-end and cross-flow filtration devices. For cross-flow filtration, the feed flow rate Q_a is much greater than the permeate flow rate Q_f. For dead-end filtration, $Q_a = Q_f$. Filtration results from the pressure difference $\Delta P = P_+ - P_-$ through the membrane*

14.4. Modeling Darcy's law through an analogy with the flow inside a network of capillary tubes

Darcy's law models the flow at a spatial scale larger than that of a pore. Inside the pores and microchannels running through the porous medium, the flow consists of an assembly of jets, as Figure 14.7 attempts to illustrate. At one point in the porous medium, velocity $\vec{u}$ that appears in Darcy's law is an average value over a volume whose size is greater than the dimension of the pores. Darcy's law, written in its generalized forms [14.4] or [14.5], therefore describes the flow at a scale which is greater than the size of the pores. Yet, this remains a local formulation. The heterogeneity of the medium can be taken into account through the spatial variations of permeability. Rigorous derivations of Darcy's law consist in averaging the local equations of fluid mechanics over a representative elementary volume (REV) of

a size greater than that of the pores and smaller than the dimensions of the porous medium. The formalism of these derivations is too complex to be presented here. We shall content ourselves with a simplified derivation of Darcy's law, which builds upon an analogy between the flow in a porous medium and that in a network of capillary tubes running through the medium. This proof utilizes the results regarding the Poiseuille flow (see Chapter 1).

A porous medium (Figure 14.7(b)) of thickness L is thus represented by a network of circular capillary tubes of diameter D. The length of each tube is denoted by l. It is greater than the thickness L of the porous medium, due to the tortuosity of the channels running through the porous medium. We, therefore, write $t = l/L$.

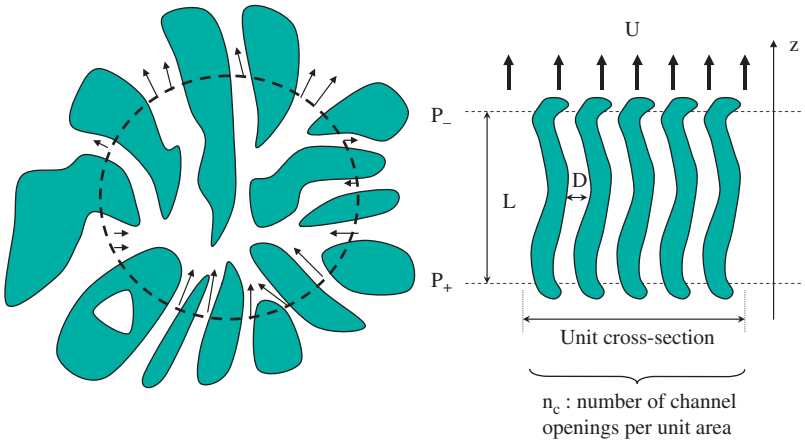

Figure 14.7. *Porous medium. (a) Representation at the scale of a representative elementary volume (REV) of a size greater than the scale of a pore. (b) Representation by a network of capillary tubes*

If a pressure variation $\Delta P = P_+ - P_-$ is applied between the inlet and outlet of a circular cylindrical tube of length l and diameter D, the flow rate that passes through the tube is given by the solution of the Poiseuille flow for a fluid of dynamic viscosity μ:

$$Q_{\text{tube}} = \frac{\pi}{128\mu}\frac{\Delta P}{l}D^4 \qquad [14.25]$$

(Chapter 1, equation [1.25]). This relation supposes that the flow is sufficiently slow to remain laminar. We return to this point later. In addition, the curvature of the capillary tube is also neglected.

By representing the porous medium with a number n_c of capillary tubes passing through a unit surface in the *Oxy* plane, we deduce from [14.25] that the discharge velocity across the surface of the porous medium is:

$$U = n_c Q_{tube} = \frac{n_c \pi D^4}{128 \mu t} \frac{\Delta P}{L} \qquad [14.26]$$

The tortuosity t is introduced in [14.26] in order to express the Darcy law in terms of the thickness of the porous medium rather than the length of the tubes. We recover in [14.26] the first form of Darcy's law (equation [14.1]). The intrinsic permeability can then be expressed as a parameter depending on the geometrical characteristics of the capillary tube network:

$$k = \frac{n_c \pi D^4}{128 t} \qquad [14.27]$$

This expression is of little interest so long as the diameter D and the number of capillaries n_c per unit surface are not related to the known geometrical characteristics of the porous medium. This further step is taken as per the Kozeny–Carman model.

14.5. Modeling permeability, Kozeny–Carman formula

The geometrical parameters of the porous medium are the grain size d and the number of grains per unit volume n_p. The geometrical parameters of the network of capillary tubes are the diameter D of the tubes and the number of tubes n_c passing through a unit surface in the *Oxy* plane. Tortuosity t is a common parameter of the porous medium and the capillary-tube network model. The Kozeny–Carman formula expresses, based on [14.27], the dependence of k on d, t, and ε, establishing a link between n_c and D, on the one hand, and between n_p and d, on the other. These relations are obtained under the hypothesis that the porous medium and the network of capillary tubes have the same porosity ε and the same specific area a_s.

For a granular medium consisting of spherical balls, the porosity and specific areas are given by:

$$1 - \varepsilon = n_p \frac{\pi d^3}{6} \quad \text{and} \quad a_s = n_p \pi d^2 \qquad [14.28]$$

Hence:

$$a_s \frac{d}{6} = 1 - \varepsilon \qquad [14.29]$$

For the capillary-tube network medium, the porosity and specific area are:

$$\varepsilon = n_c \frac{\pi D^2}{4} \frac{l}{L} = n_c \frac{\pi D^2}{4} t \quad \text{and} \quad a_s = n_c \frac{\pi D l}{L} = n_c \pi D t \qquad [14.30]$$

The equivalent relation to [14.29] is written as:

$$a_s \frac{D}{4} = \varepsilon \qquad [14.31]$$

Comparing [14.29] with [14.31] leads to:

$$D = \frac{2\varepsilon}{3(1-\varepsilon)} d \qquad [14.32]$$

$$n_c = \frac{9(1-\varepsilon)^2}{\pi \varepsilon d^2 t} \qquad [14.33]$$

$$k = \frac{\varepsilon^3}{72(1-\varepsilon)^2 t^2} d^2 \qquad [14.34]$$

The latter relation is more often used in the form:

$$k = \frac{\varepsilon^3}{36 h_K (1-\varepsilon)^2} d^2 \qquad [14.35]$$

which is known as the Kozeny–Carman law, using the empirical coefficient $h_K = 4.5 \pm 1$.

d	2 μm	60 μm	200 μm	2 mm
k (m^2)	4.4×10^{-15}	4.0×10^{-12}	4.4×10^{-11}	4.4×10^{-9}

Table 14.1. *Permeability values calculated using the Kozeny–Carman formula (equation [14.35]) for a porous medium consisting of spherical balls of diameter d. The porosity is $\varepsilon = 0.4$*

Table 14.1 lists a few values for the intrinsic permeability of a porous medium, calculated using the Kozeny–Carman relation. It illustrates several essential properties of the Kozeny–Carman relation and of the notion of permeability, which it is important to remember:

– Intrinsic permeability k is a very small quantity. It depends mainly on the grain size, and decreases strongly when the grain size decreases.

– k increases when porosity increases. However, for a deposited bed, porosity does not vary much (in the interval $0.3 < \varepsilon < 0.5$), except for some particular materials used as filter aids, which have a porosity of the order of 0.9. When added to wastewater, they contribute to maintain a higher level of porosity in the sludge cake deposited on the membrane during a filtration process.

14.6. Ergun's relation

Darcy's law is valid only for a sufficiently slow flow, which is laminar inside the porous medium. The validity criterion for Darcy's law is expressed by a Reynolds number, written using the length scale $\sqrt{k}$ that characterizes the porous medium. The following criterion for the validity of Darcy's law is generally agreed upon:

$$Re = \rho u\sqrt{k} / \mu < 10 \qquad [14.36]$$

For a Reynolds numbers exceeding the value of 10, Ergun's relation:

$$\frac{\Delta P}{L} = -\left\{\frac{36h_K(1-\varepsilon)^2}{\varepsilon^3 d^2}\mu U + \frac{6h_B(1-\varepsilon)}{\varepsilon^3 d}\rho_f U^2\right\} \qquad [14.37]$$

with $h_K = 4.5 \pm 1$ and $h_B = 0.3 \pm 0.1$, is a commonly used extension of Darcy's law. The pressure difference ΔP and the thickness L of the porous medium are defined as in Figure 14.1. In the first term on the right-hand side, we recognize the Darcy's law associated with the Kozeny–Carman relation. The second term, which is owed to Burke and Plummer, takes into account the effect of turbulence in the flow inside the porous medium. Its modeling is classical; the pressure gradient associated with the Burke and Plummer's term does not depend on the fluid's viscosity, but varies with the density of the fluid and the squared velocity.

Ergun's relation is applied not only to very porous beds but also to non-deposited granular media such as fluidized beds, as we study in Chapter 15.

14.7. Draining by pressing

Draining by pressing is a common operation for a person who presses a sponge in order to wring the maximum possible amount of liquid out of it. It is also used in industrial processes aiming to reduce the water content in a sludge. From a mechanical point of view, modeling the filtration of the liquid within the porous medium (Darcy's law) needs be complemented, in order to take into account the

deformation process of the solid skeleton of the porous medium, which results from pressing and produces the draining of the liquid.

Figure 14.8(a) shows the geometry for which the dynamics of draining by pressing is formalized. The porous medium is placed between two plates inside a vertical column. The lower plate is fluid tight, whereas the upper plate is porous. The porous upper plate is subjected to a vertical force of intensity R_s. This force compresses the porous medium, whose thickness $H(t)$ diminishes over time as the liquid leaves through the porous upper plate. We denote by $U(z,t)$ the throughflow velocity inside the porous medium, which is oriented along the Oz axis. Incompressibility results in $U(z,t)$ being positive and increasing with z, since the liquid can only leave through the top in the configuration shown in Figure 14.8. We denote by $U_s(t) = U(H(t),t)$ the draining velocity through the upper plate.

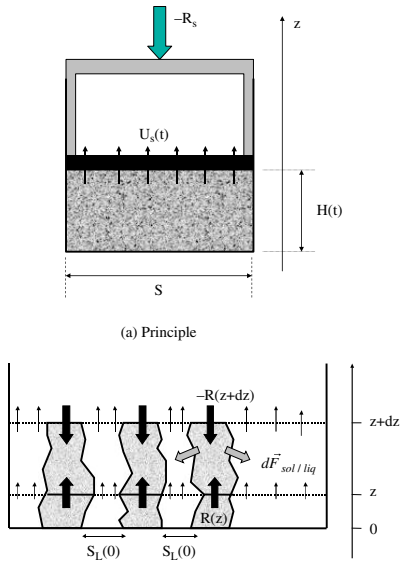

Figure 14.8. *Sketch of draining by pressing*

It is assumed that the characteristics of the porous medium – pressing and filtration – are homogeneous in any plane perpendicular to the Oz axis. Consequently, all the quantities involved in the problem depend on time t and position z, but not on x and y. Figure 14.8(b) represents a slice of porous medium between planes z and $z + \mathrm{d}z$. Within that slice, solid- and liquid-filled zones are identified. The force R_s applied on the porous medium at its surface is only partially

transferred to the solid. The remainder is retransferred to the fluid in order to force it out of the porous medium. We denote by $R(z)$ the total force applied on the solid surface at altitude z by the solid underneath. By convention, $R(z) > 0$, and the boundary condition at the surface of the porous medium is $R(H(t)) = R_s$.

Formalizing the problem requires several steps, different in nature, which are treated in sequence.

14.7.1. *Draining the liquid*

We denote by $\varepsilon(z,t)$ the porosity inside the porous medium. This varies with z. It is observed that pressing does not occur simultaneously in the entire layer. The porous medium is gradually compressed from the top to the bottom of the layer. Conservation of the liquid mass links $U(z,t)$ to $\varepsilon(z,t)$:

$$\frac{\partial U}{\partial z} = -\frac{\partial \varepsilon}{\partial t} \qquad [14.38]$$

The liquid flow is deduced from Darcy's law:

$$-\frac{\partial P}{\partial z} = \frac{\mu}{k(\varepsilon)} U(z,t) \qquad [14.39]$$

with $P(z,t)$ the pressure of the liquid inside the porous medium.

14.7.2. *Mechanical equilibrium of forces applied on the solid skeleton and on the liquid*

It is assumed that the intrinsic permeability of the porous medium is small. Compression of the porous medium is controlled by the draining of liquid out of the porous medium, which is slow. The pressing of the granular medium therefore depends chiefly on the permeability k and the viscosity μ of the liquid. The equilibrium of mechanical forces exerted on the solid is verified at all times. Since the presence of liquid inside the porous medium prevents the instantaneous compression of the cake, the force $\mathrm{d}\vec{F}_{\mathrm{liq/sol}}$ exerted by the liquid on the solid through all solid–liquid surfaces within the slice of porous medium between z and $z + \mathrm{d}z$ planes contributes to the equilibrium of forces applied on the solid, which is written as follows for the component directed along $\vec{k}$:

$$-R(z+\mathrm{d}z)+R(z)+\mathrm{d}\vec{F}_{\mathrm{liq/sol}}\cdot\vec{k}=0 \qquad [14.40]$$

By virtue of the principle of action and reaction, the solid subjects the fluid within the porous medium to a force $\mathrm{d}\vec{F}_{\mathrm{sol/liq}}=-\mathrm{d}\vec{F}_{\mathrm{liq/sol}}$ which establishes a pressure field in the porous medium. As it flows slowly, the liquid is almost at equilibrium, which is written in a similar manner to [14.40] for the same slice:

$$-P(z+\mathrm{d}z)S_L(z+\mathrm{d}z)\vec{k}+P(z)S_L(z)\vec{k}+\mathrm{d}\vec{F}_{\mathrm{sol/liq}}.\vec{k}=0 \qquad [14.41]$$

Here, $S_L(z)$ is the throughflow crosssection, which varies with z as a result of changes in porosity:

$$\varepsilon(t,z)=S_L(t,z)/S \qquad [14.42]$$

Here, S is the cross-section of the column. Equations [14.40]–[14.42], together with the action–reaction principle, lead to:

$$\frac{\partial R}{\partial z}=-S\frac{\partial(P\varepsilon)}{\partial z} \qquad [14.43]$$

whose first integral is:

$$R(z,t)=-SP(z,t)\varepsilon(z,t)+R_s \qquad [14.44]$$

using the boundary conditions $R(H(t))=R_s$ and $P(H(t))=P_{\mathrm{atm}}=0$ at the surface of the porous medium to determine the constant of integration. We thus have:

$$P(z,t)=\frac{R_s-R(z,t)}{S\varepsilon(z,t)} \qquad [14.45]$$

Using basic principles of algebra, we derive from [14.38], [14.39], and [14.45]:

$$\frac{\partial\varepsilon}{\partial t}=\frac{\partial}{\partial z}\left\{\frac{k(\varepsilon)}{\mu S}\frac{\partial}{\partial z}\left(\frac{R_s-R(z,t)}{\varepsilon(z,t)}\right)\right\} \qquad [14.46]$$

14.7.3. *Force transmission in the structure*

The delicate matter is to separate the fraction of the forces transmitted to the solid structure from those transmitted to the liquid, in order to determine $R(z,t)$,

and then the evolution of $\varepsilon(z,t)$ by solving [14.46]. Hypotheses regarding the mechanical behavior of the solid structure need to be introduced at this stage. We discuss in the following the simplest behavior we may think of, because discussing more sophisticated models is relatively peripheral to the physical principles on which we are focused, and such discussion necessitates a specialist debate that is out of place here.[3]

We consider the simplest possible behavior for force transmission within the solid structure. Before the application of the force to press the cake ($R(z,t)=0$), the porosity of the porous medium is homogeneous. It is designated by $\varepsilon_{\max}$. At the end of the experiment, the porosity again becomes homogeneous within the cake (this is denoted by $\varepsilon_{\min}$). The pressure is then equal to the atmospheric pressure throughout the liquid, and $R(z,t)=R_s$. We assume that, at all points in the porous medium, the force transmitted to the structure is related to the porosity of the medium at the same location. Additionally, we adopt a linear relationship which verifies the conditions both at the beginning and end of the experiment. This leads us to represent mathematically the following behavior observed in the $\varepsilon_{\min}<\varepsilon<\varepsilon_{\max}$ and $0<R<R_s$ intervals as:

$$R_s - R = R_s \frac{\varepsilon - \varepsilon_{\min}}{\varepsilon_{\max} - \varepsilon_{\min}} \qquad [14.47]$$

The quantity:

$$\chi = \{S(\varepsilon_{\max} - \varepsilon_{\min})\} / \{\varepsilon_{\min} R_s\} \qquad [14.48]$$

is the compressibility coefficient of the cake. The linear behavior of the porous medium in compression, expressed by [14.47], can be associated with an elastic behavior law, although we do not imagine it to be reversible (when the force is relaxed, the cake does not recover its initial thickness). The coefficient $E=1/\chi$ is therefore interpreted as the Young's modulus of the material, characterizing its subsidence for a given force.[4] Introducing [14.47] and 14.48] into [14.46] yields:

$$\frac{\partial \varepsilon}{\partial t} = \frac{\partial}{\partial z}\left\{\frac{k(\varepsilon)}{\mu\chi}\frac{1}{\varepsilon^2}\frac{\partial \varepsilon}{\partial z}\right\} \qquad [14.49]$$

3 A useful complement is found in G. Baluais, "Post-traitements à la filtration" (brochure J 3 502), *Techniques de l'Ingénieur*, volume Génie des Procédés.
4 See Chapter 6, section 6.3.

Despite its simplifications, this model has the advantage of highlighting the fact that the phenomenon behaves like a diffusion process, which both presses the solid structure and drains the liquid, starting at the top and progressing to the bottom of the cake.

14.7.4. *Characteristic time of draining by pressing*

It is relatively easy, albeit a little tedious, to calculate the space and time variations of porosity during a draining by pressing operation. By taking an average porosity to introduce an average diffusion coefficient into [14.49], a resolution using a Laplace transform leads to an expression of the solution.[5] It is noted that the characteristic time of draining by pressing takes on the form:

$$t_{\text{press filtration}} \approx \frac{H_0^2 \mu \chi}{k} \qquad [14.50]$$

which involves the initial thickness H_0 of the cake, its permeability k, and the dynamic viscosity μ of the liquid, along with the compressibility coefficient of the cake. The order of magnitude of the amount of liquid discharged by the draining by pressing operation is:

$$V_{\text{press filtration}} \approx H_0 R_s \chi \qquad [14.51]$$

Area S intervenes indirectly through R_s, which is the total force exerted on the surface S.

14.8. The reverse osmosis process

We have indicated in the introduction to this chapter that physico-chemical processes related to the diffusion of constituents or to their solubility in the fluid inside a dense membrane should be taken into account in order to model membrane separation of very small particles dispersed in a fluid. We discuss this aspect now, by describing the reverse osmosis process.

5 See again G. Baluais, "Post-traitements à la filtration" (brochure J 3 502), *Techniques de l'Ingénieur*, volume Génie des Procédés.

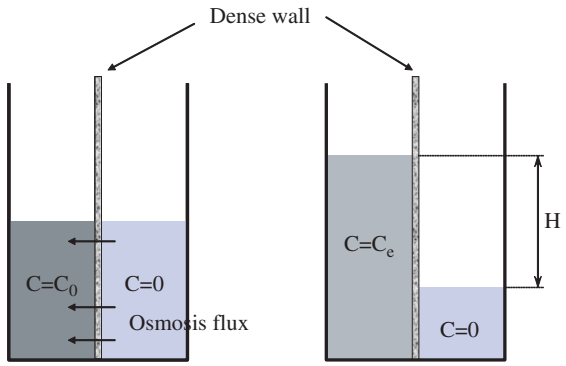

Figure 14.9. *Osmosis phenomenon and notion of osmotic pressure*

The implementation of Darcy's law is modified when the particles are very small and in sufficiently high concentration, due to osmosis which then occurs through a membrane. The notion of osmotic pressure is easily brought to the fore by carrying out the experiment depicted in Figure 14.9. Consider a jar partitioned into two compartments by a dense porous wall. The membrane is semi-permeable: it lets solvent molecules through, but retains very small particles whose size is of the order of a few nanometers. Initially (Figure 14.9(a)), equal volumes of a liquid are introduced into both the compartments. The right-hand side compartment contains pure solvent, while in the left-hand side compartment the same solvent contains very small particles with a concentration C_0. The experiment shows that this situation is not at equilibrium. Some solvent transits from the right compartment to the left compartment until the liquid inside the compartment containing the particles stabilizes at a level that is higher than the level in the right compartment by a height H (Figure 14.9(b)). The pressure difference across the porous wall is then $P_{\text{osm}} = \rho g H$. This quantity is called the osmotic pressure.

The osmotic pressure is, in fact, related to a diffusion process between the right and left compartments. If the concentration of particles is sufficiently high inside the left compartment, and the mass fraction of water is lower in the left compartment than in the right compartment, then a flow of water occurs by diffusion from right to left through the membrane. For the case illustrated in Figure 14.9(b), the water level stabilizes in the left compartment when the advection flow from left to right due to the pressure difference (Darcy's law) is equal and opposite to the diffusion flux due to osmosis. In other words, the osmotic pressure allows the diffusion flux to be quantified.

The value of the osmotic pressure is calculated using the van't Hoff relation for osmosis:

$$P_{\text{osm}} = C_e RT \qquad [14.52]$$

This relation is formally identical to the ideal gas law, since C_e is the concentration of particles in mol·m^{-3}, T the absolute temperature, and R the universal gas constant (R = 8.31 J mol^{-1} K^{-1}). The Van't Hoff relation is in fact derived from the difference of chemical potentials of the solvent on either side of the porous membrane, owing to the presence of particles in the left compartment.

Osmotic pressure in salt water is easy to calculate. For a salt concentration of 10 g L^{-1}, we obtain P_{osm} = 8.5 bar at a temperature of 25°C. The molar mass of NaCl being 58 g (35 g + 23 g), 10 g L^{-1} of salt correspond to 345 mol·m^{-3} of ions. Now, it is observed that a factor 2 appears, since NaCl dissociates into Na^+ and Cl^- ions (i.e. there are 172.5 mol·m^{-3} of Na^+ ions and 172.5 mol·m^{-3} of Cl^- ions). The main finding is that the osmotic pressure is very high because, for a reasonable concentration of particles in g L^{-1}, the concentration of particles in mol m^{-3} is large if the particles are very small.[6]

Effects of the notion of osmotic pressure are observed in everyday life:

– The absorption of water by plants: a plant absorbs any water deposited on its leaves due to the presence of mineral salts inside the plant.

– Flowers are dried out if watered with seawater. The salt in the salt water on the leaves causes the water contained inside the plant to move to the outside.

– Raw ham is prepared by drying it thanks to having sprinkled it with salt, just like salt dispersed in box where snails are left for some time to help them disgorge before being cooked.

In order to filter a solution containing very fine particles, as is the case when seawater is to be desalinated, it is therefore necessary to apply, between the compartment containing the particles (upstream) and the downstream compartment, a pressure difference $\Delta P = P_+ - P_-$ greater than the osmotic pressure. As long as $\Delta P - P_{\text{osm}} < 0$, the flux of solvent is an osmosis flux. Filtration occurs for $\Delta P - P_{\text{osm}} > 0$. This is termed reverse osmosis, since the flux of solvent is in the

6 Some authors use the term solute, rather than particles, to refer to molecules dispersed in a fluid. However, it may be noted that modeling the dynamics of such elements builds on the same foundations introduced in this part for spherical particles. For example, it is common to rely on Stokes' law in modeling diffusion through Brownian movement (Chapter 16, section 16.3).

opposite direction to the osmosis flux. The effective pressure variation producing the filtration (or reverse osmosis) flow is $\Delta P - P_{\text{osm}}$. Darcy's law (equation [14.1]) can be used simply to evaluate the flow rate, by writing:

$$\frac{\mu U}{k} = \frac{\mu}{k}\frac{Q}{S} = \frac{\Delta P - P_{\text{osm}}}{L} \qquad [14.53]$$

This explains why reverse osmosis processes employ very high-pressure levels. An exercise at the end of this chapter examines various aspects of the dimensioning of a seawater desalination process.

14.9. Energetics of membrane separation

The high pressures employed in membrane separation processes, in particular when the particles are very minute, as we have seen in the previous section with the reverse osmosis case, do not mean that membrane separation is a costly process in terms of energy. The pressure drop between the upstream and downstream sides of the membrane is an amount of energy per unit volume of fluid treated which is irretrievably lost when passing through the membrane. Thus, 1 kWh is spent to filter 1 m^3 of water with $\Delta P = 36$ bar. If the aim is to supply potable water, the cost is modest in comparison with the price of supplying 1 m^3 of potable water. This evaluation sets aside the constraints of a high-pressure membrane separation process (safety, mechanical forces, pumps to supply high pressure, etc.), which also have an impact in energy terms. It is, however, worth recalling that membrane separation processes are energy efficient, particularly in comparison with thermal processes (distillation).

14.10 Application exercises

Exercise: Study of a seawater desalination process

In order to desalinate seawater in a small-sized plant, it is envisaged to use a hollow-fiber module (Figure 14.10), the sketch of which has been found in the Techniques de l'Ingénieur.[7] Salt water flows inside circular cylindrical hollow fibers of inner diameter 40 μm and outer diameter 80 μm through which the permeate (salt free) is filtered by reverse osmosis as it passes from the inside to the outside of the fibers. In this cross-flow filtration device, a substantial fraction of the salt feed flow rate leaves without being filtered.

7 Brochure J 2791, "Filtration membranaire (OI, NF, UF): Présentation des membranes et des modules", J.C. Remigy and S. Desclaux, *Techniques de l'ingénieur*, Génie des procédés.

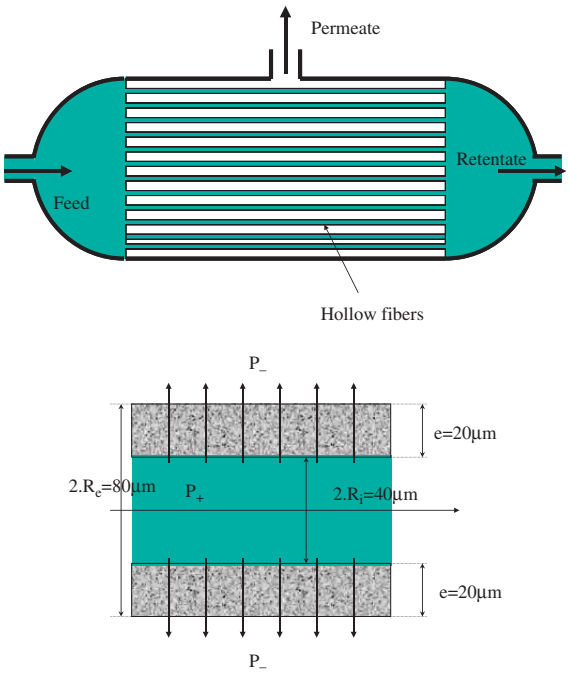

Figure 14.10. *Hollow fiber module*

The concentration of salt in the seawater is assumed equal to 35 g L^{-1}. The molar mass of sodium is 23 g and that of chlorine is 35 g. Based on this information, now:

– Calculate the osmotic pressure.

– Provide an order of magnitude for the permeability of a membrane allowing the filtration of particles whose size is 10^{-9} m. Evaluate the membrane resistance to filtration for one hollow fiber.

– The filtration plant under consideration would have an inlet pressure of 70 bar and an outlet pressure of 1 bar. Evaluate the flow rate of filtered water in liters per day and square meter of filtration area.

– The compactness of the filtration device is important. Remiguy and Declaux indicate a filtration area of the order of 15,000 m^2 for a module whose volume is 1 m^3. For a 1 m^3 module, evaluate:

- The flow rate of filtered water in cubic meters per day.

- The number of houses that could be supplied on a daily basis, based on Western standards of consumption.

- The total length of the fibers contained in the module.

- The volume occupied by the fibers inside the module.

From a process point of view, why is it so important to use small-diameter hollow fibers?

– The high pressures involved raise the issue of the mechanical strength of the hollow fibers, whose thickness is particularly small. The pressure difference between the inside and outside is balanced by a force $\vec{T}$ which stretches the fiber (Figure 14.11). For a small element of hollow fiber, of length L along the fiber axis (perpendicular direction to the plane of the figure) and corresponding to an arc of angle $2\mathrm{d}\theta$, the equilibrium of forces in the $\vec{e}_r$ direction is written as

$$LR_i 2\mathrm{d}\theta P_+ - LR_e 2\mathrm{d}\theta P_- - 2\sin(\mathrm{d}\theta)T = 0$$

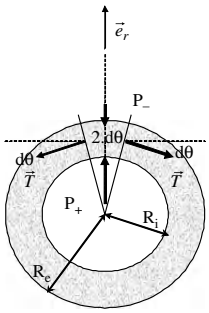

Figure 14.11. *Equilibrium of forces exerted on a hollow fiber*

The stretching force is related to the normal stress $T = \sigma L(R_e - R_i)$, which is easily calculated under the small-angle hypothesis:

$$\sigma = \frac{R_i P_+ - R_e P_-}{(R_e - R_i)}$$

Hollow fibers used in reverse osmosis can be made of cellulose acetate or of polyamide. Maximal stresses (beyond which the material breaks) are as follows:

– for cellulose acetate: $\sigma_{\max} \approx 10 - 110$ MPa .

– for polyamide: $\sigma_{\max} \approx 78$ MPa .

Calculate the stretching stress for the conditions applicable in this exercise.

Explain why the fiber does not break.

Chapter 15

Particles Within the Gravity Field

In this chapter, we discuss several aspects of the mechanical behavior of particles situated within the gravity field.

The density ρ_s of the particles often differs from the density ρ_f of the fluid in which they are immersed. Within the gravity field, this produces a relative movement of the particles with respect to the fluid, either upward (rising) or downward (settling), depending on whether the particles are less or more dense than the fluid. In section 15.1 we study how to evaluate the fall velocity of a rigid spherical particle in a fluid at rest, before discussing in section 15.2 the settling of a set of particles. The relative gravitational movement of a small-sized fluid particle is then discussed in section 15.3 for a gas bubble in a liquid, a drop of liquid in a gas, or a drop of non-miscible liquid in another liquid.

We then study, in sections 15.4 and 15.5, how the stirring of a fluid can maintain a dispersed set of particles in suspension. Practitioners of underwater diving have remarked that water becomes turbid in the event of a storm; sediments are kept in suspension within the water layer by turbulence. In a fluid at rest, Brownian motion can also maintain a colloidal suspension (e.g. paint), which is composed of very fine particles. Both physical awareness and observation show that the denser and the larger the particles are, the greater is the energy of turbulence or the molecular stirring energy required to keep the particles in suspension.

Finally, we present in section 15.6 the mechanical principles governing fluidized beds. By directing an upward fluid stream through a bed of particles deposited on a sieve, it is observed that the flow of the fluid inside the bed places the particles in

suspension when the flow rate exceeds a critical value, and keeps them in a state of stirring that is steady on average.

15.1. Settling of a rigid particle in a fluid at rest

Consider an isolated solid particle placed in a fluid at rest. If the density ρ_s of the particle is greater than the density ρ_f of the fluid, the particle settles in the gravity field. In the reverse situation, it rises.

The Stokes experiment consists in dropping a spherical particle of diameter D where $\rho_s > \rho_f$. The ball rapidly reaches a constant fall velocity $\vec{W}_c$ parallel to the gravitational acceleration $\vec{g}$. When steady-state velocity is reached, the equilibrium of the forces applied on the ball reduces to the equilibrium between the reduced weight $\vec{F}_G$ (difference between the weight and Archimedes' force) and the hydrodynamic drag force $\vec{F}_R$ exerted by the fluid flow on the particle.

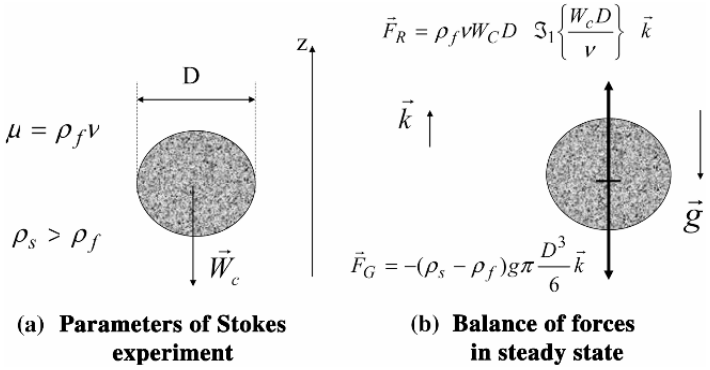

Figure 15.1. *Parameters of the Stokes experiment of dropping a spherical ball in a fluid at rest, and balance of forces*

The parameters of the Stokes experiment are recapitulated in Figure 15.1. The reduced weight $\vec{F}_G$ is written as:

$$\vec{F}_G = -(\rho_s - \rho_f) g \pi \frac{D^3}{6} \vec{k}, \qquad [15.1]$$

where $\vec{k}$ designates a unit vector in the direction opposite to gravity. The Stokes experiment is a classical problem, which we have discussed in section 3.4 as an

exercise in dimensional analysis. We recall its main results here. The hydrodynamic drag force, which resists the relative displacement of the particle with respect to the fluid, is the result of pressure and friction forces exerted by the fluid flow on the particle. The order of magnitude of viscous forces exerted on the particle is:

$$F_v \approx \rho_f \nu W_c D \qquad [15.2]$$

Dimensional analysis of the forces establishes that the hydrodynamic drag force (friction force and pressure force exerted on the particle) takes on the following form, which involves the undetermined function $\Im_1$:

$$\vec{F}_R(W_c, \rho_f, \nu, D) = \rho_f \nu W_C D \quad \Im_1\left\{\frac{W_c D}{\nu}\right\} \quad \vec{k}\,, \qquad [15.3]$$

where ν is the kinematic viscosity of the fluid.

In a steady-state regime, the equality of magnitudes of $\vec{F}_G$ and $\vec{F}_R$ leads to expression of the fall velocity as a functional relation between two non-dimensional numbers:

$$\Im_2\left\{\frac{W_c D}{\nu}, \frac{(\rho_s - \rho_f) g D^2}{\rho_f \nu W_c}\right\} = 0 \qquad [15.4]$$

This formulation, even if we were able to express function $\Im_2$, is not easy to use because the fall velocity appears in both dimensionless numbers. Consequently, it is expressed in an equivalent manner as a relation $\mathrm{Re} = \Im\{\mathrm{Ar}\}$ between the Reynolds number and Archimedes' number:

$$\mathrm{Re} = \frac{W_c D}{\nu} \quad \text{and} \quad \mathrm{Ar} = \frac{(\rho_s - \rho_f) g D^3}{\rho_f \nu^2} \qquad [15.5]$$

Archimedes' number Ar does not depend on the fall velocity, but only on the physical characteristics of the particle and the fluid.

In the asymptotical case where the Reynolds number is very small, as well as when it is very large, the form of the relation linking the Reynolds number to Archimedes' number can be determined. The order of magnitude of the pressure force exerted on the particle is written as a function of the scale P of the pressure variations on the surface of the particle,

$$F_P \approx P D^2 \qquad [15.6]$$

The order of magnitude of P is established on the basis of the orders of magnitude of the various terms in the Navier–Stokes equation. For a low Reynolds number, dimensional analysis of the Navier–Stokes equations[1] shows that the pressure scale P is such that the pressure force is of the same order of magnitude as the viscous force. Consequently, with [15.2]:

$$F_R \approx \rho_f \nu W_c D\,, \qquad [15.7]$$

and the fall velocity, derived from the equality of the magnitudes of the gravity force and the hydrodynamic force, is therefore expressed as:

$$W_c \approx \frac{(\rho_s - \rho_f) g D^2}{\rho_f \nu} \qquad [15.8]$$

In contrast, for high Reynolds numbers, the pressure term in the Navier–Stokes equation is of the same order of magnitude as the nonlinear term (which itself, by definition, is large compared to the viscous term), and the viscous force is negligible. We therefore have successively:

$$F_R \approx \rho_f W_c^2 D^2 \qquad [15.9]$$

$$W_c \approx \sqrt{\frac{(\rho_s - \rho_f) g D}{\rho_f}} \qquad [15.10]$$

Both laws relating to the fall of velocity, [15.8] and [15.10], are recalled in Table 15.1 in their dimensional and non-dimensional forms. In the laminar regime, the coefficient of proportionality 1/18 is exact,[2] whereas it is empirical in the turbulent regime. Also included in the table is the Van Allen correlation, which covers the intermediate domain $32.9 < \mathrm{Ar} < 1.04 \times 10^5$. This empirical correlation is very commonly used, as it corresponds to the characteristics of typical particles, particularly in natural environments (coastal shorelines, lakes, and rivers).

When using Stokes, Van Allen, or Newton correlations, it is necessary to check, by estimating the value of Archimedes' number, if it is indeed in the domain of validity of the correlation. Discrepancies can be very large in the case of error.

---

1 See application exercise (section 3.4) in Chapter 3.

2 In a laminar regime, the exact expression of the friction force exerted on a rigid particle is $F_v = 3\rho_f \nu W_c D$. This very classical relation will be used in this chapter and the subsequent ones.

Archimedes' number	$\mathrm{Ar} = \dfrac{(\rho_s - \rho_f) g D^3}{\rho_f \nu^2}$	Characterizes the physical properties of the fluid and particle Determines the settling regime
Reynolds number	$\mathrm{Re} = \dfrac{W_c D}{\nu}$	$\mathrm{Re} = \Im(Ar)$

	Domain of validity, Archimedes' number	Dimensional form of W_c	Non-dimensional form
Laminar regime $W_{c\text{Stokes}}$ Stokes' law	$\mathrm{Ar} < 32.9$	$\dfrac{(\rho_s - \rho_f) g D^2}{18 \rho_f \nu}$	$\mathrm{Re} = \dfrac{\mathrm{Ar}}{18}$
Intermediate regime Van Allen's law	$32.9 < \mathrm{Ar} < 1.04 \times 10^5$		$\mathrm{Re} = 0.153 \mathrm{Ar}^{0.71}$
Turbulent regime $W_{c\text{Newton}}$ Newton's law	$\mathrm{Ar} > 1.04 \times 10^5$	$\sqrt{3 \dfrac{(\rho_s - \rho_f) g D}{\rho_f}}$	$\mathrm{Re} = (3\mathrm{Ar})^{0.5}$

Table 15.1. *Settling velocity W_c of a rigid spherical particle in a fluid at rest, as a function of the physical characteristics of the fluid and particle*

15.2. Settling of a set of solid particles in a fluid at rest

The settling of a set of particles in a fluid at rest may depart significantly from the laws presented in the previous section for an isolated particle. This is mainly due to two phenomena:

– The formation of clusters

A sufficiently dense set of particles (in terms of the number of particles per unit volume) can give rise to clusters (often also called flocs), which gather particles together. Inter-particular forces such as the Van der Waals forces and electrostatic forces are responsible for these phenomena. The Van der Waals force is attractive. It therefore promotes the formation of clusters. The electrostatic force is repulsive, and opposes it. We have briefly described in section 13.2.5 the interparticular forces and their effects, but we shall not discuss these issues any further. It is nonetheless useful to recall that, generally speaking, the more spontaneous is the formation of clusters, the smaller is the size of elementary particles. For natural particles, sediments are said to be cohesive (silts) when the elementary particles have a size under 60 μm. Particles of a size greater than 60 μm are non-cohesive; they are referred to as sands.

As both the Van der Waals forces and the electrostatic forces are of electrical origin, the presence of ions in the liquid influences the formation of clusters. It is thus found that the formation of flocs is promoted for cohesive sediments in seawater in comparison to what is observed in fresh water.

The formation of clusters in a fluid is encouraged if the concentration in particles is sufficient and if a sufficient level of stirring is maintained in the fluid, as both parameters increase the probability that the particles will move sufficiently close to one another for the inter-particular forces to act and form clusters. On the other hand, a high level of turbulence breaks up the clusters whose size is too large.

While the occurrence of cluster formation can be relatively well predicted using the tools presented in Chapter 13, it is much more difficult to determine the size of flocs and their density. For practical applications, one can reasonably consider calculating the fall velocity of a cluster using the laws of fall velocity established in the previous section, provided the cluster's size D_a and density ρ_a are involved. The density of the cluster depends on the porosity p inside the cluster (Figure 15.2). Its value is intermediate between those of the fluid and solid, which tends to slow down the settling movement. On the other hand, the size of the cluster is greater than that of the elementary particles, which tends to increase the fall velocity. The effect of the size usually prevails. This explains the use of flocculants in a purification plant or a swimming pool to accelerate settling by forming clusters of elementary particles.

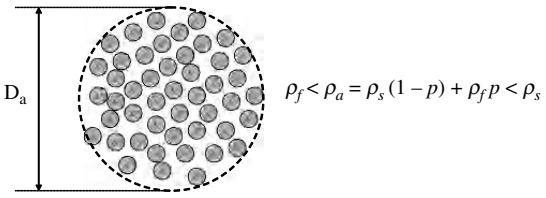

Figure 15.2. *Characteristics of clusters*

– The phenomenon of hindered settling

When the particles are in sufficiently large number inside the fluid, their settling velocity is slowed down in comparison to that of an isolated particle, because the downward movement of particles has to be compensated by the upward displacement of an equal volume of fluid. The proximity of particles to one another hinders the rise of the fluid and slows down settling. Such a situation is represented in Figure 15.3(a), which depicts the settling of a set of particles inside a closed column.

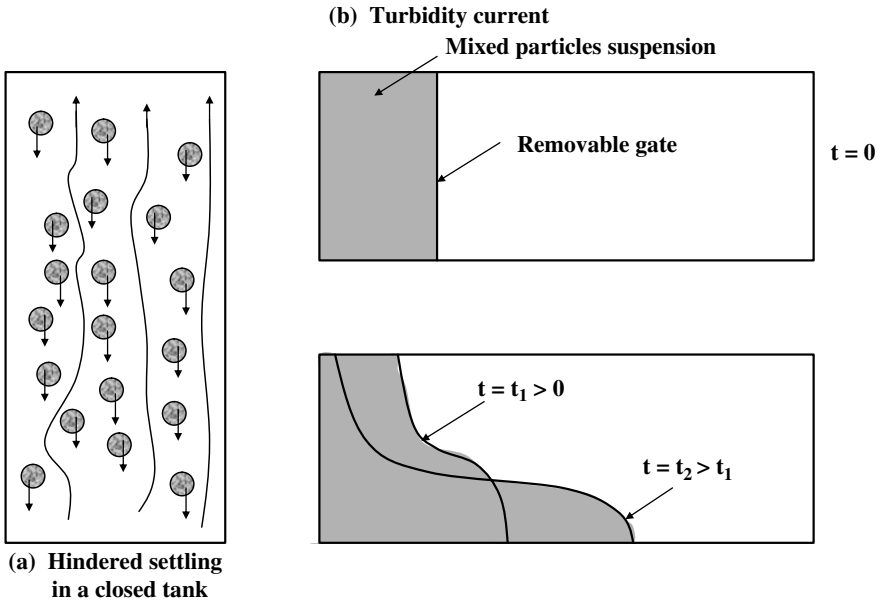

Figure 15.3. *Hindered settling (a) and turbidity current (b)*

The impediment to settling is not negligible as soon as the ratio of the average distance ℓ between two particles to the diameter D of the particles is of such an order of magnitude that $\ell / D < 5$. This situation may be reached for moderate concentrations of particles. For example, for spherical particles of density $\rho_s = 3,000$ g/L dispersed in a fluid with a concentration $C = 10$ g/L, the number of particles per unit volume is $N = 6C / \pi\rho_s D^3$. The average distance between the particles (Chapter 13, Table 13.2) equals $\ell / D \approx N^{-1/3} / D = (\pi\rho_s / 6C)^{1/3} = 5.4$ (the value does not depend on the particle diameter). In such a situation, the particles may draw the surrounding fluid with them as they settle. One consequence of this is represented in Figure 15.3(b), which shows the principle of a laboratory experiment in which a turbidity current occurs. A channel is initially divided into two parts by a removable partition. The right-hand-side part is filled with clear water and the left-hand-side part contains a concentrated suspension of particles homogeneously mixed. When the removable partition is taken away and the stirring that keeps the particles in suspension is simultaneously stopped, the particles are seen to settle, drawing the surrounding fluid with them. This generates a flow of the particulate mixture, which spills onto the bottom of the channel in a turbidity current that moves in time from left to right. Beyond the interest of this type of flow for studying phenomena that occur in natural environments, this experiment shows that, if the

concentration of particles is sufficiently high, the fluid/particle mixture behaves like an "equivalent fluid" whose density is:

$$\rho_h = \rho_f + \frac{(\rho_s - \rho_f)}{\rho_s} C \qquad [15.11]$$

ρ_h is called the wet (or total) density. Such phenomena explain why we have introduced this quantity in Chapter 13 (equation [13.6] and Table 13.2) as a characteristic quantity of a particulate medium.

15.3. Settling or rising of a fluid particle in a fluid at rest

The most common fluid particles are an air bubble in a liquid, a drop of water in a gas, or a drop of a non-miscible liquid dispersed in another liquid (oil drops in water, for example). The settling or rising of a fluid particle in a fluid at rest is modified relative to the case of a rigid particle discussed in section 15.1, because of friction stresses applied by the flow outside the particle set the fluid inside the particle in motion. The flow needs to be determined both inside and outside the particle, while verifying the continuity of velocity and stress at the surface of the fluid particle. This solution depends on the value of the Reynolds number associated with the settling velocity, $\mathrm{Re} = W_c D / \nu_c$ as well as on the ratio $\kappa = \mu_d / \mu_c$ of the dynamic viscosities of the fluids inside (dispersed phase) and outside (continuous phase) the particle. The Reynolds number is identical to the one introduced in section 15.1 for a rigid particle, but the subscript *c* is used to specify that ν_c is the kinematic viscosity of the fluid outside the particle. We only present here the results regarding a small-sized particle, for which the Reynolds number is sufficiently small. The solution to the problem was provided independently by Hadamard and Rybczynski[3] at the beginning of the 20th Century. It is written, in a formulation equivalent to Stokes' law for a rigid particle as given in Table 15.1, by bringing in Archimedes' number:

$$\mathrm{Re} = \frac{W_c D}{\nu_c} = \frac{\mathrm{Ar}}{6}\left\{\frac{1+\kappa}{2+3\kappa}\right\} = \frac{(\rho_d - \rho_c) g D^3}{6\rho_c \nu_c^2}\left\{\frac{1+\kappa}{2+3\kappa}\right\} \qquad [15.12]$$

This law, which is indeed verified for $\mathrm{Re} < 0.1$, is the counterpart to Stokes' law for a rigid particle. As a matter of fact, Stokes' law is obtained as a limiting case when $\kappa \to \infty$. For such low values of the Reynolds number, the deformation of the fluid particle by the stress field applied to its surface is negligible, and the particle may be considered to retain its spherical shape (see Chapter 13, section 13.3).

3 Hadamard, 1911, C. *R. Acad. Sci. Paris*. Vol. 152, 1735–1738. Rybczynski, 1911, *Bull. Krakow Acad. Sci.* A, 40–46.

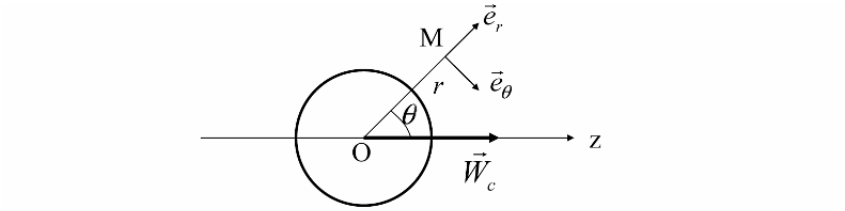

a. Spherical coordinate system with its origin O at the center of the particle, oriented along the velocity $\overrightarrow{W_c}$.

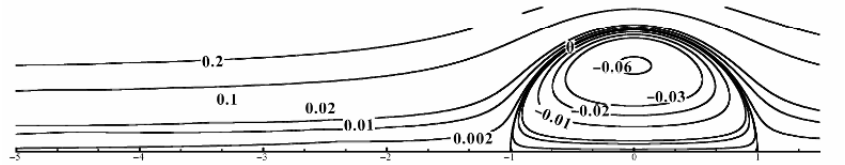

b. Air bubble in water ($\kappa = 0$, $W_c = 3W_{c\text{Stokes}} / 2$).

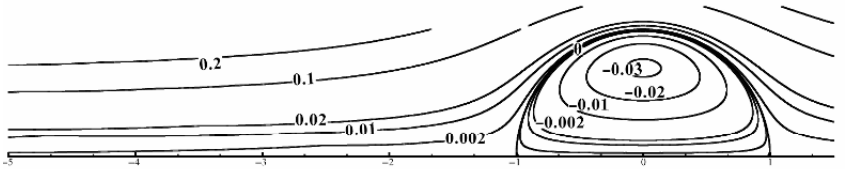

c. Liquid drop in another liquid ($\kappa = 1$, $W_c = 6W_{c\text{Stokes}} / 5$).

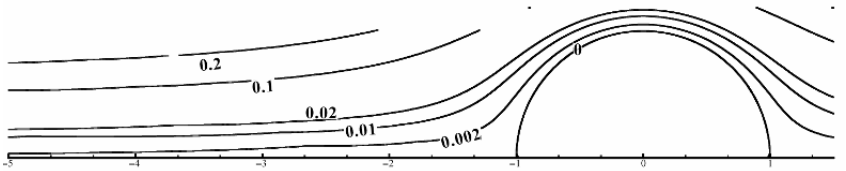

d. Asymptotical case of the rigid particle ($\kappa - \propto$, $W_c = W_{c\text{Stokes}}$).

Figure 15.4. *Streamlines, in the relative frame attached to the center of the particle, of the flow at a low Reynolds number (Re = 0.01) inside and outside a spherical fluid particle. The particle is moving within the fluid at the gravitational settling velocity* $\overrightarrow{W_c}$ *(Figure by A. Saboni)*

In Figure 15.4, the streamlines inside and outside the fluid particle have been plotted for a spherical particle moving at a velocity W_c, equal to the gravitational fall or rise velocity within the surrounding fluid. The flow is described in the

spherical coordinate system illustrated in Figure 15.4(a). The origin of the coordinate system is at the center O of the particle and moves with velocity $\overrightarrow{W_c}$ along the *Oz* axis. The relative velocity of the fluid $\vec{u}(r,\theta,\varphi) = u_r\vec{e}_r + u_\theta\vec{e}_\theta + u_\varphi\vec{e}_\varphi$ in the frame attached to the center of the particle is expressed at any point by its three velocity components in the spherical coordinate system (O, $\vec{e}_r$, $\vec{e}_\theta$, $\vec{e}_\varphi$). Angle ϕ determines the position of the meridian plane passing through the *Oz* axis and containing point M. Any one particle remains inside a given meridian plane. The steady-state solution for the velocity field, which is axisymmetric about the *Oz* axis without a rotational component about that axis, is derived from the stream function ψ via the relation:

$$u_r(r,\theta) = -\frac{1}{r^2\sin\theta}\frac{\partial\psi}{\partial\theta},\ u_\theta(r,\theta) = \frac{1}{r\sin\theta}\frac{\partial\psi}{\partial r}, \text{ and } u_\varphi(r,\theta) = 0 \qquad [15.13]$$

The characteristics of the particle and fluid are such that the Reynolds number is low $(\mathrm{Re} = W_c D/\nu_c = 0.01)$. The contour lines of the dimensionless stream function $4\psi(r,\theta)/W_c D^2$ are plotted in Figure 15.4 for three values of the viscosity coefficient $\kappa = \mu_d/\mu_c$. The streamline $\psi = 0$ is positioned, by convention, on the surface of the fluid particle. The contour lines represent the trajectories, outside or inside the fluid particle, of the flow in the reference frame attached to the particle in translation.

The asymptotical case $\kappa \to \infty$ (Figure 15.4(d)) is that of the rigid particle described in section 15.1, whose motion velocity is the velocity $W_{c\mathrm{Stokes}}$ given in Table 15.1. The velocity of the fluid flow goes to zero at the surface of the particle, and there is no flow inside the particle. For the low Reynolds number considered, the flow does not produce a separation at the rear of the particle for any of the three cases. The $\kappa = 0$ case is very similar to that of an air bubble in water. The kinematic viscosity of air, at room temperature, is 15 times larger than that of water, but its dynamic viscosity is 55 times lower than the dynamic viscosity of water, as the density of air is small compared to that of water. The $\kappa = 1$ case is illustrative of a drop of liquid in another liquid. Liquid drops encountered in liquid–liquid extraction problems have a viscosity ratio κ that usually varies in the interval $0.05 < \kappa < 10$. By virtue of [15.12], the relative velocity of the particle increases as κ decreases, going from the value of $W_{c\mathrm{Stokes}}$ (Table 15.1) for $\kappa \to \infty$ to $6W_{c\mathrm{Stokes}}/5$ for $\kappa = 1$ (liquid drop in a liquid), and then to $3W_{c\mathrm{Stokes}}/2$ for $\kappa = 0$ (gas bubble in a liquid).[4] While the streamlines are similar in the air bubble and liquid drop cases, the velocities are significantly larger inside the air bubble than in the liquid drop,

4 The friction force exerted on an air bubble in water is $F_v = 2\rho_f \nu W_c D$.

because when comparing the first case with the second, the absolute value of the minimum inside the particle is higher and the velocity W_c serving for plotting the dimensionless value of the stream function is larger in the first case.

For a Reynolds number exceeding 0.1, nonlinear terms have to be taken into account to determine the settling velocity of a spherical fluid particle. From correlations given in literature,[5] it is possible to derive the variation of the settling or rising velocity with the viscosity ratio κ and the Reynolds number Re inside the interval $0.1 < \mathrm{Re} < 400$. For a value of the Reynolds number greater than 400, the resolution of the flow can no longer be formulated in the same context, as the deformation of the spherical particle has to be taken into account.

Although the results presented in this section show that a small-sized fluid particle settles more rapidly than a solid particle of the same size, such differences are sometimes ignored, and, in certain cases, the settling laws of a solid particle are used for a fluid particle. Phenomena of interface contamination by surfactants are observed in some cases; these stiffen the interface and block the flow inside the fluid particle.[6]

15.4. Particles being held in suspension by Brownian motion

It is commonly observed that stirring is capable of keeping particles in suspension, counteracting the gravitational settling of particles when $\rho_s > \rho_f$. We consider in this section the sustenance of particles in suspension under the sole effect of Brownian motion. This approach is completed in section 15.5 with the case of turbulent flows. It is assumed that particles are numerous. We are therefore dealing not with maintaining a single particle in suspension, but with maintaining a population of particles present in a fluid, their concentration being denoted by $C(x,y,z,t)$.

For a particle of mass m, Brownian motion, which consists in random molecular stirring of the particle due to the temperature of the medium, is characterized by a kinetic energy that increases with medium temperature:

$$\frac{1}{2}m\overline{\left(\frac{\mathrm{d}\vec{x}}{\mathrm{d}t}\right)^2} = \frac{1}{2}kT \qquad [15.14]$$

5 See Saboni, Alexandrova & Gourdon, *Chemical Engineering J.*, Vol. 98(1–2), pp. 175–182 2004.

6 Surfactant effects are discussed in the review paper by Magnaudet and Eames, "The motion of high-Reynolds number bubbles in homogeneous flows", *Ann. Rev. Fluid Mech.*, Vol. 32, pp. 659–708 2000.

This quantity is the average kinetic energy of a particle selected from a set of particles, as indicated by the bar over the squared velocity. T is the absolute temperature and $k = 1.38 \times 10^{-23}$ J K^{-1} is Boltzmann's constant.

Brownian motion disperses the particles. In [15.14], $\vec{x}(t)$ designates the instantaneous displacement of a particle from an original position. These displacements are governed by the fundamental law of dynamics. The forces applied to the particle are the thermal agitation force of the Brownian motion and the friction force exerted by the flow, which opposes the relative movement of the particle with respect to the fluid. We therefore write:

$$m\frac{\mathrm{d}^2\vec{x}}{\mathrm{d}t^2} = \vec{F}_{\text{friction}} + \vec{F}_{\text{agitation}} = -3\pi\rho_f \nu D\frac{\mathrm{d}\vec{x}}{\mathrm{d}t} + \vec{F}_{\text{agitation}} \qquad [15.15]$$

The friction force is evaluated using Stokes' law for a spherical particle of diameter D (see section 15.1). Assuming that the fluid is not experiencing a solid-body motion, the relative velocity of the particle with respect to the fluid is $\mathrm{d}\vec{x}/\mathrm{d}t$. The agitation force is time dependent. The Brownian motion is modeled assuming that the direction of the agitation force is entirely random. Forces are uncorrelated from one time point to another, but their intensity is linked to the energy of Brownian motion (equation [15.14]). Under these hypotheses, the mathematical theory of Brownian agitation states that time-averaged displacements are such that:

$$\frac{1}{2}\overline{|\vec{x}(t)|^2} = \frac{kT}{3\pi\rho_f \nu D}t \qquad [15.16]$$

for a set of particles whose position at time $t = 0$ is $\vec{x}(t=0) = \vec{0}$. This result stems from the integration of [15.15] and the statistical averaging of displacements over a set of particles. The form of [15.16] is remarkable. While we have eschewed mathematical proofs,[7] we do recognize in [15.16] the classical result for a diffusion phenomenon,[8] where the increase in time of the size $L(t)$ of a zone in which the particles are dispersed follows a law of the form $L(t) = \sqrt{\kappa t}$. It is therefore possible to associate with Brownian motion a diffusion coefficient, the value of which is linked to the agitation energy of particles and to the viscosity of the fluid that slows down the displacement of the particles:

$$\kappa = \frac{kT}{3\pi\rho_f \nu D} \qquad [15.17]$$

7 They can be found in Chapter 3 of *Colloidal Dispersions*, Russel, Saville and Schowalter, Cambridge University Press, 1989.
8 See Chapter 8.

For a set of particles whose concentration is $C(x,y,z,t)$, the space and time evolution of concentration can thus be obtained as the solution of the advection-diffusion equation:

$$\frac{\partial C}{\partial t} + (\vec{u} + \overrightarrow{W_c}) \cdot \nabla C = \kappa \Delta C \,, \qquad [15.18]$$

in which the dispersion of particles by Brownian motion appears via the diffusion coefficient κ. Particles are carried in the flow with a velocity $\vec{u} + \overrightarrow{W_c}$, which is the sum of the velocity $\vec{u}$ of the fluid and the relative velocity $\overrightarrow{W_c}$ of the particles with respect to the fluid, due to settling.

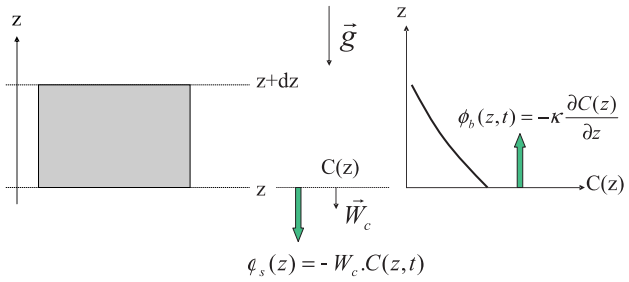

Figure 15.5. *Mass balance of particles in suspension in a slice of fluid. Evaluation of the settling flux* $\varphi_S(z)$ *and of the flux* $\varphi_b(z)$ *associated with Brownian motion agitation.*

Let us now consider the sustenance in suspension, by Brownian motion, of particles that are denser than the surrounding fluid, as depicted in Figure 15.5. Gravity tends to cause the particles to settle with velocity $\overrightarrow{W_c}$ parallel to the gravitational acceleration. Following the conventions given in Figure 15.5, the vertical direction Oz is oriented in the opposite direction to gravity. We assume the situation to be homogeneous in any plane perpendicular to the z direction. Dependence on the x and y coordinates is ignored both for concentration $C(z,t)$ and for the mass flux of particles per unit surface through a plane perpendicular to the Oz axis, denoted by $\varphi(z,t)$. The flux $\varphi(z,t)$ is, by convention, positive if the flux of particles is directed upward.

The mass balance of the particles contained in a slice of fluid located between the z and z + dz planes is written as:

$$\frac{\partial \{C(z,t)\mathrm{d}z\}}{\partial t} = \phi(z,t) - \phi(z + \mathrm{d}z, t) \qquad [15.19]$$

The flux is expressed as the sum of the settling flux $\varphi_s(z,t)$ associated with the fall of particles and the flux $\varphi_b(z,t)$ due to Brownian motion agitation:

$$\varphi(z,t) = -W_c C(z,t) - \kappa \frac{\partial C(z,t)}{\partial z} \qquad [15.20]$$

Because it is customary to do so, the fall velocity W_c of the settling movement is taken positive, although the velocity is oriented in the opposite direction to the *Oz* axis. The minus sign before W_c therefore ensures that the settling flux is actually downward. The flux associated with Brownian motion agitation is modeled using Fick's law with diffusivity κ. A positive flux corresponds to a concentration profile that decreases with increasing *z*, as represented in Figure 15.5.

The steady state, for which the population of particles is kept in suspension, is obtained when the flux $\varphi(z,t)$ is independent from *t* and *z*. It is necessarily equal to zero if no particle flow is imposed at the top and bottom of the column. We therefore have:

$$\varphi(z) = -W_c C(z) - \kappa \frac{\partial C(z)}{\partial z} = 0 \qquad [15.21]$$

Integrating [15.21] shows that the concentration of particles decreases exponentially when going upward along the *z* direction:

$$C(z) = C_o \exp\left\{-\frac{W_c}{\kappa} z\right\} \qquad [15.22]$$

This relation takes on a very simple form when the particles are very small and the fall velocity is given by Stokes' law (Table 15.1). Introducing also the expression for the diffusion coefficient of Brownian motion (equation [15.17]), equation [15.22] is readily expressed in terms of the mass *m* of the spherical particle:

$$C(z) = C_o \exp\left\{-\frac{(\rho_s - \rho_f)}{\rho_s} \frac{mgz}{kT}\right\} \qquad [15.23]$$

It is remarkable that the viscosity of the fluid does not intervene in the vertical distribution of the particles, even though this parameter influences both the fall velocity of the particle and the value of the diffusion coefficient associated with Brownian motion.

The constant of integration C_o, which is the reference concentration taken at $z = 0$, is undetermined at this stage. The model needs to be completed with a model characterizing the phenomena occurring at the lower and upper ends of the water column (such as a model describing the entrainment of a particle from the bottom),

in order to determine the value of concentration C_o. Nevertheless, the effectiveness of Brownian motion to sustain the suspension can be evaluated on the basis of [15.23]. For a volume of height h, the ratio of concentrations at the top and bottom of the column is:

$$\frac{C(h)}{C(0)} = \exp\left\{-\frac{(\rho_s - \rho_f)}{\rho_s}\frac{mgh}{kT}\right\} < 1 \qquad [15.24]$$

The particles are concentrated in the lower part of the column if $(\rho_s - \rho_f)mgh / \rho_s kT >> 1$, whereas the suspension is quasi-homogeneous if $(\rho_s - \rho_f)mgh / \rho_s kT << 1$. This dependence on the quantity $(\rho_s - \rho_f)mgh / \rho_s kT$ is significant, as the variation is exponential.[9] It can therefore be considered that Brownian motion maintains the particles in suspension on the vertical plane if:

$$\frac{(\rho_s - \rho_f)}{\rho_s}\frac{mgh}{kT} < 1 \qquad [15.25]$$

For particles of density ρ_s = 3,000 g/L, immersed in water at a temperature of 300 K, this criterion indicates that the particles are maintained in suspension by Brownian motion over a height of 10 cm if their diameter is smaller than 16 nm. The inevitable conclusion of this is that Brownian motion can only maintain very small particles in suspension. These are termed colloidal suspensions.

15.5. Particles being held in suspension by turbulence

The sustenance of particles in suspension under the action of turbulence is modeled in identical fashion to what has been done for Brownian agitation. Under the same hypothesis whereby no particles are fed into the bottom or top of the fluid layer, the steady-state distribution of particles along the vertical axis of the fluid layer corresponds to an average mass flow of particles that is zero at all points. We can therefore return to [15.21], replacing the diffusive flux associated with Brownian motion with the turbulent concentration flux, namely:

$$\varphi(z) = -W_c C(z) + \overline{w'c'} = 0 \qquad [15.26]$$

The mixing length model (Chapter 8, section 8.6) can be used to express the turbulent concentration flux $\overline{w'c'}$. We write:

$$\varphi(z) = -W_c C(z) - \kappa_t \frac{\partial C}{\partial z} \qquad [15.27]$$

9 See Exercise 15.I at the end of this chapter.

The turbulent diffusion coefficient is evaluated using the turbulent velocity u_{rms} and the integral scale ℓ_t:

$$\kappa_t = u_{\text{rms}} \ell_t \qquad [15.28]$$

If the characteristics of turbulence are homogeneous within the water layer, the vertical distribution of the particle concentration is exponential, as in [15.22]:

$$C(z) = C_o \exp\left\{-\frac{W_c}{u_{\text{rms}}}\frac{z}{\ell}\right\} \qquad [15.29]$$

The effectiveness of turbulence at maintaining the suspension is quantified by the ratio of the fall velocity to the turbulent velocity. This dimensionless parameter is called the Rouse number:

$$\text{Rou} = \frac{W_c}{u_{\text{rms}}} \qquad [15.30]$$

For Rou > 4, the concentration level decreases very strongly on a vertical profile between two points spaced apart by a length equal to the integral scale; suspension sustenance by turbulence is then weak. In contrast, if Rou < 0.5, the concentration level decreases by only 40% between its value at a given position and its value at a distance of one integral scale above. In the latter case, turbulence effectively maintains the particles in suspension.

The abilities of Brownian motion and turbulence to maintain suspensions are of rather different orders of magnitude, as evidenced by a comparison between the turbulent diffusion coefficient and the diffusion coefficient due to Brownian motion. Typical turbulent velocities are of the order of centimeters per second, while the scale of turbulence is usually larger than a centimeter. In water, the turbulent diffusion coefficient κ_t is greater than 10^{-4} m^2 s^{-1} (the turbulent Reynolds number is greater than 100 in order to be in a turbulent regime). On the other hand, for particles of diameter $D = 10$ nm in water at a temperature $T = 300$ K, the diffusion coefficient of particles by Brownian motion is $\kappa = 4.4 \times 10^{-11}$ m^2 s^{-1}. While Brownian motion cannot maintain in suspension particles of a size greater than a few nanometers, turbulence can.[10]

10 The analogy between turbulence and the Brownian motion goes further. The turbulent diffusion coefficient is evaluated as the product of the turbulent velocity by the integral scale of turbulence. Likewise, the coefficient of diffusion by Brownian motion is the product of the agitation velocity $u_b = \sqrt{kT/m}$ with the displacement scale of the particles,

15.6. Fluidized beds

Fluidized beds find numerous industrial applications, for example, in chemical reactors employing catalysts, in waste incineration furnaces, or for the desiccation of solids. Fluidization makes it possible to provide a very good contact between the fluid and solid. The exchange surface is at a maximum and the fluid is replenished. Transfers are therefore facilitated. The stirring of particles also allows for good homogenization within the bed. This is sometimes useful from a thermal viewpoint; temperature is more homogeneous and the occurrence of hot spots, a classic drawback of fixed beds, is thus avoided.

15.6.1. *Flow regimes*

The principle of fluidization is represented in Figure 15.6. A mass M_p of particles is initially deposited on a sieve inside a vertical column of cross-sectional area *S*. An upward flow of fluid is forced through the porous bed. As long as the velocity of the vertical fluid flow remains low, the bed remains lying on the grid. The particles are put in suspension when the velocity exceeds a certain level. This marks the onset of a fluidization regime. The particles are subjected to stirring movements, but they remain trapped inside the fluidized bed. The thickness H_f of the fluidized bed stabilizes at a certain level. The greater the flow rate, the more thick the bed and the more dispersed the particles.

The control parameters for the experiment described in Figure 15.6 are the mass of particles per unit surface, M_p / S, the area-averaged empty-bed velocity of the fluid in the column, $U = Q/S$, the density ρ_s of the particles, and the density ρ_f of the fluid. The diameter *D* of the particles, as will be seen in section 15.6.3, chiefly influences the fluid flow in a porous medium, jointly determining with the kinematic viscosity ν of the fluid the minimum fluidization velocity U_{mf} and the terminal entrainment velocity U_t, between which a steady-state fluidization regime is obtained. Furthermore, for a given velocity *U* of the fluid, the thickness of the fluidized bed increases if the diameter of the particles decreases, for the same mass of particles in the column.

$\ell_b = u_b m / 3\pi\mu D$. The length ℓ_b is directly derived from the integration of [15.15], when the Brownian agitation force is zero. u_b is typically of the order of 1 m/s for a particle of diameter D = 10 nm and density ρ_s = 3,000 g/L, whereas ℓ_b is of the order of 10^{-11} m when the fluid is water. Velocities are large and displacements are small.

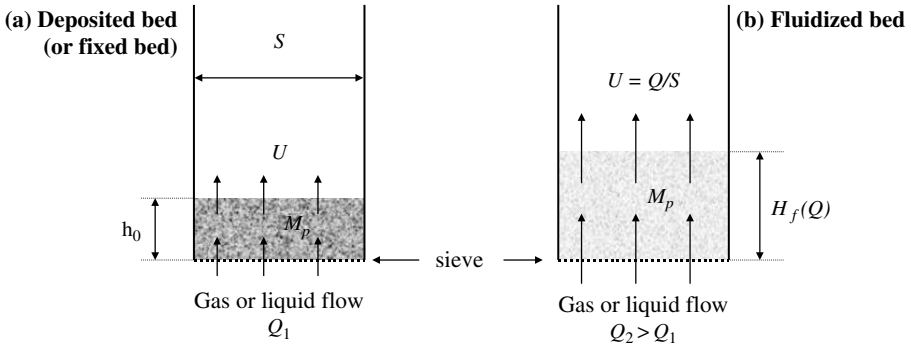

Figure 15.6. *Fluidization of a solid particle bed in a vertical stream*

The typology of flows is more complex for gas/solid fluidization than it is for liquid/solid fluidization. The reason for this is that the density ratio between the solid and the fluid is much larger for the gas/solid pair. Five regimes may be distinguished in gas/solid fluidization, and are illustrated in Figure 15.7. The change from one regime to another is brought about by increasing the area-averaged velocity of the gas.

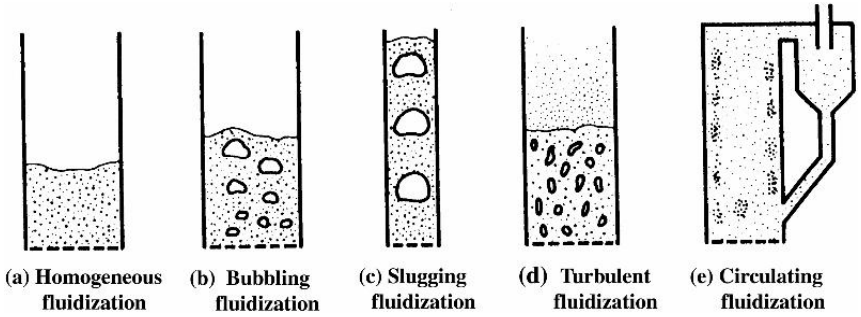

Figure 15.7. *Gas/solid fluidization regimes (figure reproduced from C. Laguérie, "Techniques de mise en contact entre phases solides et gazeuses", Techniques de l'Ingénieur, Traité de Génie des Procédés)*

The characteristics of different regimes are as follows:

– *Homogeneous fluidization:* the thickness of the fluidized bed increases as the gas velocity increases. The porosity in the bed subsequently increases but remains homogeneous within the bed. The upper surface of the bed is clearly identifiable. The movements of particles inside the bed are small.

– *Bubbling fluidization:* bubbles form at the bottom of the fluidized bed and grow by coalescence while ascending, until they burst at the surface of the bed. These bubbles are visually identifiable; they do not contain any particles. The bed becomes inhomogeneous in terms of porosity. The formation of bubbles produces pressure fluctuations within the bed.

– *Slugging fluidization:* the size of the bubbles reaches the width of the column. A stratification of the bed is then observed in the vertical direction, characterized by alternate layers of particles in suspension and particle-free gas. The surface of the bed oscillates as gas bubbles pass through. Pressure fluctuations are substantial.

– *Turbulent fluidization:* stirring within the bed is very strong, fragmenting the bed into small elements of fluidized bed and gas bubbles. The surface of the bed becomes difficult to identify. Pressure fluctuations decrease. Some particles may be carried away in the gas flow. This regime differs from the bubbling regime by the very powerful stirring occurring inside the bed.

– *Circulating fluidization:* the upper surface of the bed is no longer clearly visible. The particles are gradually carried away in the gas flow. However, downward movements of small lumps of particles may be observed along the walls. This is in fact no longer a fluidized bed regime, since there exists a solid-body motion of particles, or of a fraction thereof.

The notions of bubbling or slugging fluidization regime Vanish for a liquid/solid fluidized bed. The transition from a homogeneous regime to a turbulent regime is continuous, with the turbulent stirring of particles increasing with the velocity of the liquid.

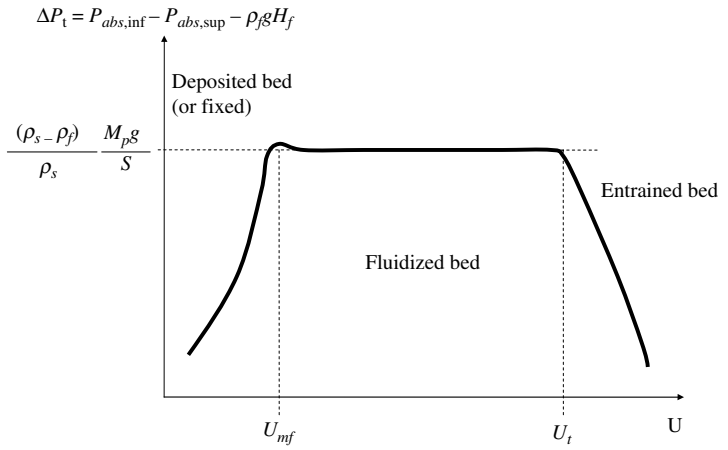

Figure 15.8. *Evolution of the head drop across a fluidized bed as a function of fluid velocity*

The fluidization regime is obtained when the velocity U of the flow lies between the minimum fluidization velocity U_{mf} and the terminal entrainment velocity U_t. From a mechanical standpoint, the major characteristic of fluidized beds is that the head variation ΔP_t between the underside and top side of the fluidized bed is independent from the velocity U of the fluid when the bed is in a fluidization state. This result is illustrated in Figure 15.8. The property is easily verified experimentally. It allows us to delineate the conditions for which the bed is fluidized. As long as the bed remains settled ("fixed bed"), the head loss grows with the velocity of the fluid. The head loss decreases again when the velocity exceeds the value for which the particles are carried away. For this reason, results regarding fluidized beds are given according to the fluid velocity.

It is readily understood that the terminal entrainment velocity U_t is equal to the fall velocity W_c of the particles constituting the bed. The fall velocity is the maximum relative velocity that a particle can have in a fluid at rest, whereas the terminal entrainment velocity is the maximum relative velocity that the fluid can have with respect to a stationary particle without carrying it away. The classical laws for the fall velocity of a spherical particle in a fluid at rest (Stokes', Van Allen's, or Newton's law – see section 15.1 and Table 15.1) are therefore used to estimate the terminal entrainment velocity.

15.6.2. *Mechanical equilibrium in a fluidized bed*

The momentum theorem explains why the head variation ΔP_t across a fluidized bed is independent of the area-averaged velocity. The use of the momentum theorem requires the hypothesis that the flow is in a steady-state regime. In reality, particles are stirred (even actively so, if the fluidization is turbulent) but the position of particles remains steady on average, since the particles are trapped inside the bed whose thickness is constant. The momentum theorem is therefore applied by considering average quantities. The mechanical balance is analyzed in two stages, first by considering the mechanical system consisting of all the particles, and second by considering the fluid volume surrounding the particles. Figure 15.9 depicts the control volumes considered. In this application, only the balance of forces along the vertical direction is considered.

15.6.2.1. *Application of the momentum theorem to the system constituted by the particles*

The mechanical system considered consists of the particles in the fluidized bed. Assuming that the particles are stationary on average, the balance of forces along the vertical reduces to the equilibrium between gravity forces and the hydrodynamic force exerted by the fluid flow past the particles. Gravity forces are the difference

between the total weight of the particles and the Archimedes' force exerted by the fluid on the particles. This force, called *reduced weight*, can be written as:

$$F_{G,z} = -(\rho_s - \rho_f) N_p \frac{\pi D^3}{6} g = -\frac{(\rho_s - \rho_f)}{\rho_s} M_p g \qquad [15.31]$$

This expression includes, besides the solid and fluid densities, the diameter D of the particles (which are assumed to be spherical), the number N_p of particles in the bed, the total mass M_p of the particles, and the gravitational acceleration g. The minus sign appears because of the orientation of the Oz axis. The balance of the hydrodynamic force $F_{f/p,z}$ exerted by the fluid flow on the particles with reduced weight yields:

$$F_{f/p,z} = \frac{(\rho_s - \rho_f)}{\rho_s} M_p g \qquad [15.32]$$

This is oriented upward.

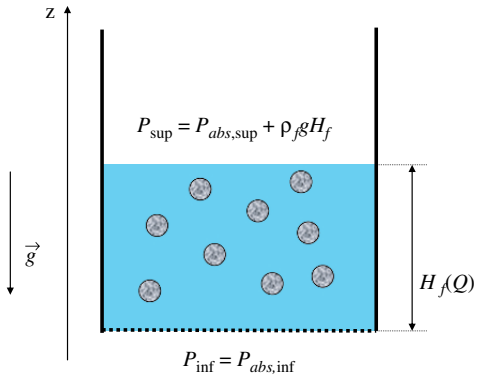

Figure 15.9. *Application of the momentum theorem to a fluidized bed*

15.6.2.2. *Application of the momentum theorem to the fluid surrounding the particles*

We now consider, as the mechanical system, the fluid that surrounds the particles. The control volume considered is indicated in Figure 15.9 as the shaded rectangle containing the particles, excluding the particles themselves. The surface of the particles is therefore part of the surface surrounding the control volume.

Since, by using the reduced weight, Archimedes' force has been subtracted from the weight of the particles, the pressures used hereafter for momentum balance over

the fluid phase will be pressures $P_{\text{upper}} = P_{\text{abs,upper}} + \rho_f g H_f$ and $P_{\text{lower}} = P_{\text{abs,lower}}$ at the top and bottom surfaces of the layer, from which the hydrostatic pressure has been deducted.[11] The quantity:

$$\Delta P_t = P_{\text{lower}} - P_{\text{upper}} = P_{\text{abs,lower}} - P_{\text{abs,upper}} - \rho_f g H_f \quad [15.33]$$

is the head variation between the bottom and top of the fluidized layer, since the mean streamwise velocity is identical in both cross sections. H_f is the thickness of the bed.

The momentum flux is conserved between the lower boundary (incoming flux) and the upper boundary of the domain (outgoing flux). The balance of vertical forces applied to the volume is therefore limited to the pressure forces applied on the lower and upper boundaries, the friction force exerted by the side wall on the fluid (denoted by $F_{\text{lat},z}$), and the force $F_{p/f,z}$ (pressure and friction) exerted by the particles on the fluid, which is equal and of opposite direction to $F_{f/p,z}$ by virtue of the action/reaction principle. Using the notations for pressure indicated in Figure 15.9, the momentum theorem (equation [2.18] of Chapter 2) can therefore be written along the vertical direction as

$$-P_{\text{lower}} S + P_{\text{upper}} S = -F_{f/p,z} + F_{\text{lat},z} \quad [15.34]$$

Forces are positive when they are oriented upward along the *Oz* axis. With [15.32] and [15.33], [15.34] becomes:

$$\Delta P_t = \frac{(\rho_s - \rho_f)}{\rho_s} \frac{M_p}{S} g - \frac{F_{\text{lat},z}}{S} \quad [15.35]$$

If the column is sufficiently wide, the friction force exerted by the side wall on the fluid becomes negligible compared to the force exerted by the particles on the fluid, because the lateral surface is reduced for the same amount of particles (the thickness of the bed is smaller). This leads to:

$$\Delta P_t = P_{\text{lower}} - P_{\text{upper}} = P_{\text{abs,lower}} - P_{\text{abs,upper}} - \rho_f g H_f = \frac{(\rho_s - \rho_f)}{\rho_s} \frac{M_p}{S} g \quad [15.36]$$

Conservation of the mass of particles:

$$M_p = CSH_f = \rho_s (1-\varepsilon) S H_f \quad [15.37]$$

provides an alternative expression for the head variation given by [15.36] based on the concentration C in particles or the porosity ε within the bed.

11 The link between hydrostatic pressure and Archimedes' force was discussed in section 1.8 of Chapter 1.

Relation [15.36] establishes some essential results:

– It demonstrates that the head variation across the bed is independent from the flow rate, for a fluidized bed of a given mass.

– It establishes a link between the head variation and the reduced weight of the particles. In a way, a fluidization experiment could be used as scales, since the pressure measurements allow the determination of the mass of the bed using the plateau measured on a plot such as in Figure 15.8.

– Knowing the mass of a fluidized bed, it is easy to determine the porosity of the bed using mass conservation (equation [15.37]), through a simple height measurement.

15.6.3. *Fluid flow in a fluidized bed*

The fluid flow in a fluidized bed is related to a flow in a porous medium. The solid lattice constituted by the particles slows down the flow and produces a head loss. For the fluidized bed, the situation is more complex than for a settled bed. As the velocity of the fluid is increased, the thickness H_f of the bed grows and its porosity ε increases. These two quantities are not geometrical data characterizing the bed; they vary according to the fluid flow. The more the bed expands via the fluidization process, the greater its permeability becomes. Because of the increase in fluid velocity and the increase in the permeability k of the bed resulting from fluidization, the critical Reynolds number $\mathrm{Re} = \rho_f u\sqrt{k}/\mu = 10$ (which sets the limit for the validity of Darcy's law) is often exceeded for a fluidized bed. It is therefore necessary to call upon other models, such as Ergun's relation (section 14.6), which extends Darcy's law into the turbulent regime, in order to describe the flow in the fluidized bed. With the notations used for the fluidized bed, Ergun's correlation is written as:

$$\frac{\Delta P_t}{H_f} = \left\{ \frac{36 h_K (1-\varepsilon)^2}{\varepsilon^3 D^2} \mu U + \frac{6 h_B (1-\varepsilon)}{\varepsilon^3 D} \rho_f U^2 \right\} \qquad [15.38]$$

($h_K = 4.5 \pm 1$ and $h_B = 0.3 \pm 0.1$). In [15.38], ΔP_t, U, H_f, and ε are variables. Ergun's relation is associated with the dynamic equilibrium of the bed [15.36] and mass conservation [15.37]. By means of these two additional relations, the characteristics of the fluidized bed can be completely determined for a given fluid velocity. By introducing [15.36] and [15.37], relation [15.38] is transformed into a relation linking porosity with the velocity of the fluid:

$$\varepsilon^3 = \left\{ 2 h_K (1-\varepsilon) \frac{U}{W_{c\mathrm{Stokes}}} + 18 h_B \left(\frac{U}{W_{c\mathrm{Newton}}} \right)^2 \right\} \qquad [15.39]$$

$W_{c\text{Stokes}}$ is the expression of the Stokes' fall velocity for small particles, and $W_{c\text{Newton}}$ that of the Newton fall velocity for large particles (see Table 15.1). Relation [15.39] shows that the porosity of the bed (and therefore its thickness) increases with velocity. The porosity and thickness of the bed also increase when the diameter of the particles diminishes. Relation [15.39] can be used to evaluate the minimum fluidization velocity U_{mf} theoretically. This only requires solving the second-degree equation constituted by [15.39], by taking the porosity equal to the porosity ε_0 of the settled bed (derived from the mass balance [15.37] if the mass M_p of the bed and the thickness H_{f0} of the settled bed are known).

	$U / U_t =$	Usage limits
Lewis–Bowerman	$1.09 \quad \varepsilon^{8.47}$ $0.89 \quad \varepsilon^{2.97}$ $0.72 \quad \varepsilon^{2.32}$	$\mathrm{Re}_t < 2$ $2 < \mathrm{Re}_t < 500$ $\mathrm{Re}_t > 500$; $\varepsilon < 0.9$
Richardson–Zaki	ε^n with $\begin{cases} n = 4.65 + 20\dfrac{D}{\Phi} \\ n = \left(4.4 + 18\dfrac{D}{\Phi}\right)\mathrm{Re}_t^{-0.03} \\ n = \left(4.4 + 18\dfrac{D}{\Phi}\right)\mathrm{Re}_t^{-0.1} \\ n = 4.4\,\mathrm{Re}_t^{-0.1} \\ n = 4.4 \end{cases}$	$\mathrm{Re}_t < 0.2$ $0.2 < \mathrm{Re}_t < 1$ $1 < \mathrm{Re}_t < 200$ $200 < \mathrm{Re}_t < 500$ $\mathrm{Re}_t > 500$

Table 15.2. *Correlations characterizing the fluid flow in a fluidized bed. U is the mean streamwise velocity, D the diameter of the particles, U_t the terminal entrainment velocity (equal to the fall velocity of the particle – see Table 15.1), and Φ the diameter of the column. $Re_t = U_t D / \nu$.*

Engineers often use the Lewis–Bowerman and Richardson–Zaki correlations to characterize fluidized beds by determining porosity as a function of the flow velocity. These correlations, empirical in nature, are recapitulated in Table 15.2. While the diameter of the column is taken into account by the Richardson–Zaki correlation, its effect remains very weak as long as the size of the particles is small compared to the diameter of the column. Comparing the Lewis–Bowerman and Richardson–Zaki correlations with Ergun's relation, expressed in the form [15.39],

confers some physical sense to these empirical correlations. The three relations determine the variations of porosity inside a fluidized bed with the velocity of the flow, and the characteristics of the particles are demonstrated through the fall velocity. The values of fall velocity in Stokes and Newton regimes appear explicitly in Ergun's relation, while the fall velocity for the particles and the fluid is directly used in Lewis–Bowerman and Richardson–Zaki correlations.

15.7. Application exercises

Exercise 15.I: Distribution of particles in suspension and grain size sorting resulting from settling

A granular set is constituted by weighing from three classes of homogeneous sand particles (the density of sand is taken equal to 3,000 g/L). The set includes:

– 200 g of particles of diameter $d_1 = 1$ mm

– 200 g of particles of diameter $d_2 = 100$ μm

– 200 g of particles of diameter $d_3 = 10$ μm

The shape of the particles will be assimilated to spheres, and the cohesive character that might be shown by the smaller particles will be neglected.

1. The particles are mixed in water at room temperature in a rectangular vessel with a side $L = 20$ cm, wherein the water height is $H = 150$ cm. Determine the fall velocity of each of the three particles. It is postulated that the particles are in sufficiently low concentrations that each particle settles with the fall velocity of an isolated particle.

2. Stirring is maintained inside the tank. The characteristics of turbulence are homogeneous within the tank, with the following values: $u_{\mathrm{rms}} = 3$ cm/s and $\ell_t = 5$ cm. Determine the concentration profile within the tank while turbulence is sustained, and calculate for each class of particles the concentrations at the top and bottom of the tank. Assume all particles to be in suspension. Comment on the results obtained. For the three particle diameters, calculate the height Z_s above the bottom for which the upper part of the tank ($Z_s < z < H$) contains a single particle.

3. At time $t = 0$, stirring is stopped and it is assumed that turbulence Vanishes instantaneously. Using the height Z_s obtained in Question 2, determine the settling time for each class of particles. Characterise the grain size distribution in the settled bed. It will be assumed that the grain size distribution is homogeneous in the different deposited layers, and that small particles do not slip between larger ones to fill in the gaps.

Exercise 15.II: Fluidization of a bimodal distribution of particles

We considered in this exercise a fluidization plant to incinerate waste, the grain size analysis of which shows that the grain size distribution is bimodal: 15% of the particles by mass have a size between 100 and 400 μm, and the remaining 85% have a size between 2 and 10 mm.

The density of the solid constituting the particles is taken equal to $\rho_s = 3{,}000$ kg/m^3 and the density of the gas as $\rho_f = 1$ kg/m^3. The kinematic viscosity of air is $\nu = 1.5 \times 10^{-5}$ m^2/s.

1. Inside a column whose cross-sectional area on the ground is $S = 1$ m^2, a mass of waste $M_p = 300$ kg is deposited on a grid. In the absence of flow, the height of the waste bed is $H = 15$ cm. Determine the porosity inside the bed.

2. A first stage involves examining the possibility of selecting experimental conditions such that the entire waste is fluidized. Determine the velocity U_{max} that the upward gas flow should not exceed.

3. Using Ergun's relation, show that it is not possible to fluidize the entire bed at the flow velocity U_{max}. Discuss a way of selecting the size D of the particles to calculate the coefficients in Ergun's relation, and evaluate the extent to which the result depends on this selection.

4. Would the conclusion of Question 3 be modified if more or less waste were put into the column?

5. Describe a fluidization regime that can be performed in the column. Suggest a velocity value, for which it could be verified that such a fluidization regime can actually be set up.

6. Why is it important to dimension such a plant in a closed loop regarding the gas flow?

Chapter 16

Movement of a Solid Particle in a Fluid Flow

This chapter deals with the movement of a small solid particle in a fluid flow. We start by presenting the equations governing particle movements, which we refer to as the Basset, Boussinesq, Oseen, and Tchen (BBOT) equations, to name a few key contributors to this modeling. Rather than deriving the equations, we endeavor to identify and discuss the physical meaning of the different terms: acceleration, added mass, Basset term, etc.

This approach is embodied by applying the BBOT equations to describe the behavior of a particle in three configurations of particular significance by their applications:

1. the movement of a fluid particle under the effect of gravity in a fluid at rest,
2. the movement of a particle in a unidirectional sheared fluid flow, and
3. the centrifugation of a particle in a rotating flow.

The BBOT equations allow the determination of the characteristic time with which the dynamics of a solid particle placed in a fluid flow adapts to its environment. This chapter is quite theoretical, although we have presented few derivations. This enables the reader to understand the hypotheses used in Chapters 15 (behavior of particles within gravity field) and 17 (centrifugation).

In section 16.5, we discuss the lift force applied on a particle in a unidirectional flow. This force is not taken into account by the BBOT equations. Finally, we conclude with the application of the results presented in this chapter to laminar flows, and then to turbulent flows (section 16.7).

16.1. Notations and hypotheses

We consider a spherical particle whose radius we denote by a. The mass of the particle is $m_p = \rho_s 4\pi a^3 / 3$, whereas $m_f = \rho_f 4\pi a^3 / 3$ is the mass the fluid would have had if it occupied the volume of the particle.

$\vec{Y}(t)$ designates the vector describing the trajectory of the particle in the fluid. We denote by $V_i(t)$ the three velocity components of the particle, expressed in the Cartesian coordinate system (O, x, y, z) = (O, x_1, x_2, x_3).

The particle is placed in a fluid flow which is assumed to be known. We designate by $u_i(\vec{x},t)$ the three components of the fluid's velocity field, which verify the Navier–Stokes equations:

$$\rho_f \left\{ \frac{\partial u_i}{\partial t} + \vec{u} \cdot \nabla u_i \right\} = -\frac{\partial p}{\partial x_i} + \rho_f \nu \Delta u_i \qquad [16.1]$$

The velocity vector $u_i(\vec{Y}(t),t)$ is the velocity the fluid would have had at the location where the fluid particle is situated at time t, if the particle were not there. We denote by $W_i(t) = V_i(t) - u_i(\vec{Y}(t),t)$ the relative velocity of the particle with respect to the fluid.

The velocity scale of the fluid flow is designated by U and its spatial scale by L. The modeling will apply to laminar as well as turbulent flows. The Reynolds number of the fluid flow,

$$\mathrm{Re}_f = \frac{UL}{\nu} \qquad [16.2]$$

(where ν is the viscosity of the fluid), may be small or large.

The particle's displacement will be calculated assuming that the particle is small. This hypothesis translates not only into the geometrical condition,

$$\frac{a}{L} << 1\,, \qquad [16.3]$$

but also into hydrodynamic conditions specifying that the relative fluid flow with respect to the particle is a low-Reynolds-number flow. This results in three conditions on the velocity scale U of the fluid, on the scale W_p of the relative

velocity of the fluid with respect to the particle, and on the angular rotational velocity ω of the particle:

$$\left.\begin{aligned} \mathrm{Re}_{p,U} &= \frac{Ua^2}{L\nu} << 1 \\ \mathrm{Re}_{p,W} &= \frac{W_p a}{\nu} << 1 \\ \mathrm{Re}_{p,\omega} &= \frac{\omega a^2}{\nu} << 1 \end{aligned}\right\} \qquad [16.4]$$

The movement of the particle is described in the following under the four hypotheses ([16.3] and [16.4]).

16.2. The Basset, Boussinesq, Oseen, and Tchen equation

Writing the fundamental law of dynamics to describe the movement of the particle requires a balance of forces exerted on the particle. These forces are gravity on one hand and the hydrodynamic forces exerted by the fluid flow on the particle on the other hand. The particle disturbs the velocity field $u_i(\vec{x},t)$ of the flow in its vicinity in such a manner as to verify the boundary conditions on the surface of the particle. The difficulty of the problem lies in calculating the perturbed velocity field in order to then derive therefrom the hydrodynamic forces which apply on the particle. While, as stated above, the fluid flow may be laminar or turbulent, hypotheses [16.3] and [16.4] mean that the perturbation of the velocity field caused by the particle is laminar. This is a dramatic simplification, but we will find in this chapter that the problem nevertheless remains very complex. A solution within the framework of the theory of creeping flows[1] is incomplete; the nonlinearities of the flow need to be considered in order to incorporate certain phenomena, such as the lift force exerted by a flow on a particle, into the theory. Rather than replicate here the calculations leading to the equations of motion for a small particle in a fluid flow, we merely state the final result and refer the reader to a few major publications. Our aim is first and foremost to discuss the result of this modeling, by elucidating the physical meaning of the different terms and by recalling the hypotheses of the modeling. This process will build upon the study of several application cases.

1 A creeping flow is a flow for which nonlinear terms are neglected in the Navier–Stokes equations, and the pressure gradient balances out the viscous terms. The book by Happel and Brenner (*Low Reynolds Number Hydrodynamics*, Kluwer Academic Publishers, 1991) discusses these questions.

In the following we resume the notations used by Maxey and Riley (1983)[2] and write the Basset, Boussinesq, Oseen, and Tchen (BBOT) equations in a form that is quasi-identical to that of Maxey and Riley. This formulation is interesting insofar as it highlights the relative movement of the particle with respect to the fluid. The three components $W_i(t)$ of the particle's relative velocity with respect to the fluid are obtained by solving the following differential equations:

$$\left(\overbrace{m_p}^{\mathbf{I}} + \overbrace{\frac{1}{2}m_f}^{\mathbf{II}}\right)\frac{\mathrm{d}W_i}{\mathrm{d}t} + \overbrace{6\pi a^2\mu\int_0^t \frac{1}{\sqrt{\pi\nu(t-\tau)}}\frac{\mathrm{d}W_i}{\mathrm{d}\tau}\mathrm{d}\tau}^{\mathbf{VI}} + \overbrace{6\pi a\mu W_i}^{\mathbf{IV}} =$$

$$\overbrace{-m_p\frac{\mathrm{d}u_i}{\mathrm{d}t} + m_f\frac{\mathrm{D}u_i}{\mathrm{D}t}}^{\mathbf{V}} + \overbrace{(m_p - m_f)g_i}^{\mathbf{III}} + \overbrace{\pi a^3\mu\Delta u_i}^{\mathbf{IVcorr}}$$

$$\underbrace{-\frac{1}{2}m_f W_j\frac{\partial u_i}{\partial x_j} + \frac{1}{20}a^2 m_f\frac{\mathrm{D}(\Delta u_i)}{\mathrm{D}t}}_{\mathbf{IIcorr}} + \underbrace{\pi a^4\mu\int_0^t \frac{1}{\sqrt{\pi\nu(t-\tau)}}\frac{\mathrm{d}(\Delta u_i)}{\mathrm{d}\tau}\mathrm{d}\tau}_{\mathbf{VI}} \qquad [16.5]$$

The differences with the equations obtained by Maxey and Riley are the corrections brought in by Auton (1987, 1988). An in-depth discussion of these equations can be found in the book by Michaelides.[3]

The notations appearing in [16.5] have already been introduced, with the exception of the two time derivatives. Indeed, equation [16.5] distinguishes between:

– the particle-tracking time derivative:

$$\frac{\mathrm{d}u_i}{\mathrm{d}t}(\vec{Y}(t),t) = \left(\frac{\partial u_i}{\partial t} + V_j\frac{\partial u_i}{\partial x_j}\right)(\vec{x} = \vec{Y}(t)) \qquad [16.6]$$

2 Maxey and Riley, 1983, "Equation of motion for a small rigid sphere in a non-uniform flow", *Physics Fluids*, Vol. 26(4), 883–889. Gatignol published a similar study the same year (*J. Mécanique Théorique et Appliquée*, 1983, Vol. 2(2), 143–154).

3 Michaelides, *Particles, Bubbles and Drops* (World Scientific 2006). The equations [16.5] correspond to those given by Michaelides, which incorporate the corrections made by Auton (1987, *J. Fluid Mech.*, Vol. 183, 199–218) and Auton, Hunt & Prud'homme (1988, *J. Fluid Mech.*, Vol. 197, 241–257).

and

– the fluid-tracking time derivative:

$$\frac{\mathrm{D}u_i}{\mathrm{D}t}(\vec{Y}(t),t) = \left(\frac{\partial u_i}{\partial t} + u_j \frac{\partial u_i}{\partial x_j}\right)(\vec{x} = \vec{Y}(t)) \qquad [16.7]$$

both these derivatives being taken at the position of the particle center.

In the left-hand side of [16.5] are gathered the terms related to the unknowns W_i and on the right-hand side are the forcing terms associated with the velocity field of the fluid flow and with gravity. In [16.5], the numerals I–VI identify various terms that influence the movement of the particle:

Term I is the acceleration of the particle with respect to the fluid, the generic term in the equation of motion.

Term II is called the "added mass" term, as it is equivalent to adding a mass of fluid to that of the particle in order to calculate the contribution of acceleration. This only appears when the particle accelerates or decelerates with respect to the fluid, that is, in a transient regime. It is physically interpreted by the fact that, in order to accelerate the particle, some momentum also has to be imparted onto the fluid surrounding the particle. The added mass term depends heavily on the difference between the density of the particle and that of the fluid. For a particle in air, the added mass term is negligible, whereas it is significant for a particle in water. The experience of waterskiing allows us to verify that the force required to lift a stationary skier from the water is far larger than that applied if the skier starts from a pontoon. When the relative velocity of the particle with respect to the fluid becomes constant, the effect of added mass fades away, because the surrounding fluid has acquired the necessary momentum. The coefficient 1/2 associated with the added mass corresponds to the case of a spherical particle. Two terms (IIcorr terms) related to the concept of added mass also appear on the right-hand side. These corrections with respect to the formulation of Maxey and Riley are due to Auton.

Term III is the reduced weight of the particle, which is the difference between the weight of the particle and the buoyancy force that applies to it. We recall that the buoyancy force is the result of hydrostatic pressure forces applied on the particle (see Chapter 1).

Term IV is the friction force applied by the fluid on the particle in a steady-state regime. As the Reynolds number is small, we recover here the classical result associated with Stokes' law (Chapter 15, Table 15.1). A complementary friction term (IVcorr term) appears on the right-hand side, and is linked to the shear of the velocity field of the fluid flow.

Element V consists of two terms representing pressure and inertia effects applied to the particle. These intervene in centrifugation processes, among others. It will be seen that the first term in V corresponds to the centrifugal force applied to the particle, and the second to the pressure force applied on the particle by the local pressure gradient.

Terms VI are called "Basset terms". Indeed, they render an effect of the history of the particle's movement with respect to the fluid. The Basset terms that appear in [16.5] are associated with an initial condition for which it is assumed that the perturbation of the velocity field is zero at time $t = 0$ when the particle is placed in the flow at a given location and with a given velocity, except at the particle's surface where a non-slip condition is applied.

16.3. Movement of a particle subjected to gravity in a fluid at rest

The BBOT equations lead to the classic results on the sedimentation of a small particle within the gravity field when the surrounding fluid is at rest. They describe the acceleration of the particle which is dropped with zero velocity, and determine the characteristic time needed to reach Stokes' fall velocity. Since $u_i \equiv 0$, equations [16.5] simplify into:

$$\left(m_p + \frac{1}{2}m_f\right)\frac{\mathrm{d}W_1}{\mathrm{d}t} + 6\pi a^2\mu\int_0^t \frac{1}{\sqrt{\pi\nu(t-\tau)}}\frac{\mathrm{d}W_1}{\mathrm{d}\tau}\mathrm{d}\tau + 6\pi a\mu W_1 = (m_p - m_f)g \qquad [16.8]$$

The velocity component with index 1 has been chosen to be oriented along the direction of gravity and [16.8] is the BBOT equation in that direction. In the other two directions, the equations reduce to the same equation without the right-hand side. This results in $W_i(t) = 0$ for $i = 2$ and $i = 3$, since $W_i(t = 0) = 0$. The particle's movement occurs in the direction of gravity.

In a steady-state regime, the first two terms equal zero, thus reverting to Stokes' law (see Table 15.1 of Chapter 15) for the fall velocity of a small spherical particle:

$$W_{c\mathrm{Stokes}} = \frac{2(\rho_s - \rho_f)a^2 g}{9\mu} \qquad [16.9]$$

This result helps underscore the fact that the BBOT equations apply only to small-size particles (equation [16.4]).

The transient stage during which the particle accelerates is described by the BBOT equations. Neglecting the Basset term in a first step, differential equation [16.8] simplifies into the form:

$$\frac{\mathrm{d}V_1}{\mathrm{d}t} + \frac{1}{t_p} V_1 = \frac{1}{t_p} W_{c\mathrm{Stokes}} \qquad [16.10]$$

The solution of [16.10] is $V_1(t) = W_{c\mathrm{Stokes}} \left\{ 1 - \exp(-t/t_p) \right\}$, which involves the characteristic time of the transient regime:

$$t_p = \left(2 \ \frac{\rho_p}{\rho_f} + 1 \right) \frac{a^2}{9\nu} \qquad [16.11]$$

Numerical applications for common cases (Table 16.1) show that the particle reaches, after a very short time, a velocity value very close to Stokes' fall velocity. The time t_p does not depend on the nature of the force that produces the flow (in this case, gravity), since it stems from the left-hand-side terms in [16.8], but only on the properties of the fluid and the particle. It is substantially shorter for a particle in water than for a particle in air, owing to the fact that the ratio ρ_p / ρ_f is much lower in the former case. The added mass term is negligible for a particle in air. In any case, the smaller the particle, the shorter the time t_p.

Fluid	ρ_p / ρ_f	ν (m^2/s)	Characteristic time t_p (s)		
Air	3,000	1.5×10^{-5}	1.1×10^{-5}	1.1×10^{-3}	1.1×10^{-1}
Water	3	10^{-6}	1.9×10^{-7}	1.9×10^{-5}	1.9×10^{-3}
Diameter d of the particle (μm)			1	10	100

Table 16.1. *Characteristic time t_p (in s) of the acceleration of a particle in a fluid, according to the diameter d of the particle and to the fluid's properties*

The Basset term is a friction term which is added in a transient regime. In the present case, $\mathrm{d}W_1/\mathrm{d}\tau > 0$, the Basset term is positive and the friction associated with this term is added to the steady-state friction force $6\pi a \mu W_1$. Because of the Basset

term, the particle takes more time to reach the limiting velocity $W_{c\text{Stokes}}$ than evaluated as time t_p. Non-dimensionalizing the velocity by $W_{c\text{Stokes}}$, and time by t_p, allows the differential equation [16.8] to be written in the following non-dimensional form:

$$\frac{\mathrm{d}W_1}{\mathrm{d}t} + \frac{3}{\sqrt{2\dfrac{\rho_p}{\rho_f}+1}} \int_0^t \frac{1}{\sqrt{\pi(t-\tau)}} \frac{\mathrm{d}W_1}{\mathrm{d}\tau}\mathrm{d}\tau + W_1 = 1 \qquad [16.12]$$

This formulation shows that the relative significance of the Basset term depends only on the density ratio between the particle and the fluid (more specifically, it does not depend on the size of the particle or on the viscosity of the fluid). Figure 16.1 compares the time evolution of the velocity of a particle dropped with zero velocity in the gravity field, obtained by taking into account the Basset term and by omitting it. The two cases with a Basset term correspond to a particle in air or water. It is verified that the Basset term has almost no effect for the particle in air ($\rho_p / \rho_f = 3{,}000$). For the particle in water ($\rho_p / \rho_f = 3$), the Basset term slows down the particle's acceleration, but the characteristic time of the acceleration remains short (for the values indicated in Table 16.1). The characteristic time (defined by $V(t'_p)/W_{c\text{Stokes}} = (1-\exp(-1))$), obtained by taking into account the Basset term, is $t'_p = 3.31\ t_p$.

The Basset term incorporates, via the time integral, the recent history of the particle's movement. The quantity $1/\sqrt{\pi(t-\tau)}$ inside the integral allows for a damping of the history effect the further back we go in time. The Basset term becomes asymptotically zero when approaching a steady state. Indeed, if $\mathrm{d}W_1/\mathrm{d}\tau = 0$ for $t > t_s$, we then have:

$$\int_0^t \frac{1}{\sqrt{\pi(t-\tau)}} \frac{\mathrm{d}W_1}{\mathrm{d}\tau}\mathrm{d}\tau \approx \frac{1}{\sqrt{\pi t}} \int_0^{t_s} \frac{\mathrm{d}W_1}{\mathrm{d}\tau}\mathrm{d}\tau \text{ for } t>>t_s \qquad [16.13]$$

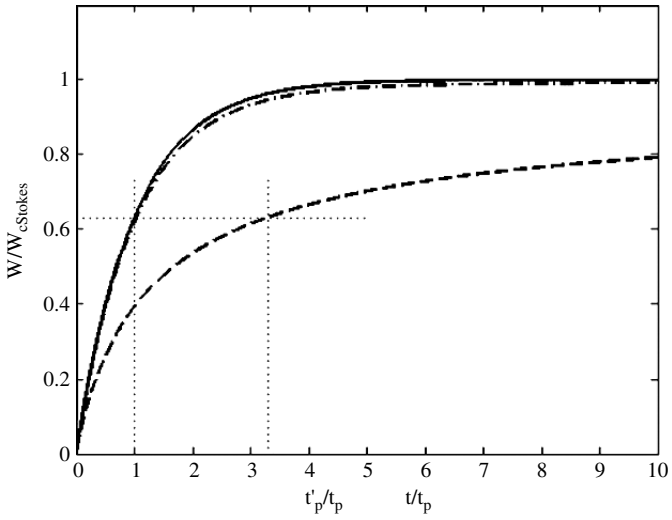

Figure 16.1. *Evolution of the velocity of a particle dropped in the gravity field. _____: calculation without Basset term (equation [16.10]), -.-.-.: calculation with Basset term for* $\rho_p / \rho_f = 3{,}000$ *; ----: calculation with Basset term for* $\rho_p / \rho_f = 3$

16.4. Movement of a particle in a steady, unidirectional shear flow

We now analyze the movement of a particle in a steady unidirectional sheared flow obtained by solving the BBOT equations. Gravity is not taken into account. The fluid flow occurs in the direction with index 1, and the velocity gradient is along the direction with index 3, which translates into:

$$u_1 = u_x(z) \quad u_2 \equiv 0 \quad u_3 \equiv 0 \qquad [16.14]$$

denoting by z the coordinate with index 3 to facilitate interpretation of the figures.

Writing the BBOT equations does not pose any problem in this particular case. The forcing terms are zero for directions 2 and 3, which are perpendicular to the direction of the fluid flow (equations [16.16] and [16.17]). In the direction of the fluid flow (equation [16.15]), non-zero forcing terms related to the gradient of the fluid flow (IIcorr and IVcorr terms in [16.5]) remain. For element V in [16.5], the term related to the fluid-tracking material derivative is zero since $u_3 \equiv 0$. Only the term related to the particle-tracking material derivative is non-zero. This is written by bringing in the relative velocity component, since $W_3 = V_3$.

$$\left(m_p + \frac{1}{2}m_f\right)\frac{\mathrm{d}W_1}{\mathrm{d}t} + 6\pi a^2\mu\int_0^t \frac{1}{\sqrt{\pi\nu(t-\tau)}}\frac{\mathrm{d}W_1}{\mathrm{d}\tau}\mathrm{d}\tau + 6\pi a\mu W_1$$
$$= -m_p W_3\frac{\mathrm{d}u_x}{\mathrm{d}z} + \pi a^3\mu\frac{\mathrm{d}^2u_x}{\mathrm{d}z^2} - \frac{1}{2}m_f W_3\frac{\mathrm{d}u_x}{\mathrm{d}z} \qquad [16.15]$$
$$+ \pi a^4\mu\frac{\mathrm{d}^3u_x}{\mathrm{d}z^3}\int_0^t \frac{1}{\sqrt{\pi\nu(t-\tau)}}W_3\mathrm{d}\tau$$

$$(m_p + \frac{1}{2}m_f)\frac{\mathrm{d}W_2}{\mathrm{d}t} + 6\pi a^2\mu\int_0^t \frac{1}{\sqrt{\pi\nu(t-\tau)}}\frac{\mathrm{d}W_2}{\mathrm{d}\tau}\mathrm{d}\tau + 6\pi a\mu W_2 = 0 \qquad [16.16]$$

$$(m_p + \frac{1}{2}m_f)\frac{\mathrm{d}W_3}{\mathrm{d}t} + 6\pi a^2\mu\int_0^t \frac{1}{\sqrt{\pi\nu(t-\tau)}}\frac{\mathrm{d}W_3}{\mathrm{d}\tau}\mathrm{d}\tau + 6\pi a\mu W_3 = 0 \qquad [16.17]$$

The solutions of equations [16.16] and [16.17] are of the same nature as those obtained in section 16.3. The relative velocities W_2 and W_3 rapidly tend toward zero if there is an initial velocity in these directions. The characteristic time of the transient regime is identical to [16.11]:

$$t_p = \left(2\ \frac{\rho_p}{\rho_f} + 1\right)\frac{a^2}{9\nu} \qquad [16.18]$$

Thus, the particle's movement aligns itself very rapidly with the direction of the fluid flow.

Equation [16.15] is solved in a similar manner. The velocity of the particle in direction 1 becomes asymptotically, in a steady-state regime,

$$V_1(z,t) = u_x(z) + \frac{a^2}{6}\frac{\mathrm{d}^2u_x}{\mathrm{d}z^2} \qquad [16.19]$$

The shear of the fluid flow produces a relative velocity of the particle with respect to the fluid. The difference is often very small. For a Poiseuille flow, for example, the velocity of the particle is less than the velocity of the fluid, but the correction is of the order of $(a/L)^2$, which is very small (equation [16.3]).

It is important to analyze the forces exerted on the particle in terms of drag force and lift force. The drag force $F_{//}$ is the component of the hydrodynamic force exerted on the particle, projected onto the direction of the particle's relative velocity with respect to the fluid, while the lift force $F_{\perp}$ is the component perpendicular to

that direction. In Figure 16.2 we specify the notations and sketch the balance of forces exerted on the particle by the fluid flow. When the directions of the particle and fluid velocities are not parallel, the lift and drag are not always simple to interpret from a physical point of view. On the other hand, when the movement of the particle has aligned with the direction of the fluid flow, it is important to note that the BBOT equations correspond to a lift force that becomes zero. The shear of the fluid flow produces only a drag force:

$$F_{//} = \pi a^3 \mu \frac{\mathrm{d}^2 u_x}{\mathrm{d}z^2}, \qquad [16.20]$$

which is balanced by the friction resulting from the relative movement of the particle with respect to the fluid.

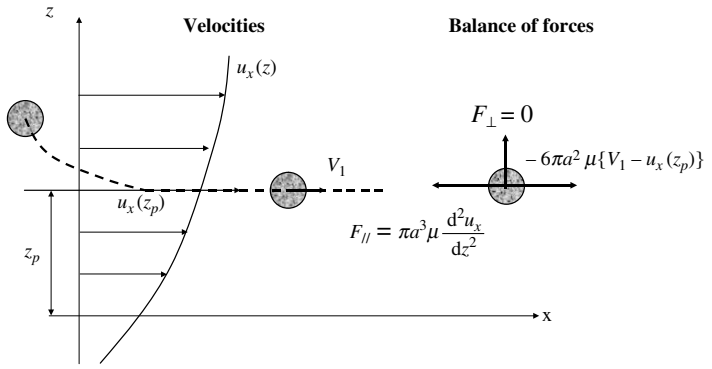

Figure 16.2. *Movement of a fluid particle and balance of forces in a unidirectional sheared flow, modeled by the BBOT equations. The trajectory of the particle, in dashed lines, becomes parallel to the direction of the fluid flow*

16.5. Lift force applied to a particle by a unidirectional flow

The example discussed in the previous section using the BBOT equations shows that the trajectory of a solid particle tends to align with the direction of the fluid flow. The fluid flow does not exert a lift force on the particle, even if it possesses a velocity gradient in the direction perpendicular to that of the flow. This result contradicts some observations of fluid mechanics. The lack of a lift force, for example, does not allow fluid particles to migrate in the direction perpendicular to the direction of the flow, or the fluid to pick up a particle lying on a wall. The study of the lift force has given rise to a considerable amount of research, of which we summarize a few important results. The reader will find in the book by Michaelides[4]

4 Michaelides, *Particles, Bubbles and Drops* (World Scientific, 2006).

a precise history of that work. In the following, we only mention a few essential articles.

We shall study successively the lift force applied on a particle in a fluid flow in an infinite medium and then the case where the particle is near a wall.

16.5.1. *Lift force exerted on a particle in a fluid flow in an infinite medium*

Figure 16.3 depicts two configurations for which theoretical evaluations of the lift force are established. The case of Figure 16.3(b) has prompted numerous studies, aiming at the following:

– Understanding how the shearing of the velocity field produces a lift force. We will focus on the case where the shear is uniform ($\mathrm{d}u_x / \mathrm{d}z = G$ = constant).

– Understanding the role of the particle's rotation. Two cases are usually considered: (i) the particle can rotate freely without friction about an axis that is perpendicular to the plans of the flow; the shear of the fluid flow then causes the particle to rotate; and (ii) the particle is prevented from rotating.

– Understanding the effect of the relative movement of the particle with respect to the fluid, in the direction of the fluid flow. W_1 denotes the relative velocity of the particle with respect to the fluid.

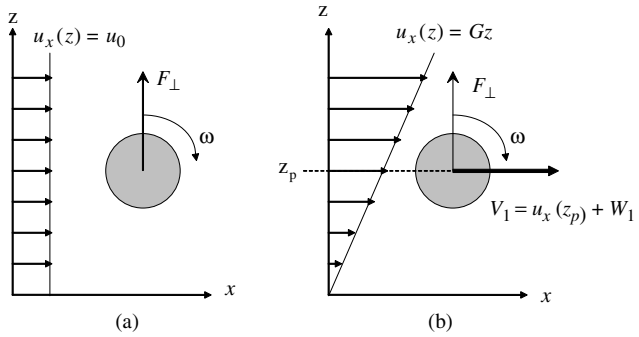

Figure 16.3. *Configurations for studying the lift force exerted on a particle in a fluid flow in an infinite medium. (a) Magnus effect: in a uniform flow the particle is rotated about a fixed axis. (b) The particle moves in the direction of a fluid flow with constant shear. Two sub-cases are considered: (i) the particle is prevented from rotating ($\omega = 0$); (ii) the particle rotates without friction under the effect of shear ($\omega = G/2$).*

The first case (Figure 16.3(a)) is that of the very classic Magnus effect for a high-Reynolds-number flow. If a rotation with angular velocity ω about the *Oy* axis

is forced on a particle of radius a placed in a uniform fluid flow u_0 (such that $u_0 a / \nu >> 1$) along the Ox direction, a lift force is generated on the particle in the Oz direction:

$$\vec{F}_{\perp} = \frac{3}{4} m_F \vec{u} \times \vec{\Omega} = \frac{3}{4} m_F u_0 \omega \vec{k} \ . \qquad [16.21]$$

The rotation vector is $\vec{\Omega} = \omega \vec{j}$ for the configuration of Figure 16.3(a). Viscosity is absent from relation [16.21], and the force is of an inertial nature. While the rotation of the particle produces, because of viscous friction, a rotating movement of the fluid around the particle, in a steady-state regime the kinematics of the flow is independent from viscosity. The pressure along the streamlines that pass the particle is calculated using Bernoulli's theorem, and only the velocity on the surface of the particle intervenes to vary the pressure. The Magnus effect is well known to aerodynamicists, since it is the analogy with the potential flow past a rotating cylinder that explains the lift applied to a thin aircraft wing at incidence. It also explains the effects obtained when a tennis player uses topspin on a ball or slices it.[5]

Let us now consider the configuration of Figure 16.3(b). The fluid, in an infinite medium, has a constant-shear flow $(\mathrm{d}u_x / \mathrm{d}z = G)$. The particle has a relative movement with velocity W_1 in the Ox direction of the fluid flow. Similar hypotheses to [16.4], meaning that the particle is small, are:

$$\left.\begin{aligned} &\mathrm{Re}_{p,W} = \frac{W_1 a}{\nu} << 1, \\ &\mathrm{Re}_{p,\omega} = \frac{\omega a^2}{\nu} << 1, \\ &\text{and } \mathrm{Re}_{p,G} = \frac{G a^2}{\nu} << 1 \end{aligned}\right\} \qquad [16.22]$$

The theoretical difficulties in calculating the lift force are significant. It was proved by Bretherton[6] that no lift force is exerted on a body of revolution by a parallel flow if we remain within the scope of the theory of creeping flows (removing nonlinear terms from the Navier–Stokes equations). It is therefore necessary to take into account the inertial (nonlinear) terms. This difficulty had been identified in 1910 by Oseen, who had indicated that the nonlinear terms cannot be

5 These notions refer to the category of *potential flows*, which are not discussed in this book despite their importance in fluid mechanics, as their applications are not common in process engineering. The reader may refer to the book by Batchelor, *An Introduction to Fluid Mechanics* (Cambridge University Press, 1967), in particular sections 6.4–6.7.

6 Bretherton (1962, *J. Fluid Mech.,* Vol. 14, 284–304).

neglected if the location is sufficiently far from the center of the particle. For the characteristics of the flow under consideration, we naturally introduce the two length scales related to the slip velocity:

$$L_{W1} = \frac{\nu}{W_1}, \qquad [16.23]$$

or to the shear:

$$L_G = \sqrt{\frac{\nu}{G}}. \qquad [16.24]$$

The solution for the flow around the sphere cannot be calculated properly beyond these distances without taking into account the nonlinearities associated respectively to the relative velocity of the particle with respect to the fluid or to the shear of the fluid flow. The conditions [16.22] whereby the particle is small simply mean that $L_{W1} / a >> 1$ and $L_G / a >> 1$.

Mathematical developments solving for the flow around the particle distinguish the inner region within the distance $\min\{L_{W1}, L_G\}$ from the center of the particle, where the flow is essentially governed by viscosity, and the outer region beyond that distance, where nonlinearities have to be taken into account. The general solution of the problem needs to merge the solutions between both domains.

Saffman[7] showed that viscosity produces, for the configuration of Figure 16.3(b), a lift force:

$$\vec{F}_{\perp} = 6.42 \mu W_1 a^2 \sqrt{\frac{G}{\nu}} \vec{k}, \qquad [16.25]$$

oriented as indicated in Figure 16.3(b) in terms of the directions of the flow and shear. The ratio of the lift force to the drag force (of magnitude $6\pi\mu W_1 a$) is of the order of $\sqrt{\mathrm{Re}_G}$; it is therefore small compared to the drag force. The lift force obtained by Saffman is identical whether the particle can rotate freely or its rotation is blocked. If the particle can rotate freely, its rotational speed establishes itself at $\omega = G/2$, so as to cancel out, in a steady-state regime, the rotation torque exerted by the fluid flow on the particle. The independence of the lift force from the rotation of the particle can be understood by noting that the ratio of the lift force after Saffman [16.25] to the lift force related to the Magnus effect is of the order of

7 Saffman (*J. Fluid Mech.*, 22, 385–400 1965) and (*J. Fluid Mech.*, 31, 624 corrigendum 1968). McLaughlin (*J. Fluid Mech.*, 224, 261–274 1991).

$1/\sqrt{\mathrm{Re}_G}$. Saffman's mathematical developments are subject to the condition $W_1 << \sqrt{G\nu}$ (i.e. $L_G << L_{W1}$), which, in practice, is restrictive with respect to typical conditions. Either the fluid's viscosity has to be very high or the relative velocity of the particle with respect to the fluid has to be particularly small.

McLaughlin generalized Saffman's work for an arbitrary value of the ratio $\varepsilon = \sqrt{G\nu} / W_1 = L_{W1} / L_G$ (Saffman studied the case where $\varepsilon = \infty$). The lift force is expressed in the form

$$\vec{F}_\perp = \frac{9}{\pi} \mu W_1 a^2 \sqrt{\frac{G}{\nu}} J(\varepsilon) \vec{k} \,. \qquad [16.26]$$

In Table 16.2 we provide a few values of functional $J(\varepsilon)$. For ε tending toward infinity, $9J(\varepsilon = \infty)/\pi = 6.46$, so that [16.26] is very close to Saffman's result. The factor $J(\varepsilon)$ decreases by a factor of 100 when ε diminishes from infinity to 0.25. The lift force changes direction for $\varepsilon \approx 0.22$. $J(\varepsilon)$ tends toward zero when ε tends toward zero (the shear goes to zero). For $\varepsilon > 0.25$, the value of $J(\varepsilon)$ is sufficiently large for the lift force to differ only slightly depending on whether the particle can rotate freely or its rotation is prevented. This no longer holds for $\varepsilon < 0.25$ as the absolute value of $J(\varepsilon)$ becomes very small.

ε	$J(\varepsilon)$	ε	$J(\varepsilon)$	ε	$J(\varepsilon)$	ε	$J(\varepsilon)$	ε	$J(\varepsilon)$
0.025	−0.000013	0.2	−0.012	0.5	0.74	0.9	1.58	5.0	2.23
0.05	−0.00028	0.25	0.028	0.6	1.02	1.0	1.69	10.0	2.247
0.1	−0.0047	0.3	0.12	0.7	1.26	1.5	1.98	20.0	2.252
0.15	−0.015	0.4	0.41	0.8	1.44	2.0	2.09	∞	2.255

Table 16.2. *Values of the function $J(\varepsilon)$ related to McLaughlin's formula [16.26]*

Also, for the configuration of Figure 16.3(b), Auton[8] obtained the lift force:

$$\vec{F}_\perp = \frac{1}{2} m_F (\vec{u} - \vec{V}) \times \mathrm{curl}(\vec{u}) = \frac{1}{2} m_F W_1 G \vec{k} \,, \qquad [16.27]$$

which is worthy of some comment, as the hydrodynamic conditions differ from those studied previously. Auton's calculation is inviscid, with the fluid slipping on the surface of the particle. Result [16.27] differs from that of the Magnus effect, despite the similarity of the equations, because the calculation does not take into account a possible rotation being imparted to the particle. The lift force obtained by

8 Auton (*J. Fluid Mech.*, Vol. 183, 199–218 1987).

Auton results from the deformation in the velocity curl field produced by the presence of the spherical particle. The calculation is performed under the sole condition that the shear is small, that is, $Ga / W_1 << 1$. Auton's result applies mainly to large-size particles and not to small particles in the sense of [16.4]. Viscosity cannot be neglected for small particles, and it is found that the lift force given by relation [16.26] or [16.27] is $1/\sqrt{\mathrm{Re}_G}$ larger than what Auton's calculation predicts, unless $J(\varepsilon)$ is small in the conditions considered.

16.5.2. *Lift force exerted on a particle in the vicinity of a wall*

The proximity of a wall influences the lift force applied on a particle. Figure 16.4 shows three configurations studied more specifically.

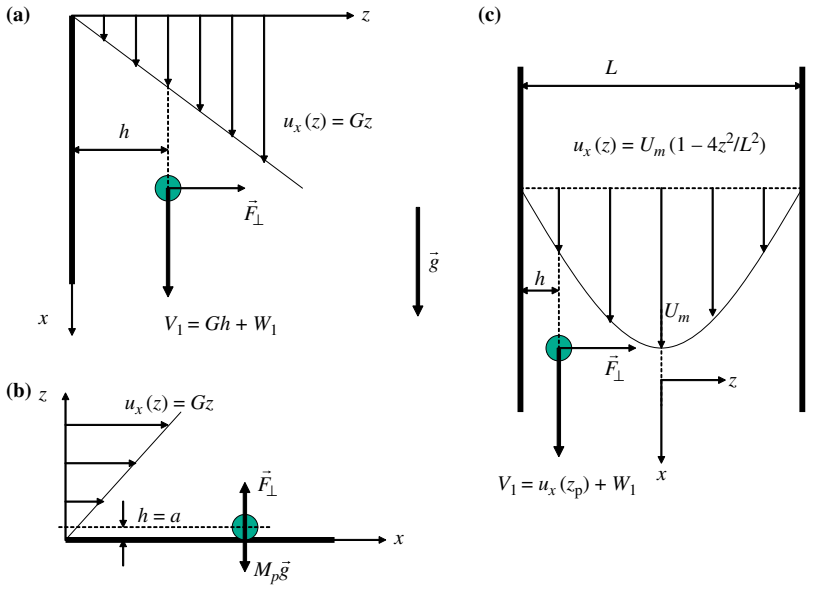

Figure 16.4. *Configurations for studying the lift force exerted on a particle placed in a fluid flow near a wall. (a) Homogeneous shear flow where the direction of the flow is parallel to the direction of gravity. (b) Particle deposited on a wall perpendicular to the direction of gravity. Homogeneous shear flow. (c) Particle in a plane Poiseuille flow whose direction is parallel to the direction of gravity*

Configuration Figure 16.4(a) is modified, compared to that of Figure 16.3(b), by the addition of a plane wall at $z = 0$. The distance from the center of the particle to the wall is denoted by h. The diagram is rotated by 90° with respect to Figure 16.3 in

order to represent conventionally the case where the direction of the flow is parallel to the direction of gravity. Thus, if the particle is denser than the fluid, this configuration depicts the simple case where the influence of the wall on the gravitational sedimentation of the particle is studied.

A comparison of the distance h between the center of the particle and the wall with the scales $L_{W1} = \nu / W_1$ and $L_G = \sqrt{\nu / G}$ (equations [16.23–16.24]) helps assess the nature of the effect of the wall on the lift force applied to the particle. If $h << \min\{L_{W1}, L_G\}$, the wall crosses the inner zone of the flow around the particle. The solution in that zone, for which the contribution of the inertial terms is negligible, can satisfy both the boundary conditions on the particle and on the wall. If $h \approx \min\{L_{W1}, L_G\}$, the wall is situated in the outer zone of the flow around the particle. The effect of the wall on the lift force involves the inertial terms. Finally, if $h >> \max\{L_{W1}, L_G\}$, then the wall is too far to alter the lift force.

When the wall is situated in the inner zone around the particle and the relative velocity W_1 is non-zero ($h << \min\{L_{W1}, L_G\}$), Cherukat and McLaughlin[9] have established that the lift force takes on the form:

$$\vec{F}_{\perp} = \rho_F W_1^2 a^2 I(\kappa, \Lambda_G)\vec{k} \qquad [16.28]$$

with the length ratio $\kappa = a / h$ (note that $\kappa < 1$ necessarily) and the velocity ratio of the fluid flow to the relative velocity of the particle $\Lambda_G = Ga / W_1$. We have $\Lambda_G > 0$ if the particle is faster than the fluid (as in Figure 16.4(a)) and $\Lambda_G < 0$ if the reverse is true. Expression [16.28] has the remarkable property of being independent of viscosity. Results of numerical calculations were used by Cherukat and McLaughlin to tabulate the functional $I(\kappa, \Lambda_G)$ into the following correlations:

$$\begin{aligned} I(\kappa, \Lambda_G) &= (1.7716 + 0.2160\kappa - 0.7292\kappa^2 + 0.4854\kappa^3) \\ &-(3.2397/\kappa + 1.145 + 2.084\kappa - 0.9059\kappa^2)\Lambda_G \\ &+(2.0069 + 1.0575\kappa - 2.4007\kappa^2 + 1.3174\kappa^3)\Lambda_G^2 \end{aligned} \qquad [16.29]$$

for a non-rotating sphere, and:

$$\begin{aligned} I(\kappa, \Lambda_G) &= (1.7631 + 0.3561\kappa - 1.1837\kappa^2 + 0.8452\kappa^3) \\ &-(3.2414/\kappa + 2.6760 + 0.8248\kappa - 0.4616\kappa^2)\Lambda_G \\ &+(1.8081 + 0.8796\kappa - 1.9009\kappa^2 + 0.9815\kappa^3)\Lambda_G^2 \end{aligned} \qquad [16.30]$$

9 Cherukat and McLaughlin (*J. Fluid Mech.*, Vol. 263, 1–18 1994).

when the sphere can rotate freely under the effect of shear. The figures plotted in the article by Cherukat and McLaughlin help interpret relations [16.29] and [16.30]. When the sphere is sufficiently far from the wall ($h/a > 5$), the wall repels the particle ($I > 0$) if the particle is moving faster than the fluid ($\Lambda_G < 0$), whereas it attracts it in the reverse situation. When the particle is near the wall (h/a close to 1), the wall repels the particle ($I > 0$) irrespective of the sign of Λ_G (and therefore of the sign of the relative velocity W_1), except inside an interval of positive values of Λ_G (between 0 and 2.5) for which slightly negative values of I are obtained. The rotation of the particle is generally found to have little impact on the lift force.

The particular case for which the relative velocity W_1 is zero is worth discussing. The term "neutral particles" is used, in the sense that, for the configuration of Figure 16.4(a), the particle has the same density as the fluid, and therefore does not settle in the gravity field. The asymptotic limit of [16.28], associated with the correlation [16.29] or [16.30], when W_1 tends toward zero, is written as:

$$\vec{F}_{\perp} = \rho_F G^2 a^4 (2.0069 + 1.0575\kappa - 2.4007\kappa^2 + 1.3174\kappa^3)\vec{k} \qquad [16.31]$$

for a sphere that is prevented from rotating, and:

$$\vec{F}_{\perp} = \rho_F G^2 a^4 (1.8081 + 0.8796\kappa - 1.9009\kappa^2 + 0.9815\kappa^3)\vec{k} \qquad [16.32]$$

for a sphere that can rotate freely. As $\kappa = a/h < 1$, it can be verified that the force $\vec{F}_{\perp}$ is always oriented in the same direction as $\vec{k}$, which means that the shear in the velocity field produces a force which repels the particle away from the wall.

In the case where the wall is situated in the outer region with respect to the center of the particle ($h > \max\{L_{W1}, L_G\}$), a previous study by McLaughlin[10] shows that the wall exerts an additional force which attracts or repels the particle depending on whether the particle is moving parallel to the wall faster or slower than the fluid. This force:

$$\vec{F}_{\perp,\text{wall}} = -1.713\pi\mu W_1 a^2 \sqrt{\frac{G}{\nu}} \left(\frac{L_G}{h}\right)^{5/3} \vec{k}\,, \qquad [16.33]$$

is added to the lift force [16.26] calculated by McLaughlin (1991) in an infinite medium. The minus sign in [16.33] indicates that the additional force is oriented in the opposite direction to the shear-induced lift force (when $J(\varepsilon) > 0$). The wall-induced additional lift force decreases to zero when h increases.

10 McLaughlin (*J. Fluid Mech.*, Vol. 246, 249–265 1993).

Cherukat's and McLaughlin's relations also enable the determination of the lift force exerted by a boundary layer flow on a particle that is settled at rest on a horizontal plane (Figure 16.4(b)). In that case, $\kappa = 1$ and $\Lambda_G = -1$ since $V_1 = Ga + W_1 = 0$. By substituting these values, we infer from [16.29] that $I = 9.29$ and:

$$\vec{F}_{\perp} = 9.29\rho_F G^2 a^4 \vec{k} \,. \qquad [16.34]$$

This expression enables the determination of the conditions for which the fluid flow entrains the particle in suspension, if the particle is denser than the fluid and the gravity force is perpendicular to the wall (Figure 16.4(b)). For that to occur, the lift force must exceed the reduced weight of the particle, which leads to the condition:

$$G = \frac{\mathrm{d}u_x}{\mathrm{d}z} > \sqrt{\frac{4\pi}{3\times 9.29}\frac{(\rho_p - \rho_f)g}{\rho_f a}} \,. \qquad [16.35]$$

The gradient of the velocity field determines the takeoff condition.

There is considerable literature concerning the lift force exerted on a particle in a Poiseuille flow. The current development of microfluidics opens new prospects for such works, which have historically been strongly motivated by applications in the medical field for understanding the transport of blood cells in arteries and veins. We consider the situation of Figure 16.4(c) where the walls are parallel to the direction of gravity. The pioneering experiments of Segré and Silberberg[11] have demonstrated the lateral migration of rigid neutral particles (equality of densities between the fluid and particles). An inhomogeneous distribution of particles occurs in a cross section of the flow, with a maximum concentration around the radial position $r = 0.6R$. Work on the lift force exerted on a particle in a homogeneously sheared flow (configuration of Figure 16.4(a)), which we have previously mentioned, provides the mathematical framework to study the case of Poiseuille flows, with the concepts of inner and outer zones around the particle for discussing the phenomena producing the lift force. It is however not sufficient to completely study the case of Poiseuille flows. Shear decreases linearly in a Poiseuille flow when moving from the wall toward the center of the pipe. In a similar manner to what is demonstrated by Cherukat and McLaughlin (1994) in a homogeneously sheared flow, it is observed in a Poiseuille flow that the wall exerts a lift force which repels a particle located near the wall. In the central part of the pipe, the shear becomes small. The ratio $\varepsilon = \sqrt{G\nu}/W_1 = L_{W1}/L_G$ of the inertial scale L_{W1} to the inertial scale L_G

11 Segré and Silberberg (*J. Fluid Mech.*, Vol. 14, 115–135 1962) and (*J. Fluid Mech.*, Vol. 14, 136–157 1962).

becomes small at the center of the pipe. Referring to the work of McLaughlin (1991) for a homogeneously sheared flow in an infinite medium, we can understand that the lift force exerted on a particle, although smaller in magnitude in the central part of the pipe than it is near the wall, pushes toward the wall a particle situated in the central part whereas it repels it away from the wall when it is close to it. This is indeed the phenomenology observed experimentally by Segré and Silberberg and highlighted by theoretical studies. We limit ourselves to citing a few important articles,[12] from which it is easy to reconstitute a comprehensive bibliography. The calculations by Asmolov (1999) highlight the difference in the direction and order of magnitude of lift forces between the near-wall region and the central part of the pipe for different values of the Reynolds number $\mathrm{Re}_c = U_m L / \nu$ of the Poiseuille flow (U_m is the velocity maximum of the Poiseuille flow, Figure 16.4(c)). This work builds on previous research by Schoenberg and Hinch (1989) and Hogg (1994). Schoenberg and Hinch's work, in particular, sets out the specificity of the Poiseuille flow. The curvature of the Poiseuille flow causes a pressure gradient effect, which also contributes to repelling particles situated in the central part of the pipe toward the walls.

16.6. Centrifugation of a particle in a rotating flow

To conclude our inventory of a few application cases of the BBOT equations, we now consider a rotating flow about *Oz* axis, omitting gravity. In the cylindrical coordinate system (Figure 16.5), the only non-zero velocity component is the azimuthal component. We consider a velocity field for the flow in the form:

$$\begin{aligned} u_r &\equiv 0 \\ u_\theta(r) &= \omega r + \frac{A}{r} \\ u_z &\equiv 0 \end{aligned} \qquad [16.36]$$

The rotating flow is the combination of a solid-body rotation flow and a vortex flow. As will be seen in Chapter 17, this case corresponds to many configurations for which centrifugal separation is implemented. Theoretically speaking, such flows verify the property $\Delta\vec{u} \equiv 0$. This property greatly simplifies the BBOT equations. It also makes it easier to identify the terms and mechanisms responsible for centrifugal separation.

12 Schonberg and Hinch (*J. Fluid Mech.*, Vol. 203, 517–524 1989), Hogg (*J. Fluid Mech.*, Vol. 272, 285–318 1994), Asmolov (*J. Fluid Mech.*, Vol. 381, 63–87 1999).

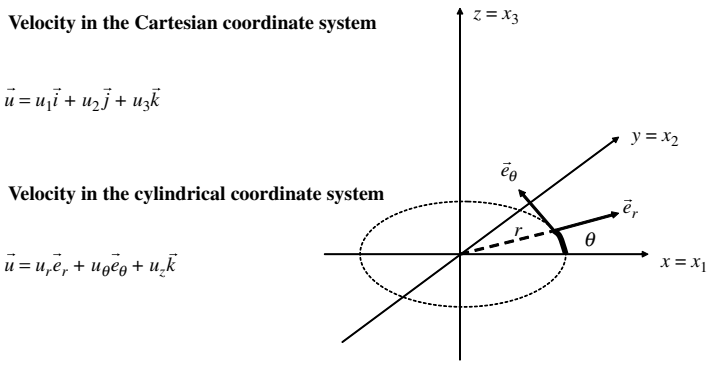

Figure 16.5. *Cartesian coordinate system and cylindrical coordinate system notations*

As the BBOT equations [16.5] are written in the Cartesian coordinate system (O,x_1,x_2,x_3), the first step is to transcribe the velocity field into the Cartesian coordinate system:

$$\begin{aligned} u_1(x_1,x_2,x_3) &= -u_\theta(r)\frac{x_2}{r} \\ u_2(x_1,x_2,x_3) &= u_\theta(r)\frac{x_1}{r} \\ u_3(x_1,x_2,x_3) &= 0 \end{aligned} \qquad [16.37]$$

In this configuration, the BBOT equations [16.5] are written as:

$$\begin{aligned} (m_p + \frac{1}{2}m_f)\frac{\mathrm{d}W_i}{\mathrm{d}t} + 6\pi a^2\mu\int_0^t \frac{1}{\sqrt{\pi\nu(t-\tau)}}\frac{\mathrm{d}W_i}{\mathrm{d}\tau}\mathrm{d}\tau + 6\pi a\mu W_i = \\ -m_p\frac{\mathrm{d}u_i}{\mathrm{d}t} + m_f\frac{Du_i}{Dt} - \frac{1}{2}m_f W_j\frac{\partial u_i}{\partial x_j} \end{aligned} \qquad [16.38]$$

Since $\Delta\vec{u} \equiv 0$, the only non-zero quantities on the right-hand side of [16.5] pertain to terms V and IIcorr. Analyzing the three terms on the right-hand side of [16.38] leads to the identification of the centrifugal separation mechanism. These terms equal zero for the direction parallel to the axis of rotation ($i = 3$). For $i = 1$ and $i = 2$, the first two terms are written as:

$$\begin{aligned} -m_p\frac{\mathrm{d}u_1}{\mathrm{d}t} + m_f\frac{\mathrm{D}u_1}{\mathrm{D}t} &= -m_p\left(u_1\frac{\partial u_1}{\partial x_1} + u_2\frac{\partial u_1}{\partial x_2}\right) + m_f\left(V_1\frac{\partial u_1}{\partial x_1} + V_2\frac{\partial u_1}{\partial x_2}\right) \\ -m_p\frac{\mathrm{d}u_2}{\mathrm{d}t} + m_f\frac{\mathrm{D}u_2}{\mathrm{D}t} &= -m_p\left(u_1\frac{\partial u_2}{\partial x_1} + u_2\frac{\partial u_2}{\partial x_2}\right) + m_f\left(V_1\frac{\partial u_2}{\partial x_1} + V_2\frac{\partial u_2}{\partial x_2}\right) \end{aligned} \qquad [16.39]$$

Bringing to the fore the relative velocities of the particle with respect to the fluid, $W_1 = V_1 - u_1$ and $W_2 = V_2 - u_2$, leads to:

$$\begin{aligned} -m_p \frac{\mathrm{d}u_1}{\mathrm{d}t} + m_f \frac{Du_1}{Dt} &= m_f \left(W_1 \frac{\partial u_1}{\partial x_1} + W_2 \frac{\partial u_1}{\partial x_2} \right) - (m_p - m_f) \left(u_1 \frac{\partial u_1}{\partial x_1} + u_2 \frac{\partial u_1}{\partial x_2} \right) \\ -m_p \frac{\mathrm{d}u_2}{\mathrm{d}t} + m_f \frac{Du_2}{Dt} &= m_f \left(W_1 \frac{\partial u_2}{\partial x_1} + W_2 \frac{\partial u_2}{\partial x_2} \right) - (m_p - m_f) \left(u_1 \frac{\partial u_2}{\partial x_1} + u_2 \frac{\partial u_2}{\partial x_2} \right) \end{aligned} \quad [16.40]$$

so that the right-hand sides of equation [16.38] for $i = 1$ and $i = 2$ are:

$$\begin{aligned} &-m_p \frac{\mathrm{d}u_1}{\mathrm{d}t} + m_f \frac{Du_1}{Dt} - \frac{1}{2} m_f W_j \frac{\partial u_1}{\partial x_j} \\ &\quad = \frac{1}{2} m_f \left(W_1 \frac{\partial u_1}{\partial x_1} + W_2 \frac{\partial u_1}{\partial x_2} \right) - (m_p - m_f) \left(u_1 \frac{\partial u_1}{\partial x_1} + u_2 \frac{\partial u_1}{\partial x_2} \right) \end{aligned} \quad [16.41a]$$

$$\begin{aligned} &-m_p \frac{\mathrm{d}u_2}{\mathrm{d}t} + m_f \frac{Du_2}{Dt} - \frac{1}{2} m_f W_j \frac{\partial u_2}{\partial x_j} \\ &\quad = \frac{1}{2} m_f \left(W_1 \frac{\partial u_2}{\partial x_1} + W_2 \frac{\partial u_2}{\partial x_2} \right) - (m_p - m_f) \left(u_1 \frac{\partial u_2}{\partial x_1} + u_2 \frac{\partial u_2}{\partial x_2} \right) \end{aligned} \quad [16.41b]$$

Substituting the velocity field [16.37] into [16.41], we can write [16.38] in the form:

$$\begin{aligned} &(m_p + \frac{1}{2} m_f) \frac{\mathrm{d}W_1}{\mathrm{d}t} + 6\pi a^2 \mu \int_0^t \frac{1}{\sqrt{\pi \nu (t-\tau)}} \frac{\mathrm{d}W_1}{\mathrm{d}\tau} \mathrm{d}\tau + 6\pi a \mu W_1 \\ &= (m_p - m_f) \frac{u_\theta^2}{r} \frac{x_1}{r} - \frac{1}{2} m_f \left\{ x_2 \frac{\partial}{\partial r} \left(\frac{u_\theta}{r} \right) \left(W_1 \frac{x_1}{r} + W_2 \frac{x_2}{r} \right) + W_2 \frac{u_\theta}{r} \right\} \end{aligned} \quad [16.42a]$$

$$\begin{aligned} &(m_p + \frac{1}{2} m_f) \frac{\mathrm{d}W_2}{\mathrm{d}t} + 6\pi a^2 \mu \int_0^t \frac{1}{\sqrt{\pi \nu (t-\tau)}} \frac{\mathrm{d}W_2}{\mathrm{d}\tau} \mathrm{d}\tau + 6\pi a \mu W_2 \\ &= (m_p - m_f) \frac{u_\theta^2}{r} \frac{x_2}{r} + \frac{1}{2} m_f \left\{ x_1 \frac{\partial}{\partial r} \left(\frac{u_\theta}{r} \right) \left(W_1 \frac{x_1}{r} + W_2 \frac{x_2}{r} \right) + W_1 \frac{u_\theta}{r} \right\} \end{aligned} \quad [16.42b]$$

$$(m_p + \frac{1}{2} m_f) \frac{\mathrm{d}W_3}{\mathrm{d}t} + 6\pi a^2 \mu \int_0^t \frac{1}{\sqrt{\pi \nu (t-\tau)}} \frac{\mathrm{d}W_3}{\mathrm{d}\tau} d\tau + 6\pi a \mu W_3 = 0 \quad [16.43]$$

The next step is to transcribe these equations into the cylindrical coordinate system by expressing the BBOT equations for the radial and azimuthal components of the particle's velocity:

$$V_r = V_1 \frac{x_1}{r} + V_2 \frac{x_2}{r} \text{ and } V_\theta = -V_1 \frac{x_2}{r} + V_2 \frac{x_1}{r}. \quad [16.44]$$

Likewise, the radial and azimuthal components of the particle's relative velocity with respect to the fluid are:

$$W_r = W_1 \frac{x_1}{r} + W_2 \frac{x_2}{r} \text{ and } W_\theta = -W_1 \frac{x_2}{r} + W_2 \frac{x_1}{r}. \quad [16.45]$$

The BBOT equation for the radial component is obtained by multiplying respectively [16.42a] and [16.42b] by x_1 / r and x_2 / r, then summing the two equations. Lengthy but not especially difficult calculations yield the following equation, in which the relative velocities in the Cartesian coordinate system W_1 and W_2 are eliminated to bring forth the relative velocities W_r and W_θ in the cylindrical coordinate system:

$$\begin{aligned}&(m_p + \frac{1}{2} m_f) \frac{\mathrm{d}W_r}{\mathrm{d}t} + (m_p + \frac{1}{2} m_f) \left(- \frac{W_\theta^2}{r} - \frac{W_\theta u_\theta}{r} \right) + 6\pi a \mu W_r \\ &= (m_p - m_f) \frac{u_\theta^2}{r} - \frac{1}{2} m_f W_\theta \frac{u_\theta}{r}\end{aligned} \quad [16.46]$$

In order to simplify the calculations, we have omitted the Basset terms, which have been found not to alter the nature of the physics. These essentially amount to an additional friction term, which slows down the adaptation of the particle's movement to the surrounding flow, but this adaptation remains very rapid anyway. On the left-hand side, the second term appears when the acceleration is expressed while changing the reference frame. Transferring this term to the right, we infer:

$$(m_p + \frac{1}{2} m_f) \frac{\mathrm{d}W_r}{\mathrm{d}t} + 6\pi a \mu W_r = (m_p - m_f) \frac{u_\theta^2}{r} + m_p \left(\frac{W_\theta^2}{r} + \frac{W_\theta u_\theta}{r} \right) + \frac{1}{2} m_f \frac{W_\theta^2}{r} \quad [16.47]$$

The acceleration term in [16.47] is written on the basis of coordinates r and θ and the radial and azimuthal components of the particle's velocity, since the coordinate change verifies with [16.44]:

$$\frac{\mathrm{d}W_r}{\mathrm{d}t} = \frac{\partial W_r}{\partial t} + V_r \frac{\partial W_r}{\partial r} + \frac{V_\theta}{r} \frac{\partial W_r}{\partial \theta} + V_z \frac{\partial W_r}{\partial z} = \frac{\partial W_r}{\partial t} + V_1 \frac{\partial W_r}{\partial x_1} + V_2 \frac{\partial W_r}{\partial x_2} + V_z \frac{\partial W_r}{\partial z} \quad [16.48]$$

By a similar procedure, the BBOT equation for the azimuthal component is obtained by multiplying respectively [16.42a] and [16.42b] by $-x_2 / r$ and x_1 / r, and then summing the two equations. This leads to:

$$(m_p + \frac{1}{2} m_f)\left(\frac{\mathrm{d}W_\theta}{\mathrm{d}t} + \frac{W_r W_\theta}{r}\right) + 6\pi a \mu W_\theta = \frac{1}{2} m_f W_r r \frac{\partial}{\partial r}\left(\frac{u_\theta}{r}\right) - m_p W_r \frac{u_\theta}{r} \quad [16.49]$$

The equation for the axial component remains [16.43].

The left-hand-side terms in equations [16.43], [16.47], and [16.49] are in identical form to those derived when we studied the fall of a small particle within the gravity field (section 16.3) or its displacement in a unidirectional fluid flow (section 16.4). The time periods characterizing the acceleration phase of the particle are identical (equations [16.11] and [16.18]). We recall that these were short. Our discussion regarding the Basset terms (section 16.3) also transposes to the case of centrifugation.

We conclude from [16.43] that the relative velocity of the particle $W_3 = W_z$ in the direction of the axis of rotation goes to zero rapidly if the W_z was non-zero at the initial time. As the velocity u_z of the flow in that direction is zero [16.36], the trajectory of the particle is rapidly confined to a particular plane perpendicular to the axis of rotation.

The forcing terms for the relative movement in that plane of the particle with respect to the fluid bring forth in [16.47] and [16.49] terms of different natures:

– The $(m_p - m_f)u_\theta^2 / r$ term in [16.47] is the one that causes the centrifugation of particles in the axial direction (equation [16.47]). The particle moves away from the axis of rotation if $\rho_p > \rho_f$. It moves toward it if the reverse is true. The term $m_p u_\theta^2 / r$ corresponds to the centrifugal force. The term $-m_f u_\theta^2 / r$ is the pressure force exerted by the rotating flow on the particle. We will establish that in Chapter 17 (section 17.3). The term $(m_p - m_f)u_\theta^2 / r$ is essentially balanced with the friction term $6\pi a \mu W_r$, thus determining the relative radial velocity W_r of centrifugation.

– The other terms appearing in [16.47] and [16.49] are akin to Coriolis forces for movement in a rotating reference frame. Transposing the criteria [16.4] according to which the flow has a low Reynolds number, the rotating flow must be such that:

$$\frac{u_\theta}{r}\frac{a^2}{\nu} << 1 \text{ and } \frac{\partial u_\theta}{\partial r}\frac{a^2}{\nu} << 1$$

Under these conditions, we verify that these Coriolis terms are small compared to the centrifugation terms. The relative velocity of the particle in the azimuthal direction is also small relative to the relative velocity in the radial direction ($W_\theta / W_r << 1$).

In a rotating flow, the BBOT equations therefore describe a centrifugation movement of a small particle, the characteristics of which are driven by rather simple mechanisms. The duration of the transient regime before equilibrium between the centrifugal forcing term and the friction is very short. The centrifugation process is described approximately by:

$$6\pi a \mu W_r \approx (m_p - m_f)\frac{u_\theta^2}{r} \qquad [16.50]$$

The difference between the centrifugal force and the pressure force exerted by the rotating flow on the particle, which generates centrifugation, is balanced by the (drag-like) friction force associated with the relative radial movement of the particle with respect to the fluid. This result will be used in Chapter 17.

16.7. Applications to the transport of a particle in a turbulent flow or in a laminar flow

The examples of application of the BBOT equations discussed in this chapter allow some useful guidance to be drawn in order to elucidate and justify the hypotheses formulated in the other chapters of this part. By keeping in mind that these equations are obtained for small particles, the following points should be emphasized:

– The characteristic time t_p of the transient regime leading to the adaptation of the particle's movement in the fluid flow is short. Mechanical equilibrium is reached very rapidly between the forcing terms of the particle's movement and the viscous drag force resisting the relative movement of the particle with respect to the fluid. We have used this result in Chapter 15 by assuming, in the context of gravitational separation, that the relative velocity of a particle with respect to the fluid is equal to the fall velocity of a particle. We shall revert to it in Chapter 17 (section 17.3) when discussing centrifugal separation.

– The Basset terms (terms VI in equation [16.5]) are additional drag terms which intervene during a transient regime. Their significance depends on the value of the density ratio ρ_p / ρ_f. They are negligible for particles in a gas. They are not negligible when the densities of the particle and fluid are comparable, although they do not modify the order of magnitude of the characteristic time t_p of the transient regime, which remains very short. For this reason, they are often ignored.

– The BBOT equations have enabled the introduction of the added mass effect, which intervenes during the acceleration and deceleration phases of the particle in the fluid. In a transient regime, the added mass is essential for a bubble in a liquid ($\rho_p / \rho_f << 1$), because the bubble has to transmit momentum to the liquid in order to be able to accelerate itself.

– The centrifugation of a particle in a rotating flow is governed by the centrifugal force linked to the rotation of the fluid flow and by the pressure force exerted by the fluid flow on the particle (terms V in [16.5]). We will use this result in Chapter 17 (section 17.3).

– For a steady unidirectional sheared flow, we have found (section 16.4) that the trajectory of a small fluid particle rapidly aligns with direction of the fluid flow. The hydrodynamic force exerted on the fluid particle is essentially the drag force $-6\pi\mu a W_i$. We have used this result on various occasions in this part (Chapter 15, section 15.4 regarding Brownian motion, among others). The BBOT equations do not bring forth a lift force. Our review of lift forces (section 16.5) shows that, for small particles, the magnitude of the lift force is small compared to that of the drag force. This explains why the lift force is not taken into account in the BBOT equations.

The application of the results presented in this chapter is differentiated depending on whether the movement of a particle is considered in a laminar or in a turbulent flow.

16.7.1. *Application to laminar flows*

The development of microfluidics makes the study of the movement of a small particle in a laminar flow an especially dynamic topic nowadays. The contents of this chapter, without having gone into the detail of theoretical developments, show the complexity and difficulty of the subject. A pertinent modeling of the movement of a particle, in order to encompass phenomena such as the resuspension of particles from walls or the migration of particles in a direction perpendicular to the flow streamlines, should incorporate the lift force exerted on a particle, even though it is much weaker than the drag force.

16.7.2. *Application to turbulent flows*

For a particle in a turbulent flow whose characteristic scales of velocity and length are denoted respectively by u_{rms} and ℓ_t, the results described in this chapter mean that the movement of the particle aligns with the direction of the turbulent fluid flow if the characteristic time t_p of the transient regime, during which the

movement of the particle adapts to the surrounding fluid flow, is small compared to the characteristic time $\tau_t = \ell_t / u_{\text{rms}}$ of turbulence, which is often the case ($t_p << \tau_t$). In such a situation, the BBOT equations justify modeling the transport of a particle as a random walk process, wherein the movement of the particle adapts rapidly to follow the variations of the turbulent flow. The turbulent diffusion process described in Chapter 8 results in the migration of particles perpendicularly to the direction of the mean flow much faster than the lift force contributes to it. That is the reason why we have presented in Chapter 15 (section 15.5) the sustenance in suspension of particles within a turbulent flow as a balance between the sedimentation flux and the turbulent diffusion flux. The lift force remains essential for determining whether a particle deposited on the bottom can be resuspended (as we have done with equation [16.35]). However, in conditions where turbulence is sufficiently strong to maintain a cloud of particles in suspension, the model presented in section 15.5 of Chapter 15 shows that the concentration of particles in suspension decreases exponentially when moving upward from the bottom. The suspension is associated with a mobile layer of sediments on the bottom (bed-load layer), and the displacement of particles cannot be considered in a restricted way by focusing on a single, isolated particle, as we have just done in this chapter. Literature on sediment transport in natural environments tackles the problems of resuspension in a turbulent flow and the dynamics of dense fluid/particle layers.[13]

13 See the books by Nielsen (*Coastal Bottom Boundary Layers and Sediment Transport*, World Scientific, 1992) and Fredsoe and Deigaard (*Mechanics of Coastal Sediment Transport*, World Scientific, 1992).

Chapter 17

Centrifugal Separation

Centrifugal separation of solid particles in a fluid, but also of non-miscible droplets in another liquid or of gas bubbles in a liquid, is a frequently employed process. Its principle has already been described in the previous chapter on the basis of the BBOT equations.

This chapter deals with several important applications. It describes in sections 17.4–17.7 the principles of dimensioning apparatus such as centrifuge decanters, centrifugal separators, centrifugal filters, and hydrocyclones. It seeks to describe the dimensioning methodology by considering simple but illustrative configurations based on real-life cases. It is not a substitute for technical documentation regarding centrifugal apparatus, which can be found in various technical publications.[1] The flow models employed are rudimentary. The flows encountered in centrifugal apparatus are classified into two typical flows, solid-body rotation on the one hand and vortex flows on the other hand. These are described in section 17.2. In order to understand the reasons that cause either of those flows to be produced in the different apparatus for centrifugal separation, it is necessary to have some theoretical knowledge, such as the notions of circulation and velocity curl, as well as Kelvin's theorem. These are introduced in section 17.1.

---

1 This chapter was partly inspired by the handouts of the course taught at ENSIC by N. Midoux (Les opérations unitaires mécaniques du génie chimique, ENSIC-CRIFIC Document).
The following references, of a more technical character, are also mentioned: Rivet, P., *Guide de la séparation liquide-solide* (Ed. Idexpo, Cachan) 1981.
Houot, R. and Joussemet, R., "Classification hydraulique en dimensions", *Techniques de l'ingénieur*, *traité Génie des Procédés*, document J 3130.

Separation criteria are fundamentally different depending on whether the fluid flow is of solid-body rotation type or vortex type. By way of example, the quality of separation is affected when the flow rate through a centrifugal separator is increased, while the inverse property is obtained in a hydrocyclone.

17.1 Rotating flows, circulation, and velocity curl

A fluid flow is usually termed a rotating flow when it is possible to identify an *Oz* axis about which the fluid particles have a movement of rotation. This notion is simple to visualize when the flow is steady and the trajectory followed by a fluid particle is closed curve. When this is not the case, the concepts of circulation and velocity curl (or vorticity) need to be introduced in order to define the notion of a rotating flow.

The circulation of a flow along a closed line *C* is defined by:

$$\Gamma(t) = \oint_C (\vec{u}.\vec{t})\ \mathrm{d}l \qquad [17.1]$$

Virtual curve *C* can be chosen arbitrarily, irrespective of the kinematics of the flow. $\vec{t}$ is the unit vector tangential to curve *C* and d*l* an element of length along *C* (Figure 17.1). $\vec{u}(\vec{x},t)$ is the velocity vector along curve *C*. In the most general case, the circulation $\Gamma(t)$ varies in time. In a steady-state regime, when the closed line *C* is a trajectory traveled by a fluid particle in the same direction, Γ is necessarily non-zero. The existence of a non-zero circulation along certain suitably chosen closed curves allows a rotating flow to be characterized.

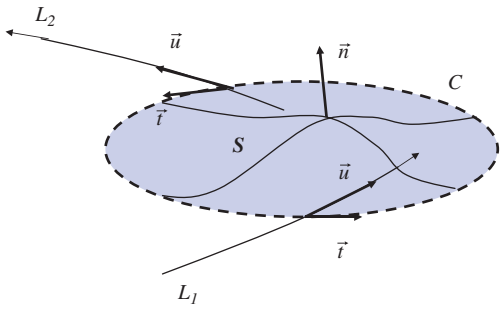

Figure 17.1. *Circulation of a flow over a closed curve. Lines L_1 and L_2 are streamlines of the flow. The virtual curve C is in dashed lines. Vectors $\vec{t}$ are tangent to it. The surface S to which vector $\vec{n}$ is normal is bounded by curve C*

The vorticity of a flow is defined as the curl vector of the velocity field. This is calculated at any point in the flow using:

$$\vec{\omega} = \overrightarrow{\text{curl}}(\vec{u}) = \begin{pmatrix} \dfrac{\partial u_z}{\partial y} - \dfrac{\partial u_y}{\partial z} \\ \dfrac{\partial u_x}{\partial z} - \dfrac{\partial u_z}{\partial x} \\ \dfrac{\partial u_y}{\partial x} - \dfrac{\partial u_x}{\partial y} \end{pmatrix}. \qquad [17.2]$$

(u_x, u_y, u_z) are the velocity components in a Cartesian coordinate system (x,y,z). Circulation is mathematically related to vorticity. It can be proved that the circulation of a flow around a closed curve *C* is equal to the flux of vorticity through any (non-closed) surface *S* bounded externally by *C*, which is written as:

$$\Gamma = \oint_C \vec{u}.\vec{t} \;\; \mathrm{d}l = \iint_S \overrightarrow{\text{curl}}(\vec{u}) \cdot \vec{n} \;\; \mathrm{d}s \,. \qquad [17.3]$$

$\vec{n}$ is the normal vector at a point on surface *S* and d*s* is the area of an element. As a consequence of relation [17.3], if a flow has a non-zero circulation along a closed curve *C*, the flow possesses non-zero vorticity in a domain going through surface *S*.

The practical interest of discriminating between flows based on their rotational or irrotational character results from Kelvin's theorem, one main consequence of which is that, *in the absence of viscosity, it is impossible for an irrotational flow to spontaneously become rotational.* Vorticity can only be produced in a flow at the boundaries of the domain, through the action of viscosity. It only appears within the fluid by transport or diffusion from the boundaries. Vorticity is produced in boundary layers near the walls.

We are therefore led to classify rotating flows based on whether they are *rotational* or *irrotational*. The flow is irrotational at a given point (or in a given domain) if the velocity curl vector is zero at that point (or at all points in that domain). It is rotational at a point if the velocity curl vector is not zero at that point. This classification is relevant, since the property whereby a flow is irrotational or rotational is conserved when a particle is followed in its movement.

When it is possible to identify naturally an *Oz* axis about which the fluid rotates, the movement is often described in the cylindrical coordinate system whose main axis is the *Oz* axis (Figure 17.2). The three velocity components are the radial component u_r, the azimuthal component u_θ, and the axial component u_z. While we have already familiarized ourselves with the use of the cylindrical coordinate

system in Chapter 1, the azimuthal velocity component was always zero in the examples treated. In this chapter, the main velocity component is the azimuthal component u_θ which characterizes rotation. The flow also often exhibits symmetry of revolution with respect to the *Oz* axis. The three velocity components then depend not on the angle θ, which locates the point where velocity is observed, but only on the distance r to the axis and to the position z. The u_r and u_z components determine the flow in a meridian plane, which is often referred to as secondary flow. The Navier–Stokes equations, expressed in a cylindrical coordinate system, are recalled from Table 1.1 (Chapter 1). The velocity curl vector, expressed in a cylindrical coordinate system, is added.

Navier–Stokes equations in cylindrical coordinates

$$\rho\left\{\frac{\partial u_r}{\partial t}+u_r\frac{\partial u_r}{\partial r}+\frac{u_\theta}{r}\frac{\partial u_r}{\partial \theta}+u_z\frac{\partial u_r}{\partial z}-\frac{u_\theta^2}{r}\right\}=-\frac{\partial p}{\partial r}+f_r+\mu\left\{\frac{\partial}{\partial r}\left(\frac{1}{r}\frac{\partial(ru_r)}{\partial r}\right)+\frac{1}{r^2}\frac{\partial^2 u_r}{\partial \theta^2}+\frac{\partial^2 u_r}{\partial z^2}-\frac{2}{r^2}\frac{\partial u_\theta}{\partial \theta}\right\}$$

$$\rho\left\{\frac{\partial u_\theta}{\partial t}+u_r\frac{\partial u_\theta}{\partial r}+\frac{u_\theta}{r}\frac{\partial u_\theta}{\partial \theta}+u_z\frac{\partial u_\theta}{\partial z}+\frac{u_r u_\theta}{r}\right\}=-\frac{1}{r}\frac{\partial p}{\partial \theta}+f_\theta+\mu\left\{\frac{\partial}{\partial r}\left(\frac{1}{r}\frac{\partial(ru_\theta)}{\partial r}\right)+\frac{1}{r^2}\frac{\partial^2 u_\theta}{\partial \theta^2}+\frac{\partial^2 u_\theta}{\partial z^2}+\frac{2}{r^2}\frac{\partial u_r}{\partial \theta}\right\}$$

$$\rho\left\{\frac{\partial u_z}{\partial t}+u_r\frac{\partial u_z}{\partial r}+\frac{u_\theta}{r}\frac{\partial u_z}{\partial \theta}+u_z\frac{\partial u_z}{\partial z}\right\}=-\frac{\partial p}{\partial z}+f_z+\mu\left\{\frac{1}{r}\frac{\partial}{\partial r}\left(r\frac{\partial u_z}{\partial r}\right)+\frac{1}{r^2}\frac{\partial^2 u_z}{\partial \theta^2}+\frac{\partial^2 u_z}{\partial z^2}\right\}$$

Incompressibility

$$\frac{1}{r}\frac{\partial(ru_r)}{\partial r}+\frac{1}{r}\frac{\partial u_\theta}{\partial \theta}+\frac{\partial u_z}{\partial z}=0$$

Velocity curl

$$\overrightarrow{\mathrm{curl}}(\vec{u})=\begin{bmatrix}\frac{1}{r}\frac{\partial u_z}{\partial \theta}-\frac{\partial u_\theta}{\partial z}\\ \frac{\partial u_r}{\partial z}-\frac{\partial u_z}{\partial r}\\ \frac{1}{r}\frac{\partial(ru_\theta)}{\partial r}-\frac{1}{r}\frac{\partial u_r}{\partial \theta}\end{bmatrix}$$

Table 17.1. *Navier-Stokes equations, incompressibility, and velocity curl expressed in a cylindrical coordinate system with axis Oz*

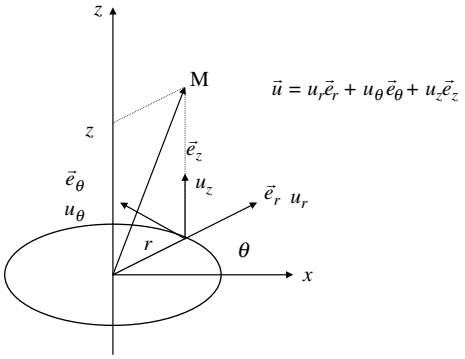

Figure 17.2. *Definitions of the position of a point M and the velocity vector in a circular cylindrical coordinate system of axis Oz*

The centrifugal flows considered in this chapter are those dominated by rotation. The azimuthal component of the velocity is preponderant, that is, $u_r << u_\theta$ and $u_z << u_\theta$ in the cylindrical coordinate system. In such a configuration, the flow tends to become two-dimensional in a plane perpendicular to the *Oz* axis. The u_r and u_θ components of the velocity are quasi-independent from coordinate *z*. The proof of this property goes beyond the scope of this chapter.[2] Our goal is to describe the centrifugation of solid particles in a rotating flow. We simply choose to consider steady-state axisymmetric fluid flows, whose velocity and pressure fields possess the following kinematic characteristics:

$$\begin{aligned} &u_r(r) \\ &u_\theta(r) \\ &u_z(r,z) \\ &p(r,z) \end{aligned} \qquad [17.4]$$

in the fluid domain, outside the wall boundary layers.

The second restriction within which we shall place ourselves is that of high-Reynolds-number flows, that is, $\mathrm{Re} = VR/\nu >> 1$. V is the velocity scale of the azimuthal component and R is a characteristic dimension of the flow in the *Oxy* plane. Viscosity will therefore be negligible outside the boundary layers, and the properties resulting from Kelvin's theorem will be applicable.

2 The reader may refer to the book by H.P. Greenspan, *The Theory of Rotating Fluids* (Cambridge University Press, 1968).

17.2. Some examples of rotating flows

17.2.1. *Solid-body rotation in a rotating tank*

We consider (Figure 17.3) a circular cylindrical tank of radius R initially filled (the tank being stationary) with liquid up to a height H_o. The tank walls are rotated about the Oz axis with an angular speed ω. The upper surface of the liquid is in contact with air through an interface on which the atmospheric pressure prevails. In the cylindrical coordinate system, the steady-state solution for the flow is in the form:

$$\begin{aligned} u_r &\equiv 0, \\ u_\theta &= u_\theta(r), \\ u_z &\equiv 0 \end{aligned} \qquad [17.5]$$

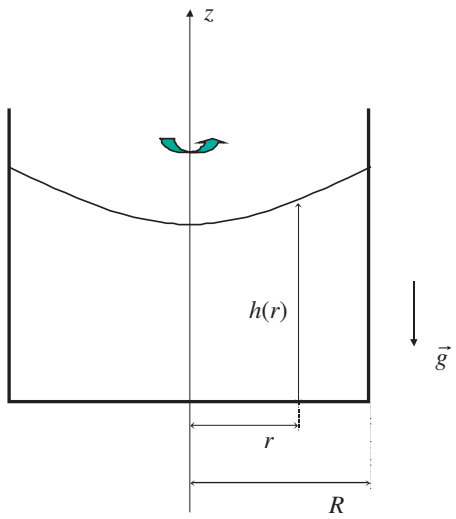

Figure 17.3. *Profile of the free surface for a solid-body rotation flow in a rotating tank*

The velocity components have to satisfy the Navier–Stokes equations, satisfy the conditions of incompressibility, and verify the following boundary conditions:

– on the sidewall: $u_\theta(R,\theta,z) = \omega R$ [17.6]

– on the bottom: $u_\theta(r,\theta,z=0) = \omega r$ [17.7]

– at the free surface: $p(r,\theta,z=h(r)) = P_{\text{atm}}$ [17.8]

One of the unknowns to be determined is the position $h(r)$ of the free surface relative to the bottom of the tank.

In our problem, the gravitational acceleration vector is oriented downward along Oz, that is, $f_r = f_\theta = 0$ and $f_z = -\rho g$. With [17.5], the Navier–Stokes equations reduce to:

$$-\rho \frac{u_\theta^2}{r} = -\frac{\partial p}{\partial r}, \qquad [17.9a]$$

$$0 = \mu \frac{\partial}{\partial r}\left(\frac{1}{r}\frac{\partial (r u_\theta)}{\partial r}\right), \qquad [17.9b]$$

$$0 = -\frac{\partial p}{\partial z} - \rho g\ . \qquad [17.9c]$$

Because of the symmetry of revolution, the pressure does not depend on angle θ. The velocity field verifies the condition of incompressibility. The only solution to [17.9] that verifies the boundary conditions [17.6] and [17.7] is:

$$u_\theta(r,\theta,z) = \omega r\ . \qquad [17.10]$$

The pressure field is determined by solving the Navier–Stokes equations for the radial and axial components. We obtain:

$$p(r,\theta,z) = -\rho g z + \frac{1}{2}\rho \omega^2 r^2 + A\ , \qquad [17.11]$$

which should verify boundary condition [17.8]. From this, we derive the parabolic shape of the free surface:

$$h(r) = -\frac{P_{\text{atm}}}{\rho g} + \frac{1}{2}\frac{\omega^2}{g} r^2 + \frac{A}{\rho g}\ . \qquad [17.12]$$

Constant A is determined by the conservation of the volume of liquid. This leads to:

$$h(r) = H_o + \frac{\omega^2}{2g}\left(r^2 - \frac{R^2}{2}\right). \qquad [17.13]$$

This simple solution has certain characteristics which are important to note:

– The flow is rotational. The curl vector, which is oriented along the *Oz* axis, is uniform in the domain:

$$\overrightarrow{\text{curl}}(\vec{u}) = \begin{bmatrix} 0 \\ 0 \\ 2\omega \end{bmatrix} \qquad [17.14]$$

– The free surface has the shape of a parabola (Figure 17.3), where the thickness of the fluid is smallest at the center. There is a radial pressure gradient which balances the centrifugal force, as shown by the Navier–Stokes equation [17.9a] for the radial component of the velocity.

It is not straightforward to determine the transient solution that leads to the solid-body rotation of the fluid starting from rest. The solution of the Navier–Stokes equations in the form ($u_r = 0$, $u_\theta(r,z,t)$, $u_z = 0$), for which the azimuthal component u_θ evolves in time under the effect of a process of vorticity diffusion from the lateral circular wall toward the tank axis, does not portray reality. A secondary flow ($u_r \neq 0$ and $u_z \neq 0$) actually occurs, which carries vorticity from the boundary layer on the horizontal bottom wall into the water layer. Boundary layers play a key part in rotating flows; they allow steady-state flows to be established more rapidly.[3]

17.2.2. *Vortex flow*

A second, very classical rotating flow is the vortex flow, of which a practical example in hydrocyclones will be seen in section 17.2.3. For now, let us seek a simple solution of the Navier–Stokes equations, in the form given by [17.5], which is steady and irrotational. The general solution of [17.9b] for the azimuthal component of the velocity can be written as:

$$u_\theta(r) = Ar + \frac{B}{r}. \qquad [17.15]$$

3 See also Greenspan, *The Theory of Rotating Fluids*. The book by Stern (*Ocean Circulation Physics*, Academic Press, 1975) also discusses the role of boundary layer flows in a rotating fluid.

The vorticity of the velocity field is:

$$\overrightarrow{\text{curl}}(\vec{u}) = \begin{bmatrix} 0 \\ 0 \\ 2A \end{bmatrix}. \qquad [17.16]$$

The flow is irrotational if $A = 0$. The irrotational flow, called a vortex flow, takes on the form:

$$u_\theta(r) = \frac{\Gamma}{2\pi r}. \qquad [17.17]$$

The vortex is characterized by the quantity Γ, which is the circulation of the flow along a circle of radius r (this observation explains the 2π factor in [17.17]). The circulation is the same irrespective of the radius r of the circle considered. The velocity is infinite on the Oz axis. Vorticity is zero except on the axis ($r = 0$), where it reaches an infinite value.

To avoid difficulties linked to the singularity at $r = 0$, an eddy- (or vortex-) type flow is commonly modeled using Rankine's model:

$$\begin{aligned} u_\theta(r) &= \frac{\Gamma}{2\pi a^2} r \quad \text{for } r < a \\ u_\theta(r) &= \frac{\Gamma}{2\pi r} \quad \text{for } r > a \end{aligned} \qquad [17.18]$$

a is the radius of the eddy. The flow is irrotational outside a disk of radius a, whereas it is a solid-body rotation flow for $r < a$. The velocity is at a maximum at $r = a$. The radial profile of the azimuthal velocity is plotted in Figure 17.4. It is easily verified that the circulation is equal to the vorticity flux, as dictated by [17.3]. The Rankine vortex is characterized by two quantities: the circulation Γ and the radius a. The radial variation of pressure is calculated by integrating the Navier–Stokes equation for the radial component of the velocity,

$$-\rho \frac{u_\theta^2}{r} = -\frac{\partial p}{\partial r} \qquad [17.19]$$

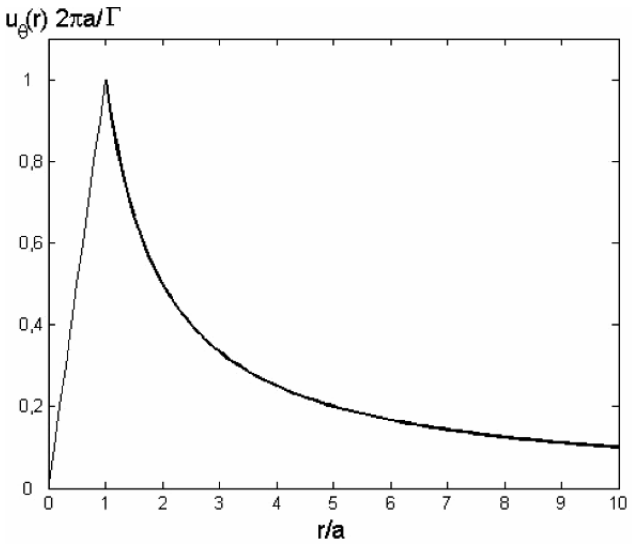

Figure 17.4. *Rankine vortex model*

For the Rankine model, we deduce:

$$\begin{aligned} p(r,z) &= p_0 + \rho\frac{\Gamma^2}{4\pi^2 a^4}\frac{r^2}{2} \quad \text{for } r < a \\ p(r,z) &= p_0 + \rho\frac{\Gamma^2}{4\pi^2 a^2} - \frac{\Gamma^2}{4\pi^2}\frac{1}{2r^2} \quad \text{for } r > a \end{aligned} \qquad [17.20]$$

The smaller the radius a, the more localized the pressure variations at the vicinity of the Oz axis. This is an observation that can be made by looking at a bathtub being emptied. When a rotation sets in, the flow is of vortex type. It is common to observe a deep depression in the free surface entering the drain orifice, which is characteristic of a vortex flow and quite different from the parabolic shape observed for solid-body rotation flow (Figure 17.3).

The Rankine model is of great practical interest, although it is not an exact solution of the Navier–Stokes equations. In the presence of viscosity, the vorticity discontinuity at $r = a$ is removed. The radius a of the vortex widens in time if a secondary flow does not counteract the effect of viscosity.

17.2.3. *Flow in a hydrocyclone*

Hydrocyclones are centrifugal separators which enable the separation of solid particles that are denser than the fluid, or of less dense particles (those are often non-miscible droplets in another liquid). Such apparatus present the advantage of not including any moving parts. The rotation results from the winding of the flow in a circular cylindrical cavity.

Figure 17.5 shows the geometry of a hydrocyclone. While the case represented corresponds to an apparatus for separating particles denser than the fluid, the hydrodynamic principles described in this section are general. They apply, unless specifically indicated otherwise, to both the cases that will be considered in section 17.7 regarding separation.

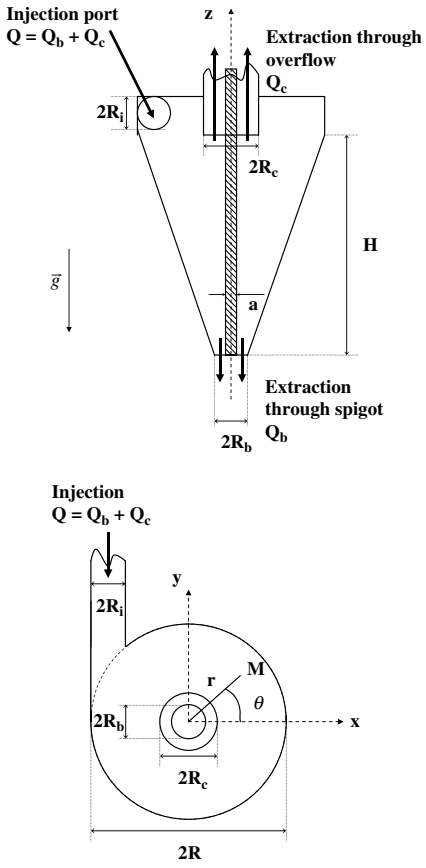

Figure 17.5. *Hydrocyclone for separating particles that are denser than the fluid*

The apparatus, which has axisymmetric geometry with respect to the vertical *Oz* axis parallel to the direction of gravity, consists of two cavities on top of each other. The fluid is fed tangentially into the upper cavity through an aperture of radius R_i. The injection flow rate is denoted by Q. The lower cavity, of circular conical shape, has a radius that decreases gradually. Extraction is performed via two apertures. If the operating conditions have been carefully selected, the particles that are denser than the fluid are discharged in their entirety through the lower aperture, called the apex or the spigot (radius R_b), while the fluid flow is mainly extracted through the upper aperture (the overflow, of radius R_c). The circular geometry causes the fluid to acquire a rotating movement as soon as it enters the upper cavity.

17.2.3.1. *Rotating flow and angular momentum conservation*

In the inlet section of the apparatus, it is simpler to express the velocity components in the Cartesian coordinate system (O,*x*,*y*,*z*). Assuming the flow to be rectilinear and uniform, these are, in the inlet section:

$$u_x \equiv 0$$

$$u_y \equiv -\overline{V} = -Q / \pi R_i^2 \qquad [17.21]$$

$$u_z \equiv 0$$

The velocity components are denoted by (u_x, u_y, u_z) in the Cartesian coordinate system (O,*x*,*y*,*z*) and (u_r, u_θ, u_z) in the circular cylindrical coordinate system (O,*r*,θ,*z*). $\overline{V}$ designates the mean streamwise velocity in the inlet section where the flow is irrotational $(\vec{\omega} = \overrightarrow{\text{curl}}(\vec{u}) = \vec{0})$.

At high Reynolds numbers, if transit through the apparatus is fast, vorticity does not have enough time to diffuse. Kelvin's theorem results in the flow being irrotational in the part of the apparatus through which the flow passes. It is therefore also irrotational in the outlet sections (spigot and overflow). This result has two consequences:

1. The rotating flow is of vortex type in the hydrocyclone. This is modeled by a Rankine vortex of radius a and circulation Γ, using equation [17.18]. The radius a depends directly on the geometrical contraction ratios R_b/R and R_c/R between the radius of the upper cavity and those of the extraction apertures.

2. In the outlet sections (spigot and overflow), the radial and axial velocity components u_r and u_z equal zero in the rotationally zone (r < a). The flow passes through annular sections $a < r < R_b$ for the spigot and $a < r < R_c$ for the overflow. In these sections, it is assumed that the flow is uniform, namely:

Spigot:

$$u_z(r,\theta,0) = 0 \quad \text{for } r < a$$

$$u_z(r,\theta,0) = -\frac{Q_b}{\pi(R_b^2 - a^2)} = -\overline{W}_b \quad \text{for } a < r < R_b \qquad [17.22]$$

Overflow:

$$u_z(r,\theta,H) = 0 \quad \text{for } r < a$$

$$u_z(r,\theta,H) = \frac{Q_c}{\pi(R_c^2 - a^2)} = \overline{W}_c \quad \text{for } a < r < R_c$$

Q_b and Q_c are the outgoing flow rates through the two outlet apertures. Mass conservation dictates that $Q = Q_b + Q_c$. The fraction of the flow that passes through either outlet section is determined by a head loss calculation developed hereinafter.

The radius a is necessarily less than the geometrical radii R_b and R_c of the spigot and overflow, in order to let the fluid out. In Figure 17.5, the vortex core $r < a$ is hatched to indicate that there is no flow in that zone.

A simple argument based on the conservation of angular momentum allows the circulation Γ of the vortex to be calculated. In a steady-state regime, the angular momentum integrated over the volume of the apparatus is constant. The conservation of this quantity stipulates that the angular momentum flux integrated over the inlet section of the apparatus is equal to the sum of the angular momentum fluxes through both outlet sections. In the following, the focus is only on the axial component of the angular momentum (along $\vec{k}$). The flux $\overrightarrow{Q\Omega}_z$ of the axial component $(\overrightarrow{OM} \times \vec{u})_z$ of angular momentum through a surface S is written as:

$$\overrightarrow{Q\Omega}_z = \rho \iint_S (\overrightarrow{OM} \times \vec{u})_z \ (\vec{u} \cdot \vec{n}) \ \mathrm{d}s \,. \qquad [17.23]$$

By convention, the normal $\vec{n}$ is oriented in the direction of the discharge flow.

In the injection section S_i we have $(\overrightarrow{OM} \times \vec{u})_z = -x\overline{V}$. The integral [17.23] is readily calculated over the surface of the inlet section. We obtain $\overrightarrow{Q\Omega}_z = \rho(R - R_i)\overline{V}^2 \pi R_i^2$, bringing to fore the distance $(R - R_i)$ between the Oz axis and the center of the inlet section.

In the two outlet sections, $(\overrightarrow{OM} \times \vec{u})_z = ru_\theta(r) = \Gamma / 2\pi$ is constant in the irrotational zone ($r > a$) owing to [17.18]. The integral [17.23] is therefore easily calculated, $\overrightarrow{Q\Omega}_z = \rho\Gamma Q / 2\pi$. There is no point in distinguishing the spigot from the overflow. The equality of angular momentum flux between the inlet and the outlets enables the vortex circulation to be determined:

$$\Gamma = Q\frac{2(R - R_i)}{R_i^2} \qquad [17.24]$$

This relation, which shows the remarkable property that the circulation of the vortex is proportional to the flow rate through the apparatus, is very satisfactorily verified experimentally[4] at high Reynolds numbers.

17.2.3.2. *Vortex radius and extracted flow rates through the spigot and overflow*

To the best of our knowledge, there is no simple (and unanimously accepted) model for determining the diameter *a* of the vortex. In practice, *a* mainly depends on the radii R_b and R_c of the outlet apertures. It does not vary much with the flow rate when the Reynolds number is large.

In Figure 17.5, the radius of the spigot R_b is smaller than the radius R_c of the overflow. This holds for a hydrocyclone separating particles that are denser than the fluid. The volume flow rate of the dispersed phase is small compared to the volume flow rate of the continuous phase. The apparatus design is made in such a way that all particles are extracted through the spigot with a flow rate of the continuous phase which is reduced as much as possible, while the maximum possible amount of the continuous phase flows through the overflow. The condition $R_b < R_c$ contributes to achieving this goal by reducing the extraction area of the spigot relative to that of the overflow.

We have not distinguished the flow rates Q_b and Q_c in order to calculate the circulation of the vortex (equation [17.24]). However, it is necessary to know Q_b and Q_c in order to determine the $u_r(r)$ and $u_z(r,z)$ velocity components of the secondary flow and infer therefrom the particle separation properties of the

4 This theory and the concepts of head losses in a rotating flow, presented hereinafter, build on the work summarized by W.S. Lewellen, ("A review of confined vortex flows", NASA Contractor Rep. N° 1772 1971).
Measurements (Escudier, Bornstein, Zehnder, *J. Fluid Mech.*, Vol. 98, 49–63 1980.) carried out in conditions where the radius *a* is very small disprove that the axial velocity component is zero inside the vortex core ($r < a$). However, the area of the rotational zone is small, and the flow rate through it is very small. Circulation is also estimated satisfactorily using [17.24] in that case.

apparatus, as will be done in section 17.7. The flow rates Q_b and Q_c are set by the head losses associated with the operation of the apparatus. The associated head losses in a hydrocyclone are quantitatively significant. They mainly occur at the hydrocyclone outlet, during extraction through the spigot and overflow, because the rotational kinetic energy is then dissipated. Compared to these head losses, the head loss inside the apparatus itself is small. It is the head losses at the apparatus outlet that determine the flow rate through the apparatus and set the fractional flow rates exiting through the spigot and overflow.

Head losses along two streamlines, one exiting through the spigot and the other through overflow, are depicted in Figure 17.6 from the hydrocyclone inlet to the two downstream reservoirs, the first one collecting the particles with a fraction of the continuous phase and the second the remainder of the continuous phase.

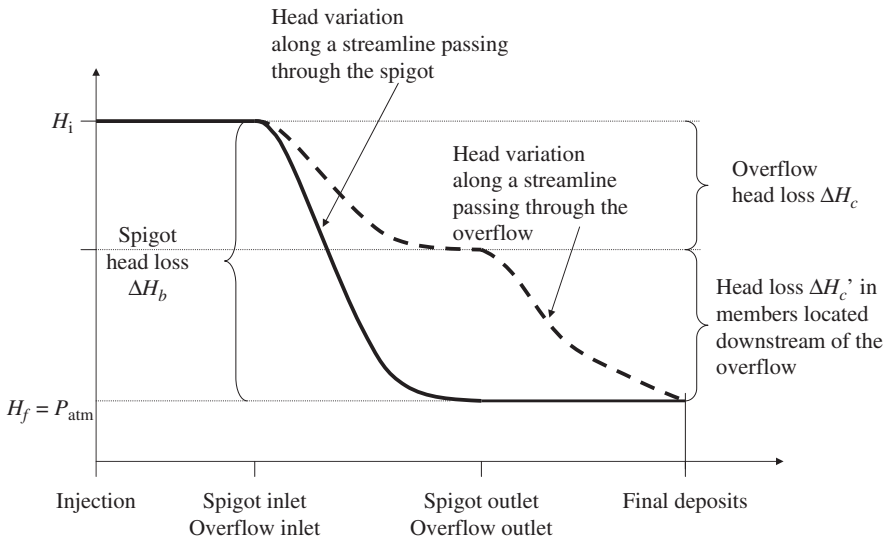

Figure 17.6. *Head variation across a hydrocyclone for a streamline passing through the spigot or overflow*

It is assumed that the spigot opens into the atmosphere. The only head loss along the streamline exiting through the spigot is produced upon exit of the flow through the spigot. It results from the sudden expansion at the outlet of the spigot and from the dissipation of the rotational flow. It is therefore written as:

$$H_i - P_{\text{atm}} = \Delta H_b(\rho\frac{\Gamma^2}{a^2}, \rho\overline{W}_b^2, a, R_b)\,. \qquad [17.25]$$

This depends on the rotational energy, the kinetic energy associated with the mean stream-wise velocity in the spigot, and also the geometrical scales of the spigot.

If the overflow is extended by a pipeline leading to the downstream basin, the head loss induced by the outlet through the overflow (of the same nature as [17.25]) is complemented by an additional head loss $\Delta H_c'$ downstream of the overflow, owing to the length of the pipe, to the sudden expansion at the exit of that pipe into the downstream basin, and to a valve with is usually used to adjust the flow rate passing through the overflow. The head variation between the apparatus inlet and the downstream basin, along the streamline passing through the overflow, is written as:

$$H_i - P_{\text{atm}} = \Delta H_c(\rho\frac{\Gamma^2}{a^2}, \rho\overline{W}_c{}^2, a, R_c) + \Delta H_c'(\rho\overline{W}_c{}^2, a, R_c)\,. \qquad [17.26]$$

The overall flow rate Q passing through the apparatus is the sum of the flow rates exiting through the spigot and overflow. It is related to the mean stream-wise velocities $\overline{W}_b$ and $\overline{W}_c$ in the spigot and overflow:

$$Q = Q_b + Q_c = \pi\overline{W}_b(R_b^2 - a^2) + \pi\overline{W}_c(R_c^2 - a^2)\,. \qquad [17.27]$$

In [17.25] and [17.26], the circulation Γ depends on the flow rate Q (equation [17.24]). Without going any further into modeling, which would lead us to treat a particular case, it can be seen simply that equations [17.25–17.27] enable the determination, for a head variation $H_i - P_{\text{atm}}$ between the inlet and outlet, of the overall flow rate going through the apparatus (hence the circulation of the vortex), and the mean stream-wise velocities in the spigot ($\overline{W}_b$) and the overflow ($\overline{W}_c$). The solution depends on the hydraulic circuit in which the hydrocylone is implemented. Since [17.25] and [17.26] determine $\overline{W}_b$ and $\overline{W}_c$, respectively, it is found that the flow rate $Q_b = \pi\overline{W}_b(R_b^2 - a^2)$ will be smaller compared to $Q_c = \pi\overline{W}_c(R_c^2 - a^2)$, the larger the ratio R_c / R_b is.

17.2.3.3. *Kinematics of the secondary flow*

A few streamlines of the secondary flow in a meridian plane of the hydrocyclone (θ = constant) are sketched in Figure 17.7. The secondary flow is determined by the radial and vertical components of the velocity. Under the hypothesis that the rotational component is dominant, the flow has a two-dimensional structure (equations [17.4]). Only the axial component of the velocity varies with z. The variation with z is linear, resulting from the conditions of incompressibility.

The $u_r(r)$ and $u_z(r,z)$ components are related through incompressibility, which is written, denoting by $h(r)$ the height inside the hydrocyclone, as:

$$\frac{1}{r}\frac{\partial(ru_r)}{\partial r} = -\frac{\partial u_z}{\partial z} = -\frac{u_{z+}(r) - u_{z-}(r)}{h(r)}. \qquad [17.28]$$

$u_{z+}(r)$ and $u_{z-}(r)$ are the values of the vertical velocity on the upper boundary ($z = H$) and on the lower boundary ($z = H - h(r)$). Integrating [17.28] for the vertical component leads to:

$$u_z(r,z) = u_{z+}(r)\frac{h(r) - H + z}{h(r)} + u_{z-}(r)\frac{H - z}{h(r)} \qquad [17.29]$$

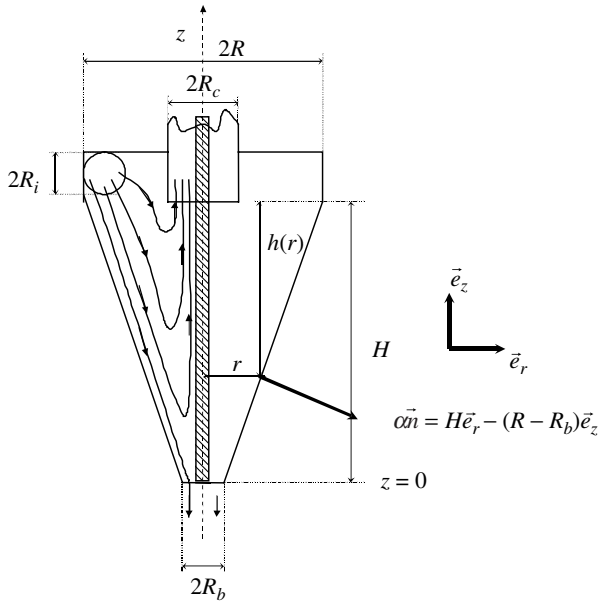

Figure 17.7. *Secondary flow in an (O,r,z) plane of a hydrocyclone*

The function $u_{z+}(r)$ is given by the boundary conditions on the upper boundary:

$$\begin{aligned} u_{z+}(r) &= u_z(r,H) = \frac{Q_c}{\pi(R_c^2 - a^2)} \quad \text{for } a < r < R_c \\ u_{z+}(r) &= u_z(r,H) = -\frac{Q}{\pi(R^2 - R_c^2)} \quad \text{for } R_c < r < R \end{aligned} \qquad [17.30]$$

On the lower boundary, the resolution is different depending on whether r is smaller or larger than the radius R_b of the spigot:

For $a < r < R_b$

$$u_{z-}(r) = u_z(r,0) = -\frac{Q_b}{\pi(R_b^2 - a^2)} . \qquad [17.31]$$

As $h(r) = H$, the $u_z(r,z)$ component is directly derived from [17.29] using [17.30] and [17.31], and the $u_r(r)$ component is determined by integrating [17.28] with [17.30] and [17.31]. The constant of integration is deduced from the condition $u_r(r = a) = 0$. The result is given hereafter in [17.35].

For $R_b < r < R$, the velocity at the bottom is parallel to the conical wall, which results in the following relation between $u_r(r)$ and $u_{z-}(r)$:

$$u_r(r) = u_{z-}(r)\frac{R - R_b}{H}, \qquad [17.32]$$

using the components of the normal vector to the wall indicated in Figure 17.7. Thanks to [17.32], the function $u_{z-}(r)$ is eliminated from [17.28], which becomes:

$$(R - r)\frac{\partial(ru_r)}{\partial r} - ru_r = -\frac{R - R_b}{H} ru_{z+} \qquad [17.33]$$

since $h(r) = H(R - r)/(R - R_b)$. The function $u_{z+}(r)$ is constant in the two intervals $R_b < r < R_c$ and $R_c < r < R$, as stated by the boundary conditions [17.30]. In each of the intervals $R_b < r < R_c$ and $R_c < r < R$, the solution of the differential equation [17.33] takes on the form:

$$u_r(r) = A + \frac{B}{r} + \frac{C}{r(R - r)} \qquad [17.34]$$

Constants A and B are determined from equation [17.33] for the boundary condition [17.30]. Constant C ensures the continuity of $u_r(r)$ at $r = R_b$, then $r = R_c$.

The solving procedure described above, which appears tedious but presents no real difficulty, leads to complete calculation of the secondary flow:

for $a < r < R_b$

$$u_r(r) = \frac{1}{2\pi H}\frac{(a^2 - r^2)}{r}\left\{\frac{Q_c}{(R_c^2 - a^2)} + \frac{Q_b}{(R_b^2 - a^2)}\right\}$$
$$u_z(r,z) = \frac{Q_c}{\pi(R_c^2 - a^2)}\frac{z}{H} + \frac{Q_b}{\pi(R_b^2 - a^2)}\frac{(z-H)}{H}$$

for $R_b < r < R_c$

$$u_r(r) = \frac{(R - R_b)}{2\pi H}\frac{1}{r(R-r)}\left\{Q_c\frac{(R_c^2 - r^2)}{(R_c^2 - a^2)} - Q\right\} \qquad [17.35]$$
$$u_z(r,z) = \frac{Q_c}{\pi(R_c^2 - a^2)} + \frac{(z-H)(R-R_b)}{2\pi Hr(R-r)^2}\left\{Q_c\frac{(2rR - R_c^2 - r^2)}{(R_c^2 - a^2)} + Q\right\}$$

for $R_c < r < R$

$$u_r(r) = -\frac{Q(R - R_b)}{2\pi H(R^2 - R_c^2)}\left\{1 + \frac{R}{r}\right\}$$
$$u_z(r,z) = -\frac{Q}{\pi(R^2 - R_c^2)}\left\{1 + \frac{(H-z)}{2H}\frac{(R-R_b)}{r}\right\}$$

This velocity field will be used in section 17.7 in order to determine the conditions of separation for solid particles.

17.3. The principle of centrifugal separation

The principle of centrifugation of a particle within a rotating flow has already been treated in section 16.6 of Chapter 16 using the BBOT equations. Here, we formulate differently the behavior of a particle in a rotational flow, using a physical approach that sets out the main forces governing the dynamics.

We consider an axisymmetric fluid flow rotating about an axis *Oz*. The rotation dominates, that is, $u_r << u_\theta$ and $u_z << u_\theta$. This hypothesis is, to a very large extent, verified in centrifugal separators, as the rotational speeds are commonly of the order of 1,000–6,000 rpm. It is therefore postulated that the structure of the flow is of the form given by equation [17.4]. In a steady-state regime, the terms associated with components u_r and u_z are negligible in the Navier–Stokes equation for the radial component of the velocity. We therefore write:

$$-\rho_f\frac{u_\theta^2}{r} = -\frac{\partial p}{\partial r}. \qquad [17.36]$$

There is in the fluid a radial pressure gradient which balances the centrifugal force applied on a fluid particle.

Let us now consider a spherical particle of diameter d and density ρ_s, placed in the fluid flow. We denote by u_{rp}, $u_{\theta p}$, and u_{zp} the radial, azimuthal, and axial components of the particle's velocity in the cylindrical coordinate system of axis Oz. The main results from Chapter 16 are the following:

– The relative movement of the particle with respect to the fluid occurs along the radial direction $\vec{e}_r$. The azimuthal and axial velocity components of the particle and fluid are identical ($u_{\theta p} = u_\theta$ and $u_{zp} = u_z$).

– The particles are small. This means, in particular, that the Reynolds number based on the relative velocity of the particle with respect to the fluid and on the diameter of the particle is small, i.e. $\mathrm{Re}_{pW} = |u_{rp} - u_r| d / \nu << 1$.

– The dynamics of the particle's relative movement with respect to the fluid is governed by the action of three forces oriented along the radial direction $\vec{e}_r$: (i) the centrifugal force F_{rc} applied to the particle's mass, (ii) the pressure force F_{rp} exerted by the fluid flow on the particle, and (iii) the friction force F_{rf} resisting the relative movement of the particle with respect to the fluid.

The centrifugal force is written as:

$$F_{rc} = m_p \frac{u_{\theta p}^2}{r_p} \qquad [17.37]$$

with r_p designating the distance from the particle to the Oz axis (Figure 17.8).

Since the particle is small, the friction résistance to the relative radial displacement of the particle with respect to the fluid is expressed by Stokes' law (Chapter 15, section 15.1):

$$F_{rf} = -3\pi\mu d(u_{rp} - u_r) . \qquad [17.38]$$

The total pressure force exerted on the particle is the integral of the pressure force exerted at every point of the sphere's surface. This integral is transformed into a volume integral by virtue of the Ostrogradsky formula:

$$-\iint_S p(\vec{r}_p + \vec{r}\,')\ \vec{n}\ \mathrm{d}s = -\iiint_V \nabla p(\vec{r}_p + \vec{r}\,')\ \mathrm{d}V \qquad [17.39]$$

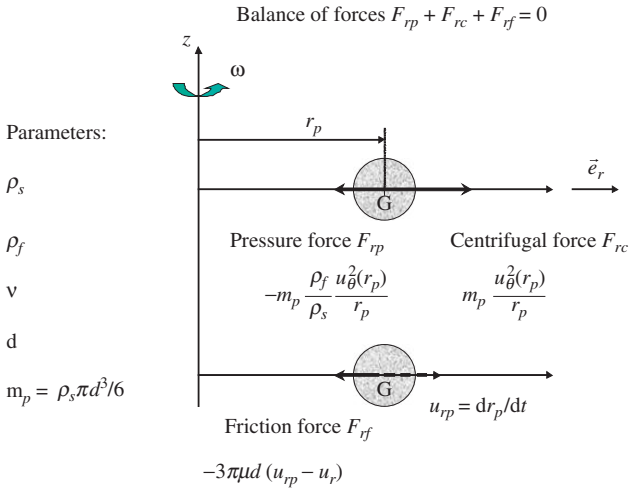

Figure 17.8. *Principle of centrifugal separation – balance of forces on a particle*

The vector $\vec{r}\,'$ locates a point inside the sphere or at its surface with respect to the center of the particle and $\vec{r}_p$ locates the position of the particle's center. S and V designate the surface area of the sphere and its volume, respectively. The pressure force expressed by [17.39] is a vector. As the only non-zero component of the pressure gradient is along the radial direction (equation [17.36]), the pressure force is in the radial direction. Its value is:

$$F_{rp} = -\iiint_V \frac{\partial p}{\partial r}(\vec{r}_p + \vec{r}\,')\ \mathrm{d}V \approx -\frac{\partial p}{\partial r}(\vec{r}_p)\ \iiint_V \mathrm{d}V = -\frac{\partial p}{\partial r}(\vec{r}_p)\ \frac{\pi d^3}{6} \qquad [17.40]$$

The approximation made in [17.40] consists in retaining only the first non-zero term of the integral of the Taylor expansion of the pressure gradient. Using [17.36] leads to:

$$F_{rp} = -\rho_f \frac{u_\theta^2(r_p)}{r_p}\frac{m_p}{\rho_s}\,. \qquad [17.41]$$

With equations [17.37], [17.38], and [17.41] expressing the forces exerted on the particle, the fundamental law of dynamics applied to the particle is stated as:

$$\begin{aligned}(m_p + \frac{1}{2}m_f)\frac{\mathrm{d}u_{rp}}{\mathrm{d}t} &= F_{rf} + F_{rp} + F_{rc} = \\ & m_p(1-\frac{\rho_f}{\rho_s})\frac{u_{\theta p}^2(r_p)}{r_p} - 3\pi\mu d(u_{rp} - u_r)\end{aligned} \qquad [17.42]$$

in the radial direction. Equation [17.42] is a simplified form which incorporates the predominant terms that we have identified while studying the BBOT equations. Relation [17.42] takes into account the added mass, yet it omits the Basset terms, among others. The new viewpoint introduced here is the calculation of the pressure force, which is not very apparent in the BBOT equations.

The last result from Chapter 16 to be employed is regarding the acceleration of a particle within the fluid flow. For a small particle, the equilibrium between the three forces F_{rc}, F_{rp}, and F_{rf} is reached in a time of the order of:

$$t_p = \left(2\frac{\rho_s}{\rho_f} + 1 \right) \frac{d^2}{36\nu}. \qquad [17.43]$$

The numerical estimations carried out in Chapter 16 (Table 16.1) show that this time is short (more so for a particle in water than for a particle in air), so that the acceleration in [17.42] can be neglected and the equilibrium between the above-mentioned three forces can be considered verified at all times.

The equilibrium of the three forces is depicted in Figure 17.8. Having neglected the acceleration, this can be translated by transforming [17.43] into the form:

$$u_{rp} = \frac{\mathrm{d}r_p}{\mathrm{d}t} = u_r(r_p) + \frac{(\rho_s - \rho_f)d^2}{18\mu} \frac{u_\theta^2(r_p)}{r_p} = u(r_p) + W_c \frac{u_\theta^2(r_p)}{g r_p}. \qquad [17.44]$$

As shown by equation [17.44], the radial velocity of centrifugation can be naturally expressed by bringing in Stokes' gravitational sedimentation velocity W_c (Table 15.1 in Chapter 15). This formulation makes it possible to establish a link with gravitational separation. The ratio $u_\theta^2(r_p)/gr_p$ is called the effectiveness coefficient of the centrifugal separation. The radial velocity of centrifugation is usually much larger than the gravitational settling velocity, because the effectiveness coefficient is large. The interest of centrifugal separators is to accelerate separation in comparison to gravitational separation processes.

The similarities between gravitational separation and centrifugal separation are strong. Equation [17.44] shows that the action of rotation is quantified by the difference between the density of the particle and that of the fluid. If $\rho_s > \rho_f$, the particle is centrifuged. In the reverse case, the particle experiences a movement toward the rotation axis (this is the case for air bubbles in a liquid, for example). The driving force is the difference between the centrifugal force exerted on the particle

and the pressure force exerted by the fluid. For gravitational separation, the driving force is the difference between the weight of the particle and the buoyancy force, which is the resultant of hydrostatic pressure forces exerted on the particle.

17.4. Centrifuge decanters

Centrifuge decanters are apparatus of a relatively elementary design. They are used for a coarse separation of particles, for example, in order to increase concentration in sludge. They are also encountered in the medical field for separating blood constituents such as platelets and leukocytes. In order to clarify a fluid with a high degree of quality, other apparatus need to be employed, such as centrifugal separators, which we shall discuss in section 17.5.

In the following, we successively apply the principle of centrifugal separation to the configuration of discontinuous decanter and then to that of a continuous decanter.

17.4.1. *Discontinuous centrifuge decanters*

Figure 17.9(a) shows a discontinuous decanter. The rotating part is a basket inserted in a fixed closed housing. The basket is rotated with an angular speed ω, which is maintained for a duration T_c. The particles contained in the fluid are gradually centrifuged toward the inner sidewall of the basket, on which a cake starts to thicken. Once the apparatus is stopped, the liquid is drained. The basket can be removed or the cake detached from the basket by a scraper, and then evacuated by a pipe.

Figure 17.9(b) describes the operating principle of a discontinuous centrifuge decanter. The fluid has a movement of solid-body rotation. If R designates the inner radius of the basket, it is considered that a particle is separated as soon as it touches the inner circular surface of the basket. For the configuration depicted in Figure 17.9(b), the housing is initially not completely filled with liquid. In an established flow regime, if the rotation is very fast, air is confined into a quasi-cylindrical circular tube, centered on the rotation axis. We denote by R_i its diameter. The centrifugation time T_c of all of the particles is the one required to centrifuge a particle initially located at the radial position R_i up to the radial position R. Equation [17.44] can be written, for solid-body rotation ($u_\theta(r_p) = \omega r_p$), as:

$$\frac{\mathrm{d}r_p}{\mathrm{d}t} = \frac{(\rho_p - \rho_f) d^2 \omega^2}{18\mu} r_p \,. \qquad [17.45]$$

(a)

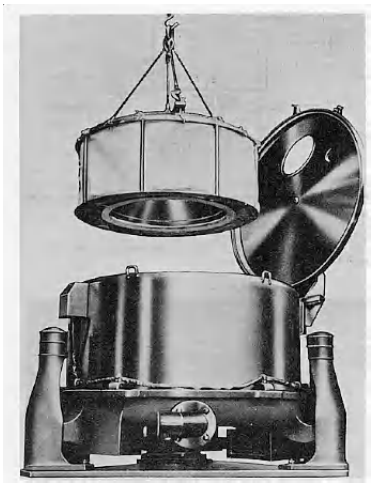

(Figure reproduced from P. Rivet, *Guide de la séparation liquide–solide*)

(b)

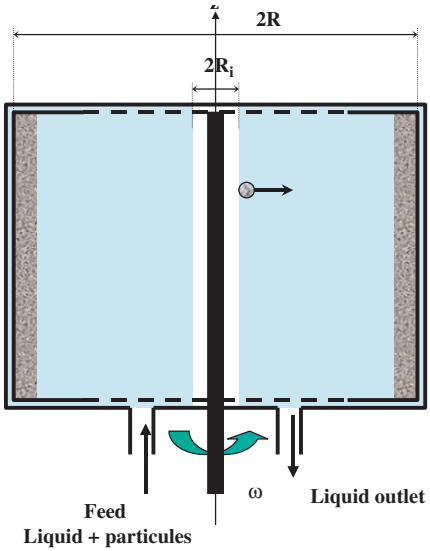

Figure 17.9. *Discontinuous centrifuge decanter with removable basket*

Integration leads to:

$$T_c = \frac{18\mu}{(\rho_p - \rho_f)d^2\omega^2}\ln\left(\frac{R}{R_i}\right). \qquad [17.46]$$

It would take an infinite time to centrifuge a particle located on the rotation axis ($R_i = 0$), as the centrifugal force is zero on the rotation axis. It is therefore desirable to fill the settling tank only partially if the particles are to be centrifuged in totality.

If the duration of operation $T_{\text{operation}}$ is less than time T_c, only the particles contained in the annular space:

$$R_1 = R \ \exp\left\{-\frac{(\rho_p - \rho_f)d^2\omega^2 T_{\text{operation}}}{18\mu}\right\} < r < R \qquad [17.47]$$

are separated. The effectiveness of settling is calculated as the ratio of the mass of particles agglomerated into a cake to the mass of particles introduced into the settling tank. If the concentration of particles is homogeneous in the suspension introduced into the settling tank, and if the settling tank is completely filled ($R_i = 0$), the effectiveness of the settling operation is simply the ratio of the volume of the annular space, defined by $R_1 < r < R$, to the total volume of the settling tank:

$$E = 1 - \frac{R_1^2}{R^2} = 1 - \exp\left\{-\frac{(\rho_p - \rho_f)d^2\omega^2 T_{\text{operation}}}{9\mu}\right\}. \qquad [17.48]$$

This dimensioning highlights several remarkable properties:

– The effectiveness of settling is independent from the dimensions of the settling tank.

– The effectiveness mainly varies with the size of the particles and the rotational speed, and it is very selective. For particles of density ρ_s = 3,000 g/L and size d = 1 μm in water, a centrifugation of duration $T_{\text{operation}}$ = 1 min has an effectiveness E = 0.036 for ω = 500 rpm and E = 0.995 for ω = 6,000 rpm. With common operating parameters, a settling tank will therefore easily separate particles whose size is in the order of microns.

– The centrifugation time calculated using relation [17.46] is short. In practice, we need to add the time required to impart the rotation on the basket and establish solid-body rotation.

17.4.2. *Continuous centrifuge decanters*

A sketch of a continuous centrifuge decanter is presented in Figure 17.10. The apparatus is fed continuously with a flow rate Q of fluid and particles, with the same flow rate (without particles) being tapped from another aperture. The extraction of particles is not continuous; they build up on the inner wall of the basket, like in the discontinuous decanter.

In the diagram shown in Figure 17.10, the fluid and particles are introduced into the bottom of the housing. They enter the annular section $R_i < R < R_e$ inside the basket through orifices provided at the base of the basket. The rotation is imparted to the fluid as they pass through. The fluid then ascends vertically in the central part of the basket and leaves from the top of the basket through an overflow, while the particles are centrifuged toward the inner sidewall of the basket.

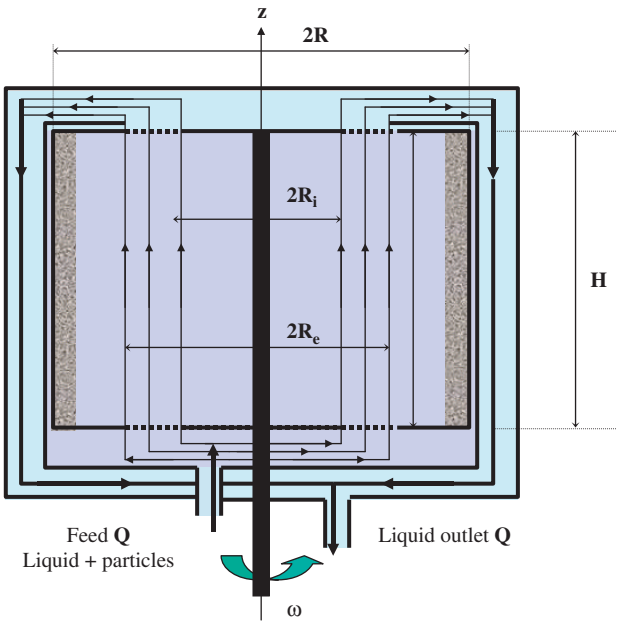

Figure 17.10. *Diagram of a continuous centrifuge decanter*

In the cylindrical coordinate system, the velocity components of the fluid are:

$$\begin{aligned} u_r(r) &\equiv 0 \\ u_\theta(r) &= \omega r \qquad \text{for } R_i < R < R_e \,. \\ u_z(r) &= Q / \pi(R_e^2 - R_i^2) \end{aligned} \qquad [17.49]$$

With [17.44], the velocity components of a fluid particle in the same domain are:

$$\begin{aligned} u_{rp} &= \frac{(\rho_p - \rho_f)\omega^2 d^2}{18\mu} r_p \\ u_{\theta p}(r_p) &= \omega r_p \\ u_{zp}(r_p) &= Q / \pi(R_e^2 - R_i^2) \end{aligned} \,. \qquad [17.50]$$

Denoting by H the height of the basket, the time taken by a particle to cross the basket vertically is $T_s = \pi(R_e^2 - R_i^2)H / Q$. This is the residence time in the apparatus and the time available to centrifuge a particle. All particles are centrifuged if a particle entering at the base of the basket at the radial position $r_p = R_i$ has a radial position $r_p(T_s) > R_e$. The trajectory starting from point ($r_p = R_i$, $z_p = 0$) is obtained by integrating:

$$\frac{\mathrm{d}r_p}{u_{rp}} = \frac{\mathrm{d}z_p}{u_{zp}} \qquad [17.51]$$

with the velocity components as per [17.50]. The criterion $r_p(T_s) > R_e$ leads to the separation criterion:

$$Q < \frac{(\rho_p - \rho_f)d^2\omega^2\pi H(R_e^2 - R_i^2)}{18\mu\, Ln(R_e / R_i)}, \qquad [17.52]$$

which means that all particles are retained in the apparatus.

Relation [17.52] is interpreted as a criterion on the residence time. The flow rate should therefore remain below a limiting value, for a specified rotation, in order for the resistance time inside the apparatus to be sufficiently long for achieving the centrifugation of all particles. It is verified from [17.52] that widening the annular spacing R_e - R_i does not improve the efficiency of separation.

17.5. Centrifugal separators

Centrifugal separators are used to clarify a liquid. These apparatus can commonly trap particles as minute as 0.1 μm.

Figure 17.11(a) presents the diagram of disc-stack centrifuge. The apparatus rotates with an angular speed ω about its axis of symmetry. It contains stacked truncated cones (radii R_e and R_i, angle α, number of inter-vane channels N and spacing e between two cones). The supply of fluid (density ρ_f and dynamic viscosity μ) and particles (diameter d and density ρ_s) is central, around the axis. The flow rate, denoted by Q, is radially distributed on the bottom wall of the rotating housing, then ascends along the cylindrical sidewall. By then, separation is already performed to a large extent, with a substantial fraction of the particles forming a cake on the cylindrical sidewall. The flow leaves the apparatus by going through inter-vane gaps between the stacked truncated cones. The finer particles are

separated when passing between the vanes if their trajectories touch the upper vane, under which they then slide due to the effect of the centrifugal force, before returning toward the cake.

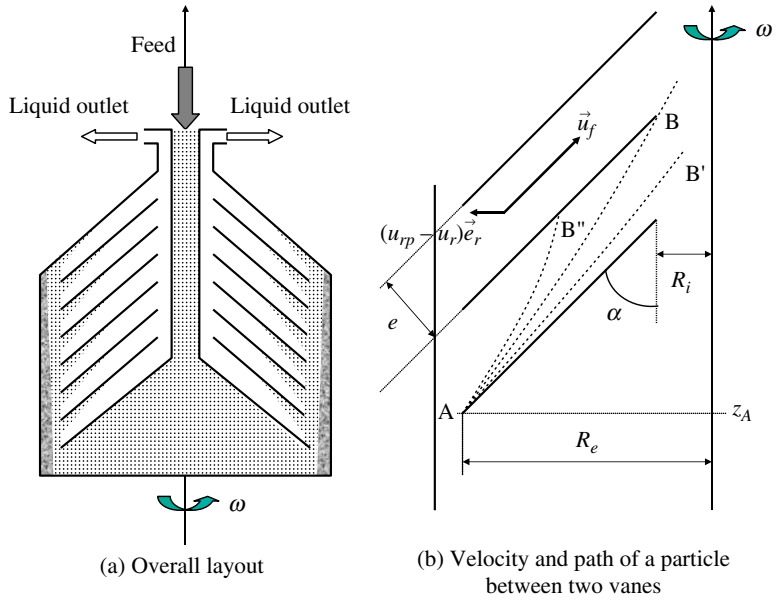

Figure 17.11. *Disc-stack centrifuge (figure adapted from P. Rivet, Guide de la séparation liquide–solide)*

The separation criterion for a particle of diameter d and density ρ_s is determined by calculating the trajectory of a particle between the vanes. Figure 17.11(b) represents the motion of particles in an inter-vane channel. The velocity of the fluid $\vec{u}_f$ is parallel to the vanes. The relative velocity of the particle with respect to the fluid, denoted by $(u_{rp} - u_r)\vec{e}_r$, results from centrifugation. It is calculated using equation [17.44]. It is assumed that the rotation of the fluid and particles is a movement of solid-body rotation. The velocity components of the particles are therefore:

$$\begin{aligned} \frac{\mathrm{d}r_p}{\mathrm{d}t} &= u_{rp} = -u_f \sin\alpha + \frac{(\rho_p - \rho_f) d^2 \omega^2}{18\mu} r_p \\ u_{\theta p} &= \omega r_p \\ \frac{\mathrm{d}z_p}{\mathrm{d}t} &= u_{zp} = u_f \cos\alpha \end{aligned} \quad . \qquad [17.53]$$

The velocity u_f of the fluid varies with the radial coordinate. Through mass conservation:

$$u_f(r) = \frac{Q}{2\pi Ne}\frac{1}{r}. \qquad [17.54]$$

It must be pointed out that assuming solid-body rotation in the channels between the vanes implies that angular momentum is not conserved. Conservation of angular momentum would make the fluid and the particles increase their rotational speed as they get closer to the rotation axis. However, a secondary flow is produced by the boundary layers on the cones, which counteracts the increase in rotational speed in the spaces between the vanes. This mechanism explains how solid-body rotation can be maintained within the channels, when the spacing is small $(e \ll (R_e - R_i))$.[5] The trajectories of solid particles are determined by integrating the differential equation:

$$\frac{\mathrm{d}r_p}{\mathrm{d}z_p} = \frac{u_{rp}}{u_{zp}} = -tg\alpha\left\{1 - \frac{(\rho_p - \rho_f)d^2\omega^2 Ne\pi}{9\mu Q\sin\alpha}r_p^2\right\} = -tg\alpha\left\{1 - \frac{r_p^2}{R^2}\right\} \qquad [17.55]$$

The quantity:

$$R = \sqrt{\frac{9\mu Q\sin\alpha}{(\rho_p - \rho_f)d^2\omega^2 Ne\pi}} \qquad [17.56]$$

has the dimension of a length. We consider the case where $R > R_e$. In the opposite case, the flow rate is too low, a particle cannot enter the inter-vane space, and the retention of all particles by the apparatus is necessarily performed.

In Figure 17.11(b), trajectories are sketched that correspond to different particle sizes. If the particle is very fine, centrifugation is very weak. The trajectory of the particle differs only slightly from that of a fluid particle (trajectory AB′). The particle leaves the inter-vane channel without touching the top wall. A particle is only retained in the apparatus if it is sufficiently large. In that case, its trajectory touches the upper vane (trajectory AB″), and then slides in the opposite direction under the upper vane because of the effect of the centrifugal force. The limiting trajectory, for which the particle enters at A and touches the upper vane at its end B, corresponds to a particle size $d_{\min}$ such that all particles whose size d is greater than

5 We do not describe the mechanism in further detail, as this would require substantial developments regarding boundary layers in a rotating flow.

$d_{\min}$ are separated by the apparatus, while particles whose size is less than $d_{\min}$ are only partially trapped.

Integrating the differential equation [17.55] poses no real difficulty. The trajectory of a particle entering an inter-vane gap at A ($r_p = R_e$, $z_p = z_A$) is written as:

$$z_p - z_A = \frac{R}{tg\alpha}\left\{Argth\left(\frac{R_e}{R}\right) - Argth\left(\frac{r}{R}\right)\right\}. \qquad [17.57]$$

The particle is separated if $z_p(R_i) - z_A > (e + (R_e - R_i)\cos\alpha) / \sin\alpha$, that is, if:

$$R\cos\alpha\left\{Argth\left(\frac{R_e}{R}\right) - Argth\left(\frac{R_i}{R}\right)\right\} > e + (R_e - R_i)\cos\alpha\,. \qquad [17.58]$$

When the gap is sufficiently narrow ($R_i / R << 1$), a Taylor expansion of [17.58] leads to the separation criterion:

$$Q < \frac{(\rho_p - \rho_f)d^2\omega^2}{9\mu}\frac{\pi(R_e^3 - R_i^3)}{3tg\alpha}N\,. \qquad [17.59]$$

Equality is obtained for the particle size $d_{\min}$. The result does not depend on the spacing e between two conical vanes. This is the result of the Taylor expansion associated with the hypothesis $R_i / R << 1$.

The separation criterion [17.59] is analogous to that obtained for the continuous centrifugal decanter (equation [17.52]). The differences are only geometrical. For both cases, increasing the fluid flow rate Q leads to a reduction in the effectiveness of separation. The time of residence inside the apparatus conditions the separation effectiveness. It is also found that separation is improved by increasing the number of cones. This amounts to an increase in the separation areas (the particle thus has more chances of touching a wall). This is a general property of centrifugal or gravitational settling systems.

17.6. Centrifugal filtration

The cakes collected on the walls of a centrifugal decanter or centrifugal separator retain a substantial amount of water. A complementary process is often required to more thoroughly dehydrate the cake. Drying and centrifugal filtration are such processes.

We describe in the following the principle of centrifugal filtration, by considering in Figure 17.12 a geometry similar to the geometry of a discontinuous decanter previously considered in Figure 17.9. The basket, which rotates with angular speed ω, is provided with slits and lined with a filter web. Water is removed by a process of filtration through the cake and the filter web, the driving force of which is the centrifugal force. The generalization of Darcy's law, in order to incorporate the centrifugal force, is written in the circular cylindrical coordinate system in the radial direction:

$$\frac{\mu}{k} u_r(r) = -\frac{\partial p}{\partial r} + \rho_f \frac{u_\theta^2(r)}{r} . \qquad [17.60]$$

$u_r(r)$ is the radial component of the throughflow velocity in the filter medium and $u_\theta(r)$ the azimuthal component of the velocity; k designates the permeability of the filter medium. The extension of Darcy's law is similar to what we have done in Chapter 14 (section 14.2) in order to take gravity into account.

As in a centrifuge decanter, the rotational flow is a solid-body rotation ($u_\theta(r) = \omega r$). The filtration process is axisymmetric. At any time, the flow rate through any cylinder of radius r is identical. The radial filtration velocity is related to the permeate flow rate by $Q = 2\pi H r u_r(r)$, and [17.60] becomes:

$$\frac{\partial p}{\partial r} = \rho_f \omega^2 r - \frac{\mu Q}{k 2\pi H r} . \qquad [17.61]$$

H is the height of the centrifugal filter, as indicated in Figure 17.12.

The filtration flow rate is determined by integrating [17.61] over the thickness of the different filter media and using the continuity of pressure at the different interfaces. The procedure is identical to the one followed in Chapter 14 (section 14.3.2) to introduce the notion of membrane resistance to filtration. In the present case (Figure 17.12), three layers can be distinguished:

1. The layer of liquid outside the cake ($R_i(t) < r < R_g$). The thickness of this layer diminishes in time as the filtration progresses. The balance of the centrifugal force with the pressure gradient applies to this layer (equation [17.61] with infinite permeability).

2. Cake ($R_g < r < R$), whose permeability is denoted by k_g.

3. Filter web ($R < r < R + H_f$). We denote by k_f its permeability and H_f its thickness.

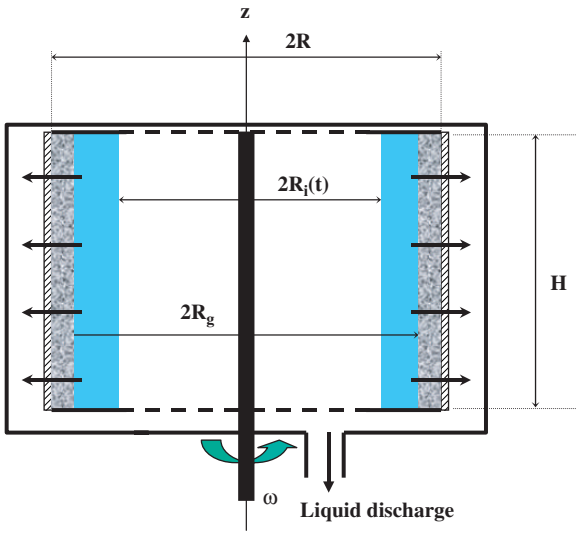

Figure 17.12. *Centrifugal filtration with circular cylindrical geometry*

Integrating [17.61] over each of the three layers leads to:

$$P_1 - P_{\text{atm}} = \rho_f \omega^2 \frac{(R_g^2 - R_i^2)}{2}, \qquad [17.62]$$

$$P_2 - P_1 = \rho_f \omega^2 \frac{(R^2 - R_g^2)}{2} - \frac{\mu Q}{k_G 2\pi H} \ln\left(\frac{R}{R_g}\right), \qquad [17.63]$$

$$P_{\text{atm}} - P_2 = \rho_f \omega^2 \frac{((R + H_f)^2 - R^2)}{2} - \frac{\mu Q}{k_F 2\pi H} \ln\left(\frac{R + H_f}{R}\right) \qquad [17.64]$$

P_1 and P_2 are respectively the pressure values at the interfaces between the liquid and the cake and between the cake and the filter. The pressure that prevails at the exit of the filter and at the liquid/air interface internal to the apparatus is the atmospheric pressure. By summing equations [17.62–17.64], the filtration rate Q is determined as a function of rotation and the geometrical characteristics:

$$\rho_f \omega^2 \frac{((R + H_f)^2 - R_i^2)}{2} = \frac{\mu Q}{2\pi H} \left\{ \frac{1}{k_g} \ln\left(\frac{R}{R_g}\right) + \frac{1}{k_f} \ln\left(\frac{R + H_f}{R}\right) \right\} \qquad [17.65]$$

As $H_f << R$, this expression simplifies so as to bring in the filter web's resistance, $R_f = H_f / k_f$:

$$\rho_f \omega^2 \frac{(R^2 - R_i^2(t))}{2} = \frac{\mu Q(t)}{2\pi HR}\left\{\frac{R}{k_g}\ln\left(\frac{R}{R_g}\right) + R_f\right\} \qquad [17.66]$$

The permeate flow rate $Q(t)$ decreases in time with the increase of the radius $R_i(t)$ of the air cylinder. A spin-drying process, which corresponds to the draining of filter media, is entered when the air/liquid interface is inside the cake ($R_g < R_i(t) < R$). Equation [17.66] then transforms into:

$$\rho_f \omega^2 \frac{(R^2 - R_i^2(t))}{2} = \frac{\mu Q(t)}{2\pi HR}\left\{\frac{R}{k_g}\ln\left(\frac{R}{R_i(t)}\right) + R_f\right\}, \qquad [17.67]$$

since the fraction of the cake that intervenes in the filtration process is $R_i(t) < r < R$. For both cases considered in equations [17.66] and [17.67], the permeate flow rate is determined after transforming either equation into a differential equation for $R_i(t)$ by means of the kinematic relation inferred from the mass balance:

$$Q(t) = 2\pi HR_i \frac{\mathrm{d}R_i}{\mathrm{d}t}(t) \qquad [17.68]$$

Commercially available centrifugal filters and spin-dryers are of very diverse geometries. We do not describe them here, but we wished to point out how the dimensioning of these apparatus is akin to that of a filtration device, and how the centrifugal force intervenes as the driving force of filtration.

17.7. Hydrocyclones

The fluid flow in a hydrocyclone has been described in section 17.2.3. Hydrocyclones are used for separating particles that are denser than the fluid or for separating lighter elements (oil droplets, for example). In the first case, the particles are thrown onto the conical sidewall of the apparatus and then extracted through the spigot. In the second, the droplets migrate toward the *Oz* axis of the apparatus and are extracted via the overflow.

The shape of the apparatus is similar in both cases. They mainly differ by a change in the ratio of the diameter $2R_b$ of the spigot to that of the overflow $2R_c$. As the flow rate of the dispersed phase is lower than that of the continuous phase, it is necessary to reduce as much as possible the flow rate extracted through the spigot with respect to the one that comes out via the overflow, in order to separate particles that are denser than the fluid. The spigot diameter $2R_b$ is smaller than the diameter $2R_c$, as in the example of Figure 17.5. Conversely, the spigot diameter will be greater than that of the overflow if we wish to separate a dispersed phase consisting of droplets less dense than those in the continuous phase, in such a way as to extract most of the continuous phase through the spigot while the dispersed phase comes out through the overflow. A head loss calculation, the principle of which has been described in section 17.2.3, determines the flow rates Q_b and Q_c exiting the spigot and the overflow as a function of the geometry of the apparatus and the hydraulic circuit in which it is placed.

17.7.1. *Separation by a hydrocyclone of particles that are denser than the fluid*

Figure 17.13 represents the separation by a hydrocyclone of dispersed phase consisting of particles that are denser than the fluid. This very classical configuration is simplified with respect to those represented in Figures 17.5 and 17.7, since the spigot opens into a closed cavity (underflow box). The fluid flow rate extracted via the spigot is zero in this case, and $Q = Q_c$. Under the effect of centrifugation, the particles are first carried by the flow until they reach the conical wall of the cyclone. They then slide downward because of gravity along the wall until they exit through the spigot. The angle θ of the cone has to be sufficiently small for the projection parallel to the wall of the centrifugal force (which is oriented upward) not to be greater than the projection of the gravity force. If that were to be the case, the particles would ascend.

Figure 17.13 helps us understand simply the criterion guaranteeing that any particle of diameter d and density ρ_s is separated, as it exits via the spigot. We consider a particle entering the lower cavity at point A. The dashed arrow joining point A to point B represents the trajectory of the particle. At A ($r = R_c$, $z = H$), the radial velocity of the particle is the sum of the fluid's velocity (equation [17.35]) and the relative velocity of the particle with respect to the fluid due to centrifugation (equation [17.44]):

$$u_{rp}(R_c, H) = -\frac{Q(R - R_b)}{2\pi H(R - R_c)R_c} + \frac{(\rho_p - \rho_f)d^2}{18\mu}\frac{u_\theta^2(R_c)}{R_c} \qquad [17.69]$$

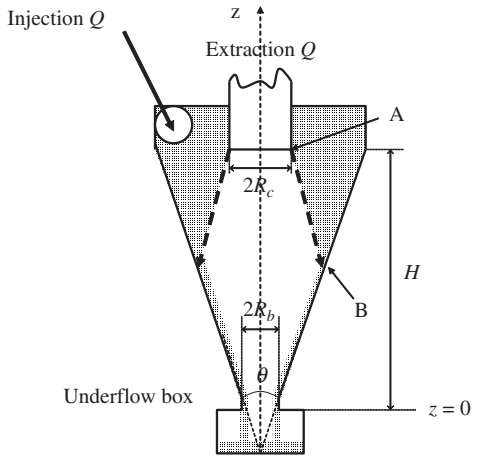

Figure 17.13. *Separation, by a hydrocyclone, with an underflow box, of particles that are denser than the fluid. The dispersed phase is shaded*

As the rotational flow is of vortex type (equation [17.18]), with the circulation given by [17.24], we infer:

$$u_{rp}(R_c, H) = -\frac{Q(R - R_b)}{2\pi H(R - R_c)R_c} + \frac{(\rho_p - \rho_f)d^2}{18\mu}\frac{Q^2(R - R_i)^2}{\pi^2 R_i^4 R_c^3} \qquad [17.70]$$

The particle entering at A is in the most unfavorable position to be separated. If this particle reaches the underflow box, then all the particles entering the apparatus will do the same. The trajectory AB drawn in Figure 17.13 is such that $u_{rp}(R_c, H) > 0$. Otherwise, the particle enters the extraction section of the overflow. It is then immediately carried into the overflow. The criterion for no particle to come out through the overflow is therefore $u_{rp}(R_c, H) > 0$. It follows that:

$$Q > \frac{9\pi\mu R_i^4}{(\rho_p - \rho_f)d^2 H}\frac{(R - R_b)R_c^2}{(R - R_i)^2 (R - R_c)} \qquad [17.71]$$

The separation condition remains $u_{rp}(R_c, H) > 0$ when there is one discharge flow per nozzle, but the flow rates Q_b and Q_c need to be known in order to express the criterion in a form similar to [17.71].

Relation [17.71] gives the separation condition for any particle of size d introduced into the hydrocyclone. The equality determines the maximum size d_{max} of the particles so that all of them flow out through the spigot. By comparison with the results obtained for centrifuge decanters (equation [17.52]) and separators (equation [17.59]), it is found that the larger the flow rate is, the more effective the separation performed by a hydrocyclone will be. In the previous two cases, the flow rate should not exceed a certain value. This remarkable result, which seems surprising at first glance, since the residence time diminishes when the flow rate increases, is explained by the fact that the intensity of the vortex increases with the squared flow rate.

Engineers commonly use what they call the partition curve to characterize separation by a hydrocyclone. An example is represented in Figure 17.14. The ratio of the mass of particles exiting through the spigot to the mass entering at the inlet is plotted versus particle size. Hydrocyclones are sometimes also used to perform grain size sorting operations. If a fluid simultaneously contains large particles and fine particles, it is possible to select the operating conditions in such a manner that all the large particles will be extracted via the spigot and a maximum of fine ones come out through the overflow.[6]

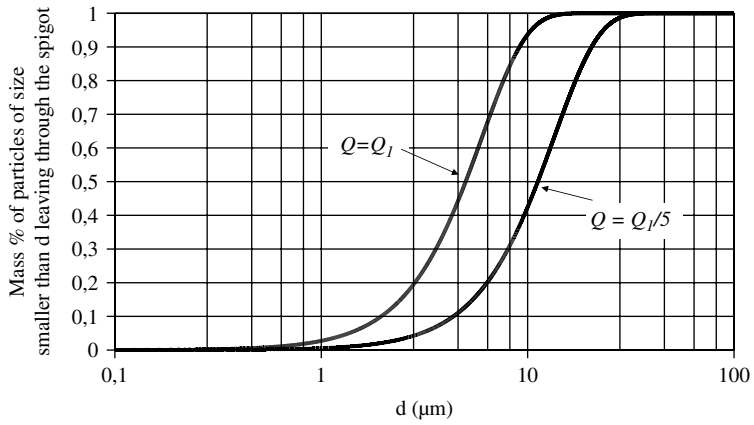

Figure 17.14. *Partition curve of a hydrocyclone for two values of the flow rate*

The main benefit of hydrocylones is their simplicity. In mechanical terms, they do not consist of any moving parts. However, these apparatus cause a substantial head loss, since the energy of rotation is lost. Moreover, the separation characteristics of a hydrocyclone are closely dependent on the head losses at the

6 This case is suggested as an exercise at the end of this chapter.

apparatus outlets, which set the flow rates extracted through the spigot and overflow. Adjusting the operating parameters of a hydrocyclone to perform a mechanical separation operation can prove delicate.

17.7.2. *Separation by a hydrocyclone of particles less dense than the fluid*

When the particles are less dense than the carrier fluid, centrifugation gathers the particles onto the apparatus axis. The dispersed phase is often constituted of droplets (of oil, for example) or air bubbles. These coalesce to form a continuous tube on the axis. The lighter phase is extracted via the overflow, while the heavier phase is tapped through the spigot. This situation is depicted in Figure 17.15. The geometry of the configuration in Figure 17.15(a) is similar to that considered in Figure 17.13 for the separation of particles that are denser than the fluid. For a droplet of size d, the most difficult particle to extract via the overflow is the one entering the upper part of the apparatus at A. If it leaves through the overflow, all particles of the same size will do the same. The trajectory AB of this particle is drawn in Figure 17.15(a). The particle leaves through the overflow if the vertical velocity at B is positive, whereas it will be extracted via the spigot if that velocity component is negative at that point. Based on the velocity field [17.35], it can be established that the criterion for all droplets of size d to be extracted via the overflow is that the axial position of point B be above the point where the vertical velocity becomes zero. This is expressed, using [17.35], by:

$$\frac{z(B)}{H} > \frac{1}{1+\dfrac{Q_c(R_b^2-a^2)}{Q_b(R_c^2-a^2)}} = \frac{1}{1+\dfrac{\overline{W}_c}{\overline{W}_b}} \qquad [17.72]$$

$\overline{W}_b$ and $\overline{W}_c$ are the mean stream-wise velocities in the spigot and overflow. Relation [17.72] translates into a criterion that is analogous to [17.71], but this requires calculating the trajectory AB for known flow rates Q_b and Q_c. Equation [17.72] shows that it is preferable to have a moderate stream-wise velocity through the spigot, so as to allow the dispersed phase to descend sufficiently low without risk of it being entrained through the spigot. This geometrical drawback can be overcome by blocking the spigot at its center (Figure 17.15(b)).

The different cases of centrifugal separation treated in sections 17.4–17.7 of this chapter implement three steps: (i) determination of the velocity field of the fluid, (ii) determination of the velocity of a particle by incorporating the centrifugation term (equation [17.44]), and (iii) formulation of a physical criterion ensuring that all particles entering the apparatus are separated. It is sought to identify the particle entering the apparatus that will be the most difficult to separate. The mathematical

calculation that follows is then either a trajectory calculation or a direct criterion on the velocity of the particle at one point. The exercise at the end of this chapter allows this approach to be implemented autonomously.

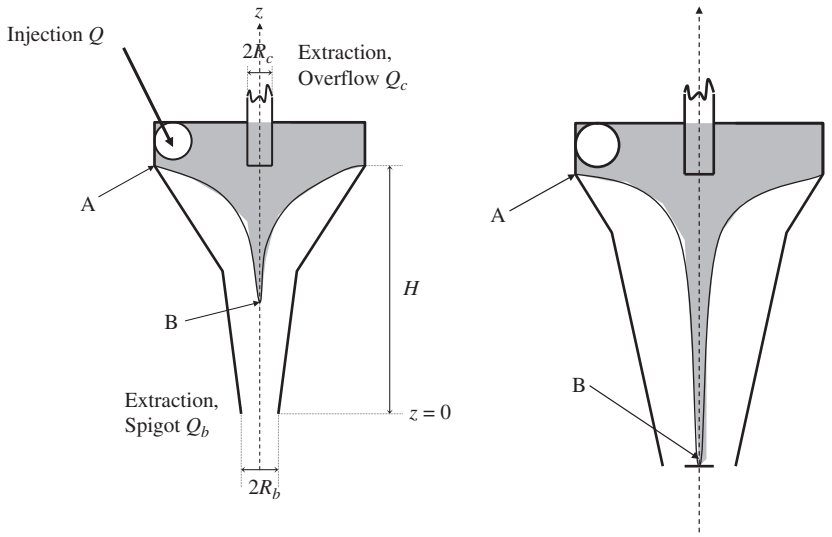

(a) Configuration with an open spigot (b) Configuration with a blocked spigot

Figure 17.15. *Separation by a hydrocyclone of droplets less dense than the fluid. The dispersed phase, which is shaded, is extracted via the overflow*

17.8. Energetics of centrifugal separation

It is not easy to accurately calculate the energy consumption of centrifugal separation. The general idea is that the energy of the rotational flow, which is the sum of the kinetic energy and the pressure energy, is lost in the apparatus. These are substantial energy consumptions.

For a discontinuous centrifuge decanter, such as that illustrated in Figure 17.9(b), the kinetic and pressure energy of a particle located at a radial distance r from the rotation axis are deduced from equations [17.10] to [17.11]:

$$E_c(r) = \rho \frac{\omega^2 r^2}{2}$$
$$p(r) = P_{\text{atm}} + \rho \frac{\omega^2}{2}(r^2 - R_i^2) \qquad [17.73]$$

The total energy integrated over the liquid volume, which is lost at each operation, is:

$$E_{\text{tot}} = 2\pi H \int_{R_i}^{R} r\left(E_c(r) + p(r) - P_{\text{atm}}\right)\mathrm{d}r = \rho\omega^2 \frac{R^2}{2}\pi H(R^2 - R_i^2) \qquad [17.74]$$

It is proportional to the maximum velocity of rotation and the volume of liquid.

In a hydrocyclone, the flow is of the vortex type. The rotational velocity (equation [17.18]) and pressure (equation [17.20]) in the irrotational zone enable the calculation of the rotational energy of a particle situated at radial distance r from the rotation axis:

$$E(r) = \rho\frac{v^2(r)}{2} + p(r) = p_0 + \rho\frac{\Gamma^2}{4\pi^2 a^2} \qquad [17.75]$$

This quantity is independent of the radius r. It is necessary to know the pressure p_0 at the center of the vortex in the hydrocyclone in order to calculate the power of the dissipated rotational energy:

$$\text{Power} = \left\{p_0 + \rho\frac{\Gamma^2}{4\pi^2 a^2} - P_{\text{atm}}\right\}Q\,, \qquad [17.76]$$

but this formula makes it possible to appreciate the large increase in dissipated power when the flow rate increases, in light of the relation [17.24] linking the circulation Γ to the flow rate Q.

17.9. Application exercise

Exercise 17.I: Grain size sorting in a hydrocyclone

We study, in a simple geometrical configuration, the way a hydrocyclone can be used to sort fine and coarse particles contained in a fluid. We determine how the flow rates should be selected, based on given geometrical dimensions and particle characteristics, in order to perform this sorting in the most satisfactory manner possible.

It is assumed that the fluid contains "large" spherical particles of diameter d_1 and "fine" spherical particles of diameter d_2. The density of the solid particles is assumed to be the same and these particles are assumed to be denser than the fluid ($\rho_s > \rho_f$).

A sketch of the apparatus is shown in the Figure 17.I.1. Through the central orifice (radius R_4), a flow rate Q_2 is extracted, and it is arranged for fine particles only to come out via this orifice. Through the annular orifice between radii R_3 and R_2, a flow rate Q_1 is extracted. The operating conditions will be selected so that all the large particles exit via this orifice. A flow rate $Q_1 + Q_2$ enters the apparatus.

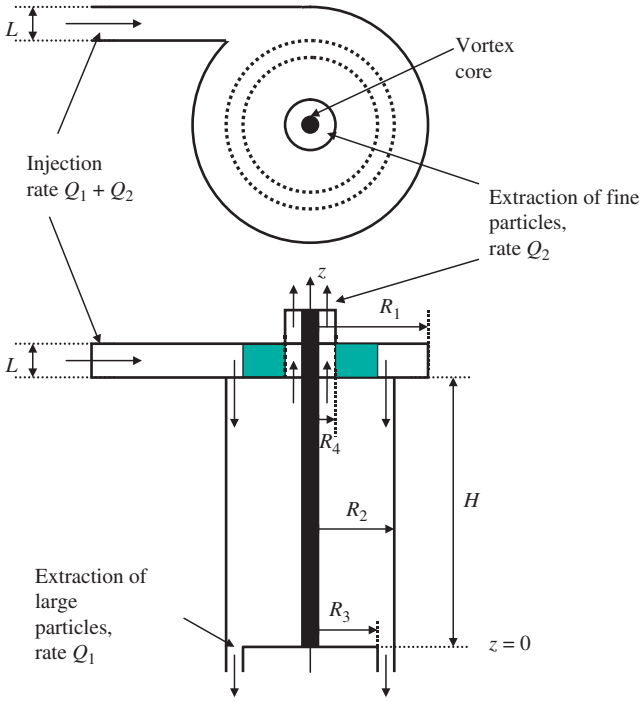

Figure 17.I.1

1. Justify that the rotational flow is of the form:

$$u_\theta(r) = \frac{\Gamma}{2\pi r} \quad \text{for } a < r < R_2$$

Why is it necessary that $a < R_4$?

Prove that the circulation of the vortex is $\Gamma = 2\pi \frac{Q_1 + Q_2}{L^2}\left(R_1 - \frac{L}{2}\right)$.

2. It is assumed that the flow is uniform in the inlet section of the lower cavity ($z = H$, $R_3 < r < R_2$) and in the outlet sections ($z = 0$, $R_3 < r < R_2$; $z = H$, $a < r < R_4$) of the apparatus. Prove that, in the cylindrical coordinate system (O,r,θ,z) whose Oz axis coincides with the apparatus axis, the field of the axial and radial components of the velocity can be modeled as follows ($z = 0$ is on the bottom):

$$u_r(r) = \frac{Q_2}{2\pi H(R_2^2 - R_3^2)} \frac{(r^2 - R_2^2)}{r} \quad \text{for} \quad R_3 < r < R_2$$

$$u_z(r,z) = -\frac{Q_2}{\pi(R_2^2 - R_3^2)} \frac{z}{H} - \frac{Q_1}{\pi(R_2^2 - R_3^2)} \quad \text{for} \quad R_3 < r < R_2$$

$$u_r(r) = -\frac{Q_2}{2\pi H} \frac{1}{r} \quad \text{for} \quad R_4 < r < R_3$$

$$u_z(r,z) = 0 \quad \text{for} \quad R_4 < r < R_3$$

$$u_z(r,z) = \frac{Q_2}{\pi(R_4^2 - a^2)} \frac{z}{H} \quad \text{for} \quad a < r < R_4$$

Which of the two components u_r and u_z is determined first? How is the second component derived from the first?

3. We denote by $r_p(t)$ and $z_p(t)$ the coordinates of a particle. Write the equations of motion for a solid particle in the domain $a < r < R_2$ under the effect of centrifugation and advection by fluid flow.

$$\frac{\mathrm{d}r_p}{\mathrm{d}t} = ? \quad \frac{\mathrm{d}z_p}{\mathrm{d}t} = ?$$

4. Write the criterion which makes it possible to ensure that the large particles come out through the annular orifice at the bottom of the apparatus.

5. Explain why a fraction of the fine particles necessarily exits through the annular orifice at the bottom, along with the large particles.

6. Write the criterion necessary for a fraction of the fine particles to exit via the central orifice. This will require verifying that the particles entering at $r = R_3$ into the domain $R_4 < r < R_3$ reach the position $r = R_4$. What happens if this is not the case? Show that, for a known radius ratio R_4 / R_3, this imposes a condition on the particle size ratio d_2 / d_1.

7. How should the flow rate Q_2 be selected to allow optimal sorting of the fine particles from the large ones, that is, to obtain the lowest possible fraction of fine particles leaving from the bottom with the large ones? Starting from the equations established in Question 3, describe the method which would enable the calculation of the fraction of fine particles exiting through the central orifice. Do not perform any differential equation resolution or integral calculation, but describe the limiting trajectory that allows its determination, by drawing it in the figure.

Chapter 18

Notions on Granular Materials

The mechanics of granular materials, which were once of interest only to specialists in geomechanics, have considerably developed, and its applications have widened to include other fields in physics. As far as processes are concerned, it has wide applications in the agri-food industry for understanding mechanics inside silos or in logistics for the transport of granular materials. A fluid dynamicist can no longer stay detached from the mechanics of granular materials. The notion of angle of repose, as well as of powder flowability, is frequently employed by engineers.

This chapter has quite modest ambitions. We limit ourselves to the introduction of a few fundamental notions about granular materials, in order to facilitate access to this field of mechanics, and to setting out what distinguishes a granular material from a fluid medium. These differences will be illustrated by two important applications:

1. The pressure distribution in a granular material at static equilibrium within the gravity field, which differs from the one that establishes itself in a fluid. The case of tanks/silos will be discussed.

2. The flow of a granular material, for example in an hourglass, which differs from that of a fluid. The reasons for this will be explained.

Flows of cohesive granular materials will not be discussed, setting aside the notion of powder flowability whose introduction requires to be complemented by drawing on examples from continuum mechanics. For non-cohesive granular materials, we shall propound a macroscopic approach, which describes phenomena within the framework of continuum mechanics. This approach, with the highly classical Janssen model (1895), enables the silo effect in pressure distribution to be

modeled, but does not entirely explain its nature. To really understand the mechanics of granular materials, we have to rely on a microscopic approach, which elucidates the discrete structure of inter-grain contacts. We will deal with this issue very briefly, being content with a description of the dilatancy mechanism and of arch phenomena in a granular material. More on this can be found in specialized publications.[1]

18.1. Static friction: Coulomb's law of friction

The mechanics of granular materials is based on the very simple concept of static friction, modeled by Coulomb's law. Considering a solid lying on a planar wall, which is horizontal with respect to the direction of gravity (Figure 18.1), it is a routine observation that the heavier the solid is, the greater will be the magnitude of the force $\vec{T}$ required to drag it or push it from rest.

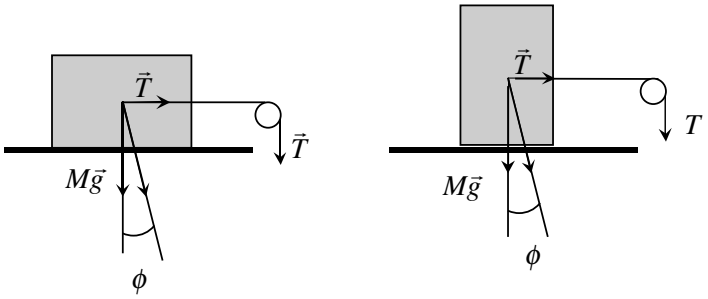

Figure 18.1. *Traction force required to initiate the movement of a solid lying on a horizontal plane. The cuboid has been rotated between the two cases and the area of the cuboid in contact with the plane is different, but the traction force* $\vec{T}$ *is identical*

These observations are made more specific by stating the following properties:

– The magnitude of the traction force $\vec{T}$ needed to move the solid is proportional to the weight Mg.

– The intensity of the traction force $\vec{T}$ does not depend on the area S of the contact surface between the solid and the supporting plane. The same force needs to be applied to move the object horizontally in both the situations depicted in Figure 18.1, between which the same solid has been rotated by a 90° angle.

---

1 These include the following two books, on which this chapter draws: Duran, J., *Sables, Poudres and Grains* (Eyrolles Sciences, 1997). *Mécanique des milieux granulaires* (collective work edited by J. Lanier, Hermès Science, 2001).

These two properties result in the relation.

$$\frac{T}{Mg} = \frac{\tau}{P} = f = tg\varphi \qquad [18.1]$$

The force and stress ratios are equal. P designates the pressure (normal stress) between the solid and the support (which is assumed to be homogeneous throughout the contact surface) and τ the friction stress at the same point associated with the traction force (tangential stress). The ratio f is the coefficient of static friction, whereas the angle ϕ between the two components of the forces applied to the solid is termed the static angle of friction. While it is independent of the area S of the surface, the friction angle does depend on the "quality" of the contact between the two surfaces, such as asperities on the two faces in contact.

Relation [18.1] is usually referred to as Coulomb's law of friction. The value of the ratio [18.1] between the tangential stress and the normal stress is the one required to initiate the movement. The associated friction angle ϕ is described as static. If the applied traction force is smaller, the solid remains stationary and resists its movement with a resistance force which is equal and opposite to the traction force applied to it. As soon as the solid starts moving, the ratio of the friction stress to the normal stress is modified and becomes less than its value in the static case. When the solid moves, the ratio f is termed the coefficient of kinetic friction. While Coulomb's law is conceptually simple, its mathematical implementation in a practical problem is delicate, as the tangential force opposing the displacement depends on the amount of force applied and its direction is opposite to the side toward which the solid is being pushed.

18.2. Non-cohesive granular materials: Angle of repose, angle of internal friction

The static friction angle introduced in the previous section corresponds to the angle of inclination that needs to be applied to the supporting plane in order to make the solid slide under the effect of gravity. This is illustrated in Figure 18.2. When the plane is sloping at an angle α, the projection of the solid's weight onto the direction perpendicular to the supporting plane is the normal force applied on the supporting plane, while the tangential traction force is the projection of the weight onto the direction parallel to the plane. When the angle of inclination α reaches the static friction angle ϕ, the ratio between the tangential stress and the normal stress becomes $tg\phi$ and the solid starts moving.

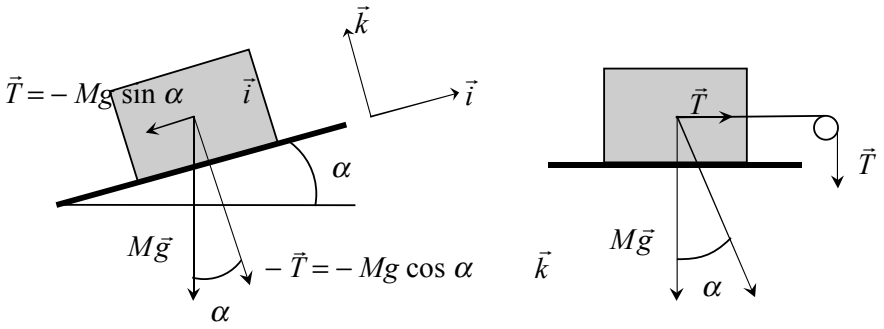

Figure 18.2. *Friction angle and sliding of a solid on an inclined plane*

These ideas can be generalized to the case of a granular bed of non-cohesive particles deposited on a plane, wherein the porosity ε is homogeneous, as illustrated in Figure 18.3.

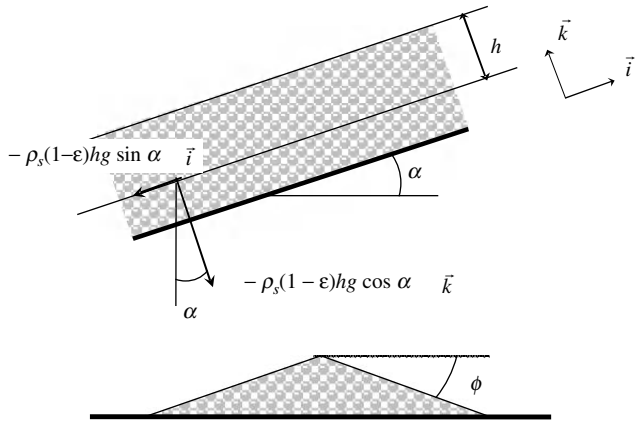

Figure 18.3. *Angle of internal friction and natural angle of repose of a granular material*

Consider a layer of particles with homogeneous characteristics (of size and shape) deposited on a plane which is inclined at an angle α on the horizontal. If the bed is at static equilibrium, the two components of the force exerted per unit surface by a surface layer of thickness h on the underlying layer are:

$$\begin{aligned} &-\rho_s gh(1-\varepsilon)\sin\alpha \ \ \vec{i} \\ &-\rho_s gh(1-\varepsilon)\cos\alpha \ \ \vec{k} \end{aligned} \qquad [18.2]$$

ρ_s is the density of the particles. These relations mean that the reaction force exerted at the lower boundary balances the weight of the layer. The ratio of the two components is $tg\alpha$; it is independent from the thickness h of the layer. It is noted that the granular layer flows if the angle α exceeds a limiting value ϕ called the angle of internal friction of the granular material. As both components of the force applied on the lower layer vary linearly with h, the departure from equilibrium occurs simultaneously for the entire granular bed deposited on the inclined plane. It then flows in its entirety.

The granular bed flows only if the inclination angle exceeds the angle of internal friction. The macroscopic friction stress, introduced for a granular material with the notion of angle of internal friction, results both from the microscopic-scale friction between grains and from the entanglement of the grains, because the particles lie in depressions formed between the particles on top of which they lie. The internal friction angle corresponds to the maximum slope of a pile of sand that is left to settle on a horizontal plane. This situation is also represented in Figure 18.3. For this reason, the internal friction angle ϕ is also called the *natural angle of repose*. In a dry medium, the natural angle of repose hardly varies and is around the value of 30° for particles such as sands. In particular, it does not depend much on the size of the particles or on the packing of the bed.

It can also be understood, by examining Figure 18.3, that the nature of the contact between the granular bed and the wall influences the stability conditions. If the wall is very smooth, the bed will flow for an inclination angle smaller than the angle of internal friction of the granular material, likewise a spring snow avalanche which leaves bare grass behind it. Consequently, the friction angle ϕ' between the grains and the wall is also introduced, defined as the ratio of the tangential stress to the normal stress characteristic of the onset of movement at the wall. In order to measure the angle of internal friction of the granular material by gradually tilting the wall, it is preferable to glue a layer of grains onto the wall so as to determine the internal friction angle ϕ rather than the friction angle ϕ' between the grains and the wall.

18.3. Microscopic approach to a granular material

Describing, at a microscopic scale, the static equilibrium within the gravity field of a granular material entails modeling the balance of forces exerted on each grain, namely the weight and the contact forces with neighboring grains. It is easier to understand this microscopic approach by studying the simplified two-dimensional configuration of the stacking of circular rollers between two vertical walls, as depicted in Figure 18.4. Each cylinder is first subjected to its own weight applied at

its center of gravity. It also undergoes forces at every point of contact with the side wall or with another cylinder.

To begin with, it is assumed that the contact forces do not involve any friction force. They are therefore normal to the contact surface. The contact force exerted on a cylinder is necessarily directed toward its center, since it can be pushed but not pulled. In Figure 18.4, the forces applied on every cylinder are drawn with a different gray level, distinguishing these forces with those applied on neighboring cylinders. The contact forces are indicated as continuous arrows, whereas the weight is shown as a dotted arrow applied at the center of gravity. In this case of static equilibrium, the contact force is simply calculated, starting with the upper cylinder. For each element, the set of forces balance one another. The sketch highlights two properties:

1. The side wall exerts a contact force on the cylinders that touch it, or conversely due to the action–reaction principle, the cylinders exert a pressure force on the vertical walls.

2. In the absence of friction, the contact forces exerted on the side walls and on the bottom increase with the height of stacking above the roller considered.

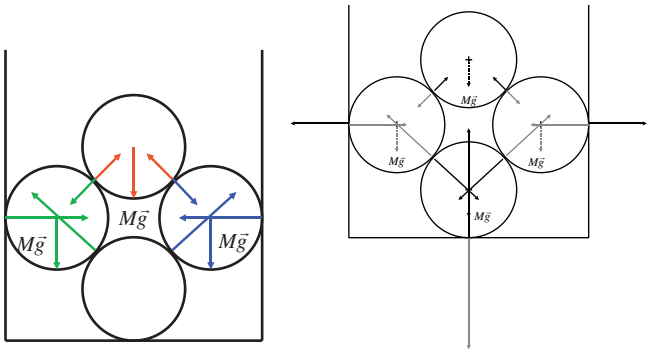

Figure 18.4. *Static equilibrium of circular cylinders between two vertical plates, in the absence of friction force. The same gray level indicates the forces applied on each cylinder. The weight is drawn as a dotted arrow and the contact forces as continuous arrows*

Let us now consider that the contacts between the rollers, and between the rollers and the side wall, involve friction forces. If we focus on one roller in contact with the side wall, it can be found that the weight of the rollers located above pushes the respective roller against the wall, on which it applies a pressure force. The contact of the roller against the wall is liable to generate at the wall a vertical friction force onto the roller, oriented upwards, which contributes to preventing its downward displacement. Its magnitude is unknown; Coulomb's law provides the maximum

magnitude of the friction force exerted by the wall on the roller. The larger the normal force applied by the roller on the wall is, the larger the friction force is. When friction is taken into account, the balance of forces on each roller, at equilibrium, can no longer be calculated without knowing the "degree of friction involvement" occurring on each grain, in the words of Duran,[2] who also mentions the "disorder in friction forces." What is clearly understood is that the friction at the wall will be able to compensate for part of the weight of the grains contained in a layer between two levels on the vertical axis.

The Reynolds dilatancy of a granular material is a phenomenon that has to be studied in order to understand how friction forces are "activated" between grains when pressure forces are applied on a granular material. The principle of dilatancy postulates that if a granular material is compressed, it must first expand to allow displacements between grains. The principle may act in a counter-intuitive way, but very simple observations help in understanding this effect. When we walk on a wet beach, for example, we find that the sand dries up around our footsteps, which proves that the surface water is sucked into the ground because the granular material expands.[3] As a result, certain volumes within the granular material subjected to compression will expand, allowing grain displacements, while other grains exert forces resisting the squeezing of the granular material by constituting a skeleton within the granular material, along which the forces balancing the weight of the granular material are transmitted. The mechanisms described indicate that the granular material takes on a discrete structure, as can be seen in Figure 18.5. On this image of a stack of cylinders, lines where strong stress is produced (lightly colored) are visible along chains that transmit forces up to the walls of the container. Figure 18.5 shows that force transmission in a granular material is heterogeneous. Arches are formed, which transmit most of the stresses. These arches carry the weight of the cylinders situated above, while the grains below are essentially subjected only to their weight. In an hourglass, the flow can sometimes be observed to stop when the formation of an arch blocks the particles.

18.4. Macroscopic modeling of the equilibrium of a granular material in a silo

We now turn to a macroscopic description, using continuum mechanics, to describe the static equilibrium of a granular materialmedium. The forces applied in the granular material are thus modeled at a scale larger than that of a grain. This approach is disproved by detailed studies, as shown by the results of the microscopic approach, but specialists[4] acknowledge that Janssen's theory (1895) satisfactorily

2 See beginning of this chapter.
3 Here, we almost repeat the words of Duran. The reader may also refer to the figure on p. 80 of Duran's book, which describes an elegant experiment for demonstrating this phenomenon.
4 Bideau and Ammi (2001).

portrays pressure variations in a silo. Another important reason for presenting it is its seminal character for the mechanics of granular materials.

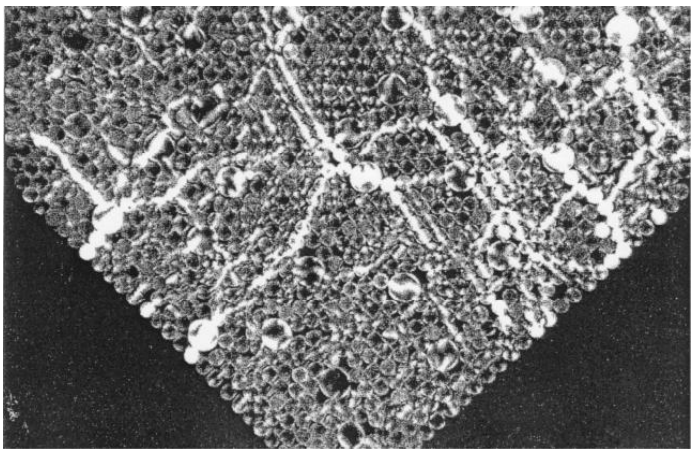

Figure 18.5. *Photo elastic image of stacked cylinders (Travers et al., 1986). Grains on which high stresses are applied appear as lighter*[5]

We now consider, in the geometry defined in Figure 18.6, the static equilibrium of a homogeneous granular material between two vertical plates located at $x = -L$ and $x = L$. We will study the equilibrium of the granular material using a continuum approach, by modeling forces inside the granular bed using the stress tensor discussed in Chapter 1. This tensor, which is necessarily symmetrical:

$$\Sigma(x,z) = \begin{pmatrix} \sigma_{xx}(x,z) & \tau(x,z) \\ \tau(x,z) & \sigma_{zz}(x,z) \end{pmatrix} \qquad [18.3]$$

models the mechanical forces within the granular material, by varying continuously in space. The force exerted at a point (x,z) through a horizontal surface by the granular material on top over the granular material below it is:

$$\begin{pmatrix} \sigma_{xx}(x,z) & \tau(x,z) \\ \tau(x,z) & \sigma_{zz}(x,z) \end{pmatrix} \begin{pmatrix} 0 \\ 1 \end{pmatrix} = \begin{pmatrix} \tau(x,z) \\ \sigma_{zz}(x,z) \end{pmatrix} \qquad [18.4]$$

5 Figure 18.5 is from the article by Bideau and Ammi (Ecoulements gravitaires: sabliers et silos, *Mécanique des milieux granulaires*, collective work edited by J. Lanier, Hermès Sciences, 2001).

while the force exerted at the same point through a vertical surface by the granular material to the right on the medium to the left is:

$$\begin{pmatrix} \sigma_{xx}(x,z) & \tau(x,z) \\ \tau(x,z) & \sigma_{zz}(x,z) \end{pmatrix} \begin{pmatrix} 1 \\ 0 \end{pmatrix} = \begin{pmatrix} \sigma_{xx}(x,z) \\ \tau(x,z) \end{pmatrix} \quad [18.5]$$

These two calculations allow us to note that components σ_{xx} and σ_{zz} are associated with normal forces through a vertical or horizontal surface, respectively. These are pressure forces. In contrast, the τ component corresponds in both cases to a force parallel to the surface, which is a friction force.

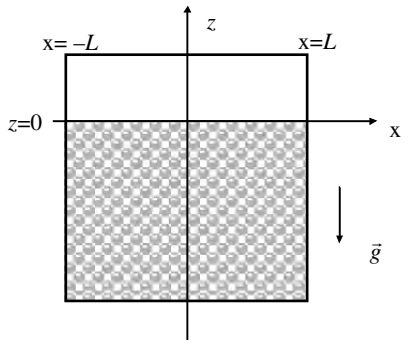

Figure 18.6. *Static equilibrium of a granular material between two vertical plates*

It has been explained previously (Figure 18.4) that the stacking of a granular material within the gravity field generates a pressure force in the *Ox* direction. The two stresses σ_{xx} and σ_{zz} are related but not necessarily equal. Janssen's model postulates a proportionality relationship between them, that is:

$$\sigma_{xx}(x,z) = K\sigma_{zz}(x,z) \quad [18.6]$$

In the following, we assume for simplicity that $K = 1$, and we denote by σ the terms σ_{xx} and σ_{zz}. While this is generally not the case in a granular material, unlike a fluid, the $K = 1$ hypothesis saves complications in formulation without altering the physical phenomena to be described. Assuming that the stresses $\tau(x,z)$ are non-zero, the model incorporates friction by a Coulomb-like approach. In an equilibrium situation, this means that:

$$\text{inside the medium } \left|\frac{\tau(x,z)}{\sigma(x,z)}\right| \leq tg\phi \text{ for } |x| < L \quad [18.7]$$

and on the wall $\left|\frac{\tau(\pm L,z)}{\sigma(\pm L,z)}\right| \leq tg\phi'$. [18.8]

Angle ϕ is the internal friction angle of the granular material and angle ϕ' the friction angle between the grains and the wall. In the following we assume these two angles to be equal.

The solution to the problem as set out by Janssen relies on the hypothesis that the limiting condition of stability is reached at the side walls. The force exerted on the granular bed by the wall at $x = L$ is:

$$\begin{pmatrix} \sigma(x,z) & \tau(x,z) \\ \tau(x,z) & \sigma(x,z) \end{pmatrix} \begin{pmatrix} 1 \\ 0 \end{pmatrix}_{x=L} = \begin{pmatrix} \sigma(L,z) \\ \tau(L,z) \end{pmatrix} \quad [18.9]$$

We necessarily have $\sigma(L,z) < 0$, as the wall presses on the bed, and $\tau(L,z) > 0$ since friction prevents the grain from falling downwards. The limiting condition of stability is written as:

$$\tau(L,z) = -\mu\sigma(L,z) \text{ with } \mu = tg\phi. \quad [18.10]$$

The condition on the $x = -L$ surface is, likewise,

$$\tau(-L,z) = \mu\sigma(-L,z). \quad [18.11]$$

At the surface of the granular material (z = 0) the stresses equal zero, that is:

$$\begin{aligned} &\tau(x,z=0) = 0 \\ &\sigma(x,z=0) = 0 \end{aligned} \quad [18.12]$$

Equations [18.10]–[18.12] are the boundary conditions for static equilibrium within the granular material under gravity, which is expressed by considering the divergence of the stress tensor at every point to be equal to the weight of the granular material per unit volume:

$$\frac{\partial\sigma}{\partial x} + \frac{\partial\tau}{\partial z} = 0 \quad [18.13]$$

$$\frac{\partial\tau}{\partial x} + \frac{\partial\sigma}{\partial z} - \rho_b g = 0 \quad [18.14]$$

$\rho_b = \rho_s(1-\varepsilon)$ is the density of the granular material.

The stress $\sigma(x,z)$ is an even function for variable x, the solution of the hyperbolic partial differential equation:

$$\frac{\partial^2\sigma}{\partial x^2}-\frac{\partial^2\sigma}{\partial z^2}=0 \qquad [18.15]$$

which is solved in the domain ($0\le x\le L,\ \ z\le 0$) with the boundary conditions derived from conditions [18.10] and [18.12]:

$$\begin{aligned} &\sigma(x,0)=0, && \frac{\partial\sigma}{\partial z}(x,0)=\rho_b g \\ &\frac{\partial\sigma}{\partial x}(0,z)=0, && \frac{\partial\sigma}{\partial x}(L,z)=\mu\frac{\partial\sigma}{\partial z}(L,z) \end{aligned} \qquad [18.16]$$

It is easy to numerically integrate the partial derivative equation [18.15], starting from the free surface, with the boundary conditions [18.16]. The pressure field $p(x,z)=-\sigma(x,z)$ is plotted in Figure 18.7 along the symmetry axis ($x=0$) and along the wall ($x=L$). The two curves are close to one another. The most important result is that the pressure levels out at a value equal to $\rho_b gL/\mu$ when depth is greater than a few times the width $2L$ of the container. The calculation was performed for an internal friction angle ϕ = 30° (i.e. μ = 0.58).

Janssen's classic analytical solution is superimposed in Figure 18.7. It only considers static equilibrium in the Oz direction (equation [18.14]), with the additional simplification that the stress $\sigma(x,z)$ (in other words, the pressure field) is uniform in any horizontal plane (independent of the coordinate x). Equation [18.14] then dictates that the stress $\tau(x,z)$ varies linearly with x. As this is an odd function due to the symmetry of the problem, we write:

$$\tau(x,z)=\tau(L,z)\frac{x}{L} \qquad [18.17]$$

Assuming now that the limiting condition of equilibrium (equation [18.10]) is reached on the wall, [18.14] thus becomes:

$$-\mu\frac{\sigma(z)}{L}+\frac{\partial\sigma}{\partial z}=\rho_b g \qquad [18.18]$$

As $\sigma(z=0)=0$, the pressure field obtained by Janssen is:

$$P_J(z)=-\sigma(z)=\frac{\rho_b gL}{\mu}\left\{1-\exp\left(\mu\frac{z}{L}\right)\right\} \qquad [18.19]$$

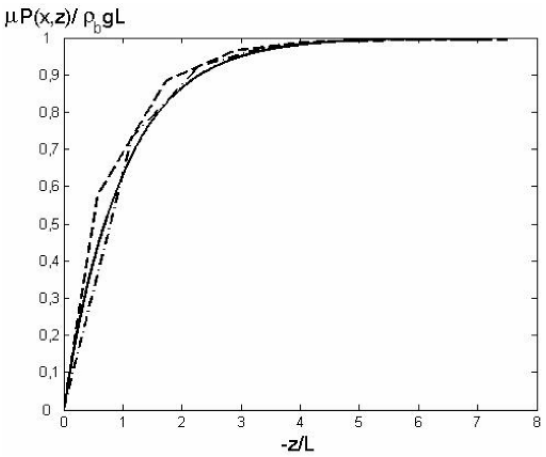

Figure 18.7. *Static equilibrium of a granular bed within the gravity field for the two-dimensional planar configuration of Figure 18.6.* μ *= 0.58. Pressure variation in the vertical direction. ____: Janssen's model, ----: 2D model, variation on the axis (x = 0), -.-.-.: 2D model, variation on the wall (x = L)*

The levelling-out pressure is

$$P_{\max} = \frac{\rho_b g L}{\mu} \qquad [18.20]$$

Figure 18.7 shows that Janssen's approximate analytical solution is quasi-identical to the previously described exact solution for 2D equilibrium. The same limiting value of pressure is obtained.

Plotting, at different depths, the variations in the *Ox* horizontal direction of the pressure (Figure 18.8(a)) and of the friction stress (Figure 18.8(b)) allow the static equilibrium in the granular bed to be analyzed. It is verified that the solution at the larger depth ($z / L = -13$) is identical for the 2D model and for Janssen's model. The pressure ratio is almost equal to 1 (Figure 18.8(a)) and the profile of the friction stress overlies the linear law [18.17]. At a smaller depth ($z / L = -1$), for the 2D model the friction stress is zero in the central part of the vessel, and pressure increases linearly with depth, which renders the pressure calculated by the 2D model higher than that predicted by Janssen's model. The friction stress follows a linear law in the zone near the wall, which widens as one moves deeper into the silo. The friction stress gradient gradually establishes itself in the silo. The levelling-out pressure is reached when the friction stress applied to positions $x = L$ and $x = -L$ is sufficiently large to carry the weight of the granular elements contained between these two points.

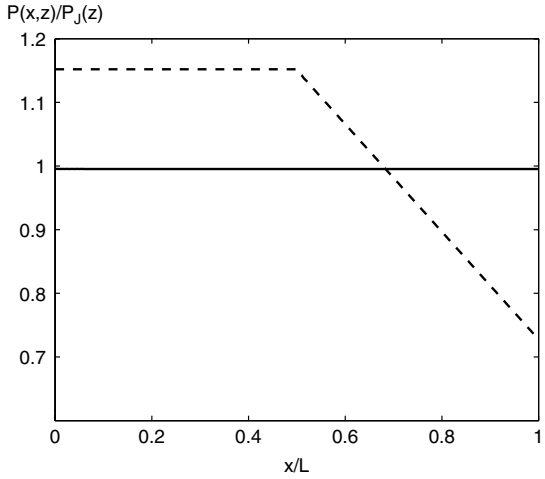

(a) Pressure profile along Ox

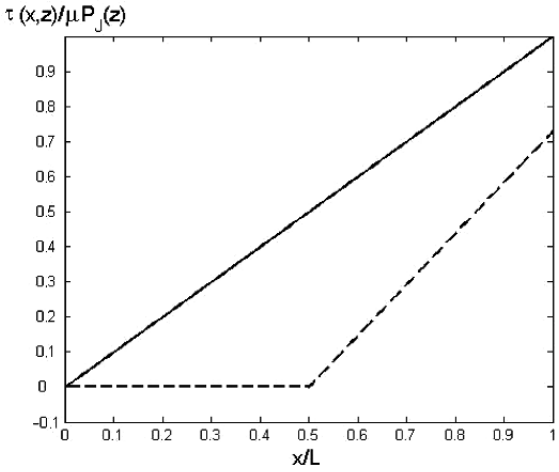

(b) Friction stress profile along Ox

Figure 18.8. *Static equilibrium of a granular bed within the gravity field for the two-dimensional plane configuration of Figure 18.6. $\mu = 0.58$. ------: 2D model, $z / L = -1$; ____: 2D model, $z / L = -13$. $P_J(z)$ is the pressure given by Janssen's model (equation [18.19])*

18.5. Flow of a granular material: example of an hourglass

The results on the pressure field, described in section 18.4, help us in understanding the flow of a granular material within the gravity field, when it

occurs. The example of the hourglass, depicted in Figure 18.9, illustrates this clearly. For a liquid, the flow velocity depends on the height h of the liquid, as stated by Torricelli's formula[6] $W = \sqrt{2gh}$.

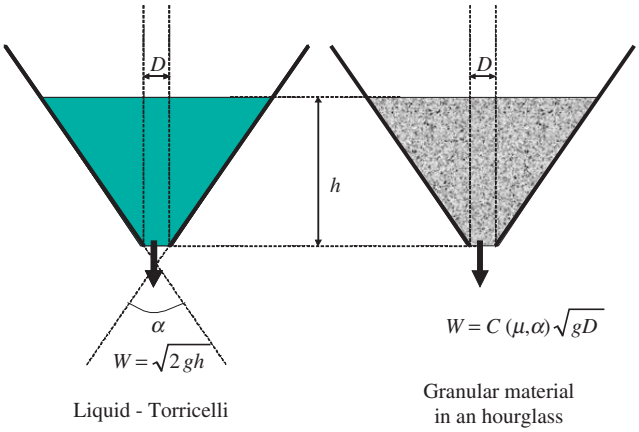

Figure 18.9. *Comparison of the flow in an "hourglass-type" geometry for a liquid (a) and a granular material (b)*

For a granular material, it is important to note that the flow velocity does not depend on the height h. The granular material flows with a constant velocity, which depends only on the characteristics of the granular material (its internal friction angle $\mu = tg\varphi$), on the diameter D of the orifice and on its opening angle α, as well as the gravitational acceleration. Dimensional analysis then yields:

$$W = C(\mu,\alpha)\sqrt{gD} \qquad [18.21]$$

This result is readily understood if one reverts to the notion of pressure field saturation set out in section 18.4. The pressure exerted on the granular material in the vicinity of the orifice is given by the width of the orifice as established by [18.20] if the height of the granular material is sufficient. The pressure is a local data, and it is this pressure value that sets the velocity. Relation [18.21] is classically converted into the well-known form of "Beverloo's law" which expresses the flow rate as a function of the same quantities:

$$Q = C(\mu,\alpha)g^{1/2}(D - kd)^{5/2} \qquad [18.22]$$

6 See Exercise 2.I in Chapter 2.

d represents the grain size and *k* is a constant which equals 1.5 for spherical grains. Unlike liquids, the flow of a granular material is subject to some unpredictability. Accidental blockage of the flow sometimes occurs due to the formation of a stable arch. This phenomenon is rarer, the smaller the grain size is compared to that of the orifice. It is usually considered that *D* should be greater than 6*d*.[7]

7 A more detailed description of these flows can be found in the article by Bideau and Ammi (2001).

Physical Properties of Common Fluids

Unless specifically stated, the values in the table below are given for conditions of temperature $T = 20°C$ and pressure $P = 1$ atm $= 1.013 \times 10^5$ Pa.

<table>
<tr><th></th><th colspan="2">Water</th><th colspan="2">Air</th></tr>
<tr><td>Density ρ
(kg m^{-3})</td><td colspan="2">998.2</td><td colspan="2">1.205</td></tr>
<tr><td>Kinematic viscosity ν
(m^2 s^{-1})</td><td colspan="2">10^{-6}</td><td colspan="2">15×10^{-6}</td></tr>
<tr><td>Dynamic viscosity μ
(Pa s = kg m^{-1} s^{-1})</td><td colspan="2">0.998×10^{-3}</td><td colspan="2">1.808×10^{-5}</td></tr>
<tr><td>Heat diffusion coefficient
k_H (m^2 s^{-1})</td><td colspan="2">1.42×10^{-7}</td><td colspan="2">2.08×10^{-5}</td></tr>
<tr><td>Prandtl number
$\mathrm{Pr} = \nu / k_H$</td><td colspan="2">7.04</td><td colspan="2">0.72</td></tr>
<tr><td>Isothermal compressibility coefficient (Pa^{-1})</td><td colspan="2">4.5×10^{-10}</td><td colspan="2">7.05×10^{-6}</td></tr>
<tr><td>Velocity of sound a
(m s^{-1})</td><td colspan="2">1486</td><td colspan="2">343</td></tr>
<tr><td>Specific heat
(J kg^{-1} K^{-1})</td><td colspan="2">$c_p = 4182$</td><td colspan="2">$c_p = 1012$
$c_v = 718$ ($T = 15°C$)</td></tr>
<tr><td rowspan="2">Surface or interfacial tension (N m^{-1})</td><td>Oil</td><td>2.0×10^{-2}</td><td>Water</td><td>7.28×10^{-2}</td></tr>
<tr><td>Mercury</td><td>3.75×10^{-1}</td><td>Mercury</td><td>4.87×10^{-1}</td></tr>
<tr><td rowspan="2">Molecular diffusion coefficient k_M
inside the fluid
(m^2 s^{-1})</td><td>Rhodamin 6G
(dye)</td><td>2.8×10^{-10}</td><td rowspan="2">Water vapor
($T = 8°C$)</td><td rowspan="2">2.39×10^{-5}</td></tr>
<tr><td>NaCl
$C = 0.01$ mol L^{-1}
$T = 25°C$</td><td>1.55×10^{-9}</td></tr>
<tr><td rowspan="2">Schmidt number
$\mathrm{Sc} = \nu / k_M$</td><td>Rhodamin 6G
(dye)</td><td>3571</td><td rowspan="2">Water vapor
($T = 8°C$)</td><td rowspan="2">0.59</td></tr>
<tr><td>NaCl
$C = 0.01$ mol L^{-1}
$T = 25°C$</td><td>577</td></tr>
</table>

Usual physical constants

Boltzmann constant	$k = 1.38 \times 10^{-23}$ J K^{-1}
Universal gas constant	$R = 8.31$ Jmol^{-1}K^{-1}
Avogadro number	$N_A = 6.02 \times 10^{23}$ atoms mol^{-1}
Permittivity in a vacuum	$1/4\pi\varepsilon_0 = 9 \times 10^9$
Charge of one electron	$e = 1.60 \times 10^{-19}$ C

Index